A NONLINEAR FINITE ELEMENT STUDY OF REINFORCED CONCRETE BEAMS

by

Akthem Abdulkarim Al-Manaseer, B.Sc.

A thesis submitted for the degree of

Doctor of Philosophy

Department of Civil Engineering

University of Glasgow

August, 1983

To

my Parents

and

my Teachers

ACKNOWLEDGEMENTS

The work described in this thesis was carried out in the Department of Civil Engineering at the University of Glasgow under the general direction of Professor A. Coull whose help and interest is gratefully acknowledged.

I wish to express my indebtedness to my supervisor, Dr. D. V. Phillips for his valuable guidance, advice and constant encouragement throughout the work.

Many thanks are due to:

Professor H.B. Sutherland whose help was most appreciated.

Dr. P. Bhatt and Dr. D. R. Green for their interest and useful discussions.

The computer staff of the Civil Engineering Department, especially Miss A. MacKinnon, Miss C. John and Mrs. A. McVey for their advice and help.

The staff members of Glasgow University Computing Service in particular Dr. W. Sharp and Mrs. D. Worster for their help in some matters relating to programming.

Many friends whose help and advice will never be forgotten.

Mrs. L. Williamson for her efficient typing.

Finally, my thanks are reserved for my family for their boundless patience, continual encouragement and financial support throughout the years.

SUMMARY

This thesis describes the development of plane stress, nonlinear finite element method of analysis for reinforced concrete beams. These include simple, deep, and T-beams, failing in flexure and in shear. The nonlinear response is assumed to be caused by concrete cracking, nonlinear biaxial stress-strain relations, and by the yielding of steel reinforcement.

The smeared crack approach was used with two models for post cracking behaviour, one with a tension stiffening effect and the other with no-tension stiffening. The endochronic theory with some adaptations was used to account for all other uncracked zones.

8-noded isoparametric elements were used for concrete representation and 3-noded isoparametric elements for steel. A modified Newton-Raphson approach, was used for solving the nonlinear problem with both the constant and variable stiffness methods. This was based on the evaluation of a tangential elasticity matrix. The unbalanced nodal forces were obtained by the method of residual forces and convergence was checked using either a force or a displacement criteria.

A nonlinear finite element program was developed where all the required aspects to model the reinforced concrete structures were included. It was a main contention of this work that the nonlinear solution parameters had such an important influence on the solution process that an extensive study was required to determine their effects. This was carried out on simple and complex beams, and suitable guide lines were established. In particular tension stiffening effects were investigated and rejected in favour of a method with no-tension

stiffening used in conjunction with controls on other solution parameters. Other parameters such as order of Gauss rule, shear retention factor, convergence tolerance, etc. were also studied in detail.

An investigation into the behaviour of a range of deep beams including perforated deep beams and beams which were heavily reinforced, was undertaken. These beams failed both in shear and flexure. In most cases crack pattern, stress distribution, and load deflection curves were used to validate, (or otherwise), the performance of the proposed models and program.

Finally a method is proposed for analysing T-beams using plane stress elements where the flange is treated separately and is connected to the web by a fictitious element. Other approximations are introduced in order to treat the problem as a two dimensional structure.

C O N T E N T S

NOTATION

Major symbols used in the text are listed below, others are defined as they first appear. Some symbols have different meanings in different contexts; these are clearly defined.

General symbols:

$\{\ \}\ ,\ \{\ \}^T$	Curly brackets denote column and row vectors
$[\ ]\ ,\ [\ ]^T$	Square brackets denote rectangular matrices
	In both cases T over the brackets denotes the transpose;
	-1 over square matrices denotes the inverse
$\|\ \|$	Straight brackets denote the absolute value
$\det\ \|\ \|$	Denotes the determinant of a square matrix

Scalars:

A_s	Cross sectional area of steel
dA	Elementary area
dv	Elementary volume
E_c	Modulus of elasticity for concrete
E_s	Modulus of elasticity for steel
E_w	Strain hardening modulus for steel
f'_c	Uniaxial compressive strength of concrete
f_{cu}	Cube strength of concrete
f_s	Stress in steel
f'_t	Tensile strength of concrete
f_y	Yield stress of steel
G, G_o	Shear modulus
h_f	Height of flange for a T-beam
I_1, I_2, I_3	First, second and third invariants of the symbol that follows in parenthesis
J_2	Second invariant of the deviator of the symbol that follows in parenthesis
K, K_o	Bulk modulus

P^e	Strain energy of an element e
P_i, $P_i(\xi,\eta)$, $P_i(\xi)$	Shape functions
P_i^*	Norm of the total applied load
Q_s	Computed ultimate load
t	Thickness of an element; time
t_f	Thickness of flange for a T-beam
u_i,v_i	Component of displacement at node i
u,v	Component of displacement in x,y
X	Distance from the outer side of a flange in a T-beam
x,y	Global cartesian coordinates in planer problems
x*,y*	Principal axes
W	Imposed potential energy due to external load
W_u	Measured ultimate load
z,z',z_o,z^*	Intrinsic time parameters
α	Aggregate interlocking factor
ζ,ζ'	Damage parameters
$\lambda,\lambda',\lambda_o$	Dilatation parameters
ξ,ξ'	Distortion parameters
η,ξ	Normalized local curvilinear coordinates
ϵ	Strain
ϵ_c	Concrete strain
ϵ_c'	Uniaxial cracking strain of concrete
ϵ_{cu}	Uniaxial crushing strain of concrete
ϵ_m	Mean strain
ϵ_s	Steel strain
ϵ_v	Volumetric strain
ϵ_{xx}, ϵ_{yy}, γ_{xy}	Strain components in global directions
$\epsilon_1,\epsilon_2,\epsilon_3$	Principal strains

ν , ν_c	Poisson's ratio for concrete
σ	Stress vector
σ_c	Stress in concrete
σ_m	Mean stress
σ_s	Steel stress
$\sigma_{xx},\sigma_{yy},\tau_{xy}$	Stress component in global directions
σ_y	Yield stress of steel
$\sigma_1,\sigma_2,\sigma_3$; $\sigma_{max},\sigma_{med},\sigma_{min}$	Principal stresses

Vectors and Matrices:

$[B]$, $[B_B]$	Strain matrix
$[D]$, $[D_c]$	Elasticity matrix
$\{F\}^e$	Nodal forces at nodes of an element e
$\{F\}^e_{\varepsilon_o}$	Nodal forces vector due to initial strains
$\{F\}^e_{\sigma_o}$	Nodal forces vector due to initial stress
$\{F\}_p$	Nodal forces vector due to distributed load per unit volume
$\{F\}_g$	Nodal forces vector due to boundary pressure
$\{F\}$	Nodal forces vector due to external load
$\{F_B\}$	Nodal forces vector for steel bars
$\{F_u\}$	Unbalanced nodal forces vector
$\{g\}$	Components of boundary pressure
$[J]$	Jacobian matrix
$[K]$, $[K_o]$, $[\bar{K}]$	Overall stiffness matrix
$[K]^e$, $[K_B]$	Element stiffness matrix

$\{P\}_i$	Vector of total applied load
$\{\bar{P}\}$	Vector of distributed load per unit volume
$\{R\}, \{R\}_n$	Vector of total imposed load
$[R]$	Rotation matrix
$\{\delta\}$	Overall displacement vector
$\{\delta_B\}, \{\delta\}_i, \{\delta\}_u$	Nodal displacements
$\{\delta\}^e$	Nodal displacements associated with element e
$\{\psi\}_i$	Vector of residual nodal forces
$\{\sigma\}, \{\sigma\}_n$	Total stress vector
$\{\sigma_o\}$	Initial stress vector
$\{\sigma_B\}$	Stress vector for bar element
$\{\sigma^P\}_n$	Inelastic stress vector
$\{\sigma_c\}_n$	Stress vector in cracked direction
$\{\sigma_p\}_n$	Principal stress vector
$\{\varepsilon\}, \{\varepsilon\}_n$	Total strain vector
$\{\varepsilon_o\}$	Initial strain vector
$\{\varepsilon_B\}$	Strain vector for bar element
$\{\varepsilon_c\}_n$	Strain vector in cracked direction
$\{\varepsilon_P\}_n$	Principal strain vector

Tensors:

δ_{ij}	Kronecker delta
$\varepsilon_{ij}, \varepsilon_{k\ell}$	Strain tensor
ε_{kk}	Volumetric strain tensor
$P_{ijk\ell}$	Fourth order tensor
σ_{ij}	Stress tensor
σ^P_{ij}	Inelastic stress tensor

σ_{kk}	Hydrostatic stress tensor
e_{ij}	Deviatoric strain tensor
e_{ij}^{e}	Elastic part of deviatoric strain tensor
e_{ij}^{p}	Inelastic part of deviatoric strain tensor
S_{ij}	Deviatoris stress tensor
S_{ij}^{p}	Inelastic deviatoric stress tensor

General abbreviations:

C	First cracking load
C_D	Specified convergence tolerance (displacement)
C_F	Specified convergence tolerance (force)
1C	First cracking model
2C	Second cracking model
COOP	Convergence tolerance
C.S.M.	Constant stiffness method
DC1	First displacement criterion
DC2	Second displacement criterion
F.D.C.	Failure indicated by displacement criterion
F.L.C.	Failure indicated by load criterion
G.R.	Gauss rule
I	Maximum limit of iterations
I.N.L.	Iterations not limited
Incr. No.	Increment number
IT = 1	Stiffnesses are updated at the beginning of the first iteration of each increment
IT = 2	Stiffnesses are updated at the beginning of second iteration of each increment
IT = 1 & 2	Stiffnesses are updated at the beginning of the first and second iteration of each increment
LC	Load criterion

Max.	Maximum
1 Mat.	One type of concrete is used
2 Mat.	Two types of concrete are used to account for confinement
N.C.	No convergence obtained
No. of Iter.	Number of iterations
N.T.S.	No tension stiffening
Ref.	Reference
T.M.1	Flange rotation method
T.M.2	Side elevation method
V.S.M.1	Similar to IT = 1 & 2
V.S.M.2	Stiffnesses are updated at the beginning of each iteration
Y	Load at first yield

Symbols used for crack plots:

/	Single open crack
⫽	Double open crack
//	Single closed crack
#	Double closed crack
⊞	Yielding of steel
*	Crushing of concrete

N.B.1 All dimensions in the figures are in mm units unless otherwise stated.

N.B.2 ε_{cu} = 0.0035 for simple beams

ε_{cu} = 0.0040 for deep beams

unless otherwise stated.

CHAPTER 1

INTRODUCTION

1.1 General

1.2 Scope and purpose

CHAPTER 1
INTRODUCTION

1.1 General

From early times builders have used material to cement stone or brick together. The first cementing material was probably mud. Sometimes this was mixed with straw to increase its strength, as was used in ancient Egypt. Other civilizations, too, have developed this concept of using two or more materials together to complement each other. For instance the Babylonians and Assyrians used naturally occurring bitumens to bind stones together.

Looking to modern times, we see that these ancient ideas are still being used. Concrete reinforced with steel is similar to straw mixed with mud. One reason why concrete is such an important construction material is because of its ability to combine with steel.

Before a reinforced structure can be designed or analysed, sufficient knowledge about the materials is required. In recent years, significant advances have been made in the understanding of concrete behaviour. However this is still incomplete. Disparities in experimental results are often observed due to difficulties in obtaining consistent test procedures and test specimens and due to the natural variability of concrete itself.

On the other hand, the behaviour of steel reinforcement is more easily measured. This is because this behaviour is predominantly uniaxi
However complexities do arise. Bond-slip between steel and concrete, dowel action under shear deformation etc. can significantly influence behaviour. Work is still in progress to improve understanding of these effects.

Development in the power of modern computing hardware has made possible the inclusion of highly complex material behaviour into methods of analysis. For reinforced concrete this would include, for example, cracking, softening and crushing of concrete, multiaxial stress response of concrete, yielding and rupture of reinforcement, bond-slip between steel and concrete. A basic aim of an analytical method is to predict such behaviour as efficiently as possible and as accurately as is necessary. This implies knowing what aspects of behaviour to include and which to discard in any given situation.

The most powerful general analytical method now available in structural analysis is the finite element method. Its basic concepts and methodology are now well established and have been published widely. New applications are being developed continuously particularly in non-linear analysis. It has proved a remarkably adaptable method, capable of including various levels of behaviour, from relatively simple to complex. It is the most useful method to employ in a general study of reinforced concrete behaviour.

A successful analysis of the nonlinear behaviour of reinforced concrete requires the following aspects to be considered:

(1) A realistic material model for concrete and steel and their interaction.

(2) An efficient discretization technique to solve the basic continuum problem (i.e. the finite element method).

(3) An efficient and reliable solution technique (i.e. the method which is used to solve the nonlinear problem).

Because behaviour is so complex, approximations have to be introduced. Each aspect defined above will have its own varying degree of complexity. The true behaviour of concrete has to be modelled by approximate theories and by test data which is subject to scatter. The finite element method is a discretization process and therefore an approximation to true behaviour. The elements (size and type) are chosen to approximate some structural behaviour which is also approximate (e.g. plane stress, thin plate bending, etc.). The numerical processes used (e.g. integration rules, equation solving techniques) introduce approximations and numerical errors. Non-linear solution procedures introduce further approximations because they are usually iterative procedures which require controls on convergence, solution step sizes, etc.

Taken together all these approximations could cause significant departures from the true behaviour. They have to be chosen carefully to avoid dubious solutions. To do this it is important to understand the nature of the approximations, how they affect solutions and how they interact.

It might be expected that the better these approximations, the more accurate the final solution. However, because of interaction between these parameters defining each approximation, certain effects might be duplicated. Then the more complex procedures might not give better results. For instance it will be shown that post cracking behaviour can be approximated to give certain overall responses. Yet these can be reproduced by controlling other numerical solution parameters instead. This type of interaction has not been given as much attention as material modelling. Neither has it been used to advantage on a rational basis to achieve more economic solutions.

The general trend in the development of methods of analysis for reinforced concrete has been to introduce more and more complications to represent detailed aspects of behaviour. But there must be doubt as to whether this is possible to do accurately or if it is even necessary. Quite often the effects being simulated are difficult to check, for instance aggregate interlocking along cracks or tension stiffening between discrete cracks. This trend must mean more expensive solutions.

Simpler approximations usually give cheaper solutions. But then it is necessary to establish practical limits of accuracy and suitability. In setting these limits, it is obviously best to compare predicted behaviour with quantities which have practical engineering significance. For reinforced concrete analysis, these would include strains, displacements, stresses, cracking patterns, failure mechanisms etc. If such a comparison shows that two different sets of approximations give similar solutions, then it would make sense to accept the cheaper and simpler method, even if the other could be given a stronger physical basis.

If detailed parametric studies are to be made on certain classes of structures, then the method of analysis must be economic to use. The simplest approximations and devices must be found which gives the required information as accurately as necessary.

In this thesis, the behaviour of different types of reinforced concrete beams have been studied. These include heavily reinforced deep beams with and without openings, and various type of T-beams. The beams failed both in shear and in flexure. Many of the available methods for designing and analysing such beams are based on empirical

formulae. Moreover these empirical formulae are normally derived for one type of beam and are not applicable if changes are made to geometry, arrangement of reinforcement, loading conditions etc.

It is both difficult and expensive to undertake comprehensive experimental studies which can isolate the influence of certain parameters so that they can be included in general theories. The finite element method should be able to isolate more conveniently these specific parameters for study. This would assist in preparing suitable practical guidelines for design and simple analysis.

In order to prepare for parametric studies, different types of approximations need to be considered. Most structures are essentially three dimensional. Moreover it is often possible to predict significant behaviour by using cheaper two dimensional approximations such as plane stress. For many structures it is obvious how to make such an approximation. Other situations are not so obvious although it would be very advantageous if such procedures could be worked out. The T-beams in this study were analysed by an adaptation of the plane stress concept.

1.2 Scope and purpose:

A main aim of this work was to develop a nonlinear plane stress finite element program which can analyse a wide range of reinforced concrete beams subjected to short term loading up to failure conditions. Another aim was to use this in conjunction with other simple approximate techniques to analyse flanged beams and to determine their limits of applicability. This work has also been coupled with devising efficient data handling processes. The ultimate purpose of this was to establish

an economical program and procedures to undertake parametric studies of beam behaviour.

Three types of elements have been used; an 8-noded isoparametric element for concrete representation, a 3-noded axial element for steel, and an "8-noded" spring pseudo-element for representing web-flange connections in T-sections. Details of these elements are explained in Chapters 2 and 8.

A review of nonlinear methods of solution and a description of the method used in this analysis is presented in Chapter 3. For the solution of the linear equations a frontal technique is employed because of its proven efficiency and wide application, whilst a variant of the modified Newton-Raphson method with both the constant and variable stiffness methods has been used to solve the nonlinear equations.

In Chapter 4 a detailed survey of available literature on the experimental behaviour of concrete and steel and its mathematical modelling is given. This is followed in Chapter 5 by a description of the models used to represent their behaviour in this work.

The endochronic theory of concrete is used to represent various aspects of concrete behaviour and a variant is developed to suit two dimensional plane stress problems. It is used to represent behaviour in the compression-compression zone, and in the tension-compression and tension-tension zones up to the cracking stage. One of the advantages of this model is that it does not distinguish between the elastic and plastic ranges and therefore does not require a yield surface. The model will act almost linearly at low load levels and plastic deformation is accounted for automatically.

For cracking and post cracking behaviour of concrete, the smeared cracking approach is used. This has been used in numerous finite element structural problems, but its performance in combination with numerical and material parameters (such as convergence tolerance, convergence criteria, numerical integration, method of updating the stiffness, shear retention factor, etc.) has not received much detailed attention. In this thesis a study of these numerical parameters and their interaction on the predicted structural behaviour will be given. In particular the use of tension stiffening stress-strain curves to represent post cracking behaviour (i.e. a gradual release of stresses in the direction perpendicular to cracks after the development of a crack) will be investigated. Tension stiffening produces a stiffer response in the load deflection curve at high load levels. However other numerical parameters can also produce a stiffer load deflection curve and it will be shown that these could be just as efficiently used as tension stiffening. This will be discussed in Chapter 6.

For steel reinforcement a bi-linear uniaxial model with some strain hardening effects has been employed. It is well known that steel behaviour can be represented quite adequately by such a model.

Other inelastic effects (such as creep and shrinkage of concrete and cyclic loading, etc.) are not included. Although these are potentially important in an overall assessment of a concrete structure, they are beyond the scope of this thesis.

Another important factor which should be considered is that of data handling; input must be as straightforward and simple as possible even for the analysis of complex structures. Irregular mesh generators and

frequent error checks on input data have been developed; and such procedures minimise errors significantly.

Presentation of output and the ease of interpretation of these results are also important from the user standpoint. For this purpose graphical output has many advantages and in this work graphical facilities were introduced to plot cracking patterns, principal stresses, and contours of stress distributions.

The theories, program and related procedures have been used to analyse different types of beam such as simple and deep beams with and without openings, panel walls, and T-beams. These analyses have been compared with results of other researchers and this will be covered in Chapters 6 - 8.

Finally, general conclusions and recommendations are presented in Chapter 9.

CHAPTER 2

FINITE ELEMENT FORMULATION

CHAPTER 2
FINITE ELEMENT FORMULATION

2.1 Introduction:

The concept of the finite element method was originally introduced for structural analysis by Turner et al.[1] and Argyris and Kelsey[2] in the mid-50's. The name "finite element" was originally coined in a paper by Clough[3] in 1960, in which the technique was presented for plane stress analysis.

Since then general progress has been so rapid that the method is now one of the most powerful tools available in structural analysis. It has also been recognized as a general numerical method for approximately solving various systems of partial differential equations with known boundary conditions. Thus its application cover a wider range of physical problems other than structural. For instance, problems arising in such fields as fluid mechanics, magneto- and electro-dynamics, temperature fields, etc., can be solved.

Zienkiewicz[4] covers the mainstream of these developments and includes a wide bibliography of the publications reflecting these activities.

The method is a general discretization procedure for solving continuum problems defined by certain classes of mathematical statements. The continuum is subdivided into finite regions termed "elements", each of which possess a finite number of unknown parameters which approximate the values of the field variables which define the problem. These field variables may be scalars, vectors, or high order tensors. These elements connect with each other through common points existing on their boundaries at which continuity and compatibility of the field variables are enforced. These common points are termed "nodes". A set of functions are chosen to define the variation of the required

field variable within each element in terms of the unknown nodal values.

In structural mechanics problems, the unknown field variables can be displacements, stresses, or both. This gives rise to the displacement (stiffness) method, the force (flexibility) method, or the hybrid method respectively. The displacement method is the most widely used because of its relative ease of formulation compared to the other methods, although advocates of the hybrid method claim that it is as easy to formulate, and perhaps more accurate[5]. This research uses the displacement method, and further details will be explained in the next section.

The finite element method is unique in the way it can formulate the properties of individual elements of any type of problem. One of its main attractions is the ease with which it can be applied to problems with geometrically complicated boundaries.

The price that must be paid for this flexibility is in the amount of numerical computation required. Usually a large number of simultaneous equations have to be solved; if more elements and nodes are included for increased accuracy, then more equations will result. However, modern methods of equation solving e.g. the frontal solutions, banded solutions[6,7], etc., have been evolved to solve these equations as economically as possible, and it is well within the power of modern computers to solve large sets of equations.

The routine solution of linear problems by the finite element method, has been well established. For instance programs for solving problems in the theory of elasticity, thin and thick plate theory, and in 3-D etc., have all been developed and have now reached a high degree of sophistication.

In recent years the most intensive work has taken place in solving nonlinear problems. The general procedure for solving such problems is to approximate the nonlinear behaviour by a series of linear solutions. Hence the linear solution procedure is a basic and important part of any nonlinear solution method. Nowadays there are numerous texts[4, 6-18] which describe the various linear methods and their applications in great detail; so a detailed description is unnecessary here, and a brief summary only will follow in the next section.

2.2 Basic steps in the finite element method:

A derivation of the displacement linear elastic finite element method will be given in conjunction with the formulation of isoparametric elements in section 2.3. First, however, the basic steps will be described in general terms.

2.2.1 Selection of element type and discretization of the continuum:

The first step is to decide on the type of element to be used, and then to subdivide the continuum or solution region into a suitable number of elements with associated nodes. In general the following points are considered in element selection:

(A) Element type:

The selection of the element will be related to the type of problem to be solved. Generally these can be grouped into four classes:

1. Plane stress/plane strain/Axisymmetric (i.e. mathematically a 2-D problem).
2. Plate bending.
3. Shells.
4. Three dimensional (solid analysis).

In each group different levels of accuracy can be obtained. This depends on the number of nodal points and corresponding degrees of freedom which are associated with the element type. Nodal points are usually placed on the boundaries of the elements, although internal nodes can also be included in certain elements in order to increase efficiency. Usually the higher the order of element (i.e. the more degrees of freedom), the more accurate and expensive it is.

It would be expected that a solution would be more accurate if more elements were used (i.e. if a finer mesh was used). However, certain basic requirements have to be satisfied when selecting an element type to ensure convergence to the correct solution as the mesh becomes finer. These can be listed as follows:

1. The displacement field within an element must be continuous.
2. The displacement model must include the constant strain states of the element, i.e. the element should be able to reproduce a constant strain field, if the nodal displacements require it.
3. The element should be able to reproduce rigid-body motions, i.e. when nodal degrees of freedom correspond to rigid-body motion, the element must exhibit zero strain and zero nodal forces. This is a special case of the constant strain criteria.
4. Elements should be compatible, i.e. there should be no inter-element gaps or overlaps. Elements that violate these requirements in a mesh are called "incompatible" or "nonconforming". However an incompatible element can be valid and convergence is obtainable, if the incompatibilities disappear with increasing mesh refinement and the element approaches a state of constant strain.

5. An element should have no preferred direction. In other words, an element should be geometrically invariant, and give the same results in whatever direction it is orientated.

Elements edges can be straight or curved; this usually depends on the number of nodes defining the element edges. For example, straight edged elements will result from 3-noded triangles or 4-noded rectangular elements; curved edged elements will result from 8-noded quadrilateral isoparametric elements, because each edge is defined by three nodes. In this work curved edged plane stress/plane strain elements are used: an 8-noded isoparametric element for concrete representation and a 3-noded isoparametric element for steel representation. The reasons for this selection will be discussed later in section 2.3.1.

(B) <u>Element size:</u>

In general the finer the mesh the better the accuracy, but at the same time the larger the computational effort required. The number of elements to be used will be decided by the type of structure to be analysed, but generally more elements are required in regions where stresses vary rapidly than in regions where they vary gradually.

However, for complex elements coarser meshes will produce efficiencies as good as fine meshes for simpler elements i.e. less elements are needed.

In structural concrete the steel reinforcement may have an effect on the way the mesh is selected. Commonly, steel is represented by placing bar elements along the side of the element. This means that the element configuration could be controlled by the position of the

reinforcement. Formulations which allow the steel to pass internally through an element [19] do not have this problem but it is at the expense of slightly greater complexity of formulation and data input. Smeared reinforcement formulation where the steel and concrete is presented as one homogeneous material also avoids this problem[20], but separate information on the concrete and steel is not usually obtainable.

In this thesis for ease of formulation bar elements are used which coincide with the sides of the elements.

(C) Element aspect ratio:

The aspect ratio for two dimensional elements is defined as the ratio of the largest dimension of the element to the smallest dimension. The optimum aspect ratio at any location within the mesh depends largely upon the difference in rate of change of displacements in different directions. For instance if the displacements vary at about the same rate in each direction, the closer the aspect ratio to unity the better the quality of the solution. Desai[14] carried out a study using different aspect ratios to analyse a beam bending problem. In the study four noded rectangular elements were used, and he found that as long as the aspect ratios were near unity, accuracy was better.

A study on the aspect ratio for the 8-noded isoparametric element was also conducted in this research. A simply supported elastic beam was analysed using aspect ratios from 0.2 to 0.94 with different mesh sizes and with 2 x 2 and 3 x 3 Gauss rules. It was concluded that the effect of changing the aspect ratio, for the range between 0.5 and 0.94

had a minor effect on the accuracy of the displacement field using 2 x 2 and 3 x 3 Gauss rules. For narrow elements with an aspect ratio of 0.2, the accuracy in the displacement field was more affected, especially when using the 2 x 2 Gauss rule, and improvement was obtained in this case when the 3 x 3 Gauss rule was used.

In practical reinforced concrete analysis it is unusual to select elements which have an aspect ratio of unity because the steel configuration will apply other constraints. However it is advisable to keep this ratio as near to unity as possible. Indeed large values, which imply long narrow elements, should be avoided because numerical problems may arise in the calculations of the stiffness, some of which might become very small.

2.2.2 Shape functions:

A shape function defines the variation of the field variable, and its derivatives, through an element in terms of its values at the nodes. Therefore shape functions are closely related to the number of nodes and hence type of element.

Often, although not always, polynomials are selected as shape functions because they are relatively easy to manipulate mathematically, particularly with regard to integration and differentiation. However, the degree of polynomial chosen will clearly depend on the number of nodes and the degrees of freedom associated with the element.

2.2.3 Element properties:

After establishing the finite element model (i.e., once the element type and its shape function have been selected), element properties have to be determined. These are expressed in terms of

matrices and related to the nodal parameters and material properties of the element. Some common matrices are the strain and stress matrices which define the strain and stress respectively at specific points in the element in terms of its nodal displacements, the elasticity matrix which is used to relate stresses to strains at certain points, and so on.

Some of these matrices combine to define the stiffness matrix which forms part of the basic equation governing the overall behaviour of the element. This equation expresses the relation between displacements and forces at element nodes in terms of the element stiffness.

$$\text{i.e.} \quad \{F\}^e = [K]^e \{\delta\}^e \qquad (2.1)$$

where $\{F\}^e$ = vector of unknown element force,

$[K]^e$ = element stiffness matrix,

$\{\delta\}^e$ = vector of unknown displacements.

This equation is general and valid for all elements.

Two main concepts are commonly used to derive this equation: functional (energy) methods and weighted residual methods. Details of these methods are given in most finite element texts [4,18]. A brief explanation of the energy method will be explained later in this chapter.

2.2.4 Assembly of element properties:

Element properties have to be assembled to express the behaviour of the entire solution region or system, or in other words, the element matrix equations have to be combined in some fashion.

In the structural displacement method, the assembly process is

based on the laws of compatibility and equilibrium. It is required that the body remains continuous, which means that neighbouring points should remain in the neighbourhood of each other after the load is applied. Also displacements of two adjacent points must have identical values for compatibility to be satisfied. The matrix equation for the system has the same form as the equations for an individual element except that they now contain terms associated with all nodes.

This equation is then modified to take into account any boundary condition of the problem. These are the physical constraints or supports that must exist so that the structure or continuum has a unique solution.

2.2.5 Solution of the system of equations:

The equations assembled in the previous section will have the form:

$$\{F\} = [K]\ \{\delta\} \qquad (2.2)$$

where $\{F\}$ = total imposed loading vector.

$[K]$ = the overall property matrix (stiffness matrix).

$\{\delta\}$ = overall displacement vector.

Commonly these equations are solved for the unknown variables by using either a direct solution method (e.g. Gauss elimination) or an iterative method (e.g. Gauss-Seidal). The method used in this research is a form of the direct solution technique and is termed the frontal method[6]. This method will be described in more detail in section 3.7.

2.2.6 Final calculation:

After solving the equations a complete solution of the problem, is obtained by evaluating quantities depending on the solved unknown

field variables. For example in stress analysis, calculation of strains follow from evaluation of the unknown nodal displacements and hence stresses can be calculated.

2.3 Isoparametric elements:

2.3.1 Introduction:

The family of isoparametric elements was first introduced by Taig[21] and Irons[22,23]. It is called isoparametric because the same interpolation function used for defining the displacement variation within the element is also used to define the element geometry.

The basic procedure is to express the element coordinates and element displacements by functions expressed in terms of the natural coordinates of the element. A natural coordinate system is a local system defined by the element geometry and not by the element orientation in the global system. Moreover these systems are usually arranged such that the natural coordinate has unit magnitude at primary external boundaries, i.e. normalization is used.

As has been previously mentioned two types of isoparametric element are used in this work. These elements, based on strain (displacement) assumptions, are the eight noded isoparametric element for concrete representation and the three noded isoparametric element for steel representation. Figure (2.1) and Figure (2.2) show these two elements and their natural coordinate systems. Note that the natural coordinates in general are not orthogonal to the global system.

A different family of isoparametric elements, based on stress-assumptions, has been introduced by Robinson[17], who called them

"isoparametric stress elements". In these the shape functions also represent the stress variation through the element. However these elements are not widely used as yet and thus in this work only the strain shape function elements are employed. Details will be explained in the following section; first however the reasons for using isoparametric elements will be summarized.

1. For a given number of degrees of freedom, complex isoparametric elements are far more accurate and versatile than simple elements. Moreover a considerable saving of computer effort is obtained, even though a complex element requires more time to formulate. This is because it requires fewer elements compared with more simple elements.
2. Data preparation is considerably reduced with complex elements, although this can be neutralized to a certain extent by automatic mesh generator schemes.
3. Numerical integration makes the evaluation of the characteristics of curved, complex elements straightforward.
4. The simultaneous description of element geometry and displacement variation by the shape functions leads to efficient and reduced computing effort.
5. Curved element sides preclude the necessity for mesh refinements where the boundaries of a structure are curved. However sometimes the reduced number of complex elements may not be adequate to represent all the geometries of a particular problem.
6. In nonlinear cracking problems isoparametric elements can predict a number of cracks in a single element without losing all of its stiffness, and these cracks can form part of different cracked zones.

7. Decay of residual forces in the nonlinear analysis should be distributed more rapidly than in simple elements, because they cover a wider area.
8. In linear elasticity for the 8-noded isoparametric element, the displacement field is not significantly affected for different aspect ratios in the range between 0.5 and 1.0.

2.3.2 Isoparametric 8-noded strain element:

(a) Shape functions:

The shape functions and their derivatives are given in Table (2.1) where $P_i(\xi,\eta)$, i=1,8 are the shape functions in the curvilinear coordinate ξ and η . These shape functions are part of the so-called serendipity family[4], and they are shown pictorially in Figure (2.3). The properties of these shape functions are such that:

$$P_i = 1 \quad \text{if } (i = j)$$

and $$P_i = 0 \quad \text{if } (i \neq j).$$

The element has 2-degrees of freedom at each node, namely the displacements u_i, v_i, giving a total of 16 degrees of freedom. Thus the displacements at a point within the element is given by:

$$u = \sum_{1}^{8} P_i(\xi,\eta)\, u_i \qquad (2.3)$$

$$v = \sum_{1}^{8} P_i(\xi,\eta)\, v_i \qquad (2.4)$$

It should be noted that the displacements u and v are parallel to the x and y and not the ξ and η axes. Similarly the position of a point within the element in global coordinates is given by:

$$x = \sum_{1}^{8} P_i(\xi,\eta)\, x_i \qquad (2.5)$$

$$y = \sum_{1}^{8} P_i(\xi,\eta)\, y_i \qquad (2.6)$$

(b) Stress and strain evaluation:

The strains within the element are readily expressed in terms of the derivatives, of the displacements, i.e.

$$\{\varepsilon\} = \{\ \varepsilon_{xx} \quad \varepsilon_{yy} \quad \gamma_{xy}\ \}^T \qquad (2.7)$$

$$= \{\ \frac{\partial u}{\partial x} \quad \frac{\partial v}{\partial y} \quad (\frac{\partial u}{\partial y} + \frac{\partial v}{\partial x})\ \}^T$$

Substituting equations (2.3) and (2.4) into equation (2.7) leads to:

$$\{\varepsilon\} = [B]\ \{\delta\} \qquad (2.8)$$

where $\{\delta\} = \{\ u_1, v_1 \quad u_2, v_2 \quad \ldots u_i, v_i \ldots u_n, v_n\ \}^T$

$=$ Element nodal deformation vector

and $[B] = [\ B_1(\xi,\eta) \quad B_2(\xi,\eta) \ldots B_i(\xi,\eta) \ldots B_n(\xi,\eta)\ ]$

$=$ the strain matrix

in which:

$$[\ B_i(\xi,\eta)] = \begin{bmatrix} \frac{\partial P_i}{\partial x} & 0 \\ 0 & \frac{\partial P_i}{\partial y} \\ \frac{\partial P_i}{\partial y} & \frac{\partial P_i}{\partial x} \end{bmatrix} \qquad (2.9)$$

Since the interpolation functions P_i are defined in terms of the curvilinear coordinates ξ and η, a transformation from local to global coordinates is required in equation (2.9). It is well known that the cartesian and the curvilinear derivatives are related by:

$$\begin{Bmatrix} \frac{\partial}{\partial x} \\ \frac{\partial}{\partial y} \end{Bmatrix} = [J]^{-1} \begin{Bmatrix} \frac{\partial}{\partial \xi} \\ \frac{\partial}{\partial \eta} \end{Bmatrix} \qquad (2.10)$$

where $[J]$ is the Jacobian matrix defined by:

$$[J] = \begin{bmatrix} \frac{\partial x}{\partial \xi} & \frac{\partial y}{\partial \xi} \\ \\ \frac{\partial x}{\partial \eta} & \frac{\partial y}{\partial \eta} \end{bmatrix} \qquad (2.11)$$

Differentiating equation (2.5) and (2.6) in accordance with equation (2.11) gives:

$$[J] = \begin{bmatrix} \frac{\partial P_1}{\partial \xi} & \frac{\partial P_2}{\partial \xi} & \text{-------} & \frac{\partial P_i}{\partial \xi} \cdots & \frac{\partial P_n}{\partial \xi} \\ \\ \frac{\partial P_1}{\partial \eta} & \frac{\partial P_2}{\partial \eta} & \text{-------} & \frac{\partial P_i}{\partial \eta} \cdots & \frac{\partial P_n}{\partial \eta} \end{bmatrix} \begin{bmatrix} x_1 & y_1 \\ x_2 & y_2 \\ \cdot & \cdot \\ \cdot & \cdot \\ \cdot & \cdot \\ \cdot & \cdot \\ x_i & y_i \\ \cdot & \cdot \\ \cdot & \cdot \\ \cdot & \cdot \\ \cdot & \cdot \\ x_n & y_n \end{bmatrix} \qquad (2.12)$$

The derivatives of equation (2.9) are now obtained using equation (2.10) and equation (2.12), i.e.

$$\begin{Bmatrix} \frac{\partial P_i}{\partial x} \\ \\ \frac{\partial P_i}{\partial y} \end{Bmatrix} = [J]^{-1} \begin{Bmatrix} \frac{\partial P_i}{\partial \xi} \\ \\ \frac{\partial P_i}{\partial \eta} \end{Bmatrix} \qquad (2.13)$$

Stress-strain relations for linear elasticity is given by:

$$\{\sigma\} = [D] \left(\{ \varepsilon \} - \{\varepsilon_o\} \right) + \{\sigma_o\} \qquad (2.14)$$

where $\{\sigma\} = \{ \sigma_{xx} \quad \sigma_{yy} \quad \tau_{xy} \}^T$

$\{\sigma_o\}$ = initial stress vector existing prior to loading.

$[D]$ = tangential elasticity matrix.

$\{\varepsilon_o\}$ = initial strain vector.

In general, the stress field can be obtained by substituting equation (2.8) into equation (2.14) i.e.

$$\{\sigma\} = [D] ([B] \{\delta\} - \{\varepsilon_o\}) + \{\sigma_o\} \qquad (2.15)$$

In nonlinear problems equation (2.15) in effect provides the key for adjusting the solution to obey the given constitutive law. This will be explained in the next chapter.

(c) Element stiffness and force evaluation:

Element stiffnesses are derived from the variational principal of minimum total potential energy. In this the total potential energy P of a structure is defined in terms of the field variable, and is then minimized with respect to this field variable, subject to specific boundary conditions. When the potential energy is at its minimum then equilibrium conditions are satisfied.

If the strain energy of an element is P^e, (which will be in terms of the nodal displacements), and the imposed potential energy due to external load is W, then the total potential energy can be defined as:

$$P = \Sigma\ P^e + W\ .$$

The minimized condition with respect to displacements can then be written as:

$$\frac{\partial P}{\partial \{\delta\}} = \Sigma \frac{\partial P^e}{\partial \{\delta\}^e} + \frac{\partial W}{\partial \{\delta\}} = 0 \qquad (2.16)$$

The element contribution to this energy is:

$$\frac{\partial P^e}{\partial \{\delta\}^e} = [K]^e \{\delta\}^e + \{F\}^e \qquad (2.17)$$

where $\{\delta\}^e$ = the displacements associated with the element,

$\{\delta\}$ = the global displacements,

$[K]^e$ = the stiffness matrix of the element,

$\{F\}^e$ = the fictitious forces acting on the element nodes which can be further defined by:

$$\{F\}^e = \{F\}^e_{\varepsilon_o} + \{F\}^e_{\sigma_o} \qquad (2.18)$$

where $\{F\}^e_{\varepsilon_o}$ = the nodal force vector due to initial strains,

$\{F\}^e_{\sigma_o}$ = the nodal force vector due to initial stresses.

The minimization of the imposed load is expressed as:

$$\frac{\partial W}{\partial\{\delta\}} = \{F\}_p + \{F\}_g - \{F\} \qquad (2.19)$$

where $\{F\}_p$ = the nodal forces due to distributed load $\{\bar{P}\}$ per unit volume,

$\{F\}_g$ = the nodal forces due to any distributed external load on boundary elements,

$\{F\}$ = any external load acting on nodes.

Substituting equations (2.17), (2.18) and (2.19)into equation (2.16) gives the minimized condition as follows:

$$\frac{\partial P}{\partial\{\delta\}} = \sum_{1}^{\text{no. of elements}} \left([K]^e \{\delta\}^e + \{F\}^e_{\varepsilon_o} + \{F\}^e_{\sigma_o} \right) + \{F\}_p + \{F\}_g - \{F\} = 0 \qquad (2.20)$$

or $$[K]\{\delta\} = \{R\} \qquad (2.21)$$

which represents the assembly of the final equilibrium equations together with prescribed boundary conditions.

It can be shown that[4]:

$$[K]^e = \int_v [B]^T [D] [B] \, dv \qquad (2.22)$$

$$\{F\}^e_{\varepsilon_o} = -\int_v [B]^T [D] \{\varepsilon_o\} \, dv \qquad (2.23)$$

$$\{F\}^e_{\sigma_o} = \int_v [B]^T \{\sigma_o\} \, dv \qquad (2.24)$$

$$\{F\}_p = \Sigma \{F\}^e_p = \Sigma -\int_v [P_i(\xi,\eta)]^T \{\bar{P}\} \, dv \qquad (2.25)$$

$$\{F\}_g = \Sigma \{F\}^e_g = \Sigma -\int_A [P_i(\xi,\eta)]^T \{g\} \, dA \qquad (2.26)$$

where $\{\bar{P}\}$ = distributed load per unit volume,

$\{g\}$ = component of boundary pressure.

For 2-dimensional problems the incremental volume dv is:

$$dv = t.dx.dy.$$

where t = the thickness of the element.

The relation between the Cartesian and the curvilinear coordinates is:

$$dx.dy = \det [J].d\xi.d\eta$$

in which $\det [J]$ is the determinant of the Jacobian matrix.

2.3.3 Isoparametric 3-noded strain element (bar element):

Bar elements are identified with a particular isoparametric 8-noded element, and any combination of four bars can be placed along the sides of an 8-noded element as shown in Figure (2.4). In general the bar elements will be defined by a single natural coordinate and thus the formulation for any one of these four possible positions of bar is identical.

(a) Shape functions:

The shape function of this element are similar to these for the 8-noded isoparametric element explained in section (2.3.2). In general the global displacements within the element are given by:

$$u = \sum_{1}^{3} P_i(\xi)\, u_i \qquad (2.27)$$

$$v = \sum_{1}^{3} P_i(\xi)\, v_i \qquad (2.28)$$

where $P_i(\xi)$ is the shape function in the curvilinear coordinate ξ.

Similarly the position of a point in the global coordinate is given by:

$$x = \sum_{1}^{3} P_i(\xi)\, x_i \qquad (2.29)$$

$$y = \sum_{1}^{3} P_i(\xi)\, y_i \qquad (2.30)$$

The shape functions and their derivatives are given in Table (2.2) and are sketched in Figure(2.5).

(b) Stress and strain evaluation:

The total strain can be written in terms of the global coordinate as:

$$\{\varepsilon_B\} = [B_B]\ \{\delta_B\} \qquad (2.31)$$

where $[B_B] = [B_{B1}(\xi)\ \ B_{B2}(\xi)\ \ B_{B3}(\xi)]$

$= $ The strain matrix

$\{\delta_B\} =$ element nodal deformation vector.

The strain matrix can be written as

$$[B_B] = \left[\frac{\partial P_1(\xi)}{\partial x}\ \ \frac{\partial P_2(\xi)}{\partial x}\ \ \frac{\partial P_3(\xi)}{\partial x}\right]$$

when the bar is parallel to one of the global coordinates (in this case the x axis). This limitation will restrict the bars to lie on the sides

of rectangular elements only.

The value of

$$\frac{\partial P_i(\xi)}{\partial x} = \frac{1}{J} \frac{\partial P_i(\xi)}{\partial \xi} \tag{2.32}$$

where $J = \{ \frac{\partial x}{\partial \xi} \} = \frac{\partial P_1}{\partial \xi} x_1 + \frac{\partial P_2}{\partial \xi} x_2 + \frac{\partial P_3}{\partial \xi} x_3$ (2.33)

Therefore:

$$[B_B] = \frac{1}{J} \left[\frac{\partial P_1(\xi)}{\partial \xi} \quad \frac{\partial P_2(\xi)}{\partial \xi} \quad \frac{\partial P_3(\xi)}{\partial \xi} \right]$$

For stress calculations only the modulus of elasticity of the bar is required. Thus the stress is obtained by

$$\{\sigma_B\} = E_s \{\epsilon_B\}. \tag{2.34}$$

where $\{\sigma_B\}$ = stress vector at the nodes of the bar.

(c) Element stiffness and forces evaluation:

The expression for stiffness and force evaluation is basically the same as for the two dimensional element, except integration is carried out in one direction only. This can be expressed for the stiffness as

$$[K_B] = \int_o^L [B_B]^T A_s E_s [B_B] dx = \int_{-1}^{+1} [B_B]^T A_s E_s [B_B] J d\xi \tag{2.35}$$

where A_s = cross section area of the bar used.

L = total length of the bar.

For internal forces the calculation can be expressed by:

$$[F_B] = \int_o^L [B_B]^T \{\sigma_B\} dx = \int_{-1}^{+1} [B_B]^T \{\sigma_B\} J d\xi \tag{2.36}$$

where $[F_B]$ = vector of nodal forces for the bar.

2.3.4 Numerical integration:

In general numerical integration is necessary for two reasons:

(1) when the value of a function of f(x,y) are known but for formula of f(x,y) is unknown;

(2) when the formula of f(x,y) is known but the analytical integration is difficult to achieve.

In this study numerical integration is required because analytical integration is impossible. For this purpose Gauss-Legendre quadrature rules have been used extensively because of their higher efficiency over other forms of quadrature. They can integrate exactly a polynomial $f(\xi)$ of degree $(2n-1)$, where n is the number of sampling points. Also they are suitable for isoparametric elements because the range of these integration rules are ± 1 which coincides with the local coordinate system of limits ± 1 on element boundaries. A general integral in terms of global coordinate can be written:

$$I = \int\int f(x,y).dx.dy$$

If we transform the global coordinate system to the normalized curvilinear coordinate then

$$I = \int_{-1}^{+1} \int_{-1}^{+1} f(\xi,\eta).\, d\xi.\, d\eta$$

Generally the Gaussian quadrature rule leads to an equation of the form:

$$I = f(\xi).d\xi = \sum_{i=1}^{m} a_i.f(\xi_i) \quad \text{in one dimension.}$$

or

$$I = f(\xi,\eta).d\xi.d\eta = \sum_{i=1}^{m}\sum_{i=1}^{m} a_j.a_i.\, f(\xi_i,\eta_i) \text{ in two-dimensions.}$$

where m = total number of integration points.

a_i, a_j = The ith and jth weighting factor.

ξ_i, η_i = coordinate of the ith integration point.

The value of a_i and ξ_i associated with the Gaussian quadrature rules are tabulated in Table (2.3). It is easy to show that with n sampling points, a polynomial of degree 2n-1 could be evaluated exactly[4].

A point which should be considered in the selection of the order of integration rule is possible matrix singularity. If the total number of unknowns in the structure-exceeds the total number of independent variables applied at the integration points, then the stiffness matrix will be singular[4].

For any one element the more Gauss points used (i.e. the higher order of integration rule), the more computational time required, so it is important to know the minimum order of rule to give the required accuracy. It is found that for exact integration 3 x 3 rule is required. However as element size decreases it would be expected that lower order rules would be adequate, but then it is necessary to determine the minimum rule that still satisfies the constant strain convergence criterion. In this limit, interelement "forces" due to a constant stress become

$$\{ F \} = \int_V \left[B \right]^T \{\sigma\} \, dv \quad .$$

Thus for convergence to the true result numerical integration must be capable of performing this integral exactly which in fact implies that:

$$\int dv = \int \det \left[J\right] \, d\xi \, d\eta$$

must be integrated exactly. For a parabolic element it is found that

a 2 x 2 point rule is the minimum required[4,8]. But this may not be the case for nonlinear analysis because local irregularities might be overlooked due to the inherent averaging process. More integration points than the minimum required may be needed to adequately describe the crack pattern and hence monitor the nonlinearized material properties with closer precision.

Further details of Gauss rule selection will be discussed in Chapter 6.

Node i	ξ_i	η_i	Shape function $P_i(\xi,\eta)$	Derivatives $\frac{\partial P_i}{\partial \xi}$	$\frac{\partial P_i}{\partial \eta}$
1	-1	-1	$\frac{1}{4}(1-\xi)(1-\eta)-\frac{1}{4}(1-\xi^2)(1-\eta)-\frac{1}{4}(1-\xi)(1-\eta^2)$	$-\frac{1}{4}(1-\eta)+\frac{1}{2}\xi(1-\eta)+\frac{1}{4}(1-\eta^2)$	$-\frac{1}{4}(1-\xi)+\frac{1}{4}(1-\xi^2)+\frac{1}{2}\eta(1-\xi)$
2	0	-1	$\frac{1}{2}(1-\xi^2)(1-\eta)$	$-\xi(1-\eta)$	$-\frac{1}{2}(1-\xi^2)$
3	1	-1	$\frac{1}{4}(1+\xi)(1-\eta)-\frac{1}{4}(1-\xi^2)(1-\eta)-\frac{1}{4}(1+\xi)(1-\eta^2)$	$\frac{1}{4}(1-\eta)+\frac{1}{2}\xi(1-\eta)-\frac{1}{4}(1-\eta^2)$	$-\frac{1}{4}(1+\xi)+\frac{1}{4}(1-\xi^2)+\frac{1}{2}\eta(1+\xi)$
4	1	0	$\frac{1}{2}(1+\xi)(1-\eta^2)$	$\frac{1}{2}(1-\eta^2)$	$-\eta(1+\xi)$
5	1	1	$\frac{1}{4}(1+\xi)(1+\eta)-\frac{1}{4}(1-\xi^2)(1+\eta)-\frac{1}{4}(1+\xi)(1-\eta^2)$	$\frac{1}{4}(1+\eta)+\frac{1}{2}\xi(1+\eta)-\frac{1}{4}(1-\eta^2)$	$\frac{1}{4}(1+\xi)-\frac{1}{4}(1-\xi^2)+\frac{1}{2}\eta(1+\xi)$
6	0	0	$\frac{1}{2}(1-\xi^2)(1+\eta)$	$-\xi(1+\eta)$	$\frac{1}{2}(1-\xi^2)$
7	-1	1	$\frac{1}{4}(1-\xi)(1+\eta)-\frac{1}{4}(1-\xi^2)(1+\eta)-\frac{1}{4}(1-\xi)(1-\eta^2)$	$-\frac{1}{4}(1+\eta)+\frac{1}{2}\xi(1+\eta)+\frac{1}{4}(1-\eta^2)$	$\frac{1}{4}(1-\xi)-\frac{1}{4}(1-\xi^2)+\frac{1}{2}\eta(1-\xi)$
8	-1	0	$\frac{1}{2}(1-\xi)(1-\eta^2)$	$-\frac{1}{2}(1-\eta^2)$	$-\eta(1-\xi)$

Table (2.1) Shape functions and derivatives for a quadratic quadrilateral.

Node	ξ_i	Shape function $P_i(\xi)$	Derivatives $\frac{\partial P_i}{\partial \xi_i}$
1	-1	$-\frac{1}{2}\xi(1-\xi)$	$\frac{-1+2\xi}{2}$
2	0	$(1-\xi)(1+\xi)$	-2ξ
3	+1	$\frac{1}{2}\xi(1+\xi)$	$\frac{1+2\xi}{2}$

Table (2.2) Shape functions and their derivatives for a 3-noded bar element.

m	i	a_i	$f(\xi_i)$
1	1	2	0
2	1	1	$-\frac{1}{\sqrt{3}}$
	2	1	$+\frac{1}{\sqrt{3}}$
3	1	$\frac{5}{9}$	$-\sqrt{0.6}$
	2	$\frac{8}{9}$	0
	3	$\frac{5}{9}$	$\sqrt{0.6}$
4	1	$\frac{1}{2}-\frac{\sqrt{30}}{36}$	$-\sqrt{\frac{3+\sqrt{4.8}}{7}}$
	2	$\frac{1}{2}-\frac{\sqrt{30}}{36}$	$+\sqrt{\frac{3+\sqrt{4.8}}{7}}$
	3	$\frac{1}{2}+\frac{\sqrt{30}}{36}$	$-\sqrt{\frac{3-\sqrt{4.8}}{7}}$
	4	$\frac{1}{2}+\frac{\sqrt{30}}{36}$	$+\sqrt{\frac{3-\sqrt{4.8}}{7}}$

Table (2.3) Weighting factors and Gaussian sampling point positions.

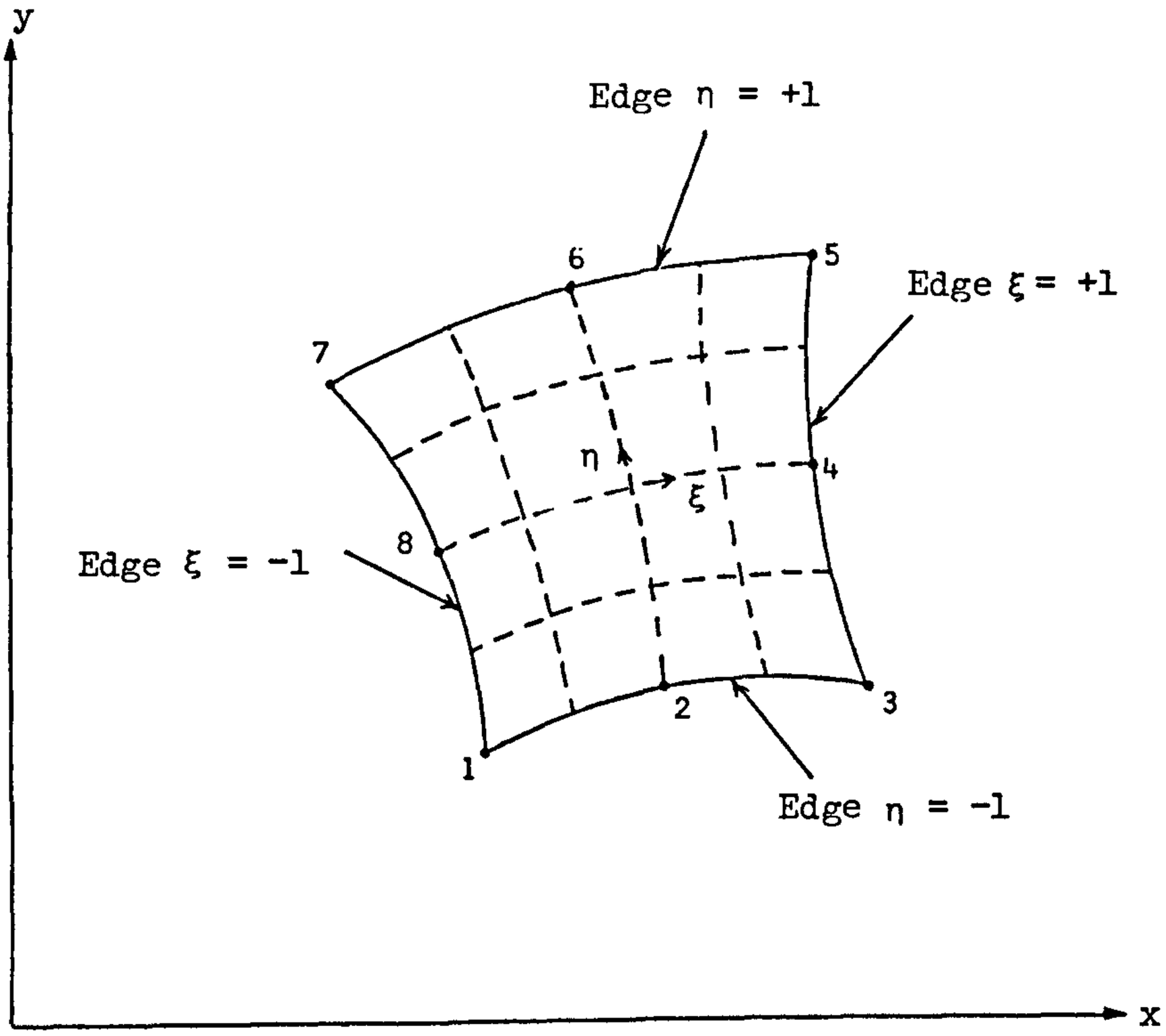

Figure (2.1) Typical 8-noded isoparametric element.

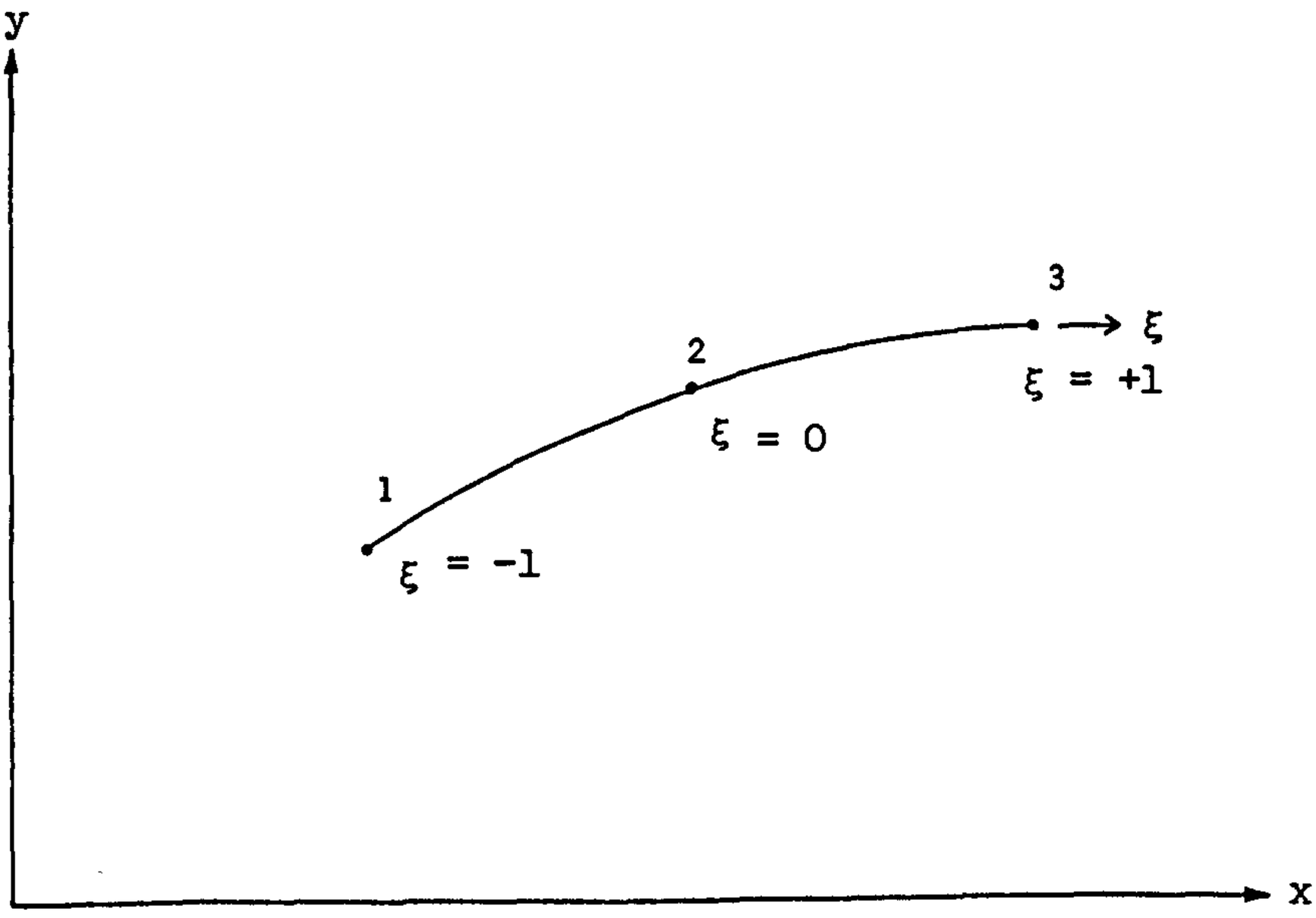

Figure (2.2) Typical 3-noded isoparametric element.

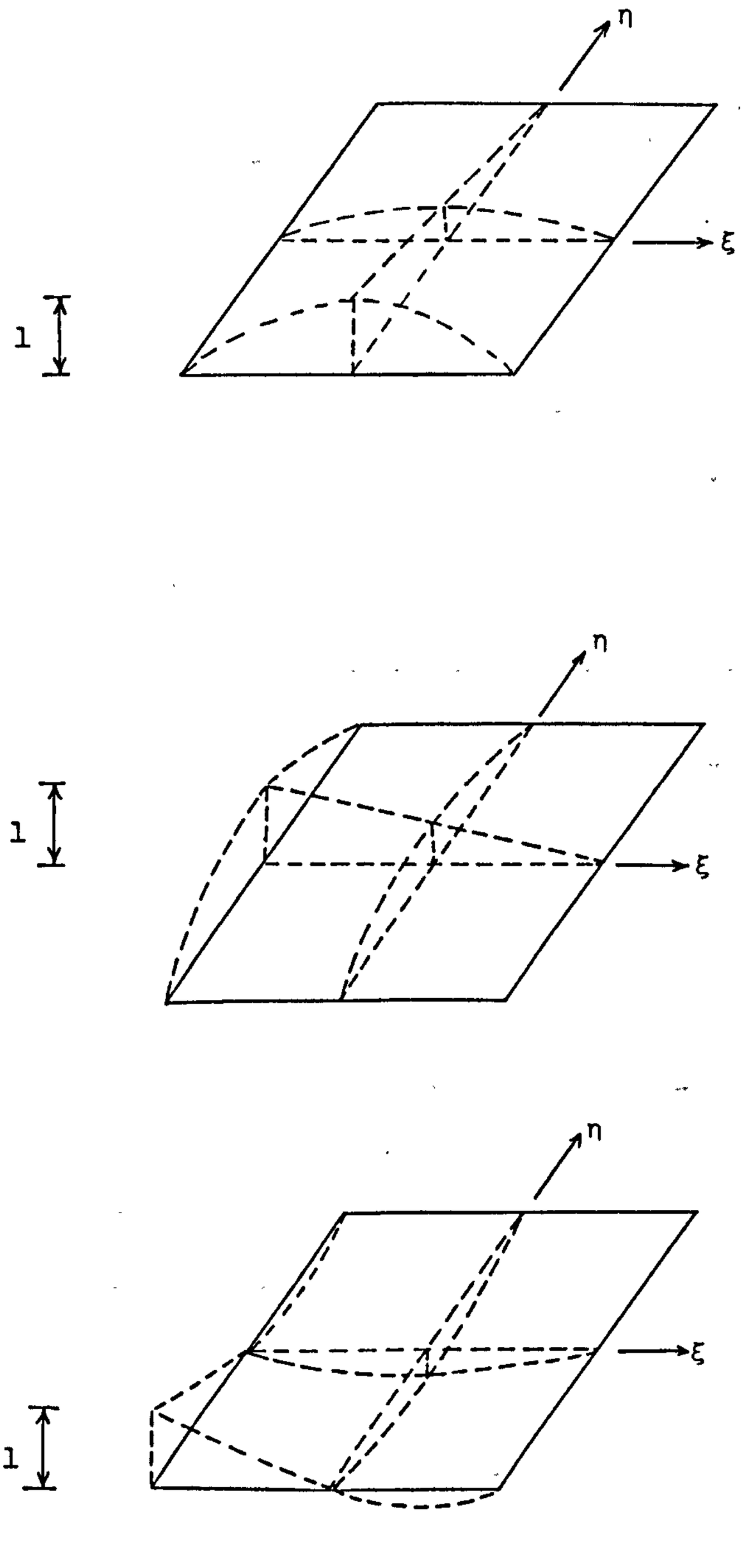

Figure (2.3) Shape functions of serendipity family for parabolic element.

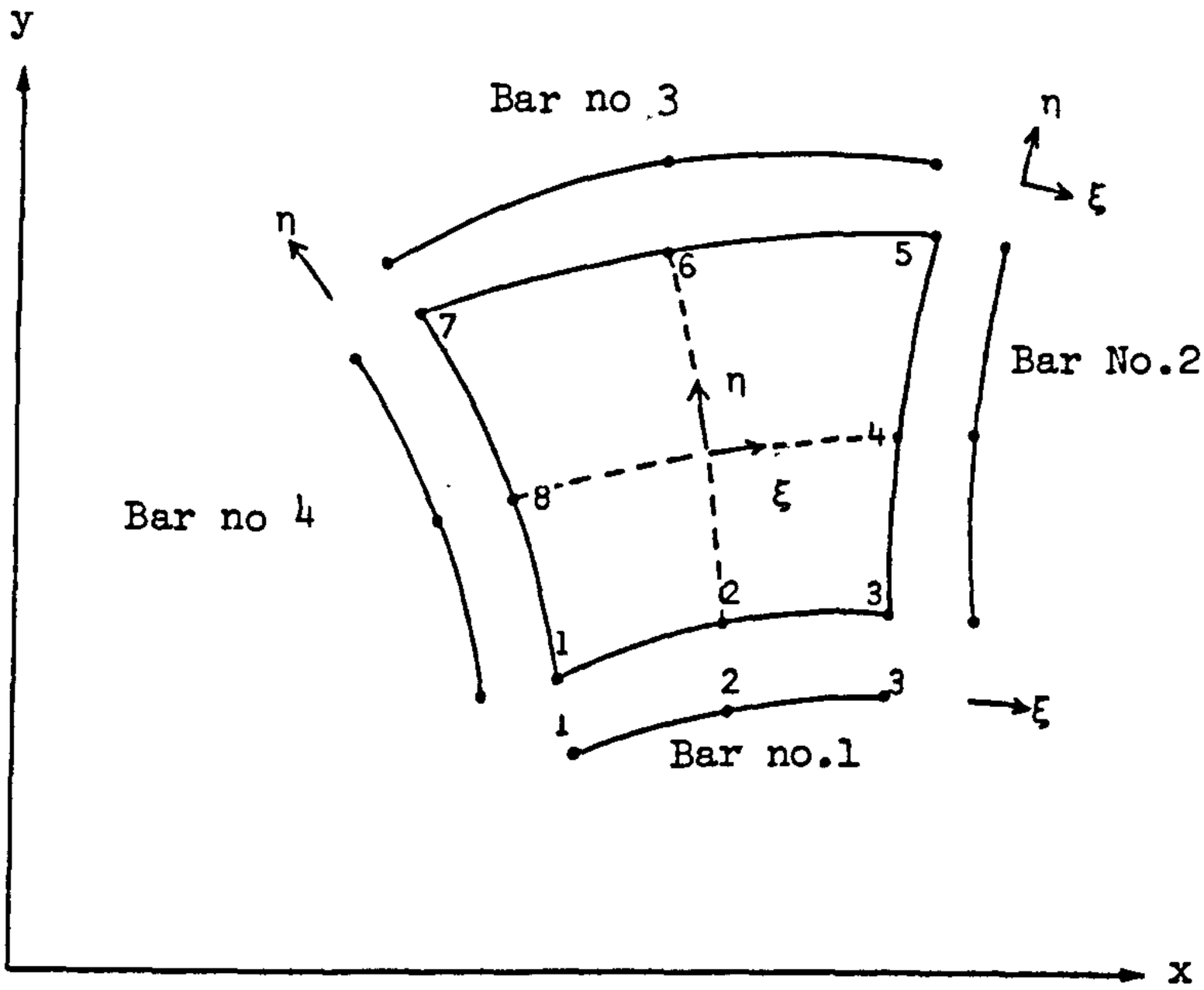

Figure (2.4) Bar element position on the isoparametric element.

$N_1(\xi) = -\frac{1}{2}\ \xi(1-\xi)$

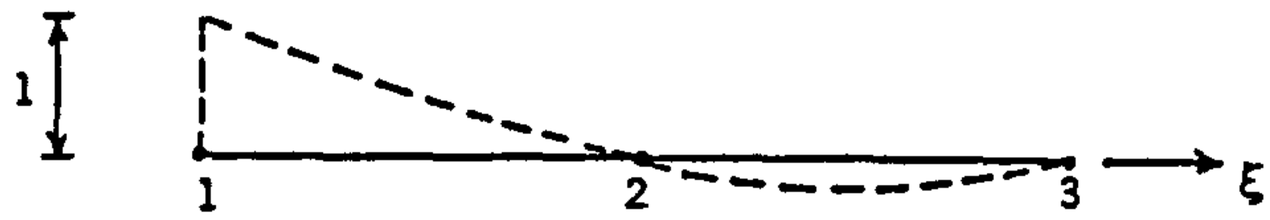

$N_2(\xi) = (1-\xi)(1+\xi)$

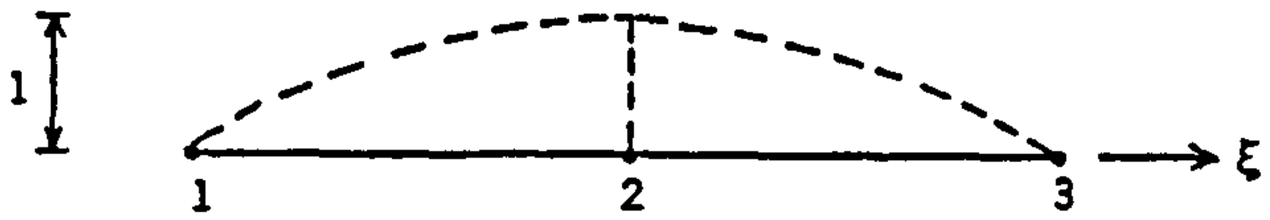

$N_3(\xi) = \frac{1}{2}\ \xi(1+\xi)$

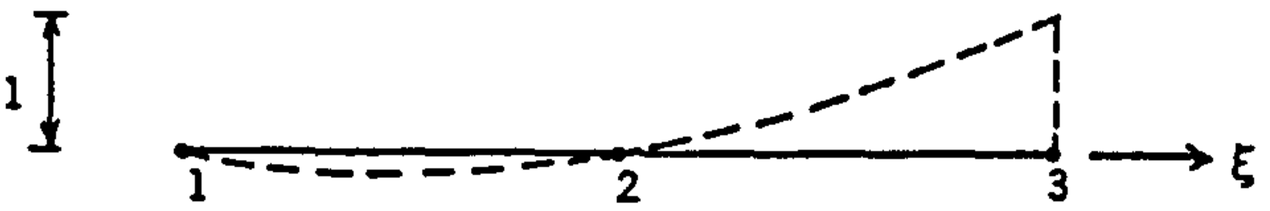

Figure (2.5) Parabolic shape functions for 3-noded bar element.

REFERENCES

1. Turner, M.J.; Clough, R.W.; Martin, H.C.; Topp, L.J., "Stiffness and deflection analysis of complex structures." J.Aero. Sci., Vol.23, 805-823, 1956.

2. Argyris, J.H.; Kelsey, G., "Energy theorems and structural analysis". Butterworth, 1960. (Collection of papers published in Aircraft Engineering in 1954 and 1955).

3. Clough, R.W., "The finite element method in plane stress analysis". Proc. 2nd conf. on Electronic Computation, ASCE, New York, 345-377, 1960.

4. Zienkiewicz, O.C., "The finite element method". McGraw-Hill, 3rd ed., 1977.

5. Spilker, R.L.; Pian, T.H.H., "Hybrid-stress models for elastic-plastic analysis by the initial-stress approach". Int. J. Num. Meth. Eng., Vol.14, 359-378, 1979.

6. Irons, B.; Ahmed, S., "Techniques of finite elements". Wiley, 1981.

7. Hinton, E., Owen, D.R.J., "Finite element programming". Academic, 1977.

8. Cook, R.D., "Concepts and applications of finite element analysis". Wiley, 2nd ed., 1981.

9. Cheung, Y.K.; Yeo, M.F., "A practical introduction to finite element analysis". Pitman, 1979.

10. Smith, I.M., "Programming the finite element method with application to geomechanics". Wiley, 1982.

11. Hinton, E.; Owen, D.R.J., "An introduction to finite element computations". Pineridge, 1979.

12. Owen, D.R.J.; Hinton, E., "Finite elements in plasticity". Pineridge, 1980.

13. Brebbia, C.A.; Connor, J.J., "Fundamentals of finite element Techniques". Butterworth, 1973.

14. Desai, C.S.; Abel, J.F., "Introduction to the finite element method". van Nostrand, 1972.

15. Rao, S.S., "The finite element method in engineering". Pergamon 1982.

16. Tong, P.; Rossettos, J.N., "Finite element method". M.I.T., 1977.
17. Robinson, J., "Integrated theory of finite element method". Wiley, 1973.
18. Desai, C.S., "Elementary finite element method". Prentice-Hall, 1979.

19. Phillips, D.V., "Non linear analysis of structural concrete by finite element methods". Ph.D. Thesis, University of Wales, 1973.

20. Krishnamoorthy, C.S.; Panneerselvam, A., "A finite element model for non-linear analysis of reinforced concrete framed structures". The Struct. Eng., Vol.55, No.8, 331-338, Aug., 1977.

21. Taig, I.C., "Structural analysis by the matrix displacement method". Engl. Electric Aviation report No.S017, 1961.

22. Irons, B.M., "Numerical integration applied to finite element methods". Conf. use of digital computers in Struct. Eng., Newcastle University, 1966.

23. Irons, B.M., "Engineering application of numerical integration in stiffness method". J.A.I.A.A., Vol.14, 2035-2037, 1966.

24. Chen, E.Y.T.; Schnobrich, W.C., "Material modelling of plain concrete". IABSE Colloquium in advanced mechanics in reinforced concrete, Delft, 1981.

CHAPTER 3

NONLINEAR METHOD OF SOLUTION

CHAPTER 3
NONLINEAR METHOD OF SOLUTION

3.1 Introduction:

This chapter presents the method used for solving the nonlinear problems described in this study and briefly compares this with others. A nonlinear solution is obtained by solving a series of linear problems in which the appropriate nonlinear conditions are satisfied to a specific degree of accuracy. This method is used because of the lack of a general approach for solving nonlinear equations.

A nonlinear structural problem must obey the basic laws of continuum mechanics, i.e. equilibrium, compatibility, and the constitutive relations of the material. Displacement compatibility is automatically satisfied in the displacement finite element technique. Common nodes between elements ensure continuity and compatibility of displacements along internal element boundaries (including the nodes) and polynomial shape functions ensure continuity and single valued displacements internally. Therefore it becomes only necessary to enforce that the nonlinear constitutive relations are correctly satisfied whilst at the same time preserving the equilibrium of the structure.

One way of achieving this is to first of all ensure that at any loading stage the stresses are consistent with the calculated displacement field and given constitutive relations. These stresses will then be statically equivalent to a set of internal nodal forces which should be in equilibrium with the external force system. Generally these forces are not the same and the differences between them are termed "residual forces"[1] which have to be removed to achieve equilibrium.

In general for a particular load level, a number of successive linear solutions are required to remove the residual forces to a desired degree of accuracy. The method is obviously iterative in nature and

the final results will depend on the factors associated with the iterative process, for example the increment size, accuracy required, the exact type of solution process employed etc. Clearly it is impossible to obtain a unique solution to a particular problem because of these many factors.

There can be several causes of nonlinear behaviour in a structure, which can be divided into two classes:

1. Nonlinear material behaviour,
2. Geometric changes (i.e. large deformations) in the structure, including changing boundary conditions.

Stress-strain relations are a major source of nonlinearity. These can vary from short-term nonlinear relationships between stress and strain such as plasticity, cracking, nonlinear elasticity, etc., to time-dependent effects such as creep, viscoelastic behaviour, shrinkage, etc. In concrete, cracks even exist before any external loading has been applied.[2,3] This is due to effects such as segregation, water gain, and bond cracks at the matrix-aggregate interface.

The second source of nonlinearity is when deflections are sufficiently large that the equilibrium equations based on the original geometry are no longer valid and need to be modified to account for the new geometry. This affects the force-displacement equations, because additional internal forces are generated due to the deflected geometry. Also if the large displacements cause large strains, then additional higher order terms must be included in the mathematical definition of strain. This results in nonlinear strain-displacement equations.[4,5]

Changes in the external boundary conditions are, in a sense, another

source of geometric nonlinearity. For example, beams on elastic foundations in which the size and location of contact zones between beam and foundation depends on the nature of the applied force. In certain circumstances, reinforced concrete structures present another example where boundary conditions change with varying load. Cracking and crushing cause separation of adjacent parts of the structure, which can be interpreted as a new geometric configuration, and this interpretation can be included in analytical procedures, such as the spring element method of Ngo et al.[6]

In this study only nonlinearity caused by the short-term nonlinear behaviour of concrete and steel is considered. These include the tensile cracking of concrete, the nonlinear stress-strain relations of concrete in compression and the yielding and work-hardening of steel. Exact details of the laws representing this behaviour will be given later in Chapter 5.

However, in general, the solution of a nonlinear problem is highly dependent on these material laws, and data used. A more accurate law ought to give a more accurate solution. But as mentioned above, the solution can also be highly dependent on the nonlinear procedure employed. Furthermore, the finite element approximations itself, e.g. element type, mesh size, Gauss rule etc., may lead to further inaccuracies.

These sources of error in the nonlinear process are inter-related in the sense that one type of approximation might counter balance another; or they might reinforce each other. In some cases certain approximations might cause a more flexible structure, such as lower order Gauss rules; other approximations might cause a more stiff structure, such as a coarse mesh; some approximations might affect the ultimate strength

such as the given tensile strength. Herein lies a major difficulty in solving a nonlinear reinforced concrete problem. With a material as variable as concrete, it is difficult enough to assess the accuracy of the material laws and data in a given situation. Add to this the effects of the basic numerical procedure, especially when dealing with cracking, and it becomes very difficult indeed to know how accurate the solution is.

It is fairly obvious that the more complex the material law the more expensive the solution; the more accurate the nonlinear method (i.e. small load increments, many iterations, low convergence tolerances, etc.), the more expensive the solution; the finer the finite element mesh or the more sophisticated the element, the more expensive the solution. Therefore if the analyst had unrestricted computing resources it would seem probable that an accurate solution could be obtained.

Since this is not possible, approximations of varying degree have to be introduced to obtain an economic solution. Then the inter-relationships mentioned above come into operation. It could be argued that certain procedures are incorporated so that a numerical solution can be adjusted to fit the known solution. These then become a sort of numerical device, even if a physical significance can be argued for them, for example tension stiffening. The problem then is what to do when the solution is not known beforehand, and guidelines are obviously necessary. It becomes important to investigate the effects of these "devices" on a solution; their accuracy, their economy and their interdependence.

If two different solution techniques give at any stage similar results within a desired accuracy (e.g. deflections, crack zones,

crushing zones, stress and strain distributions etc.), then obviously the cheaper solution is more acceptable, whatever devices were used to get there, i.e. the ends justify the means.

These points will be elaborated further when specific problems will be presented later, particularly in Chapter 6.

3.2 Numerical Techniques for Nonlinear Analysis:

3.2.1 Basic formulation:

The solutions of nonlinear problems by the finite element method are usually attempted by one of three basic techniques:

1. Incremental (step-wise procedure).
2. Iterative (Newton method).
3. Incremental-iterative (mixed procedure).

The general basis of each method is similar. For problems where only the material behaviour is nonlinear, the relationship between stress and strain is assumed to be of the form:

$$f(\sigma,\varepsilon) = 0$$

The element stiffness matrix is a function of the material properties and can be written as:

$$[K] = k(\sigma,\varepsilon)$$

The external nodal forces $\{R\}$ are related to the nodal displacements $\{\delta\}$ through the stiffnesses of the element and can be expressed by:

$$\{R\} = [K]\{\delta\}$$

which on inversion becomes:

$$\{\delta\} = [K]^{-1}\{R\}$$

$$\text{or } \{\delta\} = [k(\sigma,\varepsilon)]^{-1}\{R\} . \qquad (3.1)$$

This derivation illustrates the basic nonlinear relationship between $\{\delta\}$ and $\{R\}$, due to the influence of the material law on $[K]$.

Equation (3.1) is solved by a succession of linear approximations: The different methods of applying these linear approximations will in general lead to different load-displacement paths influencing the final solution. These methods will now be discussed in more detail.

3.2.2 Incremental method[4,7,8]

The basis of the incremental method is the subdivision of the total applied load vector into smaller load increments, which do not necessarily need to be equal. During each load increment the equation:

$$\{R\} = [K]\{\delta\}$$

is assumed to be linear, i.e. a fixed value of $[K]$ is assumed using material data existing at the end of the previous increment. Nodal displacements can then be obtained for each increment and these are added to the previously accumulated displacements. The process is repeated until the total load is reached.

The accuracy of this procedure depends on the increment size; the smaller the increments the better the accuracy, but at the same time the more computational effort required. A modification of this method is the "midpoint Runge-Kutta" method.[4] In this, the first step is to apply half the load increment and to calculate new stiffnesses corresponding to the total stresses at this value. These stiffnesses are then utilized to compute an approximation for the full load increment.

The incremental method in its original and modified form do not account for force redistribution during the application of the incremental load (i.e. no iteration process exists to restore equilibrium).

3.2.3 Iteration method:[4,5,7,8]

In the iteration method, the full load is applied in one increment. Stresses are evaluated at that load according to the material law. This gives equivalent forces which may not be equal to the external applied forces, i.e. equilibrium is not necessarily satisfied. Then, the portion of the total loading that is not balanced is calculated as the difference between the total applied load vector and internal nodal forces. These are the unbalanced nodal forces $\{F_u\}$ which are then used to compute an additional increment of displacements, and hence new stresses, which give a new set of equivalent nodal forces. This process is repeated until equilibrium is approximated to a certain degree of accuracy. When this stage is reached the total displacement is calculated by summing the displacements from each iteration.

There are many variations of this basic process and a solution depends in many ways on the method used for computation of the stiffness matrix $[K]$ and the unbalanced nodal forces $\{F_u\}$.

A) Computation of unbalanced nodal forces:

In general, the linear constitutive law can be written in the form:

$$\{\sigma\} = [D]\ (\{\varepsilon\} - \{\varepsilon_o\}) + \{\sigma_o\} \qquad (3.2)$$

where $[D]$ is a constant, linear elastic matrix, $\{\sigma_o\}$ and $\{\varepsilon_o\}$ are initial stress and strain vectors. Equation (3.2) is in essence the linear approximation for the nonlinear relation:

$$f(\sigma,\varepsilon) = 0 \qquad (3.3)$$

in any linear iteration. By adjusting any of the quantities $[D]$, $\{\varepsilon_o\}$, or $\{\sigma_o\}$, Equation (3.2) can be made to approximate Equation (3.3).

If $\{\epsilon_o\}$ is adjusted the process becomes the "initial strain" method[8] and is used when strains are expressed in terms of stress. If $\{\sigma_o\}$ is adjusted, the process is called the "initial stress" method[8], and is used when stress can be given in terms of strain.

In the initial strain method the Equation (3.2) is simplified to:

$$\{\sigma\} = [D]\,(\{\epsilon\} - \{\epsilon_o\}) \qquad (3.4)$$

Assuming $\{\epsilon_o\} = 0$ initially, Equation (3.4) is solved with an appropriate $[D]$ matrix and strain $\{\epsilon_{A1}\}$ to obtain a certain level of stress $\{\sigma_A\}$ where:

$$\{\sigma_A\} = [D]\,\{\epsilon_{A1}\} .$$

The strain which should have occurred is:

$$\{\epsilon_{A2}\} = [\bar{D}]^{-1}\,\{\sigma_A\} .$$

The difference between the strains:

$$\{\epsilon_o\} = \{\epsilon_{A2}\} - \{\epsilon_{A1}\}$$

is used as an initial strain in Equation (3.4), and the equivalent unbalanced nodal forces $\{F_u\}$ are calculated from:

$$\{F_u\} = -\int_v [B]^T[\bar{D}]\,\{\epsilon_o\}\,dv \quad .$$

These forces are removed by applying them to the structure which causes a correction to $\{\delta\}$. This process is repeated until $\{\epsilon_o\}$ or $\{F_u\}$ becomes negligible.

The steps in the initial stress method are very similar. The Equation (3.2) is now simplified to:

$$\{\sigma\} = [D] \{\varepsilon\} + \{\sigma_o\} \quad . \qquad (3.5)$$

Assuming $\{\sigma_o\} = 0$ initially, Equation (3.5) is solved with an appropriate $[\bar{D}]$ matrix and strain $\{\varepsilon_A\}$ to obtain a certain level of stress $\{\sigma_{A1}\}$ where:

$$\{\sigma_{A1}\} = [\bar{D}] \{\varepsilon_A\} \quad .$$

The stress which should have occurred is:

$$\{\sigma_{A2}\} = [\bar{D}] \{\varepsilon_A\} \quad .$$

The difference between the stresses:

$$\{\sigma_o\} = \{\sigma_{A2}\} - \{\sigma_{A1}\}$$

is used as an initial stress in Equation (3.5), and the equivalent unbalanced nodal forces $\{F_u\}$ are calculated from:

$$\{F_u\} = -\int_v [B]^T \{\sigma_o\} \, dv \quad .$$

These forces are removed by applying them to the structure to obtain a correction to $\{\delta\}$. This process is repeated until $\{\sigma_o\}$ or $\{F_u\}$ becomes negligible.

B) <u>Methods for computing stiffnesses</u>:[4,5,8]

Generally either the stiffness can be constant or variable throughout a solution. In the constant stiffness method the initial linear stiffness $[K_o] = k(\sigma_o , \varepsilon_o)$ is used at every stage in the analysis. The unbalanced nodal forces are calculated using either the initial strain or stress method.

Since calculating the stiffnesses and fully solving the equations

is an expensive operation, this method has economic advantages because the stiffness is calculated only once. Also a symmetric positive-definite matrix will always exist.[9,11,22] Its main disadvantage is that it usually requires a high number of iterations to achieve the desired accuracy, especially when cracking and yielding of reinforcement has occurred. This is due to the sudden and large changes that are caused in the stiffnesses. It has been suggested that acceleration processes could be used to speed up the solution,[9,11,22] although these have not always met with success.

In the variable stiffness method, a linear solution is performed but the $[D]$ matrix is adjusted during the iteration process. This can be done either by using a secant modulus approach or a tangential modulus approach. The initial strain or stress method can be used for the computationof the unbalanced nodal forces.

If the stiffnesses are updated during all iterations then the method is a form of the well known "Newton Raphson" method. In general the variable stiffness method requires considerably less iterations than the constant stiffness method, although a full solution is more expensive than a resolution with a constant stiffness.

However, problems could arise as reductions in stiffness could lead to negative or zero terms on the leading diagonal of the stiffness matrix. This difficulty is usually avoided by ensuring positive stiffness coefficients, and by using the residual nodal force vector concept to simulate any further loss of stiffness.

A cheaper variation of the variable stiffness approach can be obtained by using a modified "Newton Raphson" method, where the stiffnesses are only updated during certain iterations.

Figure (3.1.a) shows the different methods used for the iteration procedure.

3.2.4 Mixed method:[4,5,8,9,11,12]

In this method a combination of the incremental and iterative process is used. The load is applied in increments and the solution at that load is obtained iteratively until equilibrium is obtained.

The constant stiffness procedure can be used in which the initial stiffness $[K_o]$ is constant throughout the analysis; or the variable stiffness approach can be used with either the secant modulus or tangent modulus. Again the initial strain or initial stress method can be used for calculating the unbalanced forces during the iterative process. Figure (3.1.b) shows the different methods of the mixed procedure.

3.3 Comparison of basic methods:

One of the main advantages of the incremental procedure, is that it provides a relatively complete description of the load-deformation behaviour. The disadvantage is its difficulty in knowing in advance what increments of load are necessary to obtain a good approximation to the exact solution.

In general the iterative method is less time consuming than the incremental method. The iterative procedure is also easier to incorporate in a linear elastic program. The main disadvantage of the iterative procedure is that there is no assurance that it will converge to the exact solution. Further limitation of this method is that the displacements, stresses and strains are determined for only one increment.

The mixed procedure combines the advantage of both the incremental

and iterative procedures and minimizes the disadvantage of each method. It can give a description of the load-deformation behaviour at every load level with the desired equilibrium accuracy. The main disadvantage of this procedure is that it is more expensive, requiring a lot more computing time.

Further discussion of these techniques are adequately covered in references 4 and 5.

3.4 Method used in this work;[1,8,9]

A modified version of the mixed procedure is used in this work. In general the modified "Newton-Raphson" approach is used to evaluate the stiffnesses, with the constant stiffness and full variable stiffness methods as special cases. The stiffnesses are evaluated using a tangential elasticity matrix. For the calculation of the unbalanced nodal forces a modification of the initial stress method is used, termed the method of "Residual forces".[1] Its basic philosophy is that, at any stage, a load system equivalent to the total stress level is evaluated and checked against the applied loading system. The difference between the two will result in a set of residuals that are a measure of any lack of equilibrium. The residuals are then applied to the structure to restore equilibrium. This process is repeated until the residuals are sufficiently small. Thus for equilibrium it is required that

$$\{\psi\}_i = \int_V [B]^T \{\sigma\}\, dv - \{R\} = 0$$

where $\{\sigma\}$ are the actual stresses dependent on the given constitutive relation, $\{R\}$ lists all forces due to external loads, initial stresses ... etc., and $\{\psi\}_i$ the residual forces.

The use of the method of residual forces in the evaluation of the excess forces will ensure that residuals are not cumulative, which may not be the case when using the initial stress method.[1,9]

3.5 Convergence criteria:[8,9,11,13,14,15]

It is important to include reliable criteria which will check for the gradual elimination of the residual forces and terminate the iterative process when convergence to the desired accuracy has been achieved. The user specifies this accuracy by giving quantitative values known as convergence tolerances. In other words the user specifies the degree of accuracy of equilibrium that is acceptable. The convergence criteria can be based on various quantities; either directly on the unbalanced forces, or indirectly on displacement increments, or on changes in stress values. In this thesis two options for convergence are used. A displacement convergence criteria and a force convergence criterion.

It is difficult and expensive to check the decay of displacements or residual forces for every degree of freedom therefore some overall evaluation is preferable. This is achieved by using norms. Those used in this work will now be defined.

3.5.1 Force convergence criterion:

This criterionassumes that convergence is achieved if:

$$\frac{\Delta\psi_i^*}{P_.^*} \leq C_F$$

where $\Delta\psi_i^*$ = norm of the residuals

$$= \sqrt{\{\psi\}_i^T \{\psi\}_i}$$

and P_i^* = norm of the total applied loads

$$= \sqrt{\{P\}_i^T \{P\}_i}$$

C_F = a specific convergence tolerance

3.5.2 Displacement convergence criteria:

Two types of displacement criteria are used in which:

A) Convergence is achieved if;

$$\frac{\Delta \delta_i^*}{\delta_i^*} \leq C_D$$

where $\Delta \delta_i^*$ = norm of the displacements which have taken place during an iteration.

$$= \sqrt{\Delta\{\delta\}_i^T \Delta\{\delta\}_i}$$

and δ_i^* = norm of the total displacements from the beginning

$$= \sqrt{\{\delta\}_i^T \{\delta\}_i}$$

C_D = a specific convergence tolerance

B) Convergence is achieved if ;

$$\frac{\Delta \delta_i^*}{\delta_{Ii}^*} \leq C_D$$

where δ_{Ii}^* = norm of the total displacement in the increment at which the structure is analysed.

3.5.3 General discussion on convergence criteria:

The main function of convergence criteria is to control the number of iterations in an increment. The control is exercised by the user through the choice of convergence tolerances and the type of norm. In most cases the user will also specify a maximum number of iterations allowed, irrespective of the state of convergence. The number of iterations will influence the predicted shape of the load-deformation curve and ultimate load, e.g. too few might give an overstiff response. Hence it is of paramount importance that the user understands the factors influencing convergence behaviour and redistribution of forces. Very little information on these aspects exist in published literature, but it is clear that more is required if unreliable results are to be avoided.

Fine tolerances are theoretically desirable but can be very expensive to obtain because they quite often require a lot of iterations. They can be particularly difficult to achieve when discontinuous material laws (such as tension cracking) form part of the nonlinear behaviour. Steep discontinuities in material laws can cause large residuals and these residuals need to be redistributed. However this redistribution will cause more discontinuities and hence residuals in other parts in subsequent iterations. In such cases the rate of accumulation of residuals can be higher than the rate of distributing them. Another situation is when residuals are nearly redistributed and another discontinuity occurs which increases the residuals again and requires more iterations. These effects cause a high number of iterations which will continue until a stable crack situation is reached. In practice the initiation of particular cracks is subject to some variation, and it is arguable whether it is necessary to wait until a completely stable

crack situation has been achieved in any increment by using very fine tolerances. Therefore retarding the rate of crack propagation by specifying large tolerances or smaller number of maximum iterations could lead to satisfactory results.

In this work the load convergence criterion is the most commonly used because it works directly on equilibrium requirements. Also the displacement criterion can sometimes give misleading indications of convergence. For instance its norm could be small and decreasing yet at the same time the residual forces could be increasing due to local changes in stiffnesses.

Finally the rate of convergence depends on the method used in the solution, it is well known that constant stiffness will lead to slow convergence and this could lead to an expensive solution.[14] An accelerator process may be included to give a faster convergence, but problems may arise such as there being no guarantee that the solution will be the same as the unaccelerated solution. The accelerator process also can lead to premature instability of the solution.[9]

A more detailed discussion of these points and a numerical comparison of the use of convergence criteria will be given in Chapter 6.

3.6 Basic steps in the nonlinear method used:

1. Apply an increment of load $\Delta\{R\}_n$ and calculate the first estimate of the incremental displacement

$$\Delta\{\delta\}_n = [\bar{K}]^{-1} \Delta\{R\}_n$$

where $[\bar{K}]$, can be the initial elastic stiffness, or a tangential stiffness based on conditions prevailing at the start of the increment.

2. Calculate the total displacement and strain.

$$\{\delta\}_n = \{\delta\}_{n-1} + \Delta\{\delta\}_n$$

$$\{\varepsilon\}_n = \{\varepsilon\}_{n-1} + \Delta\{\varepsilon\}_n$$

3. Calculate the total stress $\{\sigma\}_n$ using the appropriate constitutive law:

$$f(\sigma,\varepsilon) = 0$$

4. Find the equivalent nodal forces due to $\{\sigma\}_n$, then calculate the residuals $\{\psi\}_i$

$$\{\psi\}_i = \int_v [B]^T \{\sigma\}_n \, dv - \{R\}_n$$

where $\{R\}_n$ is the total external load.

5. Check if residuals or displacements satisfy the convergence criteria. If they do apply a new load increment $\Delta\{R\}_{n+1}$ and repeat from (1).

6. If not, apply the residuals $\{\psi\}_i$ and calculate the corrective displacement $\Delta\{\delta\}_{ni}$ caused by them from

$$\Delta\{\delta\}_{ni} = [\bar{K}]^{-1} \{\psi\}_i$$

where $[\bar{K}]$ is the initial elastic stiffness, or a tangential stiffness based on conditions prevailing at the start of the iteration.

7. Go to step 2 and repeat the process until convergence conditions are satisfied.

A flow chart of this process is shown in Figure (3.2).

3.7 Frontal equation solving routine:

The simultaneous equation solving routine plays a major role in the efficiency of a finite element program. This is particularly true in a nonlinear finite element program because a lot of processing time is used in solving and resolving equations.

In this research a version of the frontal solution will be used. It was originally introduced by Irons,[18] and subsequently modified by Hinton and Owen[17]. Further improvements have been made in this work which will be described later.

The frontal solution is a very efficient direct solution process. Its main attraction is that variables are introduced at a later stage and eliminated earlier than in most other methods. Additional to this is its efficiency in the way it handles the core storage, i.e. a large number of elements can be used without the need for large storage. This is important especially when complex structures have to be analysed.

The front solver is never efficient than a band solver, and for the majority of cases is very much more efficient, especially for problems in which elements with mid side nodes are used.[19]

The main difference between a frontal and a banded solution is that the frontal solver does not store as many zero coefficients inside the band. The storage allocation in a banded solver is determined by the order in which the nodes are presented for assembly. But in a front solver the storage is determined by the order in which elements are presented. Thus for the frontal solver node numbering is irrelevant and it is the element numbering that is all important.[17,19]

The main idea of the frontal solution is to assemble the equations and eliminate the variables at the same time. As soon as the coefficients

of an equation are completely assembled from the contributions of all relevant elements, the corresponding variable can be eliminated. This means the total stiffness matrix of the structure is never formed as such, since after elimination the reduced equation is immediately transferred to back-up disc store.

The core contains, at any given instant, the upper triangular part of a square matrix containing the equations which are being formed at that particular time. These equations, their corresponding nodes and degree of freedom are termed the "Front". The number of the unknowns in the front is the "frontwidth" . The maximum size of problem which can be solved is governed by the "Maximum Frontwidth". The equations, nodes and degrees of freedom belonging to the front are termed "active"; those which are yet to be considered are "inactive"; those which have passed through the front and have been eliminated are said to be "deactivated".

During the assembly-elimination process the elements are considered each in turn according to a prescribed order. Whenever a new element is called in, its stiffness coefficients are read from disc file and summed either into existing equations, if the nodes are already active, or into new equations which have to be included in the front if the nodes are being activated for the first time. If some nodes are appearing for the last time, the corresponding equations can be eliminated and stored away on a disc file and are thus deactivated. In so doing they free space in the front which can be employed during assembly of the next element.

Although in itself the frontal solution is efficient, the periphery operations of transfer to a backing disc file is inefficient because

transfer is a very slow and costly operation, especially with a high number of elements. This situation can be improved by storing the reduced equations corresponding to the eliminated variables in core, in a temporary array termed a "Buffer area". As soon as this area is full the information is transferred to disc. The introduction of the buffer area may reduce the cost by about 50% compared with the use of ordinary backing disc store. In this research it was found that transfer to disc was very rarely required, but this, of course, depends on the size of the main core storage of the computer used.

The front width in this work was set equal to a maximum of 100, which allows about 200 isoparametric elements, to be solved. This is considerably large for this type of element.

The use of this subroutine in other computers may require change of the buffer area with respect to the size of the computer used. The buffer area in this program was set equal to 250,000.

References 16, 17, 19, 20, 21, 22 give more detail about the frontal technique.

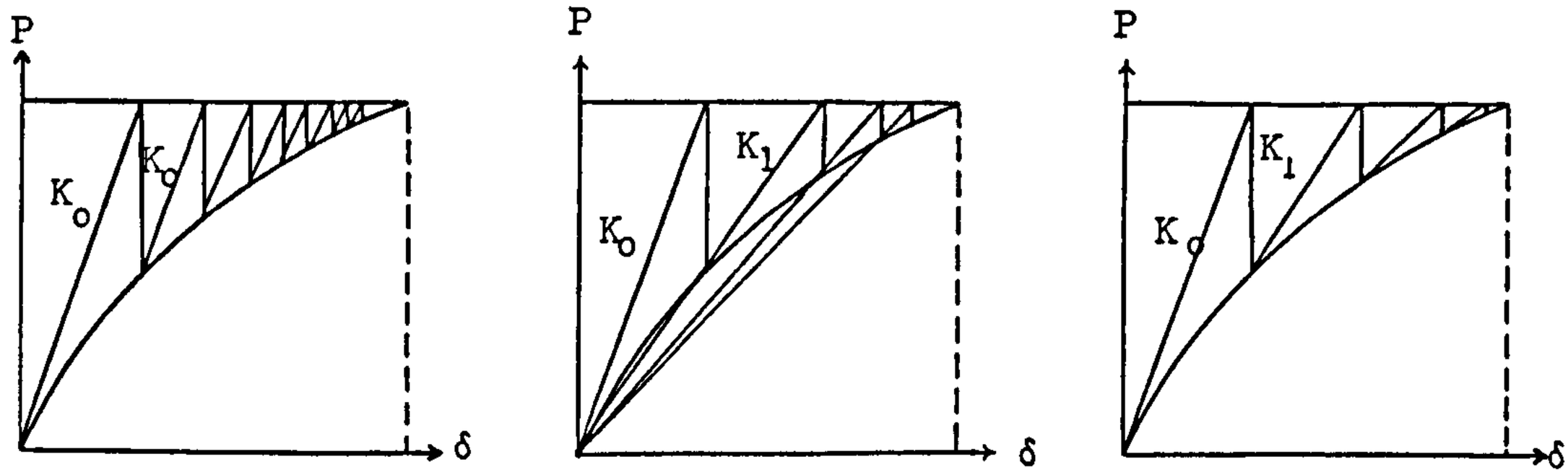

constant stiffness procedure

variable stiffness procedure

Secant Modulus Approach

variable stiffness procedure

Tangent Modulus Approach

Figure (3.1.a) Iteration Process.

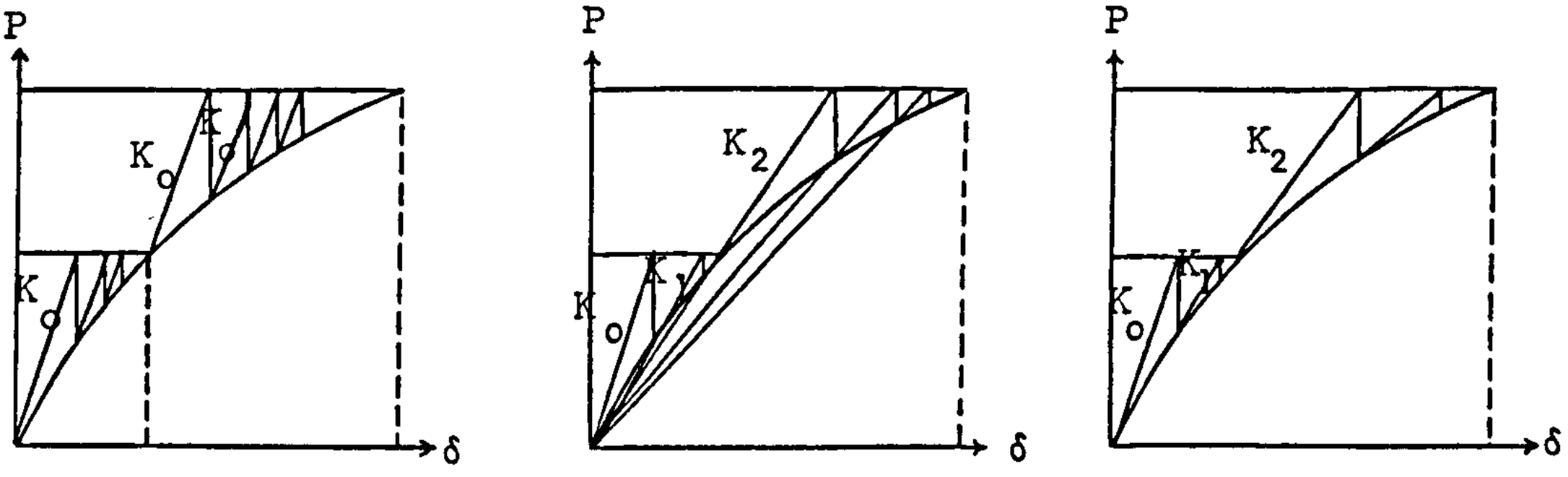

constant stiffness procedure

variable stiffness procedure

Secant Modulus Approach

variable stiffness procedure

Tangent Modulus Approach

Figure (3.1.b) Mixed Procedure.

Figure (3.1) Basic Procedure for Non Linear Solution.

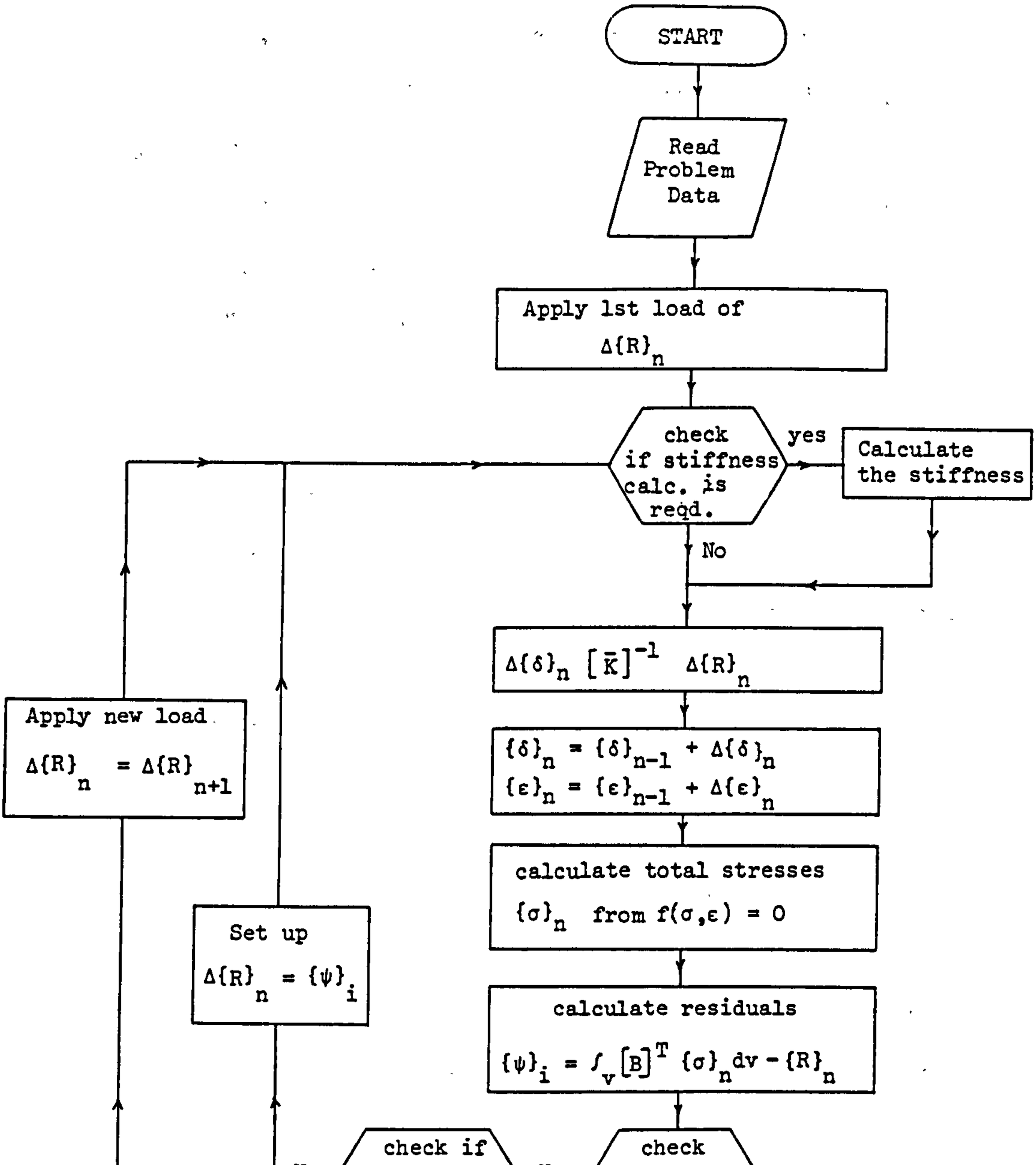

Figure (3.2) Flow Chart for Non Linear Procedure used in this Analysis.

REFERENCES

1. Nayak, G.C., "Plasticity and large deformation problems by finite element method". Ph.D. Thesis, University of Wales, Swansea, 1971.
2. Mindess, S.; Young, F.J., "Concrete". Prentice-Hall, 1981.
3. Neville, A.M., "Properties of concrete". Pitman, 3rd ed.,1981.
4. Desai, C.S.; Abel, J.F., "Introduction to the finite element method". Van Nostrand, 1972.
5. Cook, R.D., "Concepts and applications of finite element analysis". Wiley, 2nd ed., 1981.
6. Ngo, D.; Franklin, H.A.; Scordelis, A.C., "Finite element study of reinforced concrete beams with diagonal tension cracks". Report No. UC-SESM 70-19, University of California, Dec., 1970.
7. Martin, H.C.; Carey, G.F., "Introduction to finite element analysis". Tata McGraw-Hill, 1975.
8. Zienkiewicz, O.C., "The finite element method". McGraw-Hill, 3rd ed., 1977.
9. Phillips, D.V., "Non linear analysis of structural concrete by finite element methods". Ph.D. Thesis, University of Wales, 1973.
10. Zienkiewicz, O.C.; Valliappan, S.; King, I.P., "Elasto-plastic solution of engineering problems; initial stress finite element approach". Int. J. Num. Meth. Eng., Vol.1, 75-100, 1969.
11. Cope, R.J.; Rao, P.V.; Clark, L.A., "Nonlinear design of concrete bridge slab using finite element procedures". Nonlinear Design of Concrete Structures, CSE-ASCE-ACI-CEB International Symposium, University of Waterloo, Ontario, Canada, 379-407, Aug., 1979.
12. Tezcan, S.S.; Mahapatra, B.C.; Mathews, C.I., "Tangent stiffness matrices for finite elements". IABSE, Vol.30-I, 1970.

13. Cope, R.J.; Rao, P.V.; Edwards, K.R., "Nonlinear finite element analysis techniques for concrete slabs". Numerical methods for nonlinear problems, Proc. of the Int. Conf. held in University College, Swansea, 445-456, Sep .,1980.

14. Cope, R.J.; Rao, P.V., "Discussion on reference 22 ". Proc. Inst. Civ. Eng., Vol.69, Part 2, 873-874, Sep., 1980.

15. Cedolin, L.; Nilson, A.H., "A convergence study of iterative methods applied to finite element analysis of reinforced concrete". Int. J. Num. Meth. Eng., Vol.12, 437-451, 1978.

16. Hinton, E.; Owen, D.R.J., "An introduction to finite element computations". Pineridge, 1979.

17. Hinton, E.; Owen, D.R.J., "Finite element programming", Academic, 1977.

18. Irons, B.M., "A frontal solution program for finite element analysis". Int.J. Num. Meth. Eng., Vol.2, 2-32, 1970.

19. Cheung, Y.K.; Yeo, M.F., "A practical introduction to finite element analysis". Pitman, 1979.

20. Alizadeh, A.; Will, G.T., "A substructured frontal solver and its application to localized material nonlinearity". Comp. & Struct., Vol.10, 225-231, 1979.

21. Razzaque, A., "Automatic reduction of Frontwidth for finite element analysis". Int. J. Num. Meth. Eng., Vol.15, 1315-1324, 1980.

22. Duncan, W.; Johnarry, T., "Further studies on the constant stiffness method of nonlinear analysis of concrete structures". Proc. Inst. Civ. Eng., Part 2, Vol.67, 951-969, 1979.

23. Irons, B.; Ahmed, S., "Techniques of finite elements". Wiley, 1981.

CHAPTER 4

REVIEW OF CONCRETE AND STEEL BEHAVIOUR AND ITS PREVIOUS MODELLING

CHAPTER 4
REVIEW OF CONCRETE AND STEEL BEHAVIOUR AND ITS PREVIOUS MODELLING

4.1 Introduction :

A reliable prediction of the behaviour of reinforced concrete structures requires a knowledge of the behaviour of concrete in its elastic, inelastic and nonlinear ranges. A good material law should be able to produce the deformation behaviour of the structure accurately but this depends on the experimental data available. Recently, more and more experimental knowledge has become available regarding the deformation and strength properties of concrete under various loading systems. The accuracy of this data however, is often in question because of uncertainties concerning the efficiency of the various testing systems used to achieve given states of stress within specimens.

Preferably the information obtained experimentally should be combined with some basic theory in order to produce a set of mathematical formulae for use in analysis. Nowadays the power of computers is such that accurate and complex laws can be incorporated without too much difficulty. The main problem is in defining a suitable law. In recent years a lot of work has been carried out in modelling concrete and there are several ways of achieving this. A good summary is given by Chen[85].

One recent development in particular is where the material behaviour of concrete is defined in terms of several internal state variables. Known as the "endochronic theory", it appears to be very promising for describing concrete behaviour under a wide range of loading conditions. It is this method which will be particularly developed in this work.

The purpose of this chapter is to review the various methods available for defining the constitutive material laws for reinforced concrete. It will also include a discussion of relevant information about concrete and steel behaviour.

4.2 Mathematical description of the behaviour of reinforced concrete:

In the mathematical modelling of reinforced concrete there are three main areas to be examined.

1. The behaviour of concrete.
2. The response of steel reinforcement.
3. The bond-slip phenomenon between steel and concrete.

Each of these points will be discussed separately in the following sections.

4.2.1 The behaviour of concrete:

Various mathematical approaches are available for defining the stress-strain behaviour of reinforced concrete under different stress states. In this section a general description of these models will be given. However behaviour in tension zones, particularly cracking, is usually modelled separately and therefore this will be discussed separately. In fact tension cracking in general has a dominating effect on the nonlinear response and the compression model quite often takes secondary importance.

The mathematical approaches can be classified as follows:

(A) Curve fitting:

This method has been used predominately to describe uniaxial stress-strain data and numerous references are available.[6,7,8,10,11,12,72] Reviews are also given by Popovics[16], Sargin[68] and Chen[85].

Basically the method describes the uniaxial stress in terms of the strain in that direction using curve fitting techniques. The advantage of this method is that it is very easy to use in comparison to other methods. Its basic disadvantage is the lack of any underlying theory. It is simply a matter of fitting curves and formulae to a given

set of data. It is therefore doubtful whether extrapolation is possible for other concrete structures under different states of stress.

(B) Physical model of the concrete microstructure :

The basis of this method is to use a numerical method, such as the finite element method, to provide information on the behaviour of a material specimen. The specimen can be made up of difficult components, such as mortar, aggregate, aggregate/mortar, interface bond in concrete, and each component is given its own intrinsic properties. An example of this method is given in reference 45. Its advantage is that it can provide information on the behaviour of the different components in one specimen. However, this is not needed for general analysis and in any case it would be excessively expensive because of the computer time required to define the behaviour of all the components.

(C) Characterization based on a measure of damage :

This method was introduced by Romstadt[49], when he proposed a multilinear constitutive model for concrete under biaxial stress. The uniaxial stress strain curve for concrete was first divided into four regions, corresponding to the four major zones of microcracking activity. The biaxial stress space was then divided into four corresponding regions on the assumption that each represented equal amounts of damage in each zone. This damage is approximated by assuming constant mechanical behaviour in each zone. (i.e. for each region constant tangent value of Young's modulus and Poisson's ratio were found from the chord moduli for the corresponding region of the uniaxial stress-strain curve). The concept of regions with constant moduli is attractive computationally, but it seems unlikely that the dilatation and other properties of concrete can be adequately described. The theory was

developed for biaxial stress states only, but it is possible that the concept could be generalised to multiaxial stress states.

(D) Nonlinear elasticity:

In this approach the bulk modulus, shear modulus, Poisson's ratio, and Young's modulus, of concrete are expressed in terms of stress/strain variables, such as deviatoric stresses or strains, stress or strain invariants, normal and shear octahedral strains, etc. These relationships are obtained from experimental data. The moduli are usually used to formulate an isotropic matrix to represent the behaviour of concrete at a certain load level. Hypoelastic and hyper-elastic models are examples of this approximation.

Good results have been obtained using this method, but the disadvantage is that the data obtained from experimental tests may not be suitable for other types of analysis, where the conditions are different. Numerous examples of this approach can be found in references 29, 47, 48, 65, 67 and it is explained in more detail in reference 85.

(E) Modified plasticity theory:

This concept has been extended from metals to concrete and is based on the principles of the classical theory of plasticity. Examples of this method are given in references 62, 63, 64. Although some fairly good results have been obtained, the main disadvantage of this method is that some of the characteristics of classical plasticity are not valid for concrete such as the isotropic hardening of the yield surface, the large ductility, the constant plastic volume requirement etc. Also some of concrete's characteristics are difficult to represent in plasticity theory, such as stress softening after peak stress, cracking and cyclic loading. However these problems can be solved by using different laws.

(F) Endochronic theory :

An example of this theory is given in reference 49. Its basic concept is to use a pseudo-time scale called intrinsic (or endochronic) time, to define deformation in terms of strain and stress. It is capable of measuring the rate of change or damage of the internal structure of a material subjected to deformation. The endochronic model for concrete is based on an extensive set of functions which fit experimentally observed effects such as inelasticity, strain softening and hardening, hysteretic behaviour, etc. Since it is the endochronic method which is adopted in this thesis, details of its mathematical formulation will be given in the next chapter when its advantages and disadvantages will also be explained.

(G) Tension and cracking model:

In general, cracked concrete is usually modelled by a linear elastic fracture relationship. Two fracture criteria are most commonly used: the maximum principal stress criterion; and the maximum principal strain criterion. When a principal stress or strain exceeds its limiting value a crack is assumed to occur in a plane normal to the direction of the offending principal stress or strain. The maximum stress criterion is more commonly used than the maximum strain criterion, although it has been reported that the maximum strain criterion can predict stiffer behaviour than the maximum principal stress criterion[4].

In finite element analysis three different approaches have been employed for crack modelling. These are classified as follows:

(1) Smeared cracking approach:[4,20]

In this, cracks are assumed to be smeared throughout the region in a continuous fashion, such that across the region there are an infinite

number of cracks of infinite crack width. This model assumes that the concrete becomes an orthotropic material after the first crack has occurred. It is the most common model used and will also be used in this work because it is capable of predicting general description of concrete behaviour. A fuller, more detailed, description will be given in Chapter 5.

(2) Discrete cracking model:[86,87]

In this,the nodes of adjacent elements are assumed to be separated when a crack occurs. One obvious difficulty in such an approach is that the location and orientation of the cracks are not known in advance and so, geometrical restrictions are imposed by the preselected finite element mesh. This can be improved to some extent by redefinition of element nodes, but such techniques are extremely complex and time consuming. However, this model can be useful in obtaining details of the local behaviour of structures.

(3) Fracture mechanics model:[91,92]

The success of fracture mechanics in solving various types of cracking problems, has led to its use in finite element analysis of reinforced concrete structures. Fracture mechanics may be defined as the study of the stress and displacement fields in the region of crack tips in materials which are elastic, homogeneous, and isotropic, particularly at the onset of unstable crack growth (or fracture). The advantage of this method is that it will enable us to understand the mechanical behaviour of concrete more clearly, particularly with microcracking and cement/aggregate interfacial problems. The development of this method is still in progress and a lot of work is required to evaluate its validity.

4.2.2 Modelling steel reinforcement:

Steel reinforcement is generally assumed to transmit axial forces only and thus the description of its stress-strain relationship is fairly straightforward.

For simplicity in design and analysis it is usual to idealize the stress-strain curve for steel. Various different idealizations have been used and some of the more common are shown in Figure (4.1b). Normally a uniaxial elastic stress-strain curve, with a strain hardening effect is used in most structural analysis. However, for cyclic, and large strain problems an additional complexity must be included to take into account unloading and reloading effects.

4.2.3 The bond-slip phenomenon between steel and concrete:

The bond-slip relationship between concrete and reinforced steel exists because of the adhesion, friction, and mechanical interlock between concrete and steel. One of the most common methods used to represent bond-slip is the use of linkage elements. The main idea is to include a linkage element which connects the nodes of steel and concrete finite elements. This linkage element is composed of two springs perpendicular to each other which allow the transfer of forces between the separate nodes. Each spring must be given a certain stiffness, obtained from experimental tests. Normally a nonlinear bond-slip relationship, obtained from a pullout test, is assigned to the spring parallel to the bar, and a very high stiffness is given to the spring perpendicular to the bar to prevent any separation between the bar and the concrete.

An advantage of this element is that it has no physical dimension, i.e. it allows two different deformations to occur at a common node. One disadvantage is that it is difficult to incorporate, especially when a high number of reinforcing bars are used at different layers. Also it is difficult to give a realistic value for the stiffness of the springs perpendicular to the bar. Details of this method can be found in references 86, 87, 88.

Another way of accounting for bond is to use a gradual stiffening curve for concrete after cracking has occurred, and is usually called "tension stiffening". This approach is based on the fact that if the opening of a crack occurs at the same time as bond failure, it will cause some movement between the bar and the concrete. This will then cause the shear force at the contact surface between the cracks to feed tension stresses into the concrete. The concrete attached to the bar will contribute to the overall stiffness of the system. This contribution is accounted for by the gradual stiffening curve mentioned above.

An alternative way of representing this stiffening effect is to increase the steel stiffness and stress. This additional steel stress, corresponding to the same strain in the steel, represents the total tensile force carried by both the steel and concrete between the cracks.

In this thesis linkage elements are not used because of the high cost of including this element, especially for heavily reinforced structures, and also because of the lack of unified mathematical model for the bond-slip relationship.

Although tension stiffening can be defined on physical grounds,

it is essentially a numerical device rather than a bond device. Other numerical devices will be suggested on the basis of convergence criterion and will be discussed in more detail in Chapter 6.

4.3 Mechanical behaviour of concrete under different states of loading:

Concrete is a carefully proportioned mixture of cement, water, fine aggregate, and coarse aggregate. As soon as the components of concrete have been mixed together, the cement and water react to produce a cementing gel (cement paste) which bonds the fine and coarse aggregates into a stone-like material. The chemical reaction between the cement and water is an exothermic reaction producing significant quantities of heat termed hydration.

The strength of concrete is a function of the strength of the cement, the aggregate, and the interaction between the components. The water-cement ratio is also a major variable influencing the strength of the concrete. When the water-cement ratio is large, a dilute, high-shrinking, weak gel is produced. Concrete containing such gels is low in strength and lacks resistance to deterioration by weathering.

Typical stress-strain curves of aggregate and cement paste are demonstrated in Figure(4.2). It is clear that the relationship is linear except at high stress levels. The moduli of elasticity for the aggregate and the cement paste are quite different. However the combined response of these materials is markedly nonlinear. This is mainly due to the nature of the cement-aggregate bond and interim of microcracking when this bond breaks down. It has been found that a reduction in bond strength leads to an increase in the nonlinearity of the stress-strain curves. Stronger concretes exhibit a more linear

stress-strain curve, and the curve also becomes more linear when the aggregate stiffness approaches the stiffness of the matrix.

In the next section a review of the work done on the stress-strain behaviour and strength of concrete under short term loading will be given. This will be described under three stress states: uniaxial, biaxial and triaxial.

4.3.1 Uniaxial stress behaviour:

(a) Compression region:

A typical stress-strain curve for concrete subjected to uniaxial compression is shown in Figure (4.3). In general, a typical curve will show an almost linear relationship up to about 30% of its ultimate load. Although bond cracks will already exist, they are quite stable at low stresses and have little tendency to propagate. In addition, there is probably some additional crack initiation at highly localized tensile strain concentrations; these cracks also remain stable at low loads, but their formation probably accounts for the slight nonlinearity of the stress-strain curve even at low stresses.

Between about 30% and 50% of the ultimate stress, the cracks begin to propagate, but at a very slow rate. Most of the crack growth remains in the interfacial region between the aggregate and mortar. The system of bond cracks multiplies and grows in a stable fashion, and the stress-strain curve begins to show increasing curvature.

At this stage, there is very little cracking in the cement matrix. However, once the stress exceeds about 50% of the ultimate,

cracks begin to extend into the matrix. A much more extensive and continuous crack system begins to develop as matrix cracks connect the originally isolated bond cracks.

Finally, beyond about 75% of the ultimate stress more rapid crack growth occurs in the matrix, and the crack system eventually becomes unstable causing failure.

The uniaxial compressive strength of concrete is the most common measure for assessing the quality of concrete. In the UK, the characteristic cube strength of concrete, f_{cu}, is used. This is based on the strength of standard 150 mm cubes 28 days after mixing; 100 mm cubes are sometimes used if the nominal maximum size of the aggregate does not exceed 25 mm.

Generally in the USA 150 mm x 300 cylindrical specimens are tested giving the cylindrical compressive strength f'_c. These cylinders have a height to diameter ratio of 2,[1] and the cylinder strength is usually about 70-90% of the cube strength. The difference is due to the friction forces which develop between the platen plates of the testing machine and the contact face of the test specimen. These end forces produce a multiaxial stress state which increases the apparent compressive strength of concrete. The multiaxial stress effects are significant throughout the cube; in the cylinder, the specific height to width ratio will minimize this effect [89].

Much experimental work has been done on the shape of the uniaxial stress-strain curves, for examples see references 2,5-16,18-21, 68-72, 85.

Conclusions can be summarized as follows: The stress-strain relationship is influenced by the size and shape of the specimen and test procedure. This is difficult to formulate since it is affected by a large number of factors. For example a longer duration of loading leads to an increase in strains and a decrease in strength and initial modulus of elasticity.

The other important factors affecting the stress-strain curve are concrete strength, type of cement, type of aggregate, mix properties, method of curing and age. For example the stronger the concrete strength the steeper the slope of ascending and descending branches of the stress-strain curve.

(b) Tension region:

The shape of the tensile stress-strain curve is much more linear than the compressive curve.[23 - 25] This is because the stable crack propagation stage is much shorter and cracks travel very rapidly through the mortar matrix and around the aggregate paste interface [4]. It is difficult to measure the direct tensile strength of concrete, mainly because of the difficulty of applying a truly concentric pull. A method for measuring the indirect tensile strength is sometimes referred to as the "splitting tensile strength".

The test consists of loading a cylinder of 150 mm x 300 mm, across its diameter until failure occurs by splitting across the vertical

plane. The splitting tensile strength is then calculated with respect to the maximum load applied and length and diameter of the cylinder.

Generally, for practical purposes, the splitting tensile strength can be taken as $^{1}/8$ to $^{1}/12$ of the cube strength[89]. The tensile strength in flexure is known as the modulus of rupture and is obtained by testing a plain concrete beam under symmetrical two point loading applied at one third-span points. It is only a hypothetical stress based on the assumption of linear elastic behaviour up to the instant of rupture. The modulus of rupture over estimates the true tensile strength of the concrete and is used only as a comparative measure. The modulus of rupture is usually about 1½ times the splitting cylinder strength[89]. More details on the tensile strength of concrete can be found in references 23-28, 72, 73, 85, 89.

4.3.2 Biaxial stress behaviour:

A biaxial stress condition occurs if the principal stresses are acting in two directions only, and the third principal stress is zero. Early experiments were focussed primarily on the strength of concrete. But in recent years, more research has been done on the deformation and microcracking properties of concrete under biaxial loading.

Detailed reviews have been compiled from time to time: Hilsdorf[54], Rosenthal et al.[43], Kupfer et al[41], Phillips[4]. Gerstle et al. [84]. etc.

The measured response of concrete under biaxial stress appears to be subject to large variations which depends on testing and measuring techniques, even under working stress levels[77]. It has been difficult to obtain consistent behaviour for concrete under these states. Labib[3]

has summarized the main parameters influencing these inconsistencies as follows:

1. Characteristics of the concrete, such as the fractions of concrete and paste volume, aggregate particle size, distribution properties of aggregate and cement paste, and the bond at the aggregate-paste interface.
2. The size and shape of the specimen.
3. The moisture condition and temperature distribution throughout the specimen.
4. The influence of machine platens on the stress and strain distribution of the specimen.

Typical stress-strain curves for concrete under biaxial states of stress in compression-compression, tension-compression and tension-tension regions are shown in Figures (4.4), (4.5) and (4.6). These were obtained from the experimental tests of Kupfer et al.[41], where normal weight concrete specimens of dimension 20 x 20 x 5 cm. were tested. For comparison uniaxial stress-strain curves are also shown in these figures.

The relationships are essentially linear up to 40% of the failure stress, with only a small amount of permanent deformation due to microcracking taking place. Some authors refer to this point as the "initial discontinuity point" or "elastic limit". In two dimensional principal stress space this elastic limit is represented by envelope 1 in Figure (4.7). For stress states outside this envelope, larger cracks form, internal disruption of the material structure takes place, and substantial permanent deformations are produced. Envelopes 2, 3, and 4

in Figure (4.7) show the limits for other important points in the stress-strain relationship.

In this thesis only the conclusions obtained from various experimental tests will be given. The test procedures themselves can be found elsewhere, for example in, Kupfer et al.[41], Rosenthal et al.[43], Buyukoztark et al.[45], Atan et al.[46], Liu et al.[47], Tasuji et al.[52], and Cedolin et al.[67].

The conclusions can be summarized as follows:

1. The ultimate strength of concrete under biaxial compression is greater than that under uniaxial compression. The main reason for this increase is due to the confinement of microcracks.
2. The ultimate strength increase under biaxial compression, is dependent on the ratio of principal stresses, and appears to be maximum (up to about 25% higher than the uniaxial value) at a stress ratio of about 0.5, diminishing somewhat as the ratio is increased to unity.
3. The compressive stress at failure in the region of combined compression and tension decreases as the tensile stress increases.
4. The biaxial tensile strength of concrete is approximately equal to its uniaxial strength, and stress-strain curves are similar in shape in both uniaxial and biaxial tension.
5. The variation of Poisson's ratio from biaxial tension (0.18) to biaxial compression (0.2) is negligible.
6. The concrete strain corresponding to maximum stress varies from 0.002 (uniaxial) to 0.003 (biaxial).
7. Volumetric strain behaviour is described separately in Section 4.3.4.

Further details on the biaxial states of stress can be found in references, 30-55, 74-76, 85.

4.3.3 Triaxial stress behaviour:

The behaviour of concrete under multiaxial states of stress has been primarily concerned with the determination of the ultimate strength under combined stress states. Early investigations were carried out by Richart et al.[93], Balmer[59] and Akroyd[60]. These were followed after 1960, by many further studies, for example, Johnson et al.[57], Gardner[58], Liebenberg[72], Mills et al.[70], Hobbs[61], Shah et al.[65], Kotsovos et al.[22,66,78,79,80,81], Cedolin et al.[67], Murray[82], Elwi et al.[83], Gerstle et al.[84], Ahmed et al.[73].

Past examination of the response and strength of plain concrete under multiaxial states show a large scatter of results.

This thesis is not primarily concerned with the triaxial stress behaviour of concrete but a brief description will be given for completeness. Kotsovos[22] has presented good summary and also Gerstle et al.[84] discuss conclusions based on test results obtained in different laboratories where the same specimen was tested under different methods and loading systems. Typical stress-strain curves under triaxial states of stress are shown in Figure (4.9) from a test by Richart[93]. As these curves show linear behaviour up to about 30-40% of the ultimate load. Thereafter the behaviour depends on the confining pressure and concrete behaves more like a metal exhibiting apparent ductility. This is because the formation of microcracks is suppressed by hydrostatic pressure on the specimen and this apparent ductility increases as the confinement stress increases.

From different experimental data a wide range of test strains have been reported. This is due to the different machine constraints on the specimen boundaries. The boundary constraints will inhibit transverse deformation affecting the value of the moduli.

4.3.4 Definition of the dilatation of concrete:

Figure (4.8) shows the relationship between compressive stress and volumetric strain for concrete in uniaxial and biaxial compression. It is clear that volume decreases for most of the load range, but then starts to increase just before reaching failure. This dilatation is caused by the internal disruption of concrete (i.e. the progressive growth of major microcracks) under shear strains. In the uniaxial test this internal disruption starts to occur at about 75-80% of the concrete crushing stress; this can be identified by the point of inflection in Figure (4.8) and in envelope 2 in Figure (4.7).

The maximum volume which can be ultimately reached depends on the volume occupied by the various components of concrete when fully disrupted. This maximum value is approached as dilatation continues and disruption progresses. Beyond this stage of complete disruption the concrete behaves as a cohesionless material and can carry loads only if it is confined.

4.3.5 Hydrostatic pressure sensitivity:

Hydrostatic pressure sensitivity prevents the formation of micro-cracks. This causes the stiffness, failure stress, and ductility of the concrete to be effectively increased. This is seen clearly by comparing the results for triaxial tests shown in Figure (4.9). This

can also be seen by comparing uniaxial and biaxial tests, shown in Figure (4.8).

In fact concrete behaves more like a metal at high hydrostatic stresses because the formation of microcracks is completely suppressed. This aspect is particularly important under triaxial stress states when higher hydrostatic stresses are present requiring higher shear stresses to cause failure.

4.3.6 Shear across cracks:

Immediately before formation of a crack the shear stress parallel to the crack is zero because the crack is perpendicular to the principal stress. As long as there is no shearing movement of the crack surface, the shear stress parallel to the crack remains zero. However, if such movement occurs, as shown in Figure (4.10), substantial shear stresses can be developed because of the roughness of the crack surface and the presence of reinforcement bars crossing the crack. The roughness of the crack surface leads to shear transfer by aggregate interlock. This is more effective when transverse steel is present because it counteracts the tendency for the crack width to increase during shear movement. The aggregate interlock phenomenon has been investigated by a number of researchers.(94,95,96,97,98,99,100,115).

The most important observation from experimental tests is that the crack width has the largest influence on the shear stiffness, and the maximum size and shape of the coarse aggregate does not seem to influence the shear-stress/shear-strain relationship(94). Other factors such as the amount of steel crossing the crack and the orientation of reinforcement with respect to the crack, also has a substantial influence on both the ultimate shear strength and the shear stiffness(115

4.4 Mechanical behaviour of steel:

4.4.1 Brief description of steel behaviour :

Since steel reinforcement is predominantly uniaxial, it is generally not necessary to introduce the complexity of a multiaxial constitutive relationship for steel.

A typical uniaxial stress-strain diagram for steel is shown in Figure (4.1a). Initially the relationship is linear and elastic until the "proportional limit" P is reached. For a further small range of stress increase, the strain is still elastic but no longer linearly related. The "yield point" Y is then reached and this marks the start of plastic deformation. The difference between P and Y is slight for most steels and is usually neglected in practical applications. Beyond the yield point, plastic flow occurs with strain increasing at a much greater rate. Generally, stress must be increased to cause further deformation, a condition termed strain or work hardening. Eventually a maximum stress is reached at point V, after which a descending tail rapidly occurs to fracture at F.

Some materials, such as mild steel, exhibit a small but sharp drop in load after yield to a lower yield level. Thereafter strains increase plastically at more or less constant load to about ten times the yield strain. At this point the material begins to work harden, and clearly the lower yield point should be used for calculation purposes.

For practical purposes steel exists in various forms. Basically these are:

1. Plain round hot-rolled bars of either, mild steel, medium-strength steel, or high strength steel. Yield stresses vary from about 250 N/mm^2 (34,000 lb/in^2), to 360 N/mm^2 (52,000 lb/in^2), whilst

the corresponding ultimate strengths vary from 460 N/mm^2 (67,000 lb/in^2) to 600 N/mm^2 (88,000 lb/in^2).

2. Cold worked bars or drawn wire of mild, or more usually, high tensile steel bars. Such reinforcement exhibits considerably higher yield stresses (or proof stresses since most bars of this type do not have a definite yield point). Twisted round or square bars normally have proof stresses depending on the size of diameter and range from 410 N/mm^2 (60,000 lb/in^2) to 480 N/mm^2 (70,000 lb/in^2).

The Young modulus of steel is about 200 x 10^3 N/mm^2 (30 x 10^6 lb/in^2)

4.4.2 Bond-slip and dowel action:

Bond stress is the name assigned to the shearing stress parallel to the bar axis on the steel-concrete interface. This bond transfers the force from the steel bar to the surrounding concrete and vice versa. The bond between concrete and steel results from chemical adhesion, friction and mechanical interaction between the concrete and the steel.

For plain reinforced bars, chemical adhesion and friction are the major contributory factors to the bond strength (i.e. the ultimate load that is obtained before bond failure), while mechanical interaction plays a minor role. Considerable slip has been observed between the steel bar and the concrete, suggesting the loss of adhesion at relatively low stresses,[101] and that the subsequent bond resistance is due to the frictional drag on the bar at locations without adhesion. Bond failures in specimens reinforced with plain bars were characterized by the extraction of the bar from the concrete specimen.

Deformed bars were introduced to alter this behaviour pattern and

the projecting deformations, ribs or lugs, add to the bond resistance by bearing on the concrete and thereby minimizing slip considerably. As shown in Figure (4.11) the bond resistance for a deformed bar is activated at the lug interface by bearing pressure, which can be resolved into two components. One component acts parallel to the bar tending to shear the concrete along a cylindrical failure surface, while the second component acts radially and tends to create longitudinal splitting. The latter mode of failure is the more common.

Scordelis[102] has also given the following as factors which affect the ultimate bond strengths; type of loading, confining lateral reinforcement or pressure, concrete cover, bar spacing, location of splices.

Reinforced bars also act as dowels as shown in Figure (4.12), when major shear deformation occurs after the development of tension cracking and the bar will take concentrated shear force.

Many factors can effect the dowel action such as various bar diameters, specimen geometry, length of the reinforcement and its arrangement and cover of the concrete. Dowel effect becomes more important especially under cyclic loading and more work is required to be done.

Reviews on bond and dowel problems can be found in references 21, 101 - 116.

4.5 General Conclusions:

1. Reinforced concrete structures under realistic loading are subjected to a great number of influences such as tension cracking, multiaxial response, bond slip, dowel action, aggregate interlocking

etc. An accurate inclusion of all these factors in a computer program would appear to be quite impossible even though these factors and the interaction between them, must have some effect on the result of an analysis.

For the time being, because we do not have complete information regarding the different factors influencing the behaviour of concrete and steel interaction, it is more useful to use the available information in as simple a form as possible, rather than introducing complexities which still reply on approximation to known behaviour and data.

2. There is a fair scatter of test results for strength and deformation properties of concrete. This causes difficulties in forming adequate mathematical laws.

3. More experimental tests are required under biaxial states of stress to enable a clearer picture of concrete behaviour to emerge.

4. Because tension cracking has a dominant effect on the nonlinear response, care must be taken in developing methods which describe cracking behaviour.

5. In order to obtain realistic mathematical models, it is necessary to include the following factors in some fashion:

(a) A suitable multiaxial compression failure criterion.

(b) A realistic multiaxial cracking criterion in tension and suitable post-cracking behaviour.

(c) An accurate model for representing stress-strain behaviour for all multiaxial stress ranges.

(d) An adequate stress-strain curve for steel.

(e) An accurate representation for bond problems between the steel reinforcement and concrete.

6. A unified representation of uniaxial, biaxial and triaxial concrete response appears possible at low load stress levels but may break down near failure.

7. Concrete response to multiaxial stress states at working levels can be considered as linear elastic material for engineering purposes.

8. Most studies have been carried out on uniaxial modelling because of the availability of wide range of experimental work. For biaxial and triaxial modelling the problem is more difficult and requires more complexity to model the behaviour satisfactorily.

9. There are several approaches used to describe mathematically the stress-strain behaviour of concrete. The endochronic approach will be used in this thesis because it appears to have much potential for wide and accurate application.

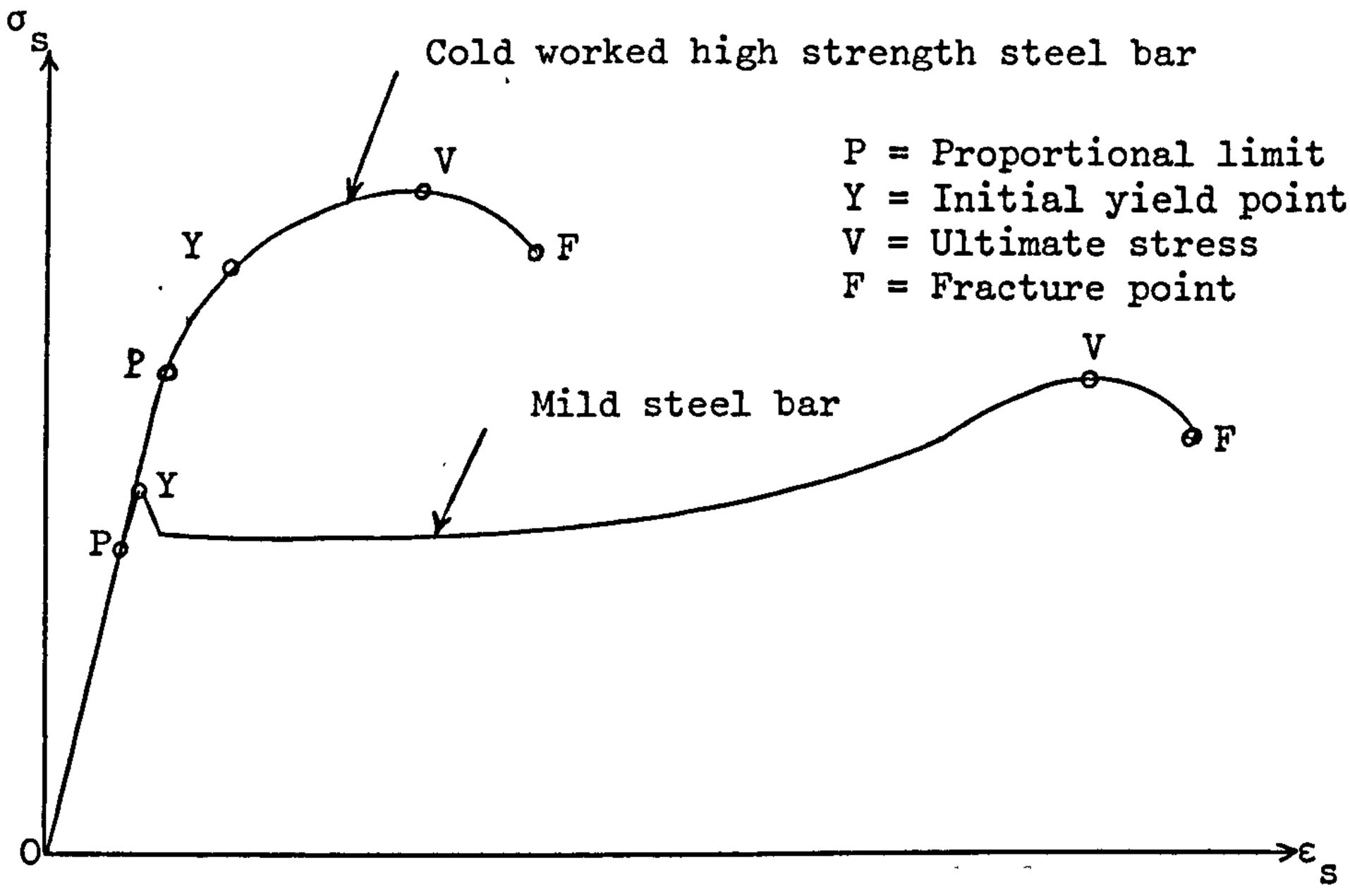

Figure (4.1a) Typical stress-strain curve.

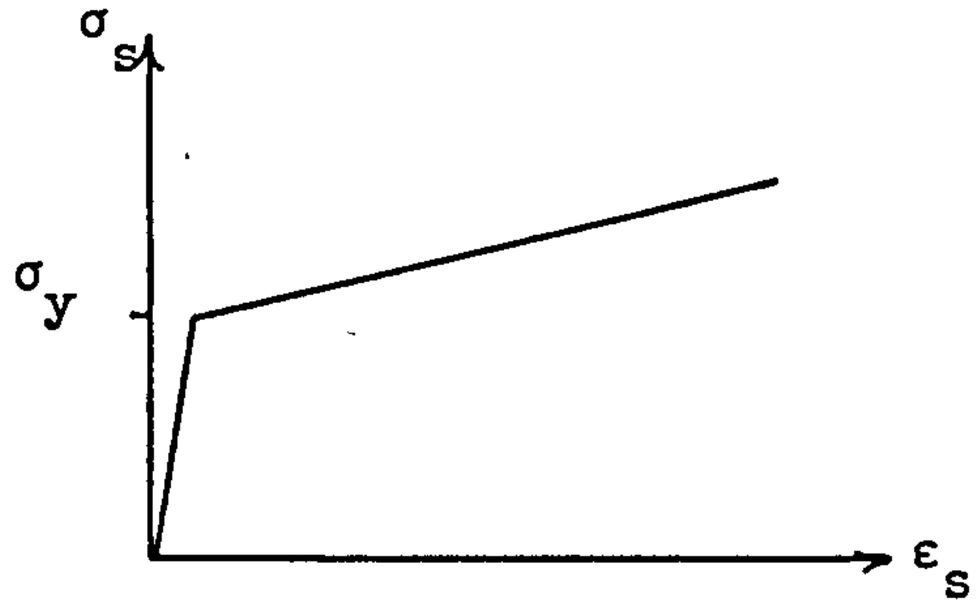

Elastic strain hardening approximation

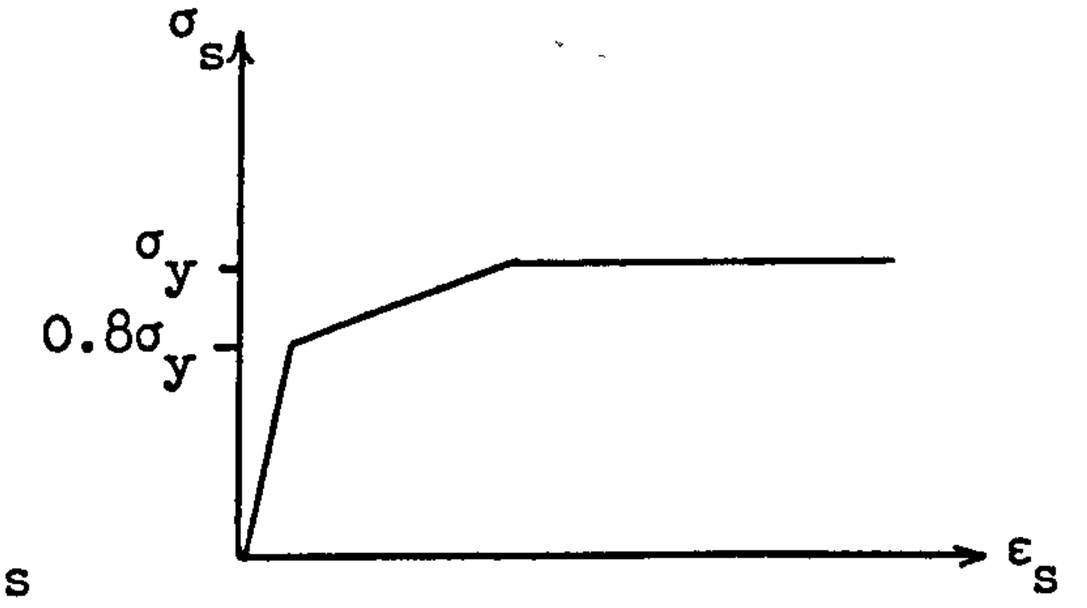

Elastic semi-perfect plastic approximation

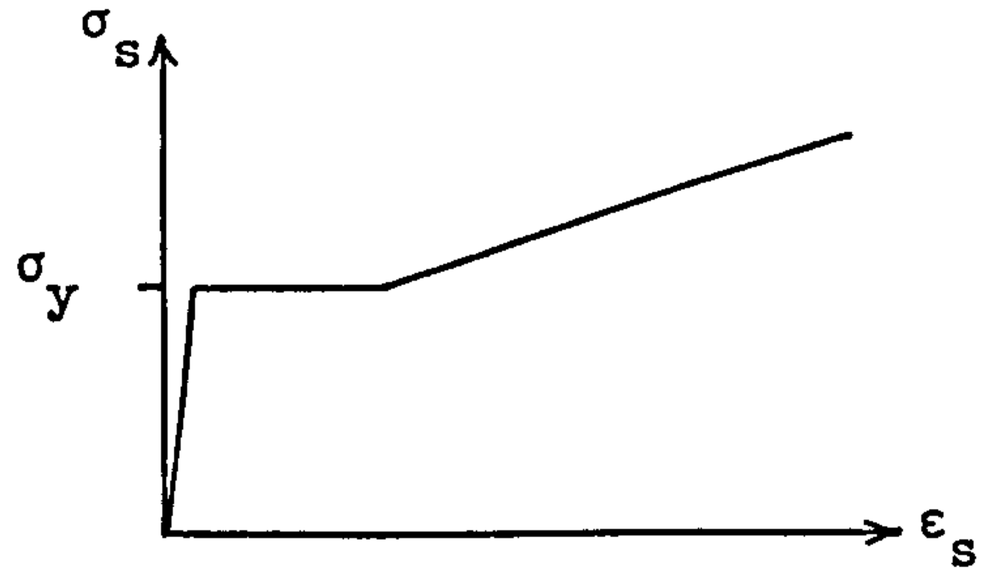

Trilinear approximation

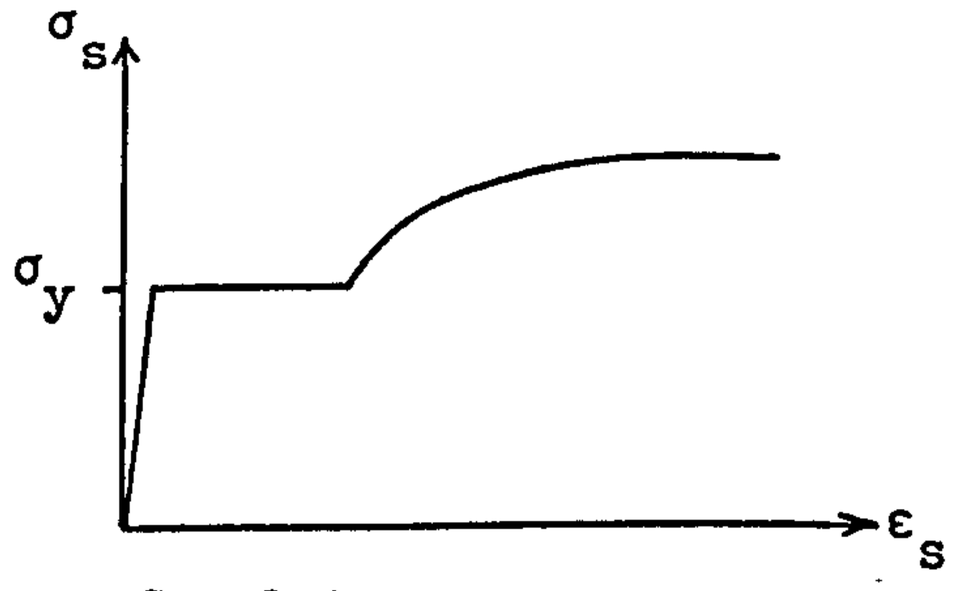

Complete curve

Figure (4.1b) Idealized stress-strain curves.

Figure (4.1) Stress-strain curve for steel reinforcement.

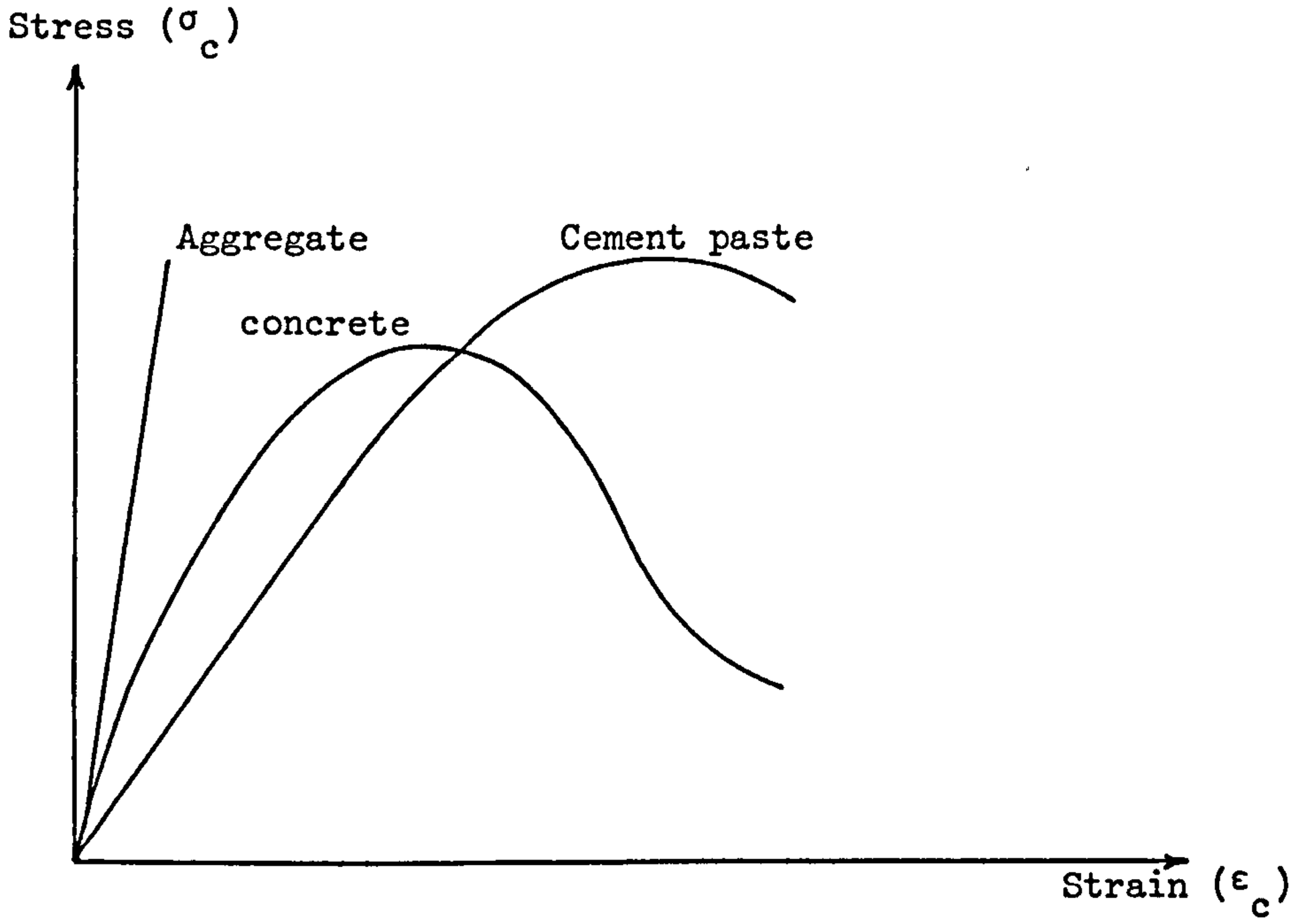

Figure (4.2) Stress-strain curve for aggregate, hardened cement paste, and concrete.

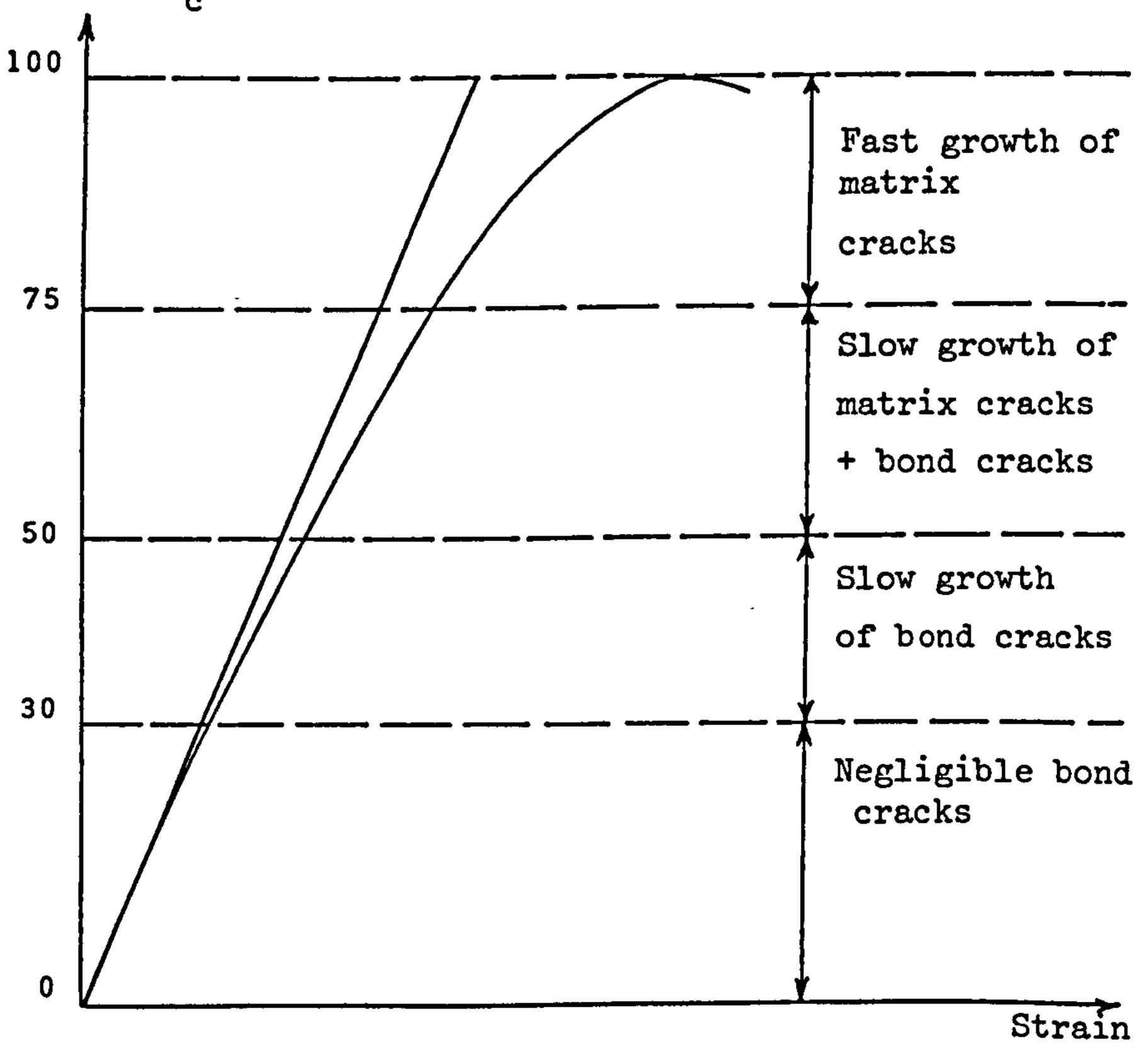

Figure (4.3) Typical stress-strain curve in uniaxial-compression.

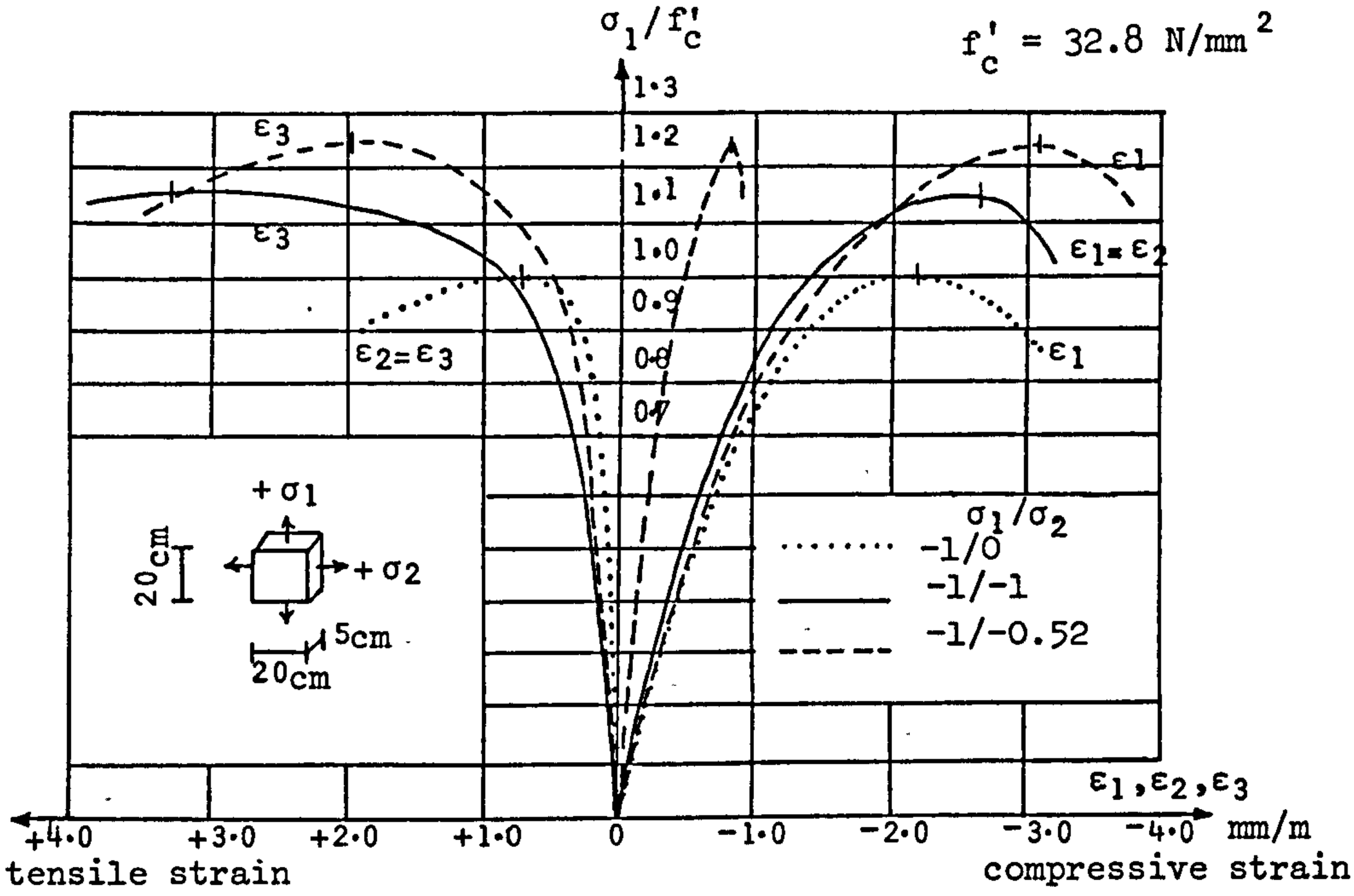

Figure (4.4) Experimental stress-strain curves for biaxial compression.(Kupfer et al.)[41]

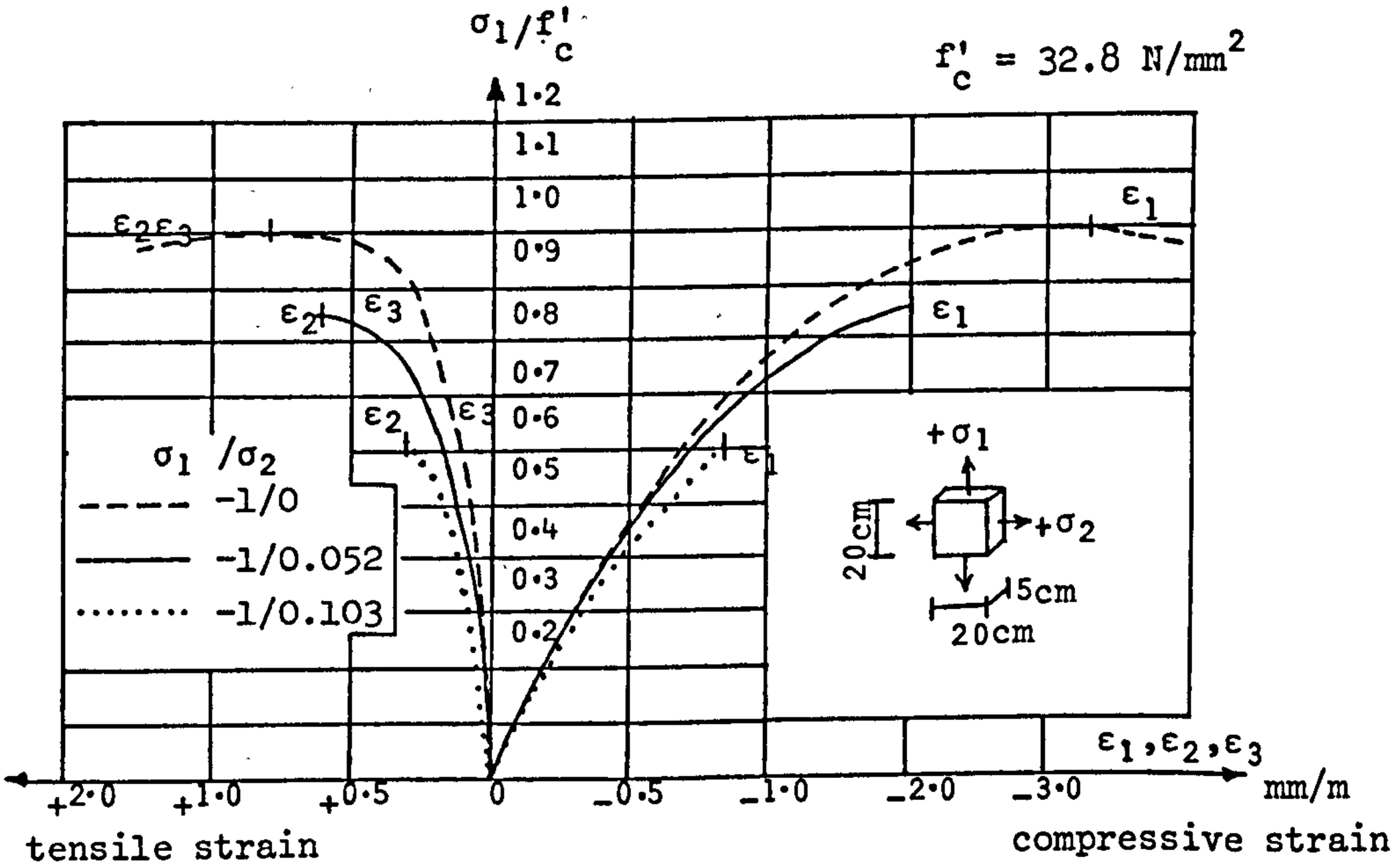

Figure (4.5) Experimental stress-strain curves for biaxial tension-compression.(Kupfer et al)[41]

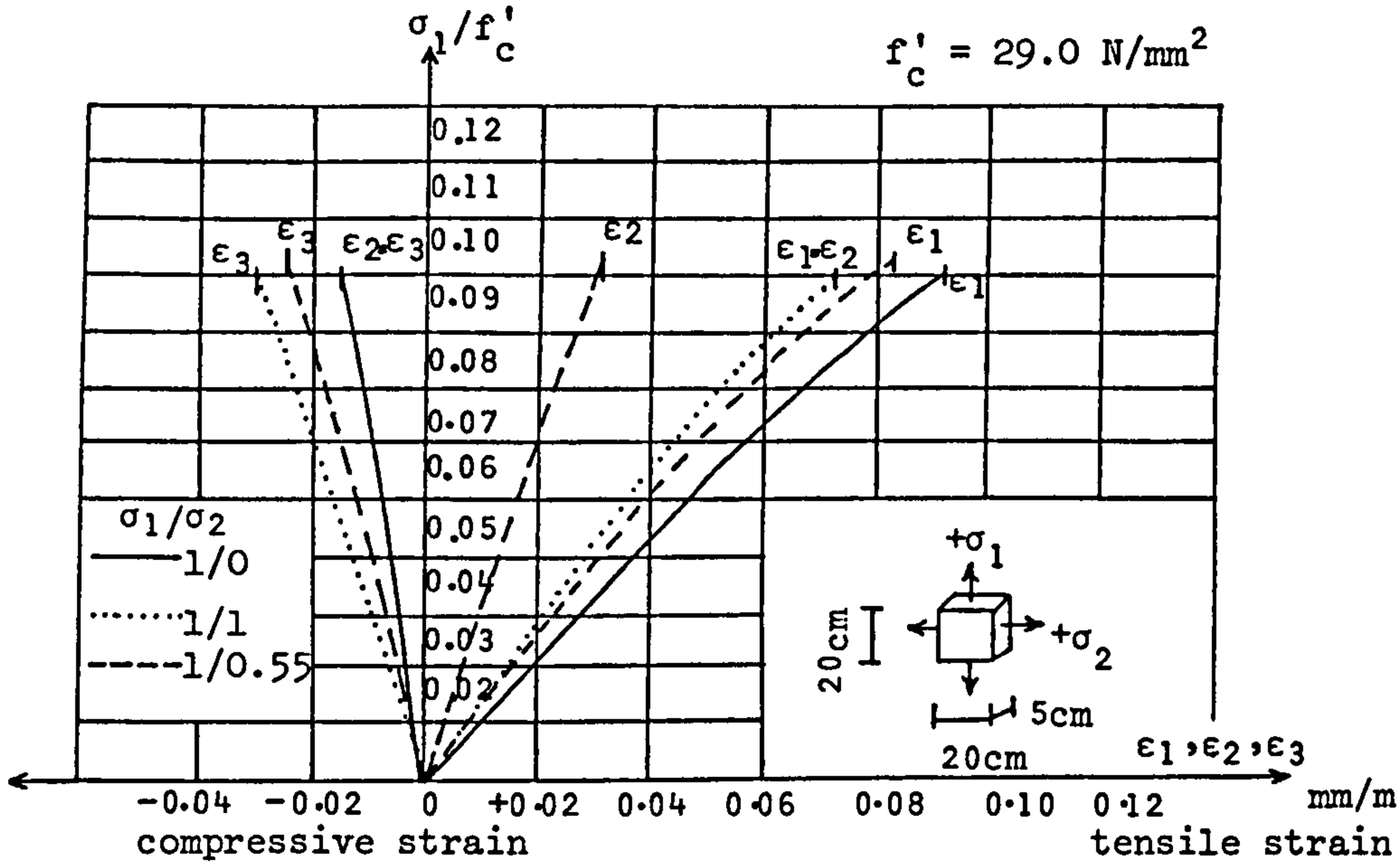

Figure (4.6) Experimental stress-strain curves for biaxial tension. (Kupfer et al.)[41]

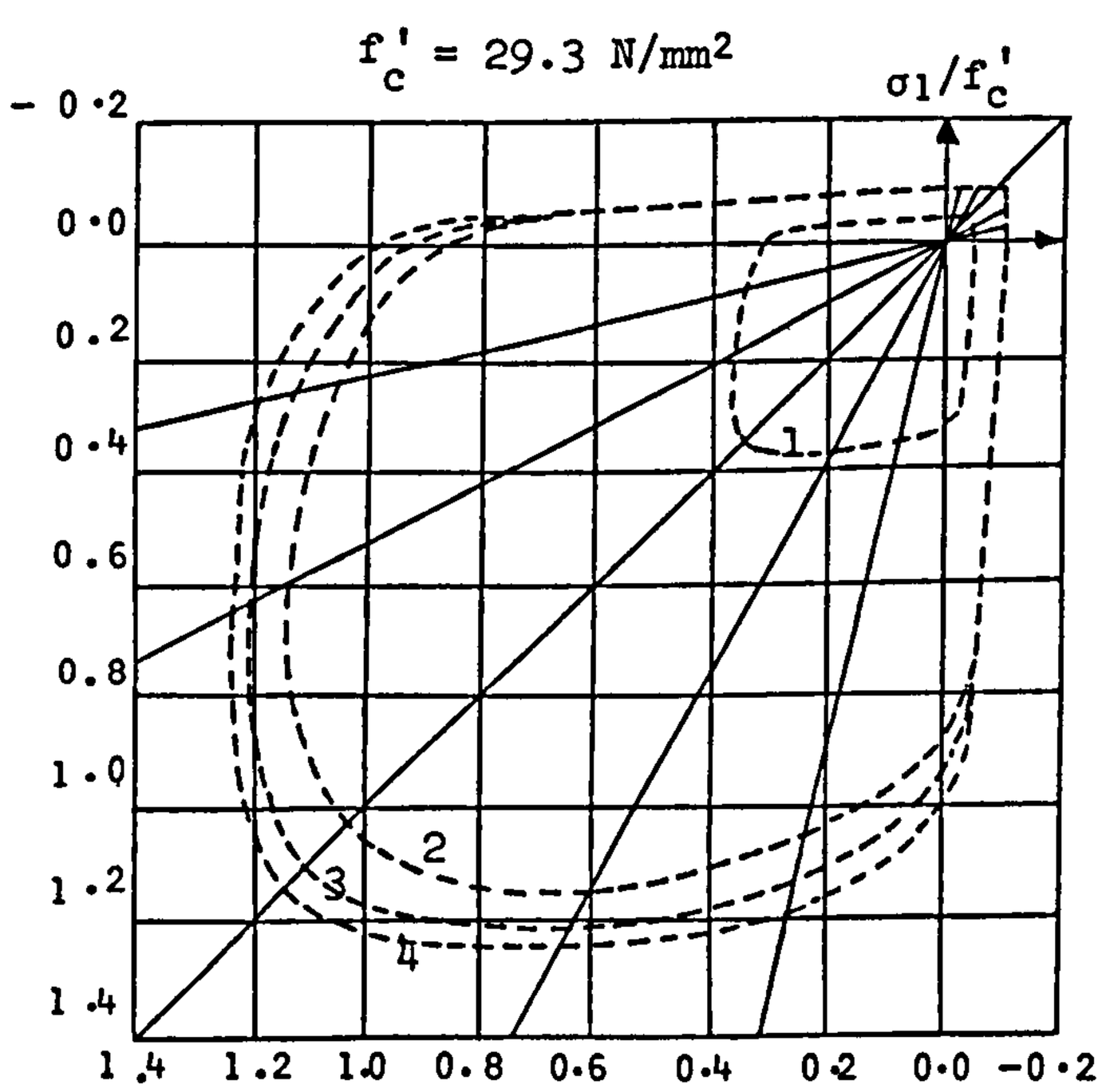

1 - Elastic limit
2 - Point of inflection
3 - Minimum volume
4 - Maximum stress

Figure (4.7) Behaviour zones under biaxial states of stress. (Kupfer et al.)[41]

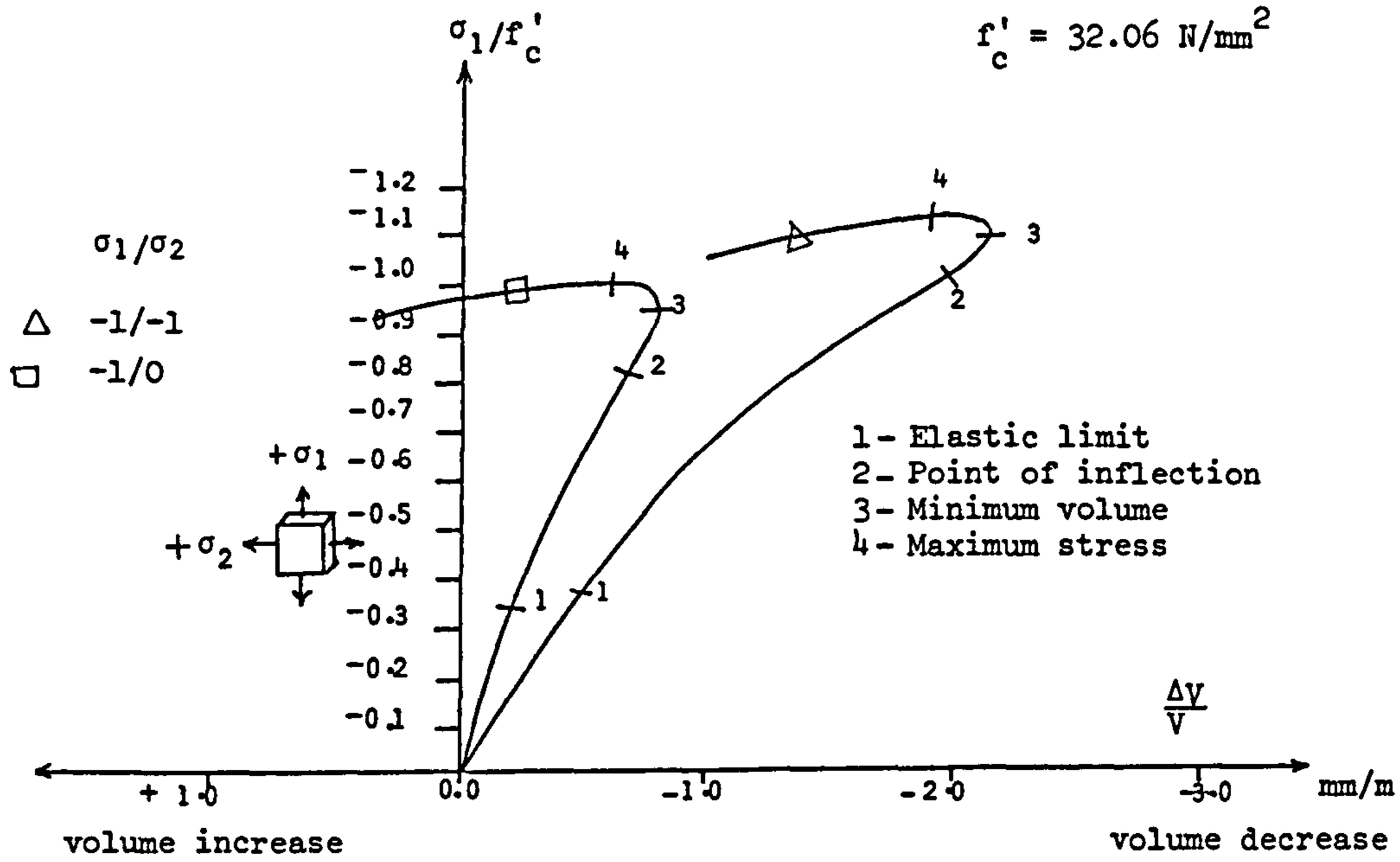

Figure (4.8) Volumetric strain of concrete under uniaxial and biaxial compression.(Kupfer et al.)[41]

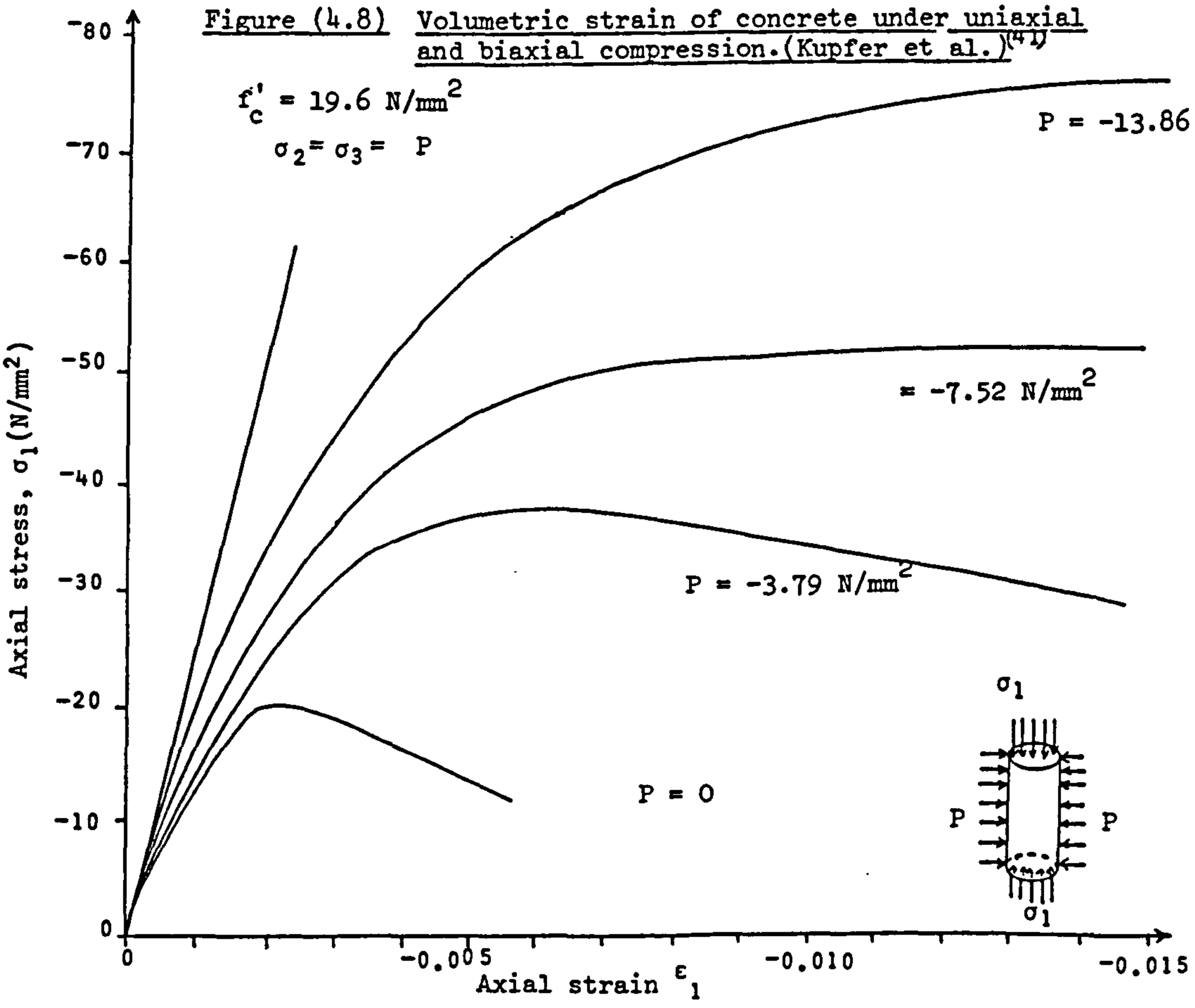

Figure (4.9) Axial stress-strain curve for triaxial compression test by Richart et al.[93]

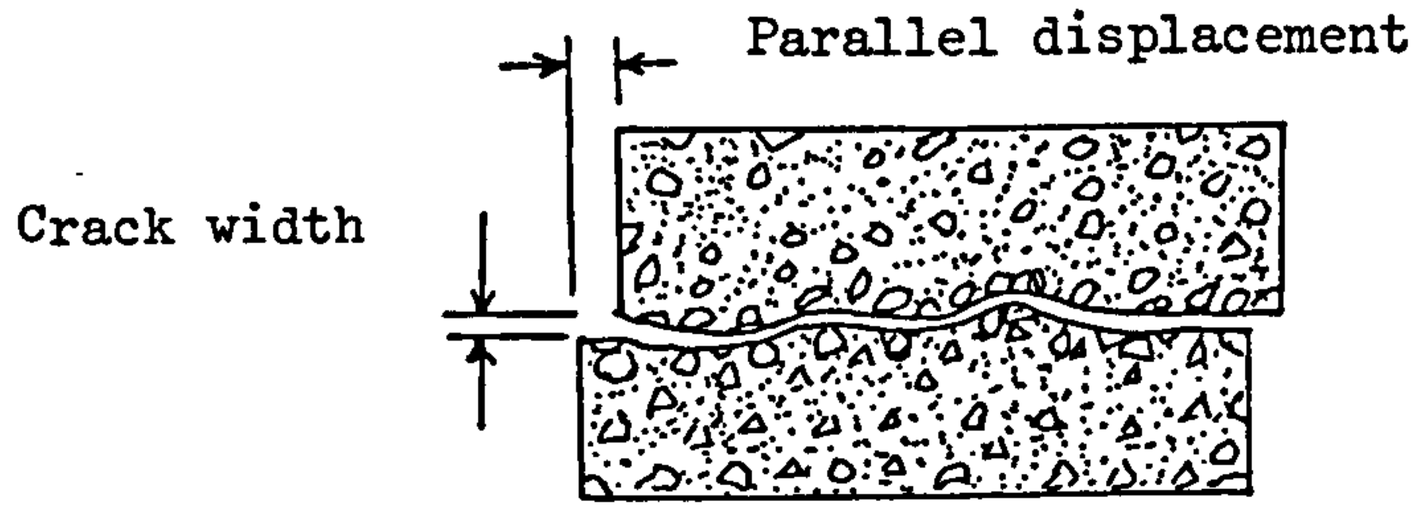

Figure (4.10) Aggregate interlocking of a cracked concrete.

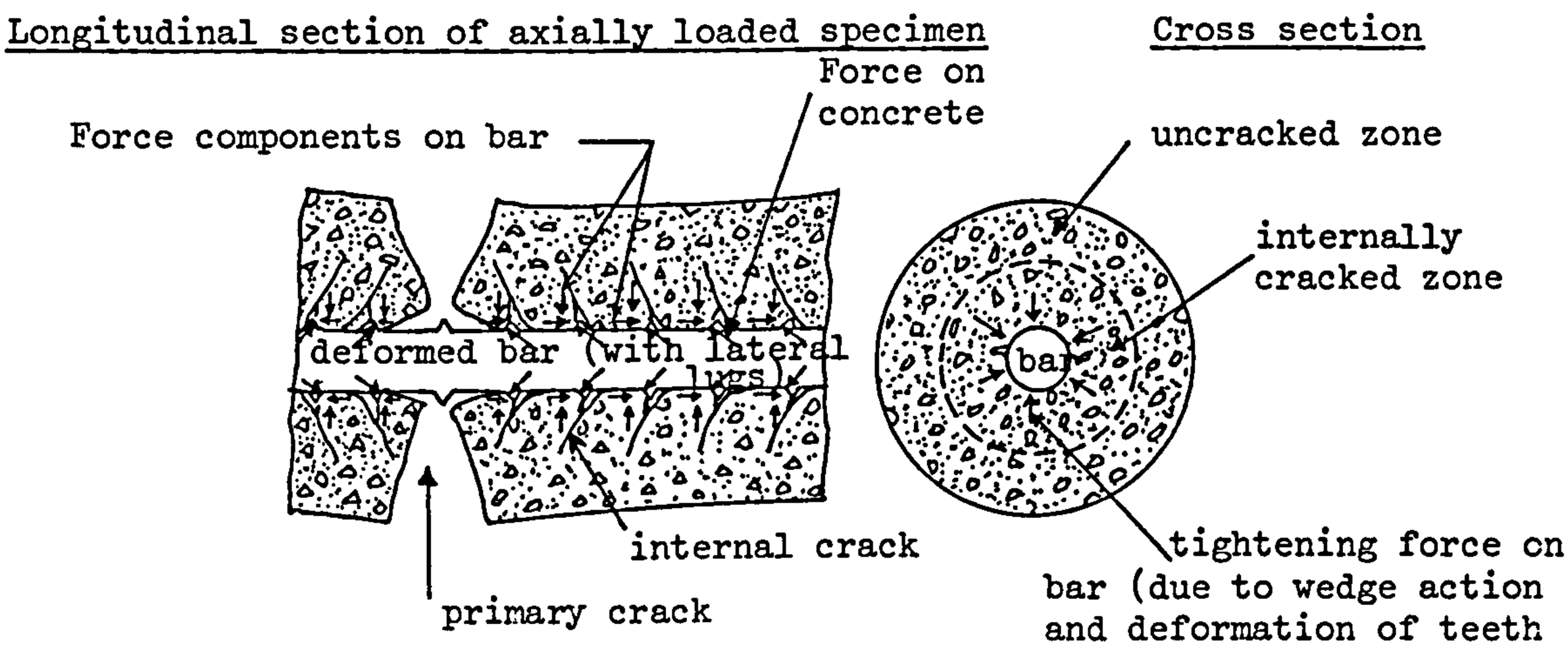

Figure (4.11) Deformation of concrete around Reinforcing Bars (after formation of internal cracks)(Taylor).[116]

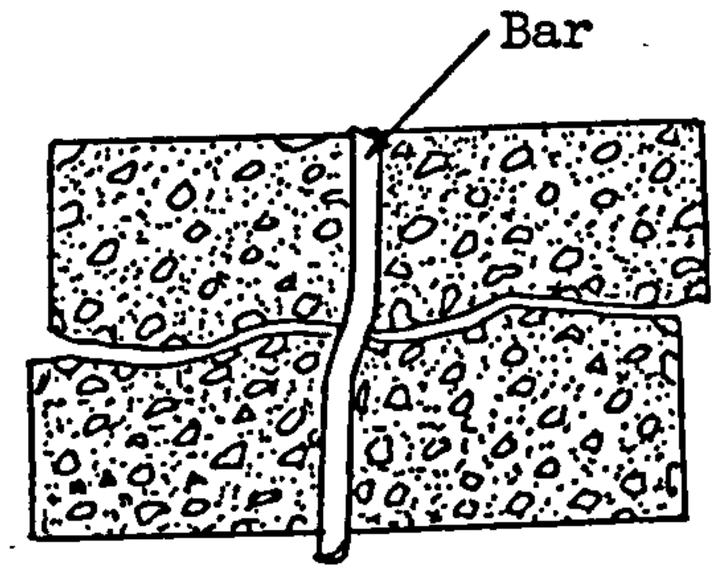

Figure (4.12) Dowel action of a reinforcing bar.

REFERENCES

1. Park, R.; Paulay, T., "Reinforced concrete structures". Wiley 1975.
2. Rüsch, H., "Versuche zur festigkeit der biegedruckzone (Experiments concerning the strength of the compression zone in bending)". Deutscher Ausschuss fur stahlbeton, Heft 120, Berlin, 1955.
3. Labib, F., "Nonlinear analysis of the bond and crack distribution in reinforced concrete members". Ph.D. Thesis, University of London, Sep., 1976.
4. Phillips, D.V., "Nonlinear analysis of structural concrete by finite element method". Ph.D. Thesis, University of Wales, 1973.
5. Shah, S.P.; Winter, G., "Inelastic behaviour and fracture of concrete". J. ACI, Vol.63, 925-930, Sep ., 1966.
6. Desayi, P.; Krishnan, S., "Equation for the stress strain curve for concrete". J. ACI. Vol.61, 345-350, May, 1964.
7. Saenz, L.P., "Discussion on reference 6". J. ACI, Vol.61, 1229-1235, Sep., 1964.
8. Tulin, L.G.; Gerstle, K.H., "Discussion on reference 6". J. ACI, Vol.61, 1236-1238, Sep., 1964.
9. Smith, G.M.; Young, L.E., "Ultimate flexural analysis based on stress-strain curve of cylinders". J. ACI, Vol.53, 597-610, Dec.,1956.
10. Richard, R.M.; Abbott, B.J., "Verstile elastic plastic stress-strain formula". J. of Eng.Mech.Div., ASCE, 511-515, Aug.,1975.
11. Popovics, S., "A numerical approach to the complete stress-strain curve for concrete". Cement &.Conc.Res., Vol.3, 583-599, 1973.

12. Ramberg, W.; Osgood, W.R., "Description of stress-strain curve by three parameters". Technical Note No.902, National Advisory Committee for Aeronautics, Washington, D.C., 1943.

13. Hognested, E., "A study of combined bending and axial load in reinforced concrete members". Bulletin No.399, Eng. Experimental Station, University of Illinois, 1951.

14. Bresler, B., "Reinforced concrete engineering". Vol.1, Wiley, 1974.

15. Kent, D.C.; Park, R., "Flexural members with confined concrete". J. of Struct. Div., ASCE, Vol. 97, 1969-1990, July, 1971.

16. Popovics, S., "A review of stress-strain relationship for concrete". J. ACI, Vol.67, 243-248, March, 1970.

17. Malhotra, V.M., "Are 4 x 8 inch concrete cylinders as good as 6 x 12 inch cylinders for quality control of concrete". J.ACI, Vol.73, 33-36, Jan., 1976.

18. Comité Européen du Béton, "International recommendation for the design and construction of concrete structures". Cement &. Conc. Res., 1970.

19. Neville, A.M., "Properties of concrete". Pitman, 1981.

20. Faherty, K.F., "An analysis of reinforced and prestressed concrete by finite element method". Ph.D. Thesis, University of Iowa, 1972.

21. Johnston, D.W.; Zia, P., "Analysis of dowel action". J. of Struct. Div., ASCE, Vol.97, 1611-1630, May, 1971.

22. Kotsovos, M.C., "Mathematical description of the deformation behaviour of concrete under generalise stress state". Interim report, Imperial College, London, Dec., 1978.

23. Hughes, B.P.; Champman, G.P., "The complete stress-strain curve for concrete in direct tension". Rilem Bulletin No.30, 95-98, March, 1966.

24. Todd, J.D., "The determination of tensile stress-strain curve for concrete". Proc. Inst. Civ. Eng., Part 1, Vol.4, 201-211, March, 1955.

25. Hughes, B.P.; Ash, J.E., "Short term loading and deformation of concrete in uniaxial tension and pure torsion". Mag.Conc. Res., Vol.20, 145-154, Sep., 1968.

26. Evans, R.H.; Marathe, M.S., "Microcracking and stress-strain curve for concrete in tension". Material and Struct., Res. and Testing No.1, 61-64, Feb., 1968.

27. Komlos, K., "Determination of the tensile strength of concrete". The Indian Conc. J., Vol.42, 68-76, Feb., 1968.

28. Madu, R.M., "Characterization of the stress-strain curves for reinforced concrete under uniaxial tension". Mag. Conc. Res., Vol.27, 210-218, Dec., 1975.

29. Coon, M.D.; Evans, R.J., "Incremental constitutive law and their associated failure criteria with application to plain concrete". Int. J. Solids & Struct., Vol.8, 1169-1183, 1972.

30. Wastlund, G., "New evidence regarding the basic strength properties of concrete". Betong, Vol.3, Stockholm, 189-205, 1937.

31. Iyengar, K.T.S. R.; Chandrashekhara, K.; Krishnaswamy, K.T., "Strength of concrete under biaxial compression". J. ACI, Vol.62, 239-249, Feb., 1965.

32. Vile, G.W.D.; Sigvaldason, O.T., "Discussion on reference 31". J.ACI, Vol.62, 1192-1195, Sep., 1965.

33. Bellamy, C.J., "Strength of concrete under combined stresses". J.ACI, Vol.58, 367-381, Oct., 1961.

34. Vile, G.W.D., "The strength of concrete under short term biaxial stresses". Int. Conf. on Structural of Concrete, London, Sep., 1965.

35. Weigler, H.; Becker, G., "Uber das bruch und veformungsverhalten von beton bei Mehrachsiger Beanspruchung". Der Bauingenieur, Heft 10, 390-396, 1961.

36. Bresler, B., Pister, K.S., "Strength of concrete under combined stresses". J. ACI, Vol.55, 321-345, Sep., 1958.

37. Goode, C.D.; Helmy, M.A., "The strength of concrete under combined shear and direct stress". Mag. Conc. Res., Vol.19, 105-112, June, 1967.

38. McHenry, D.; Karni, J., "Strength of concrete under combined tensile and compressive stress". J. ACI, Vol.29, 829-839, April, 1958.

39. Smith, G.M., "Failure of concrete under combined tensile and compressive stresses". J. ACI, Vol.25, 137-140, Oct.,1953.

40. Krishnaswamy, K.T., "Strength of concrete under combined tensile-compressive stress". Materiaux et contructions, Vol.2, 187-194, 1969.

41. Kupfer, H.; Hilsdorf, H.K., "Behaviour of concrete under biaxial stresses". J. ACI, Vol.66, 656-666, Aug., 1969.

42. Pandit, G.; Zimmerman, R.M., "Discussion on reference 41", J. ACI, Vol.67, 194-197, Feb., 1970.

43. Rosenthal, I.; Clucklich, J., "Strength of concrete under biaxial stress". J.ACI, Vol.67, 903-914, Nov.,1970.

44. Krishnaswamay, K.T.; Pandit, G.S., "Discussion on reference 43". J.ACI, Vol.68, 404-406, May, 1971.

45. Buyukozturk, O.; Nilson, A.H.; Slate, F.O., "Stress-strain response and fracture of a concrete model in biaxial loading". J. ACI, Vol.68, 590-598, Aug., 1971.

46. Atan, Y.; Slate, F.O., "Structural lightweight concrete under biaxial compression". J. ACI, Vol.70, 182-185, March, 1973.

47. Liu, T.C.Y.; Nilson, A.H.; Slate, F.O., "Stress-strain response and fracture of concrete in uniaxial and biaxial compression". J.ACI, Vol.69, 291-295, May, 1972.

48. Kupfer, H.; Gerstle, K.H., "Behaviour of concrete under biaxial stresses". J. of Eng. Mech. Div., ASCE, Vol.99, 853-866, Aug.,1973.

49. Rosmstad, K.M.; Taylor, M.A.; Herrmann, L.R., "Numerical biaxial characterization for concrete". J. of Eng.Mech. Div., ASCE, Vol.100, 935-948, Oct., 1974.

50. Darwin, D.; Pecknold, D.A., "Nonlinear biaxial stress-strain law for concrete". J. of Eng. Mech. Div., ASCE, Vol.103, 229-241, April, 1977.

51. Andenaes, E.; Gerstle, K.; Ko, H.Y., "Response of mortar and concrete to biaxial compression ". J. of Eng. Mech. Div., ASCE, Vol.103, 515-526, Aug., 1977.

52. Tasuji, M.E.; Slate, F.O.; Nilson, A.H., "Stress strain response and fracture of concrete in biaxial loading". J. ACI, Vol.75, 306-312, July, 1978.

53. Cedolin, L.; Deipoli, S., "Finite element studies of shear-critical R/c beams". J. of Eng. Mech. Div., ASCE, Vol.103, 395-410, June, 1977.

54. Hilsdorf, H., "The experimental determination of the biaxial strength of concrete". (Die Bestimmung Derzweiachsigen festigkeit von Beton) Proc., Vol.173, Deutscher Ausschuss fur Stahlbeton, Berlin, 1965.

55. Rajagopalan, K., "Discussion on reference 51". J. of Eng. Mech. Div., ASCE, Vol.104, 715, June, 1978.

56. Mills, L.L.; Zimmerman, R.M., "Compressive strength of plain concrete under multiaxial loading conditions". J. ACI, Vol.67, 802-807, Oct., 1970.

57. Johnson, R.P.; Lowe, P.G., "Behaviour of concrete under biaxial and triaxial stresses". Int. Conf. on Struct., Solid Mech. and Eng. Design in Civil Eng. Materials, Paper No.89, Southampton University, April, 1969.

58. Gardner, N.J., "Triaxial behaviour of concrete". J. ACI, Vol.66, 136-146, Feb., 1969.

59. Balmer, G.G., "Shearing strength of concrete under high triaxial stress-computation of Mohr's envelope as a curve". Report No.Sp-23, Denver, Colorado, Oct., 1949.

60. Akroyd, T.N.W., "Concrete under triaxial stress". Mag. Conc. Res., Vol.13, 111-118, Nov., 1961.

61. Hobbs, D.W., "Strength and deformation properties of plain concrete subject to combined stress". Cement &. Con. Association, Report No.42, July, 1974.

62. Chen, A.C.T.; Chen, W.F., "Constitutive relations for concrete". J. of Eng. Mech. Div., ASCE, Vol.101, 465-481, Aug., 1971.

63. Chen, A.C.T.; Chen, W.F., "Constitutive equations and punch indentation of concrete". J. of Eng.Mech.Div.,ASCE, Vol.101, 889-906, Dec.,1975.

64. Chen, A.C.T., "Constitutive relations of concrete and punch indentation problems". Ph.D. Thesis, Lehigh University, 1973.

65. Palaniswamy, R.; Shag, S.P., "Fracture and stress-strain relationship of concrete under triaxial compression". J. of Strct. Div., ASCE, Vol.100, 901-916, May, 1974.

66. Kotsovos, M.D.; Newman, J.B., "Behaviour of concrete under multi-axial stress". J. ACI, Vol.74, 443-446, Sep., 1977.

67. Cedolin, L.; Crutzen, Y.R.J.; Deipoli, S., "Triaxial stress-strain relationship for concrete". J. of Eng. Mech. Div., ASCE, Vol. 103, 423-439, June, 1979.

68. Sargin, M., "Stress-strain relationships for concrete and the analysis of structural concrete relationships". Solid Mech. Div., University of Waterloo, Canada, 1971.

69. Sahlin, S., "Effect of far-advanced compressive strains of concrete in reinforced concrete beams subjected to bending moments. Betong Vol.40, Stockholm, 1955.

70. Young, L.E., "Simplifying ultimate flexural theory of maximizing the moment of the stress block". J. ACI, Vol.57, 549-556, Nov., 1960.

71. Kriz., L.B.; Lee, S.L., "Ultimate strength of over reinforced beams". J. of Eng. Mech. Div., ASCE, 95-105, June, 1960.

72. Leibenberg, A.C., "A stress-strain function of concrete subjected to short term loading". Mag. Conc. Res., Vol.61, 345-350, March, 1964.

73. Ahmad, S.H.; Shah, S.P., "Complete triaxial stress-strain curves for concrete". J. of Struct. Div., ASCE, Vol.108, 728-742, April, 1982.

74. Ottosen, N.S., "Constitutive model for short time loading of concrete". J. of Eng. Mech. Div., ASCE, Vol.105, 127-141, Feb., 1979.

75. Murray, D.W.; Chitnuyanondh, L.; Rijub-Agha, Y.R.; Wong, C., "Concrete plasticity theory for biaxial stress analysis". J. of Eng. Mech. Div., ASCE, Vol.105, 989-1005, Dec., 1979.

76. Tasuji, M.E.; Nilson, A.H.; Slate, F.O., "Biaxial stress-strain relationships for concrete". Mag. Conc. Res., Vol.31, 217-224, 1979.

77. Gerstle, K.H., "Simple formulation of biaxial concrete behaviour". J.ACI, Vol.78, 62-68, Jan.-Feb., 1981.

78. Kotsovos, M. D. ; Newman, J.B., "A mathematical description of the deformation behaviour of concrete under complex loading". Mag. Conc. Res., Vol.31, 77-90, June, 1979.

79. Kotsovos, M. D., "Effect of stress path on the behaviour of concrete under triaxial stress states". J. ACI, Vol.76, 213-223, Feb., 1979.

80. Kotsovos, M. D., "A mathematical description of the strength properties of concrete under generalized stress, Mag. Conc. Res., Vol.31, 151-158, Sept. 1979.

81. Kotsovos, M. D.; Newman, J.B., "Mathematical description of deformational behaviour of concrete under generalized stress beyond ultimate strength". J. ACI, Vol.77, 340-346, Sept-Oct., 1980.

82. Murray, D.W., "Octahedral based incremental stress strain matrices". J. of Eng. Mech. Div., ASCE, Vol.105, 501-513, Aug., 1979.

83. Elwi, A.A.; Murray, D.W., "A 3D hypoelastic concrete constitutive relationship". J. of Eng. Mech. Div., ASCE, Vol.105, 623-641, Aug., 1979.

84. Gerstle, K.H.; Aschl, H.; Bellotti, R.; Bertacchi, P.; Kotosovos, M.D.; Ko, H.; Linse, D.; Newman, J.B.; Rossi, P.; Schickert, G.; Taylor, M.A.; Traina, L.A.; Winkler, H.; Zimmerman, R.M. "Behaviour of concrete under multiaxial stress states". J. of Eng. Mech. Div., ASCE, Vol.106, 1383-1403, Dec.,1980.

85. Chen, W.F., "Plasticity in reinforced concrete". McGraw-Hill, 1982.

86. Ngo, D.; Frankline, H.A.; Scordelis, A.C., "Finite element study of reinforced concrete beams with diagonal tension cracks". Report No. UC-SESM 70-19, University of California, Dec.,1970.

87. Ngo, D.; Scordelis, A.C., "Finite element analysis of reinforced concrete beams". J. ACI, Vol.64, 162-163, March, 1967.

88. Nilson,A.H., "Nonlinear analysis of reinforced concrete by the finite element method". J. ACI, Vol.65, 757-766, Sep. ,1968.

89. Kong, E.K.; Evans, R.H., "Reinforced and prestressed concrete". Thomas Nelson, 1981.

90. Bazant, Z.P., Bhat, P.D., "Endochronic theory of inelasticity and failure of concrete". J. of Eng. Mech. Div., Vol.102, 331-344, Aug., 1976.

91. Hillemier, B.; Hilsdorf, H.K., "Fracture mechanics studies of concrete compounds". Cement &. Con. Res., Vol.7, 523-536, 1977.

92. Bazant, Z.P., Cedolin, L., "Blunt crack band propagation in finite element analysis". J. of Eng. Mech., Div., ASCE, Vol.105, 297-315, April, 1979.

93. Richart, F.E.; Brandtzaeg, A.; Brown, R.L., "A study of the failure of concrete under combined compressive stresses". Bulletin No.185, Eng. Experimental Station, University of Illinois, 1928.

94. Paulay, T.; Loeber, P.J., "Shear transfer by aggregate interlock". Proc. of the Shear Symposium, ACI Publication SP-42, Vol.1, 1-15, 1973.

95. Morrell, P.J.B.; Chia, C.H., "A method of determining the contribution of aggregate interlock forces to the shear resistance of singly reinforced concrete beams". Proc. Inst. Civ. Eng., Part 2, Vol.69, 885-861,1980.

96. Fardis, M.N.; Buyukozturk, O., "Shear transfer model for reinforced concrete". J. of Eng. Mech. Div., ASCE, Vol.105, 255-275, April, 1979.

97. Walraven, J.C., "Fundamental analysis of aggregate interlock". J. of Struct. Div., ASCE, Vol.107, 2245-2270, Nov., 1981.

98. Gerstle, K.H., "Material modelling of reinforced concrete". IABSE Colloquium on The Advanced Mechanics of Reinforced Concrete, Introductory Report, Delft, 41-61, 1981.

99. Walraven, J.C.; Vos, E.; Reinhardt, H.W., "Experiments on shear transfer in cracks in concrete". Report No.5-79-3, Part 1, Delft University, 1979.

100. Reinhardt, H.W.; Walraven, J.C., "Crack in concrete subject to shear". J. of Struct. Div., ASCE, Vol.108, 207-224, Jan.,1982

101. Mylrea, T.D., "Bond and anchorage". J. ACI, Vol.44, 521-552, March, 1948.

102. Scordelis, A.C., "General report - Basic Problem". IASS Symposium on the nonlinear behaviour of reinforced concrete spatial structures, Vol.3, 35-70, July, 1978.

103. Lutz, L.A.; Gergely, P., "Mechanics of Bond and slip of deformed bars in concrete". J. ACI, Vol.64, 711-721, Nov., 1967.

104. Perry, E.S.; Jundi, N., "Pullout bond stress distribution under static and dynamic repeated loadings". J. ACI, Vol.66, 377-380, May, 1969.

105. Nilson, A.H., "Bond stress-slip relations in reinforced concrete". Report No.345, Cornell University, Dec., 1971.

106. Testa, R.B.; Stubbs, N., "Bond failure and inelastic response of concrete". J. of Eng. Mech. Div., ASCE, Vol.103, 295-310, April, 1977.

107. Mirza, S.M.; Houde, J., "Study of bond stress-slip relationships in reinforced concrete". J. ACI, Vol.76, 19-46, Jan., 1979.

108. Kemp, E.L.; Wilhelm W.J., "Investigation of the parameters influencing bond cracking". J. ACI, Vol.76, 47-71, Jan., 1979.

109. Jimenez, R.; White, R.N.; Gergely, P., "Bond and dowel capacities of reinforced concrete". J. ACI, Vol.76, 73-92, Jan., 1979.

110. Tassios, T.P.; Yannopoulos, P.J., "Analytical studies on reinforced concrete members under cyclic loading based on bond stress-slip relationships". J. ACI, Vol.78, 206-216, May-June, 1981.

111. Somayaji, S.; Shah, S.P., "Bond stress versus slip relationship and cracking response of tension members". J. ACI, Vol.78, 217-225, May-June, 1981.

112. Edwards, A.D.; Yannopoulos, P.J., "Local bond-stress-slip relationships under repeated loading". Vol.30, 62-72, June,1978.

113. Tepfers, R., "Lapped tensile reinforcement splices". J. of Struct. Div., ASCE, Vol.108, 283-301, Jan., 1982.

114. Venkateswarlu, B.; Gesund, H., "Cracking and bond-slip in concrete beams". J. of Struct. Div., ASCE, Vol.98, 2663-2685, Dec., 1982.

115. Mattock, A.H., "Shear transfer in concrete having reinforcement at an angle to the shear plane". ACI Publication SP-42, Vol.2, 17-42, 1973.

116. Taylor, H.P.T., "Shear stresses in reinforced concrete beams without shear reinforcement". Technical Report, TRA 407, Cem. & Con. Association, London, Feb., 1968.

CHAPTER 5

MATHEMATICAL MODELLING OF THE CONSTITUTIVE LAWS FOR REINFORCED CONCRETE

CHAPTER 5
MATHEMATICAL MODELLING OF THE CONSTITUTIVE LAWS FOR REINFORCED CONCRETE

5.1 Introduction:

In this chapter the mathematical models used for concrete and steel will be explained in detail. A brief summary of the models will be given first in this section.

For the concrete there are various conditions to consider which depend on the state of stress and the state of cracking, and different models are used to represent these various aspects of behaviour. Before the start of cracking,the endochronic model is used to represent all states of stress. But as cracks develop different paths are selected; a cracking model to represent cracking behaviour, a uniaxial-compression model to represent regions of uniaxial-compression, and failure conditions to represent the crushing of concrete.

(1) The endochronic model:

This model is used for the description of concrete behaviour in the stress regions of biaxial-compression, tension-compression, and tension-tension before the development of cracks. The same formulation is used to describe all these states. The endochronic theory was first presented for concrete by Bazant et al.[1]. in 1974 and has since been improved in various ways. It will be explained in detail in section 5.2.

(2) The cracking model:

A separate cracking model is required because the endochronic theory aspresented in this thesis does not apply for tensile cracking. Although it is possible to include this by changing some functions in the model, it is more realistic to introduce an independent criterion for tensile cracking.[4] The cracking model is primarily based on the maximum stress criterion using the uniaxial tensile strength of concrete f'_t as

a measure for crack initiation. However the maximum principal strain criterion is also included for certain cases as explained later.

For post cracking,two different models have been investigated. One assumes a sudden drop in stress in the plane perpendicular to the crack direction after a crack has occurred, and the other assumes a gradual release of the stress in this direction. Aggregate interlocking along a crack is represented by a simple factor.

This is sometimes called the shear retention factor and retains some shear capacity after cracking. The smeared crack approach is used to represent the material after cracking. This will be discussed in detail in section 5.3.

(3) The uniaxial-compression model:

The model proposed by Popovics[20] for uniaxial-compression is used in regions where a crack has occurred and compressive strains exist in the direction parallel to the crack. The reason for this procedure is because it is difficult to use the endochronic theory when a separate cracking model is included. It is difficult to change material parameters from a biaxial state into a uniaxial state. This model is explained in section 5.4.

(4) The crushing model:

A separate model is used to represent crushing of concrete. The onset of crushing is based on a crushing strain envelope for uniaxial and biaxial conditions. It is applicable for all states of stress and was formulated in this way to avoid having separate models for the Popovics and endochronic procedures. Further details are explained in Section 5.5.

A flow chart is shown in Figure (5.1), to illustrate the use of each of the models detailed above.

For steel reinforcement, a bi-linear stress-strain curve is assumed. This is explained in Section 5.6.

5.2 The endochronic model:

5.2.1 Historical review:

The endochronic theory was first proposed by Valanis[8,9] in 1971 to describe the mechanical behaviour of metals. Valanis showed that by employing a pseudo-time scale, called the intrinsic time, a constitutive equation in integral or differential form can successfully be used to describe metal behaviour, including such aspects as strain hardening, unloading and reloading, cross-hardening and continued cyclic strainings. The theory is a form of viscoplasticity theory but it does not require the specific definitions of yielding and hardening, i.e., no yield surface is needed.

Using Valanis concept, Bazant and his co-workers extended the theory to describe the behaviour of rock, sand, plain concrete, and reinforced concrete under various conditions. In 1974, Bazant[1] modified the endochronic theory to include additional parameters that can model the behaviour of sand and concrete such as inelastic dilatancy, hydrostatic pressure sensitivity, and, in the case of long-time creep, different intrinsic time scales for short-time and long time processes. In 1975 Bazant[2] showed the validity of the new model for representing multiaxial states of stress and uniaxial cyclic behaviour. Bazant et al.[4] extended the endochronic theory for

analysing the nonlinear behaviour of sand under conditions of cyclic shear.

Further modifications were carried out by Bazant et al. for concrete nonlinear behaviour in references 3, 5, 6,10. This thesis develops a version presented by Bazant et al. in reference 10. This incorporates a wide range of concrete properties such as the stress-strain curves under uniaxial, biaxial and triaxial stress states for different strengths, their failure envelopes, strain softening behaviour, inelastic strains due to hydrostatic compression, lateral strains and volume expansion, and dependance of material parameters on the strength. Bazant's version also incorporates other aspects such as cyclic loading behaviour and creep response but these were not used in this work.

Certain shortcomings of this model have been reported. For example,the original model[3] was found to give much too steep an unloading curve and too mild a degradation of elastic moduli when large creep strains occurred. Also when unloading was reversed to reloading the slope became smaller when it should have become steeper. Also, when a low stress, cyclic loading was followed by a high stress load, the response was too stiff.[13-15,17,18] Some recent papers[13,18] have been concerned with trying to modify the theory to deal with these shortcomings.

The theory is still under active study and improvement.[7,10,13,14,18,24]. However it has evolved far enough to represent concrete behaviour for the problems dealt with in this thesis. Indeed different versions of the theory have already been used in practical applications

of finite element analysis for concrete structures, for exmaple references 11,12,19.

The endochronic model in this work has been modified to be suitable for two dimensional finite element analysis. Special techniques are used to obtain the appropriate solutions, as will be explained in Section 5.2.6.

5.2.2 Basic assumption of the endochronic theory:(8)

As explained in the previous section the endochronic theory does not require the use of the concept of a yield surface and suggests instead physical interpretations in terms of damage, microcracking and internal friction. The phenomenon of distinct yielding is most common in metals and makes a sudden transition from a linear-elastic to a nonlinear plastic stress-strain response. But yielding is often a gradual transition, which makes it difficult to state precisely when it has occurred.

Thus the absence of a yield surface makes the endochronic theory useful for representing this type of behaviour. Instead,the theory includes plastic deformations whenever deformation takes place and this is useful for materials such as concrete which tend to have inelastic strains from the early stages, although initially of course they are small compared to elastic deformations.

The theory is based upon the observation that the state of stress at a point in a plastic material depends on the set of the previous states of deformation of all points in its neighbourhood; but it does not depend on the rapidity at which such deformation states have succeeded one another. In the case of such rate independent behaviour, an absolute

strain measure ξ can be introduced which is intrinsically related to the accummulated strain history of the material and which represents a sort of time in the sense that it records one event after another, but is not concerned with the actual time lapse between them. This parameter ξ is usually called "intrinsic time"[8], although it has also been termed "distortion measure"[3]. Clearly it is independent of t, the external time measured by a clock, and is solely dependent on strain increments.

This parameter ξ has to be a monotonically increasing function of deformation to ensure a uniqueness between it and the deformation history, otherwise two different states of deformation could exist simultaneously (i.e. ξ must be different for each successive state of deformation even if a particular state repeats a historically earlier one).

Valanis[8] suggested that the most useful means of ensuring that an increment of ξ was positive is to define it by the quadratic form:

$$d\xi^2 = P_{ijk\ell}\, d\varepsilon_{ij}\, d\varepsilon_{k\ell} \qquad (5.1)$$

where ε_{ij} is the strain tensor for small deformations and $P_{ijk\ell}$ is a fourth order tensor which in general may depend on ε_{ij}.

In cases where material behaviour also depends on actual time, a theory of viscoplasticity may be obtained by introducing another "time measure" ζ which is related to both the real time t as well as the strain measure ξ[8]. This can be expressed through the relationship:

$$d\zeta^2 = \alpha^2\, d\xi^2 + \beta^2\, dt^2 \qquad (5.2)$$

where α and β are scalar-valued material parameters, and ζ is called the "Intrinsic time measure", because of the analogy between ξ and real time. The total "time" is a function of the "time measure" and is called the "intrinsic time scale" z. i.e.

$$z = z(\zeta) \; ; \; \frac{dz}{d\zeta} > 0; \quad 0 \leq \zeta < \infty \qquad (5.3)$$

This scale is a property of the material at hand. The function z and the operator $P_{ijk\ell}$ of equation (5.1) must be chosen so that the observed material behaviour is modelled. As will be seen later, the stress is a function of the strain history as defined by the intrinsic time scale, z, and therefore the theory has been called "endochronic theory".

From basic thermodynamic principles, Valanis[8] obtained two relationships for the total deviatoric and hydrostatic stresses which form the basis of endochronic theory. These are as follows:

$$\text{Deviatoric stresses} \quad S_{ij} = 2\int_{z_o}^{z} G(z-z^*)de_{ij}(z^*) \qquad (5.4)$$

$$\text{Hydrostatic stresses} \quad \sigma_{kk} = 3\int_{z_o}^{z} K(z-z^*)d\varepsilon_{kk}(z^*) \qquad (5.5)$$

where z_o = intrinsic time scale at initial state

z^* = intrinsic time at $z_o \leq z^* \leq z$

z = intrinsic time scale

G = $G(z)$ = Shear modulus

K = $K(z)$ = Bulk modulus

$$\sigma_{ij} = S_{ij} + \delta_{ij} \frac{\sigma_{kk}}{3} \quad = \text{stress tensor}$$

$$\epsilon_{ij} = e_{ij} + \delta_{ij} \frac{\epsilon_{kk}}{3} \quad = \text{strain tensor}$$

The function G(z) and K(z) must be chosen such that experimental data are modelled by Equations (5.4) and (5.5).

5.2.3 Application to metals:[9]

The endochronic theory was originally applied by Valanis to model the behaviour of metals rather than concrete. These earlier theories included behaviour which was more relevant to metals but nevertheless will be briefly discussed here before showing the adaptation for concrete. The basic assumptions for metals were as follows:

1. Time effects were neglected (i.e. $z = z(\xi)$);
2. It was assumed that plastic deformations were incompressible and that the material behaves elastically under pressure. Thereby equation (5.5) becomes, $\sigma_{kk} = 3K\epsilon_{kk}$ where K is a constant;
3. It was assumed that the apparent shear modulus was given by the single exponential term $G(z) = G.e^{-\alpha z}$ where G_o is the initial shear modulus; thereby Equation (5.4) was reduced to the differential equation:

$$de_{ij} = \frac{dS_{ij}}{2G_o} + \frac{\alpha S_{ij}\, dz}{2G_o} \qquad (5.6)$$

In Equation (5.6) $\frac{dS_{ij}}{2G_o}$ is the elastic deviatoric strain increment of classical plasticity. $\frac{\alpha S_{ij}\, dz}{2G_o}$ is interpreted as

the plastic strain increment and resembles the Prandtl-Reuss equations. The difference between the endochronic and the Prandtl-Reuss theory lies in the role played by dz.

In the Prandtl-Reuss theory dz can be either positive, zero or negative and z is identified with the yield surface ($z = z(S_{ij})$ representing the loading function). Plastic deformation occurs only after the yield surface is reached and $dz > o$. When $dz \leq o$ plastic deformation does not occur.

In the endochronic theory, however, dz is always positive for a deforming material, and is not related to a yield surface. Hence, contrary to the Prandtl-Reuss theory, "Plastic" deformations are present in the endochronic plasticity theory whenever deformation takes place.

Valanis[9] applied this theory to model complex experimental results for metals and good comparisons were obtained.

5.2.4 Application to concrete:

Bazant et al.[10] extended the theory to concrete. Characteristics which had not been included for metals were now considered. These were:

1. Inelastic volumetric strain behaviour (i.e. introducing inelastic dilatancy).
2. Shear compaction effects.
3. Hydrostatic pressure sensitivity and strain-hardening and softening effects which are related to the intrinsic time z.
4. The dependence of tangent moduli (G and K) on dilatation.

5. Introducing more than one intrinsic time (i.e. ξ ,ξ', z, z') to account for differences in behaviour under deviatoric and hydrostatic stress states.

In contrast to metals, which behave linearly under hydrostatic stress, concrete undergoes inelastic deformation. Bazant et al. introduced an inelastic volumetric strain increment into the volumetric stress-strain relationship, while retaining the deviatoric stress-strain relationship in the same form as for metals. i.e.:

$$\text{Deviatoric strain} = de_{ij} = de_{ij}^{e} + de_{ij}^{P} = \frac{dS_{ij}}{2G} + \frac{S_{ij}}{2G}\,dz \qquad (5.7)$$

$$\text{Volumetric strain} = d\varepsilon_m = d\varepsilon_m^{e} + d\varepsilon_m^{P} = \frac{d\sigma_m}{3k} + \left(d\varepsilon^{o} + d\lambda + d\lambda' + \frac{\sigma_m\, dz'}{3K}\right) \qquad (5.8)$$

in which

de_{ij}^{e} = Elastic part of deviatoric strain increment.

de_{ij}^{p} = Inelastic part of deviatoric strain increment.

$d\varepsilon_m^{e}$ = Elastic part of volumetric strain increment.

$d\varepsilon_m^{P}$ = Inelastic part of volumetric strain increment.

ε_m = $\varepsilon_{kk}/3$ = mean strain.

σ_m = $\sigma_{kk}/3$ = mean stress.

e_{ij} = $\varepsilon_{ij} - \delta_{ij}\,\varepsilon_m$ = deviatoric strain tensor.

S_{ij} = $\sigma_{ij} - \delta_{ij}\,\sigma_m$ = deviatoric stress tensor.

δ_{ij} = Kronecker delta.

λ = Inelastic dilatancy.

λ'= Shear compaction.

z z' = Intrinsic times for distortion and compaction.

Four parts have been identified as forming the plastic part of the mean strain (i.e. inelastic volumetric strains) which can be written as:

$$d\varepsilon_m^{\,p} = d\varepsilon^{o} + d\lambda + d\lambda' + \frac{\sigma_m\, dz'}{3K} \qquad (5.9)$$

$d\varepsilon^{o}$ accounts for stress-independent inelastic strain, such as thermal dilatation and shrinkage. However these effects will not be given any further attention in this work and are assumed equal to zero.

The parameter λ represents a measure of the inelastic volumetric strain due to shear strains and has been called "Inelastic dilatancy" by Bazant et al. This effect is manifested in uniaxial compression tests by the increase of Poisson Ratio up to and over 0.5 when failure is imminent. An increase of λ, i.e. $d\lambda$ can be expressed as follows:

$$d\lambda = \ell(\lambda)\, L(\lambda,\varepsilon,\sigma) \qquad (5.10)$$

where $\ell(\lambda)$ is a "dilatancy-hardening function" and is represented graphically in Figure (5.2.a). This function is linearly related to λ and becomes equal to zero when λ approaches a maximum value, λ_o. Such a maximum value must exist because there is a certain maximum volume that concrete can reach after it is fully crushed. $L(\lambda,\varepsilon,\sigma)$ is a "dilatancy-softening function" and is assumed to depend on $I_1(\sigma)$ (i.e. first invariant of the stress tensor) and $J_2(\varepsilon)$ (i.e.

second invariant of deviatoric strain). The presence of $I_1(\sigma)$ incorporates the fact that dilatancy must vanish at very high hydrostatic pressure, because no cracks can open (Figure (5.2.b)). The function of $J_2(\varepsilon)$ is used because the deviatric strains cause microcracking. This function, Figure (5.2.c), assures that there is no appreciable dilatancy in cyclic compression for low strains, but allows it to be quite pronounced, but gradual, when load cycles reach into high stresses.

Bazant et al. found from practical experience that λ has a very profound effect on predicted behaviour (i.e. shape of the hysteresis loops) and the Poisson's ratio under cyclic loading. $d\xi$ in Equation (5.10) was also included because this will relate dilatancy to the deviatoric strain increment (represented by $d\xi$) and is apparently necessary as a further measure of microcracking.

Variable λ' represents the shear compaction which appears at the beginning of inelastic deformation and represents the departure from the hydrostatic pressure line as shown in Figure (5.2.d). This inelastic deformation occurs in the zone between envelope 1 and 2 of Figure (4.7) and is defined in a similar function to Equation (5.10), i.e.

$$d\lambda' = \ell'(\ell')\, L'(\lambda', \varepsilon, \sigma) d\xi \qquad (5.11)$$

The function $\ell'(\lambda')$ prevents λ' from exceeding a certain limit, and the function $L'(\lambda', \varepsilon, \sigma)$ causes $d\lambda'$ to vanish for large shear strain (i.e. large $J_2(\varepsilon)$) when shear compaction ceases.

The parameter z' is the intrinsic time associated with volume change, and models inelastic volumetric strains due to hydrostatic stress (i.e. the cumulative damage sustained by the concrete due to volume change).

This effect is mainly important at high hydrostatic pressure. The parameter z' was defined by:

$$dz' = \frac{d\zeta'}{z_2} = \frac{d\eta'}{h(\eta')z_2} \qquad (5.12)$$

where $$d\eta' = H(\sigma)d\xi' \qquad (5.13)$$

The softening function $H(\sigma)$ increases the inelastic volume change if the hydrostatic compression grows but becomes constant at higher compression levels. The less inclined medium portion of the hydrostatic curve is governed by the linear term in $h(\eta')$ and the subsequent stiffening is achieved by the quadratic term in $h(\eta')$.

The values of $d\xi$ and $d\xi'$ were reduced by Valanis[9] and Bazant et al.[10] to:

$$d\xi = |J_2(d\varepsilon)|^{1/2} = \sqrt{\frac{1}{2}\, de_{ij}\, de_{ij}} \qquad (5.14)$$

where $J_2(d\varepsilon)$ = second invariant of the deviatoric strain increment tensor de_{ij}.

and $$d\xi' = |I_1(d\varepsilon)| = |d\varepsilon_{kk}| = |d\varepsilon_{11} + d\varepsilon_{22} + d\varepsilon_{33}| \qquad (5.15)$$

where $I_1(d\varepsilon)$ = first invariant of the strain tensor increment $d\varepsilon_{ij}$.

The functions ℓ, L, ℓ', L', h and H and constant z_2 are listed in Appendix A.

The inelastic part of the deviatoric strain takes into account the sensitivity of these strains to hydrostatic pressure and attempts to present its strain-hardening and softening behaviour i.e.

$$de_{ij} = \frac{S_{ij}}{2G}\, dz \qquad (5.16)$$

where z is the intrinsic time, representing the cumulative damage sustained by concrete due to distortion. Bazant et al. expressed it as:

$$dz = \frac{d\zeta}{z_1} = \frac{d\eta}{f(\eta,\varepsilon,\sigma)z_1} \qquad (5.17)$$

where $$d\eta = F(\varepsilon,\sigma)\, d\xi \qquad (5.18)$$

The functions f and F were chosen to model the hydrostatic pressure sensitivity and the effect of strain hardening and softening behaviour. For simplicity a diagram is shown in Figure (5.2.e) which illustrates their effect on a uniaxial compressive stress-strain curve. These functions and the constant z_1 are also listed in Appendix A.

The tangent moduli (G and K) are assumed to be dependent only on the inelastic dilatation λ. The functions are selected such that G and K decrease as λ grows because, as explained earlier, λ represents the inelastic dilatancy due to shear strain and has a predominant effect on microcracking. This affects indirectly the value of Poisson's Ratio and hence G and K. The following functions were assumed to be suitable representations:

$$K = K_o\, \phi(\lambda) \qquad (5.19)$$

and $$G = G_o\, \phi(\lambda) \qquad (5.20)$$

in which $$\phi(\lambda) = \frac{1}{1 + c_5\lambda} \qquad (5.21)$$

and K_o = Initial elastic Bulk modulus = $\frac{E_o}{3(1-2\nu)}$;

G_o = Initial elastic shear modulus = $\frac{E_o}{2(1+\nu)}$

E_o = Initial Young's modulus.

ν = Initial Poisson's ratio.

The value of c_5 was deduced from experimental measurements and was found to be equal to 150. The value of $\phi(\lambda)$ is chosen in such a way that G and K cannot become negative for any value of λ and that it will yield a slower decrease of G and K with λ at high values of λ.

5.2.5 Summary of the equation of the endochronic theory:

The endochronic theory equations used in this work can now be summarized as follows:

Deviatoric strain: $$de_{ij} = \frac{dS_{ij}}{2G} + \frac{S_{ij}\, dz}{2G} \qquad (5.22)$$

Volumetric strain: $$d\varepsilon_m = \frac{d\sigma_m}{3K} + d\varepsilon^o + d\lambda + d\lambda' + \frac{\sigma_m dz'}{3K} \qquad (5.23)$$

where $$dz = \frac{d\zeta}{z_1} = \frac{d\eta}{f(\eta,\varepsilon,\sigma)z_1} \qquad (5.24)$$

$$d\eta = F(\varepsilon,\sigma)d\xi \qquad (5.25)$$

$$dz' = \frac{d\zeta'}{z_2} = \frac{d\eta'}{h(\eta')z_2} \qquad (5.26)$$

$$d\eta' = h(\sigma)\, d\xi' \qquad (5.27)$$

$$d\xi = \sqrt{J_2(d\varepsilon)} = \sqrt{\frac{1}{2}\, de_{ij}\, de_{ij}} \qquad (5.28)$$

$$d\xi' = \sqrt{|I_1(d\varepsilon)|^2} = |d\varepsilon_{11}+d\varepsilon_{22}+d\varepsilon_{33}| \qquad (5.29)$$

$$d\lambda = \ell(\lambda)\, L(\lambda,\varepsilon,\sigma)d\xi \qquad (5.30)$$

$$d\lambda' = \ell'(\lambda')L(\lambda',\varepsilon,\sigma)d\xi \qquad (5.31)$$

The remaining functions not defined above are listed in Appendix A.

Hence Bazant et al. have modelled the essential features of concrete. This involved isolating and idealizing in a rational manner the many aspects of concrete behaviour at different levels of load and at different stress states. Then suitable functions were chosen to qualitatively represent each individual part of this behaviour.

The parameters included in these functions were then determined by suitable optimization procedures based on available experimental data.

However the theory as presented is difficult to modify because of the complexity of the form of the equations and the difficulty of knowing just how the constants were determined. There appears to be much interdependence between various parameters and the different effects they represent. This makes it difficult to clarify the relative significance of each parameter and would appear to lead to over-complex relations. For similar reasons it is also difficult to judge the relative significance of the high number of experimental constants in the endochronic equations.

Simplifications need to be introduced so that the theory becomes more accessible to, and can be more easily modified by, other researchers and engineers. However, despite these remarks the theory has proved both accurate and efficient, and can represent a wide range of different concrete behaviour.

Comparisons between experimental results and those using the endochronic theory are presented in the next section. This will include a new set of experimental data not investigated by Bazant.

5.2.6 Numerical procedure for applying the endochronic theory:

An iterative process is required to obtain a good approximation of the stresses for a calculated strain increment associated with a specific increment of load. This is because the different incremental state variables (i.e. $d\xi_n$, $d\xi'_n$, $d\eta_n$, $d\eta'_n$, dz_n, dz'_n, $d\lambda_n$, $d\lambda'_n$) are unknown for the current increment. Therefore the determination of the appropriate moduli (G and K) and the final states of stress cannot be reached directly.

The basic procedure is shown in Figure (5.3) for a uniaxial case. Starting from point A the incremental variables $d\xi_n$ and $d\xi'_n$ are initially evaluated using the current incremental strain. Stresses and strains are obtained at half the current increment $(n-\frac{1}{2})$ using the initial values of G and K. From these new values for the softening and hardening functions of the endochronic theory are obtained from which the incremental variables $d\eta_n$, $d\eta'_n$, and total values at half the current increment $\eta_{n-\frac{1}{2}}$, $\eta'_{n-\frac{1}{2}}$ are evaluated. These are used to evaluate the incremental values of dz_n and dz'_n. Finally $d\lambda_n$ and $d\lambda'_n$ are evaluated using the values obtained at $\lambda_{n-\frac{1}{2}}$ and $\lambda'_{n-\frac{1}{2}}$ which are initially assumed to be equal to λ_{n-1} and λ'_{n-1}. The values of $d\lambda_n$ and $d\lambda_n$ are used to evaluate a new set of $\lambda_{n-\frac{1}{2}}$ and $\lambda'_{n-\frac{1}{2}}$ which in turn are used to evaluate the new $G_{n-\frac{1}{2}}$ and $K_{n-\frac{1}{2}}$. The values of dz_n, dz'_n, $d\lambda_n$, $d\lambda'_n$, $G_{n-\frac{1}{2}}$, $K_{n-\frac{1}{2}}$ are then used to evaluate the incremental stresses at the end of the increment (i.e. point 1 in Figure (5.3)). This process is continued until the difference between the endochronic state variables and the total stresses at the beginning and the end of this cycle is as small as desired. The main steps are described in the following:

1. Set up the 42 material constants defined in Appendix A. These remain unchanged throughout the whole analysis.

2. For any particular load level $\{P\}_{n-1}$ there will exist total strains $\{\varepsilon\}_{n-1}$, total stresses $\{\sigma\}_{n-1}$, dilatation parameters λ_{n-1}, λ'_{n-1} and intrinsic time parameter η_{n-1}, η'_{n-1}, at each point in the material. These are zero before any application of load. Material constants G_{n-1}, K_{n-1} also exist from which the tangential matrix $[D]_{n-1}$ can be calculated. Initially these are the elastic constants G_o,K_o.

3. A load increment $\Delta\{P\}_n$ is applied from which the current incremental strains$\Delta\{\varepsilon\}_n$ and stresses $\Delta\{\sigma\}_n$ are calculated using the current tangential material matrix. i.e.

$$\Delta\{\sigma\}_n = [D]_{n-1}\,\Delta\{\varepsilon\}_n \qquad (5.32)$$

Then a first estimate of the total stress vector is calculated for the current increment i.e.

$$\{\sigma\}_n = \{\sigma\}_{n-1} + \Delta\{\sigma\}_n \qquad (5.33)$$

4. Calculate the total strains $\{\varepsilon\}_{n-\frac{1}{2}}$ and stresses $\{\sigma\}_{n-\frac{1}{2}}$ which exist at half the current strain increment i.e.

$$\{\varepsilon\}_{n-\frac{1}{2}} = \{\varepsilon\}_{n-1} + 0.5\,\Delta\{\varepsilon\}_n \qquad (5.34)$$

$$\{\sigma\}_{n-\frac{1}{2}} = \{\sigma\}_{n-1} + 0.5\,\Delta\{\sigma\}_n \qquad (5.35)$$

5. Calculate the incremental variables $\Delta\xi_n$,$\Delta\xi'_n$, $\Delta\eta_n$,$\Delta\eta'_n$, Δz_n, $\Delta z'_n$, $\Delta\lambda_n$,$\Delta\lambda'_n$ for the whole increment using equations (5.22 - 5.31). $\eta_{n-\frac{1}{2}}$, $\eta'_{n-\frac{1}{2}}$ are then used to evaluate Δz_n, $\Delta z'_n$ where $\eta_{n-\frac{1}{2}} = \eta_{n-1} + 0.5\Delta\eta_n$ and $\eta'_{n-\frac{1}{2}} = \eta'_{n-1} + 0.5\Delta\eta'_n$.

Using $\Delta\lambda_n$ calculate $\lambda_{n-\frac{1}{2}}$ from the equation $\lambda_{n-\frac{1}{2}} = \lambda_{n-1} + 0.5\,\Delta\lambda_n$ to evaluate the new shear modulus $G_{n-\frac{1}{2}}$ and Bulk modulus $K_{n-\frac{1}{2}}$ which exist at this point using equations (5.19 - 5.21).

6. Define the deviatoric and hydrostatic parts of some ficticious plastic stress increment by

$$\Delta S_{ij}^{P} = 2G\,\Delta e_{ij}^{P} \qquad (5.36)$$

$$\Delta \sigma_m^{P} = 3K\Delta\epsilon_m^{P} \qquad (5.37)$$

Then by substituting the expression for inelastic strains from equation (5.7) and (5.8) into equations (5.36) and (5.37) the following expression for inelastic stress increments are obtained:

$$\Delta S_{ij}^{P} = S_{ij}\,\Delta z \qquad (5.38)$$

$$\Delta \sigma_m^{P} = 3K(\Delta\lambda + \Delta\lambda') + \sigma_m\,\Delta z' \qquad (5.39)$$

Equations (5.7) and (5.8) can be written in terms of deviatoric and volumetric stresses as:

$$\Delta S_{ij} + \Delta S_{ij}^{P} = 2G\,\Delta e_{ij} \qquad (5.40)$$

$$\Delta \sigma_m + \Delta \sigma_m^{P} = 3K\,\Delta\epsilon_m \qquad (5.41)$$

and can then be rewritten as a relation between the total stresses and strains increments as:

$$\Delta\sigma_{ij} + \Delta\sigma_{ij}^{P} = D_{ijk\ell}\;\Delta\epsilon_{k\ell} \qquad (5.42)$$

in which

$$\Delta\sigma_{ij} = \Delta S_{ij} + \delta_{ij}\,\Delta\sigma_m \qquad (5.43)$$

$$\Delta\sigma_{ij}^{P} = \Delta S_{ij}^{P} + \delta_{ij}\;\Delta\sigma_m^{P} \qquad (5.44)$$

$$D_{ijk\ell} \quad \Delta\varepsilon_{k\ell} = 2G\Delta e_{ij} + 3K\delta_{ij} \quad \Delta\varepsilon_{m} \qquad (5.45)$$

Equation (5.42) can be written in matrix form as:

$$\Delta\{\bar{\sigma}\}_n + \Delta\{\sigma^P\}_n = [D]_{n-\frac{1}{2}} \Delta\{\varepsilon\}_n \qquad (5.46)$$

where $[D]$ is the elasticity matrix based on the current values of shear and bulk modulus which is, in this procedure, evaluated at the mid point of the current increment.

The sum $\Delta\{\bar{\sigma}\}_n + \Delta\{\sigma^P\}_n$ is initially the estimated linear stress increment which consists of a ficticious inelastic stress $\Delta\{\sigma^P\}_n$ and the current stress increment $\Delta\{\bar{\sigma}\}_n$ and is illustrated in Figure (5.3).

The values of $\{\Delta\sigma^P\}_n$ can be evaluated using equations (5.38) and (5.39), and an initial estimate will be calculated for $\Delta\{\bar{\sigma}\}_n$ from which the total stress $\{\bar{\sigma}\}_n$ is calculated.

7. A convergence criterion suggested by Bazant has been used. This is defined by:

$$|\bar{\sigma}_{xx} - \sigma_{xx}| < |C_F . \sigma_{xx}| \qquad (5.47)$$

where $C_F = 0.1\%$. σ_{xx} is the cartesian stress calculated from equation (5.33) and $\bar{\sigma}_{xx}$ is the cartesian stress calculated at the end of the iteration process defined in step (6).

If equation (5.47) has not converged then go to step (4) and set up $\Delta\{\sigma\}_n = \Delta\{\bar{\sigma}\}_n$ and repeat. Alternatively if a certain number of iterations were exceeded then go to step (8).

8. Update the endochronic variables (i.e. λ_n, λ'_n, η_n, η'_n from $\lambda_n = \lambda_{n-1} + \Delta\lambda$ ...etc.) to be used for the next increment. A flow chart is shown in Figure (5.4) to illustrate this numerical process.

5.2.7 Stress strain curves obtained using the endochronic model[10]

Experimental data obtained by Hognested et al. 1955[21], Kupfer et al. 1969[22], and Tasuji et al. 1978[23] are used in this section to examine the validity of the endochronic model for predicting the uniaxial and biaxial response of concrete. The first two references were part of the experimental data used by Bazant et al. in optimizing the endochronic equations, the last reference gives a new set of data for comparison.

Figure(5.5) compares Hognested et al's. experimental results for uniaxial compressive stress-strain data for different strengths (20.7, 32.1 and 42.7 N/mm^2) with the endochronic model and Popovics formulae (which will be discussed later in this chapter). As can be seen the endochronic model exhibits very close comparison with this data. Popovic's formulae also show a good fit with the experimental data. Figure (5.6) illustrates volumetric strain changes against the uniaxial stress/strength ratio obtained from tests by Kupfer et al.. The accuracy of the endochronic model is also demonstrated here.

The experimental biaxial volume change against stress/strength ratios presented by Kupfer et al. are shown in Figure (5.7). These are compared with the endochronic model for different values of Young's modulus and Poisson's ratio. Again fairly good fits are obtained but

it would appear that the endochronic equations for volume change are fairly sensitive to changes in Young's modulus and Poisson's ratio. The comparison with the experimental work of Tasuji et al. are shown in Figures (5.8 - 5.10) for the stress ratios of 0.2, 0.5 and 1.0 with f'_c equal to 33.3 N/mm^2. Again the endochronic model predicts this data fairly closely. The figures also show the endochronic prediction for f'_c equal to 20.2, and 42.7 N/mm^2 which are the same values used by Hognested et al. under uniaxial conditions. However,there are no experimental results to compare these with, and they serve only to illustrate the different curves that can be obtained. Finally Figure (5.11) shows the good agreement between the endochronic model and Tasuji et al's. experimental biaxial ultimate strength envelope.

To conclude, this short study demonstrates that the endochronic model can successfully predict various aspects of the uniaxial and biaxial behaviour of concrete under short term monotonic conditions.

5.3 The cracking model:

As mentioned previously the cracking model is based on the smeared crack approach. This implies that an infinite number of cracks occur at a specific point if a certain cracking criterion is satisfied. This approach is used because it is capable of predicting the load deflection behaviour, general stress-strain distribution, and general cracking behaviour for most categories of reinforced concrete structures (i.e. specific local behaviour in the vicinity of discrete cracks is not the subject of this work).

The basic assumptions for this model are as follows:

1. Concrete is assumed to be a homogeneous and isotropic material before a crack develops and follows the endochronic constitutive laws as previously described.
2. A crack is assumed to occur in a plane perpendicular to the direction of the principal stress or strain which caused this crack as shown in Figure (5.12).
3. Concrete will convert to orthotropic behaviour once a crack forms. This is represented mathematically by changing the tangential matrix to represent the new orthotropic state. Some shear stresses will be retained in the new orthotropic matrix due to the effect of aggregate interlocking between cracked concrete.
4. Two models have been used to represent the uniaxial tensile stress-strain behaviour of concrete in the direction perpendicular to the crack after a crack has occurred. The first model assumes that stresses will drop immediately to zero after a certain failure criterion is satisfied. This is shown in Figure (5.13).

   The second model assumes a gradual release of stresses will occur after a certain failure criterion is satisfied. This is the tension stiffening model and is shown in Figure (5.14). As explained previously the reason for assessing two different cracking models was to compare the effect of these models on the general behaviour of the structure when they acted in conjunction with varoius numerical procedures.
5. Two fracture criteria are used; "the maximum principal stress" criterion and "the maximum principal strain" criterion.

For the first model the maximum principal stress criterion is used exclusively.

For the second cracking model both the maximum principal stress and strain criterion are used. This is to prevent numerical problems in calculating the stress when the maximum stress criterion alone was used with tension stiffening. The problem was caused by the sudden change in stiffness from an isotropic state to an orthotropic state after crack formation which leads to the elimination of Poisson's ratio effects. Figure (5.15) illustrates this point. However, inclusion of the strain criterion removes this problem because the strain criterion will ensure that the strains also reach the peak point on the uniaxial stress-strain curve.

The main steps for each model are summarized in the next two sections:

5.3.1 Procedure for the first cracking model:

1. Enter with the values of strains $\{\varepsilon\}_{n-1}$, stresses $\{\sigma\}_{n-1}$, and initial crack conditions. At the beginning of the analysis $\{\varepsilon\}_{n-1}$ and $\{\sigma\}_{n-1}$ are zero and the material is uncracked.

2. Apply a load increment of $\Delta\{P\}_n$ from which the incremental strains $\Delta\{\varepsilon\}_n$ and stresses $\Delta\{\sigma\}_n$ are calculated.

3. Calculate the total strains and stresses from:

$$\{\varepsilon\}_n = \{\varepsilon\}_{n-1} + \Delta\{\varepsilon\}_n \qquad (5.48)$$

$$\{\sigma\}_n = \{\sigma\}_{n-1} + \Delta\{\sigma\}_n \qquad (5.49)$$

4. If the concrete is initially uncracked then:

(A) Calculate the principal angle α_c from the equation:

$$\alpha_c = \frac{1}{2} \tan^{-1} \left[\frac{2\tau_{xy}}{\sigma_{xx} - \sigma_{yy}} \right] \qquad (5.50)$$

This angle is shown in Figure (5.16), and lies between -45° and $+45^\circ$.

(B) Calculate the total principal stresses $\{\sigma_p\}_n$ using the following equation:

$$\{\sigma_p\}_n = [R^{-1}]^T \{\sigma\}_n \qquad (5.51)$$

where $[R]$ is a transformation matrix and is equal to:

$$[R] = \begin{bmatrix} c^2 & S^2 & Sc \\ S^2 & c^2 & -Sc \\ -2Sc & 2Sc & c^2-S^2 \end{bmatrix} \qquad (5.52)$$

and $c = \cos \alpha_c$, $S = \sin \alpha_c$.

The matrix $[R]$ is used to calculate the principal stresses because it allows the stresses to be orientated in the proper direction with respect to the angle α_c.

(C) If $\{\sigma_p\}_n \geq f'_t$ in any single direction then a crack occurs perpendicular to the direction of $\{\sigma_p\}_n$. The angle α_c is then fixed as the permanent crack direction and the tangential elasticity matrix $[D_c]$ is updated as follows:

$$[D_c] = \begin{bmatrix} 0 & 0 & 0 \\ 0 & E_2 & 0 \\ 0 & 0 & \alpha G \end{bmatrix} \qquad (5.53)$$

if a crack occurs perpendicular to axis (1) in Figure (5.16),

$$\text{and} \qquad [D_c] = \begin{bmatrix} E_1 & 0 & 0 \\ 0 & 0 & 0 \\ 0 & 0 & \alpha G \end{bmatrix} \qquad (5.54)$$

if a crack occurs perpendicular to axis (2) in Figure (5.16). E_1 and E_2 are the tangential moduli of concrete in the direction parallel to the single crack, and α is a shear factor defining the shear resistance parallel to the crack due to aggregate interlocking.

Its value is a predetermined constant which can be set between 0.0 and 1.0, usually 0.5.

(D) If $\{\sigma_p\}_n \geq f'_t$ in both directions then two cracks occur at the same time perpendicular to each other. The angle α_c is fixed as before and the new tangential matrix is updated to:

$$[D_c] = \begin{bmatrix} 0 & 0 & 0 \\ 0 & 0 & 0 \\ 0 & 0 & \alpha G \end{bmatrix} \qquad (5.55)$$

5. If cracks already exist then

(A) Use the fixed angle of crack α_c and transform the Cartesian stresses and strains into the crack direction by:

$$\{\sigma_c\}_n = [R^{-1}]^T \{\sigma\}_n \qquad (5.56)$$

$$\{\varepsilon_c\}_n = [R] \{\varepsilon\}_n \qquad (5.57)$$

(B) If one crack already exists then check whether it is open or closed (a crack is assumed to close if the normal strain across the crack is compressive). When the crack is closed then set up

$[D_c]$ to:

$$[D_c] = \begin{bmatrix} E_1 & 0 & 0 \\ 0 & E_2 & 0 \\ 0 & 0 & \alpha G \end{bmatrix} \qquad (5.58)$$

where E_1 and E_2 are the restored elasticity moduli before cracking.

(C) Check whether a second inplane crack already exists, if not, test whether it occurs using:

$$\{\sigma_c\}_n \geq f'_t$$

and update $[D_c]$ to:

$$[D_c] = \begin{bmatrix} 0 & 0 & 0 \\ 0 & 0 & 0 \\ 0 & 0 & \alpha G \end{bmatrix} \qquad (5.59)$$

If it already exists, examine whether both cracks are open or closed by checking whether $\{\varepsilon_c\}_n$ is compressive in both directions.

If the strain only on axis (1) in Figure (5.16) is compressive then set up $[D_c]$ to:

$$[D_c] = \begin{bmatrix} E_1 & 0 & 0 \\ 0 & 0 & 0 \\ 0 & 0 & \alpha G \end{bmatrix} \qquad (5.60)$$

If the strain only on axis (2) in Figure (5.16) is compressive then set up $[D_c]$ to:

$$[D_c] = \begin{bmatrix} 0 & 0 & 0 \\ 0 & E_2 & 0 \\ 0 & 0 & \alpha G \end{bmatrix} \qquad (5.61)$$

and if the strains on both axis (1) and (2) are compressive then set up $[D_c]$ to:

$$[D_c] = \begin{bmatrix} E_1 & 0 & 0 \\ 0 & E_2 & 0 \\ 0 & 0 & \alpha G \end{bmatrix} \qquad (5.62)$$

6. Update the new Cartesian stresses according to the new tangential matrix from:

$$\{\sigma\}_n = [R]^T [D_c][R]\{\varepsilon\}_n \qquad (5.63)$$

5.3.2 Procedure for the second cracking model:

1. Calculate $\{\varepsilon\}_n$, $\{\sigma\}_n$ using the same first three stages as in the previous model.

2. If the concrete is initially uncracked then:

(A) Calculate the principal angle α_c as in the first cracking model.

(B) Calculate the total principal strains and stresses using the following equations:

$$\{\varepsilon_p\}_n = [R]^T \{\varepsilon\}_n \qquad (5.64)$$

$$\{\sigma_p\}_n = [R^{-1}]^T \{\sigma\}_n \qquad (5.65)$$

(C) If $\{\sigma_p\}_n \geq f'_t$ and $\{\varepsilon_p\}_n \geq \varepsilon'_c$, then a crack occurs perpendicular to the direction of the maximum principal stress or strain. Fix angle α_c as the permanent angle of crack and calculate the new stresses in the direction perpendicular to the crack on the principal axis using the following equation:

$$\sigma_i = f'_t - f'_t \frac{(\varepsilon_i - \varepsilon'_c)}{(\varepsilon_A - \varepsilon'_c)} \quad \text{for} \quad \varepsilon_i \leq \varepsilon_A \tag{5.66}$$

$$\sigma_i = 0.0 \quad \text{for} \quad \varepsilon_i > \varepsilon_A \tag{5.67}$$

where ε_i and σ_i represents the strain and stress in the direction perpendicular to the crack. ε_A is shown in Figure (5.14) and represents the value of strain at which the stress finally becomes zero in the part-cracking range.

(D) Calculate the stress in the direction parallel to the crack σ_j and the assumed retained shear stress τ from:

$$\sigma_j = E_j \varepsilon_j \tag{5.68}$$

and

$$\tau = \alpha G \gamma \tag{5.69}$$

where j refers to the direction parallel to the crack and γ is the calculated shear strain value. The updated stresses can then be written as:

$$\{\sigma_c\}_n = \begin{Bmatrix} \sigma_i \\ \sigma_j \\ \tau \end{Bmatrix} \tag{5.70}$$

if the crack occurred perpendicular to axis (1) in Figure (5.16).

And

$$\{\sigma_c\}_n = \begin{Bmatrix} \sigma_j \\ \sigma_i \\ \tau \end{Bmatrix} \tag{5.71}$$

if the crack occurred perpendicular to axis (2) in Figure (5.16).

(E) The new Cartesian stresses can then be calculated from:

$$\{\sigma\}_n = [R]^T \{\sigma_c\}_n \tag{5.72}$$

(F) Steps C to E are also used to check whether two cracks have occurred at the same load level and if so stresses will be updated accordingly in both directions.

(G) For the stiffness calculation in subsequent iterations $[D_c]$ is set equal to:

$$[D_c] = \begin{bmatrix} 0 & 0 & 0 \\ 0 & E_2 & 0 \\ 0 & 0 & \alpha G \end{bmatrix} \qquad (5.73)$$

when a crack occurs perpendicular to axis (1) in Figure (5.16), or is set equal to:

$$[D_c] = \begin{bmatrix} E_1 & 0 & 0 \\ 0 & 0 & 0 \\ 0 & 0 & \alpha G \end{bmatrix} \qquad (5.74)$$

if a crack occurs perpendicular to axis (2) in Figure (5.16).

When cracks occur in two directions then:

$$[D_c] = \begin{bmatrix} 0 & 0 & 0 \\ 0 & 0 & 0 \\ 0 & 0 & \alpha G \end{bmatrix} \qquad (5.75)$$

3. If cracks already exist then:

(A) Use the fixed angle of crack α_c and transform the Cartesian strains and stresses into the crack direction:

$$\{\varepsilon_c\}_n = [R]^T \{\varepsilon\}_n \qquad (5.76)$$

$$\{\sigma_c\}_n = [R^{-1}] \{\sigma\}_n \qquad (5.77)$$

(B) If one crack exists then check whether the strain perpendicular to the crack is changed from the descending to the ascending part of the stress-strain curve, then update the stress on the principal angle from

$$\{\sigma_c\}_n = [D_c]\ \{\epsilon_c\}_n$$

where

$$[D_c] = \begin{bmatrix} E_1 & 0 & 0 \\ 0 & E_2 & 0 \\ 0 & 0 & \alpha G \end{bmatrix} \qquad (5.78)$$

and calculate the new cartesian stresses from:

$$\{\sigma\}_n = [R]^T \{\sigma_c\}_n \qquad (5.79)$$

For stiffness calculations in subsequent iterations $[D_c]$ is set equal to:

$$[D_c] = \begin{bmatrix} 0 & 0 & 0 \\ 0 & E_2 & 0 \\ 0 & 0 & \alpha G \end{bmatrix} \qquad (5.80)$$

when the change of strain occurs perpendicular to axis (1) in Figure (5.16), and

$$[D_c] = \begin{bmatrix} E_1 & 0 & 0 \\ 0 & 0 & 0 \\ 0 & 0 & \alpha G \end{bmatrix} \qquad (5.81)$$

when the change of strain occurs perpendicular to axis (2) in Figure (5.16).

This criterion is used instead of using a criterion for crack

closing, and when the strains become negative then the tangential modulus for the compression zone is used.

(C) To check whether a crack exists in a second direction the same procedure for checking a crack in the first direction is used except that $[D_c]$ for the stiffness calculation is set up so that:

$$[D_c] = \begin{bmatrix} 0 & 0 & 0 \\ 0 & 0 & 0 \\ 0 & 0 & \alpha G \end{bmatrix} \qquad (5.82)$$

If a second crack already exists, then check if the strain in any single direction or both directions changes from the descending to the ascending part of the curve. Then calculate the stresses using:

$$\{\sigma_c\}_n = [D_c]\ \{\varepsilon_c\}_n \qquad (5.83)$$

where

$$[D_c] = \begin{bmatrix} 0 & 0 & 0 \\ 0 & E_2 & 0 \\ 0 & 0 & \alpha G \end{bmatrix} \qquad (5.84)$$

if the strain changes on axis (1) in Figure (5.16), or

$$[D_c] = \begin{bmatrix} E_1 & 0 & 0 \\ 0 & 0 & 0 \\ 0 & 0 & \alpha G \end{bmatrix} \qquad (5.85)$$

if the strain changes on axis (2) in Figure (5.16).

If the strains in both directions change set up:

$$[D_c] = \begin{bmatrix} E_1 & 0 & 0 \\ 0 & E_2 & 0 \\ 0 & 0 & \alpha G \end{bmatrix} \qquad (5.86)$$

The new Cartesian stresses are then updated from equation (5.83) by using:

$$\{\sigma\}_n = [R]^T \{\sigma_c\}_n \qquad (5.87)$$

For stiffness calculation $[D_c]$ remains as in equation (5.82).

5.4 The uniaxial-compression model:

Once a crack has occurred and remains open a uniaxial state of stress will exist parallel to the crack. If this stress is compressive, the simple uniaxial-compressive model proposed by Popovics[20] is used. This model is a curve fitting method represented by the following equations:

$$\sigma = f'_c \frac{\varepsilon}{\varepsilon_o} \frac{n}{n-1+(\varepsilon/\varepsilon_o)^n} \quad \text{for } \varepsilon \leq \varepsilon_o \qquad (5.88)$$

$$\sigma = f'_c \quad \text{for } \varepsilon_o < \varepsilon < \varepsilon_{cu} \qquad (5.89)$$

$$\sigma = 0.0 \quad \text{for } \varepsilon \geq \varepsilon_{cu} \qquad (5.90)$$

where σ = is the compressive stress in psi at strain ε ,

ε_o = strain at maximum stress,

f'_c = uniaxial compressive cylindrical strength in psi

$n = 0.0004\, f'_c + 1.$

ε_{cu} = uniaxial crushing strain of concrete

For ε_o the following equation was suggested by Popovics:

$$\varepsilon_o = k.(f'_c)^{0.25} \times 10^{-4} \qquad (5.91)$$

where k is a function of the type of mineral aggregate and the applied test method. From experimental data Popovics suggests values in the range of 2.12 - 2.85 for concrete. In this thesis a value of 2.7 will be used which was obtained from analysis of data taken from the work of Hognested et al.[21].

The tangential modulus of elasticity for the uniaxial curve is given by:

$$E_T = 1 - \frac{(\varepsilon/\varepsilon_o)^n \, n(n-1)}{\left[(n-1+(\varepsilon/\varepsilon_o)^n\right]^2} \qquad \frac{f'_c}{\varepsilon_o} \qquad \text{for } \varepsilon \leq \varepsilon_o \qquad (5.92)$$

$$E_T \simeq 0.0 \qquad \text{for } \varepsilon > \varepsilon_o \qquad (5.93)$$

The model is compared with experimental values obtained by Hognested et al. in Figure (5.5). It is also compared with the endochronic model and good agreement is obtained in both cases.

5.5 The crushing model:

The crushing model can follow one of two paths depending on the state of cracking.

1. Where the point is cracked, crushing is assumed to occur if the compressive strains parallel to the crack exceeds the crushing strain of concrete in uniaxial compression. Once crushing has occurred the stiffness matrix of the concrete is assumed to be zero at that point.

2. Where the point is not cracked, one of two crushing criteria can be selected. The first assumes that if the compressive principal strains in any direction exceed the uniaxial compressive strain of concrete, then the material has crushed. This criterion is shown in Figure (5.17).

   Alternatively the second criterion assumes that crushing occurs if a surface representing the compressive strains exceeds the uniaxial compressive strain of concrete. This crushing surface is defined by:

$$c(\varepsilon) = \sqrt{\varepsilon_1^2 - \varepsilon_1\varepsilon_2 + \varepsilon_2^2} - \varepsilon_{cu} \qquad (5.94)$$

where ε_1 ε_2 are the principal strains and ε_{cu} is the uniaxial compressive crushing strain of concrete. The surface is shown in Figure (5.18).

When a tensile strain exists in one direction and compressive strain in the other direction, then crushing is assumed to occur when the compressive strain exceeds the uniaxial compressive crushing strain of concrete.

5.6 Theoretical Model for Steel:

Steel behaviour is modelled by a uniaxial bilinear stress-strain curve with the strain hardening effect as shown in Figure (5.19). When steel reaches the uniaxial yield stress f_y in tension or compression, yielding is assumed to occur. For the calculation of stresses the following equations are used:

$$f_s = E_s \varepsilon_s \qquad \text{when} \quad f_s \leq f_y \qquad (5.95)$$

$$f_s = \frac{E_w}{E_s}(f_s' - f_y) + f_y \qquad f_s > f_y \qquad (5.96)$$

f_s = uniaxial stress of steel at strain ϵ_s.

f_y = yield stress of steel.

E_s = Young modulus of steel.

E_w = Hardening modulus of steel.

f'_s = Stress value if no yielding is assumed after f_y.

No reloading criterion is assumed in this model and stresses are assumed only to follow the curve of Figure (5.19).

For stiffness calculation before yielding E_s is included, but once the steel is yielded this value is replaced by the hardening modulus of steel.

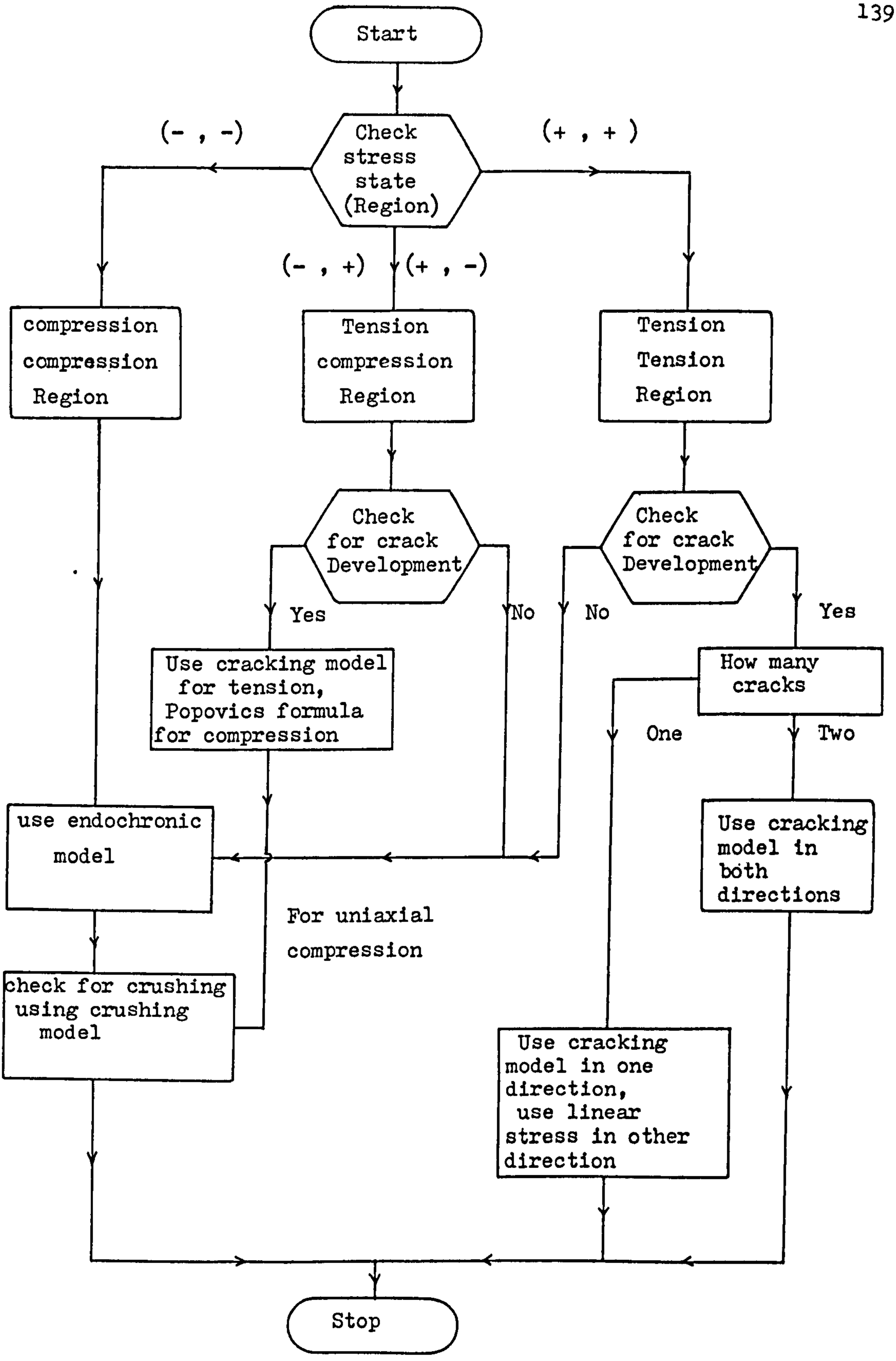

Figure 5.1 Flow chart of the concrete material model.

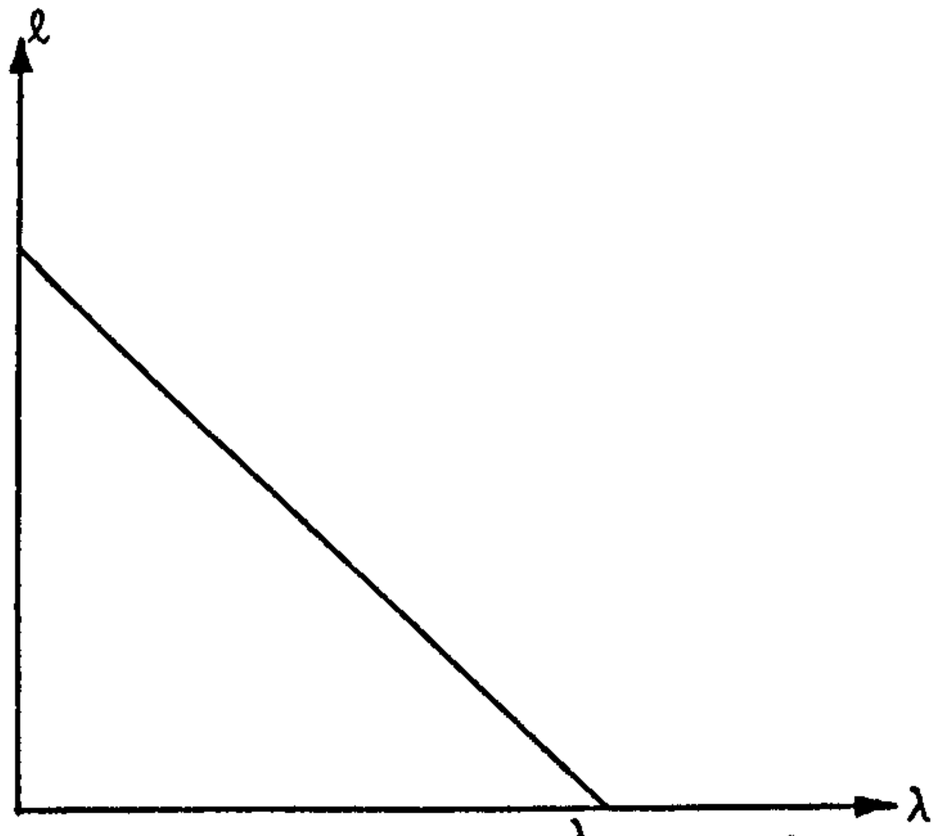

(a)

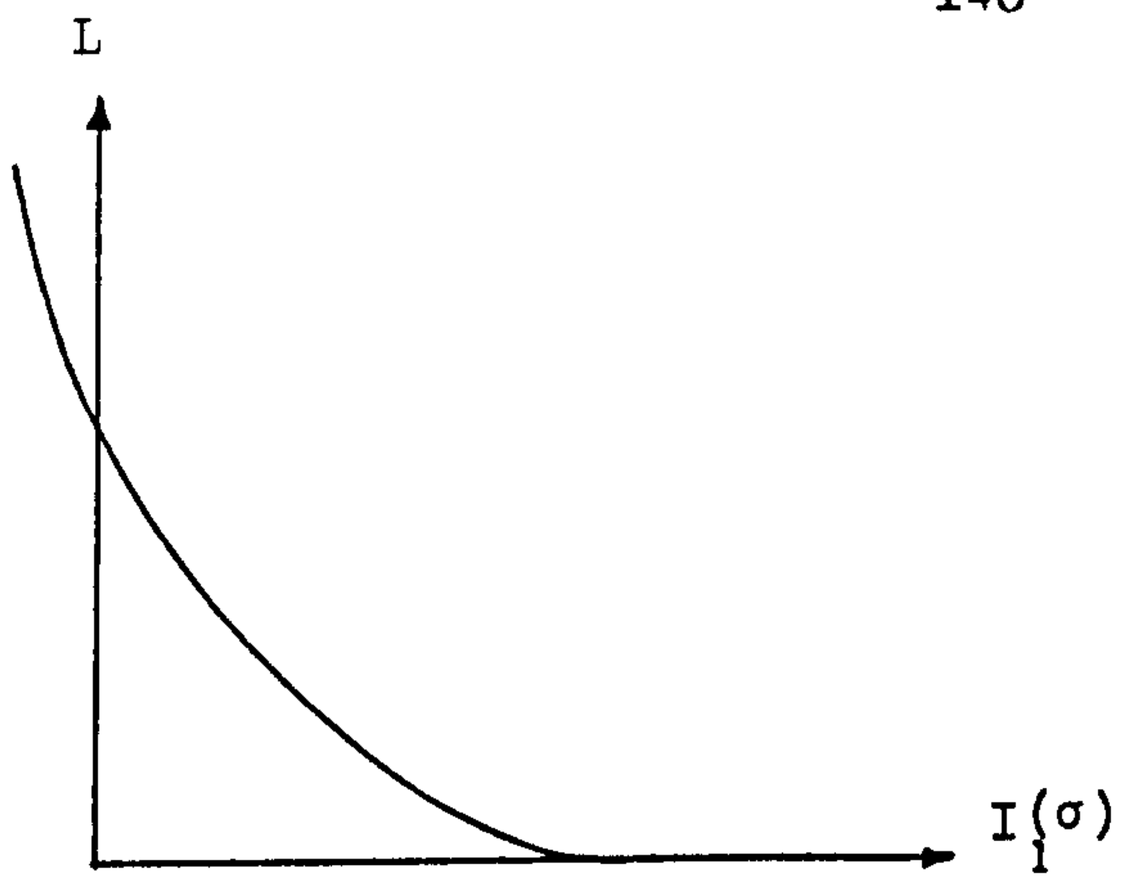

(b)

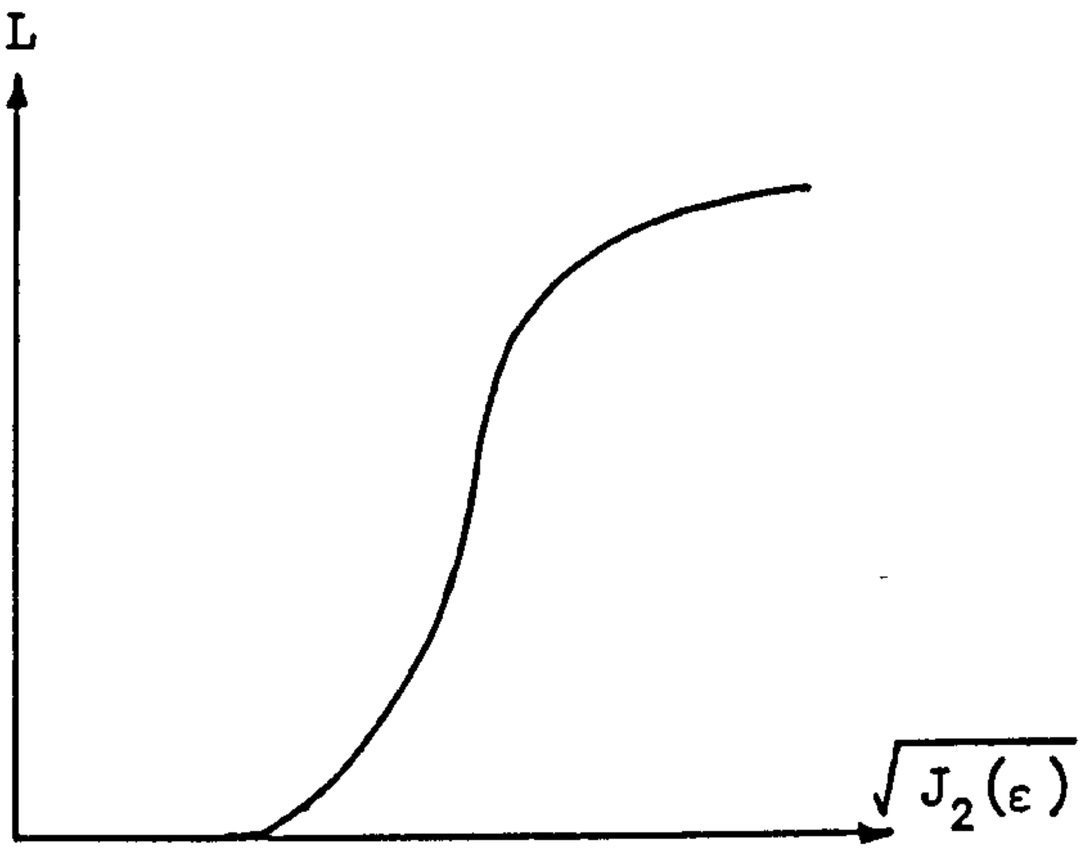

(c)

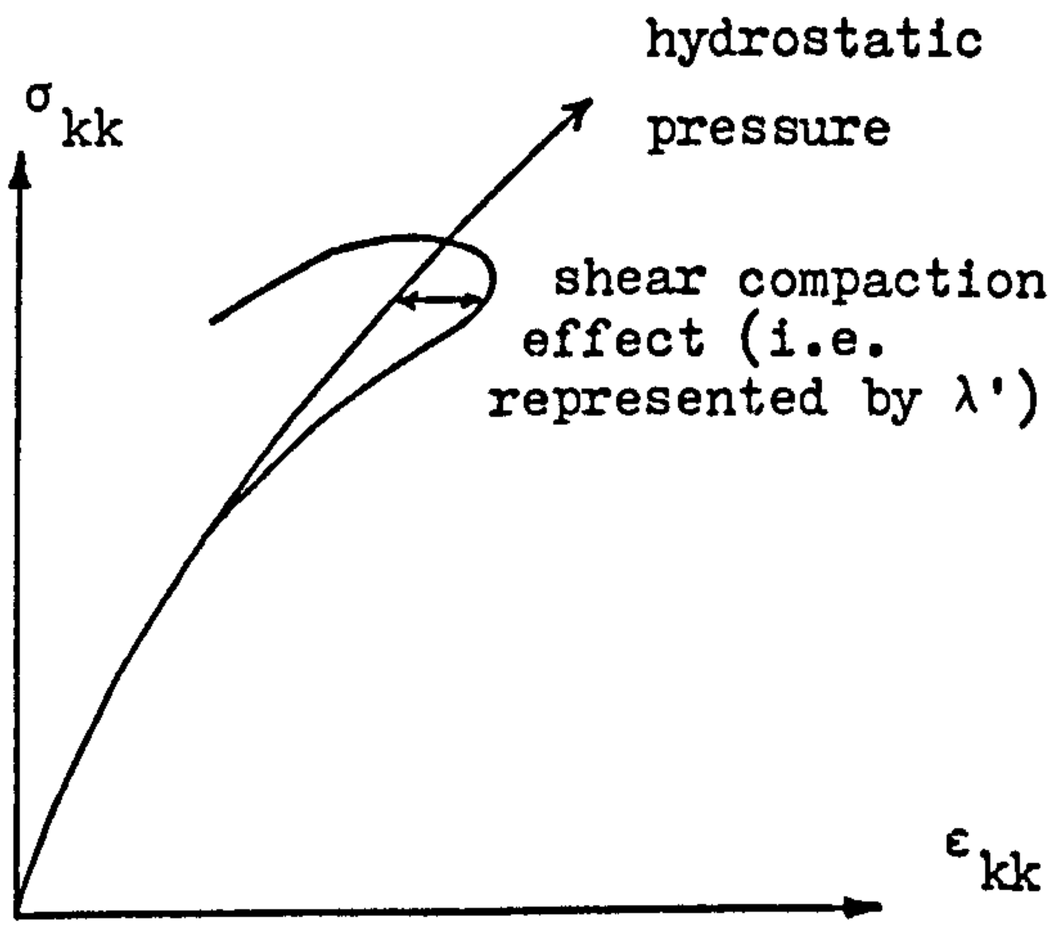

(d)

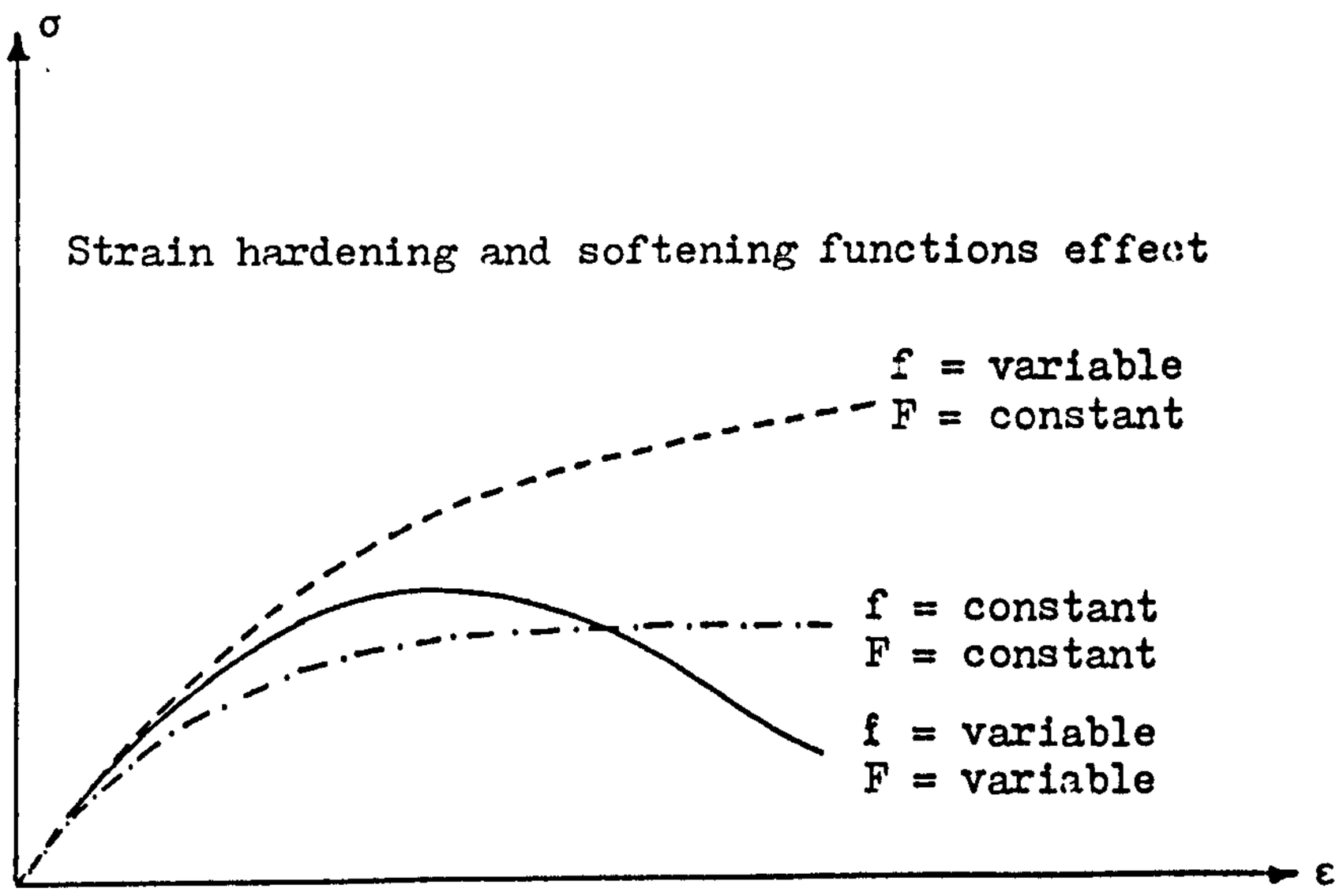

(e)

Figure 5.2 Diagram of some characteristic functions.

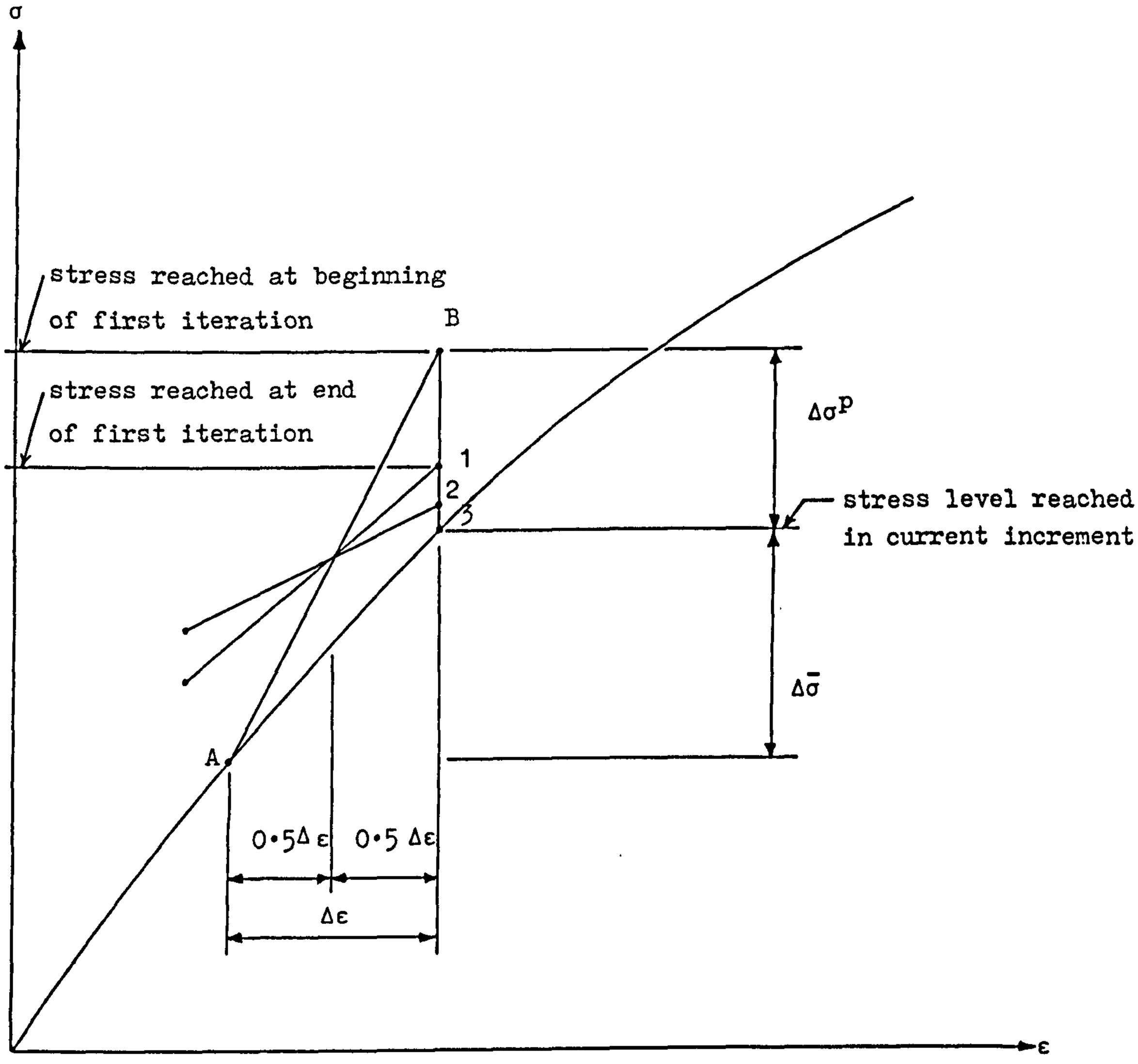

Figure 5.3 Procedure for updating the stresses for a uniaxial case using the endochronic model.

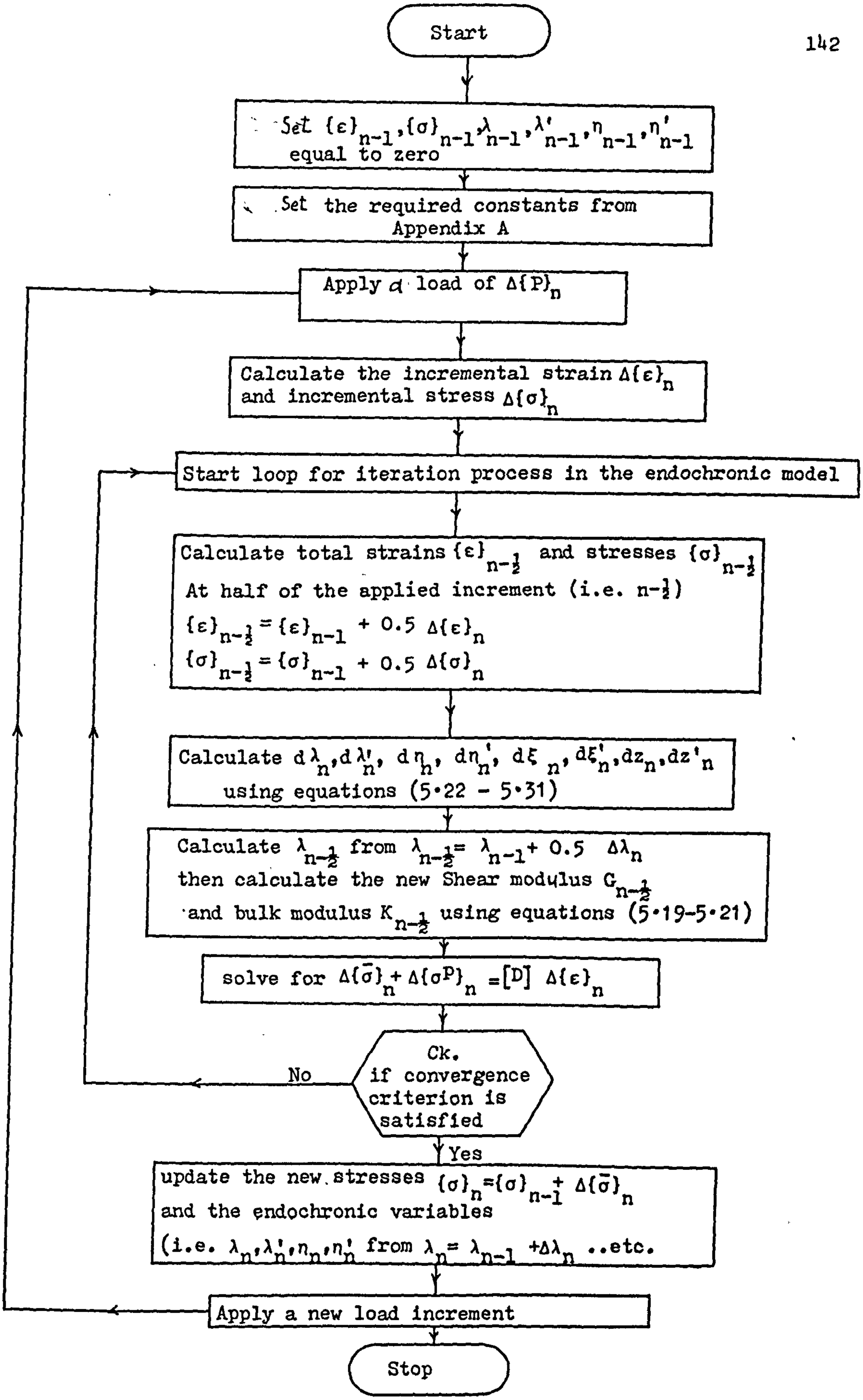

Figure 5.4 Flow chart of the endochronic numerical procedure.

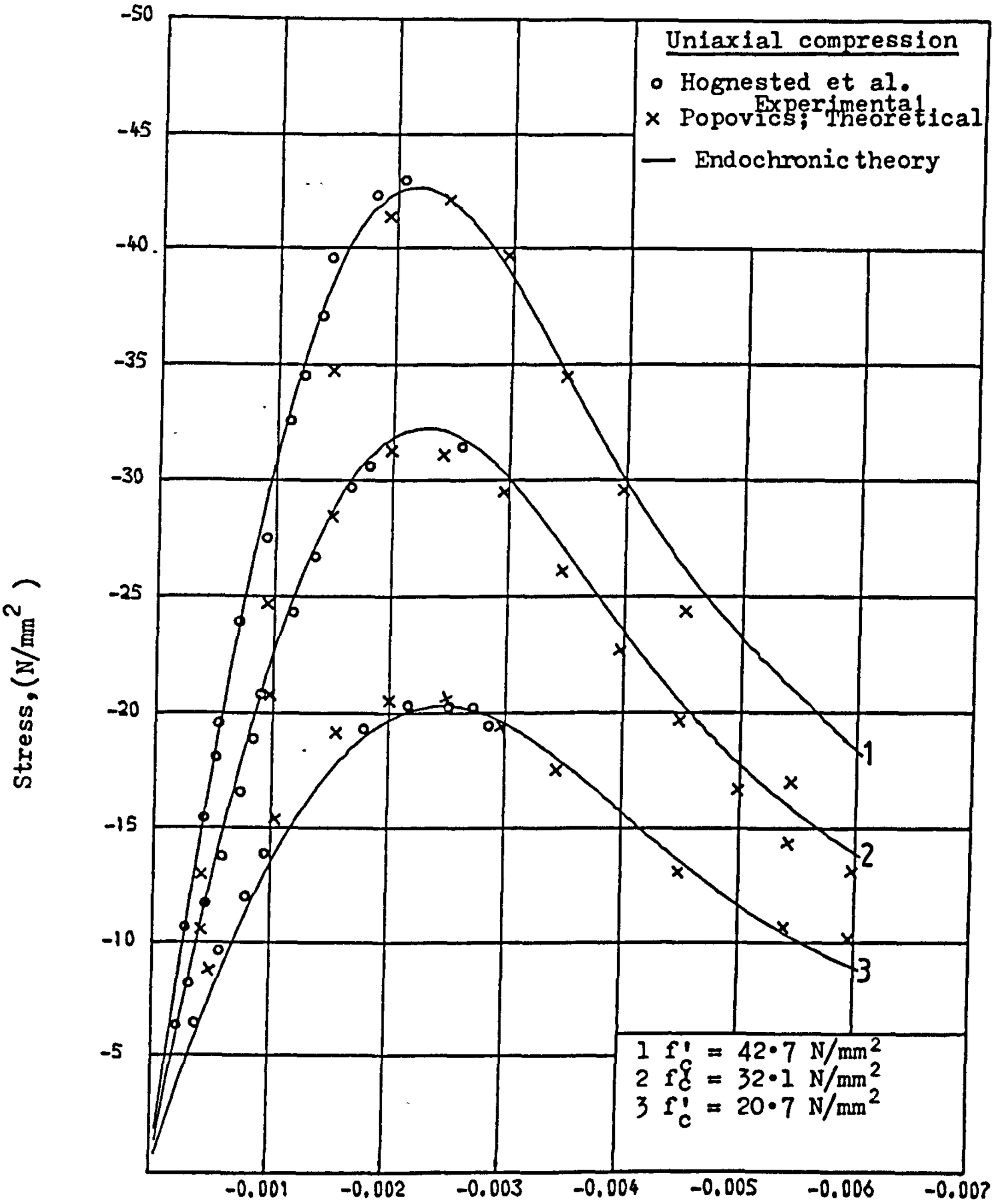

Figure (5•5) Fit of uniaxial test data of Hognested et al.

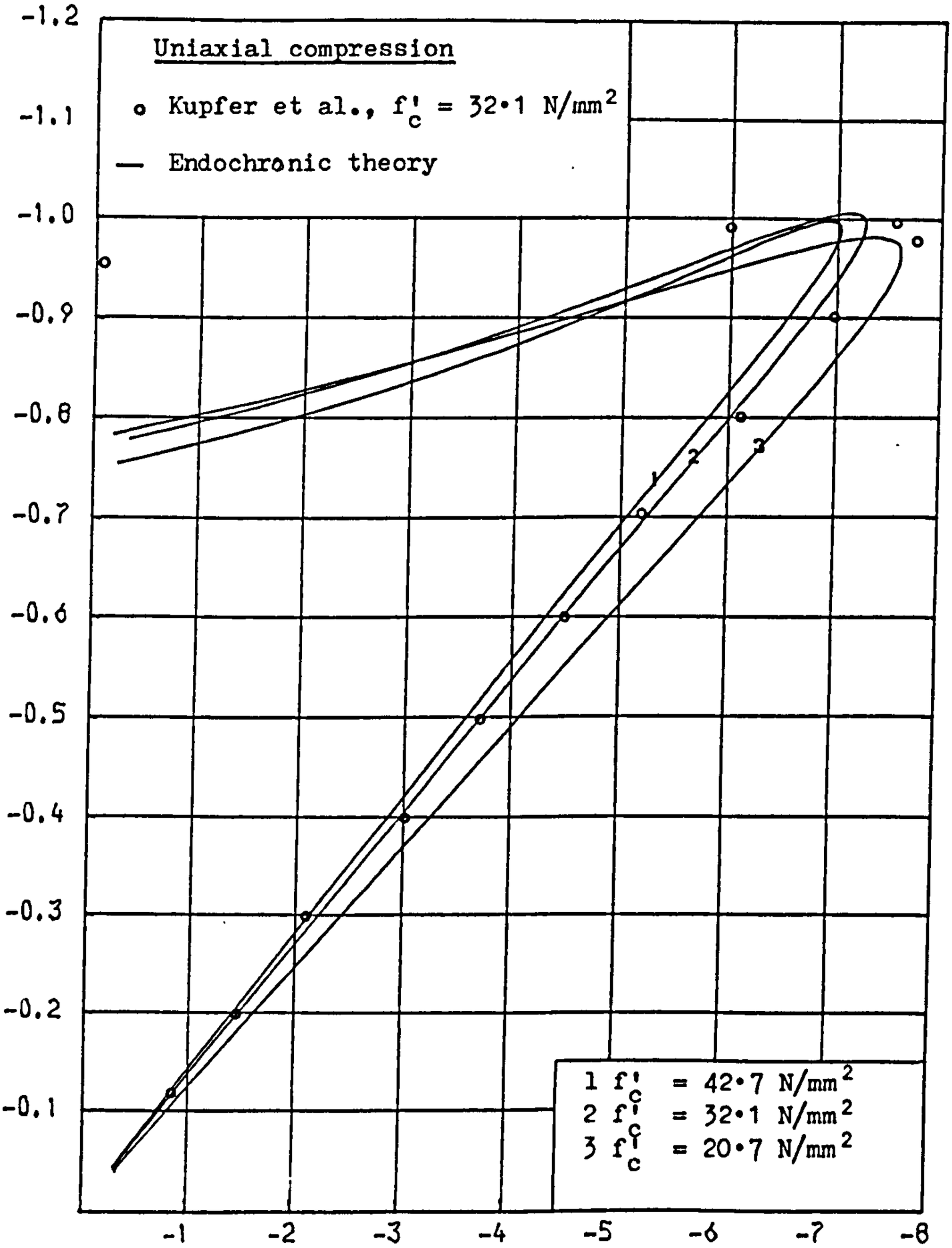

Figure (5•6) Volume change diagrams for uniaxial test.

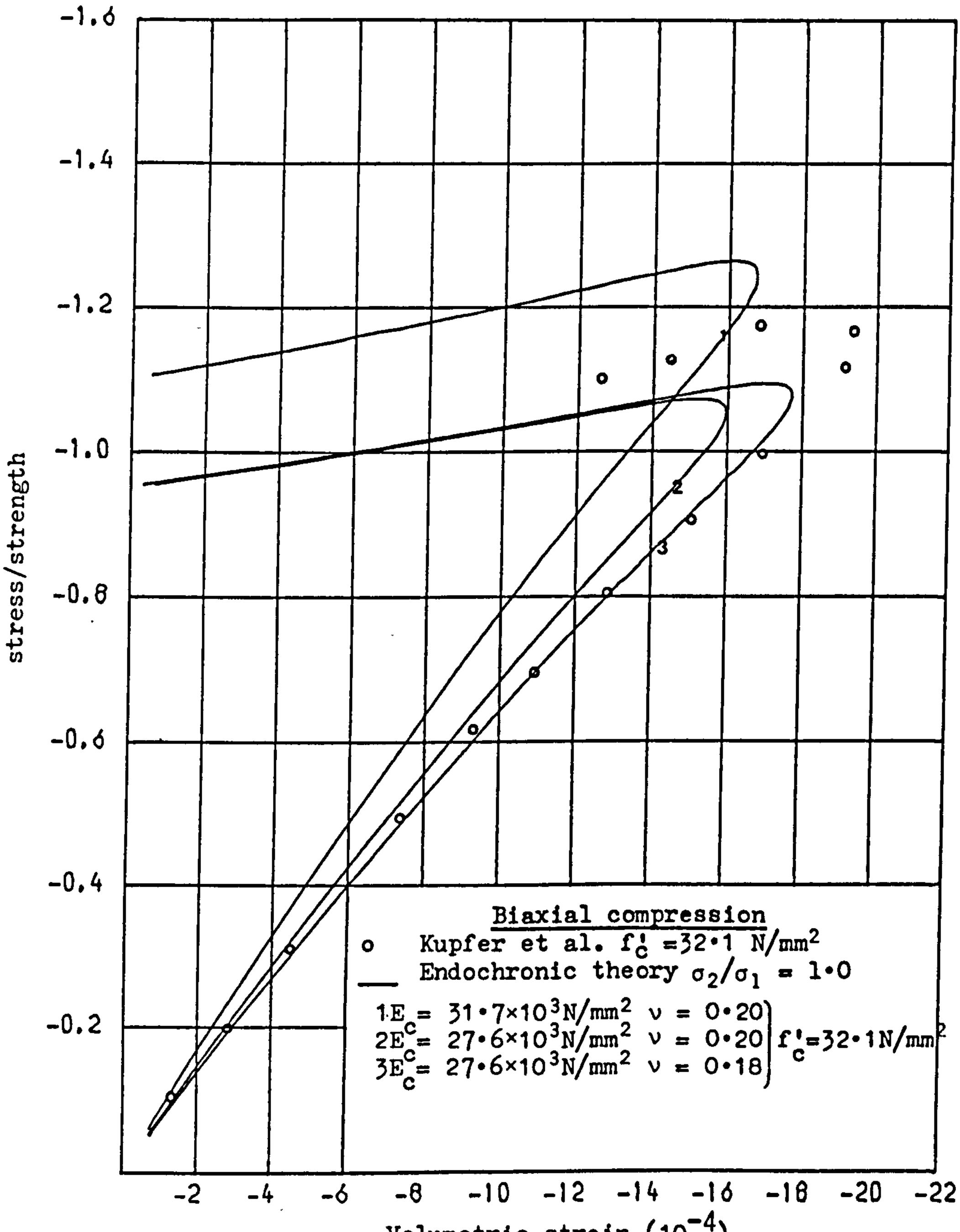

Figure (5·7) Volume change diagrams for biaxial test.

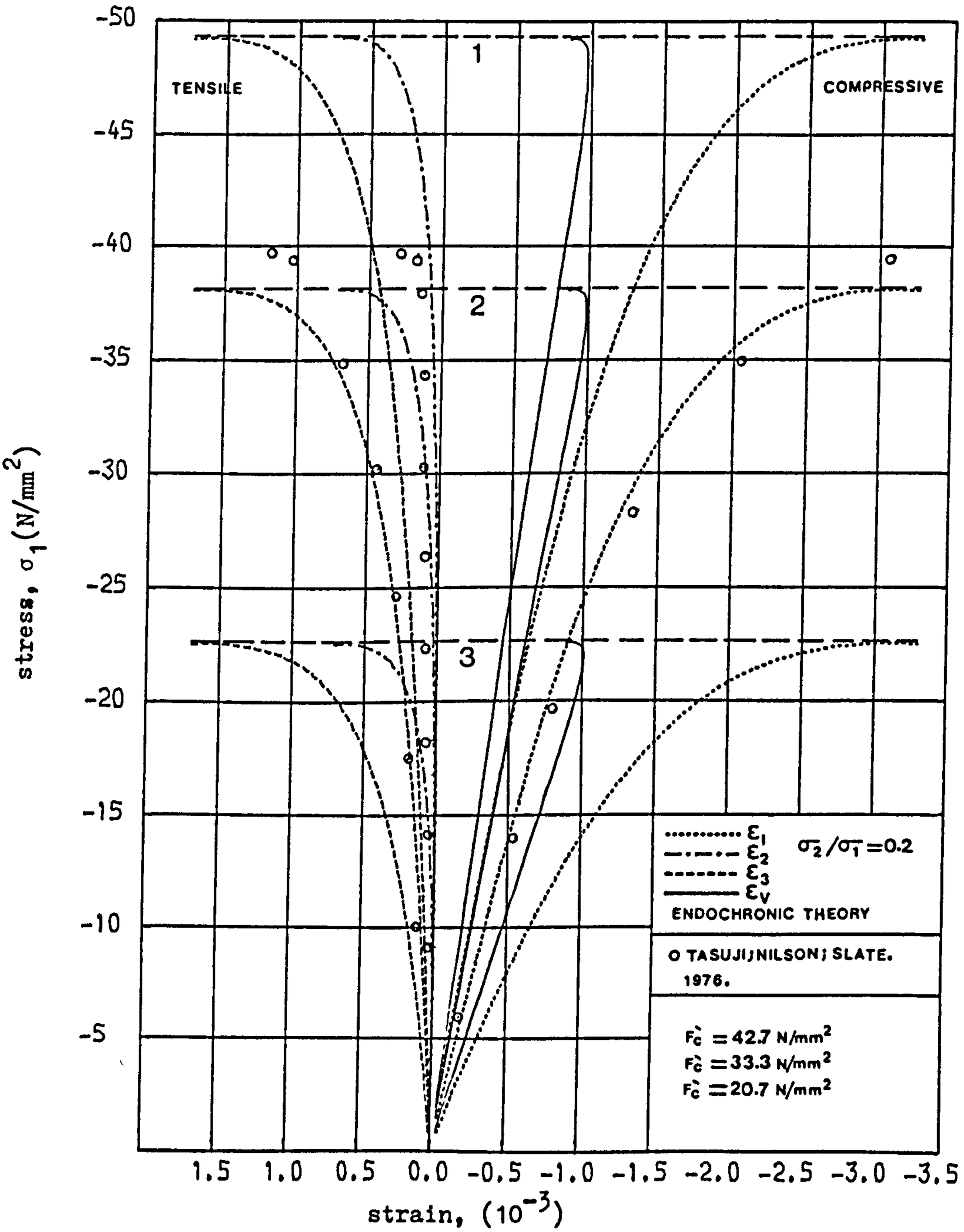

Figure (5·8) Stress-strain relationships for biaxial compression.

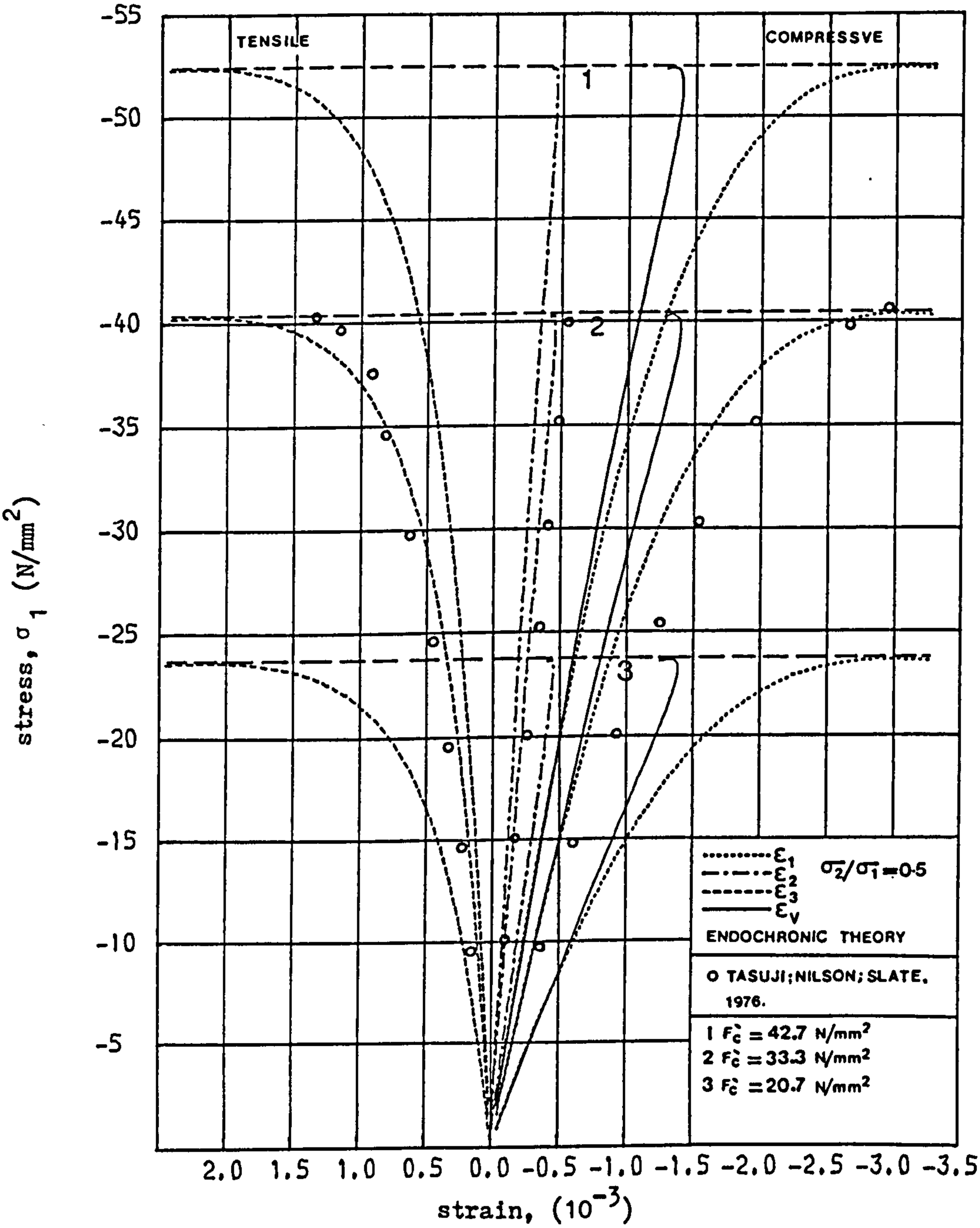

Figure (5·9) Stress-strain relationships for biaxial compression.

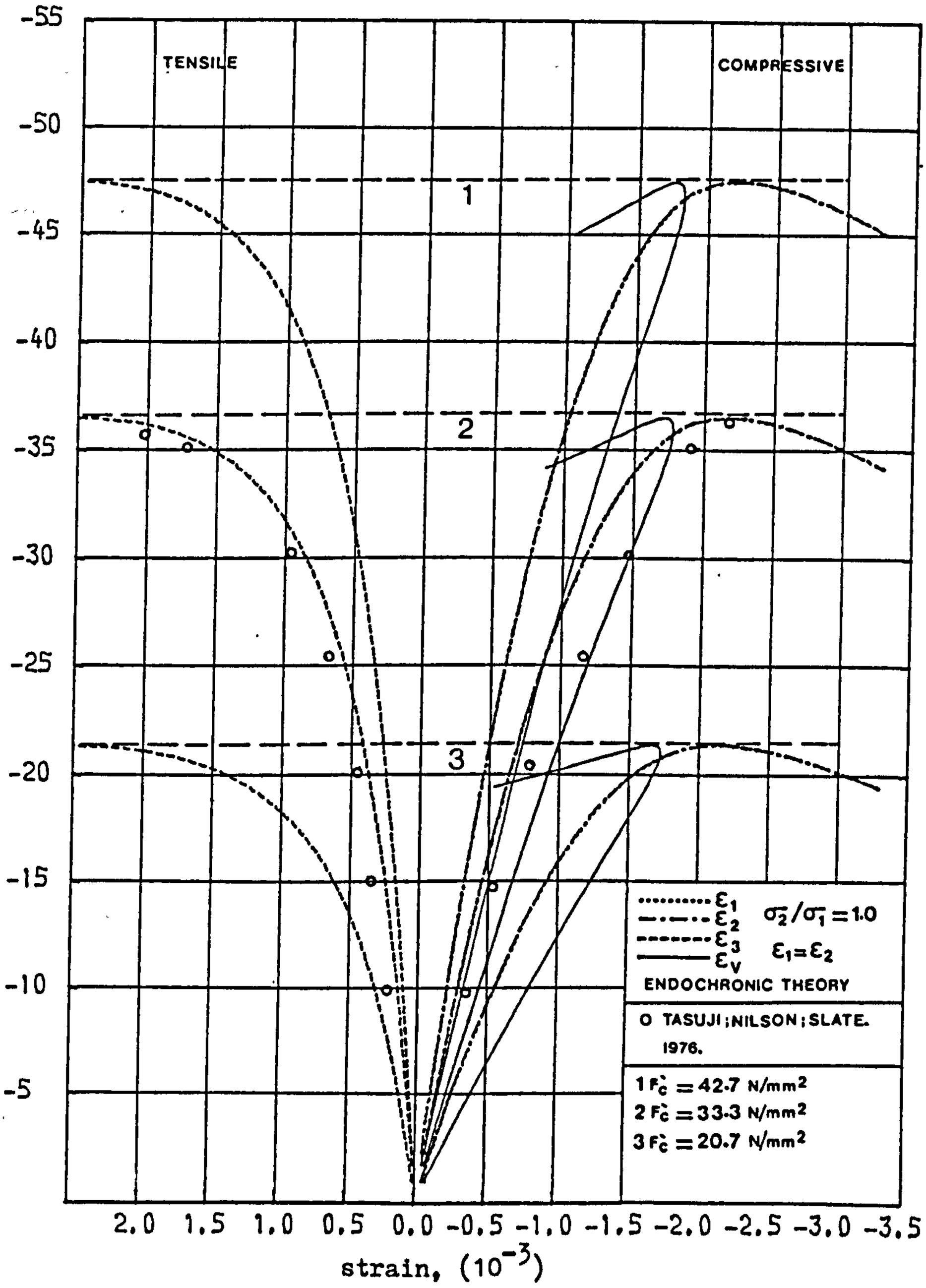

Figure (5·10) Stress-strain relationships for biaxial compression.

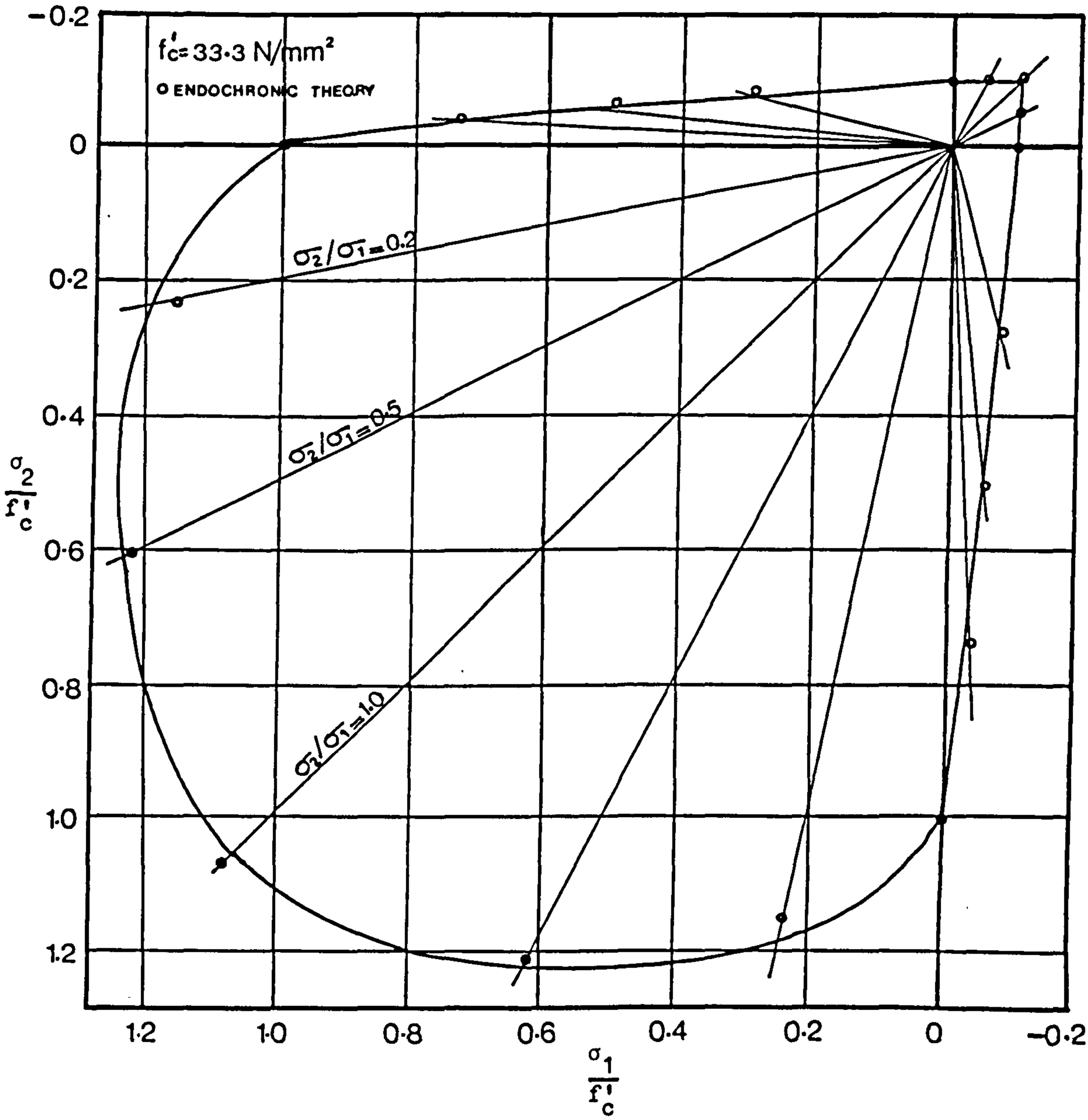

Figure (5·11) Biaxial ultimate strength envelope of concrete.

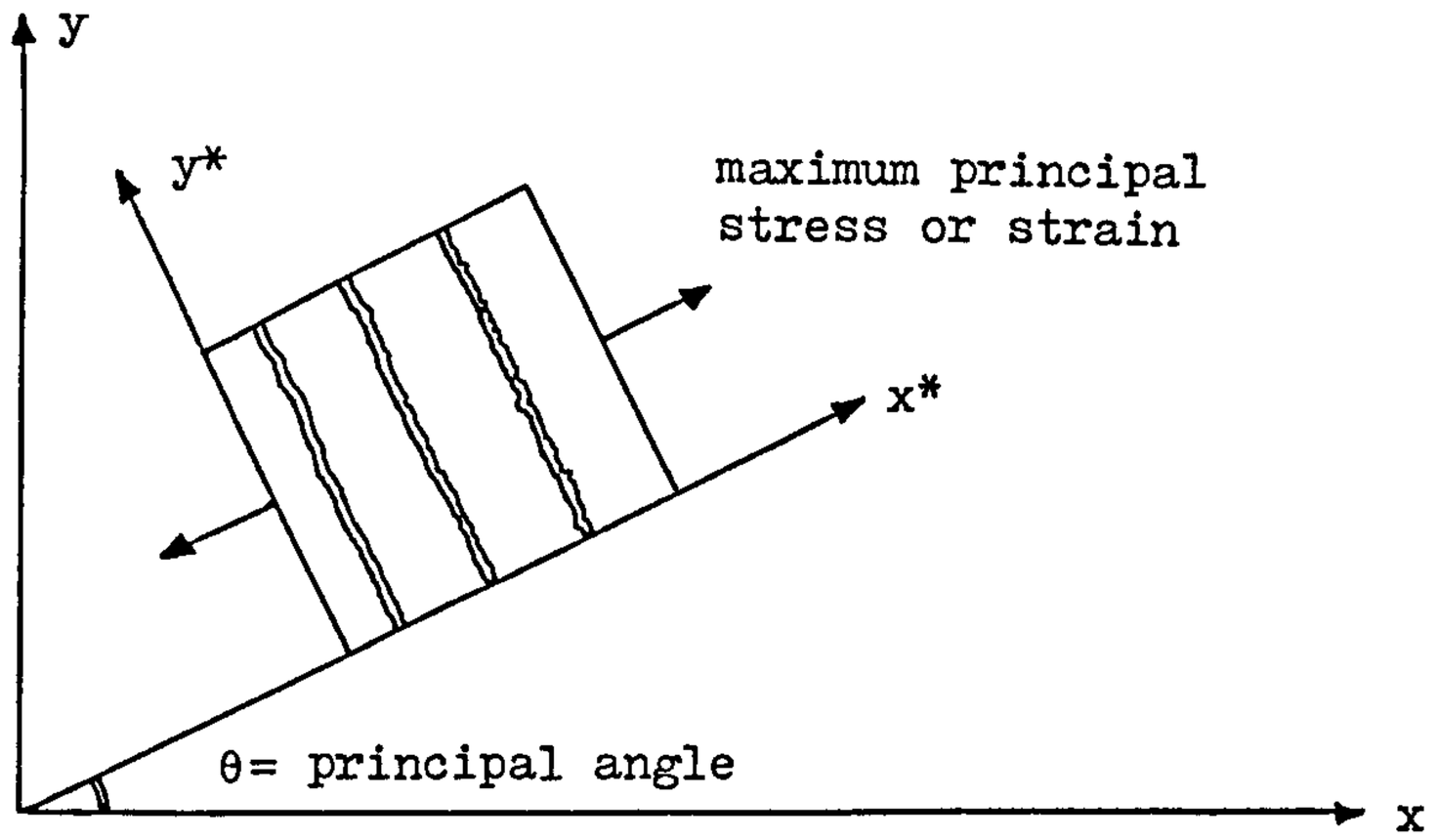

Figure 5·12 Idealization of smeared crack approach.

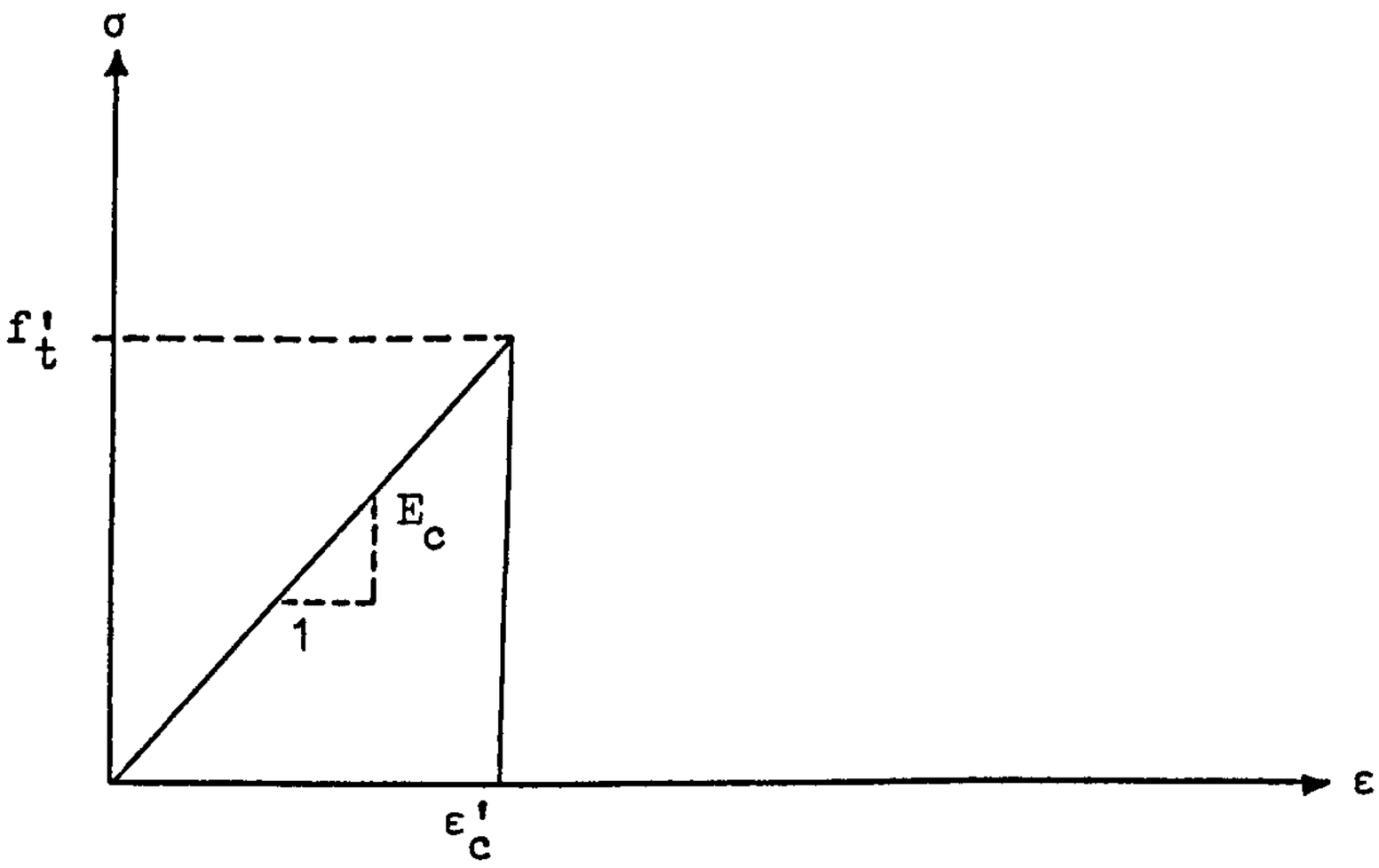

Figure 5·13 Stress-strain curve for first cracking model.

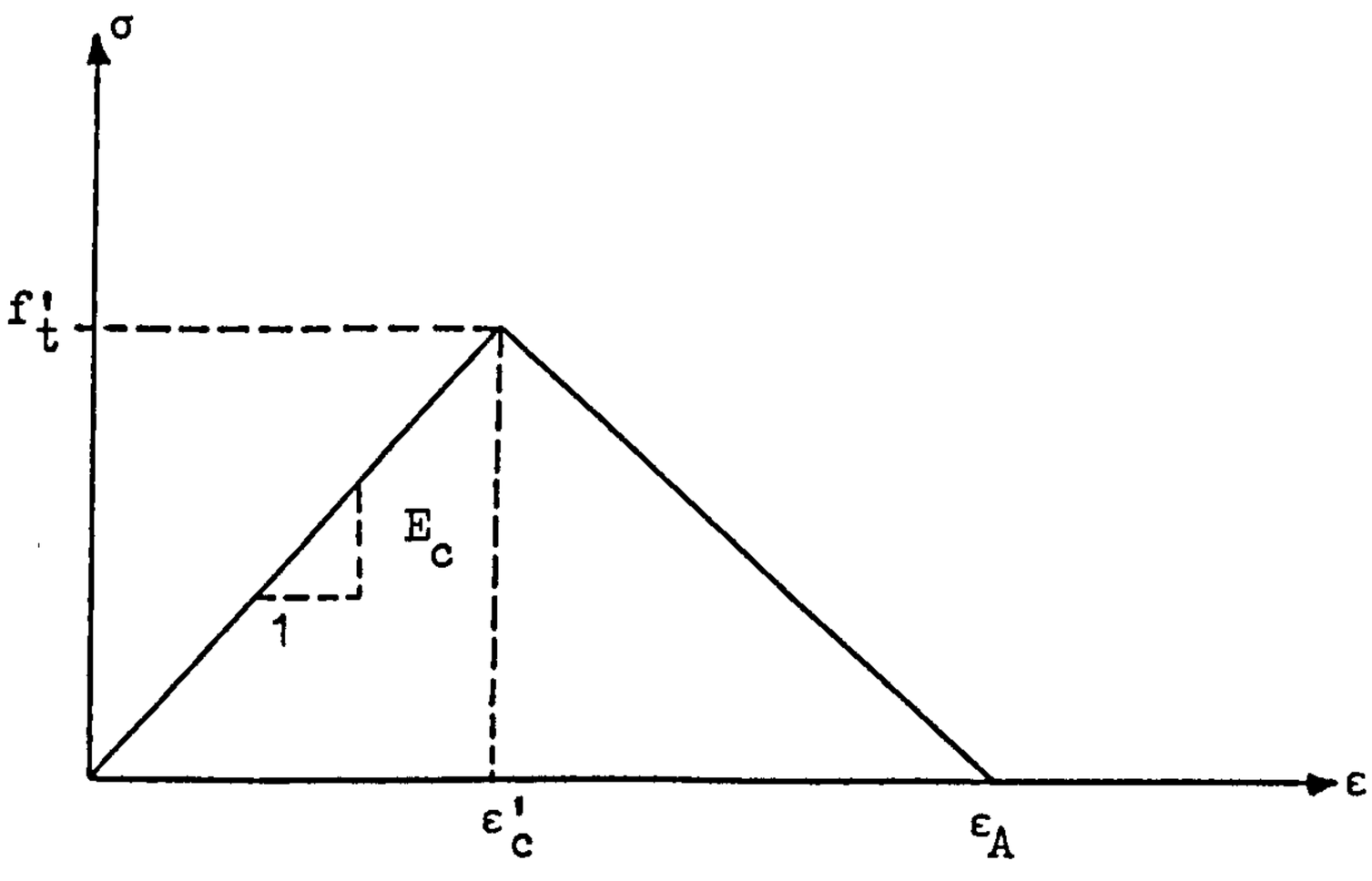

Figure 5·14 Stress-strain curve for second cracking model.

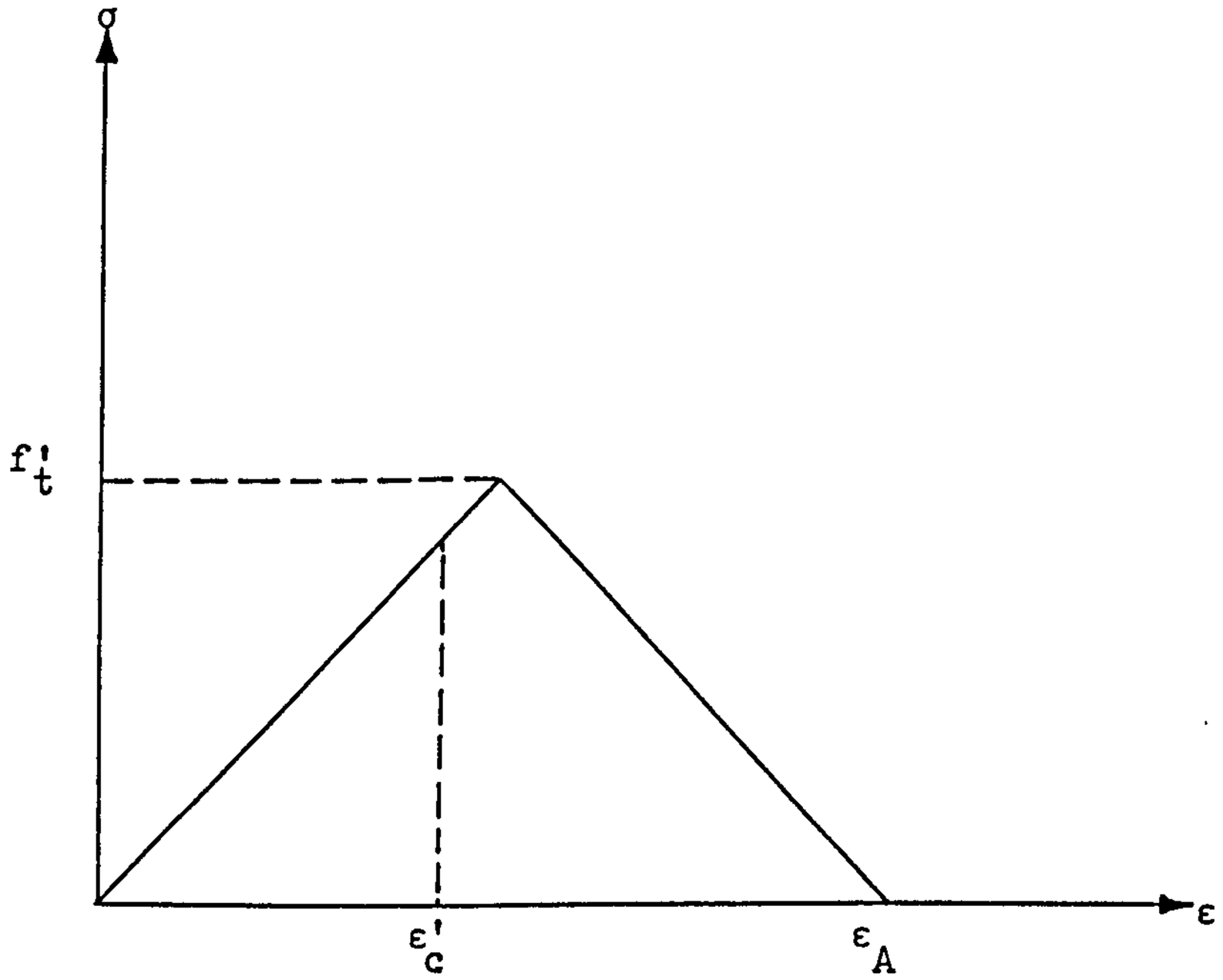

Figure 5·15 Cracking strain measured in the ascending uniaxial stress-strain curve corresponding to a cracking stress at the same load level.

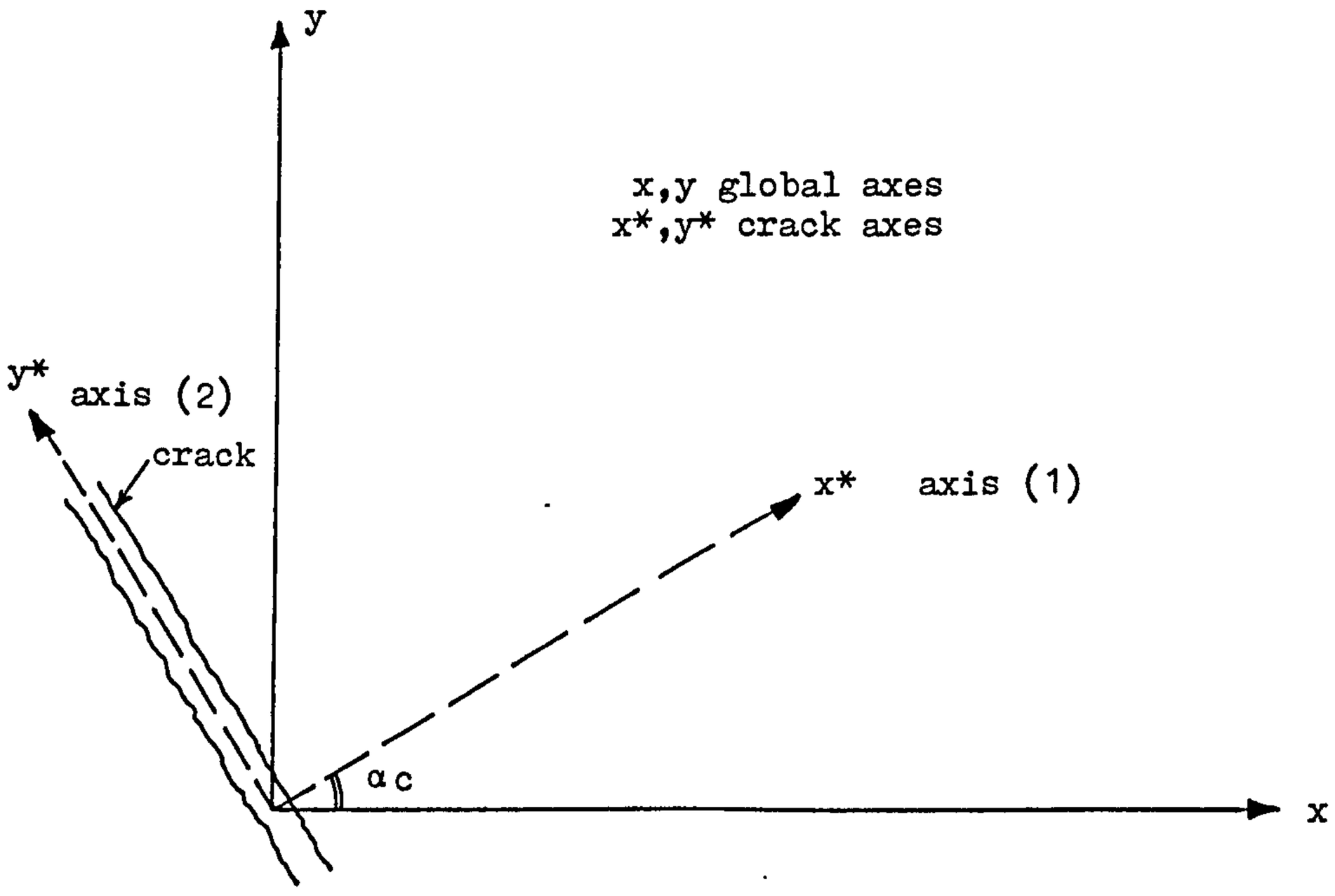

Figure 5·16 Rotation of axes.

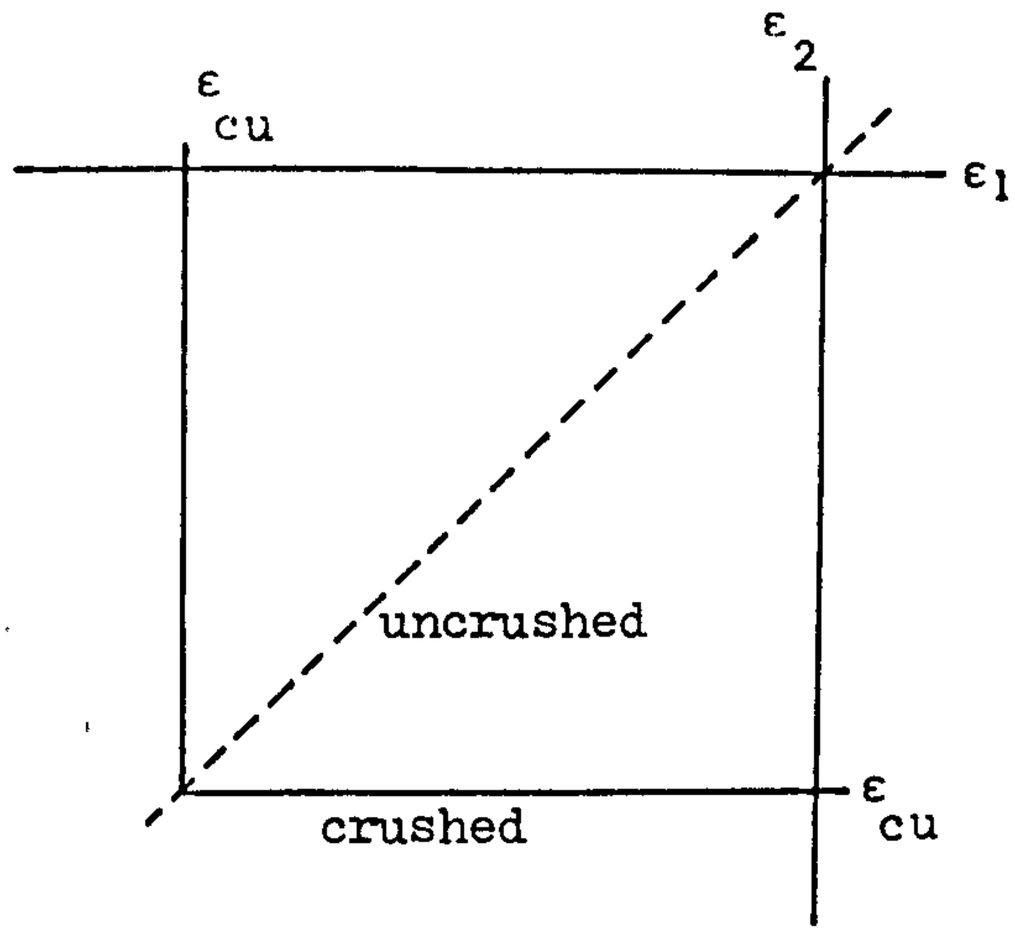

Figure 5·17 First criterion for crushing.

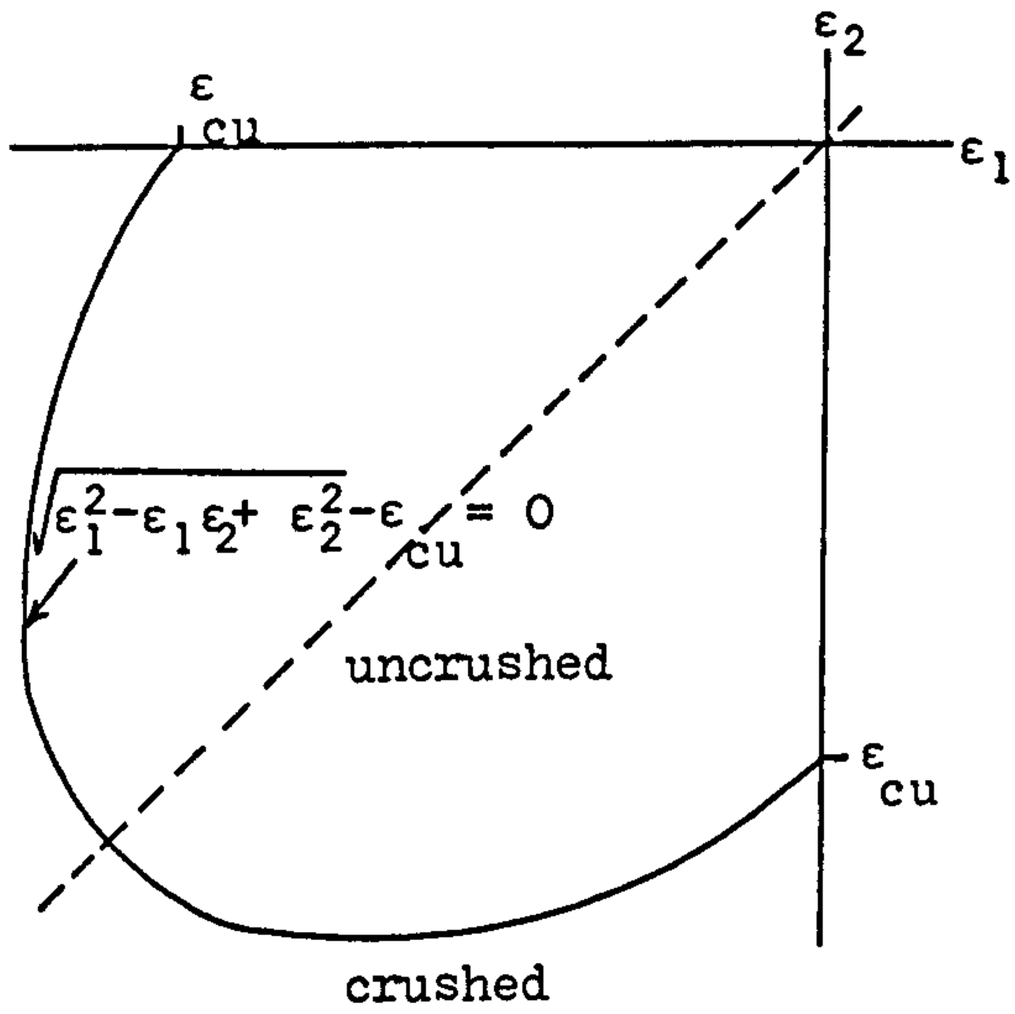

Figure 5·18 Second criterion for crushing.

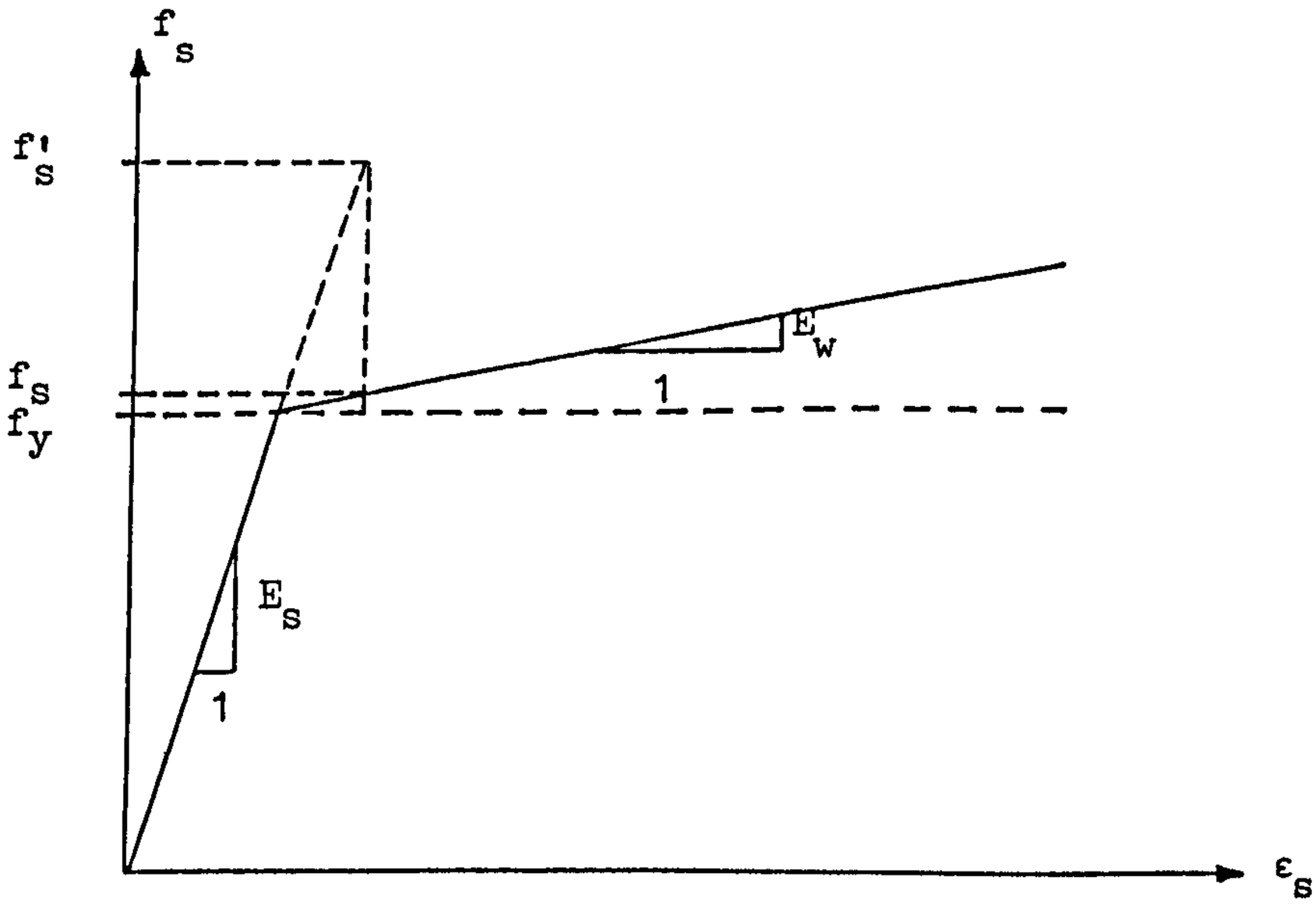

Figure 5·19 Mathematical uniaxial stress-strain curve for steel reinforcement.

REFERENCES

1. Bazant, Z.P., "A new approach to inelasticity and failure of concrete, sand, and rock: Endochronic theory". Proc. Soc. of Eng. Sci., 11th annual meeting, Duke University, Durham, 158-159, Nov., 1974.

2. Bazant, Z.P., "Some questions of material inelasticity and failure in the design of concrete structures for nuclear reactors". Trans. 3rd Int. Conf. on Struct. Mech. in Reactor Tech., London, Vol.3, Paper H1/1, Sep., 1975.

3. Bazant, Z.P.; Bhat, P.D., "Endochronic theory of inelasticity and failure of concrete". J. of Eng. Mech. Div., ASCE, Vol.102, 701-722, Aug., 1976.

4. Bazant, Z.P.; Krizerk, R.J., "Endochronic constitutive law for liquefaction of sand". J. of Eng. Mech. Div., ASCE, Vol.102, 225-238, April, 1976.

5. Bazant, Z.P.; Bhat, P.D.; Shieh, C., "Endochronic theory for inelasticity and failure analysis of concrete structures". Report No.1976-12/259, Northwestern University, Illinois, Dec., 1976.

6. Bazant, Z.P.; Bhat, P.D., "Prediction of hysteresis of reinforced concrete beams". J. of Struct. Div., ASCE, Vol.103, 153-167, Jan., 1977.

7. Bazant, Z.P., "Endochronic inelasticity and incremental plasticity". Int. J. Solids & Struct., Vol.14, 691-714, 1978.

8. Valanis, K.C., "A theory of viscoplasticity without a yield surface". Part I, General Theory, Archives of Mechanics, Vol.23, 517-551, 1971.

9. Valanis, K.C., "A theory of viscoplasticity without a yield surface". Part II, Application to mechanical behaviour of metals, Archives of Mechanics, Vol.23, 535-551, 1971.

10. Bazant, Z.P.; Shieh, C., "Endochronic model for nonlinear triaxial behaviour of concrete". Nucl. Eng. and Design, Vol.47, 305-315, 1978.

11. Arnesen, A.; Sorensen, S.I.; Bergan, P.G., "Nonlinear finite element analysis of reinforced concrete". Comp.& Struct., Vol.12, 571-579, 1980.

12. Devilliers, I., "Implementation of endochronic theory for analysis of concrete structures". Ph.D. Thesis, University of California, Berkeley, 1977.

13. Bazant, Z.P.; Shieh, C., "Hysteretic fracturing endochronic theory for concrete". J. of Eng. Mech. Div., ASCE, Vol.106, 929-950, Oct., 1980.

14. Bazant, Z.P., "Work inequalities for plastic fracturing materials". Int. J. Solids & Struct., Vol.16, 873-901, 1980.

15. Rivlin, R.S., "Some comments on the endochronic theory of plasticity". Int. J. Solids & Struct., Vol.17, 231-248, 1981.

16. Bazant, Z.P., "Advances in deformation and failure models for concrete". IABSE Colloquium in advanced mechanics in reinforced concrete, Introductory Report, Delft, 9-39, 1981.

17. Sandler, I.S., "On the uniqueness and stability of endochronic theories of material behaviour". J. of Applied Mech., Vol.45, 263-266, June, 1978.

18. Bazant, Z.P.; Kim, S., "Plastic-fracturing theory for concrete". J. of Eng. Mech. Div., ASCE, Vol.125, 407-428, June, 1979.

19. Sorensen, S.I., "Endochronic theory in nonlinear finite element analysis of reinforced concrete". Report No. 78-1, Trondheim University, March, 1978.

20. Popovics, S., "A numerical approach to the complete stress-strain curve of concrete". Cement & Con. Research, Vol.3, 583-599,1973.

21. Hognested, E.; Hanson, N.W.; McHenry, D., "Concrete stress distribution in ultimate strength design". J. ACI, Vol.27, 455-479, Dec., 1955.

22. Kupfer, H.; Hilsdorf, H.K.; Rusch, H., "Behaviour of concrete under biaxial stresses". J. ACI, Vol.66, 656-666, Aug., 1969.

23. Tasuji, M.E.; Slate, F.O.; Nilson, A.H., "Stress strain response and fracture of concrete in biaxial loading". J. ACI, Vol.75, 306-312, July, 1978.

24. Dungar, R.; Nuh, S. "Endochronic-critical state models for sand". J. of Eng. Mech. Div., ASCE, Vol.106, 951-968, Oct., 1980.

CHAPTER 6

NUMERICAL STUDY OF VARIOUS PARAMETERS AFFECTING NONLINEAR SOLUTIONS

CHAPTER 6
NUMERICAL STUDY OF VARIOUS PARAMETERS AFFECTING NONLINEAR SOLUTIONS

6.1 Introduction:

The usefulness of the finite element method for nonlinear analysis very much depends on the various numerical parameters which influence the solution. It is important to understand how these influence solutions and how they interact. Otherwise,numerical problems could arise which could cause divergence of a solution, or worse, give erroneous results even though convergence had been achieved.

Numerical parameters can be classified into three groups; solution parameters, quasi-material parameters, and actual material parameters. The quasi-material parameters are factors which are treated as if they were material properties but in fact are really numerical devices used to produce a required effect. Actual material parameters are measurable properties of a material such as the tensile strength of concrete. The most important of these parameters investigated in this work are:

(1) Solution parameters:

- (a) Convergence factors and criteria.
- (b) Number of iterations required to achieve an acceptable solution.
- (c) Method of updating the stiffness (constant or variable).
- (d) Order of Gauss rule.
- (e) Mesh size.

(2) Quasi-material parameters:

- (a) Aggregate interlocking effects.
- (b) Tension stiffening effects.

(3) Actual material parameters:

(a) Crushing criterion of concrete.

(b) Tensile strength of concrete.

(c) Young's modulus.

The object of this chapter is to establish guidelines for the nonlinear method presented here and to check the effects of the numerical parameters in the first two groups. Those in the third group will be discussed in later chapters as and when they arise.

Many of the above parameters are related to each other indirectly and in many circumstances it may be possible to obtain the same results by controlling different parameters. However, this is not a general rule. Also, one parameter could affect another parameter directly. For example, it is well known that reducing the increment size will give much faster convergence in that increment.

Information on numerical studies has only been presented by a few authors. Scordelis[1] made a comprehensive review of the available finite element methods of analysis for reinforced concrete structures. It involved information regarding such numerical parameters as tension stiffening, aggregate interlocking, dowel and shear effects. In his conclusions he stated that although much progress has been made in the modelling of concrete behaviour in recent years, many aspects still remain unsolved.

Gerstle[2] also overviewed the current state of knowledge. This included an assessment of the influence of both the elastic and inelastic material behaviour. He concluded that for the time being it is impossible to model reinforced concrete behaviour completely, because a lot of the parameters have still not been studied in sufficient detail.

He also concluded that systematic investigations of different influences, with the aim of establishing a list of priorities for specific cases, are still necessary to achieve the required compromise between reality and simplicity.

Other authors including Phillips[3], Nilson et al.[4], Duncan et al.[5] Cope et al.[6,7,8,9], and Crisfield[10] have also studied the effects of different numerical parameters. These will be discussed in later sections.

The numerical study in this chapter will be based mainly on a single span deep beam tested by Ramakrishnam[11]. This beam was chosen because a reasonable computer time was required for a full nonlinear analysis. Although this beam exhibited a flexural failure, the conclusions obtained were used in the next chapter as a guideline for the analysis of beams failing in shear. Further numerical studies are also reported there and these confirm the findings of this chapter.

At the end of this chapter, a study of a simple beam tested experimentally by Burns and Siess[12] will also be reported. This beam has often been used by various authors as a standard case and therefore it affords a useful test for the methods proposed in this thesis.

6.2 Description of the deep Beam used in the numerical study:

Figure (6.1) illustrates the single span reinforced deep beam A-1 which was one of several tested experimentally by Ramakrishnam et al[11]. The beam has a length of 686.0mm (27.0 in.) an overall depth of 381.0mm (15 in.) and was tested under two concentrated point loads. Only main tensile steel was used and this was kept as low as possible. To avoid

local failure at the load and support points special reinforcement cages were provided. A summary of the given and assumed properties of the beam are shown in Table (6.1).

The behaviour of the beam is affected by the yielding of the low percentage reinforcement. The experimental failure mode is effectively flexural, and failure occurred at a load of 107.6 kN. The experimental crack pattern is also shown in Figure (6.1).

In the finite element analysis only one half of the beam was analysed because of its symmetry. In the study 16 parabolic elements were used, as shown in Figure (6.1). A mesh convergence study showed that this relatively coarse mesh was adequate under elastic conditions, and it was assumed that it would be sufficient for the nonlinear analysis. The reinforcement was approximated by bar elements lying between the internal sides of the parabolic element.

A standard pattern of 16 load increments was specified for the total analysis; coarse increments of 9.9 kN (1 ton) for the first 10 increments, and 5 finer ones of 1.9 kN(0.2 ton) closer to failure conditions. The finer increments were used to ensure that the ultimate load could be predicted within 2% since failure was expected within that range. However a final coarse increment of 9.9 kN (1 ton) was also available just in case failure did not occur within the fine increment range, ensuring that a total load of 119.5 kN was available, if necessary. The analysis was stopped if failure had not occurred by this load value.

6.3 Parameters affecting the number of iterations and the convergence rate:

The number of iterations, convergence criteria and tolerances may

greatly affect the numerical solution path. Various authors have reported on these effects. Phillips[3] found that using the constant stiffness method produced slow convergence, especially after crack development. For the variable stiffness method he found that it was not necessary to ensure exact convergence within an increment. This was justified on the grounds that about 7-8 iterations were necessary to allow the major changes in conditions to be taken into account (i.e. stiffness changes and redistribution of stress due to cracking), that errors did not accumulate but were automatically carried forward by the concept of calculating residual forces from total stresses, and that the largest proportion of residuals (50-75%) were redistributed in the first two or three iterations.

Nilson et al.[4] carried out a numerical study on convergence for a simply supported beam. These authors stated that the important contribution to behaviour was also obtained mainly from the first one or two cycles. However, it was found that it was important to have a larger number of cycles (the authors specified 10) to provide realiable information on local stress conditions in the vicinity of the cracks, and on the extent of cracking. A guideline was given for the iterations and increments required, but no generality was claimed because the study was limited to one simple beam.

Duncan et al.[5] used the constant stiffness method and found that using small load steps rather than exactly satisfying static equilibrium at each load level a fast convergence form can be obtained. Also he found that when load increment sizes were too small and static equilibrium was satisfied, then the accuracy of the model deteriorated. He attributed this to the inexactness of the boundary conditions.

However Duncan was criticized by Cope et al.[13] for neglecting static equilibrium because it could produce a range of solutions from which there was no criterion for distinguishing the correct one.

Cope et al.[7] carried out a study of reinforced concrete slab behaviour. In this study iterations were performed at each increment until specified equilibrium and displacement norms were satisfied. Results showed that predictions of behaviour under serviceability loading, and to at least 50% overload, could be obtained with reasonable values for the norms. But for a reasonable prediction of behaviour as collapse approached, it was judged that a limit of 300 iterations was necessary.

Cope et al.[9] carried out a further study of bridge slab design which included an investigation of various numerical parameters. It was found that nonlinear numerical techniques applied to concrete structures is complicated by the lack of uniformity in stiffness degradation and by the different load - unload paths. These features make it particularly difficult to specify norms to automatically control the number of iterations to be performed.

It is clear that the convergence and iteration processes have a significant effect on an analysis, and these need to be studied in more detail. Generally the problem can be classified into three main groups:

(A) Effect of using different convergence criteria. In this work the load and displacement criterion explained in Chapter 3 will be compared.

(B) Effect of using different convergence tolerances or convergence operators (here termedCOOP for simplicity). Values varying from 1% to 20% are studied.

(C) Effect of limiting the number of iterations for specific convergence tolerances. This will be discussed only for the load criterion because the displacement criteria used in this work were found to be unreliable indicators of the decay of residuals.

In this section the following conditions were kept constant throughout the analysis:

(1) The first cracking model was used (i.e. there is no tension stiffening). Tension stiffening will be discussed in a later section.

(2) The method V.S.M.1 was used. This assumes stiffnesses are updated at the beginning of the first and second iteration in each increment. Other methods are discussed later.

(3) The three point Gauss rule was used. The effect of varying this parameter will be discussed later.

(4) The shear retention factor was kept constant and equal to 0.5. The effect of different values of this parameter are discussed in a separate section.

6.3.1 Load criterion:

Different load deflection curves using the load criterion LC (as described in section 3.5.1) are compared for convergence tolerances of 20%, 15%, 10% and 5% in Figure (6.2). Predicted failure loads are compared in Table (6.2). Iterations were continued until convergence to the specified tolerance was obtained. It can be observed that COOP = 20% gave the best fit to the experimental load deflection curve and also gave the closest ultimate load.

The actual convergence value obtained and the maximum number of iterations required for each increment are also shown in Table (6.2). For COOP = 5%, the first cracking load occurred one increment earlier, at 49.8 kN compared to COOP equal to 20%, 15%, and 10%. This was because an extra iteration was required to redistribute the inelastic stresses of the endochronic law for the more severe convergence factor, causing a slightly different load path to be followed.

Comparison of the crack pattern plotted for different load levels are shown in Figures (6.3-6.6). These load levels represent the most important stages of the behaviour. Yielding of steel and crushing of concrete are also indicated.

It can be observed that different convergence rates can cause different crack patterns for the same load level. However these patterns become more similar at the final load stages. It was also observed that in most cases the finer the convergence tolerance, the more cracks developed at earlier stages. But there are exceptions to this; an example of this is shown in Figure (6.5) and (6.6) for values of COOP = 10% and 15%, where more cracks have developed in the case of 15%. The main numerical reason for this is due to the delay of the load increment in which most of the cracks appeared and to the variation of the total number of iterations required to achieve convergence as illustrated in Table (6.2). However this type of problem may not be observed clearly for very fine tolerances because most of the cracks will be developed at an early stage, unless restrained by some other numerical device.

To study the effect of the number of iterations, analyses were carried out where the maximum number of iterations was limited to 10

and 30. Different load deflection curves using the load criterion are compared for convergence tolerances of 20%, 15%, 10% and 5% in Figures (6.7) and (6.8). Predicted failure loads are compared in Table (6.3) and (6.4). It can be observed that the load deflection curve was not affected when COOP = 20% because the maximum number of iterations required was 9. It appears that limiting the number of iterations to 30 improved the load deflection curve and predicted failure load. This improvement was even better when a limitation of 10 iterations was specified. However when a maximum number of 30 iterations was specified convergence rates were not affected up to the yielding stage except for COOP = 5% as shown in Table (6.3). But when a maximum of 10 iterations was specified, the limit was applied after the development of the first cracks, as shown in Table (6.4).

Figures (6.9), (6.10) and (6.11), (6.12) show the decay of residuals obtained throughout the iterations at load increment of 79.6 kN and 89.6 kN. It appears that the convergence rate was generally in the range of 10 - 30% for all the cases and that decay of these forces was slow.

Different load deflection curves are compared for convergence tolerances of 20% and 5% in Figure (6.13), when I.N.L. denotes "iterations not Limited" and "I" "maximum number of iteration limited" in the analysis. It can be observed that COOP = 20% gave the best fit to the experimental load deflection curve and also gave the closest ultimate load.

Further comparison was carried out for the horizontal stresses at the midspan section of the beam described in Figure (6.13), as shown in Figures (6.14) and (6.15). It was observed that the variation in the stress distribution at lower loads is higher than at the higher load levels. This is because the effect of crack development is more

significant at the lower load levels.

The following points arise from this study of the load criterion:

(1) For a high convergence of 20%, even at the 10 iterations limit, the observed load deflection, ultimate load, and crack pattern are not affected because the number of iterations never exceed 9. For a lower convergence of 15% or less these were better for 10 than 30 iterations or for no limits on the number of iterations.

(2) The ultimate loads were not significantly changed when the maximum number of iterations was limited to 30 and 10, for values of COOP = 15%, 10%, and 5%. For an unlimited number of iterations the ultimate load was considerably less.

(3) It appears that a more accurate analysis is obtained if a certain proportion of residual forces are retained within the structure at each load increment as this slows down the rate of cracking. The residuals will be largest at nodes of elements in which cracks have occurred. Limiting the number of iterations is one method of maintaining forces in the structure. This effect is important after initial stages of cracking. However no obvious criterion exists to specify these limitations.

(4) Using the high convergence tolerance is another method of maintaining the forces in the structure. It can give a constant measure of the residual forces existing in the structure and it can be used instead of limiting the number of iterations. However tension stiffening is also another method of maintaining residuals and will be discussed later.

(5) Different stress distributions are obtained at low load levels for COOP equal to 5% and 20% but this difference lessens at higher load

levels. This is because most of the cracking of concrete developed at the previous load levels and the main effect is that the stress history path has been delayed.

6.3.2 Displacement criteria:

Different load deflection curves using the first displacement criterion DC1 (as described in Section 3.5.2) are compared for convergence tolerances of 10%, 5% and 1% in Figure (6.16). Predicted failure loads are compared in Table (6.5). Iterations were continued until convergence to the specified tolerance was obtained. It can be observed that COOP = 10% gave the best fit to the experimental load displacement curve and also gave the closest ultimate load. The differences in the predicted ultimate load and the load deflection curves for COOP = 10% and 5% were not very significant.

The actual convergence value obtained and the maximum number of iterations required for each increment are also shown in Table (6.5). It can be observed that the number of iterations required for COOP = 10% and 5% were in a narrow range, and a much higher number of iterations was required when COOP was set equal to 1%. However the load criterion was used as the indicator for failure because the displacement criterion does not necessarily give any indication of an increase in residuals. Even though the displacement criterion might be satisfied, there can still be some very high residual forces not distributed: it appears that the load criterion is necessary for a more accurate estimate of the ultimate load for the size of load increment used here.

Load deflection curves using the second displacement criterion DC2 (as described in Section 3.5.2) are also compared for COOP = 10%,

5% and 1% in Figure (6.17). Predicted failure loads are compared in Table (6.6). Iterations were continued until convergence to the specified tolerance was obtained. It can be observed that COOP = 10% gave the best fit to the experimental load deflection curve and gave the closest ultimate load.

The actual convergence value obtained and the maximum number of iterations required for each increment are also shown in Table (6.6). By comparing Table (6.5) and Table (6.6) it appears that the total number of iterations required to achieve convergence in the case of 10%, and 5% was much higher when using DC2 than when using DC1. When COOP was equal to 1% almost similar numbers of iterations were required. Failure was also recognized in these cases by using the load criterion.

Points raised by the displacement criteria can be summarized as follows:

(1) Effectively, it is another method of retaining residuals and delaying their redistributions especially when used with high convergence tolerances.

(2) The first displacement criterion DC1 converges more rapidly than the second displacement criterion DC2 at convergence tolerances of 5% and 10%. But for convergence tolerance of 1% the total number of iterations required were similar. This is because the denominator in DC1 is the total displacement existing at the current stage while in DC2 the denominator has a smaller value because it is the displacement of the current increment.

(3) Both displacement criteria overestimate the ultimate load at the tolerances investigated, and the load criterion was necessary to

measure the increase of residuals at failure. The finer the tolerance the lower the predicted load.

(4) A fairly good fit was obtained with the experimental results when using COOP equal to 5% and 10% without using tension stiffening.

6.3.3 Discussion on load and displacement criteria:

Load deflection curves are compared for convergence tolerances of 20% for the load criteria LC and 10% for both displacement criteria DC1, DC2 in Figure (6.18). Close predictions of failure loads are obtained in all cases. Referring to Table (6.2), (6.5) and (6.6), it is seen that the total number of iterations required to predict failure in all cases was 25, 38, 61 for LC, DC1 and DC2. Comparison of the crack pattern plotted for different load levels are shown in Figure (6.19) and (6.20). It can be observed that crack propagations using the load criterion was slightly less than that obtained using both displacement criteria at a low load level of 69.7 kN. At a higher load level of 99.6 kN, the cracks pattern observed was fairly similar for all cases. However it appears that the load criterion predicts similar results to that of both displacement criteria and requires a fewer number of iterations to predict failure.

Finally the following points can be made:

(1) The best solutions were obtained when high convergence tolerances were used, causing a certain amount of forces to be retained. It will be shown later that a similar situation can be obtained using the tension stiffening method with lower convergence tolerances.

(2) The load criterion requires less iterations than the displacement criteria for a similar crack pattern and load deflection curve, for the convergence rates investigated.

(3) The selection of the convergence criteria and convergence tolerance is very important in predicting the behaviour of reinforced concrete, and must be considered carefully, otherwise the solution may follow a significantly different path.

6.4 Constant and variable stiffness methods:

A nonlinear solution is highly dependent on the way in which the stiffness of the structure is handled. The constant stiffness and the variable stiffness methods are the most widely used in finite element analysis. Each method has its own intrinsic advantages and disadvantages and these are explained in references 3 and 6. A brief review on the application of these methods was covered in the previous section.

The constant stiffness method as earlier explained produces slow convergence and normally a high number of iterations are required to reproduce the load deflection behaviour. Accelerator schemes have sometimes been used [3,6,9] to reduce the number of iterations required to reach a specified equilibrium stage, but they may cause instability of the solution [3]. These are not used in this work, because they add an additional numerical parameter which may complicate the numerical study.

The constant and variable stiffness methods have been used extensively by many authors, but comparison of their influence has not been reported widely, especially when used with different numerical parameters.

In this numerical study the following conditions were kept constant throughout the analysis:

(1) The first cracking model was used (i.e. no tension stiffening).

(2) The three point Gauss rule was used.

(3) The shear retention factor was kept constant and equal to 0.5.

(4) The load criterion was used to check convergence.

Different load deflection curves using the constant stiffness method C.S.M. are compared for convergence tolerances of 20% and 5%, in Figure (6.21). Predicted failure loads are compared in Table (6.7). Iterations were continued until convergence to the specific tolerance was obtained. It can be observed that failure occurred almost at the same load level in both cases, although the best load deflection was obtained for the case of COOP = 20%.

The actual convergence value obtained and the maximum number of iterations required for each increment are also shown in Table (6.7). It is clear that it is very expensive to obtain the solution using COOP = 5% because a total of 560 iterations were required compared with only 24 in the case of COOP = 20%.

A comparison of the crack patterns for different load levels is shown in Figures (6.22) and (6.23). The observation was that different crack patterns are predicted for the same load level during the early stages, but almost identical patterns were obtained near the failure condition.

Different load deflection curves using the constant stiffness method C.S.M. and variable stiffness methods V.S.M.1 and V.S.M.2 for COOP = 20% are compared in Figure (6.24). V.S.M.1 updates the stiffness at the beginning of the first and second iterations of each

increment and V.S.M.2 updates the stiffnesses at the beginning of each iteration during every increment. Predicted failure loads are compared in Table (6.8). Iterations were continued until convergence to the specific tolerance was obtained. It can be seen that V.S.M.1 and V.S.M.2 gave the best fits to the experimental load deflection curve. A close prediction of the ultimate load was obtained in all cases.

The actual convergence value obtained and the maximum number of iterations required for each increment are also shown in Table (6.8). The total number of iterations required to predict failure using the C.S.M. and the V.S.M.1 for COOP = 20% were almost similar. However V.S.M.1 is more expensive because stiffnesses are updated twice in each increment, whereas for the C.S.M. the stiffnesses are calculated once only. However for low convergence tolerances the C.S.M. requires a very high number of iterations.

Finally, different load deflection curves using a value of COOP = 20% are compared in Figure (6.25) for different cases of the variable stiffness method. In these the stiffnesses are updated either at the beginning of the first (i.e. IT = 1), or second (i.e. IT = iteration or at the beginning of both (i.e. IT = 1 & 2 or V.S.M.1). Predicted failure loads are compared in Table (6.9). Iterations were continued until convergence to the specific tolerance was obtained.

The actual convergence value obtained and the maximum number of iterations required for each increment are also shown in Table (6.9). It can be observed that the total number of iterations required in all cases was not greatly different, although IT = 1 and IT = 2 are probably more economical because the stiffness is only changed once

in the increment. However IT = 1 & 2 predicted slightly better load deflection curve and ultimate load.

Residual decay using the C.S.M. is compared in Figure (6.26) for values of COOP equal to 20% and 5% at load levels of 59.8 kN and 89.5 kN. It can be seen that for COOP = 5%, crack development mostly occurred at low load levels and a very smooth curve was obtained at higher load levels. It appears also that most of the sudden changes are occurring in the residual range of 10-30%. However the use of a high convergence will allow cracks to occur in a more gradual manner than for a low convergence because the high convergence will prevent all the cracks from appearing at an early stage.

Residual decays are also compared in Figure (6.27) for the cases studied in Figure (6.25) at a load level of 79.7 kN. The convergence tolerance of 20%, gave a very close prediction to the experimental load deflection at that load level.

The following points can be summarized:

(1) The C.S.M. method gives a stiffer load deflection curve when a high convergence of 20% is used, and gives a more flexible response when using a low convergence tolerance of 5%. Crack patterns before failure are almost the same in both cases, although this is different at lower load levels.

(2) Using COOP = 20%, produces a fairly good prediction of the load deflection curve and ultimate load for both the constant stiffness and variable stiffness method. However much better results for the load deflection were obtained when using the variable stiffness method.

(3) The V.S.M.1 method found to be better than the C.S.M. and the V.S.M.2 methods because it predicted better load deflection curve than the C.S.M. method and is cheaper than the V.S.M.2 method. However, IT = 1 & 2 (i.e. the V.S.M.1 method) also gives a slightly better prediction of the ultimate load than using IT = 1 and IT = 2.

6.5 Gauss rule:

The best order of Gauss rule to be used is usually decided after numerical tests, since the profits and pitfalls of a particular rule are hard to foresee. Often it is best to use as low an order as possible because this will require less solution time than a higher rule. Other advantages are that low orders tend to soften an element, thus countering the overly stiff behaviour associated with an assumed displacement field. Softening comes about when some higher-order terms that would otherwise contribute to strain energy happen to vanish at the Gauss points of a low-order rule. In other words, with fewer sampling points, some of the more complicated deformation modes offer less resistance (However, it is possible that certain modes will offer more resistance).[14]

In general 2 x 2 Gauss rules are required as the minimum order for the parabolic quadrilateral[15] under linear elastic conditions[16]. However Bathe et al.[19], and Cook[14] found that for non-rectangular elements or elongated quadrilaterals the 3 x 3 Gauss rules are required. This is because the low integration rules may produce zero energy deformation modes (i.e. a pattern of nodal degrees of freedom which produces a strain field that is zero at all points) which can misrepresent

element volume.

Irons et al.[17] also reported that the 8-noded isoparametric element can have what he terms "Spurious mechanisms" when 2 x 2 Gauss rules are used, (i.e. an element which can deform without generating strain energy).

It was found by Bathe[16] that an accurate response prediction in nonlinear analysis frequently required a higher order integration than that required in a linear analysis. This is because a higher integration rule is frequently required in order to capture the onset and spread of the material nonlinear condition accurately enough. Specifically, since the material nonlinearities are only measured at the integration points of the element, the use of relatively low integration order may mean that the spread of the materially nonlinear conditions through the element is not represented accurately. The use of high order numerical integration also reduces the number of possible uncertainties that can enter into the interpretation of the results of a complex analysis, and should therefore be used until sufficient experience with the response of the structure has been obtained. At that time the use of reduced integration together with less elements to idealise the structure may be considered.

These points have also been stated by Chen et al.[18], who found that integration points can only be reliable in cases where sampling points are not far away from each other and recommended,that reduced integration rules must be used with care. He also recommended that occasionally it is better to have more integration points in order to describe the crack pattern more accurately. However the selection depends very much on the problem and its actual stress distribution.

In spite of these problems, certain workers have obtained acceptable results using the low integration rules for nonlinear analysis. Phillips[3] found that 2 x 2 Gauss rules can be adopted to predict satisfactory results for the 8-noded parabolic element. Cope et al.[7] also found that using 2 x 2 Gauss quadrature with quadratic interpretation functions restricting material properties variation to a bi-linear form over an element ensure no additional numerical errors are introduced into an analysis by retaining that order of quadrature.

Obviously there is some uncertainty regarding which integration rule to use. In this section a study was carried out to ascertain the effect of changing the order of the integration rule for the program developed in this work. The shear retention factor was made equal to 0.0 and 0.5, in order to examine its contribution when used with different order of Gauss rule. For instance $\alpha = 0.0$ can produce a soft load deflection while 4 x 4 Gauss rules can produce a stiff load deflection.

The following conditions were kept constant throughout the analysis:

(1) The first cracking model was used (i.e. no tension stiffening).

(2) The method V.S.M.1 was used.

(3) The load criterion LC was used to check convergence and COOP was set equal to 20%.

Different load deflection curves using a value of α equal to 0.0 are compared for different orders of Gauss rule of 2 x 2, 3 x 3 and 4 x 4 in Figure (6.28). Iterations were continued until convergence to the specified tolerance was obtained. It was observed that failure was grossly underestimated; divergence rapidly occurring after the start of cracking. However a more stiffer load deflection was obtained as the order of Gauss rule increased.

Different load deflection curves using a value of α equal to 0.5 are compared for different orders of Gauss rules of 2 x 2, 3 x 3 and 4 x 4 in Figure (6.29). The actual convergence value and the maximum number of iterations required for each increment are shown in Table (6.10). It can be observed that 3 x 3 gave the best fit to the experimental load deflection curve and also gave the closest ultimate load. However the 4 x 4 Gauss rule gave a stiffer prediction in the load deflection curve after the start of cracking, but ultimate failure load was as that using the 3 x 3 Gauss rule.

Comparison of the crack pattern plotted for the 3 x 3 and 4 x 4 Gauss rules at two different load levels are shown in Figure (6.30). It can be observed that less cracks appeared for the 4 x 4 Gauss rule at low load levels although an almost similar pattern was produced at higher loads. However when the 2 x 2 Gauss rule was used an underestimation of the failure load also occurred, in a similar fashion to that when α was equal to zero.

The 2 x 2 Gauss rule was investigated for a finer mesh of 36 elements as shown in Figure (6.31). The 36 elements provided more Gauss rules over the depth and the width of the beam. The actual convergence value and the maximum number of iterations required for each increment are also shown in Table (6.10).

It was observed that although the predicted failure load was better for the finer mesh it still grossly underestimated the experimental failure load. However failure occurred after two increments from the start of cracking when the fine mesh was used.

The crack patterns at failure for both cases are compared in Figure (6.32). The cracks propagated in an unexpected manner, in fact some cracks appeared and propagated outside the maximum bending

moment. This suggests that the 2 x 2 Gauss rule may not be a reliable rule to use in the nonlinear analysis, and confirms the findings of Chen et al[10].

The following points can be made:

(1) Care must be taken when using low integration rules because numerical problems may arise causing the solution to diverge.

(2) Changing the order of integration when α is set equal to 0.0 does not significantly improve the predicted results.

(3) When α was not equal to zero, the 3 x 3 and 4 x 4 Gauss rules gave the best prediction to the load deflection and ultimate load but the 2 x 2 Gauss rule still gave an inferior result.

It would appear that it is the order of Gauss rule which is crucial rather than the total number of sampling points throughout the continuum. However this matter requires further investigation.

6.6 Shear reten ion factor:

As previously explained, the shear reten ion factor is an assumed numerical factor which is included in the theoretical cracking model, to take into account the reduction in shear modulus after the development of a crack. The new shear modulus is defined as $G_c = \alpha G$, where α is the shear reten ion factor, G the shear modulus before cracking, and G_c the modified shear modulus. α has been used by many investigators. For example Phillips[3] used values of α equal to 0.0, 0.5, and 1.0 and found that when α was equal to zero an underestimation of the failure load was obtained, but for α equal to 0.5, and 1.0 reasonable predictions for ultimate load could be obtained.

Suidan et al.[20] used a constant value of 0.5 in his analysis and obtained good agreement with the experimental results. Hand et al.[21] found that shear retention was necessary to preserve numerical stability in some cases. Values of 0.2 and 0.4 were used in his analysis, and no large differences arose from using these two values. Other authors assumed that this factor varies with respect to the physical phenomenon [22,23,24]. For example Cedolin et al.[22] assumed that the value of G_c decreases linearly with the crack width and that it reaches a very small value when the crack is wide.

Al-Mahaidi[23] investigated the reduction of shear modulus due to cracking, which had been used by different analysts. He found a considerable range varying from 50% to only 10% for very wide cracks.

The particular value chosen for α between 0.0 and 1.0 does not appear to be critical but values greater than zero are necessary to prevent numerical difficulties, which may occur due to the zero terms in the diagonal stiffness matrix. The presence of α is realistic since it represents the retention of some shear due to the aggregate interlock that occurs across an open crack. However the reduced shear modulus G_c more nearly represents a number of springs parallel to the crack rather than the physical reality of a rough crack in concrete.

In general terms the use of α has proved to give satisfactory results for different analyses.

In this section values of α equal to 0.0, 0.01, 0.05, 0.2, 0.5 and 1.0 will be compared. Also the effect of varying α on convergence and number of iterations will be studied. In this section the following conditions were kept constant throughout the analysis.

(1) The first cracking model was used (i.e. no tension stiffening).

(2) The method V.S.M.1 was used.

(3) The three point Gauss rule was used.

(4) The load criterion was used to check convergence and a convergence tolerance of 20% was used.

Different load deflection curves using values of α equal to 0.01,0.05, 0.5, and 1.0 are compared in Figure (6.33), and values of 0.0, 0.2, 0.5 and 1.0 are compared in Figure (6.34). Predicted failure loads are compared in Table (6.11) for α equal to 0.01, 0.05, 0.2, 0.5 and 1.0. Iterations were continued until convergence to the specified tolerance was obtained. The actual convergence value obtained and the maximum number of iterations for each increment are also shown in Table (6.11). It can be observed that $\alpha = 0.5$ gave the best fit to the experimental load deflection curve.

However, it seems that when α is increasing towards 1.0 a stiffer prediction is obtained. When α was equal to 0.0 a drastic underestimation of the failure load was obtained with instability of the solution. The following points can be summarized:

(1) The shear retention factor is an important parameter, and a value of zero should not be assumed because numerical problems appear at the stage when most of the cracks occur.

(2) As α increases towards 1.0, stiffer load deflection curves are obtained. The best load deflection curve was when α equal to0.5.

(3) The total number of iterations required to achieve convergence to a value of 20% for the tested value of α fell within a narrow range, and the minimum number was required when α was set equal to 1.0.

(4) The wide range of α varying between 0.01 and 1.0 did not significantly affect the predicted load deflection curves. If this is the case then there is no point in using more complicated methods for varying the shear on cracking surfaces unless local behaviour is required. This would seem to suggest that α is a numerical device rather than an approximation to a physical phenomenon.

6.7 Tension stiffening:

Tension stiffening was first introduced by Scanlon[25] to account for the tensile stiffening effect of concrete between cracks. He assumed that after concrete reaches its ultimate tensile strength, a primary crack will form, but the cracked concrete carries some tensile stresses perpendicular to the crack direction. As the load increases, more cracks will form,but the amount of tensile stresses carried by the concrete progressively decreases.

In another study by Gilbert et al.[26,27] different shapes were used to represent the tension stiffening effect. These are shown in Figure (6.35). Gilbert et al. also proposed a second method to account for the tension stiffening indirectly. This assumed that the retention of stresses after the development of a crack is represented by increasing the steel stresses as illustrated in the modified stress-strain curves shown in Figure (6.36). The additional stress in the steel approximates the tensile forces carried by both the steel and the concrete between the cracks. The added stress is lumped at the level of the steel and oriented in the same direction for reasons of convenience. The results obtained using the modified approach for the stress-strain curve

of steel were found to be as good as those obtained using the first method, but are in fact cheaper to obtain. Gilbert et al. also showed that the load deflection curves obtained using tension stiffening or the modified approach for steel gave much better results than that with no tension stiffening.

Lin et al.[28] found that tension stiffening has a significant influence on the post cracking response of under-reinforced concrete structures, but not on the behaviour at the ultimate stage.

Scordelis[1] also reported that tension stiffening gives a more accurate representation of stiffness for the deflection calculations, but will underestimate the maximum steel stress at an actual crack within an element, and that tension stiffening will become more difficult to represent for biaxial and triaxial stress states.

Cope et al.[6] investigated the effect of tension stiffening on concrete bridge decks and found that its effect is most significant for low reinforcement percentages. The agreement was less significant for a higher steel percentage. He suggested that further experimental work was required to understand the behaviour of tension stiffening.

Mang et al.[29] reported that neglecting tension stiffening may significantly underestimate the ultimate load.

Shirai et al.[30] assumed in his study that the bond resistance between concrete and the reinforcement bars after crack formation gives some resistance to concrete. He called this the tension stiffening effect, and its resistance gradually deteriorated with an increase in the number of cracks. A polynomial was proposed to represent the descending branch which is a function of the steel property.

From observations of tests on concrete panels Vecchio et al.[31] confirmed that tension stiffening has some effect on the ultimate strength of concrete provided that the failure occurred before all of the steel yielded.

Cope et al.[8] also found that the force contributed by tension stiffening results in a lower stress in the reinforcement than that predicted by an analysis assuming no tension stiffening. Cope et al.[9] also found that tension stiffening was not required for the design of the slabs he tested. Crisfield[10] reported that the strain softening branch (tension stiffening) can induce localized instabilities and non-unique solutions. He criticized the available literature because no mention of this had been reported.

From this review the following points can be summarized:

(1) Tension stiffening has been used by many authors, who have shown that it has a significant effect on the load deflection behaviour of the structure.

(2) Tension stiffening is another complexity in a nonlinear analysis, which was originally introduced to improve the accuracy of the results obtained. However it has been given various physical interpretations, ranging from a way of retaining stresses between discrete cracks to indirectly including bond-slip or to aggregate interlocking effects.

(3) Different approaches have been used for approximating tension stiffening, but the chosen shape of the stress-strain curve appears to be fairly arbitrary.

(4) In some studies an underestimation of the steel stresses was obtained because of tension stiffening.

The aim of this section is to study the effect of using a particular tension stiffening stress-strain curve (shown in Figure (5.14), and represented by the second cracking model) on the behaviour of the deep beam, and to try to identify the numerical processes involved. The following points will be investigated:

(A) The interaction of the convergence rate and the tension stiffening model.

(B) The effect of having different values of ε_A i.e. the strain at which the stress is equal to zero in the descending part of the stress-strain curve of concrete in tension. (It is assumed that this effect represents different shapes of tension stiffening curves).

(C) A comparison between the tension stiffening model and no tension stiffening model.

The following conditions were kept constant throughout the analysis:

(1) The method V.S.M.1 was used.

(2) The three point Gauss rule was used.

(3) The shear retention factor was kept constant and equal to 0.5.

(4) The load criterion was used to check convergence.

Different load deflection curves using a value of $\varepsilon_A = 5\varepsilon'_c$ are compared for convergence tolerances of 20%, 5% and 1% in Figure (6.37). Predicted failure loads are compared in Table (6.12). Iterations were continued until convergence to the specified tolerance was obtained. It can be observed that a value of COOP = 5% gave the best fit to the experimental load deflection curve and also gave the closest ultimate load. But it is clear that tension stiffening has a profound effect

on the solution.

The actual convergence value obtained and the maximum number of iterations required for each increment are also shown in Table (6.12). When COOP was equal to 20% only one iteration was required to reach convergence until the steel yielded. This shows that a high convergence factor with tension stiffening may overestimate the ultimate load and stiffness. It was also observed that using a small tolerance of 1% may underestimate the ultimate load and stiffness. This shows again however that the convergence tolerance is an important parameter in the control of the load deflection curve.

Comparison of the crack pattern plotted for different load levels is shown in Figure (6.38) and (6.39). It can be observed that using the high convergence of 20% with tension stiffening caused a different crack pattern from that of 5% and 1% at high load levels.

Different load deflection curves using a value of $\varepsilon_A = 10\ \varepsilon_c'$ are compared for convergence tolerances of 20%, 5%, 1% and 0.01% in Figure (6.40). Predicted failure loads are compared in Table (6.13). Iterations were continued until convergence to the specified tolerance was obtained or a limit of 350 iterations had been reached. It can be observed that COOP = 0.01% gave the closest prediction to the ultimate load.

The actual convergence value obtained and the maximum number of iterations required for each increment are also shown in Table (6.13). It can be seen that the use of high convergence produces stiffer results in the load deflection curve after the development of a crack. When a value of COOP = 20% was used, yielding was not even observed up

to a load of 119.5 kN. However when COOP was set equal to 0.01% a total of 1142 iterations were required with a limitation of 350 set as a maximum. However an almost similar load deflection curve was observed when COOP was set equal to 1% and a maximum of 162 iterations were required.

Comparisons of the crack pattern plotted for different load levels are shown in Figures (6.41) and (6.42). It was observed that COOP = 1% and 0.01% gave similar patterns.

Finally different load deflection curves for a value of $\varepsilon_A = 25\varepsilon'_c$ are compared in Figure (6.43) for values of COOP equal to 20%, 5%, 1% and 0.01%. Iterations were continued until convergence to the specified tolerance was obtained. It can be observed that the predicted results overestimate the experimental load deflection curve in all cases and the analysis was stopped at a load of 119.5 kN.

To show the effect of changing ε_A, different load deflection curves for equal values of COOP are shown in Figures (6.44 - 6.46). It can be seen that as ε_A increases so the stiffnesses and ultimate load increases. It also shows that the use of tension stiffening depends very much on such arbitrary values at ε_A, that it makes tension stiffening curves an uncertain device.

The following points can be summarized:

(1) Tension stiffening is a method of retaining some amount of stress which is not released when cracks occur.

(2) The tension stiffening method can produce satisfactory results when compared with experimental curves, but is very much inter-related to the convergence tolerance used and the value of ε_A (which is assumed to be a measure of the shape of the tension stiffening curve).

(3) When tension stiffening is used with a high convergence tolerance of 20% an overestimation of the ultimate load and a stiff load deflection curve, was produced. A small convergence produced an underestimation of the ultimate load but the value of ϵ_A should control this.

A final comparison was carried out in Figure (6.47) for, COOP = 20% with no tension stiffening, COOP = 5% with $\epsilon_A = 5\epsilon_c'$, and COOP = 1% with $\epsilon_A = 10\epsilon_c'$. Predicted failure loads are compared in Table (6.14). It can be observed that the no tension stiffening case gave the best fit to the experimental load deflection curve. The total displacement with tension stiffening was closer to the ultimate load deflection although the load deflection curve was stiffer. The number of iterations required is also shown in Table (6.14). No tension stiffening required only 25 iterations while $5\epsilon_c'$ required 58 iterations and $10\epsilon_c'$ required 162 iterations.

Comparison of the crack patterns for these cases are plotted in Figures (6.48 - 6.50). Very little difference is observed in these cases which implies that no tension stiffening with a high convergence rate gives similar results to the inclusion of tension stiffening with lower convergence rates.

6.8 Conclusions:

The main conclusions to be drawn from this chapter are as follows:

(1) A high convergence tolerance can give satisfactory results if tension stiffening is not used. A value of COOP = 20% was suggested in this work when using the load criterion. The load criterion also gave a more realiable measure of the decay of the residuals than the displacement criterion used here.

(2) Tension stiffening can produce satisfactory results but care must be taken when choosing the value of convergence tolerance and the value of strain at which the stress drops to zero. However it would appear that tension stiffening can be satisfactorily replaced by using a no tension stiffening stress-strain law with a higher convergence tolerance. This is because they both have the effect of retaining residual forces. It also has a considerable advantage in that it requires far less iterations and hence computer time.

(3) The V.S.M.1 method where the stiffnesses are updated at the beginning of the first and second iteration of each increment predicted the best results in all cases studied.

(4) The shear retention factor is an important numerical device and the wide range varying between 0.01 - 1.0 did not produce a significant effect on the load deflection curve. There is no point in using more complication for this variable in the smeared cracking approach and a value of 0.5 is suggested.

(5) Care must be taken in selecting the order of numerical integration in the prediction of nonlinear behaviour, because numerical problems can exist when using low integration rules. However, a 3 x 3 Gauss rule was found to be a realiable rule for the prediction of the concrete behaviour.

(6) The conclusions are further tested for more complex beams failing in shear in the next chapters and will be largely confirmed again.

6.9 Burns & Siess shallow beam J-4[12]:

The analysis of this beam independently assesses the conclusions drawn so far in this thesis. The beam has also been tested by various other authors[20,32,33,34] and so gives additional comparisons. The beam was tested under concentrated load and is shown in Figure (6.51). Details of the material properties are shown in Table (6.1).

Because of symmetry, only half of the beam will be considered. The finite element mesh used is shown in Figure (6.52) and the load was applied at nodal point 103.

The following assumptions were made in the analysis:

(1) The stirrups were neglected and only main steel was provided.

(2) The first cracking model was used (i.e. there was no tension stiffening).

(3) The load criterion was used with a convergence tolerance of 20%.

(4) The method V.S.M.1 was used.

(5) The shear retention factor was set equal to 0.5.

(6) The 3 x 3 Gauss rule was used.

(7) The load was applied in equal increments of 10.0 kN until failure occurred.

Different load deflection curves obtained from various authors[20,32,33,34] are compared with the present analysis in Figure (6.53). Iterations were continued until convergence to the specified tolerance was obtained. Figure (6.54) gives a clearer comparison with Sorenson's results and the results obtained in this work.

It was observed during the experiment that the cracking started at a load level of approximately 40.0 kN while the reinforcement steel yielded at a load of 156.0 kN. In this analysis, the start of cracking was

observed at load of 40.0 kN while yield of reinforcement started at load level of 150.0 kN.

Analytical cracking patterns are shown in Figures (6.55 - 6.58) and principal stress directions are shown in Figures (6.59) and (6.62). The following points are summarized:

(1) The load criterion with COOP = 20% using the V.S.M.1 and α = 0.5 gave a very good prediction compared with other investigators confirming the previous conclusions.

(2) The use of high convergence did not significantly affect the stresses in steel because the point of yielding was satisfactorily estimated.

(3) The use of elongated elements with the 3 x 3 Gauss rule adequately predicted the experimental behaviour.

Beam name	f'_c (N/mm^2)	f'_t (N/mm^2)	E_c^* (kN/mm^2)	ν_c^*	A_s (mm^2)	f_y (N/mm^2)	E_s (kN/mm^2)	E_w^* kN/mm^2)
A-1	24.1	3.1	20.6	0.15	71.0	344.8	206.9	34.5
J-4	53.0	3.77	28.4	0.20	1012.9	309.7	210.0	0.0

* Assumed values

Table (6.1) Details of material properties.

Convergence Tolerance		5%		10%		15%		20%	
Incr. No.	Load (kN)	Convergence in the Analysis (%)	No. of Iter.	Convergence in the Analysis (%)	No. of Iter.	Convergence in the Analysis (%)	No. of Iter.	Convergence in the Analysis (%)	No. of Iter.
1	9.9	1.28	1	1.28	1	1.28	1	1.28	1
2	19.9	2.85	1	2.85	1	2.85	1	2.85	1
3	29.9	4.62	1	4.62	1	4.62	1	4.62	1
4	39.8	1.07	2	6.54	1	6.54	1	6.54	1
5	49.8	4.42 C	1	8.56	1	8.56	1	8.56	1
6	59.8	4.83	56	9.33 C	27	10.63 C	1	10.63 C	1
7	69.7	4.88	156	9.47	1	14.03	24	17.74	2
8	79.7	4.75 Y	26	9.86 Y	2	12.98 Y	8	17.25	9
9	89.5	4.19	6	F.L.C.		F.L.C.		16.52 Y	2
10	99.6	F.L.C.						17.25	2
11	101.6							9.52	2
12	103.6							19.20	2
13	105.6							F.L.C.	
Total number of Iterations			250		35		38		25

Key to symbols:

C = first cracking load.
Y = load at first yield.

N.C. = No convergence obtained.
F.L.C. = Failure indicated by load criterion.
F.D.C. = Failure indicated by displacement criterion.

Convergence Tolerance		5%		10%		15%		20%	
Incr. No.	Load (kN)	Convergence in the analysis (%)	No. of Iter.	Convergence in the analysis (%)	No. of Iter.	Convergence in the analysis (%)	No. of Iter.	Convergence in the analysis (%)	No. of Iter.
1	9.9	1.28	1	1.28	1	1.28	1	1.28	1
2	19.9	2.85	1	2.85	1	2.85	1	2.85	1
3	29.9	4.62	1	4.62	1	4.62	1	4.62	1
4	39.8	1.07	2	6.54	1	6.54	1	6.54	1
5	49.8	4.42 C	1	8.56	1	8.56	1	8.56	1
6	59.8	7.06	30	9.33 C	27	10.63 C	1	10.63 C	1
7	69.7	4.78	18	9.46	1	14.03	24	17.74	2
8	79.7	21.69 Y	30	9.86 Y	2	12.98 Y	8	17.25	9
9	89.6	17.65	30	26.95	30	28.30	30	16.52 Y	2
10	99.6	97.74	30	45.57	30	51.57	30	17.25	2
11	101.6	F.L.C.		F.L.C.		F.L.C.		9.52	2
12	103.6							19.20	2
13	105.5							F.L.C.	
Total Number of Iterations			144		95		98		25

Table (6.3) Convergence effect using the load criterion (V.S.M.1),(30 iterations maximum).

Convergence Tolerance		5%		10%		15%		20%	
Incr. No.	Load (kN)	Convergence in the analysis (%)	No. of Iter.	Convergence in the analysis (%)	No. of Iter.	Convergence in the analysis (%)	No. of Iter.	Convergence in the analysis (%)	No. of Iter.
1	9.9	1.28	1	1.28	1	1.28	1	1.28	1
2	19.9	2.85	1	2.85	1	2.85	1	2.85	1
3	29.9	4.62	1	4.62	1	4.62	1	4.62	1
4	39.8	1.07	2	6.54	1	6.54	1	6.54	1
5	49.8	4.42 C	1	8.56	1	8.56	1	8.56	1
6	59.8	16.89	10	16.89 C	10	10.63 C	1	10.63 C	1
7	69.7	12.89	10	12.88	10	25.88	10	17.74	2
8	79.7	21.46 Y	10	6.21 Y	2	14.51 Y	5	17.25	9
9	89.6	19.87	10	24.71	10	19.90	10	16.25 Y	2
10	99.6	34.13	10	27.58	10	28.49	10	17.25	2
11	101.6	53.88	10	62.90	10	34.96	10	9.52	2
12	103.6	F.L.C.		F.L.C.		F.L.C.		19.20	2
13	105.5							F.L.C.	
Total number of iterations			66		57		51		25

Table (6.4) Convergence effect using the load criterion (V.S.M.1), (10 iterations maximum).

Convergence Tolerance		1%		5%		10%	
Incr. No.	Load (kN)	Convergence in the analysis (%)	No. of iter.	Convergence in the analysis (%)	No. of iter.	Convergence in the analysis (%)	No. of iter.
1	9.9	0.62	2	0.62	2	0.62	2
2	19.9	0.92	2	0.92	2	0.92	2
3	29.9	0.98	3	1.07	2	1.07	2
4	39.8	0.16	3	1.21	2	1.21	2
5	49.8	0.18 C	4	1.38 C	2	1.38 C	2
6	59.8	0.93	29	2.49	2	2.49	2
7	69.7	0.81	12	4.93	8	5.99	4
8	79.7	0.99 Y	19	3.89 Y	5	7.56	4
9	89.6	0.84	12	3.86	3	5.09 Y	3
10	99.6	0.98	34	4.73	3	9.62	3
11	101.6	1.45 F.L.C.		1.20	3	1.99	3
12	103.6			3.99	2	6.59	2
13	105.6			3.11	3	7.69	2
14	107.6			2.45 F.L.C.	3	7.66	2
15	109.6			4.28	3	3.86 F.L.C.	3
16	119.5			3.38	4	9.47	3
Total number of iterations			120	up to load 107.6 kN	42	up to load of 109.5 kN	38

Table (6.5) Convergence effect using the first displacement criterion (V.S.M.1).

Convergence Tolerance		1%		5%		10%	
Incr. No.	Load (kN)	Convergence in the analysis (%)	No. of iter.	Convergence in the analysis (%)	No. of iter.	Convergence in the analysis (%)	No. of iter.
1	9.9	0.62	2	0.62	2	0.62	2
2	19.9	0.10	3	1.83	2	1.83	2
3	29.9	0.28	3	3.16	2	3.16	2
4	39.8	0.61	3	4.74	2	4.74	2
5	49.8	0.83 C	4	4.81 C	3	6.67 C	2
6	59.8	0.93	33	4.56	16	8.45	4
7	69.7	0.81	18	3.99	8	9.49	7
8	79.7	0.97 Y	23	4.76 Y	7	8.15	4
9	89.6	0.94	29	4.68	9	9.30	5
10	99.6	3.10 F.L.C.		4.72	6	7.99	5
11	101.6			3.98	9	6.04	6
12	103.6			4.66 F.L.C.	21	5.13	8
13	105.6			F.D.C.	8	5.13	8
14	107.6					8.80 F.L.C.	4
15	109.6					7.41	4
16	119.5					F.D.C.	10
Total number of iterations			118	Up to load 103.6 kN	87	Up to load 107.6 kN	61

Table (6.6) Convergence effect using the second displacement criterion (V.S.M.1).

Convergence Tolerance		5%		20%	
Incr. No.	Load (kN)	Convergence in the analysis (%)	No. of iter.	Convergence in the analysis (%)	No. of iter.
1	9.9	1.28	1	1.28	1
2	19.9	2.85	1	2.85	1
3	29.9	4.62	1	4.62	1
4	39.8	1.07	2	6.54	1
5	49.8	4.42 C	1	8.56	1
6	59.8	4.77	44	10.63 C	1
7	69.7	4.98	235	14.67	2
8	79.7	4.48 Y	64	18.48	2
9	89.6	4.97	49	18.51	11
10	99.6	4.97	95	19.97	1
11	101.6	4.50	15	18.17	2
12	103.6	4.98	26	F.L.C. Y	
13	105.6	4.98	26		
14	107.6	F.L.C.			
Total number of iterations			560		24

Table (6.7) Convergence effect using the load criterion (C.S.M.).

Method used		C.S.M.		V.S.M.1		V.S.M.2	
Incr. No.	Load (kN)	Convergence in the analysis (%)	No. of iter.	Convergence in the analysis (%)	No. of iter.	Convergence in the analysis (%)	No. of iter.
1	9.9	1.28	1	1.28	1	1.28	1
2	19.9	2.85	1	2.85	1	2.85	1
3	29.9	4.62	1	4.62	1	4.62	1
4	39.8	6.54	1	6.54	1	6.54	1
5	49.8	8.56	1	8.56	1	8.56	1
6	59.8	10.63 C	1	10.63 C	1	10.63 C	1
7	69.7	14.67	2	17.74	2	17.74	2
8	79.7	18.48	2	17.25	9	13.55	5
9	89.6	18.51	11	16.52 Y	2	14.19 Y	2
10	99.6	19.97	1	17.25	2	16.89	3
11	101.6	18.17	2	9.52	2	8.47	2
12	103.6	F.L.C. Y		19.20	2	18.78	2
13	105.6			F.L.C.		17.05	10
14	107.6					F.L.C.	
Total number of iterations			24		25		32

Table (6.8) Convergence effect using different solution methods, (COOP = 20%).

Method used		IT = 1		IT = 2		IT= 1 & 2 (V.S.M.1)	
Incr. No.	Load (kN)	Convergence in the analysis (%)	No. of iter.	Convergence in the analysis (%)	No. iter.	Convergence in the analysis (%)	No. iter.
1	9.9	1.28	1	1.28	1	1.28	1
2	19.9	2.85	1	2.85	1	2.85	1
3	29.9	4.62	1	4.62	1	4.62	1
4	39.8	6.54	1	6.54	1	6.54	1
5	49.8	8.56	1	8.56	1	8.56	1
6	59.8	10.63 C	1	10.63 C	1	10.63 C	1
7	69.7	18.75	3	13.33	2	17.74	2
8	79.7	19.66	9	17.96	11	17.25	9
9	89.6	19.92 Y	4	15.70 Y	2	16.52 Y	2
10	99.6	18.96	2	17.67	2	17.25	2
11	101.6	9.21	2	8.68	2	9.52	2
12	103.6	F.L.C.		F.L.C		19.20	2
13	105.6					F.L.C.	
Total Number of iterations			26		25		25

Table (6.9) Convergence effect using different solution methods, (COOP = 20%).

G.R. No. of elements		2 x 2 16 elements		2 x 2 36 elements		3 x 3 16 elements		4 x 4 16 elements	
Incr. No.	Load (kN)	Convergence in the analysis (%)	No. of iter.	Convergence in the analysis (%)	No. of iter.	Convergence in the analysis (%)	No. of iter.	Convergence in the analysis (%)	No. of iter.
1	9.9	1.77	1	2.24	1	1.28	1	1.30	1
2	19.9	3.24	1	4.42	1	2.85	1	2.92	1
3	29.9	4.96	1	6.89	1	4.62	1	4.72	1
4	39.8	7.00	1	9.68	1	6.54	1	6.67	1
5	49.8	10.59 C	1	12.74 C	1	8.56	1	8.71 C	1
6	59.9	F.L.C.		19.45	12	10.63 C	1	11.07	1
7	69.7			19.54	8	17.74	2	18.59	1
8	79.7			F.L.C.		17.25	9	18.78	2
9	89.6					16.52 Y	2	19.78	7
10	99.6					17.25	2	16.61	2
11	101.6					9.52	2	10.93	2
12	103.6					19.20	2	18.90	2
13	105.6					F.L.C.		F.L.C.	
Total number of iterations			5		25		25		22

Table (6.10) Convergence effect using different integration rules with shear retension factor equal to 0.5, (V.S.M.1, COOP = 20%).

Shear retension factor		α = 0.01		α = 0.05		α = 0.2		α = 0.5		α = 1.0	
Incr. No.	Load (kN)	Convergence in the analysis (%)	No. of iter.	Convergence in the analysis (%)	No. of iter.	Convergence in the analysis (%)	No. of iter.	Convergence in the analysis (%)	No.of iter.	Convergence in the analysis (%)	No. of iter.
1	9.9	1.28	1	1.28	1	1.28	1	1.28	1	1.28	1
2	19.9	2.85	1	2.85	1	2.85	1	2.85	1	2.85	1
3	29.9	4.62	1	4.62	1	4.62	1	4.62	1	4.62	1
4	39.8	6.54	1	6.54	1	6.54	1	6.54	1	6.54	1
5	49.8	8.56	1	8.56	1	8.56	1	8.56	1	8.56	1
6	59.8	10.63 C	1	10.63 C	1	10.63 C	1	10.63 C	1	10.63 C	1
7	69.7	17.51	2	17.59	2	17.60	2	17.74	2	17.71	2
8	79.7	18.39	16	19.76	9	19.26	12	17.25	9	19.35	8
9	89.6	17.85	1	19.01 Y	3	16.15 Y	2	16.52 Y	2	18.33	1
10	99.6	19.81 Y	2	16.23	2	17.09	2	17.25	2	14.94 Y	2
11	101.6	F.L.C.		12.92	2	14.55	2	9.52	2	16.08	2
12	103.6			16.01	2	18.42	2	19.20	2	16.36	2
13	105.6			19.71	2	F.L.C.		F.L.C.		F.L.C.	
14	107.6			F.L.C.							
Total number of iterations			27		28		28		25		23

Table (6.11) Convergence effect using different shear retension factors, (V.S.M.1, COOP = 20%).

Convergence Tolerance		COOP = 20%, $5\varepsilon'_c$		COOP = 5%, $5\varepsilon'_c$		COOP = 1%, $5\varepsilon'_c$	
Incr. No.	Load (kN)	Convergence in the analysis (%)	No. of iter.	Convergence in the analysis (%)	No. of iter.	Convergence in the analysis (%)	No. of iter.
1	9.9	1.28	1	1.28	1	0.04	2
2	19.9	2.85	1	2.85	1	0.16	2
3	29.9	4.62	1	4.62	1	0.34	2
4	39.8	6.54	1	1.07	2	0.59	2
5	49.8	8.56	1	4.72 C	1	0.91 C	2
6	59.8	15.07 C	1	3.14	2	0.49	3
7	69.7	16.09	1	2.41	2	0.88	3
8	79.7	17.87	1	4.39	2	0.98	91
9	89.6	19.58	1	4.94 Y	33	0.85 Y	22
10	99.6	15.30	2	4.18	7	F.L.C.	
11	101.6	16.17	1	4.73	1		
12	103.6	17.01	1	3.26	4		
13	105.6	18.09	1	4.33	1		
14	107.6	19.15	1	F.L.C.			
15	109.6	19.71 Y	7				
16	119.5	15.50	3				
Total number of iterations			25		58		129

Table (6.12) Convergence effect using tension stiffening (V.S.M.1).

Convergence tolerance		COOP = 20%, $10\varepsilon'_c$		COOP = 5%, $10\varepsilon'_c$		COOP = 1%, $10\varepsilon'_c$		COOP =0.01%, $10\varepsilon'_c$	
Incr. No.	Load (kN)	Convergence in the analysis (%)	No. of iter.	Convergence in the analysis (%)	No. of iter.	Convergence in the analysis (%)	No. of iter.	Convergence in the analysis (%)	No. of iter.
1	9.9	1.28	1	1.28	1	0.04	2	0.0014	3
2	19.9	2.85	1	2.85	1	0.15	2	0.0009	4
3	29.9	4.62	1	4.62	1	0.34	2	0.0054	4
4	39.8	6.54	1	1.07	2	0.59	2	0.0036	5
5	49.8	8.56	1	4.72 C	1	0.91 C	2	0.0033 C	6
6	59.8	15.05 C	1	3.09	2	0.44	3	0.0040	7
7	69.7	15.98	1	2.10	2	0.62	3	0.0054	8
8	79.7	17.59	1	2.57	2	0.92	3	0.0080	9
9	89.6	19.10	1	3.80	2	0.57	5	0.0095	20
10	99.6	9.76	2	4.95	2	0.85	13	0.51	N.C. 350
11	101.6	10.57	1	3.49	2	0.97	4	0.028 Y	N.C. 350
12	103.6	11.73	1	4.90	1	0.98 Y	106	0.0099	26
13	105.6	12.45	1	4.04	2	0.71	5	0.34	N.C. 350
14	107.6	13.17	1	4.18	2	0.99	4	F.L.C.	
15	109.6	13.89	1	4.77 Y	28	0.92	6		
16	119.5	17.72	1	4.95	3	F.L.C.			
Total number of iterations			17		54		162		1142

Table (6.13) Convergence effect using tension stiffening (V.S.M.1).

Convergence Tolerance		COOP = 1%, $10\varepsilon'_c$		COOP = 5%, $5\varepsilon'_c$		COOP = 20%, N.T.S.	
Incr. No.	Load (kN)	Convergence in the analysis (%)	No. of iter.	Convergence in the analysis (%)	No. of iter.	Convergence in the analysis (%)	No. of iter.
1	9.9	0.04	2	1.28	1	1.28	1
2	19.9	0.16	2	2.85	1	2.85	1
3	29.9	0.34	2	4.62	1	4.62	1
4	39.8	0.59	2	1.07	2	6.54	1
5	49.8	0.91 C	2	4.72 C	1	8.56	1
6	59.8	0.44	3	3.14	2	10.63 C	1
7	69.7	0.62	3	2.41	2	17.74	2
8	79.7	0.92	3	4.39	2	17.25	9
9	89.5	0.57	5	4.94 Y	33	16.52 Y	2
10	99.6	0.85	13	4.18	7	17.25	2
11	101.6	0.97	4	4.73	1	9.52	2
12	103.6	0.98 Y	106	3.26	4	19.20	2
13	105.6	0.71	5	4.33	1	F.L.C.	
14	107.6	0.99	4	F.L.C.			
15	109.6	0.92	6				
16	119.5	F.L.C.					
Total number of iterations			162		58		25

Table (6.14) Convergence effect using tension stiffening, (V.S.M.1).

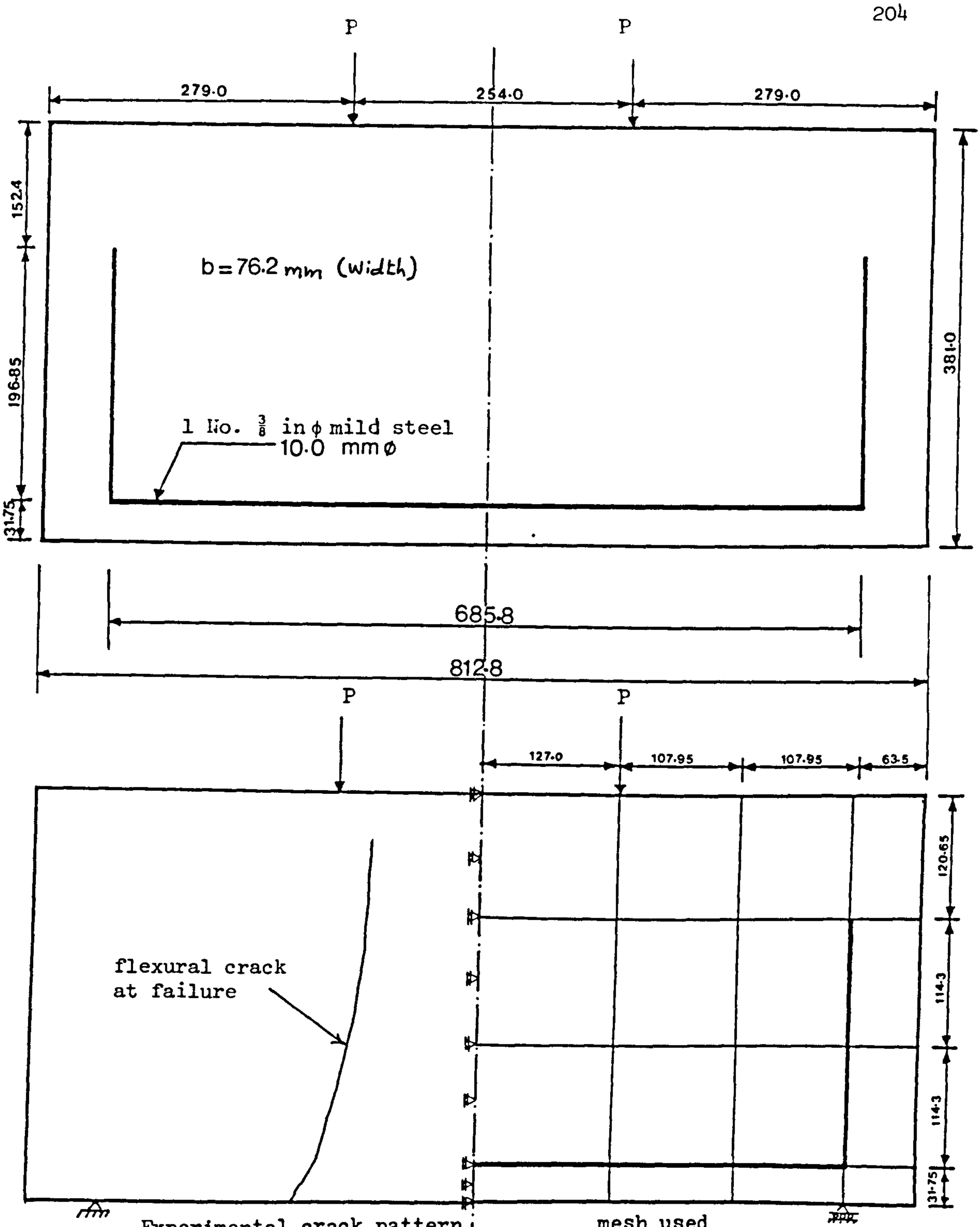

Experimental crack pattern

mesh used

Figure (6•1) Details of deep beam A-1.

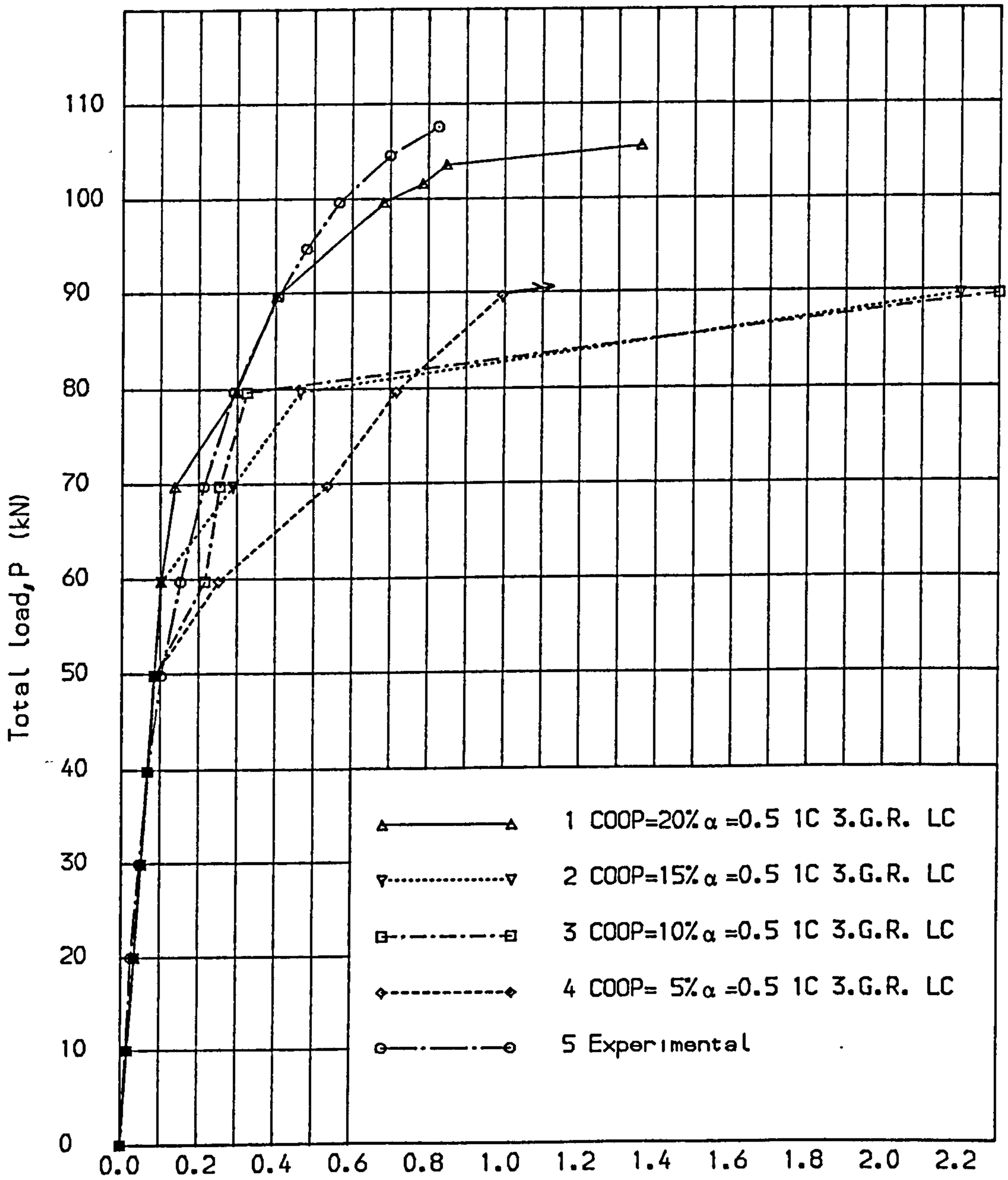

Fig. (6.2) Load deflection curves for deep beam, (V.S.M.1).

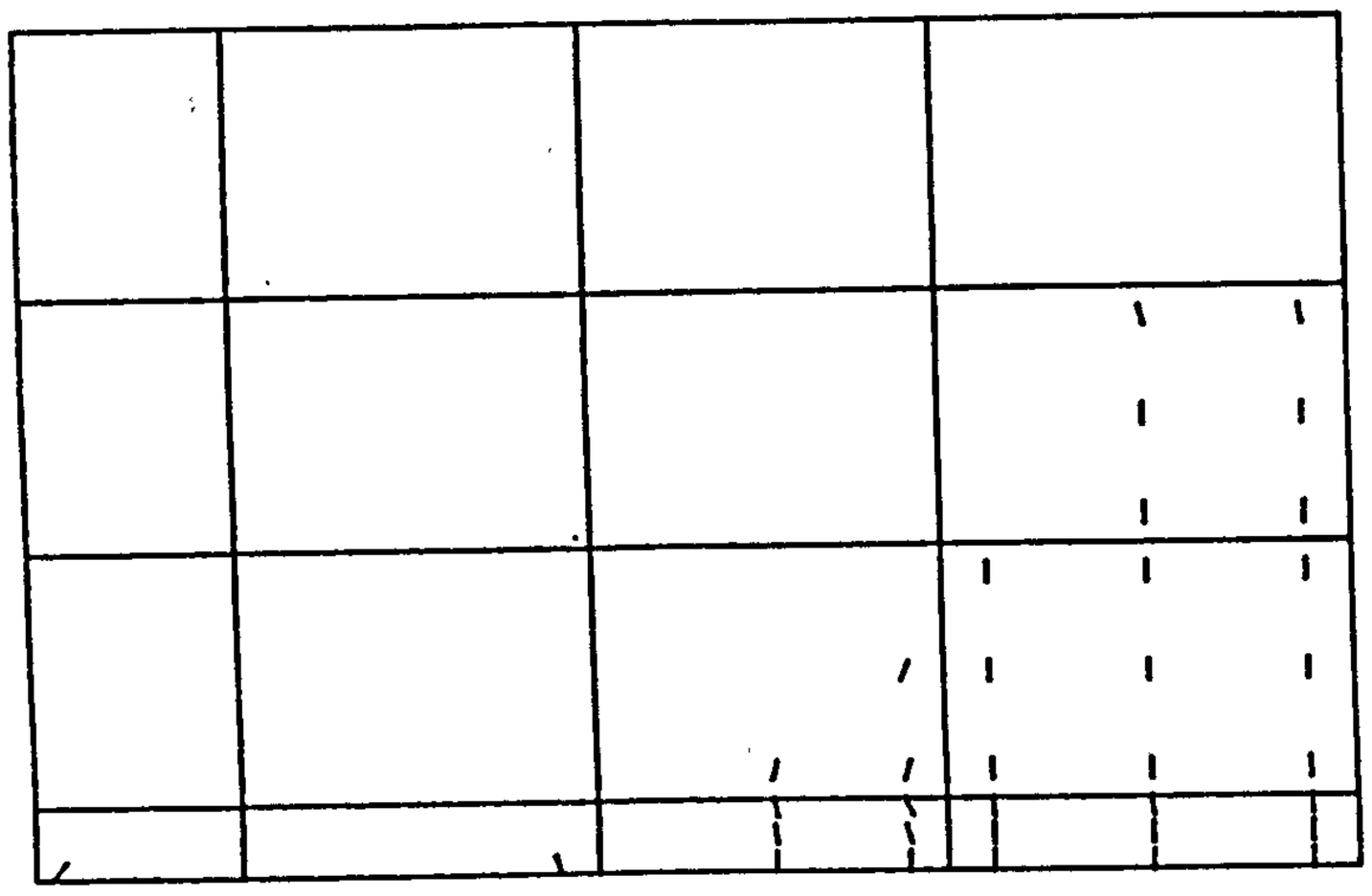

COOP = 5%

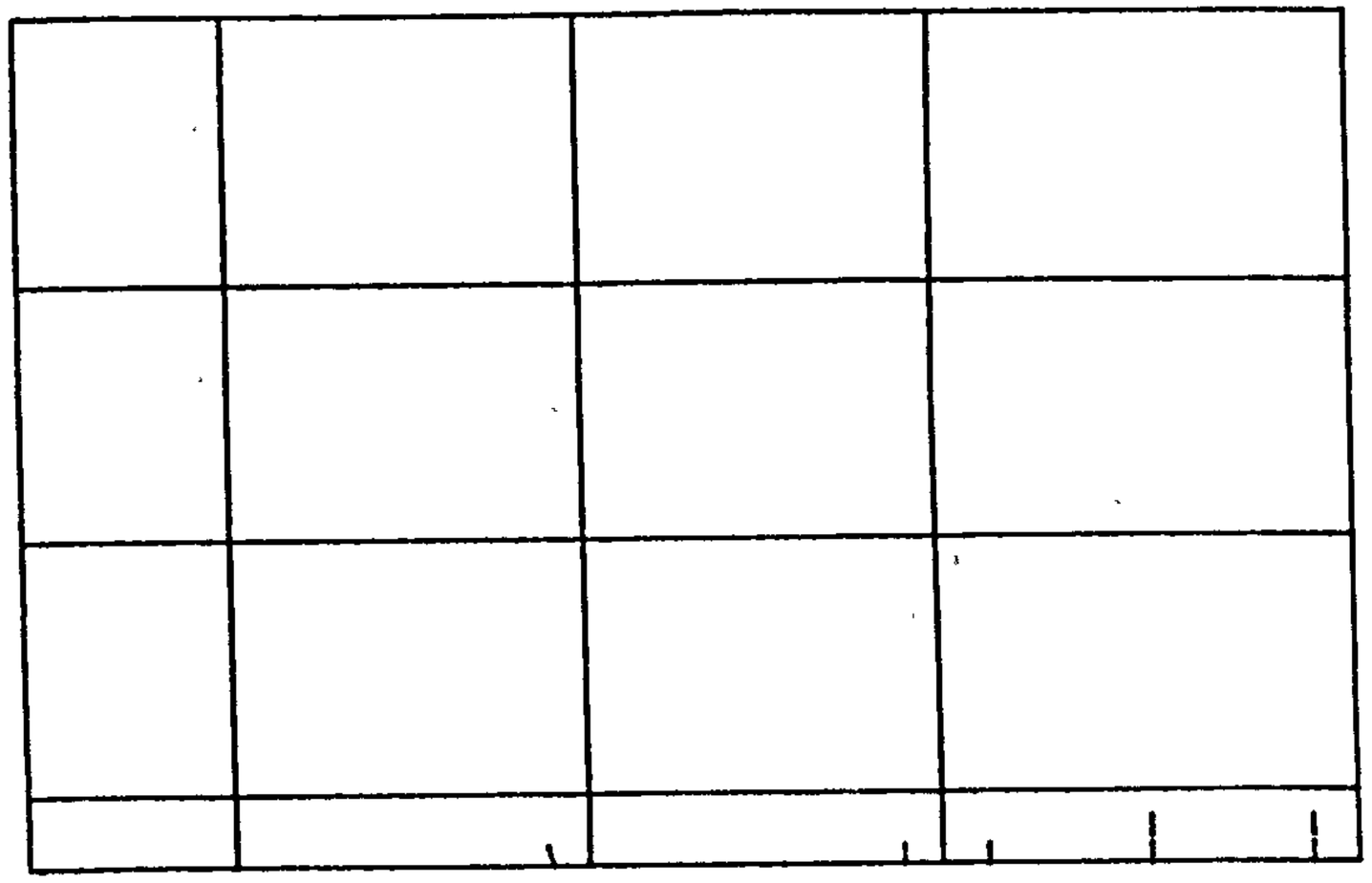

COOP = 15%

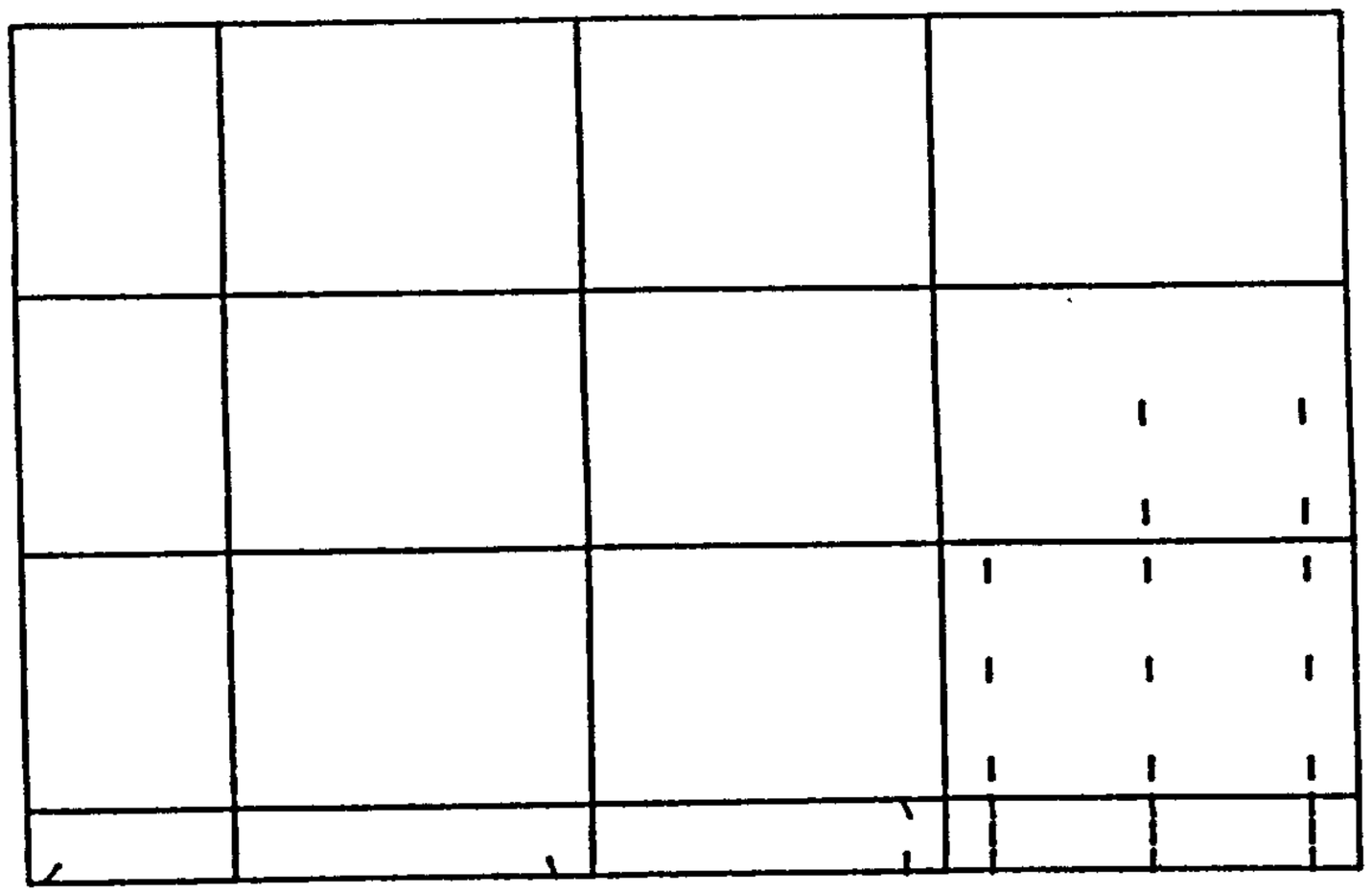

COOP = 10%

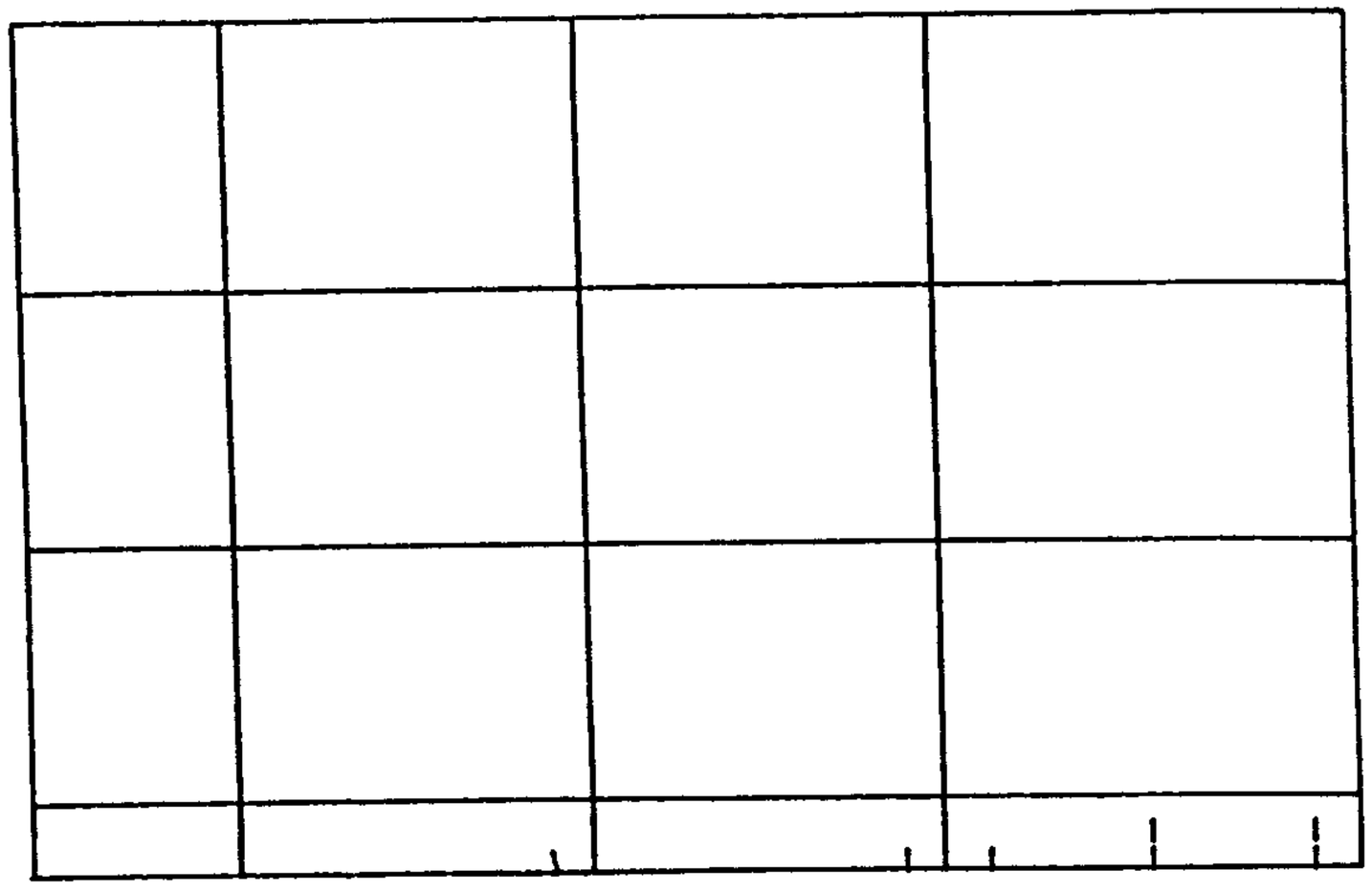

COOP = 20%

Figure (6.3) Crack patterns at load = 59·8 kN.

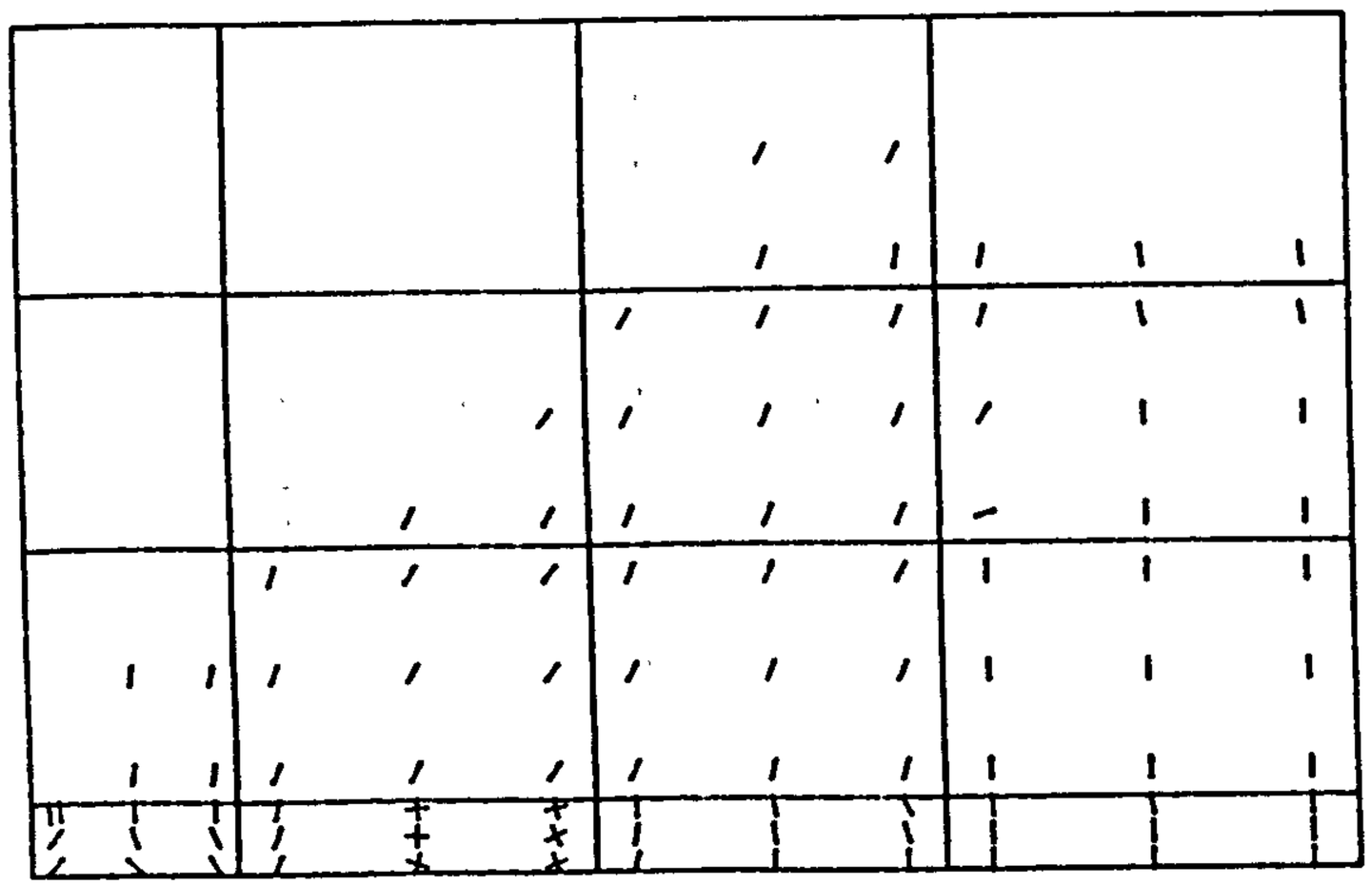

COOP = 5%

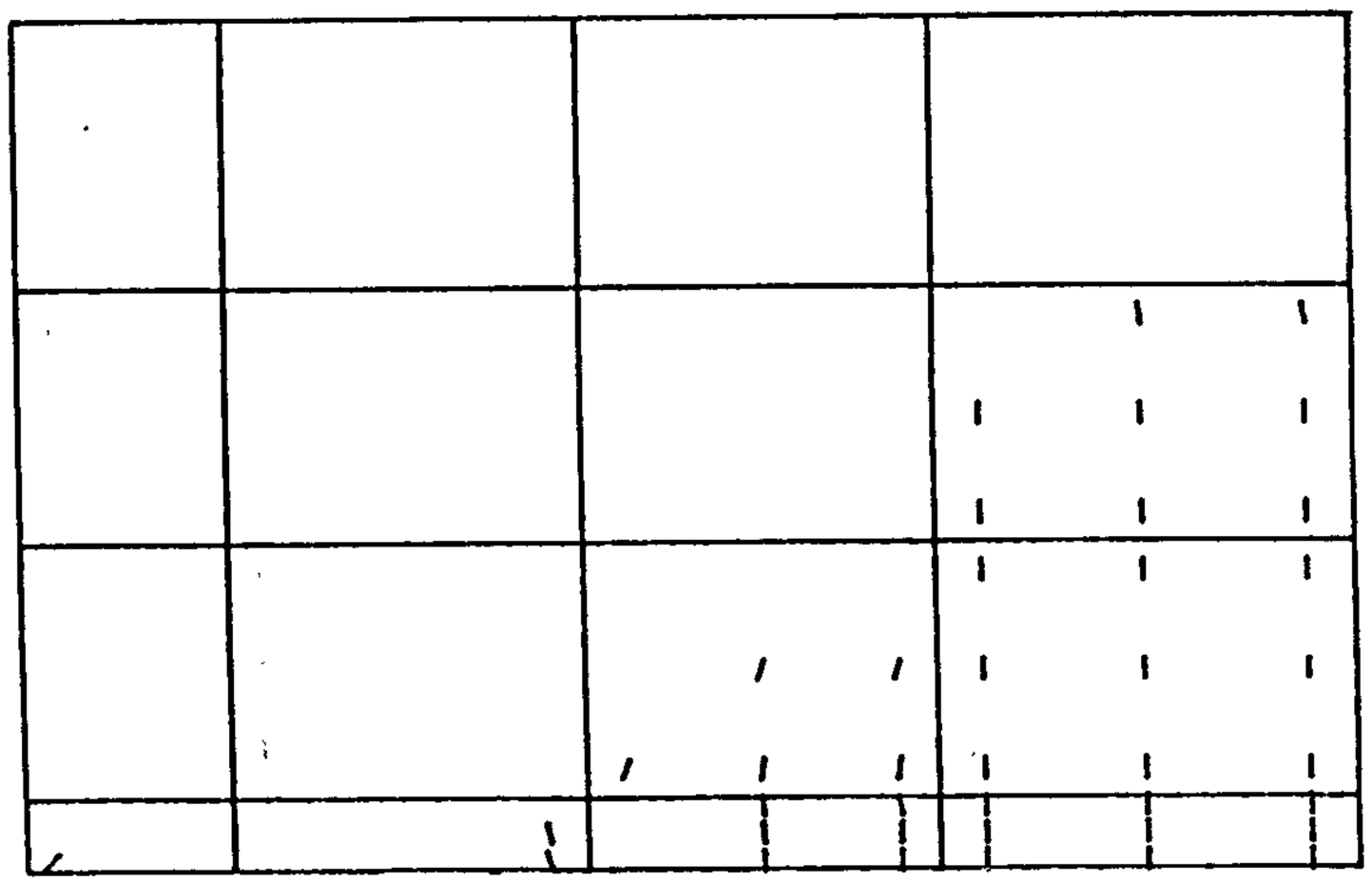

COOP = 15%

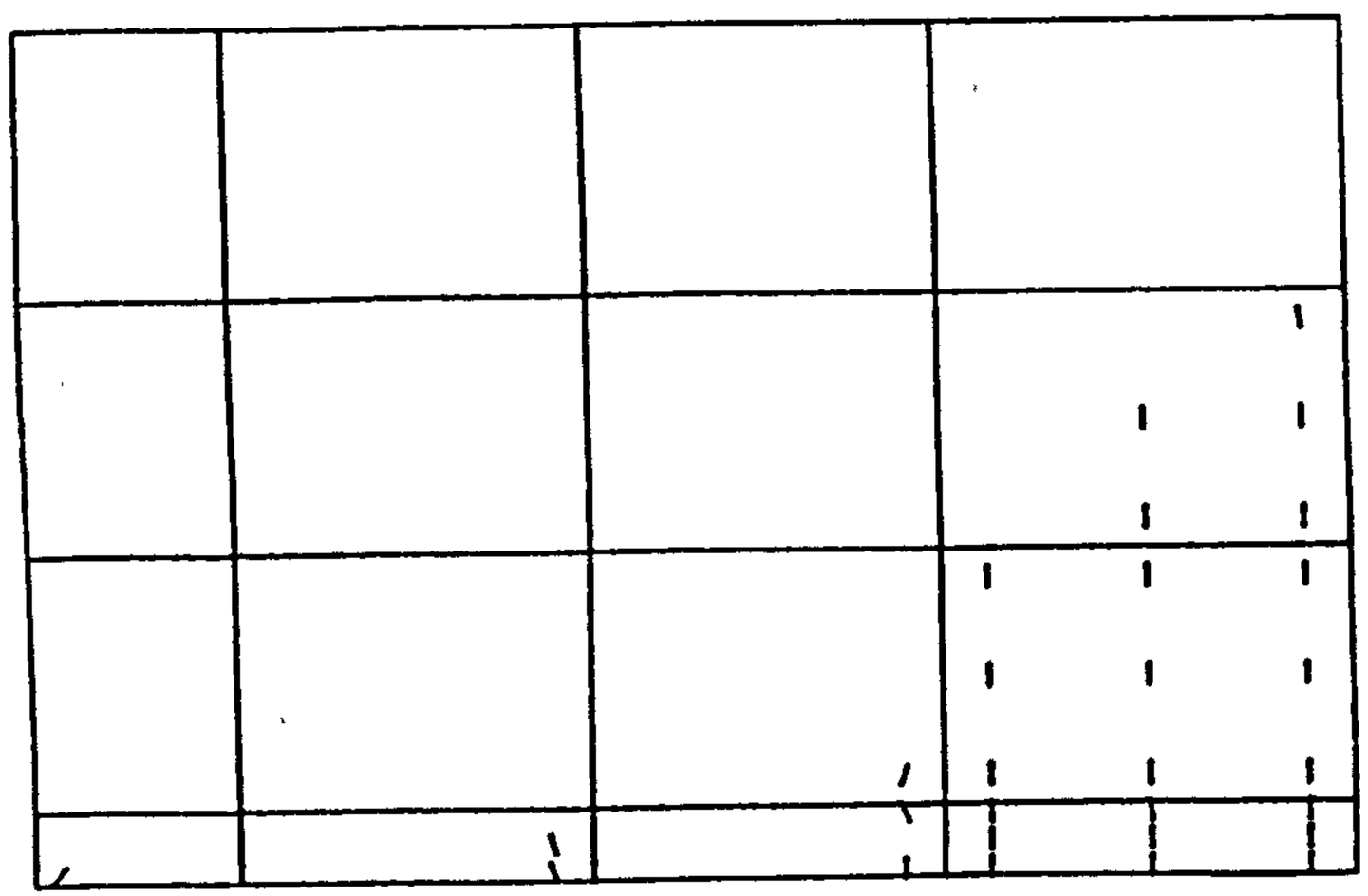

COOP = 10%

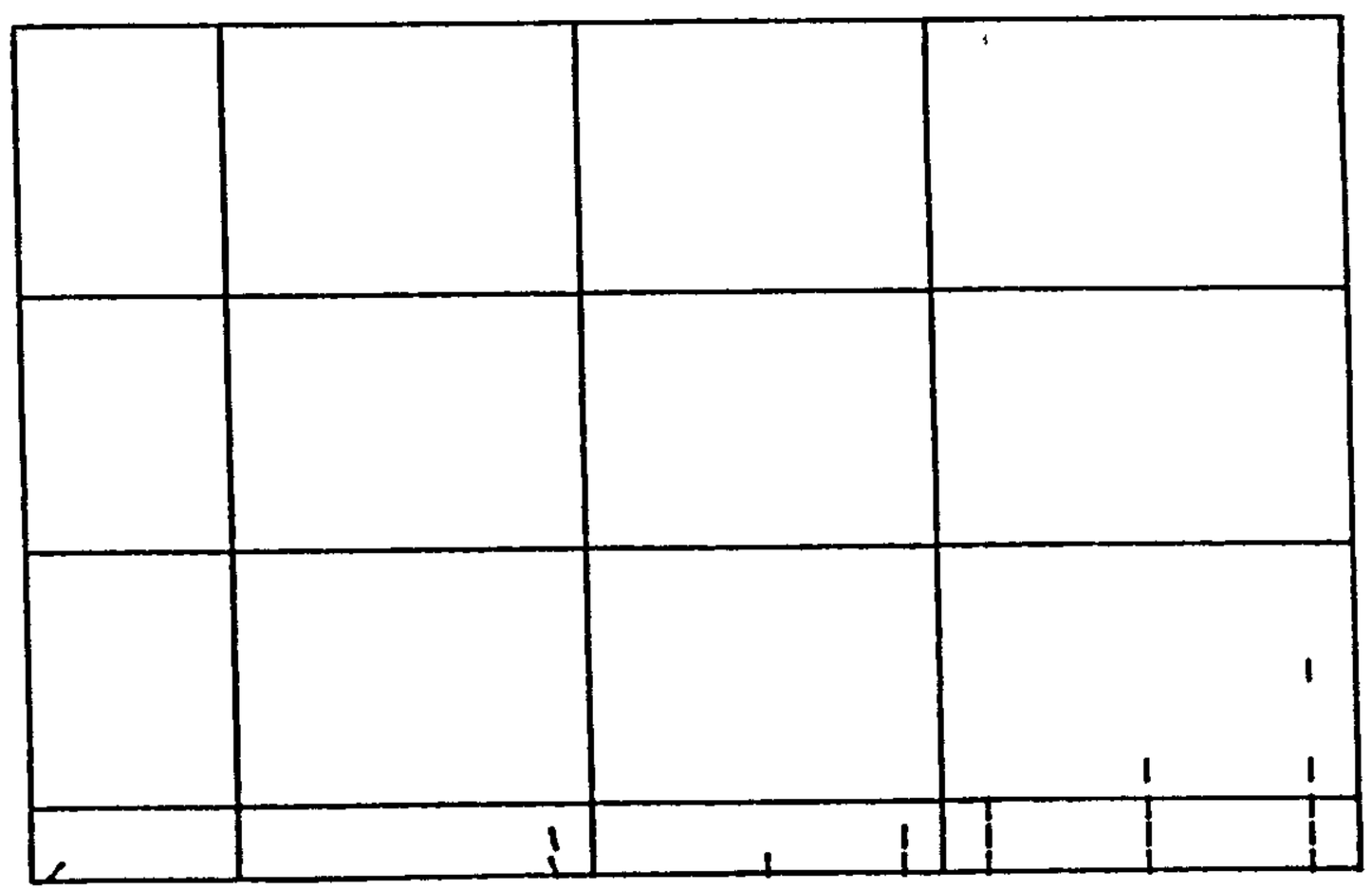

COOP = 20%

Figure (6•4) Crack patterns at load = 69•7 kN.

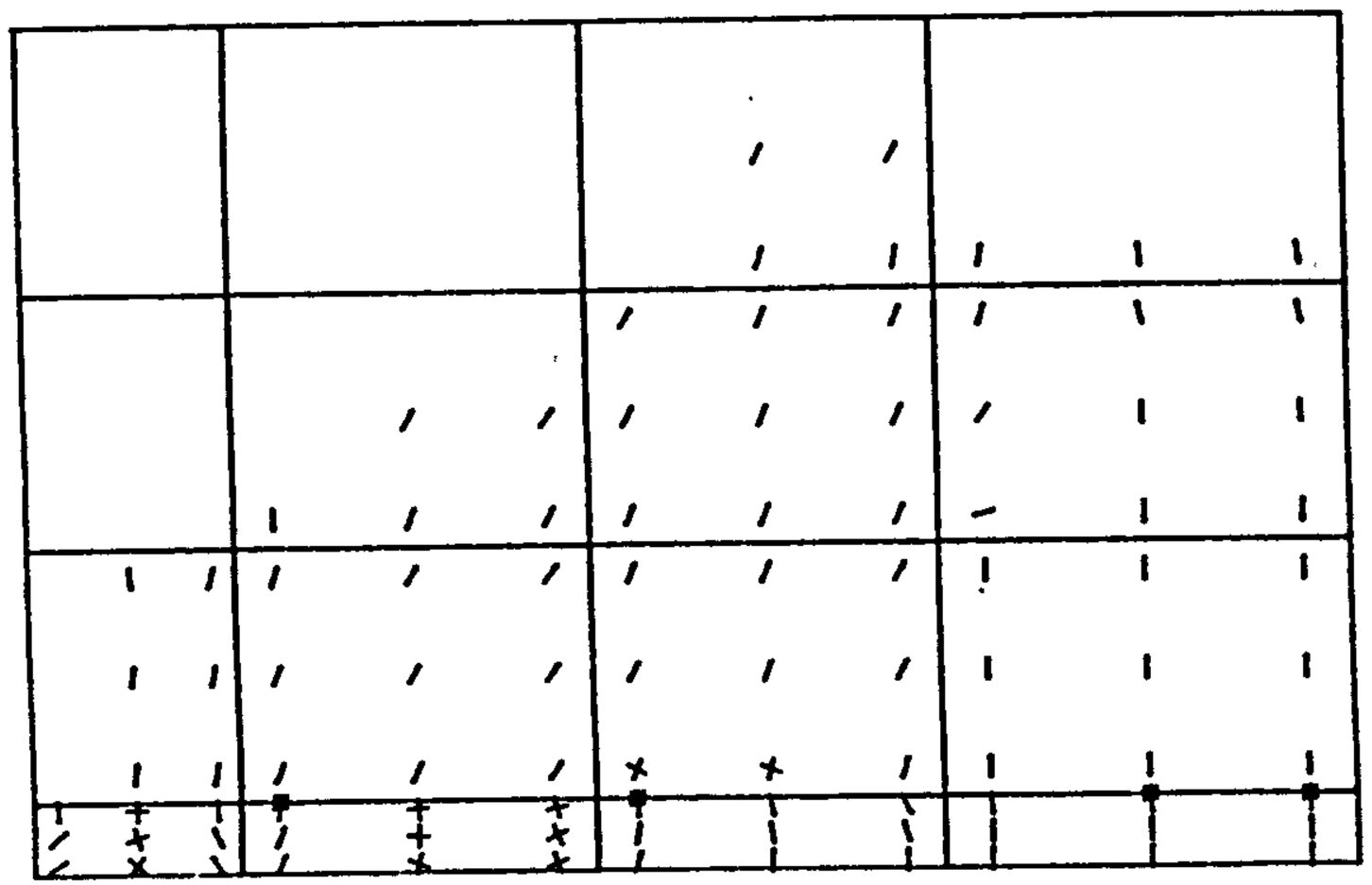

COOP = 5%

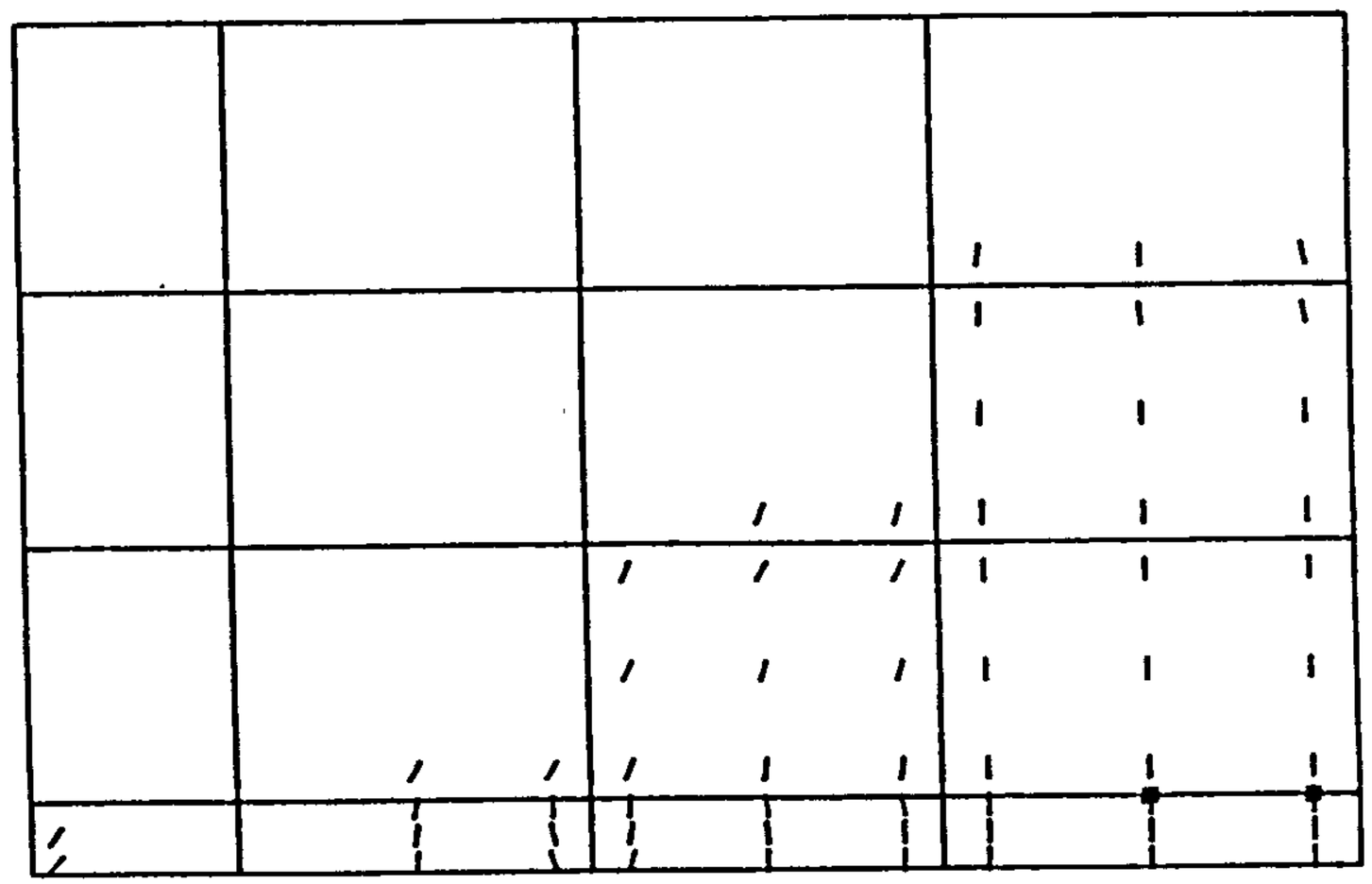

COOP = 15%

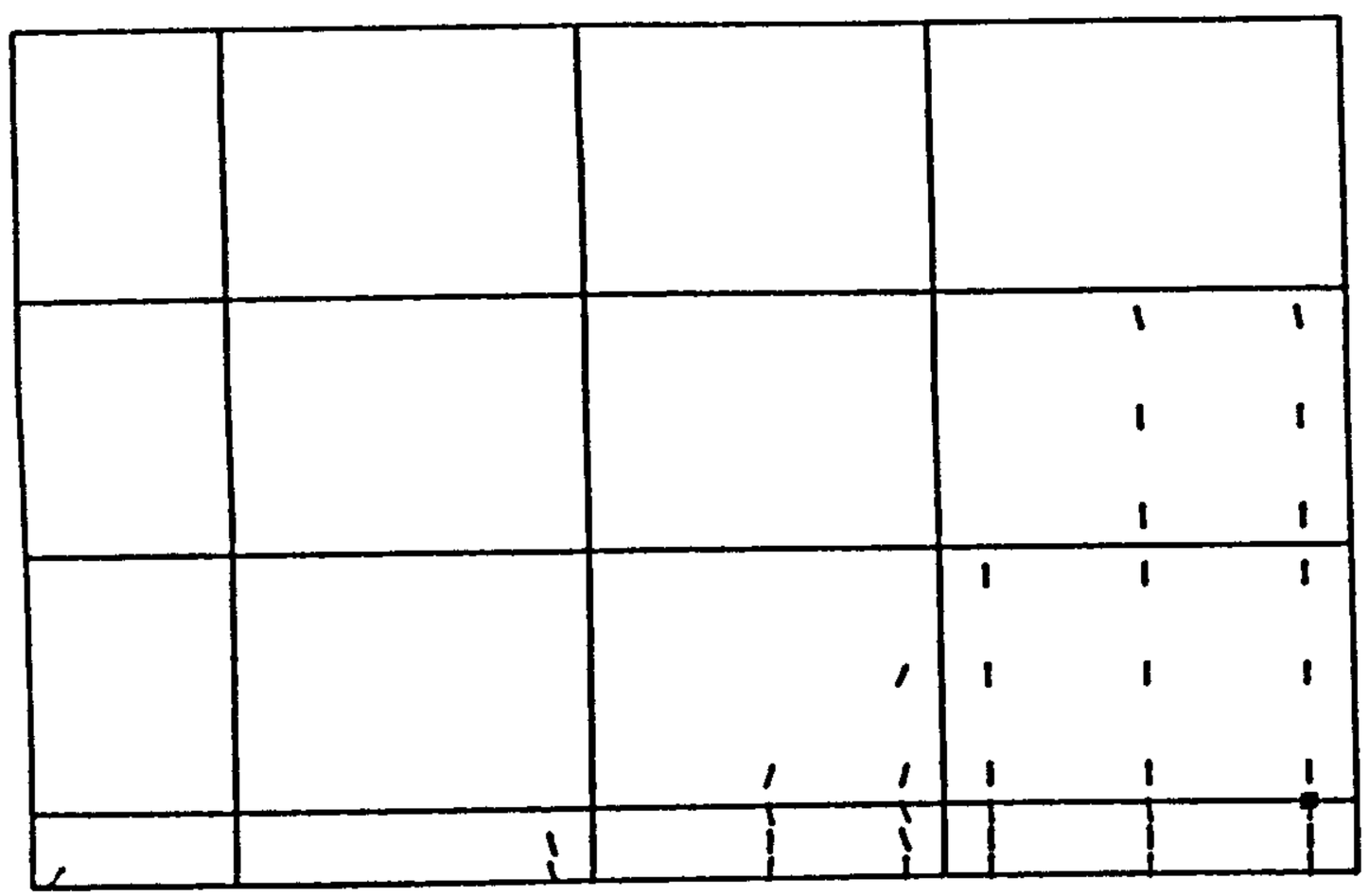

COOP = 10%

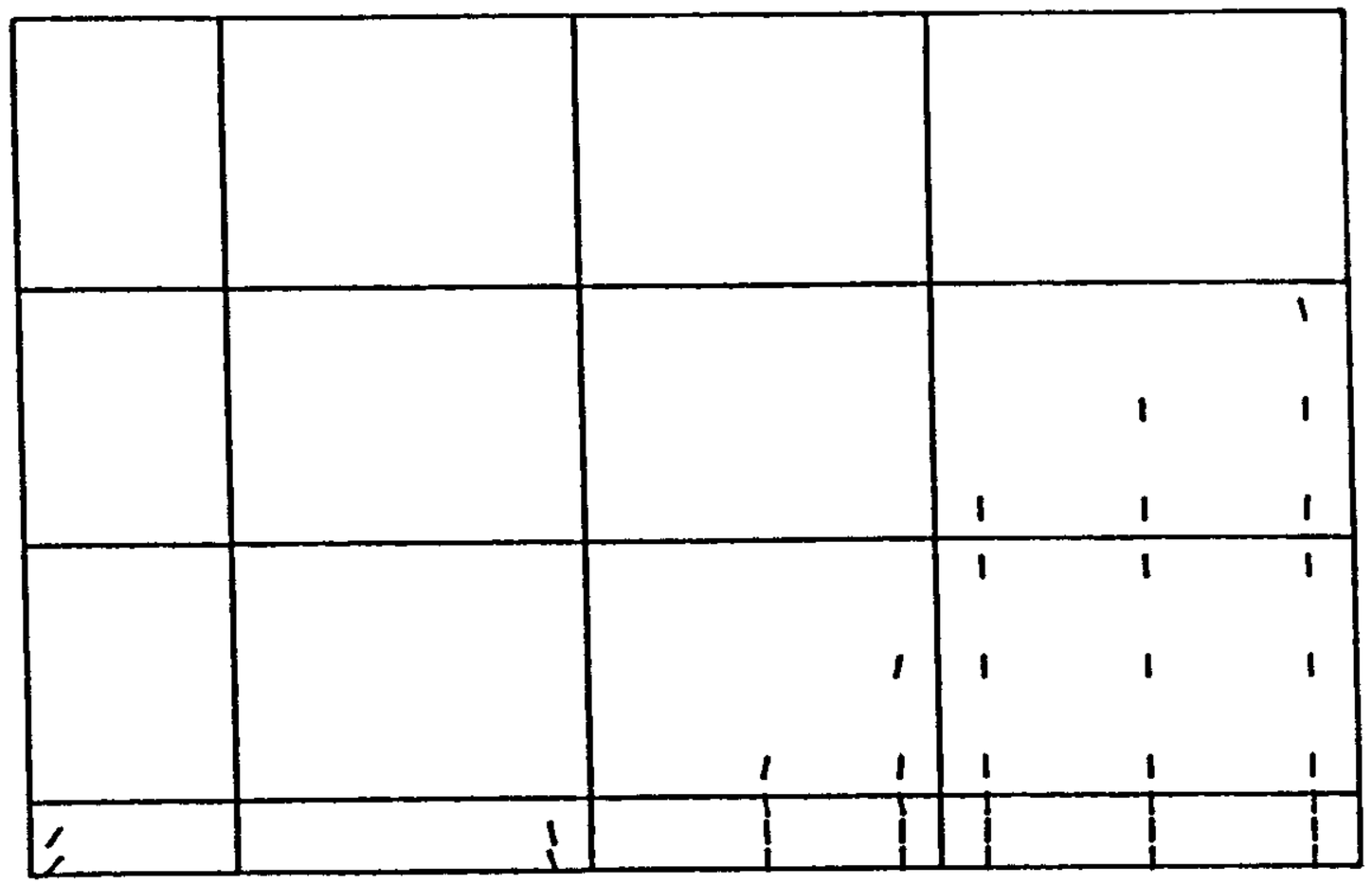

COOP = 20%

Figure (6·5) Crack patterns at load = 79·7 kN.

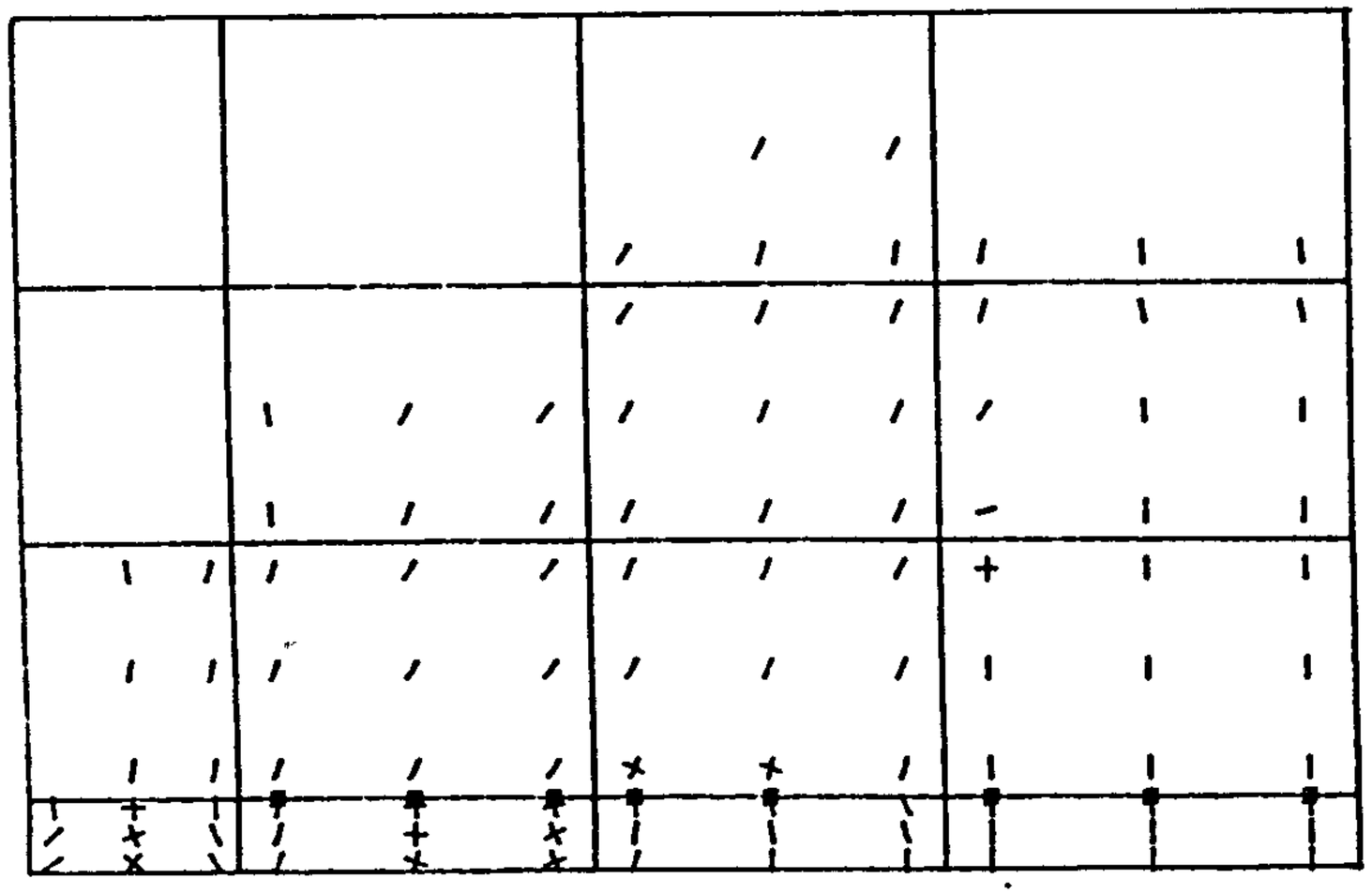

COOP = 5%

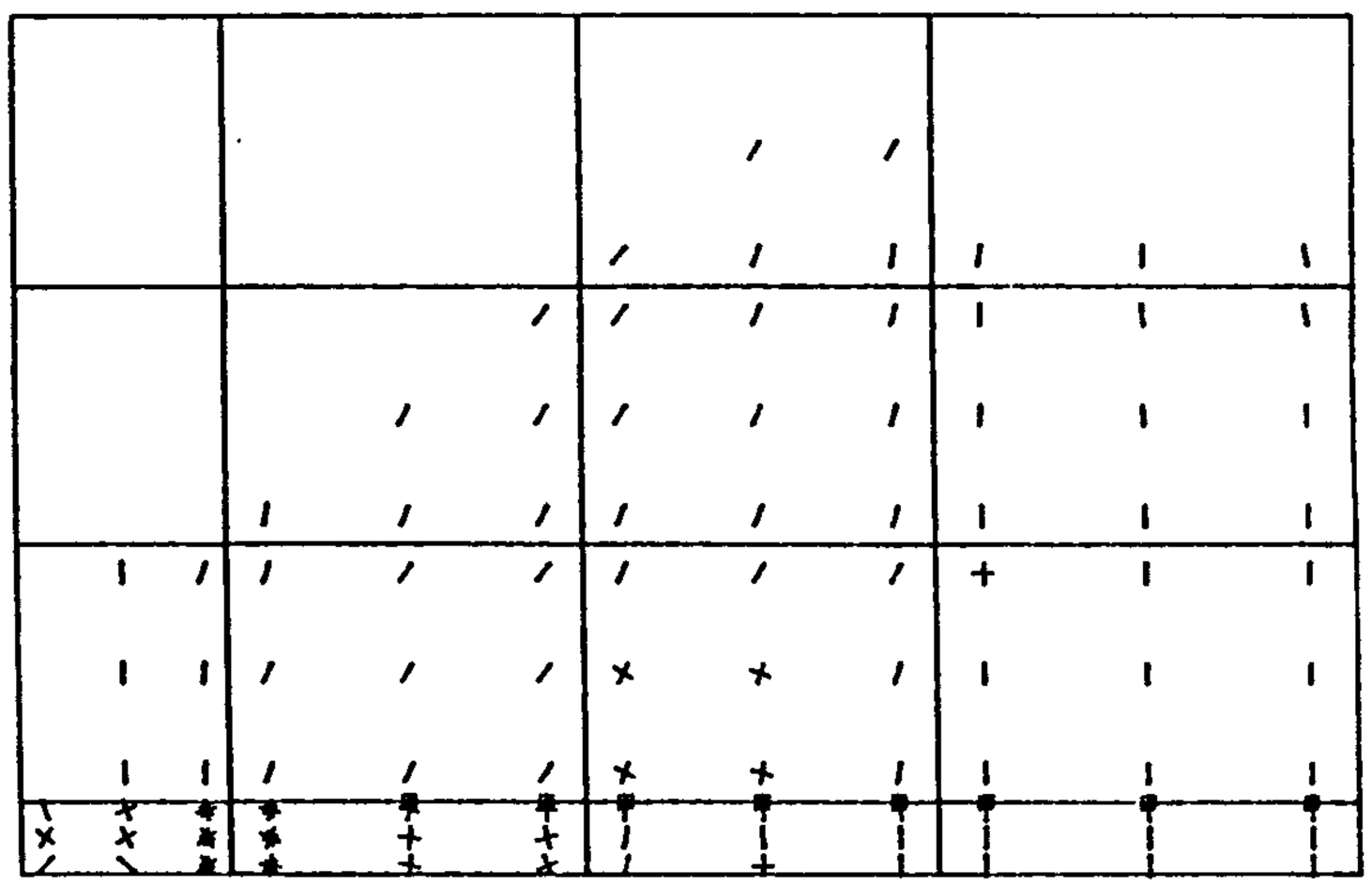

COOP = 15%

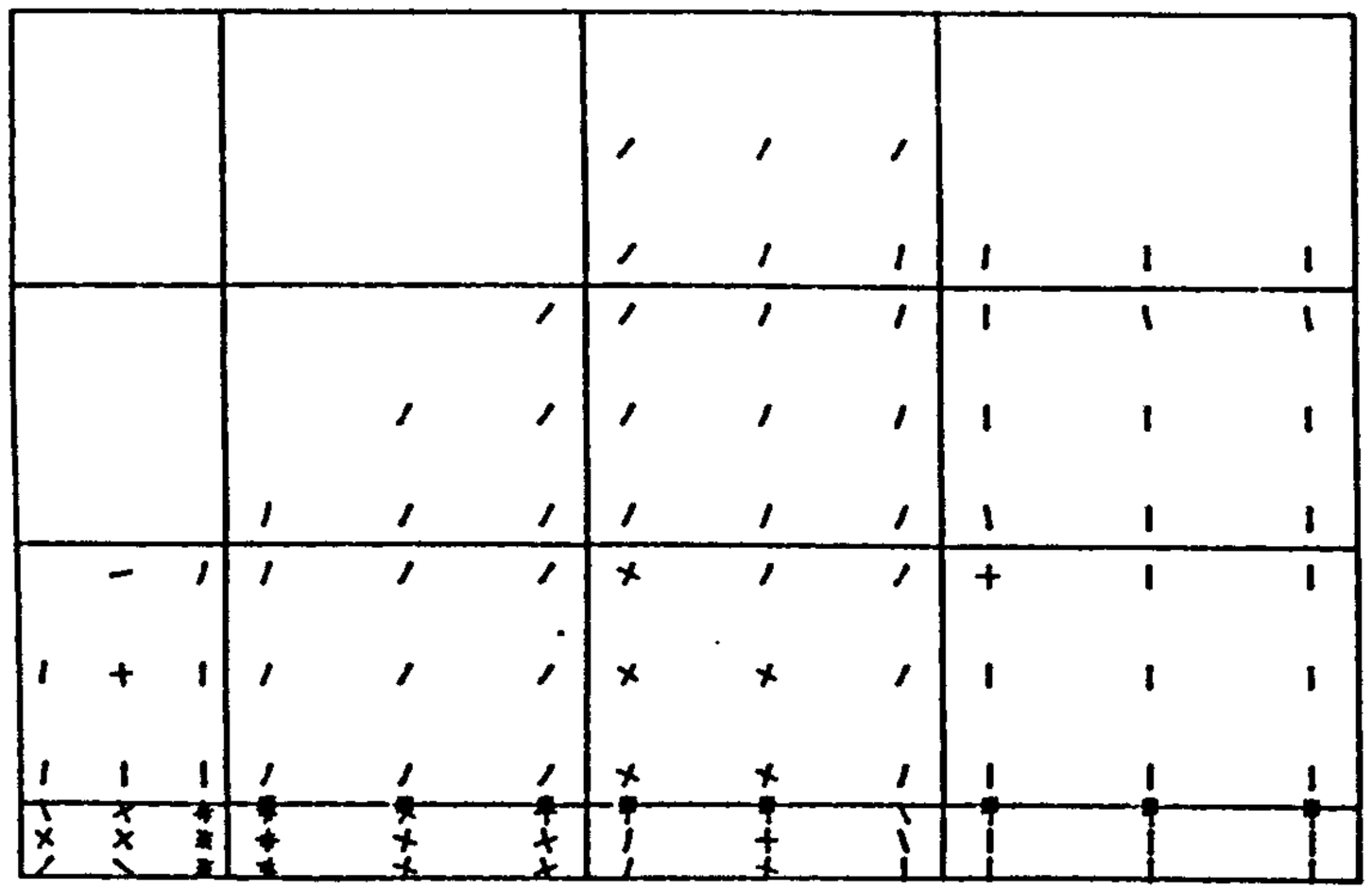

COOP = 10%

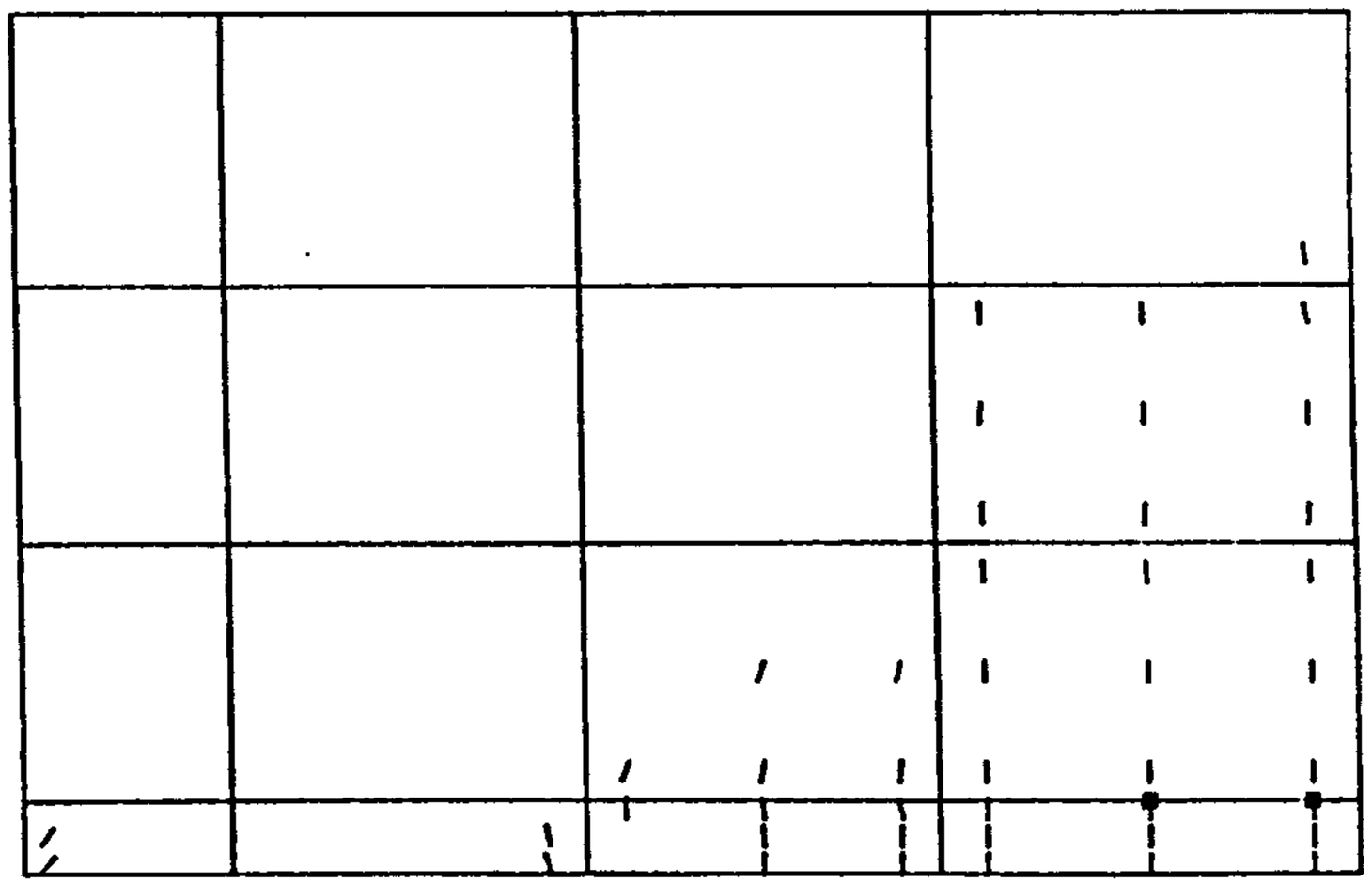

COOP = 20%

Figure (6·6) Crack patterns at load = 89·6 kN.

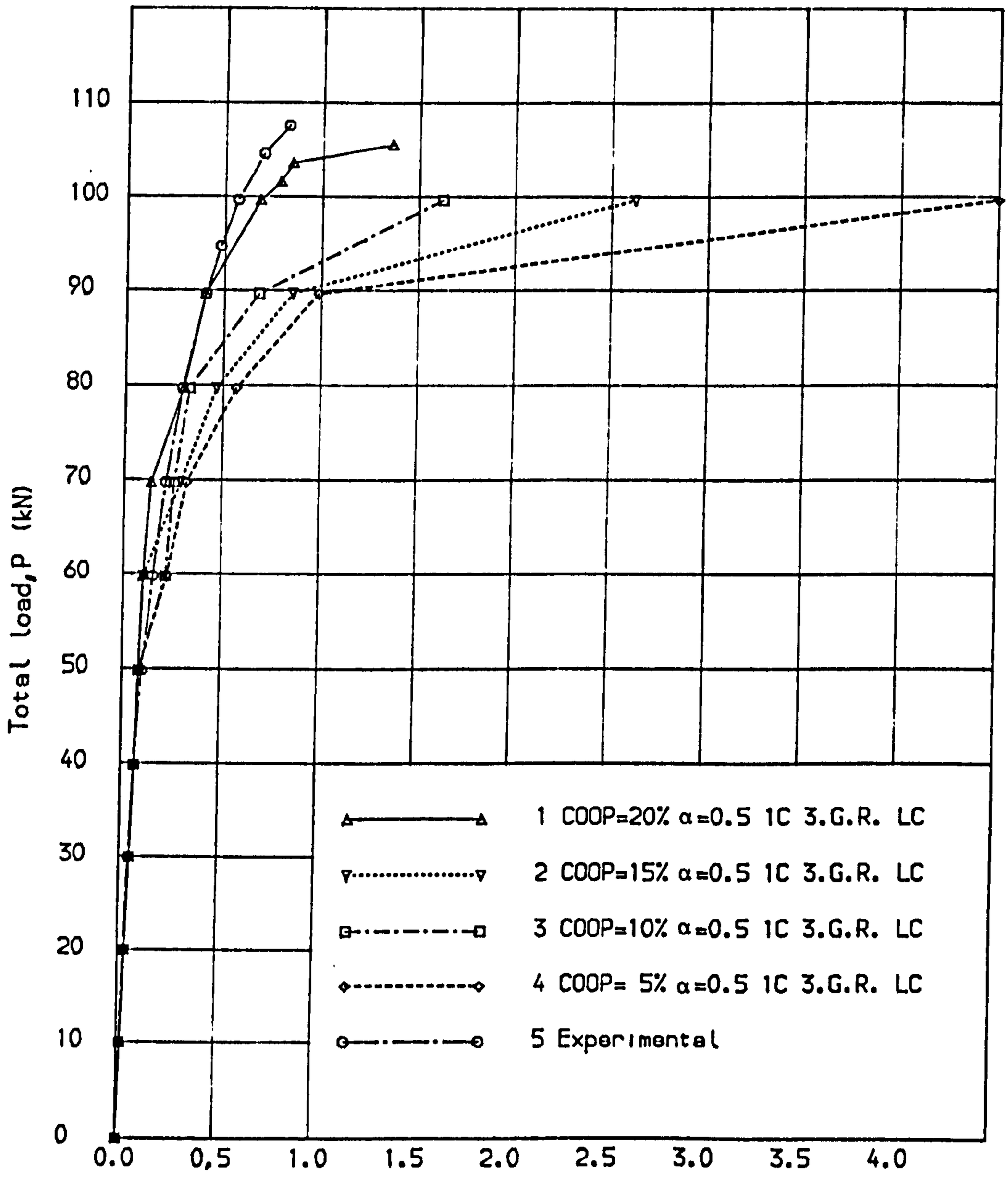

Fig. (6.7) Load deflection curves for deep beam, (V.S.M.1).

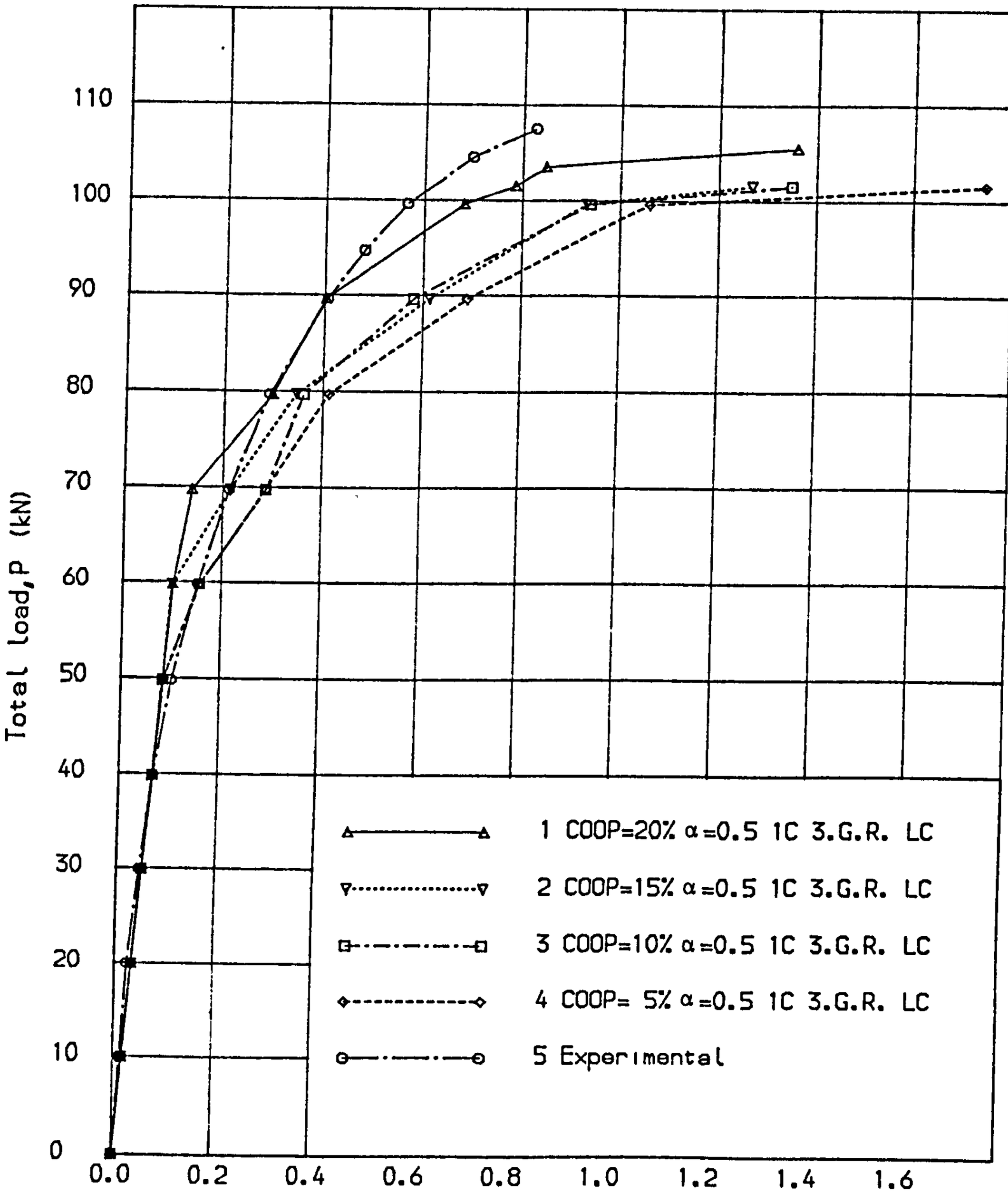

Fig. (6.8) Load deflection curves for deep beam, (V.S.M.1).

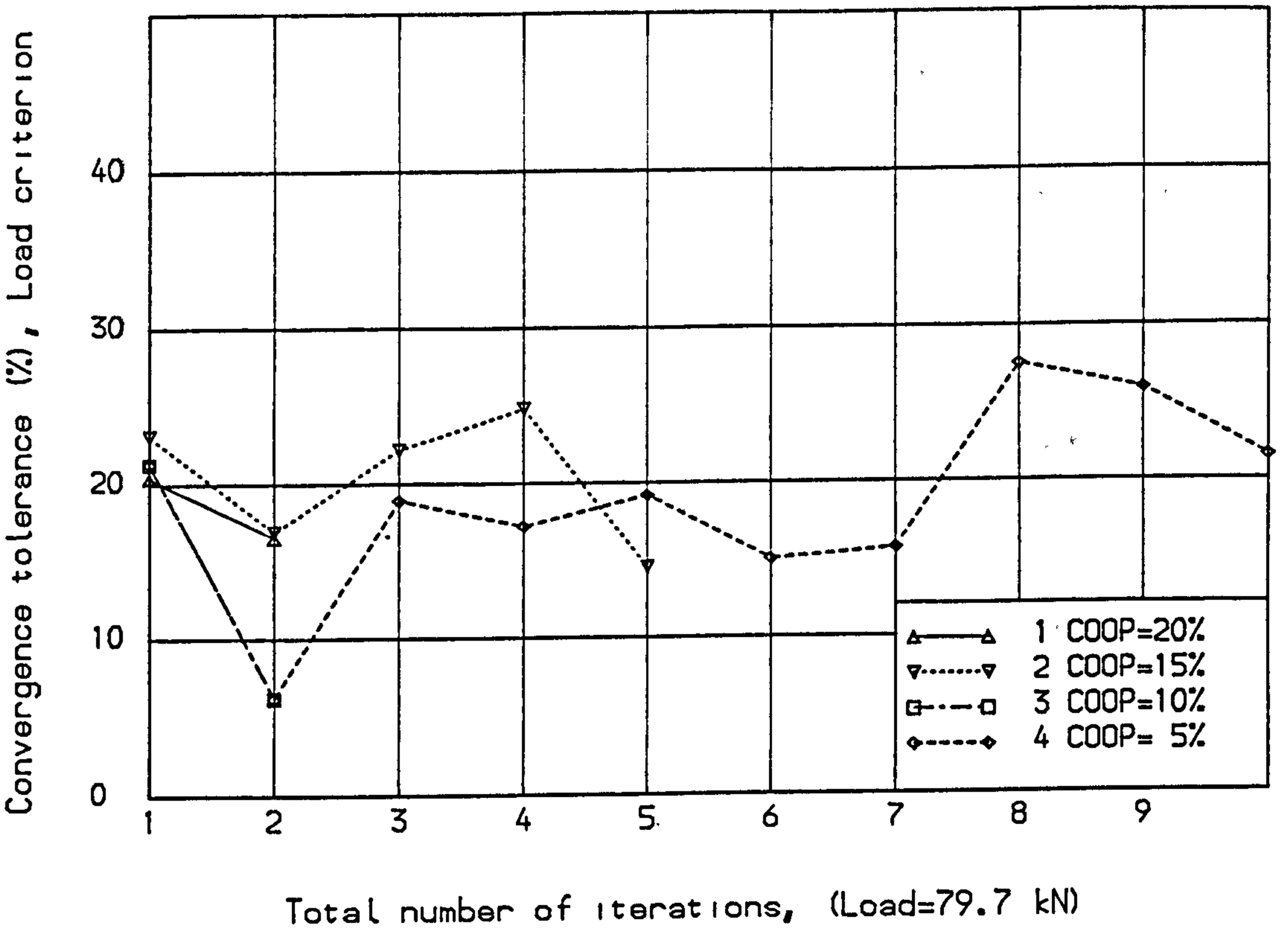

Fig. (6,9) Convergence and number of iterations (Max.=10).

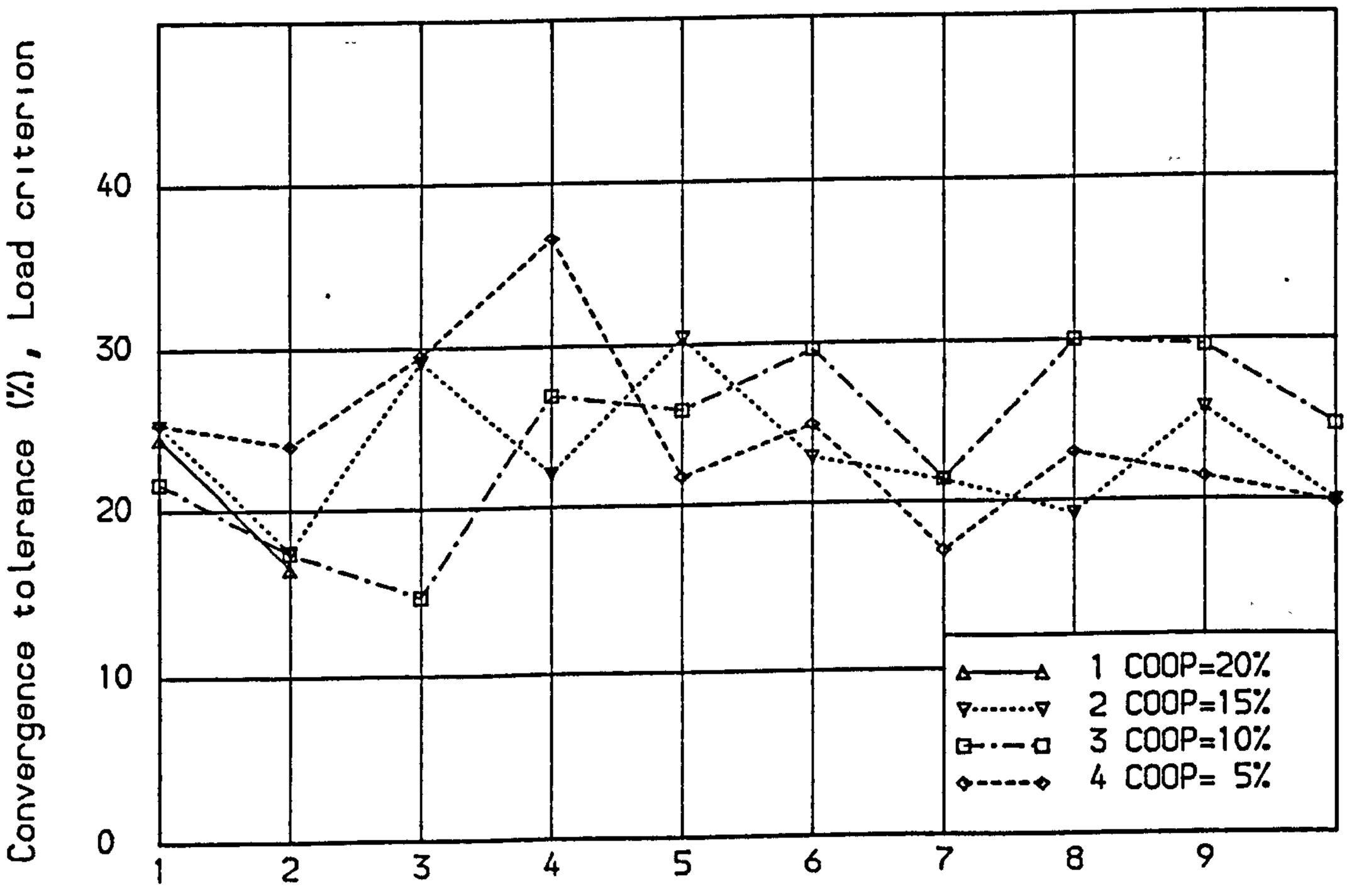

Fig. (6,10) Convergence and number of iterations (Max.=10).

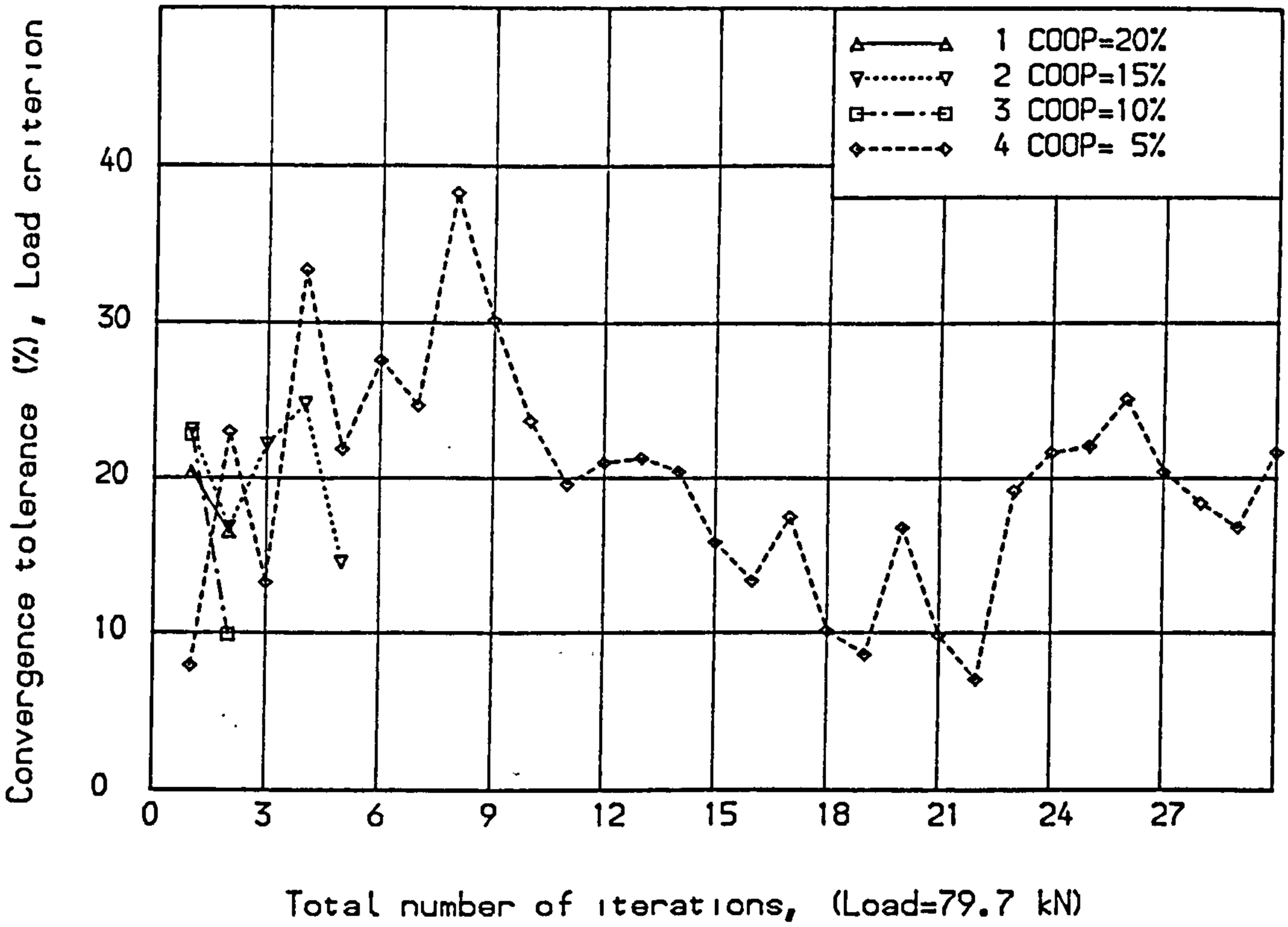

Fig. (6,11) Convergence and number of iterations (Max.=30).

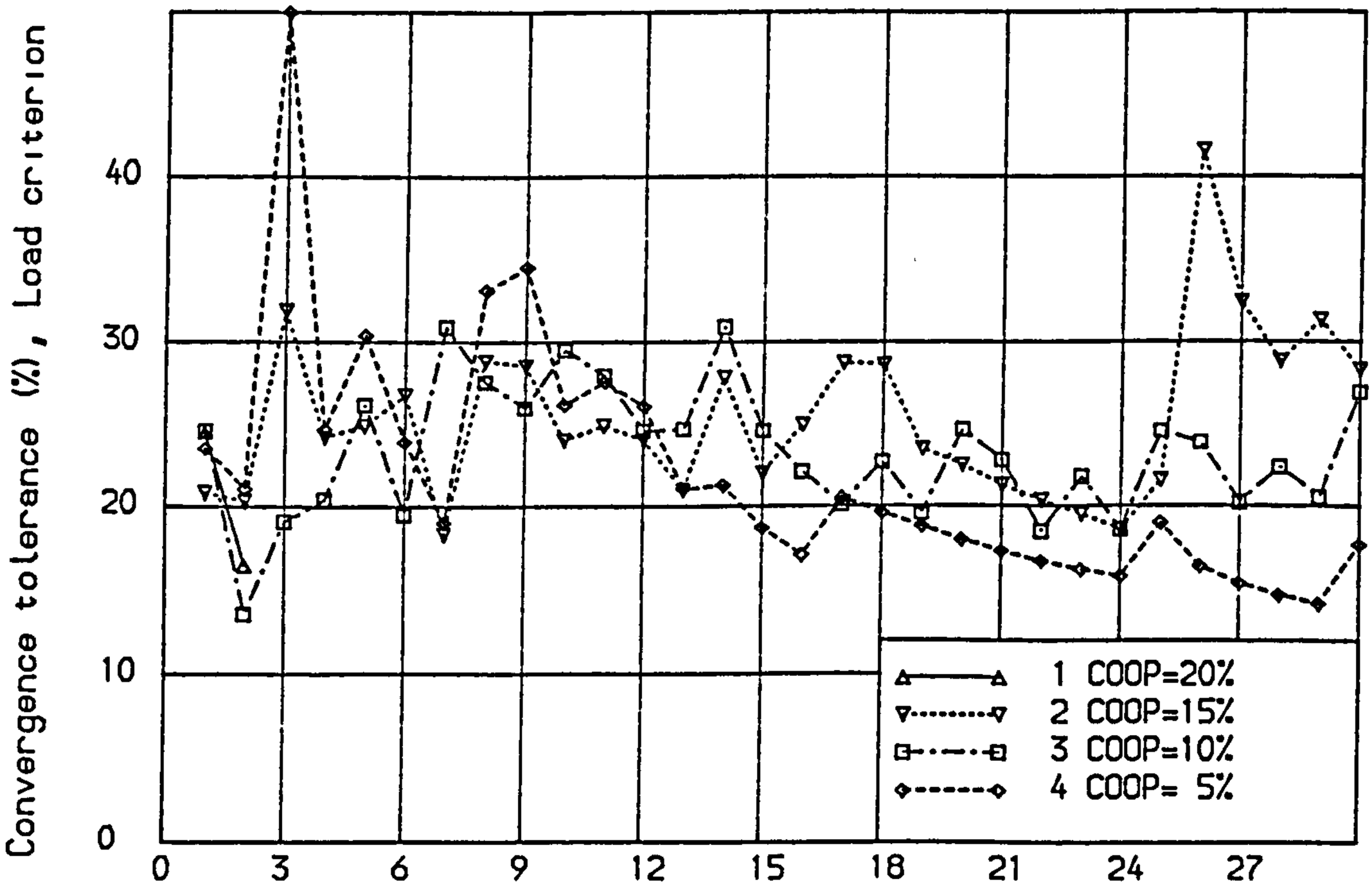

Fig. (6,12) Convergence and number of iterations (Max.=30).

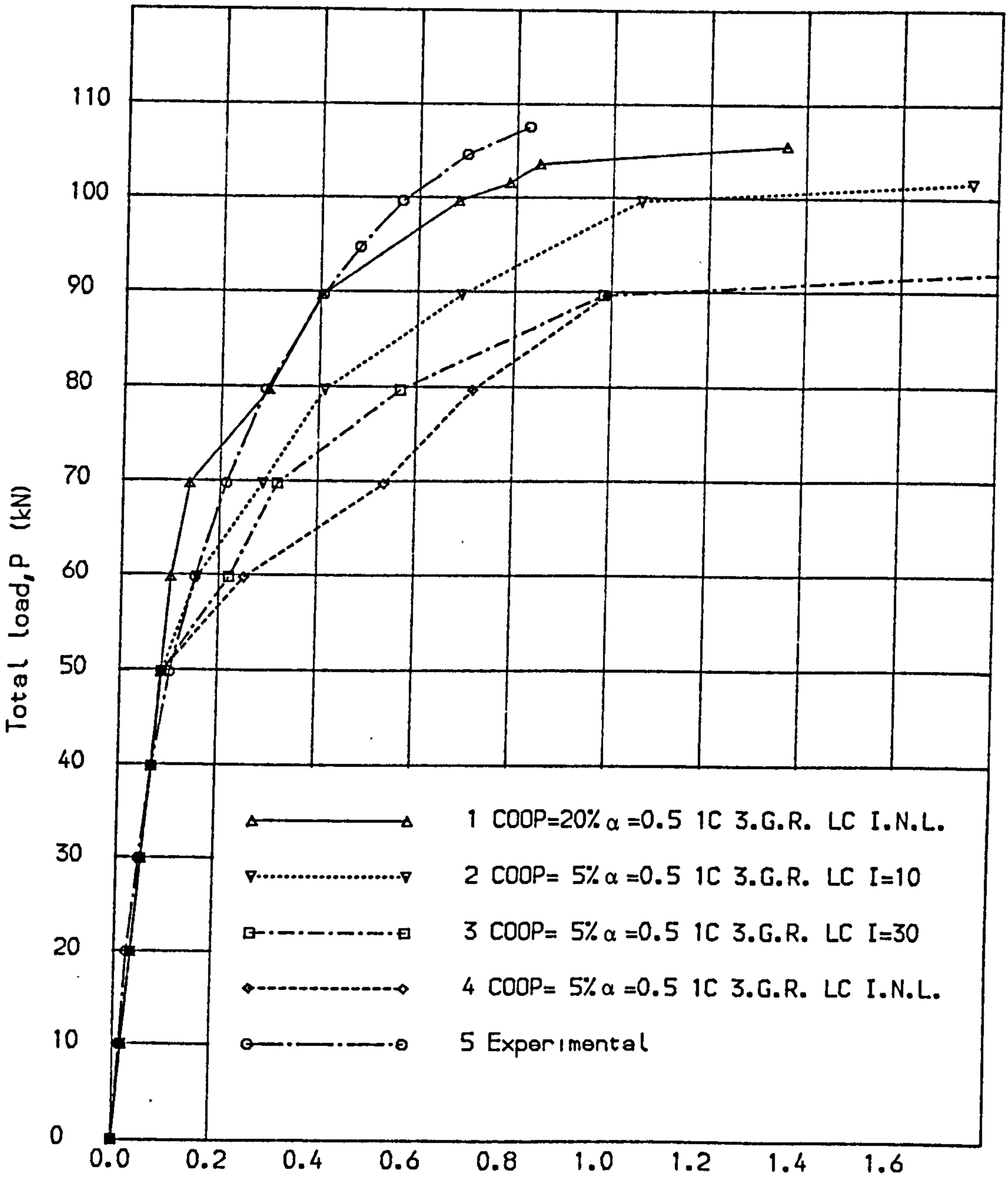

Fig. (6.13) Load deflection curves for deep beam, (V.S.M.1).

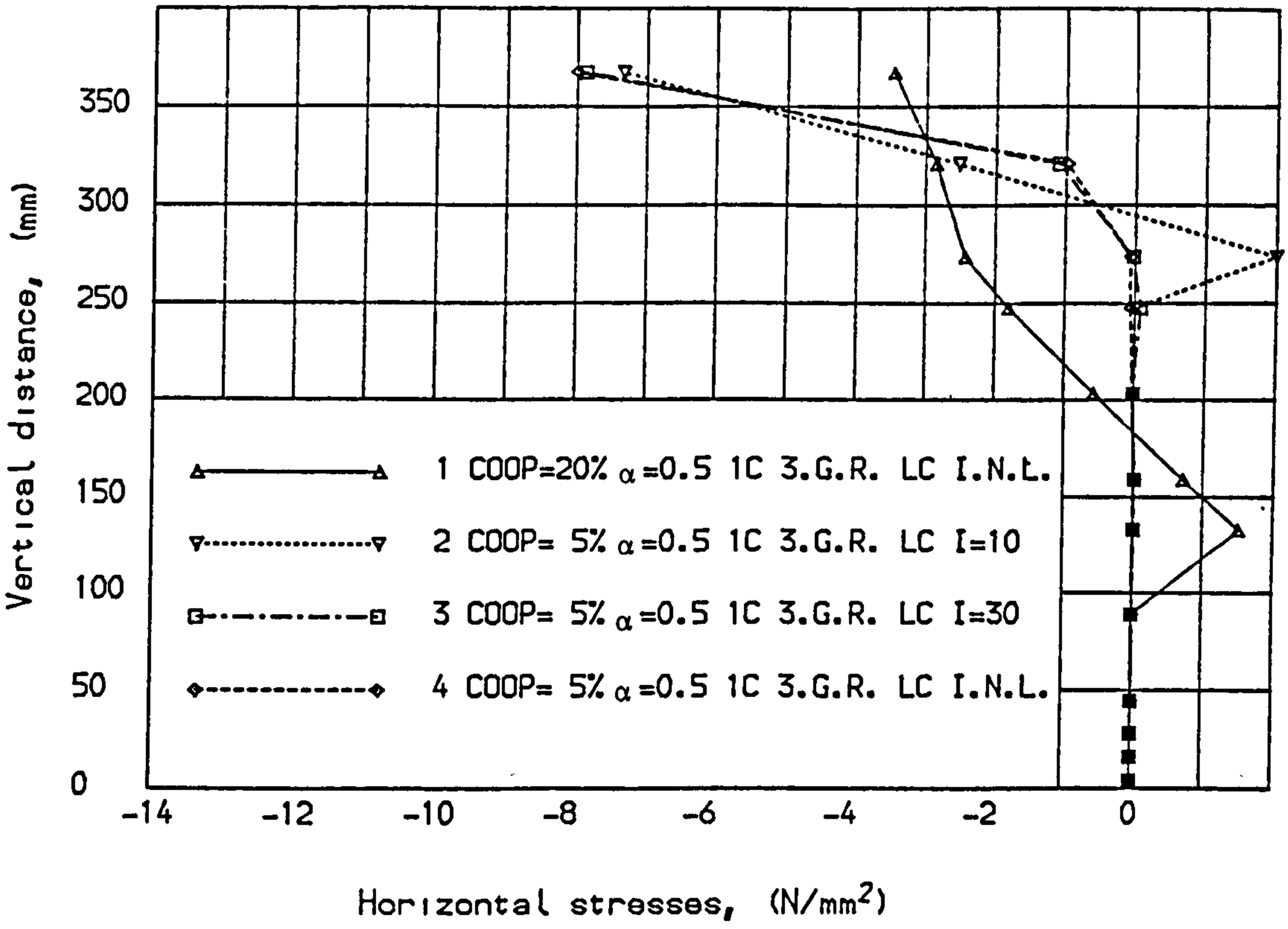

Fig. (6.14) Stress distribution at midspan section, (89.6 kN).

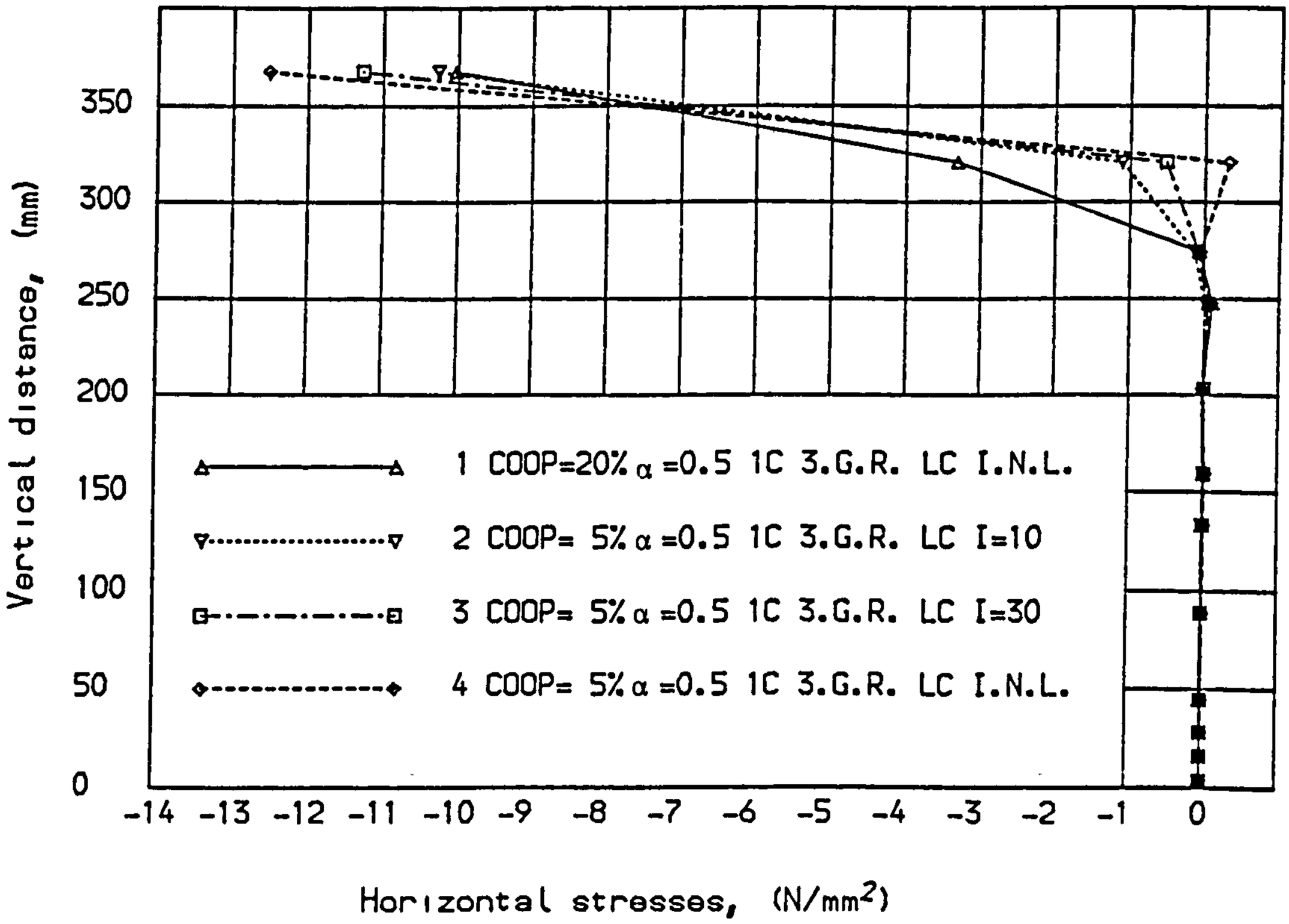

Fig. (6.15) Stress distribution at midspan section, (89.6 kN).

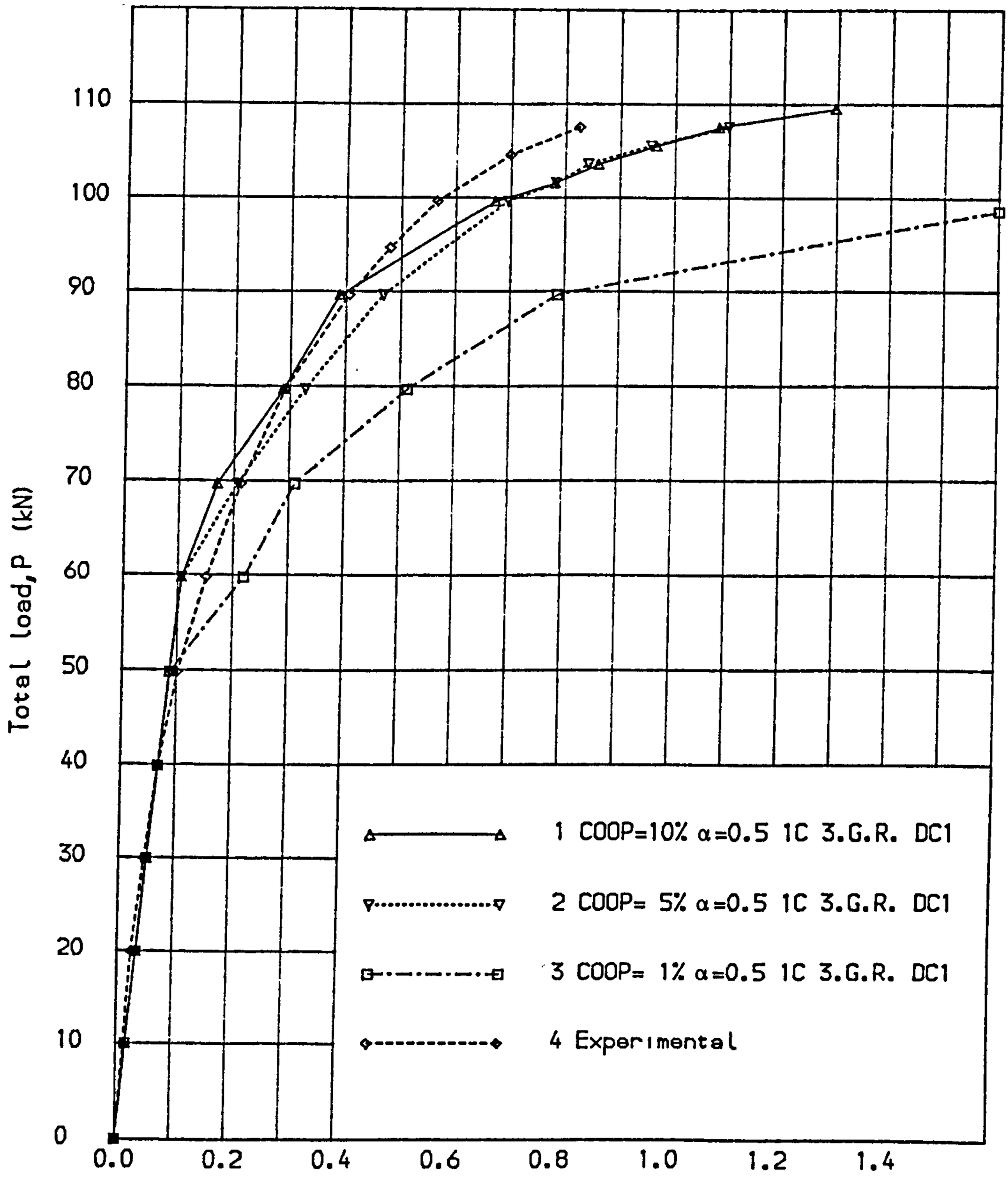

Fig. (6.16) Load deflection curves for deep beam, (V.S.M.1).

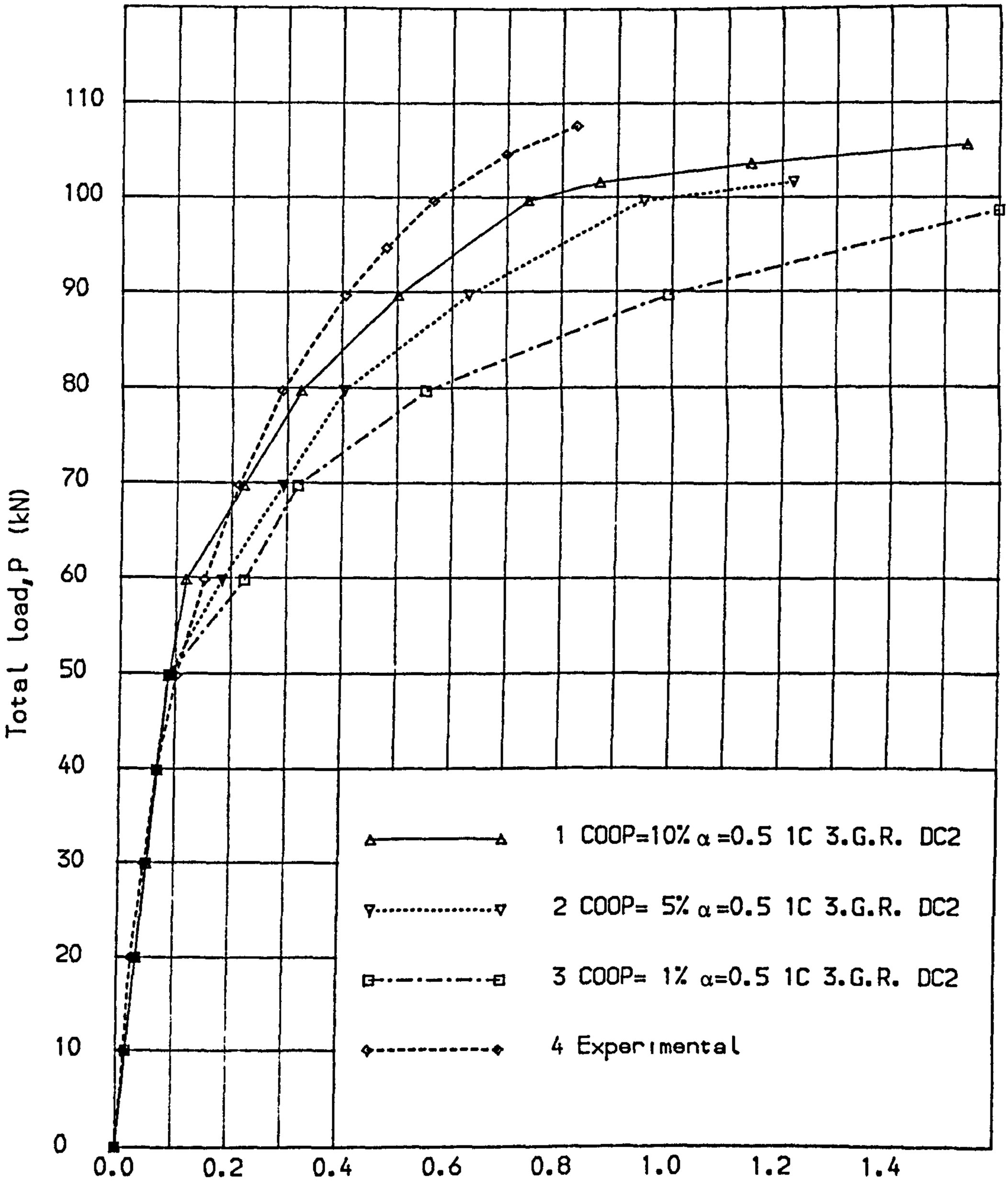

Fig. (6.17) Load deflection curves for deep beam, (V.S.M.1).

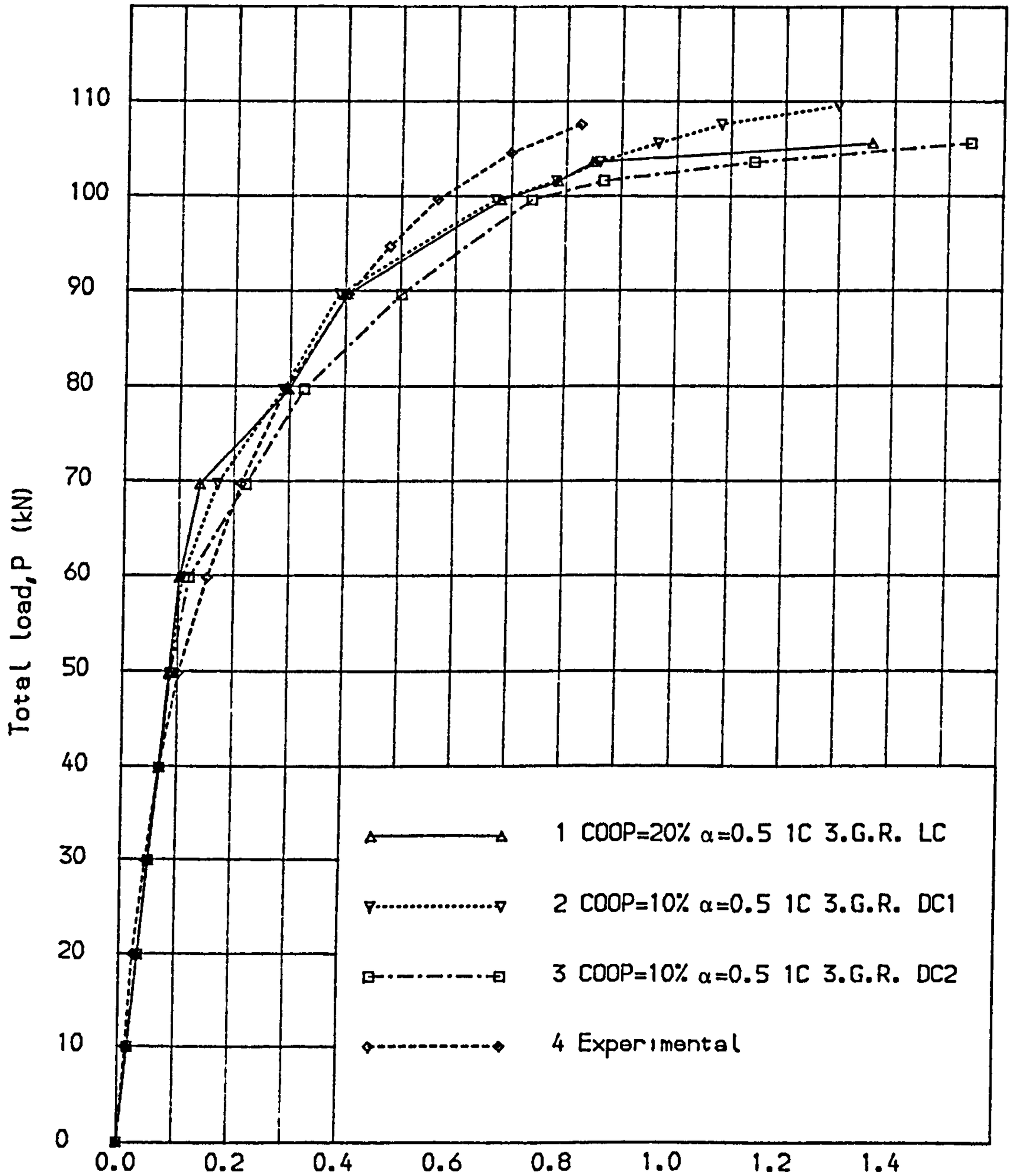

Fig. (6.18) Load deflection curves for deep beam, (V.S.M.1).

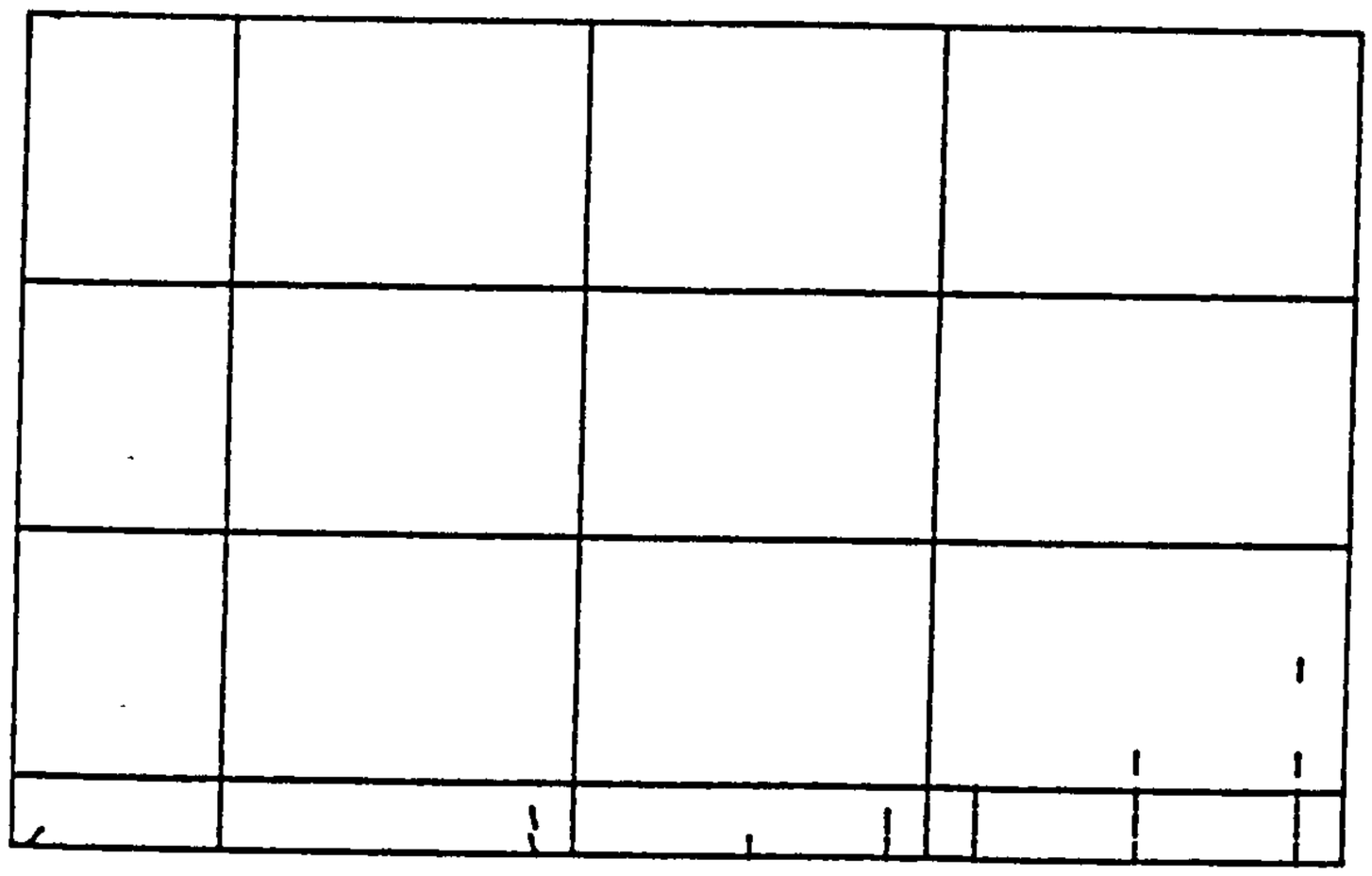

Load criterion, COOP = 20%

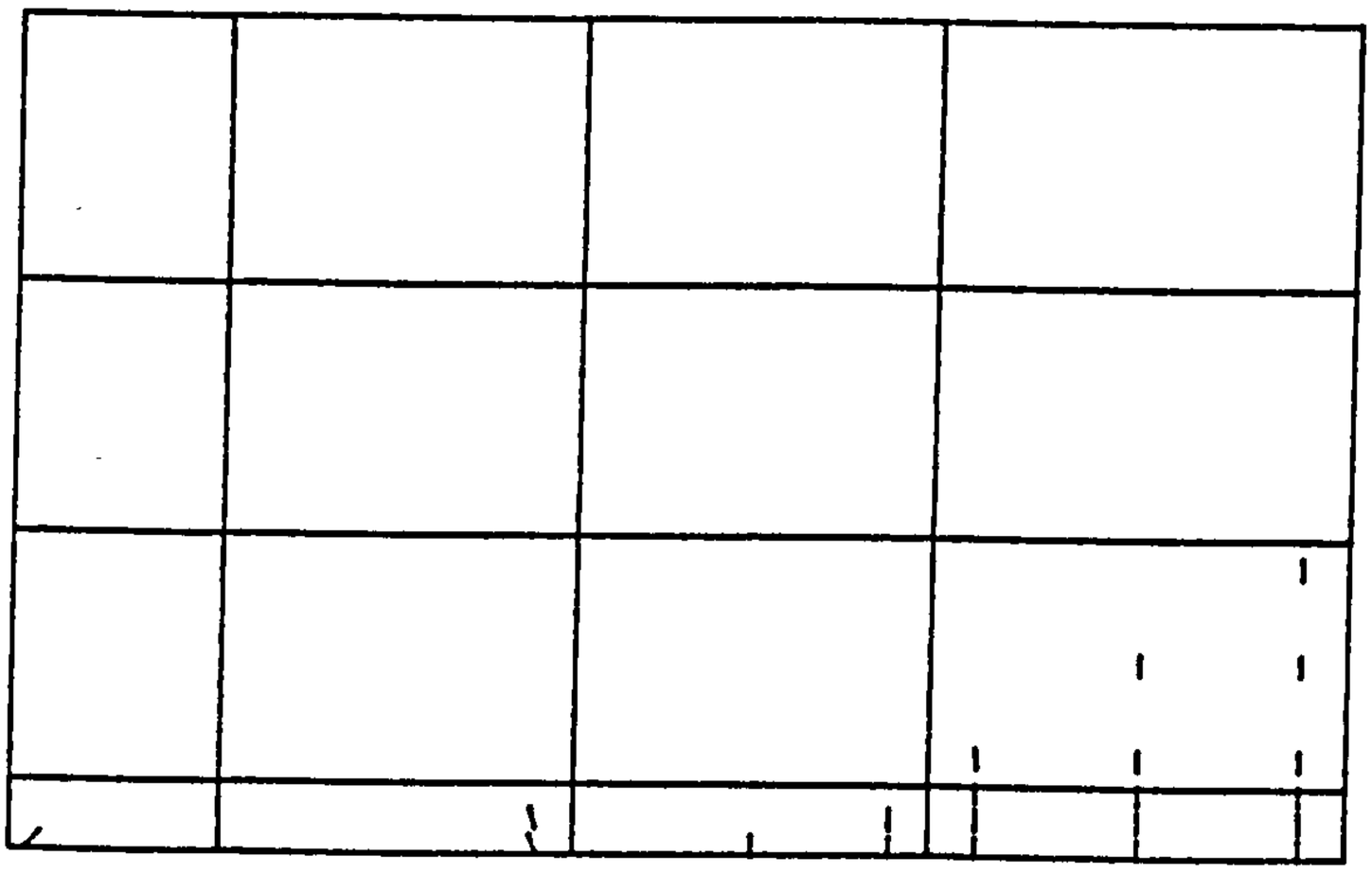

Displacement criterion 1, COOP = 10%

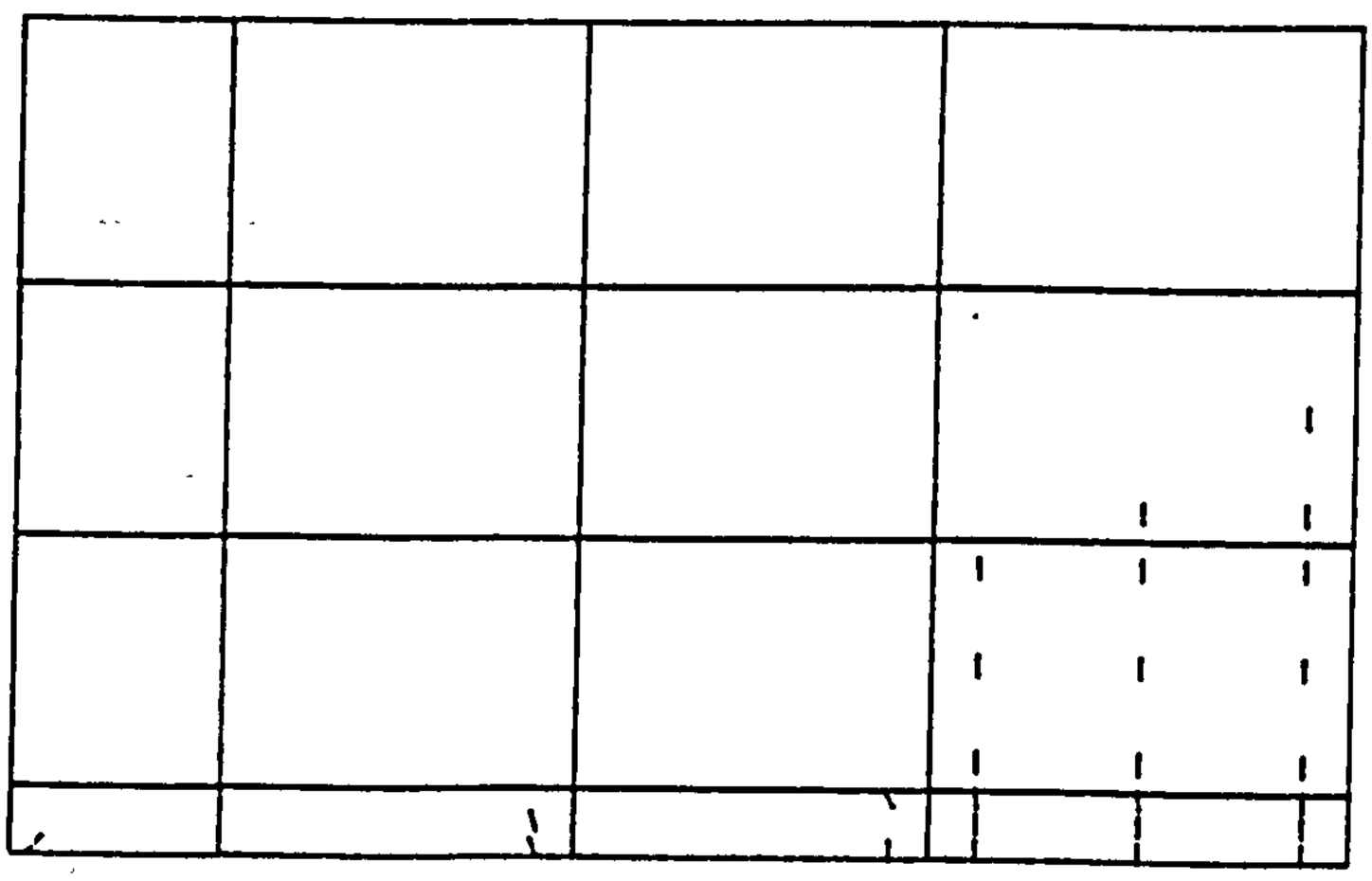

Displacement criterion 2, COOP = 10%

Figure (6·19) Crack patterns at load = 69·7 kN.

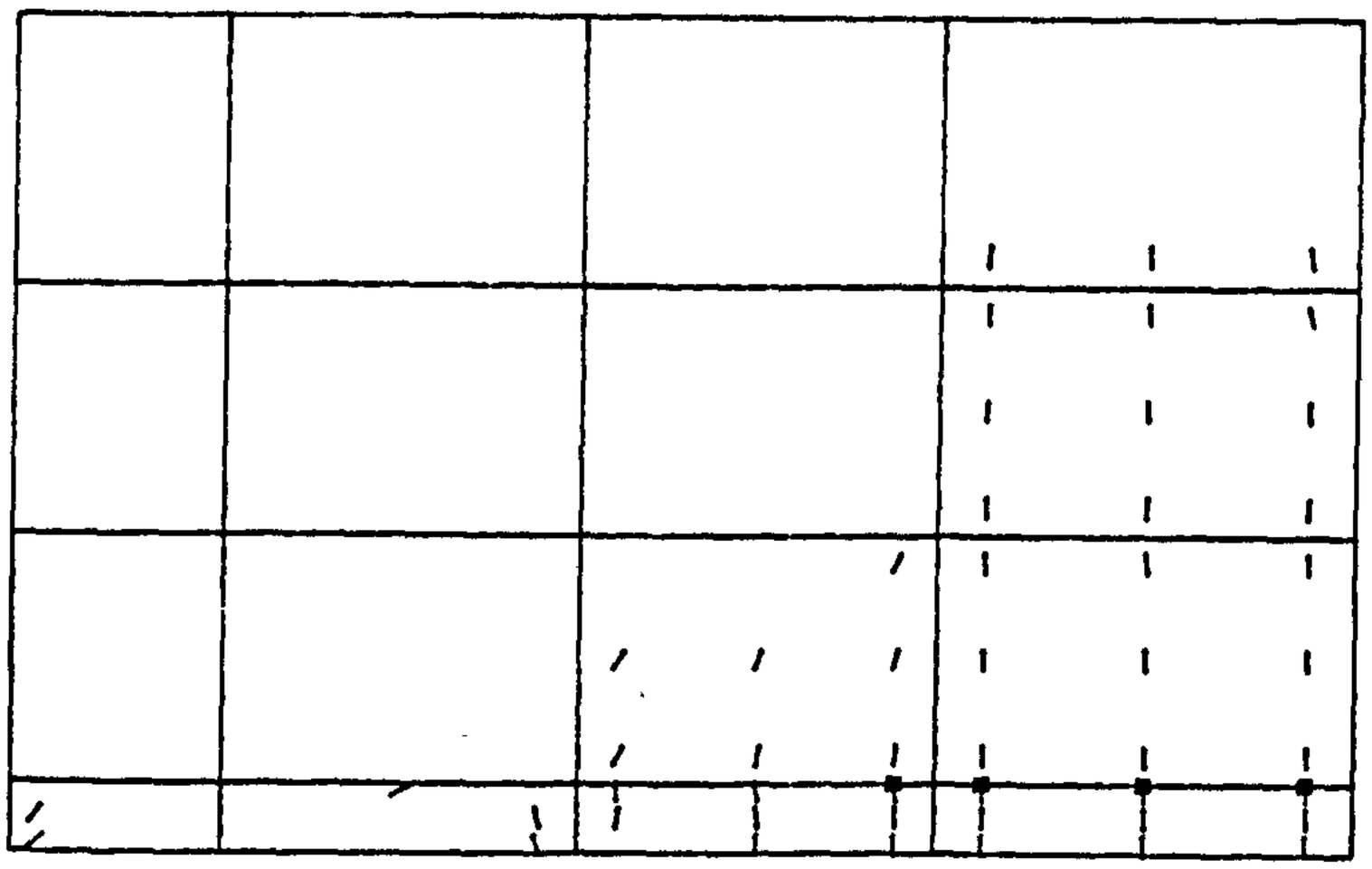

Load criterion, COOP = 20%

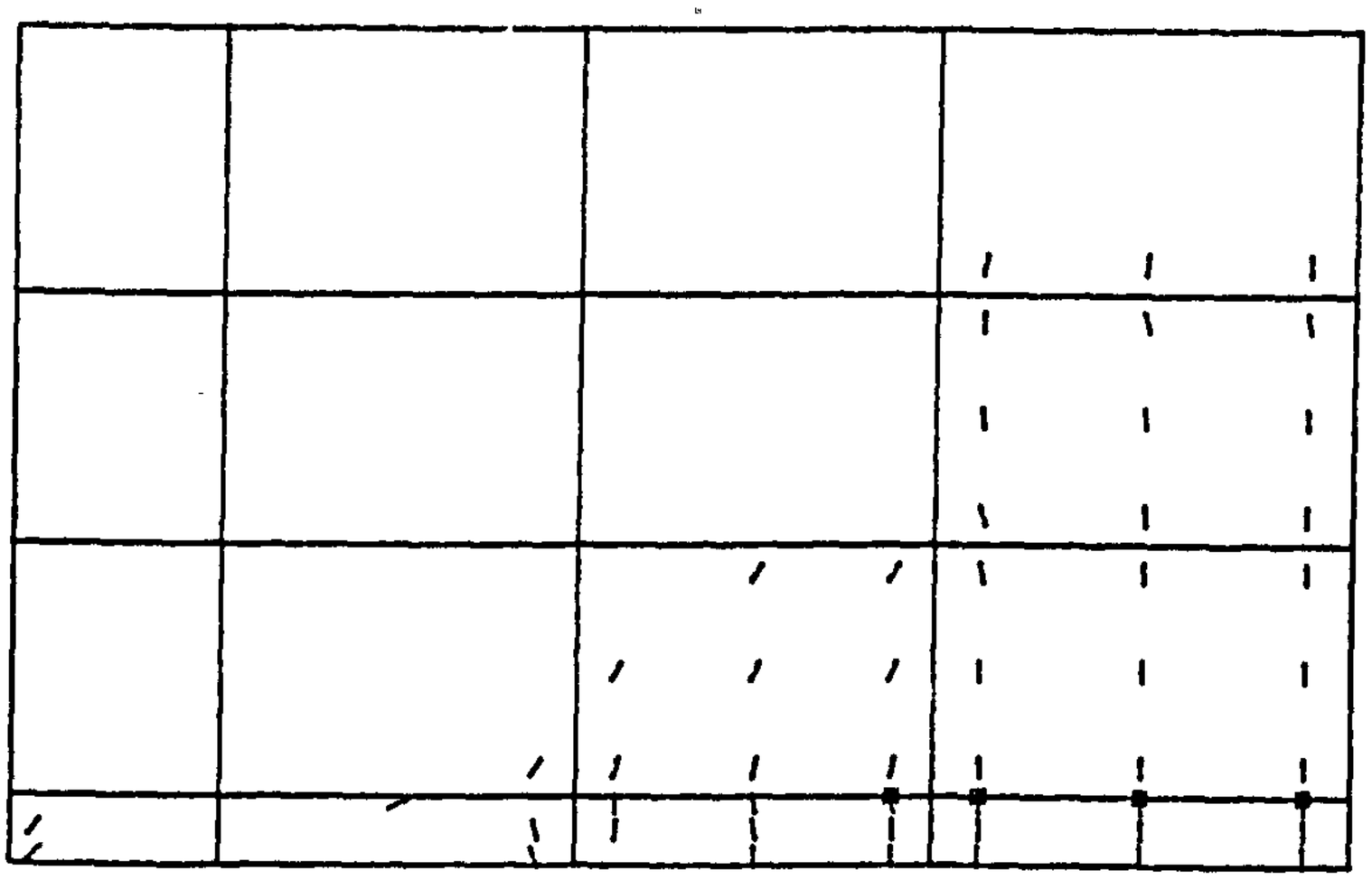

Displacement criterion 1, COOP = 10%

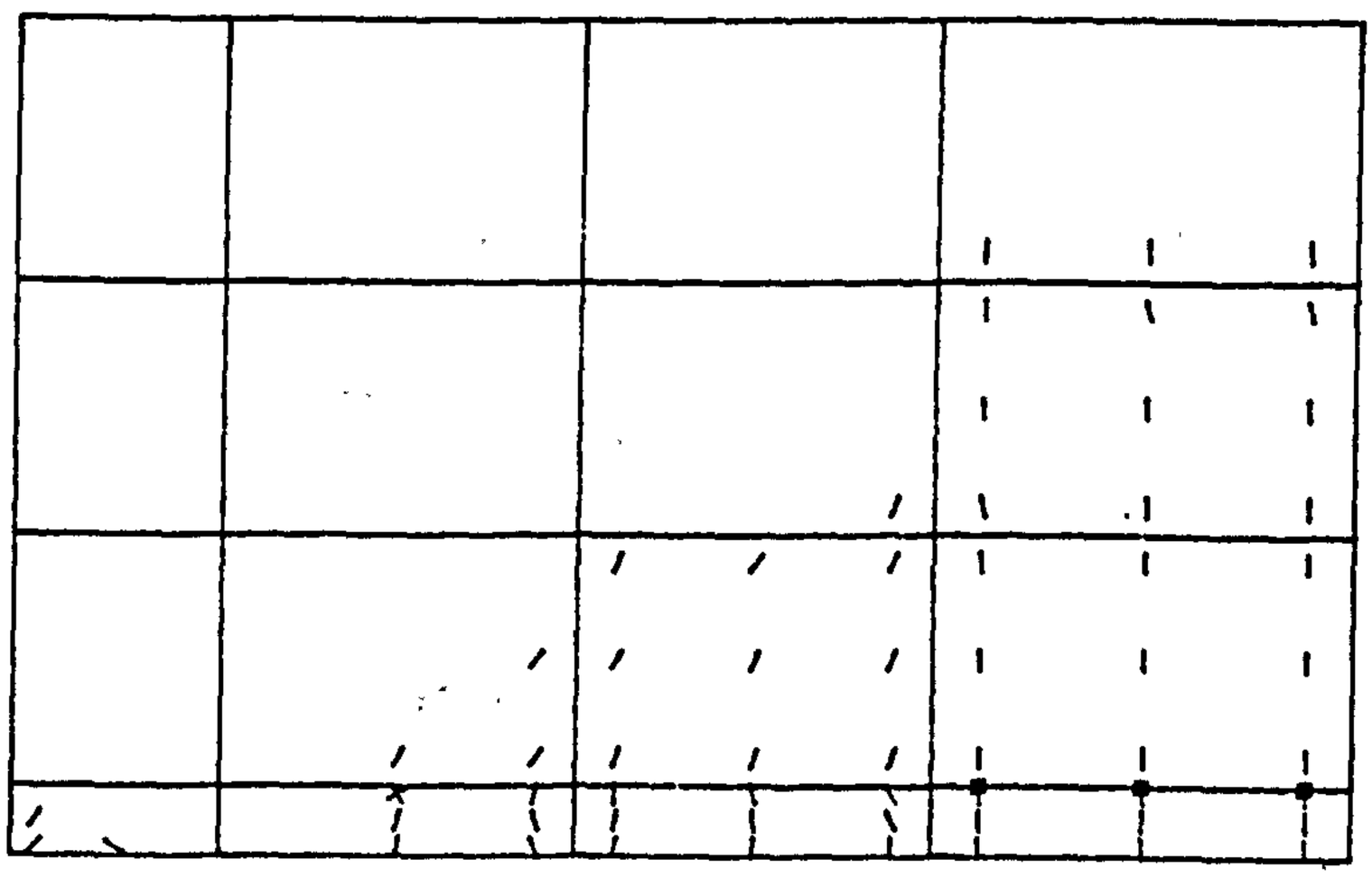

Displacement criterion 2, COOP = 10%

Figure (6•20) Crack patterns at load = 99•6 kN.

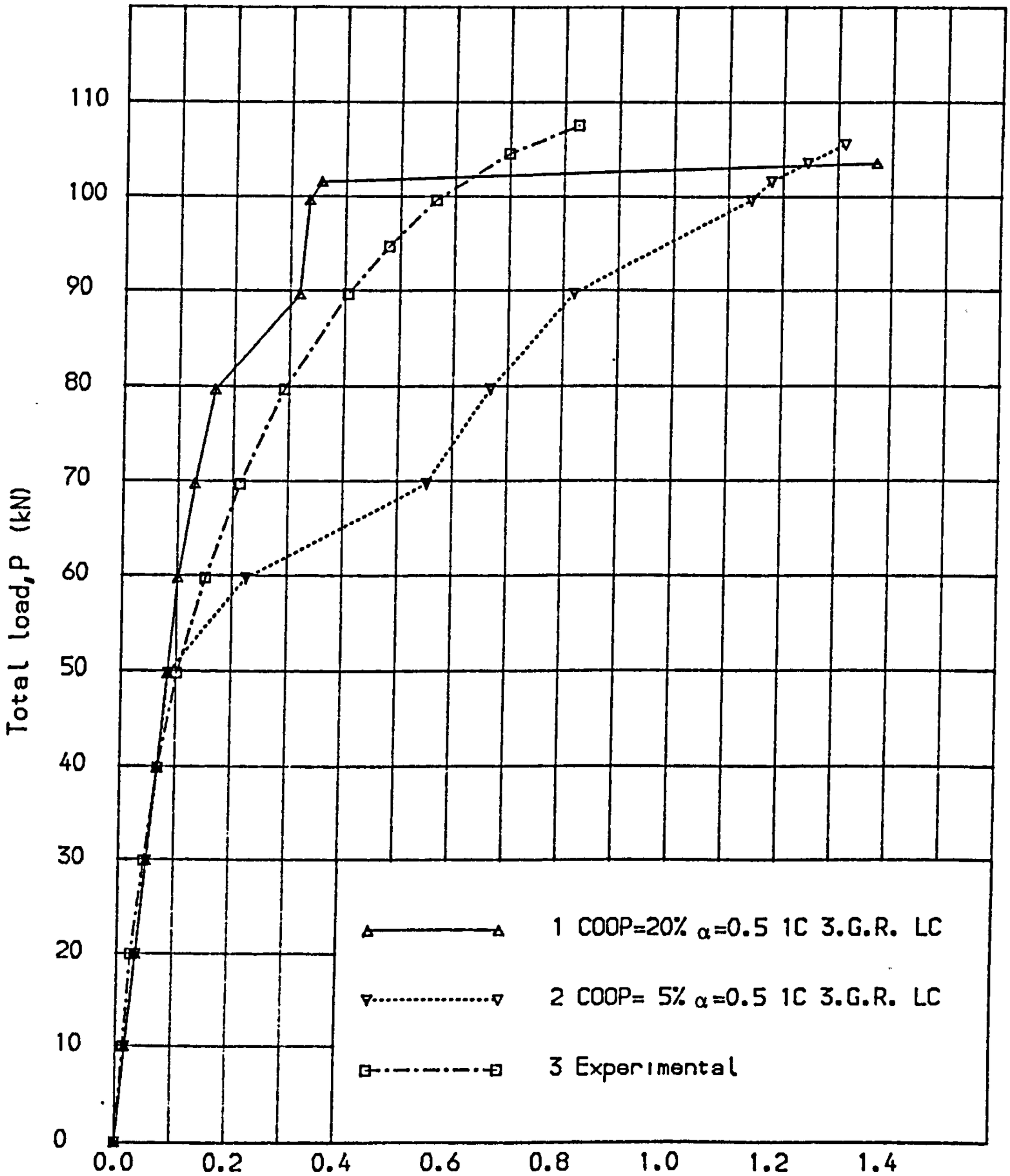

Fig. (6.21) Load deflection curves for deep beam, (C.S.M.).

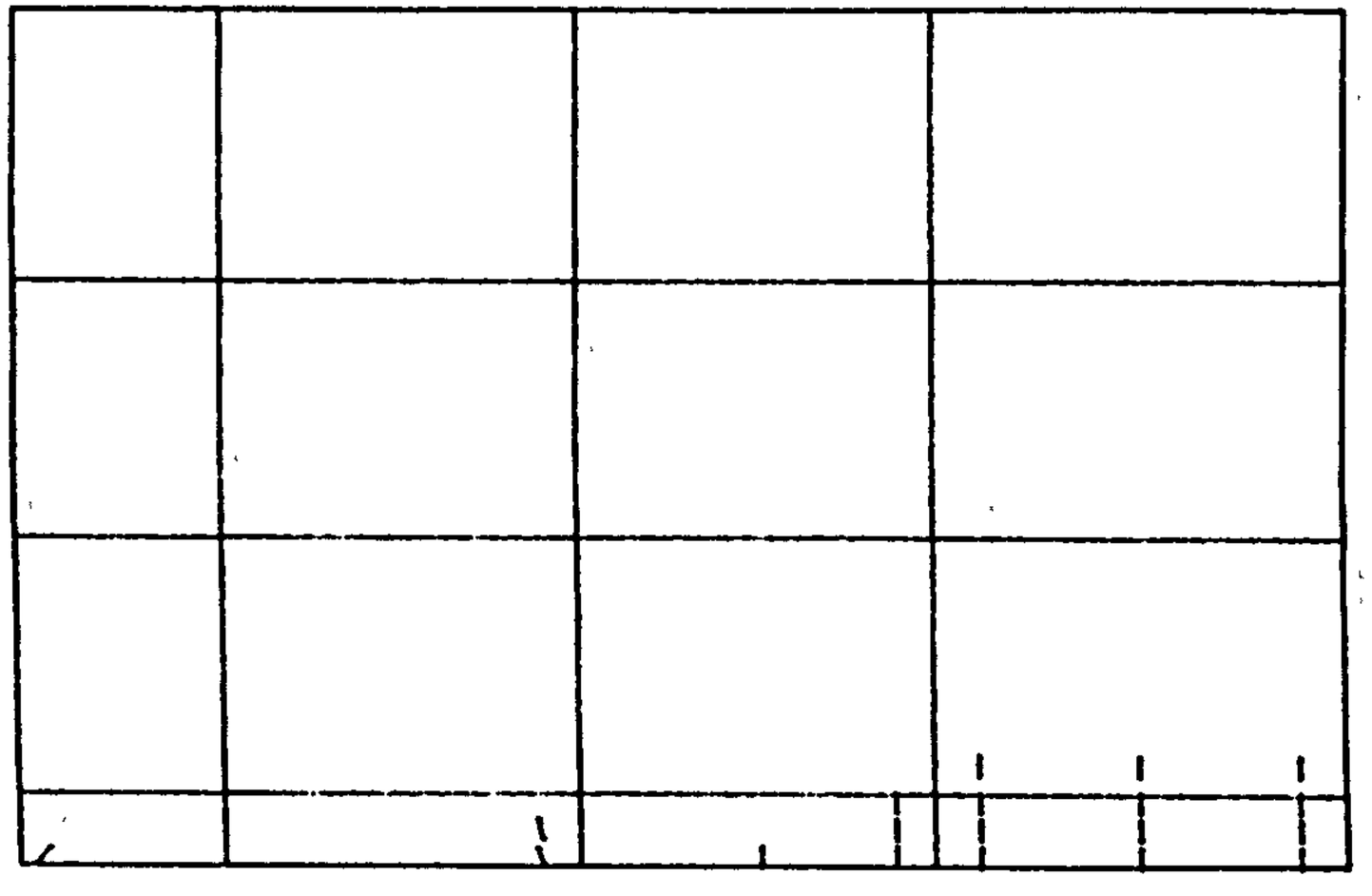

COOP = 20% , Load = 69•7 kN

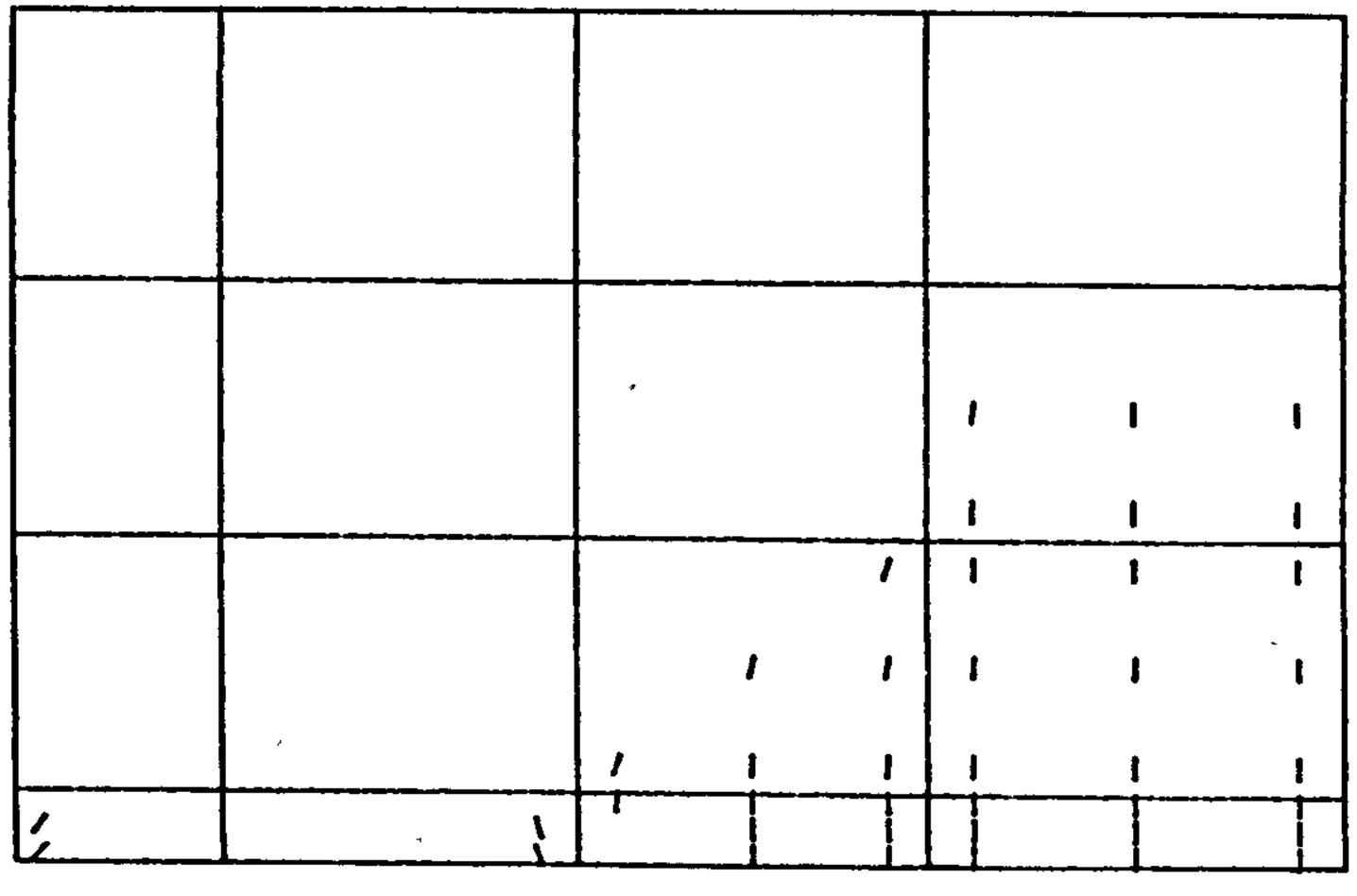

COOP = 20% , Load = 89•6 kN

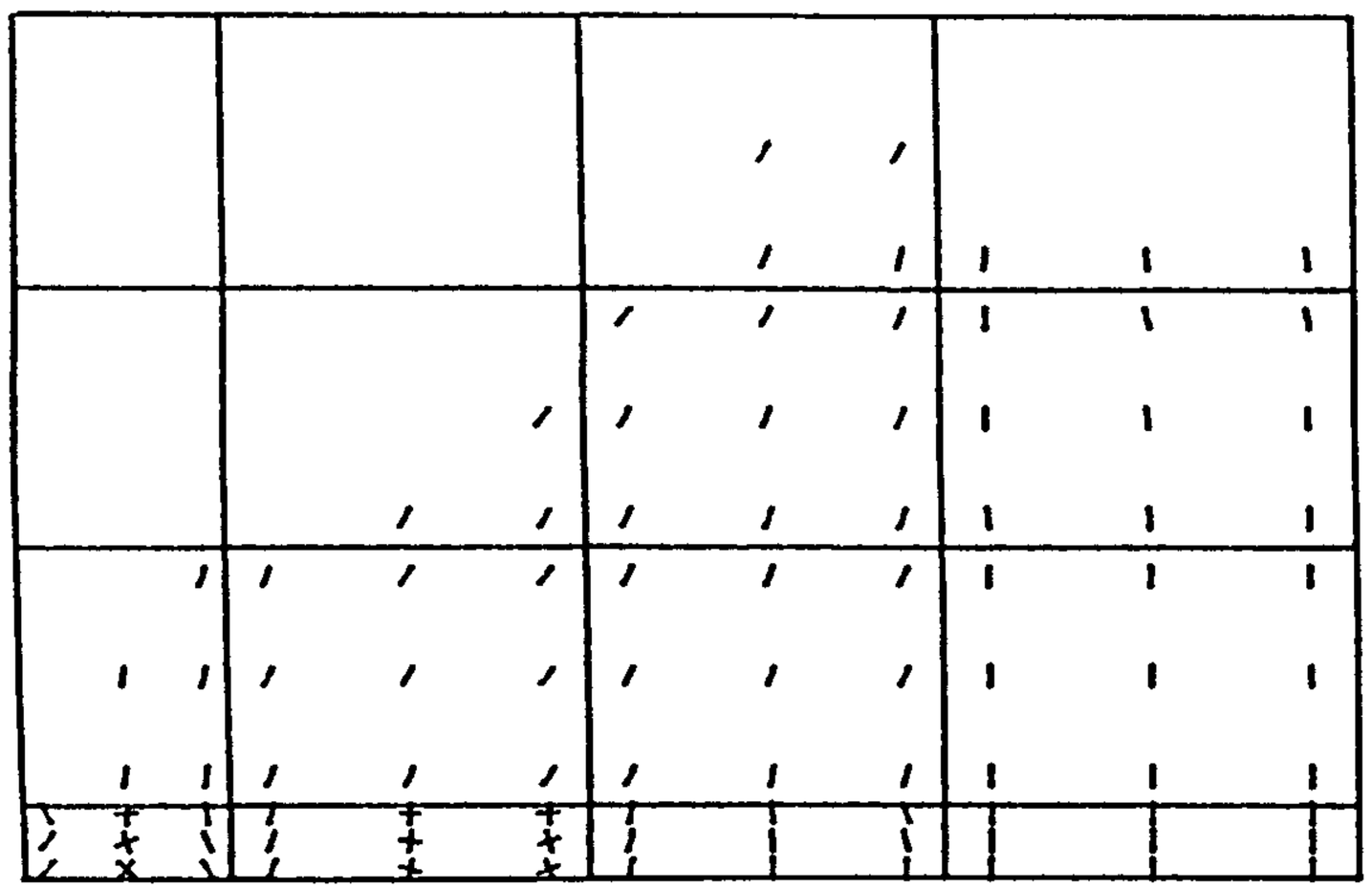

COOP = 5% , Load = 69•7 kN

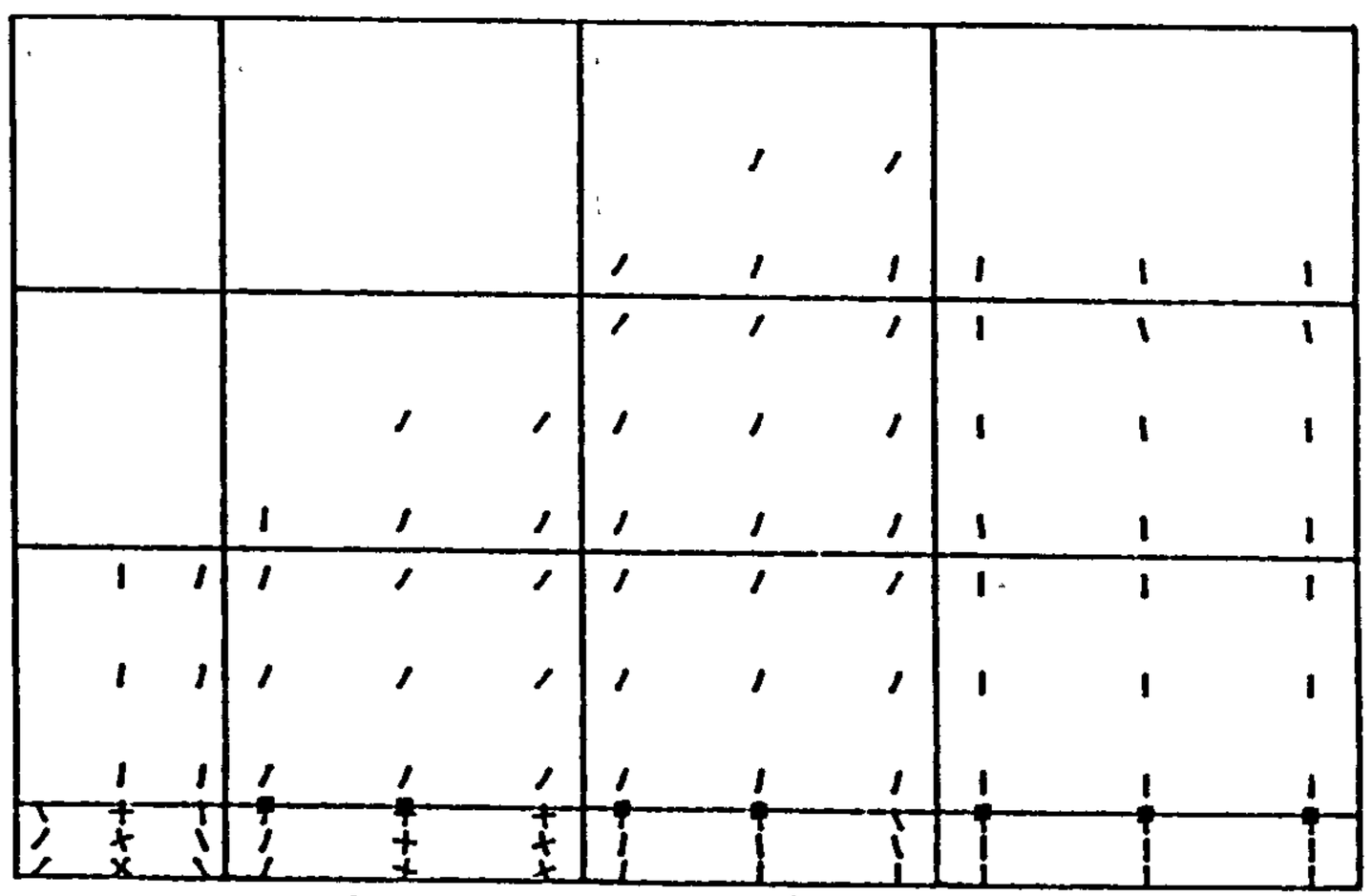

COOP = 5% , Load = 89•6 kN

Figure (6•22) Crack patterns using the constant stiffness method.

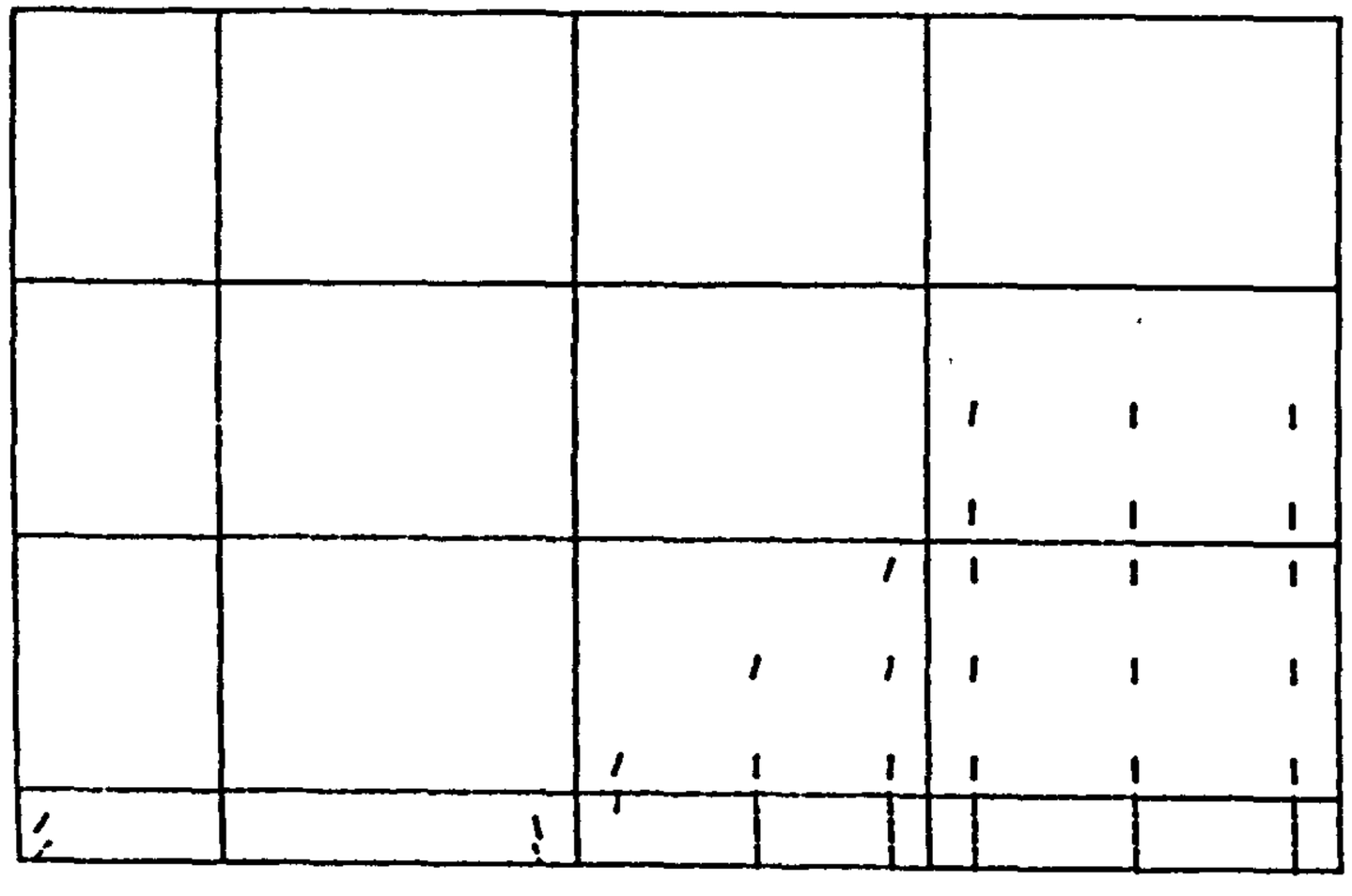

COOP = 20% , Load = 99·6 kN

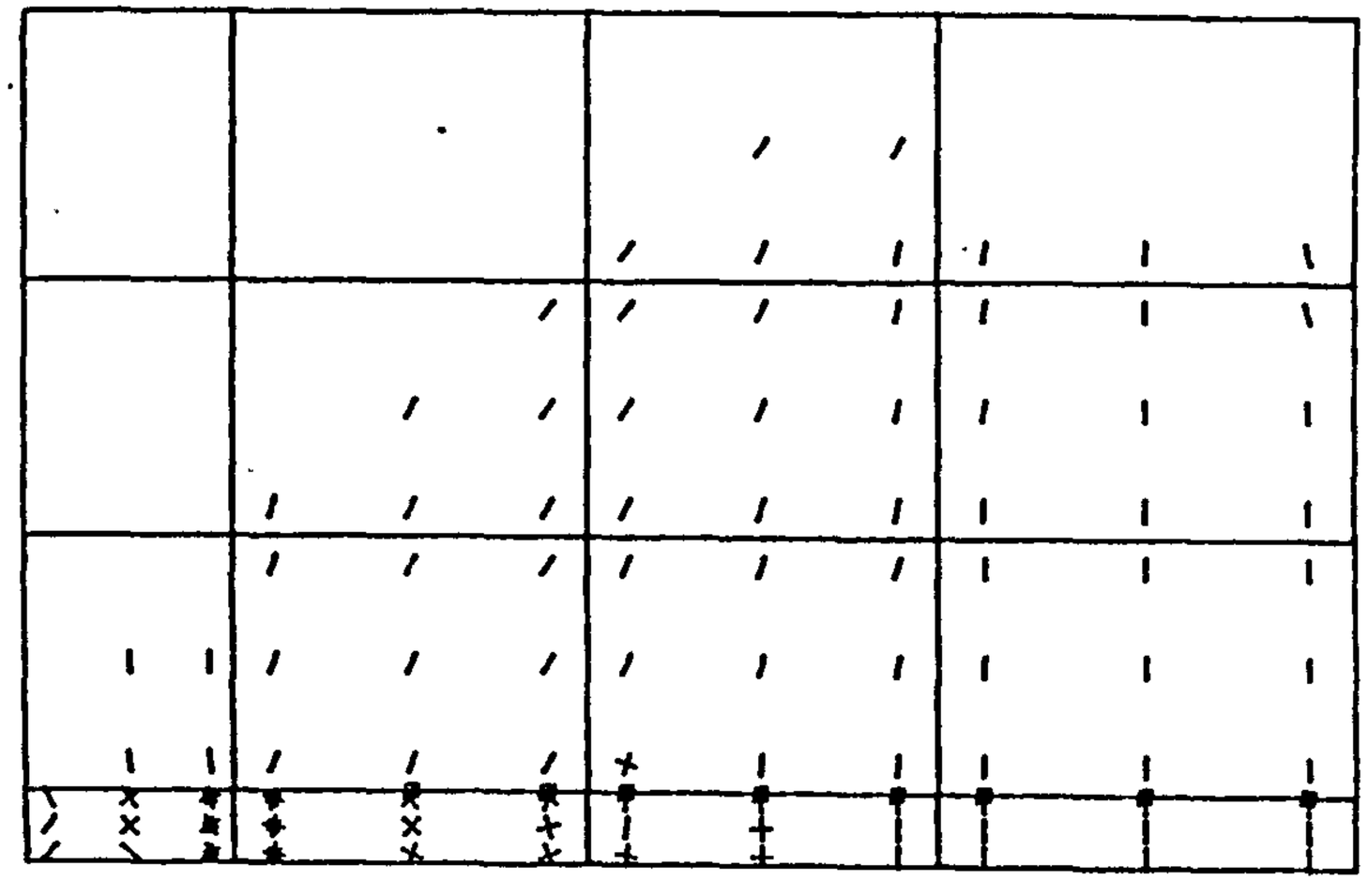

COOP = 20% , Load = 103·6 kN

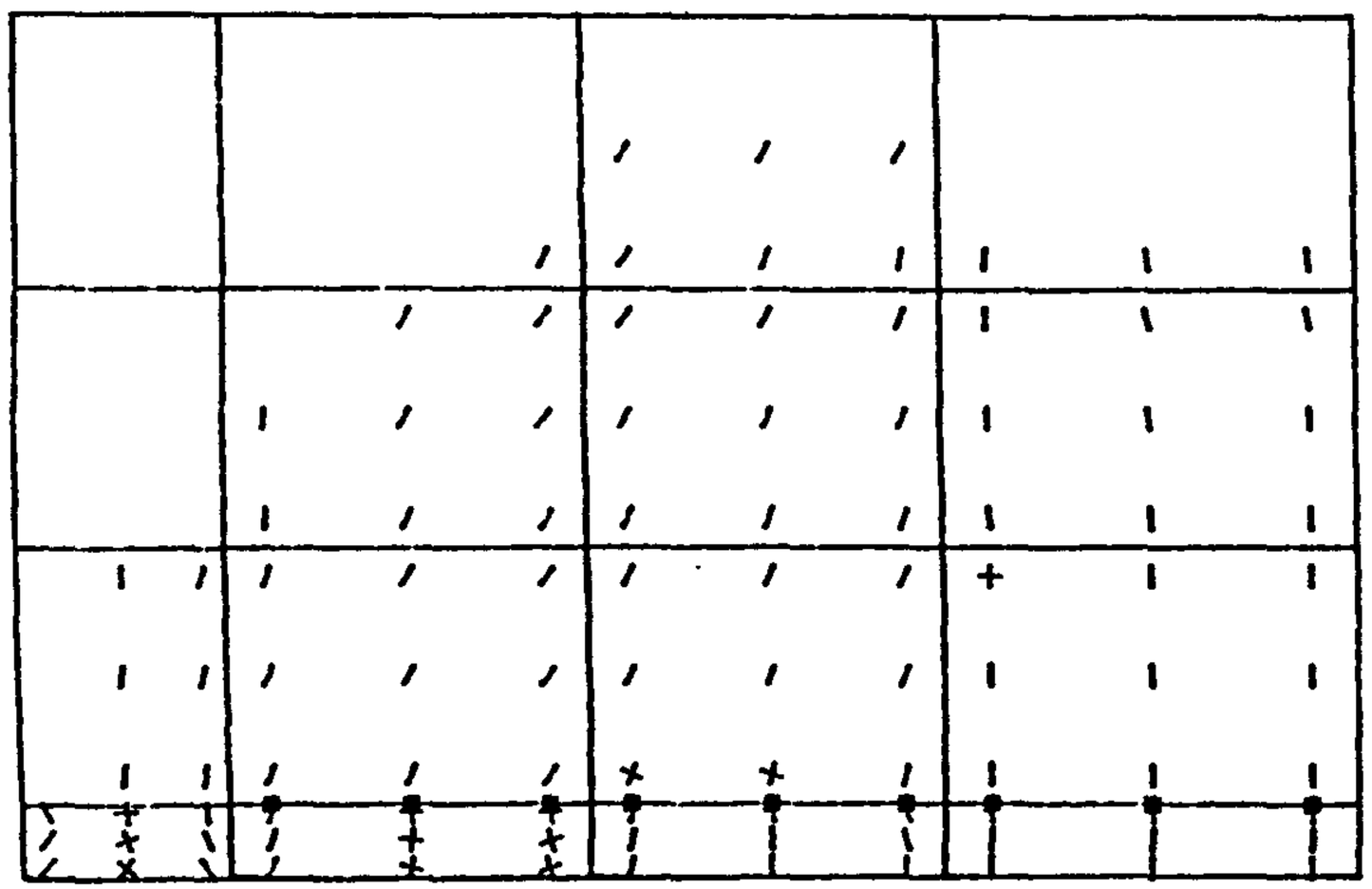

COOP = 5% , Load = 99·6 kN

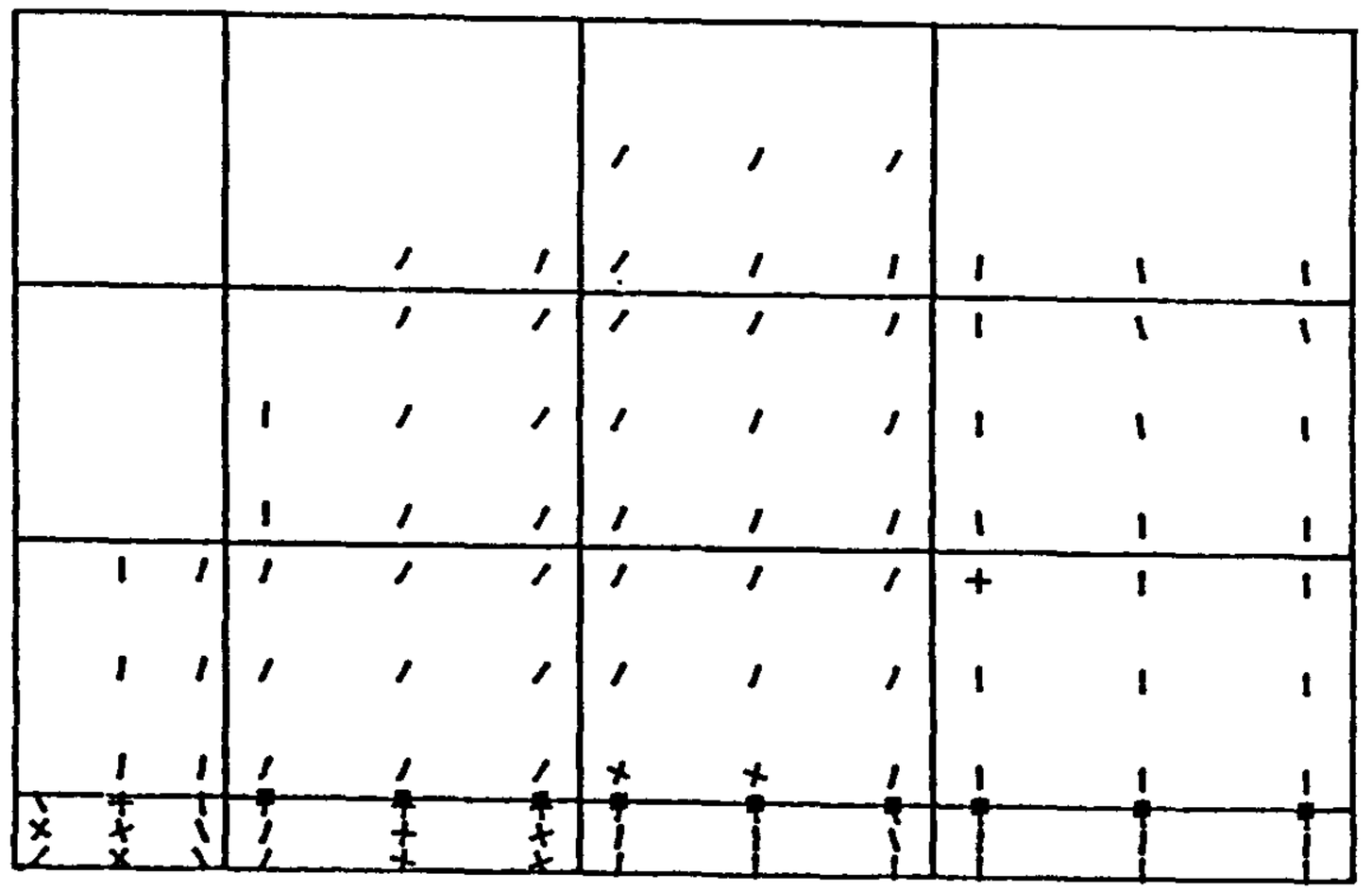

COOP = 5% , Load = 103·6 kN

Figure (6·23) Crack patterns using the constant stiffness method.

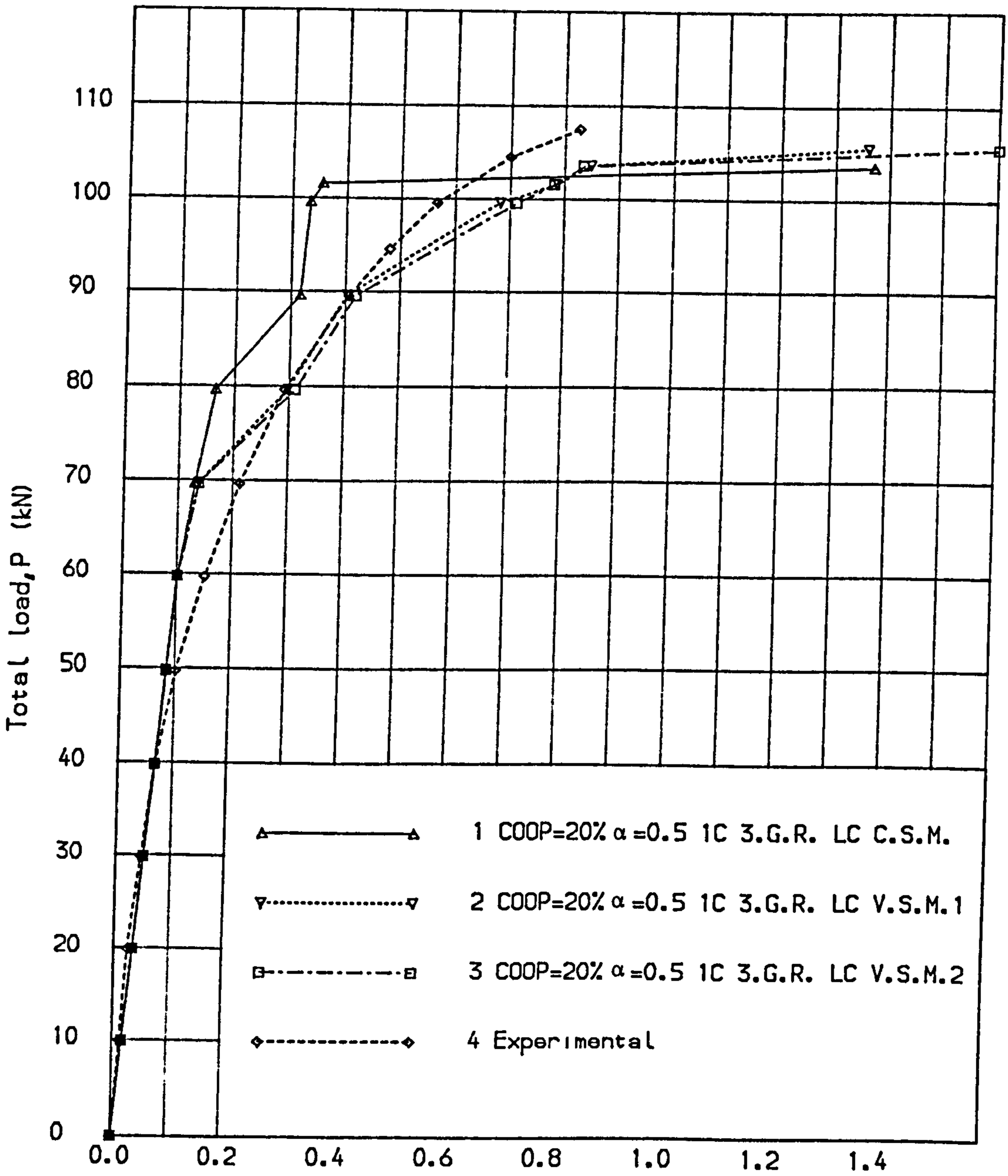

Fig. (6.24) Load deflection curves for deep beam.

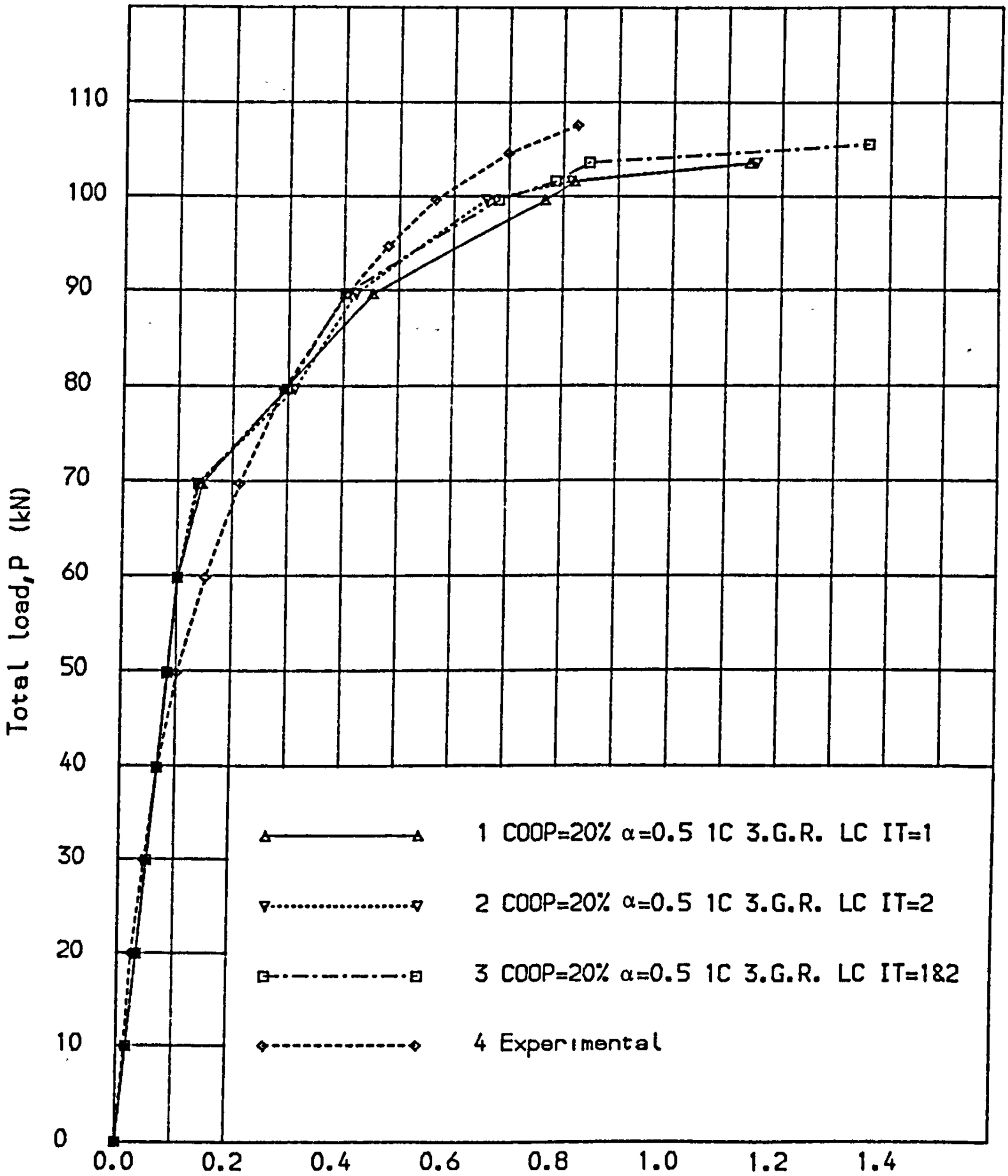

Fig. (6.25) Load deflection curves for deep beam.

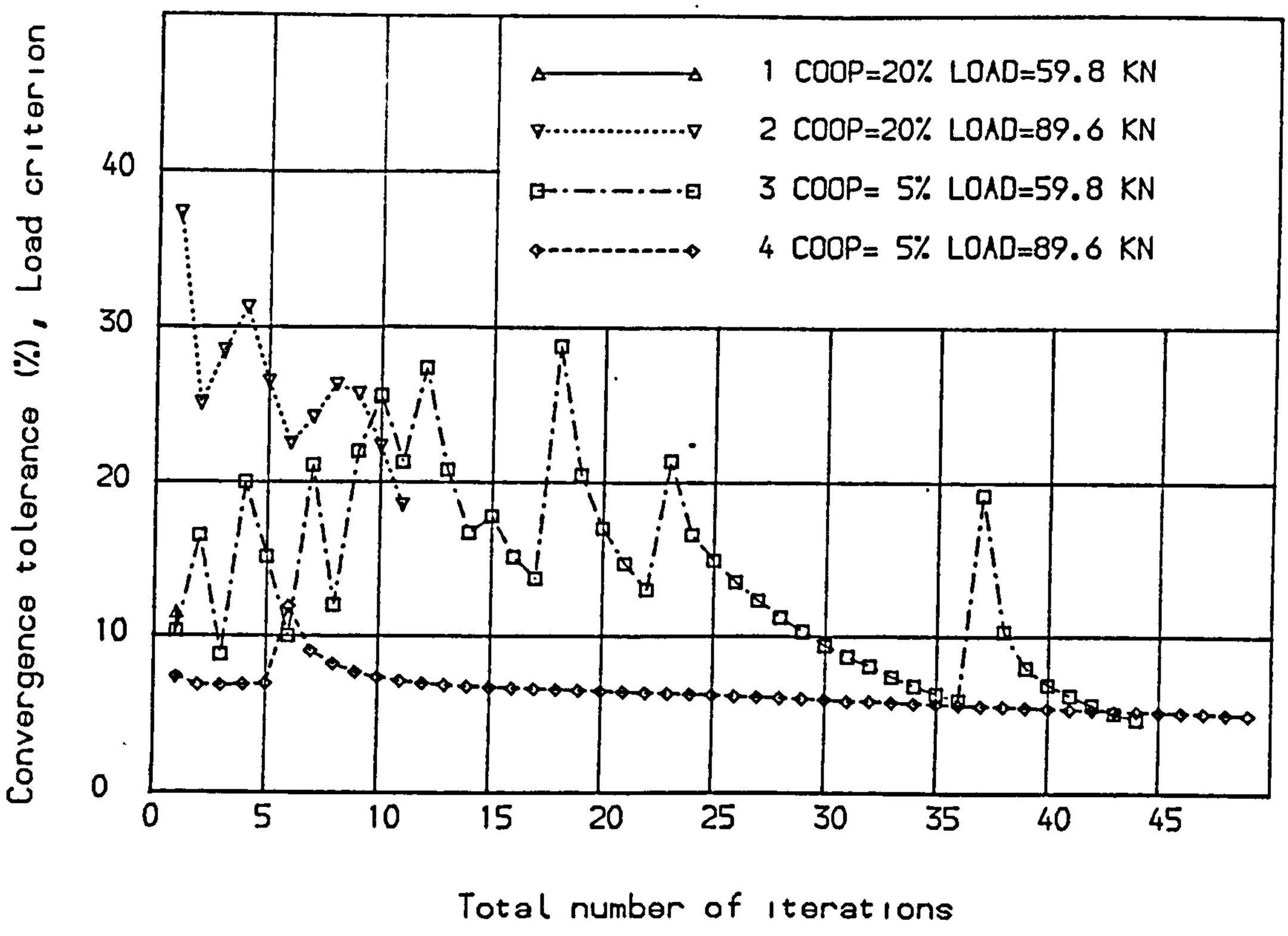

Fig. (6,26) Convergence and number of iterations, (C.S.M.).

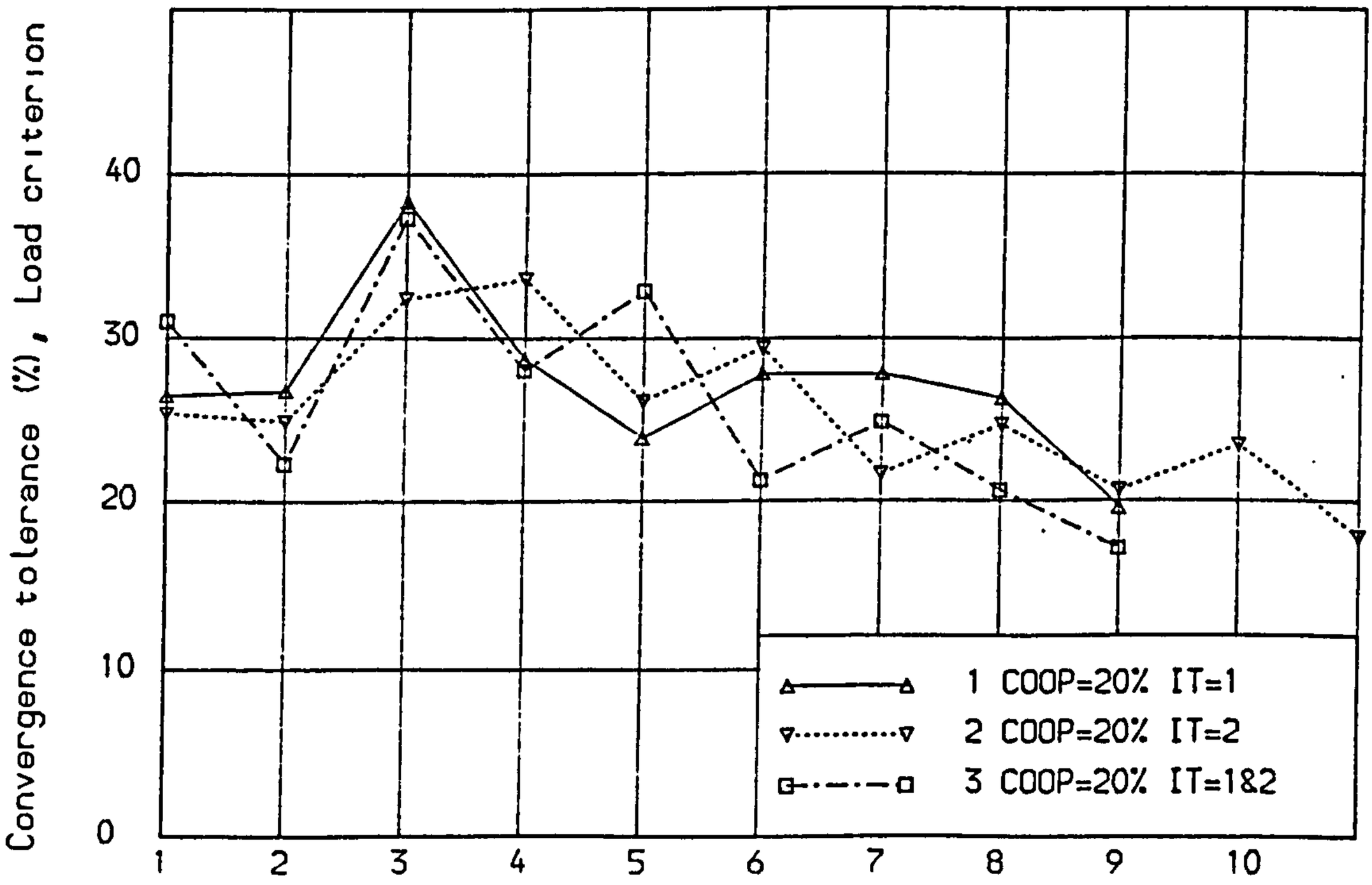

Fig. (6.27) Convergence and number of iterations, (I.N.L.).

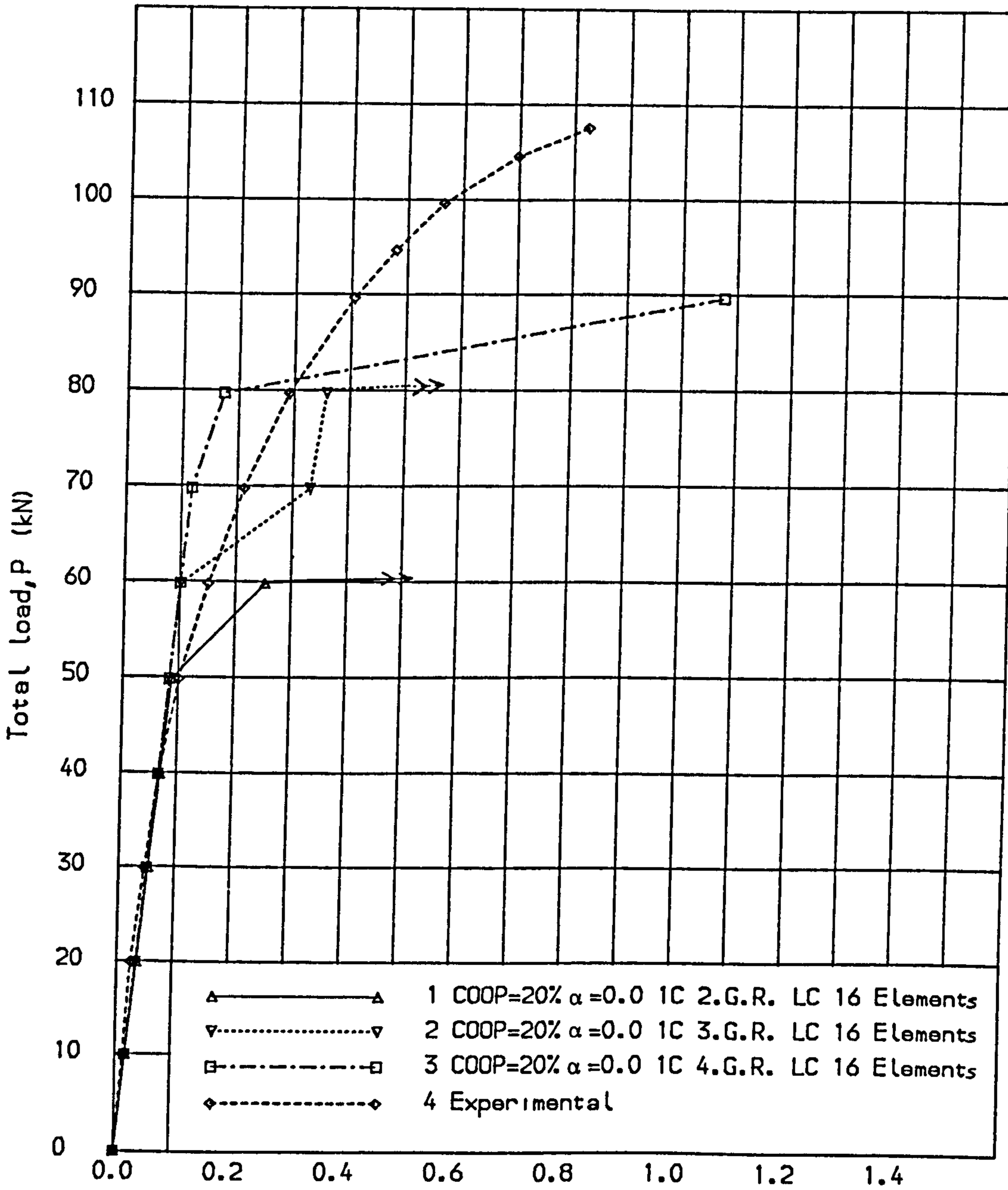

Fig. (6.28) Load deflection curves for deep beam, (V.S.M.1).

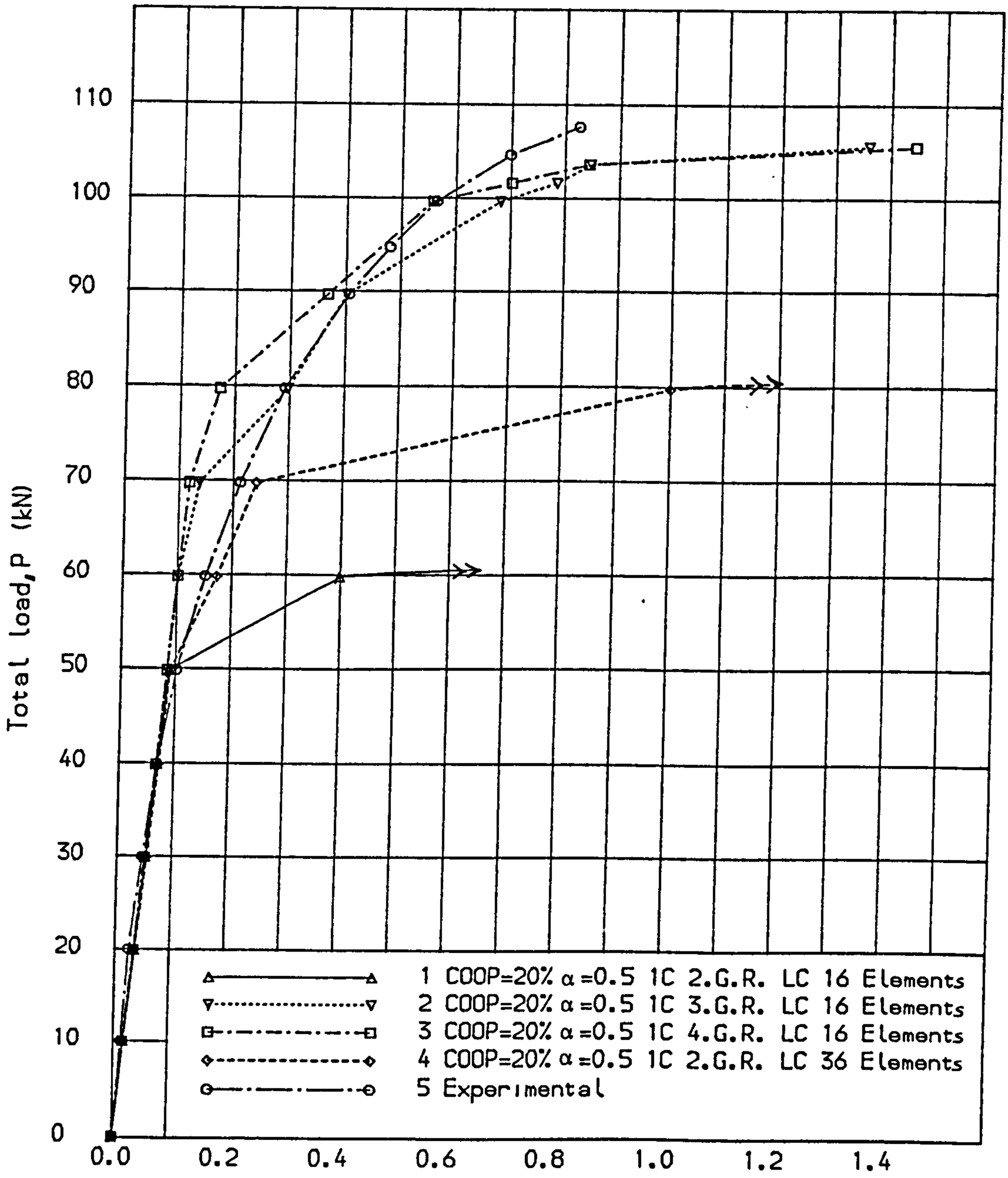

Fig. (6.29) Load deflection curves for deep beam, (V.S.M.1).

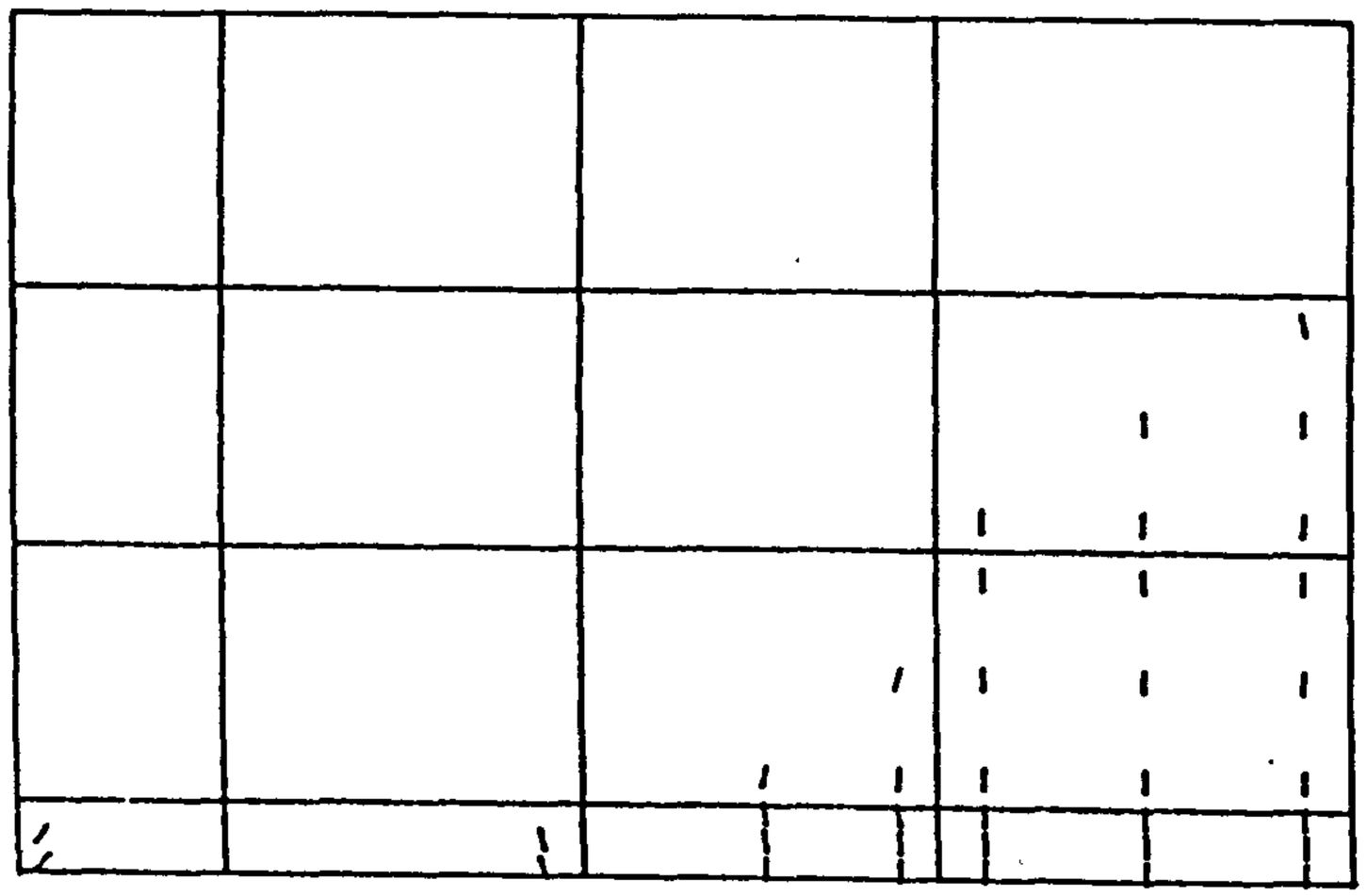

Load = 79•7 kN , 3 x 3 G.R.

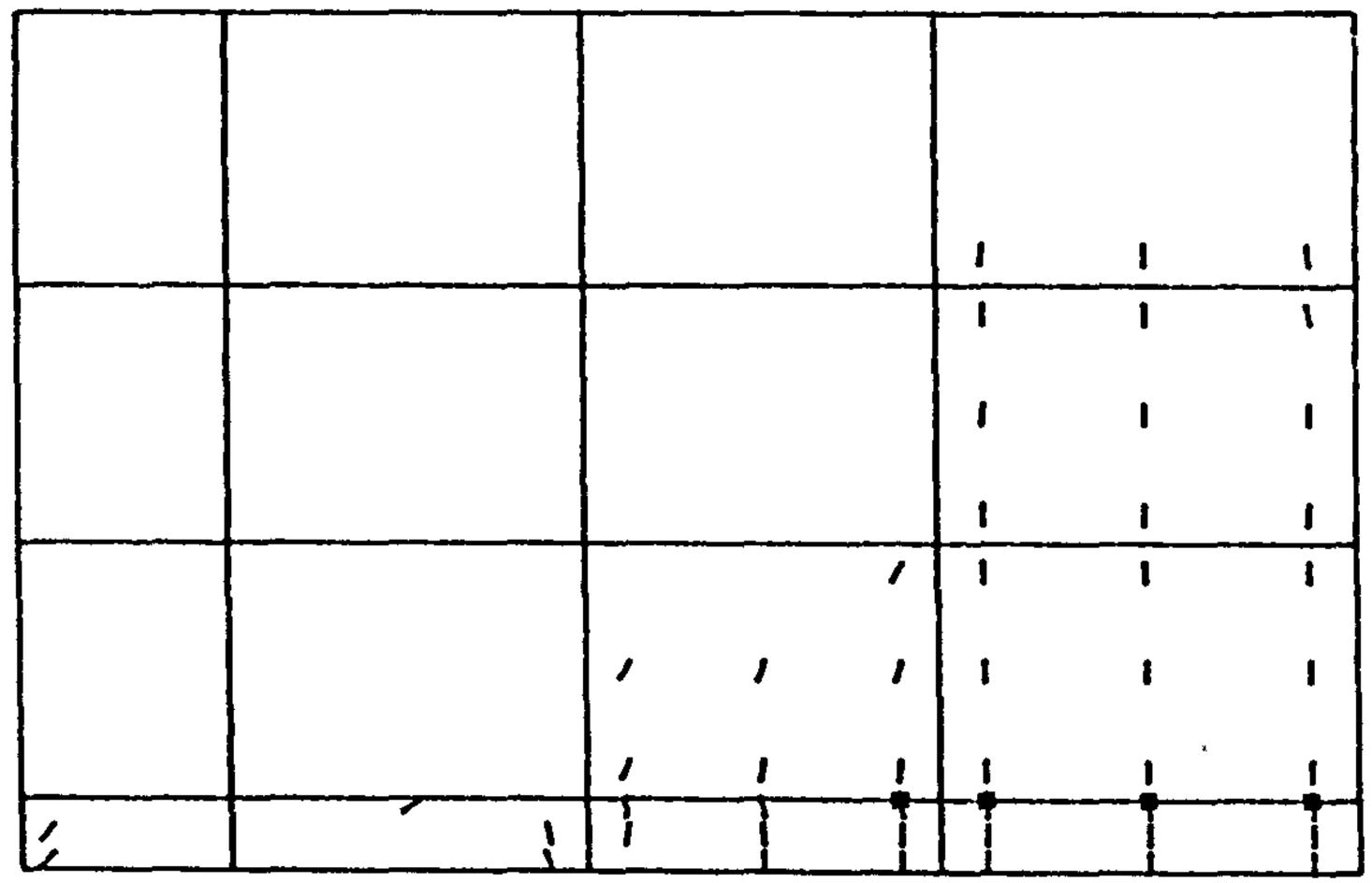

Load = 99•6 , 3 x 3 G.R.

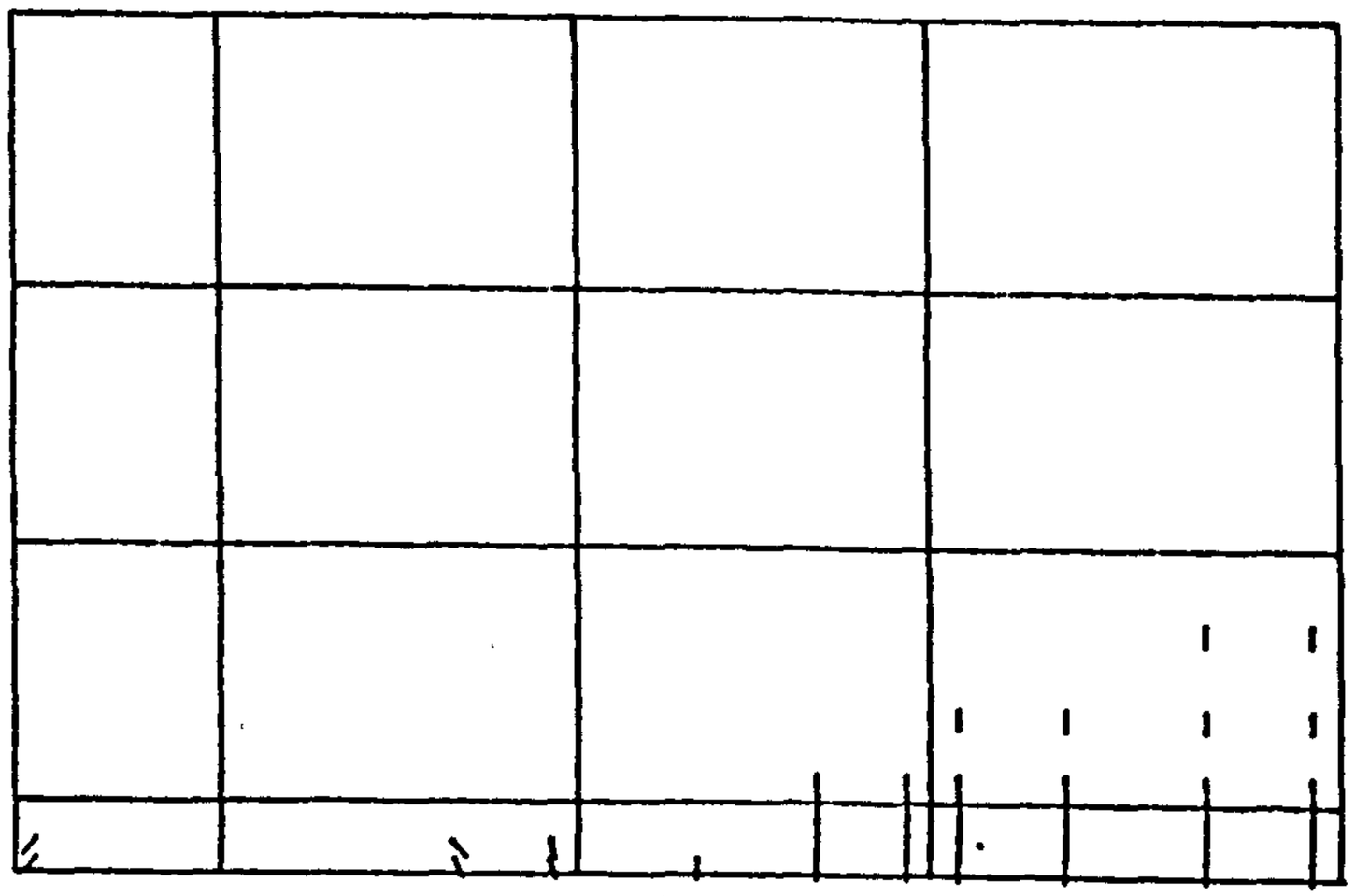

Load = 79•7 kN , 4 x 4 G.R.

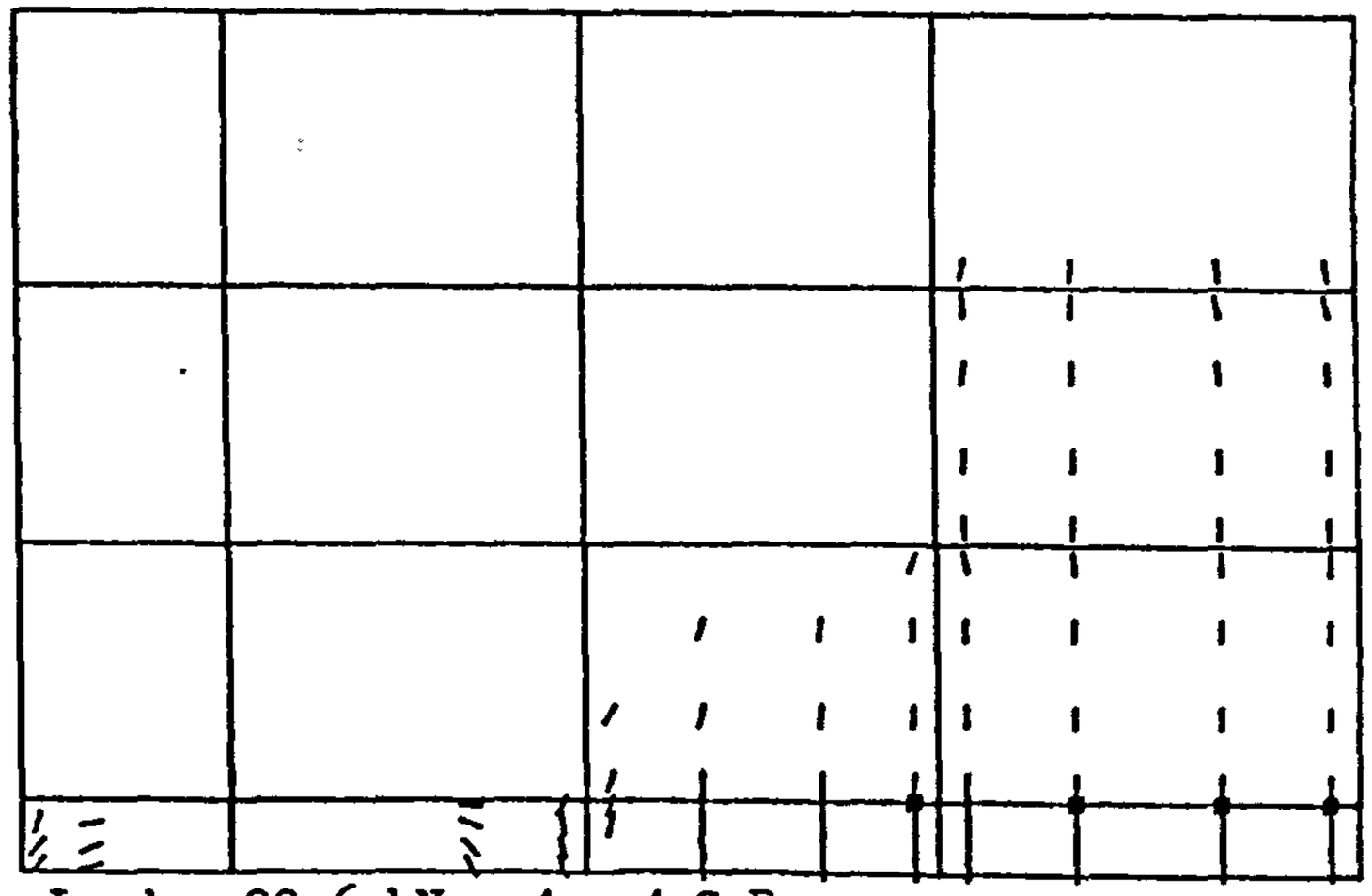

Load = 99•6 kN , 4 x 4 G.R.

Figure (6•30) Crack pattern using 3 x 3 and 4 x 4 Gauss rules (COOP = 20%).

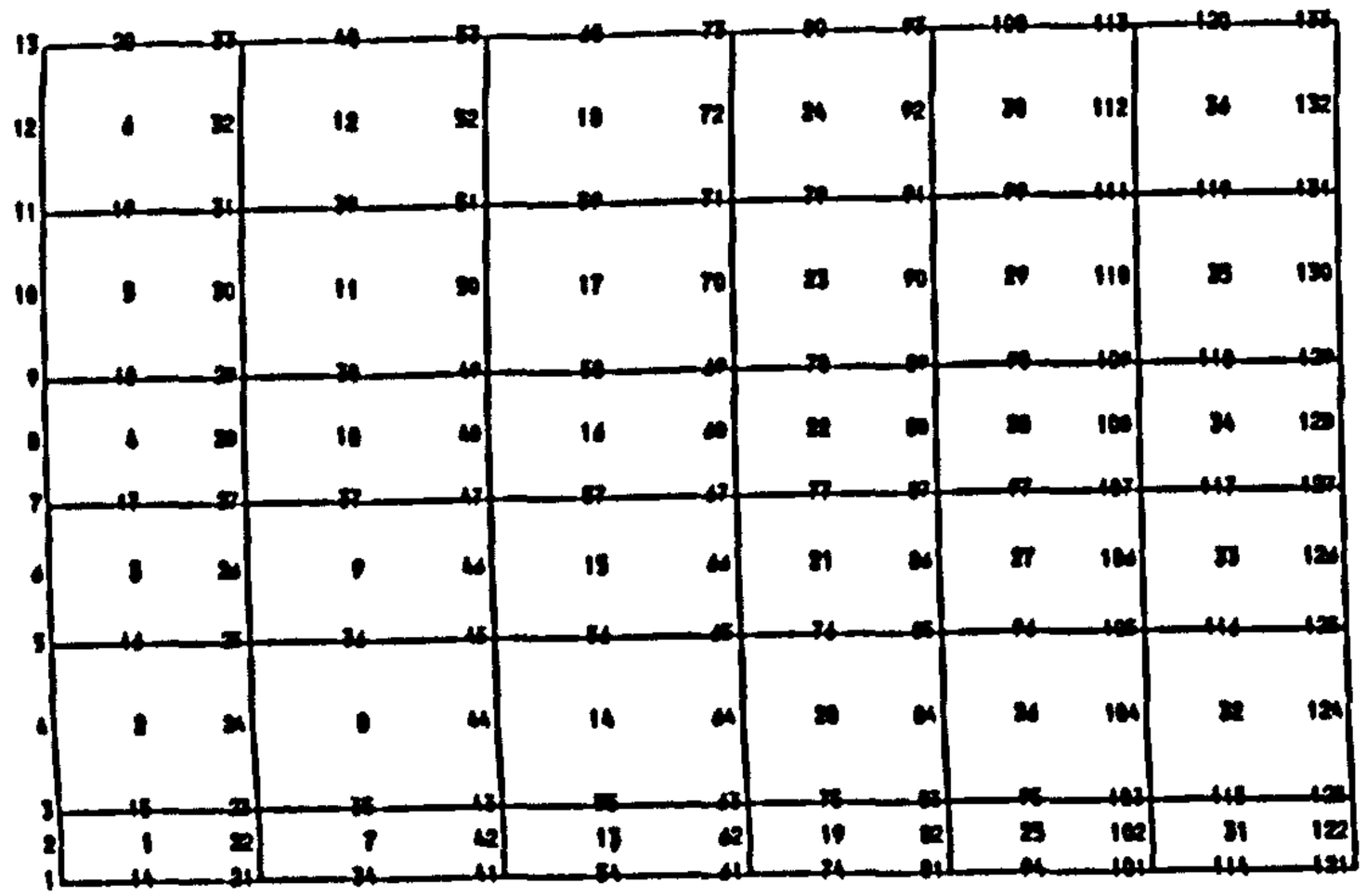

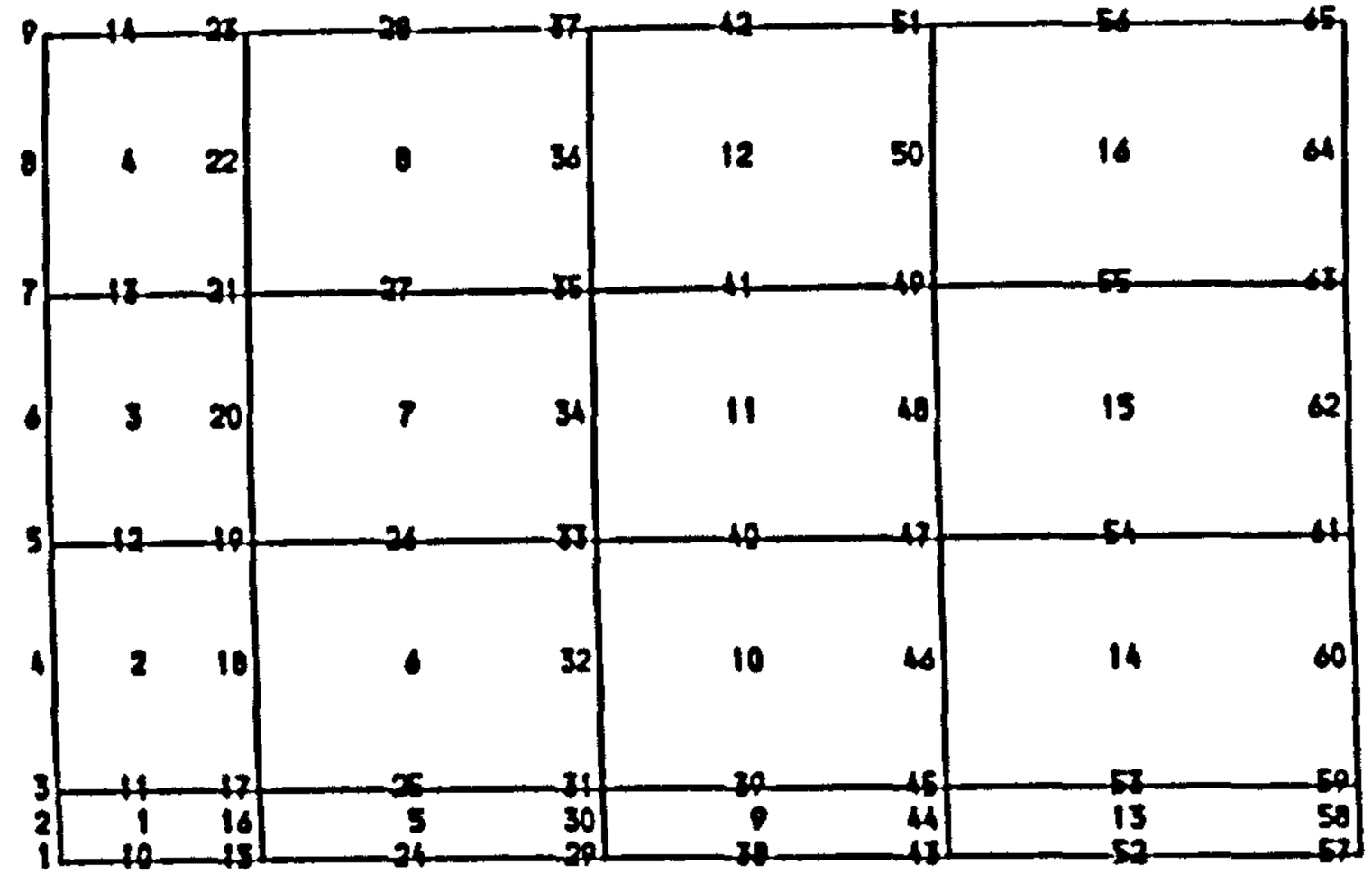

Figure (6·31) Meshes used to compare the effect of 2 x 2 Gauss rules.

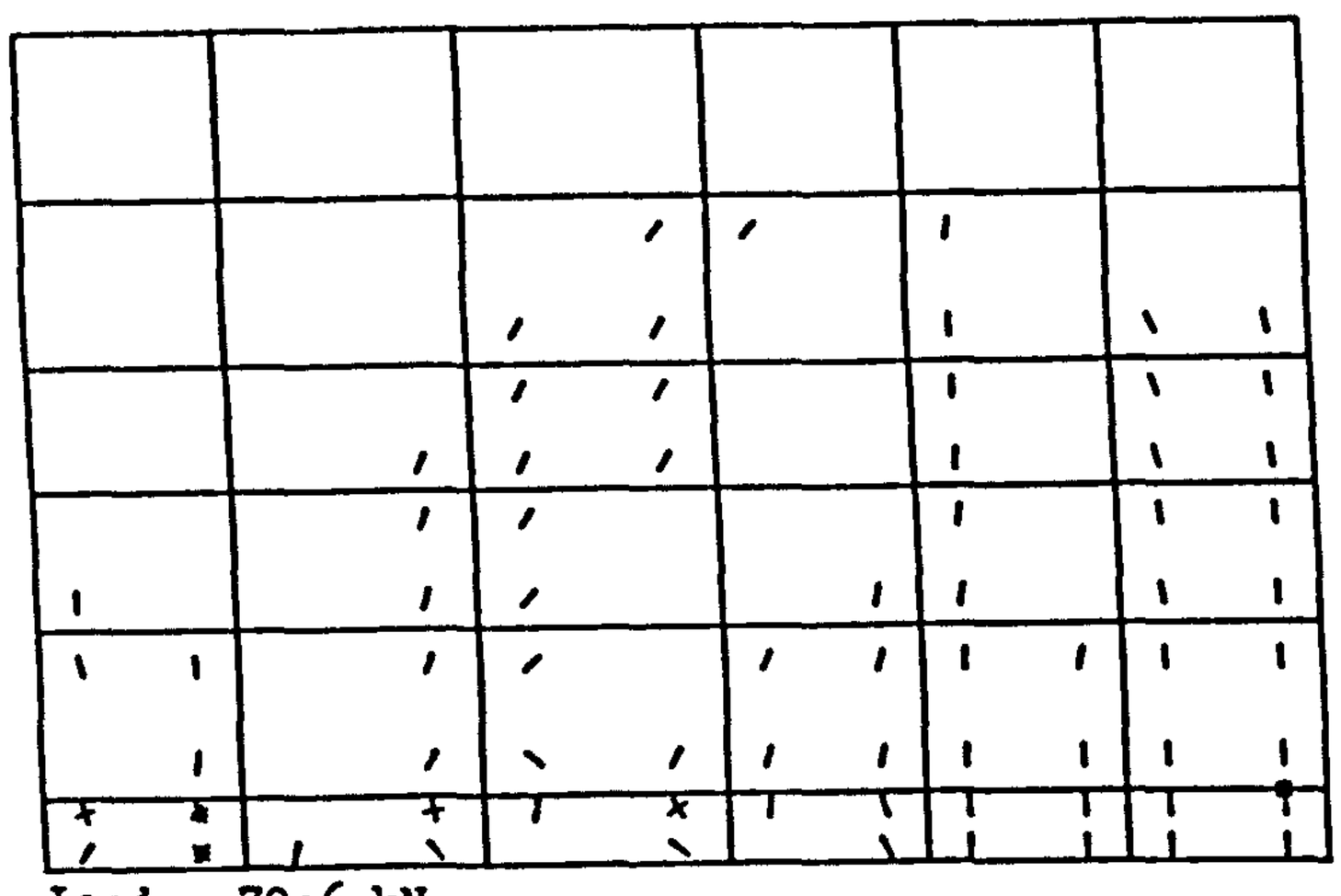

Load = 79·6 kN

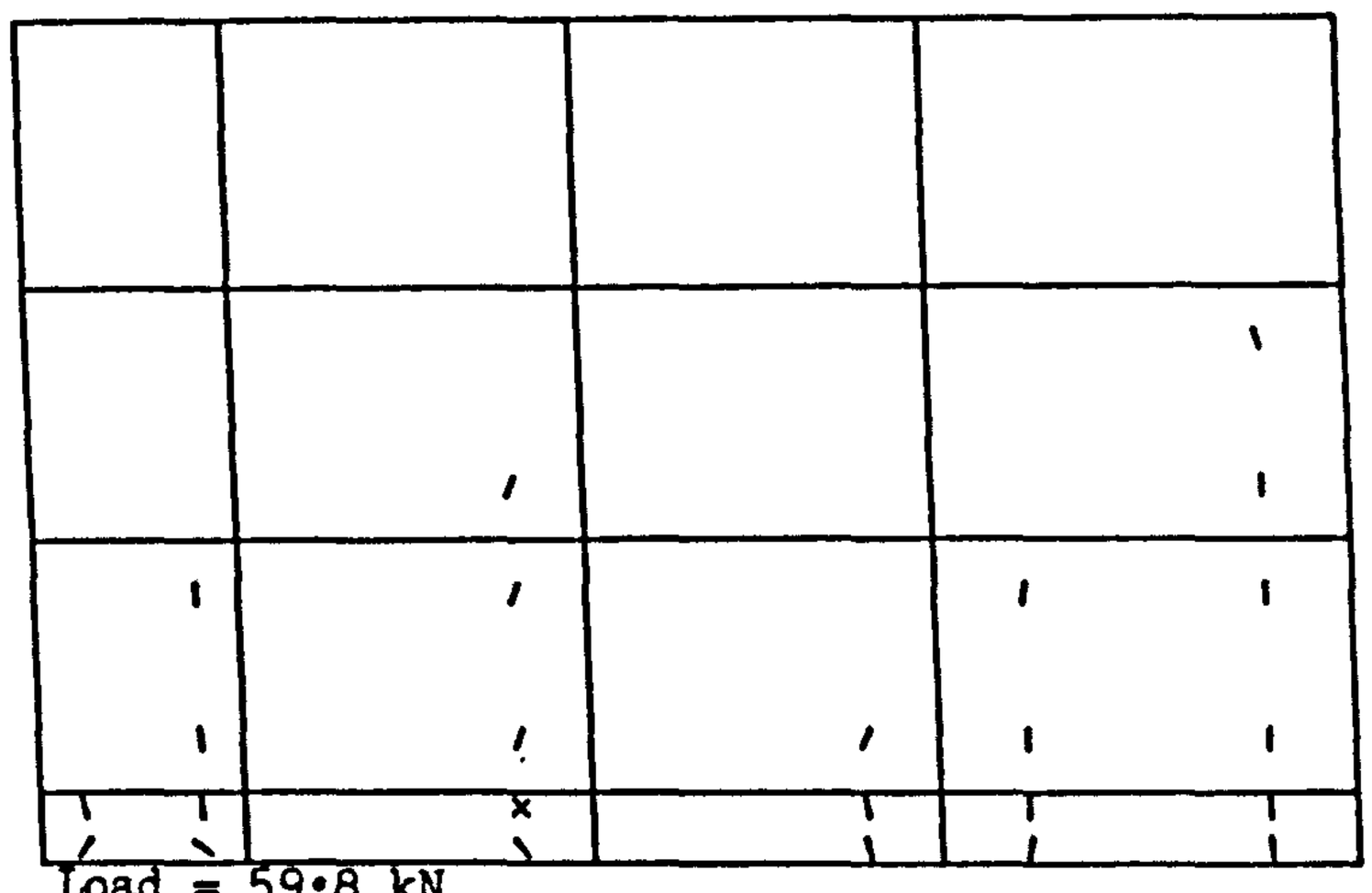

Load = 59·8 kN

Figure(6·32) Crack patterns at failure loads for the 2 x 2 Gauss rules (COOP = 20%).

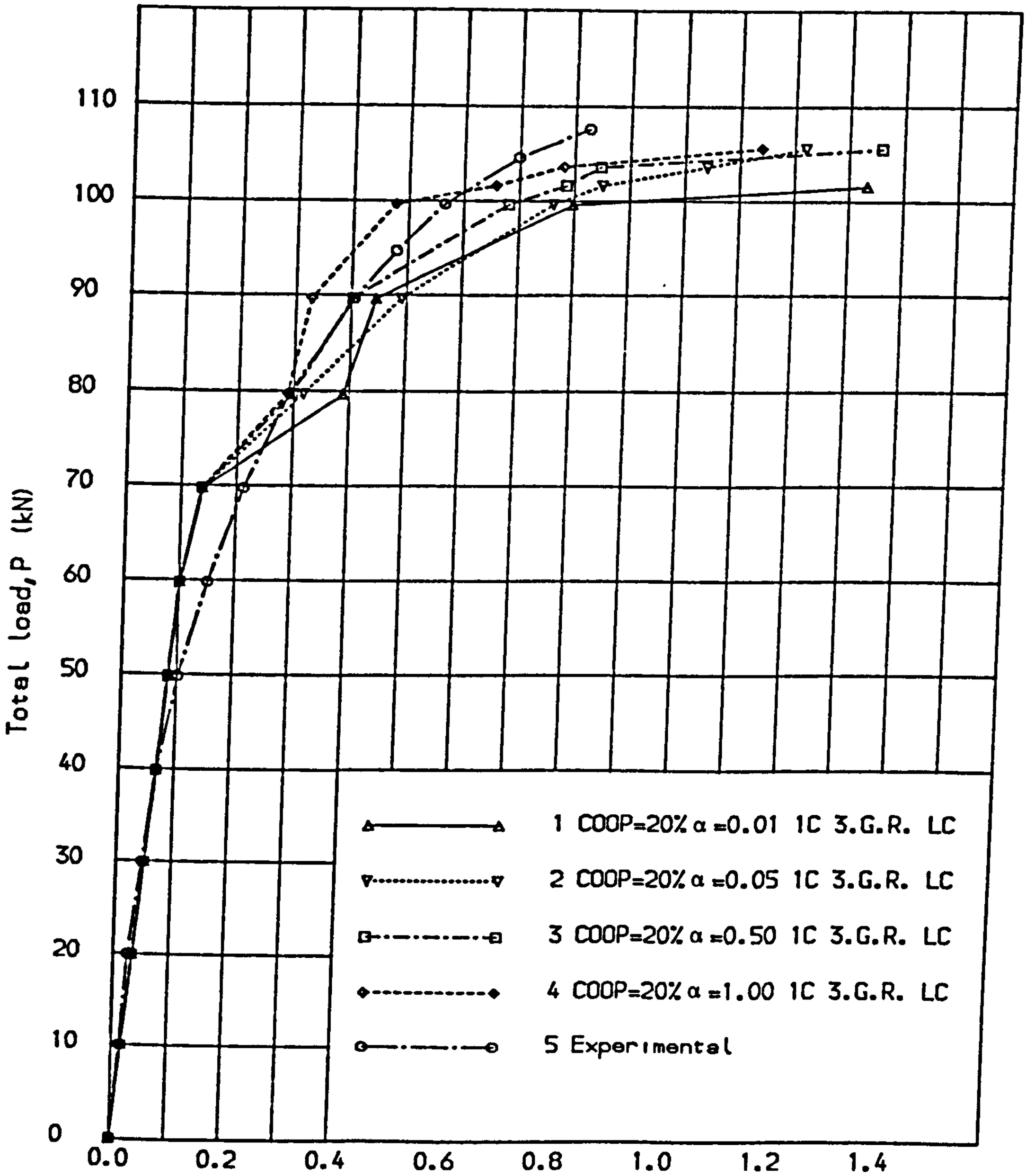

Fig. (6.33) Load deflection curves for deep beam, (V.S.M.1).

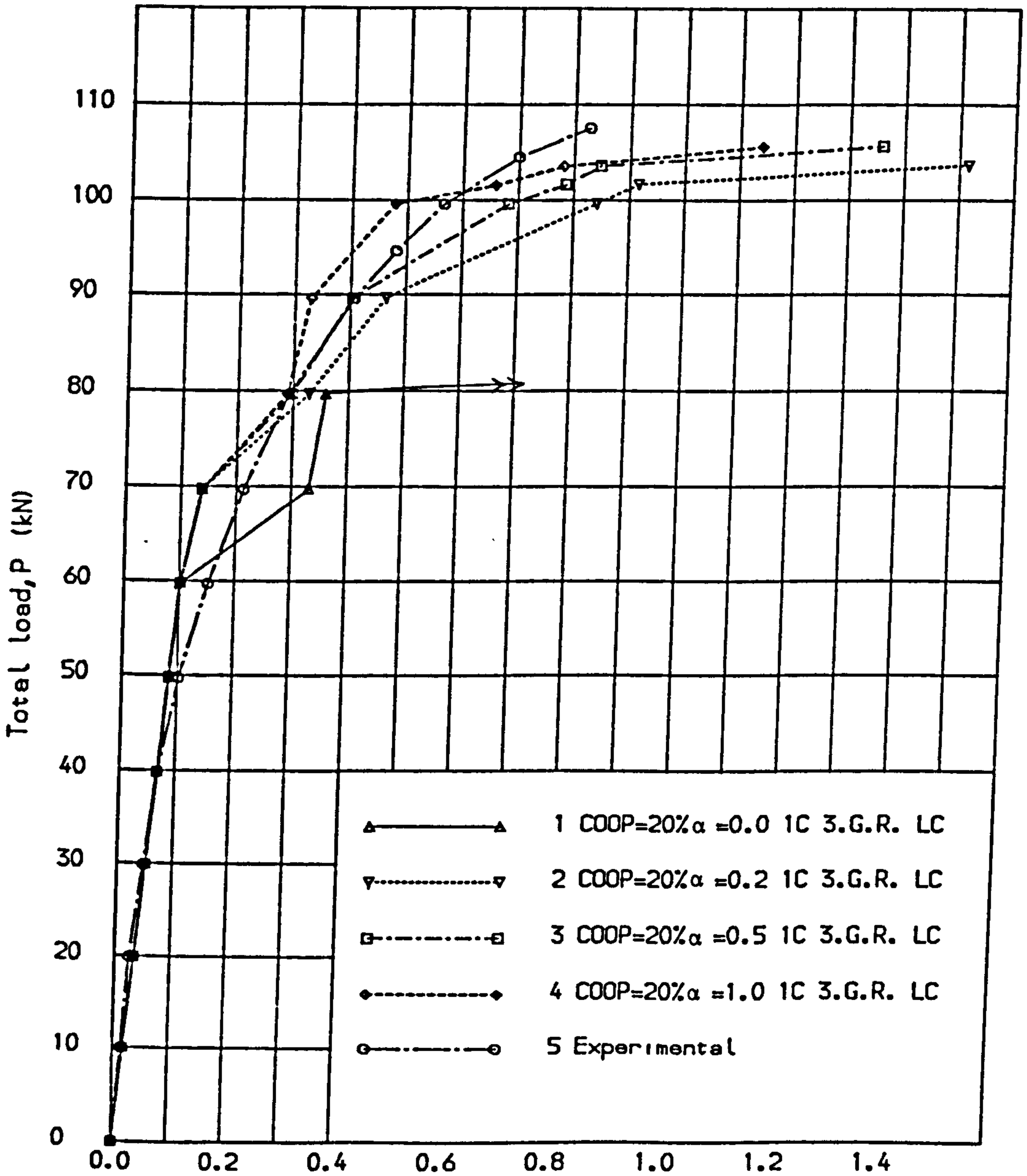

Fig. (6.34) Load deflection curves for deep beam, (V.S.M.1).

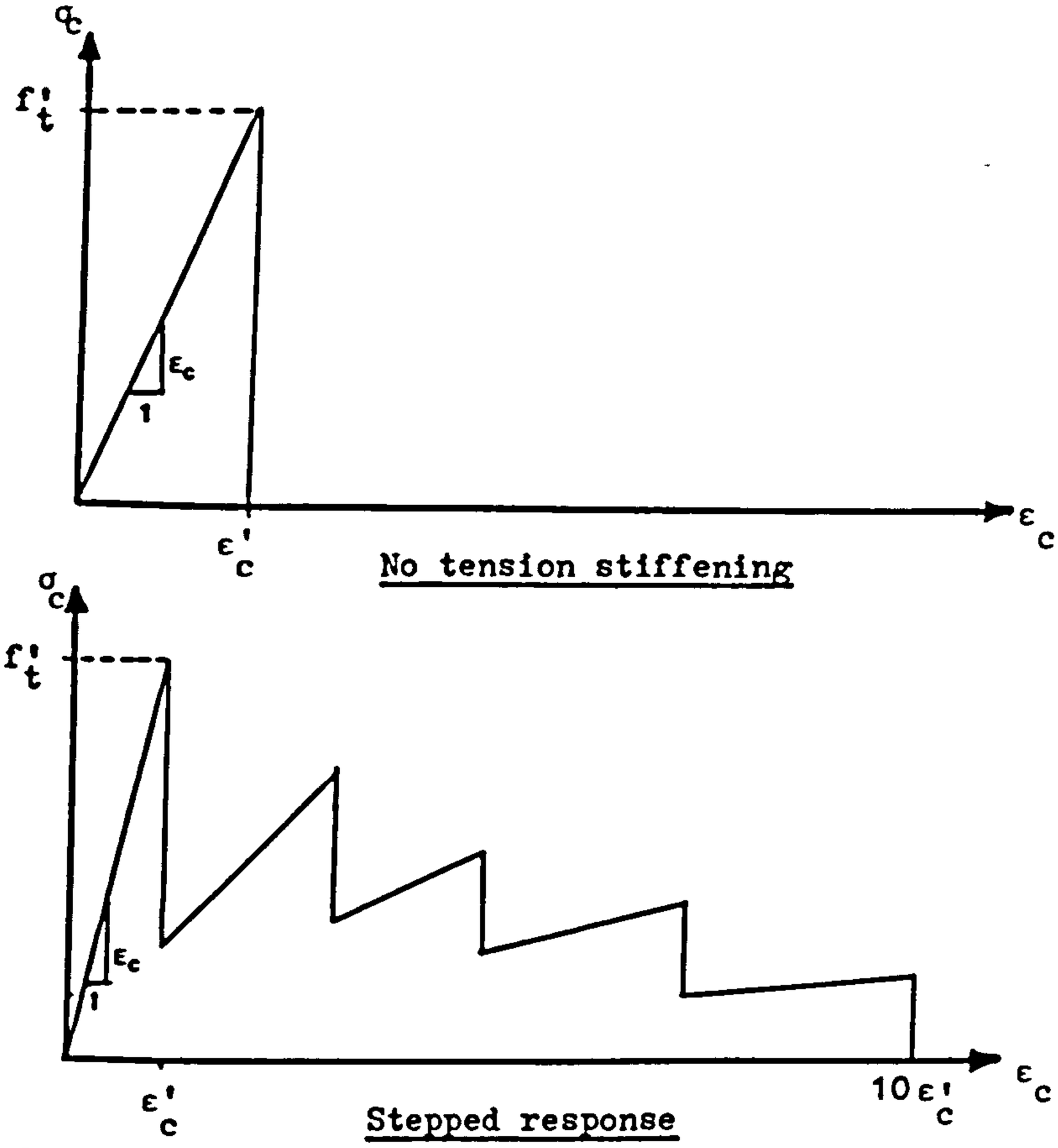

Figure (6·35) Alternative stress-strain diagrams for concrete in tension.

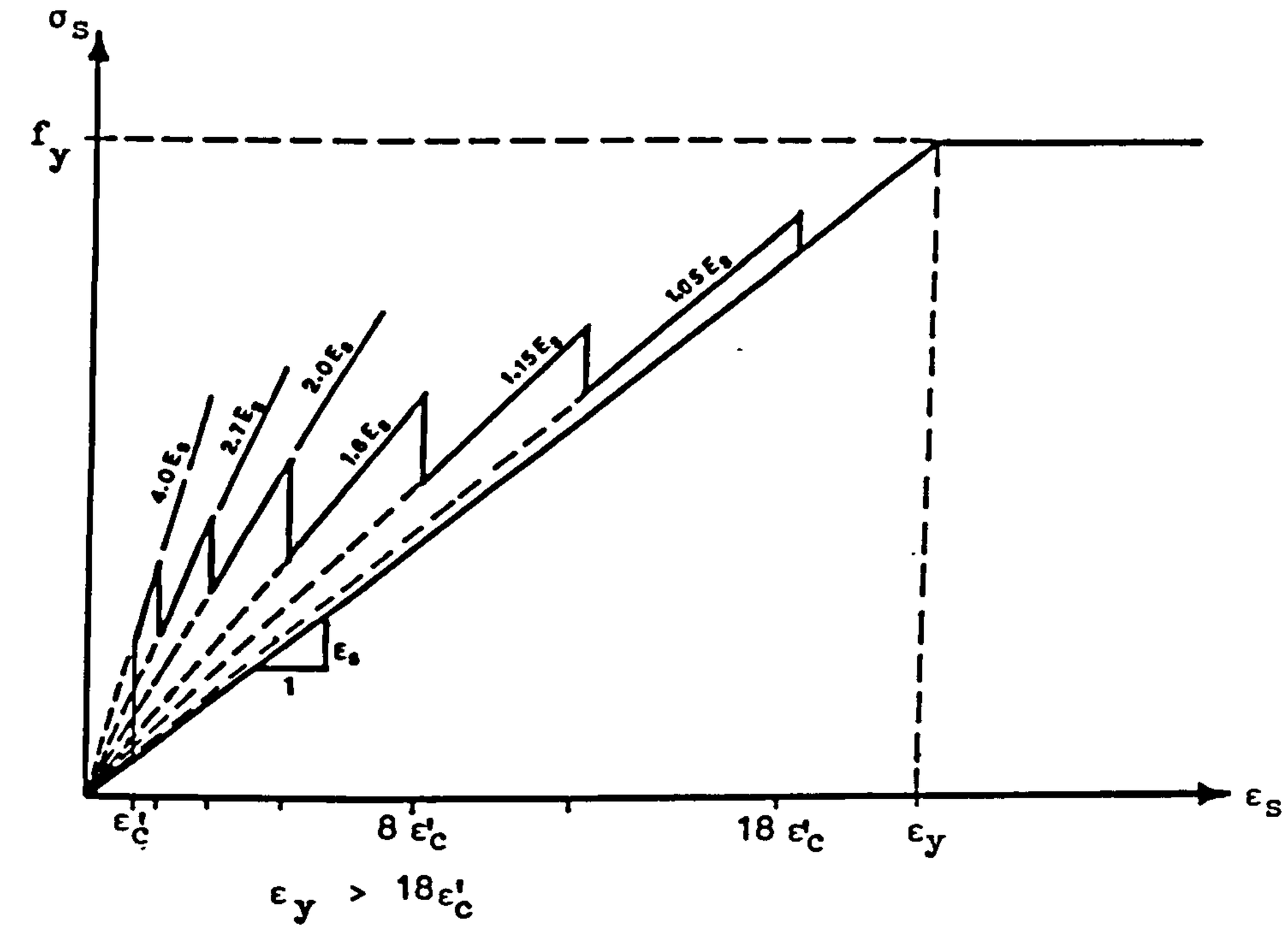

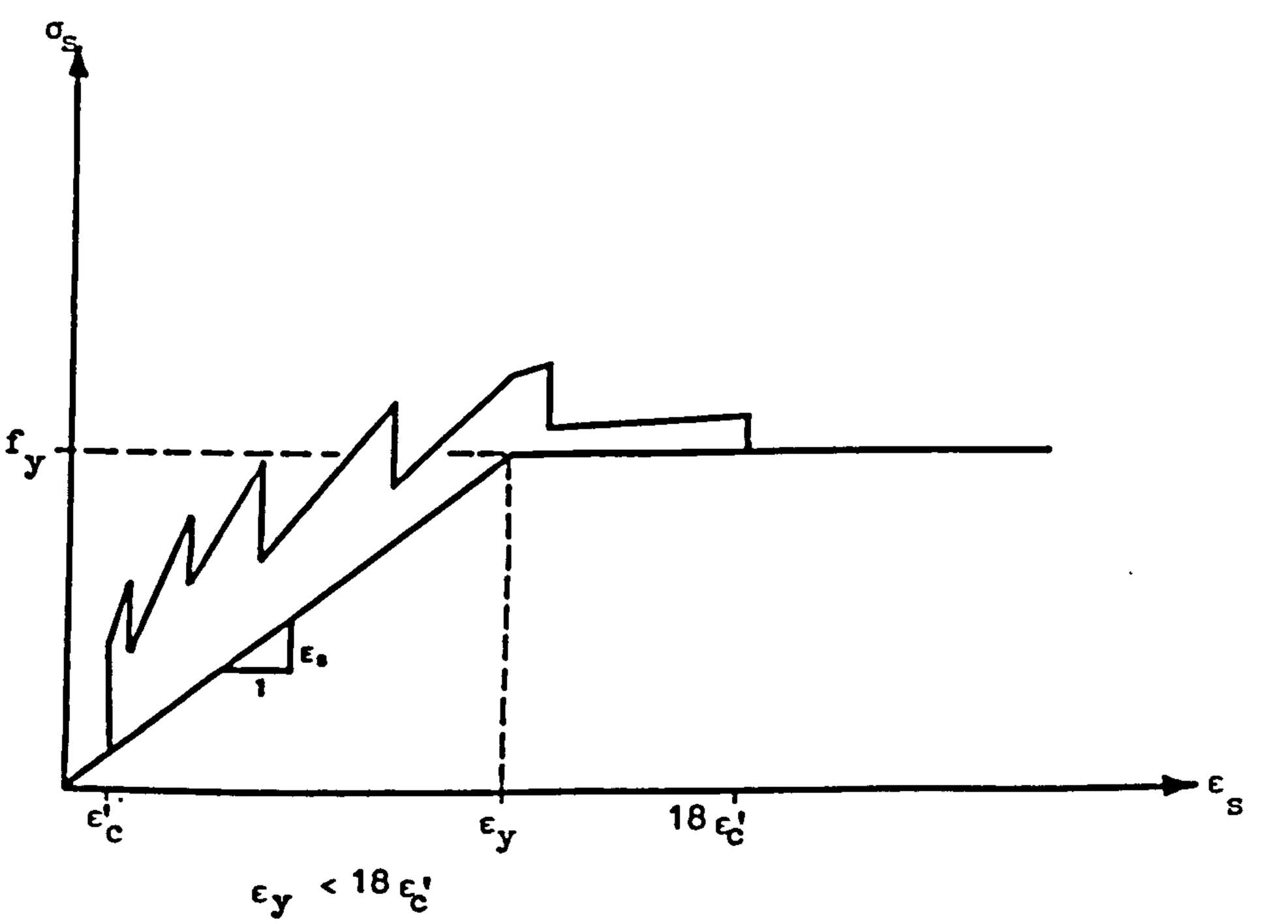

Figure (6·36) Modified stress-strain diagrams for tension steel after cracking to account for tension stiffening.

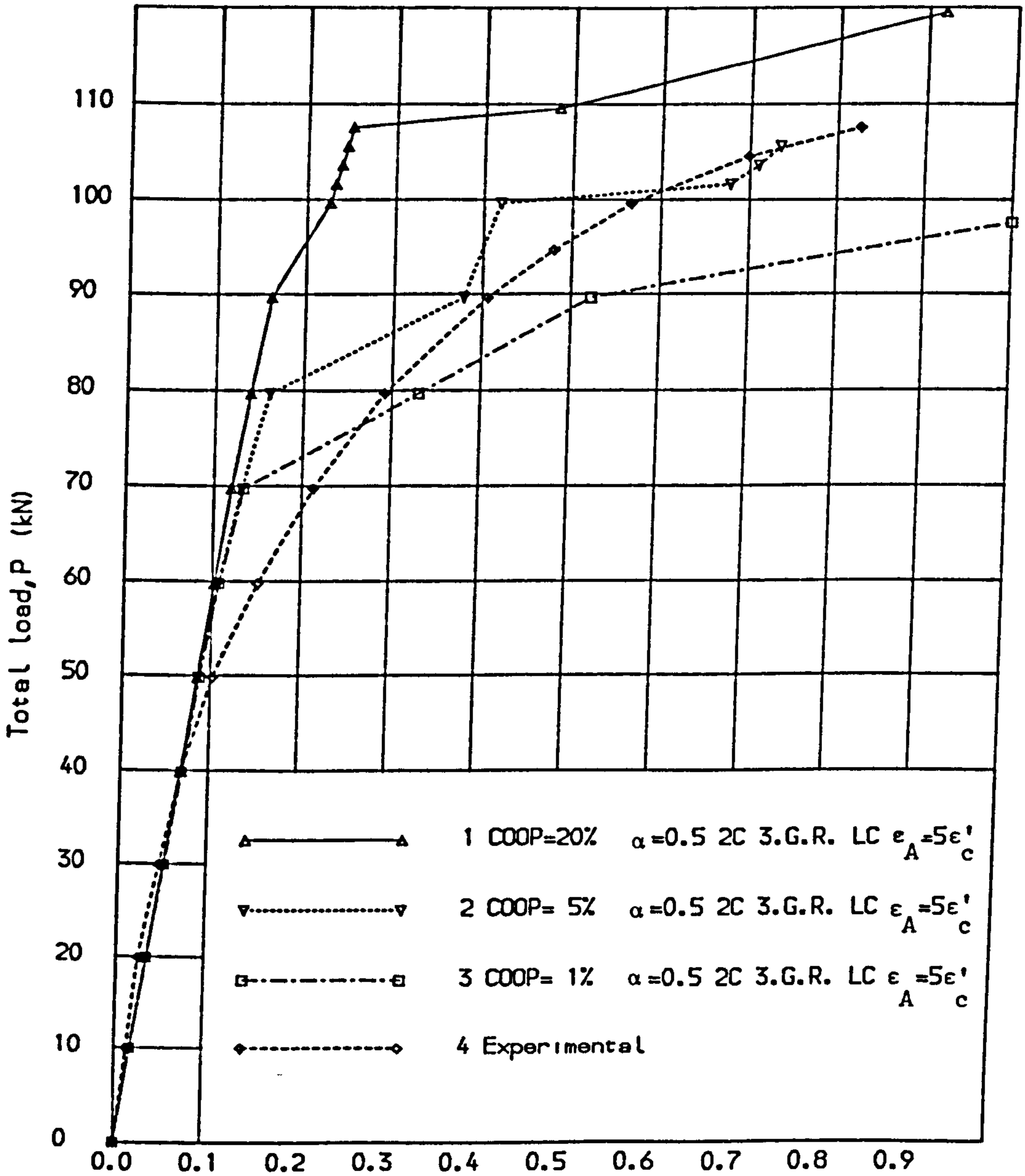

Fig. (6.37) Load deflection curves for deep beam, (V.S.M.1).

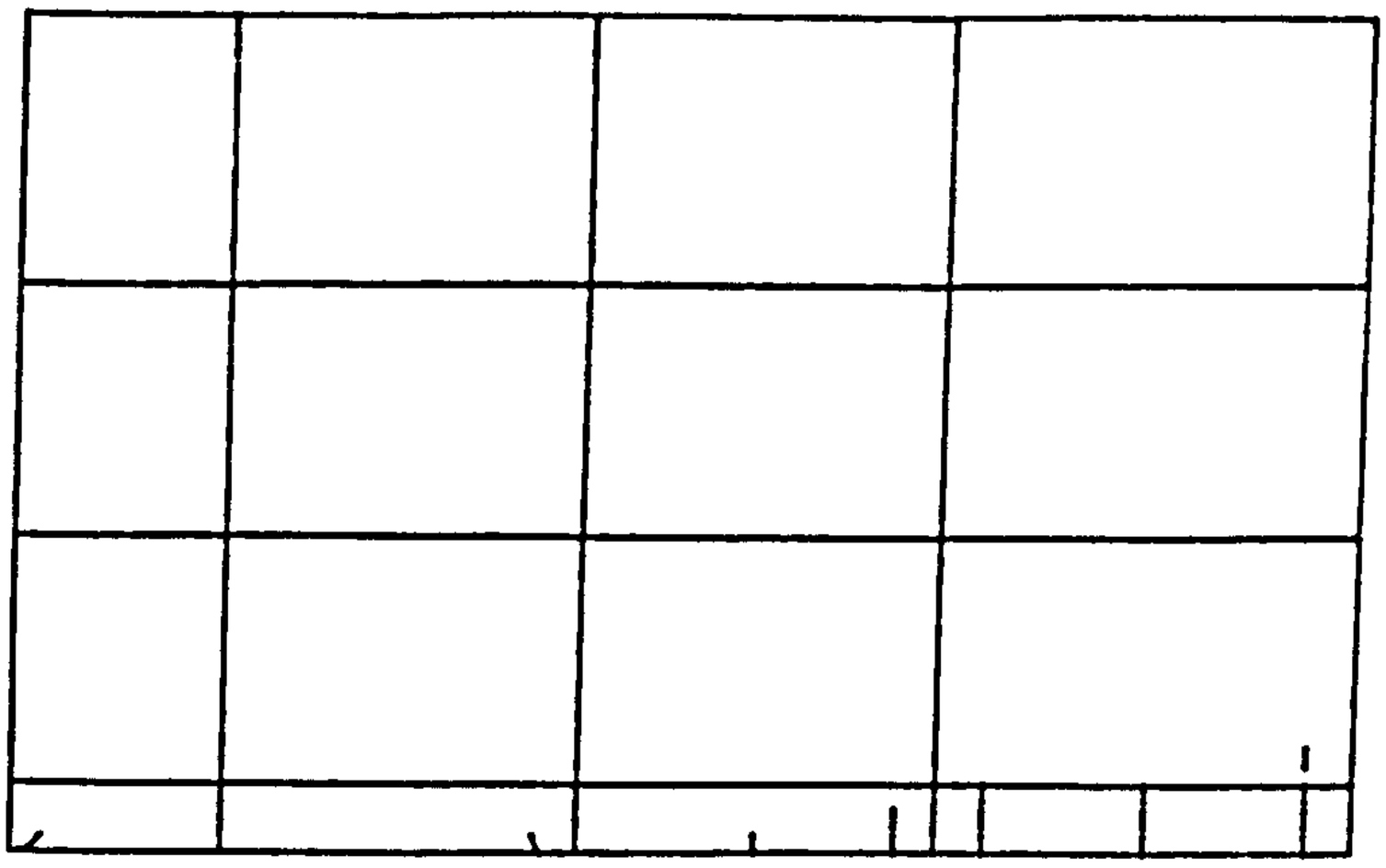

COOP = 20%

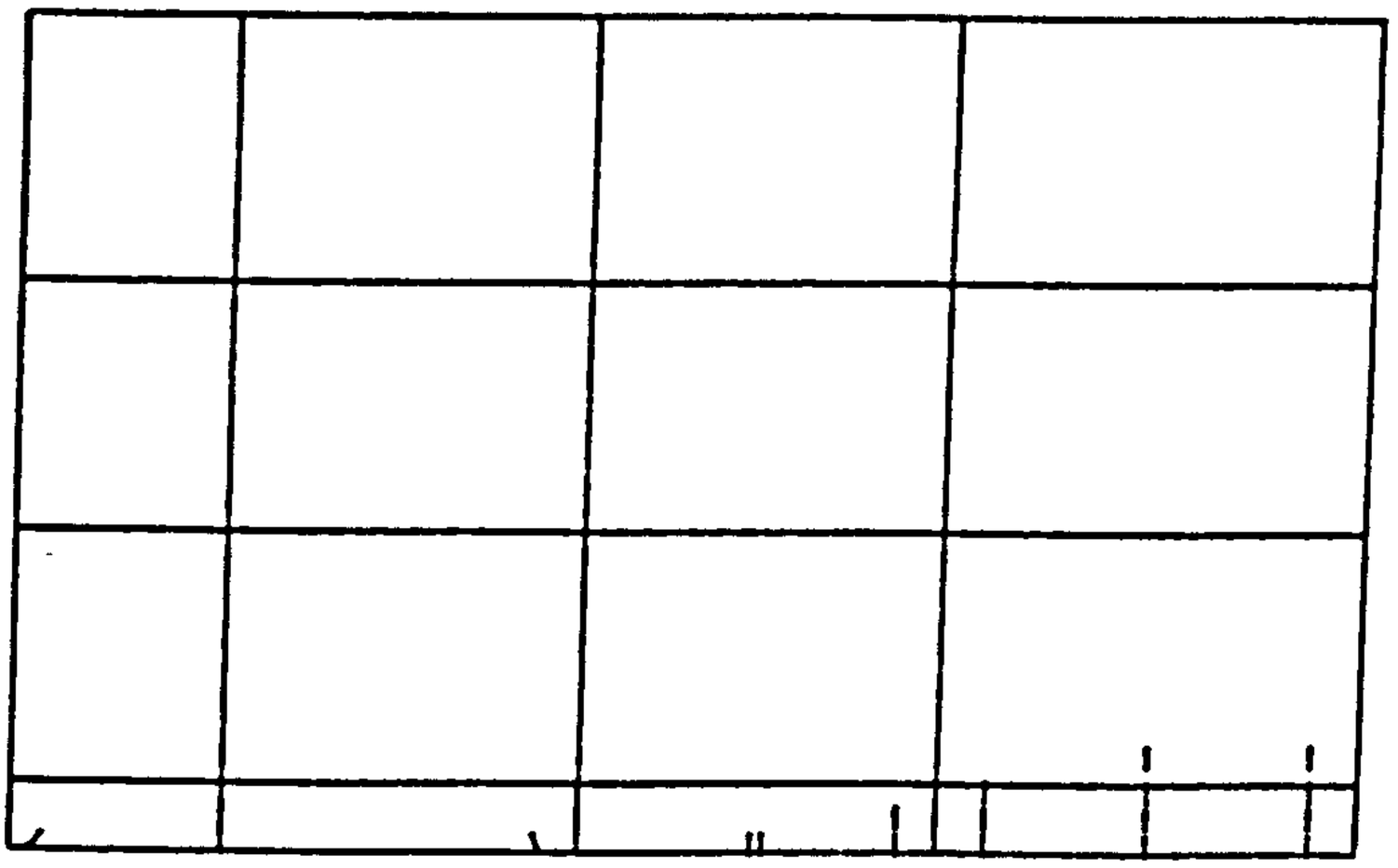

COOP = 5%

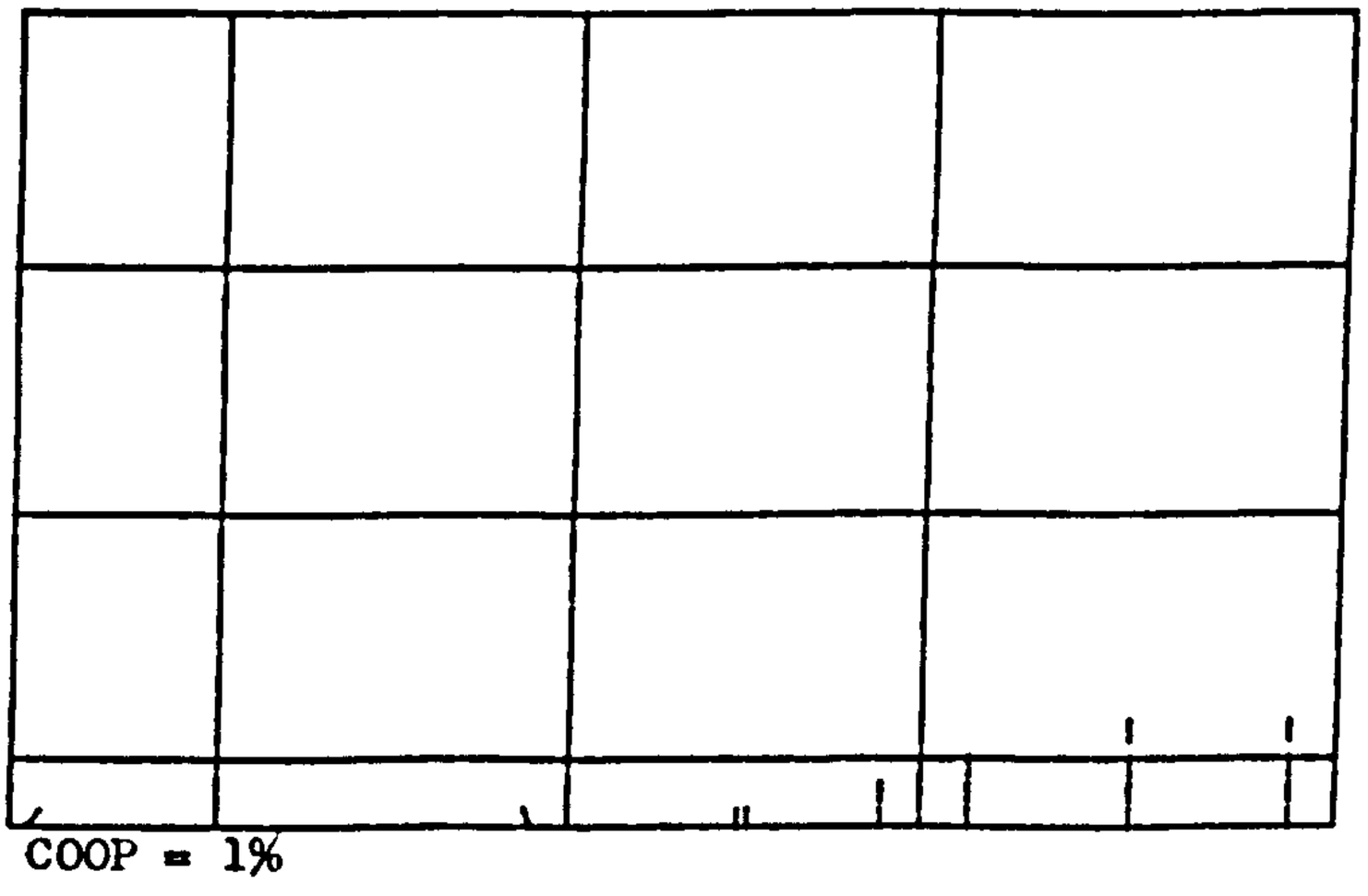

COOP = 1%

Figure (6·38) Crack pattern at load = 60·7 kN, ($\varepsilon_A = 5\ \varepsilon_c'$).

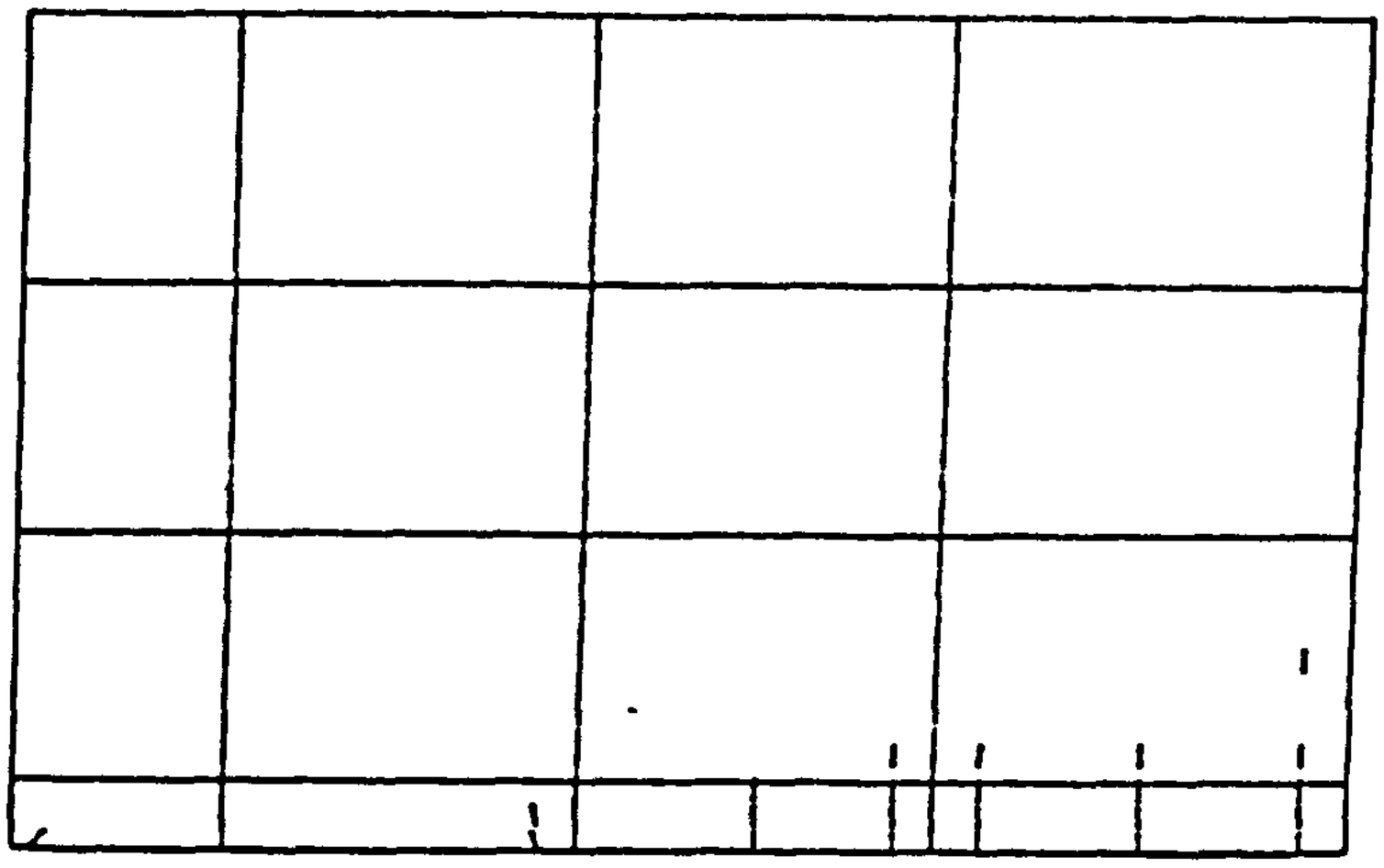

COOP = 20%

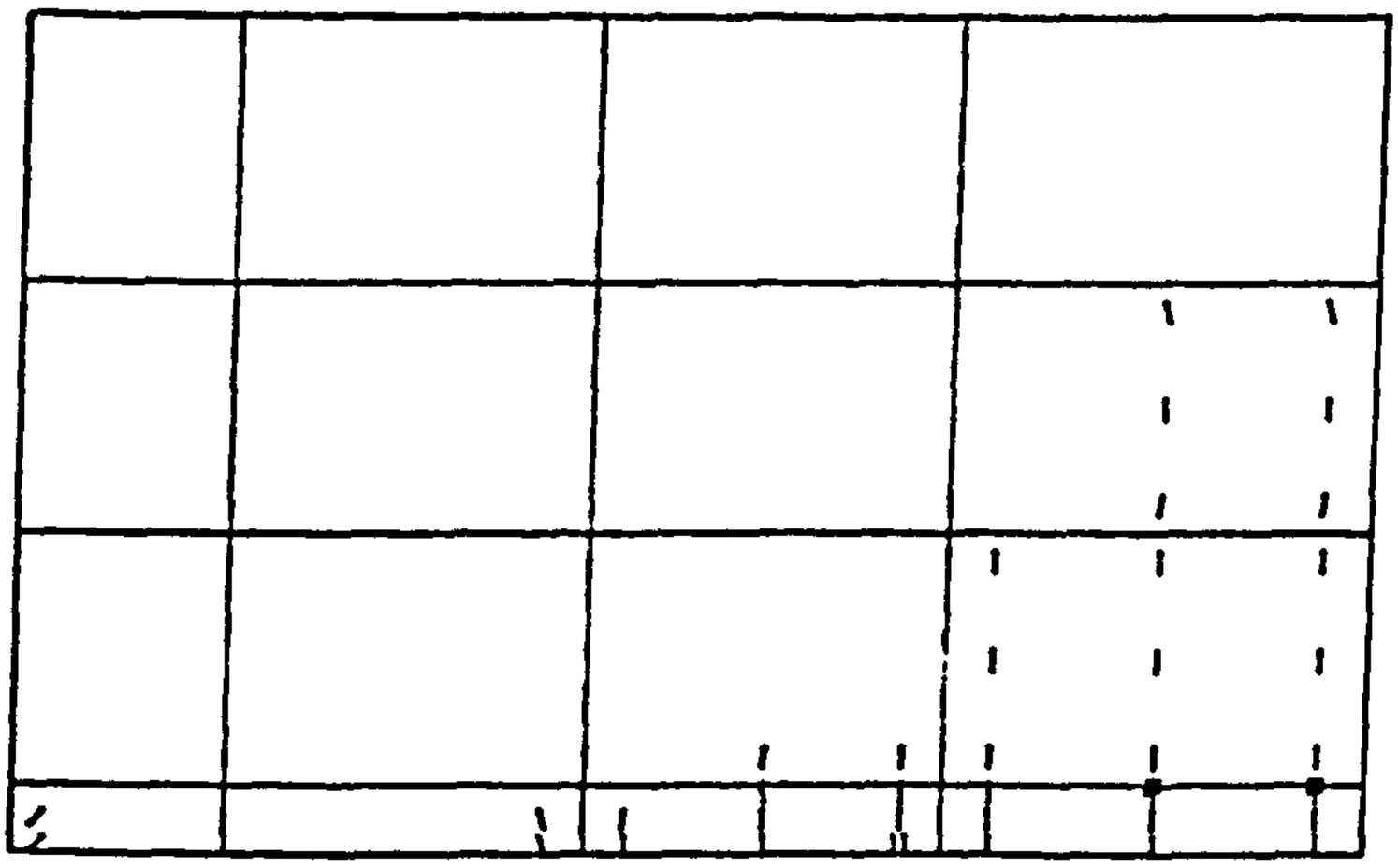

COOP = 5%

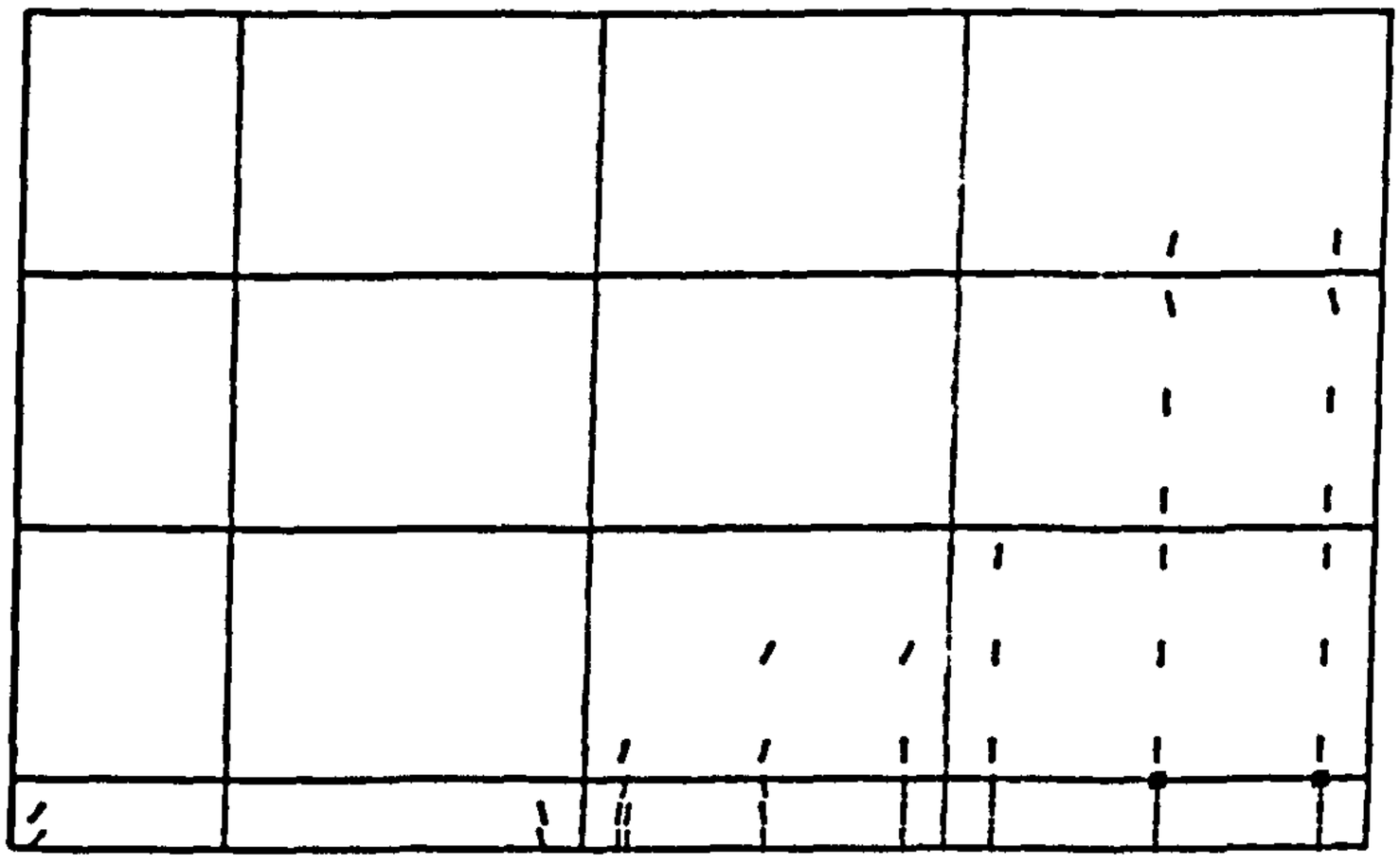

COOP = 1%

Figure (6·39) Crack pattern at load = 89·6 kN, ($\varepsilon_A = 5\ \varepsilon_c'$).

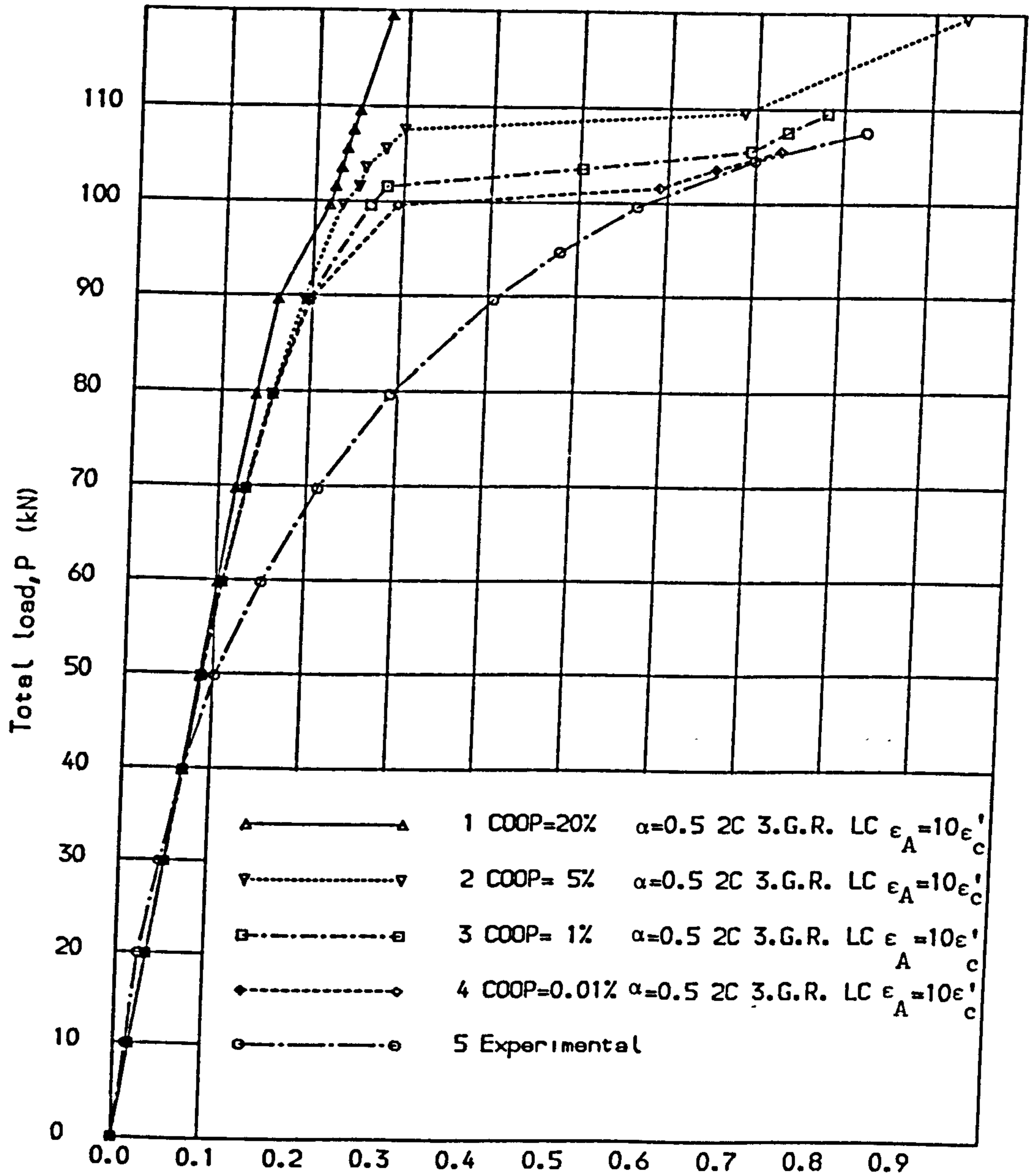

Fig. (6.40) Load deflection curves for deep beam, (V.S.M.1).

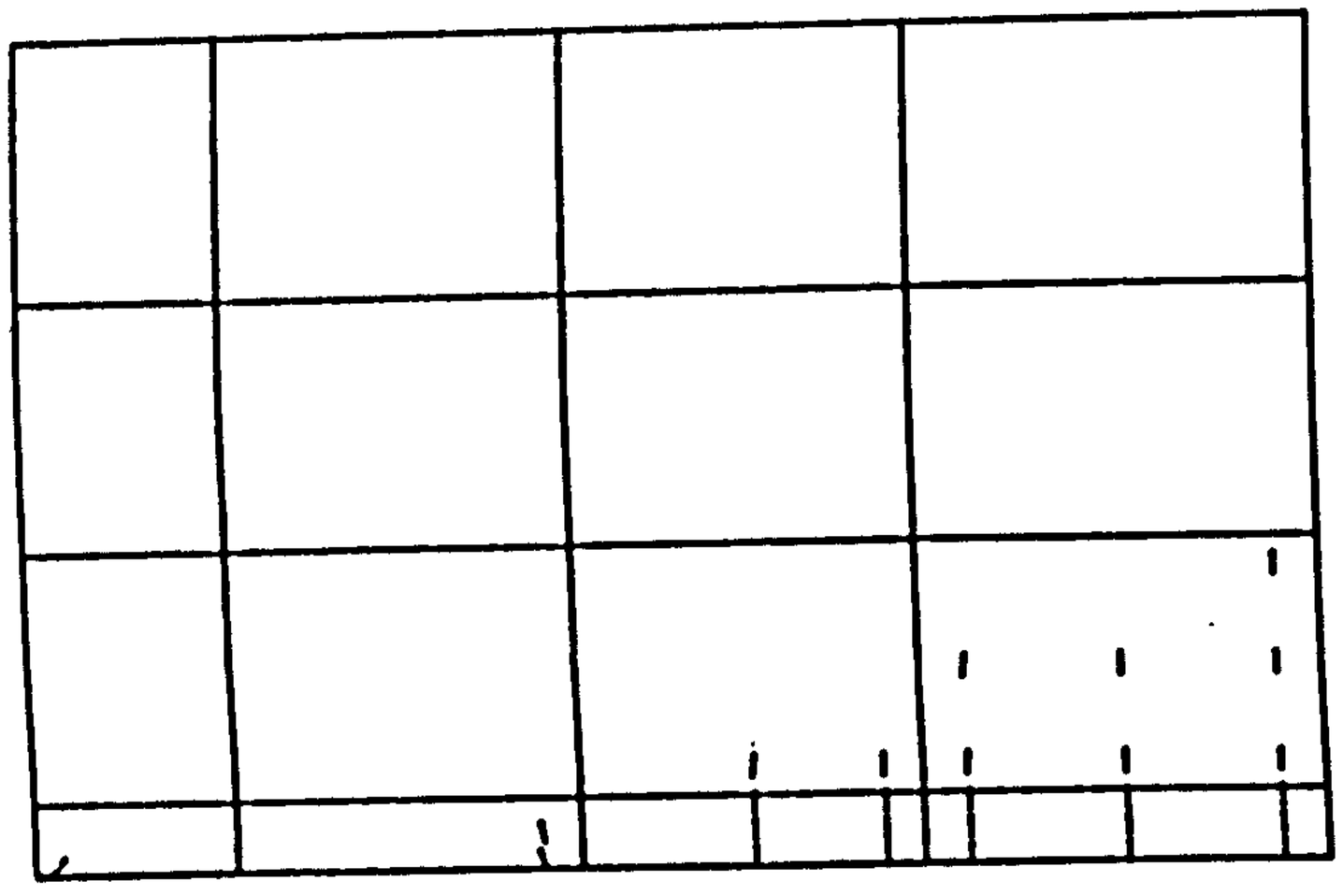

COOP = 20%

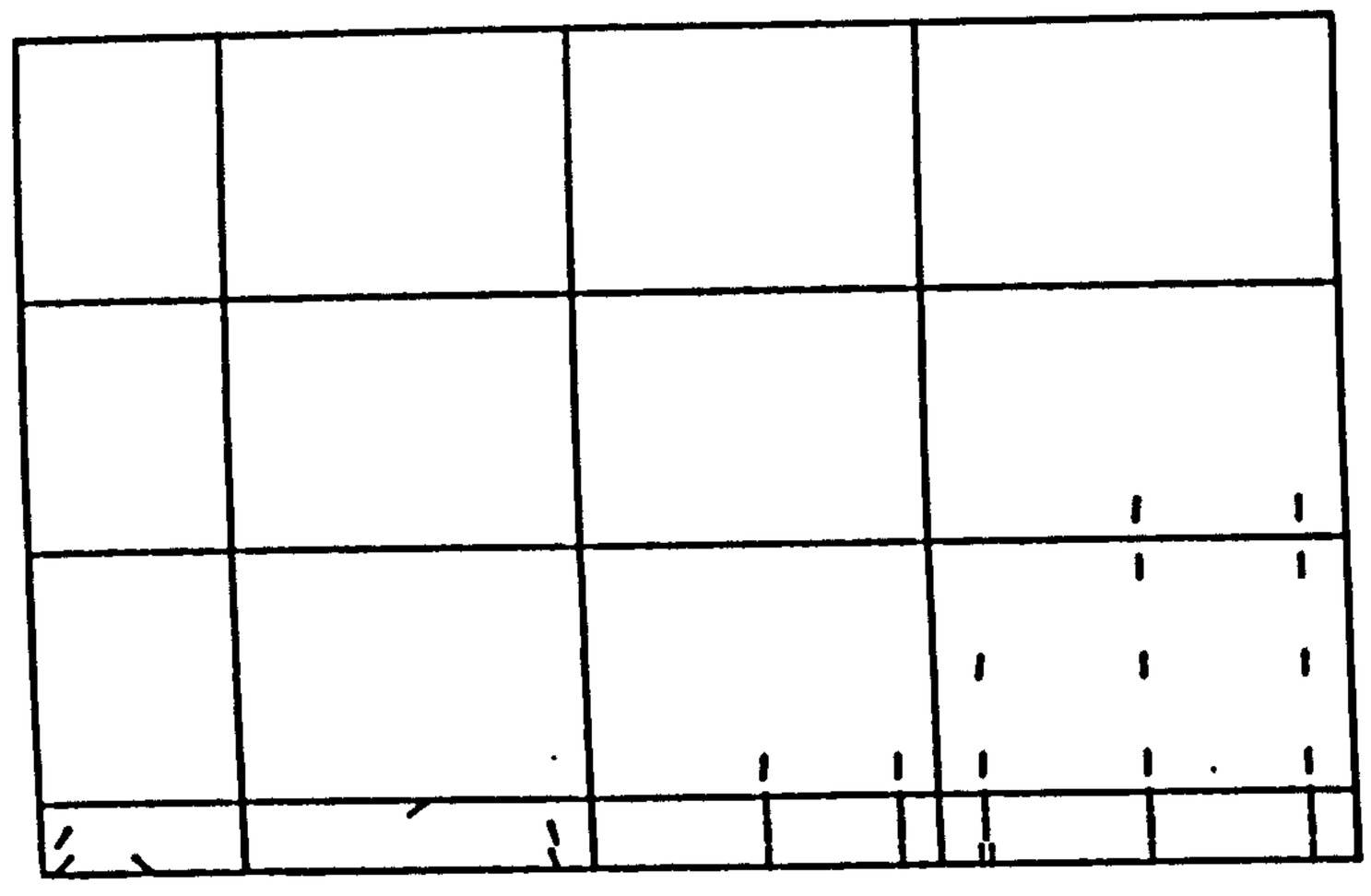

COOP = 1%

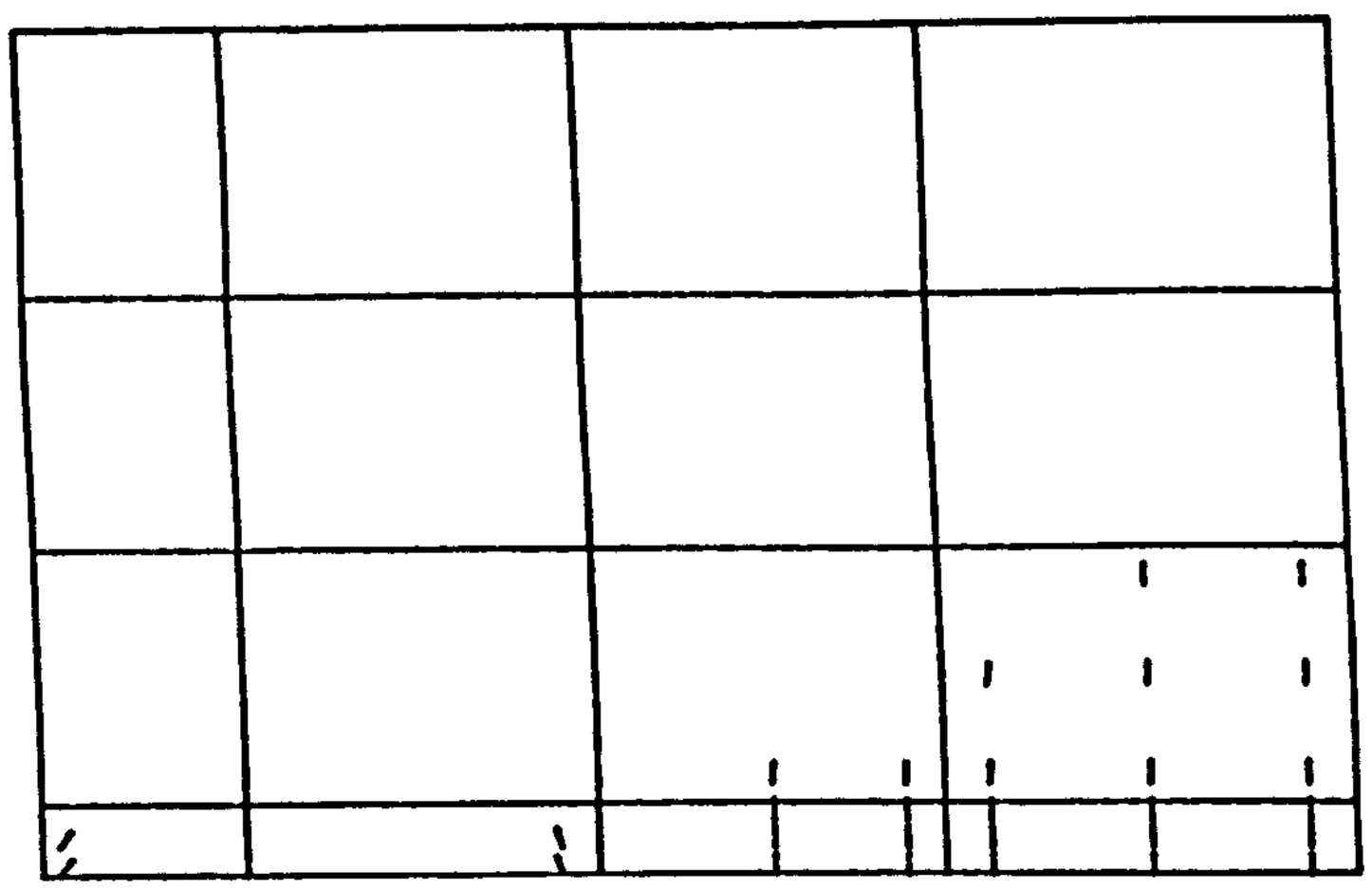

COOP = 5 %

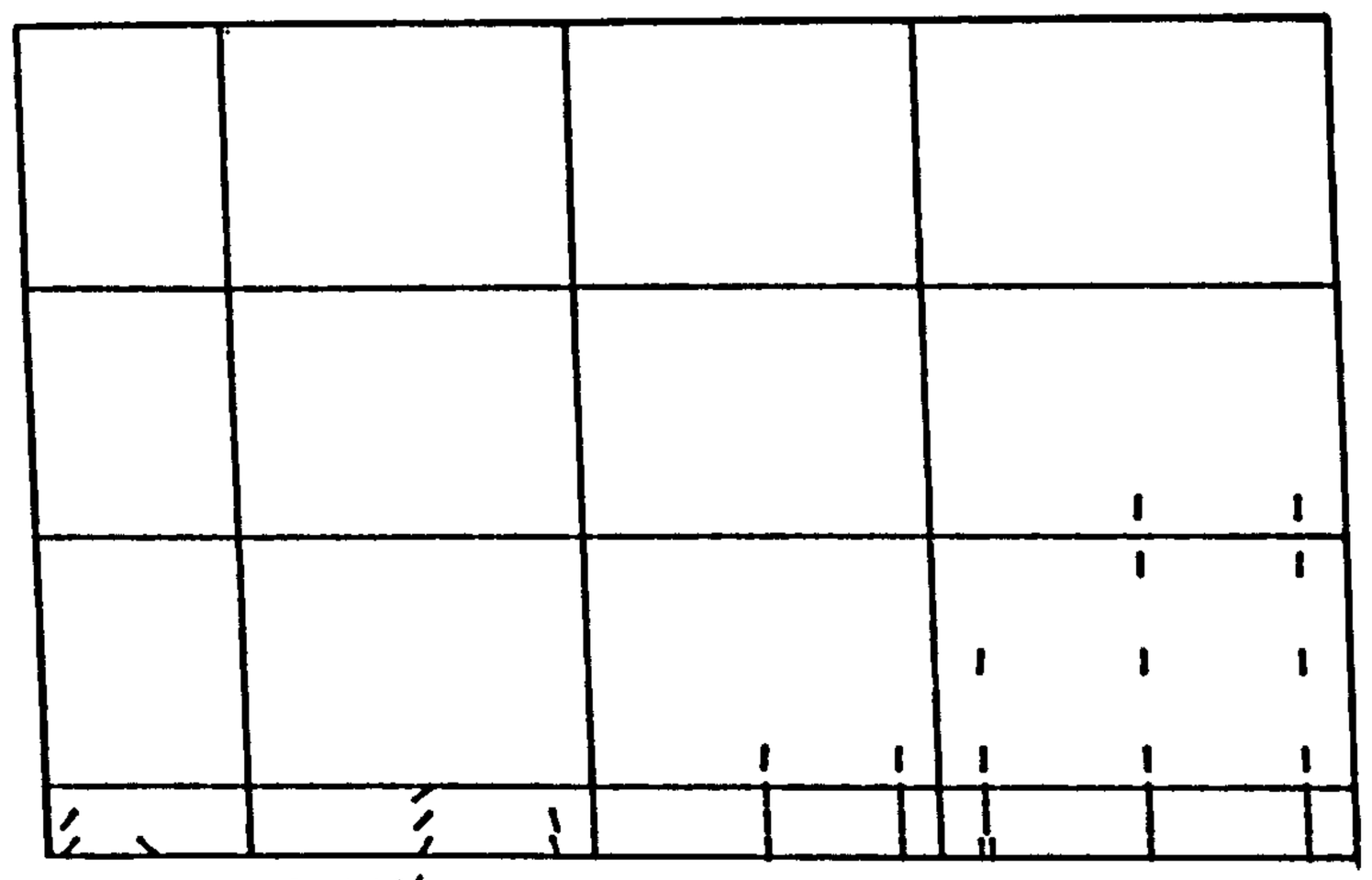

COOP = 0·01%

Figure (6·41) Crack patterns at load = 99·6 kN , ($\varepsilon_A = 10\ \varepsilon_c'$).

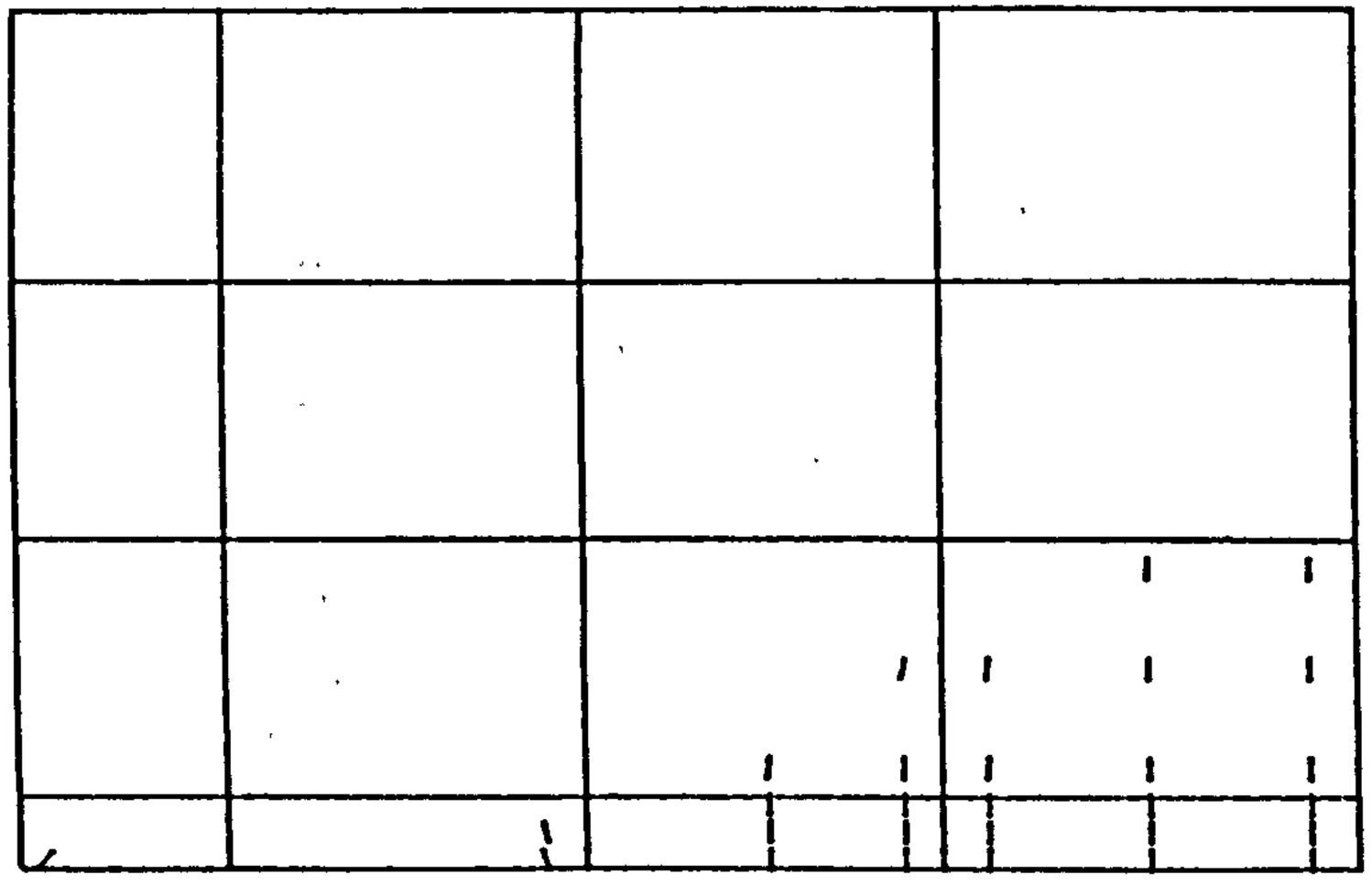

COOP = 20%

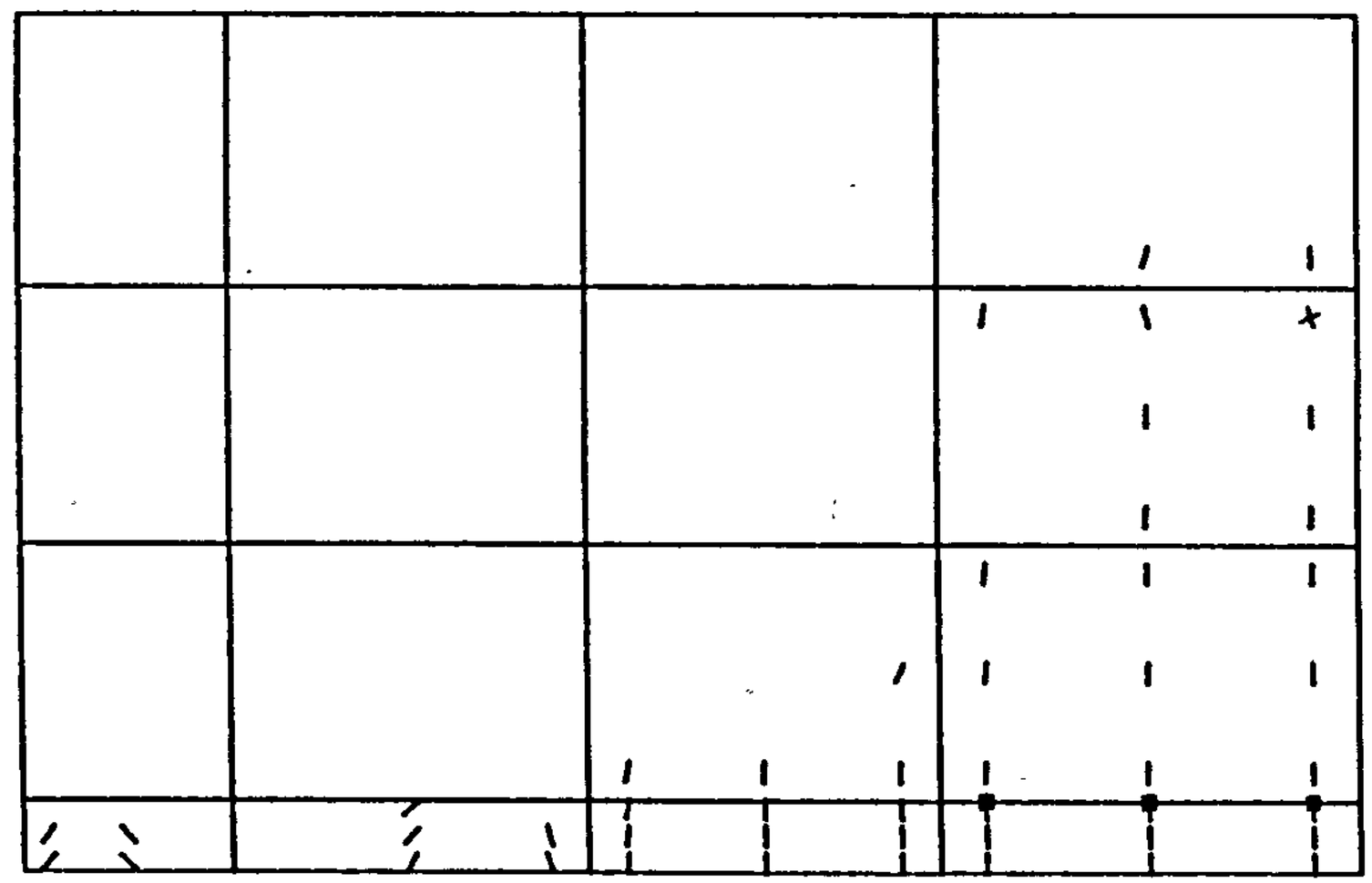

COOP = 1%

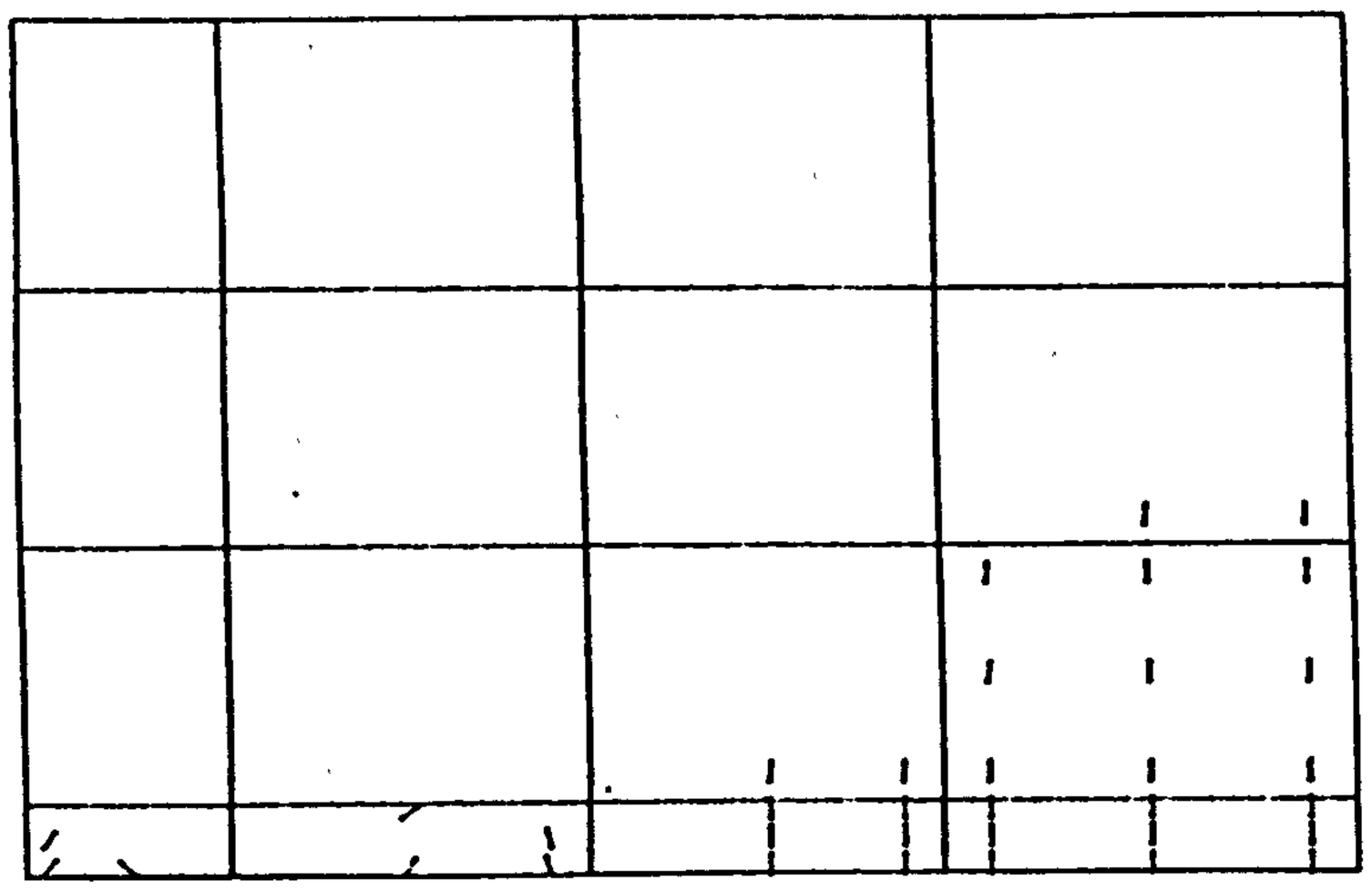

COOP = 5 %

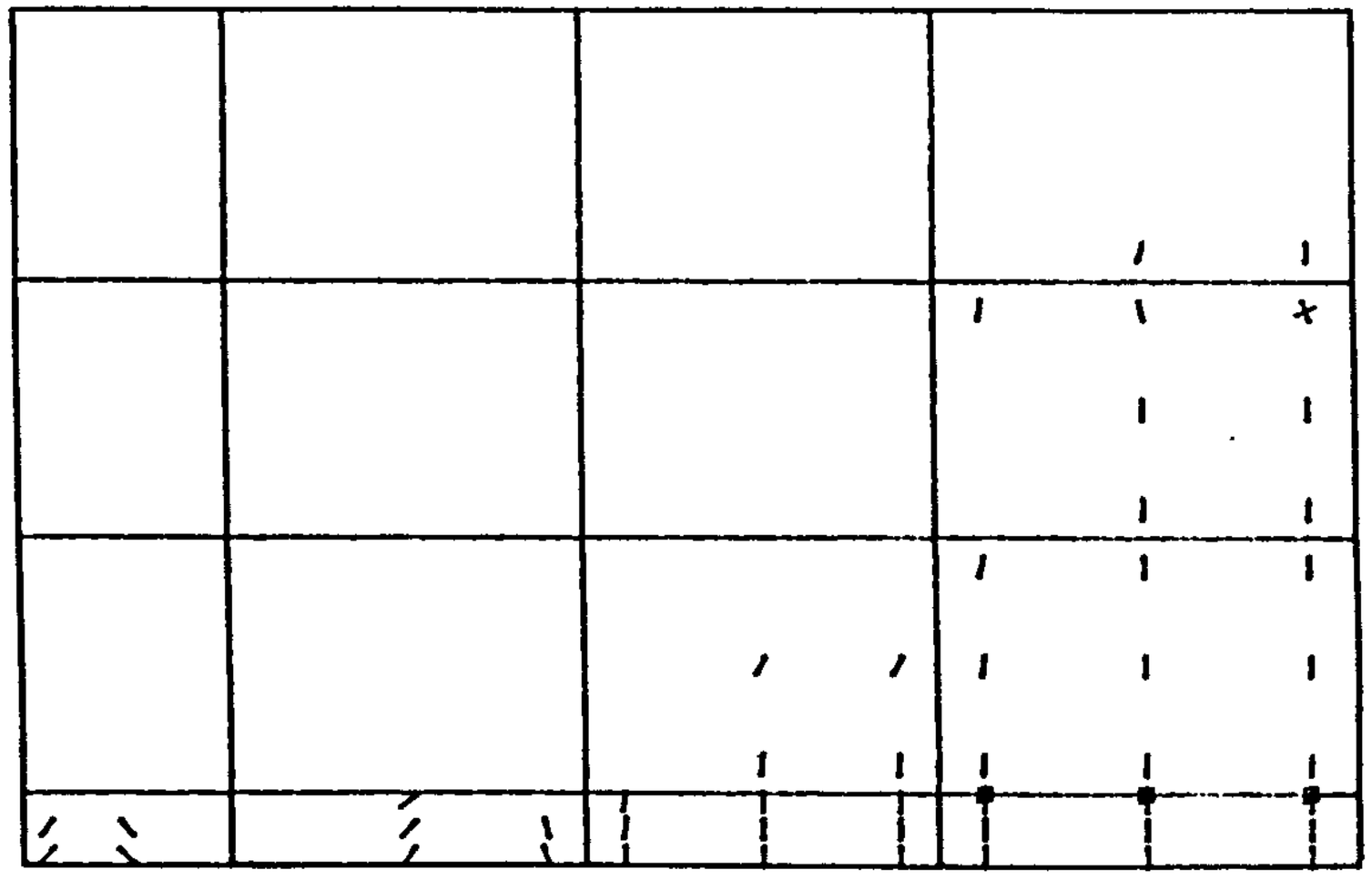

COOP = 0•01%

Figure (6•42) Crack patterns at load = 105•6 kN , ($\varepsilon_A = 10\,\varepsilon_c'$).

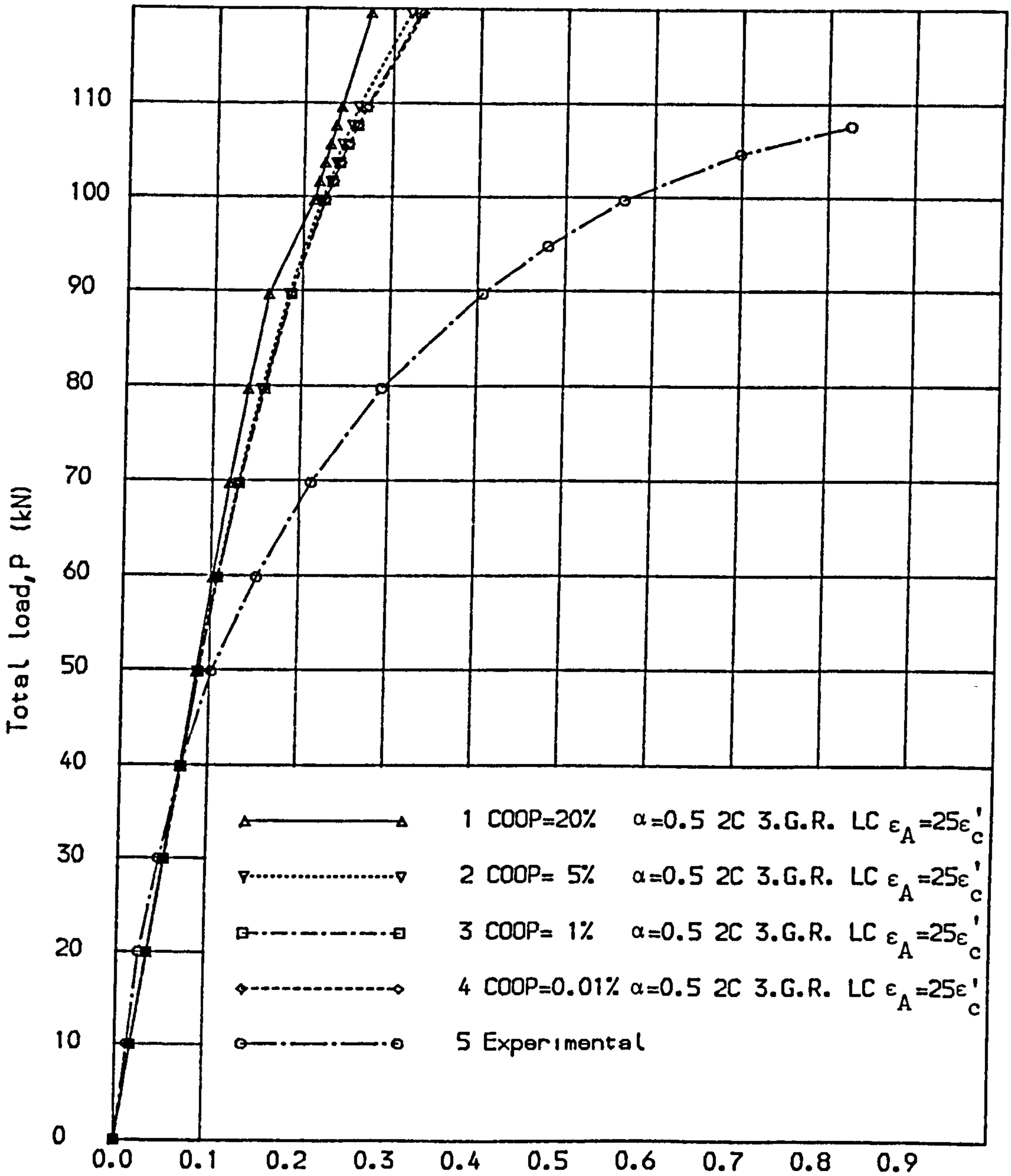

Fig. (6.43) Load deflection curves for deep beam, (V.S.M.1).

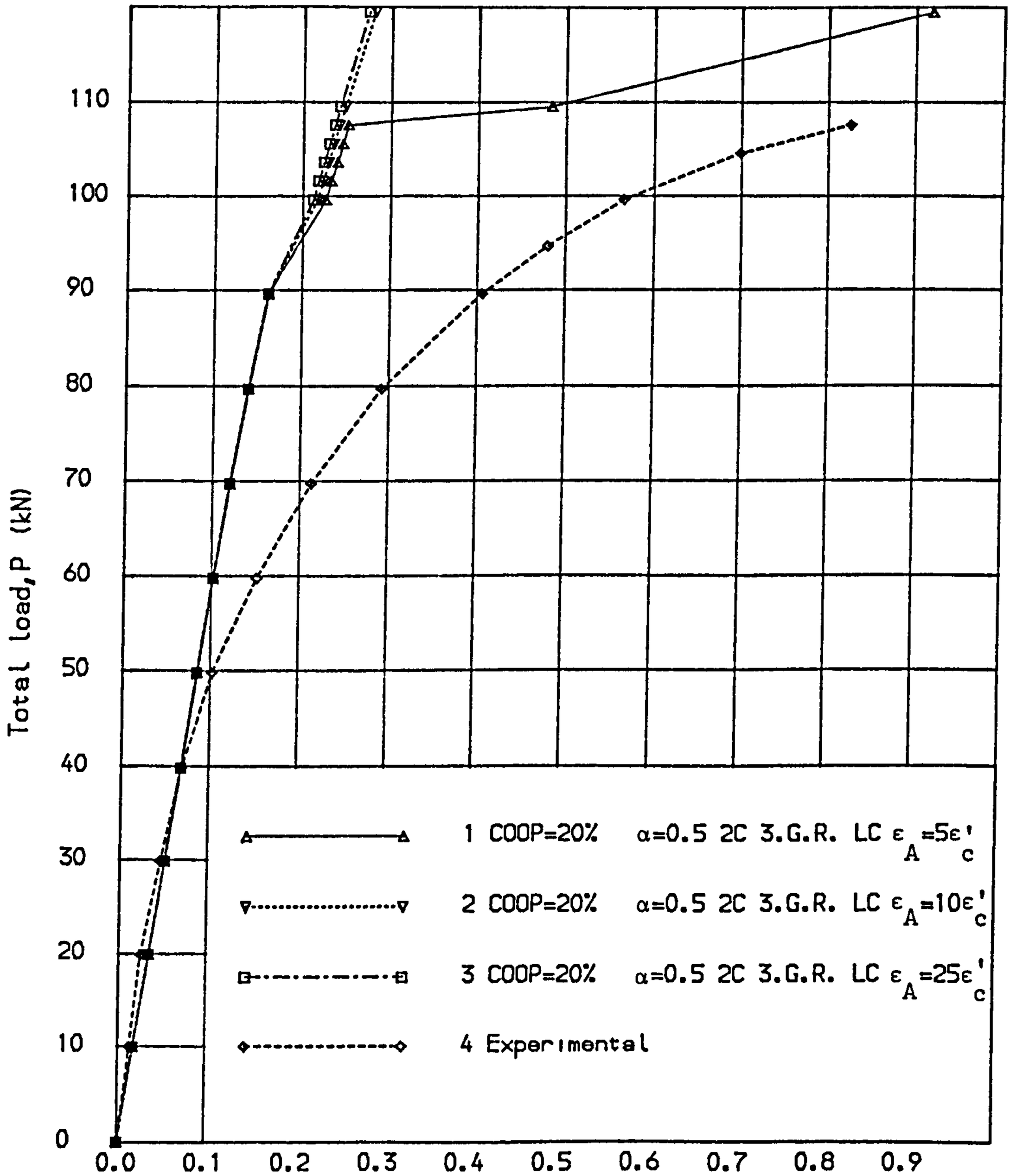

Fig. (6.44) Load deflection curves for deep beam, (V.S.M.1).

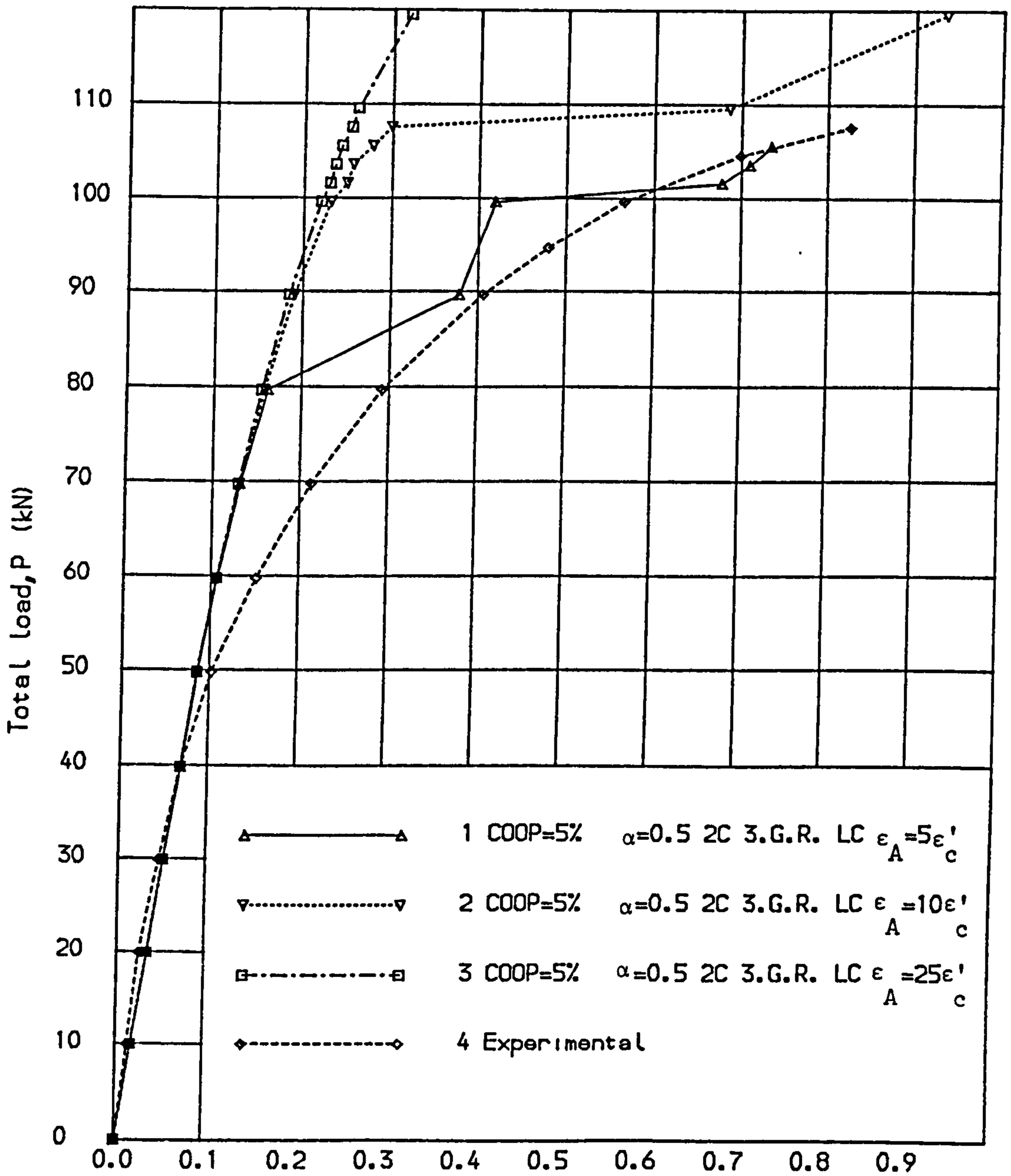

Fig. (6.45) Load deflection curves for deep beam, (V.S.M.1).

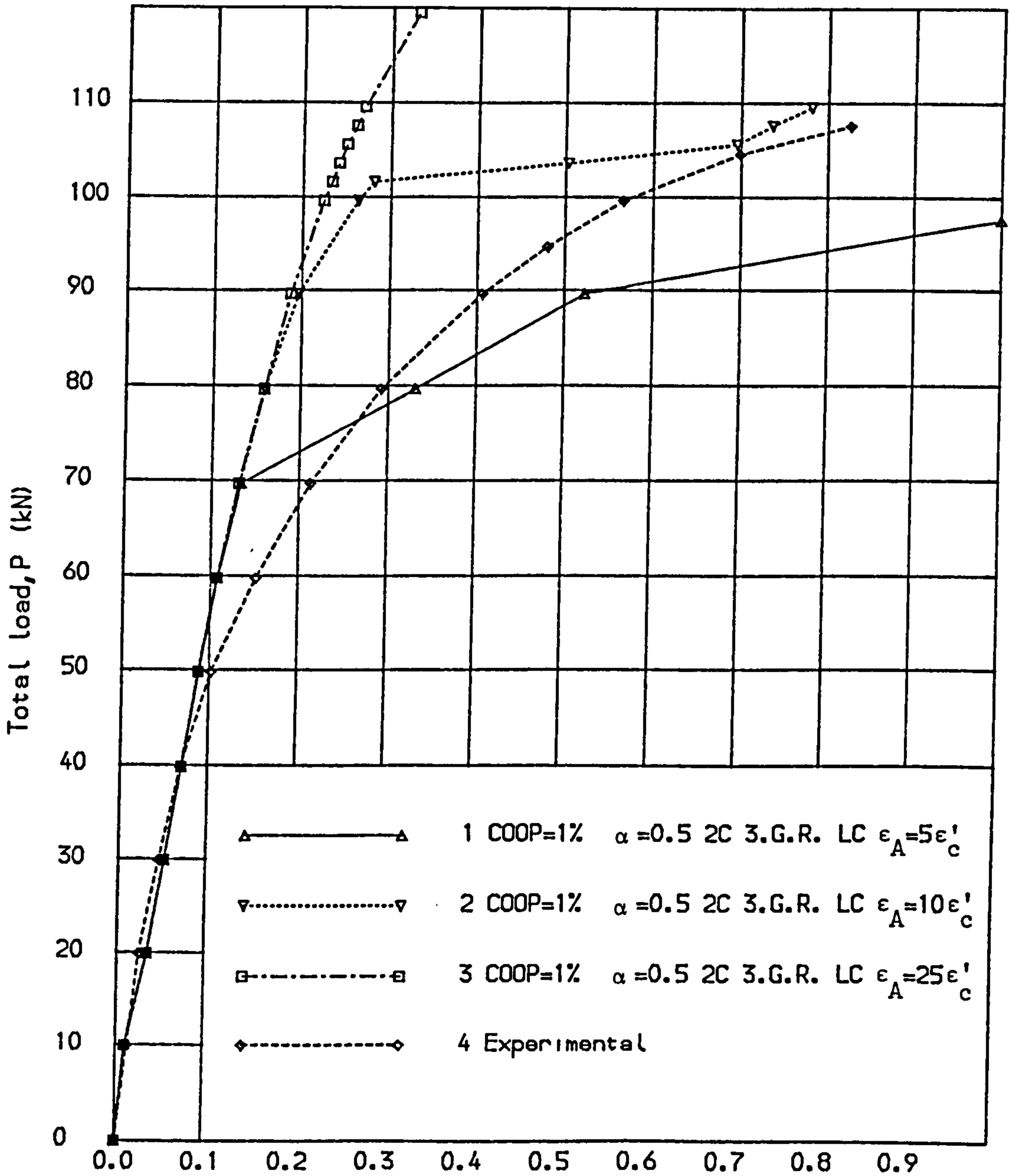

Fig.(6.46) Load deflection curves for deep beam, (V.S.M.1).

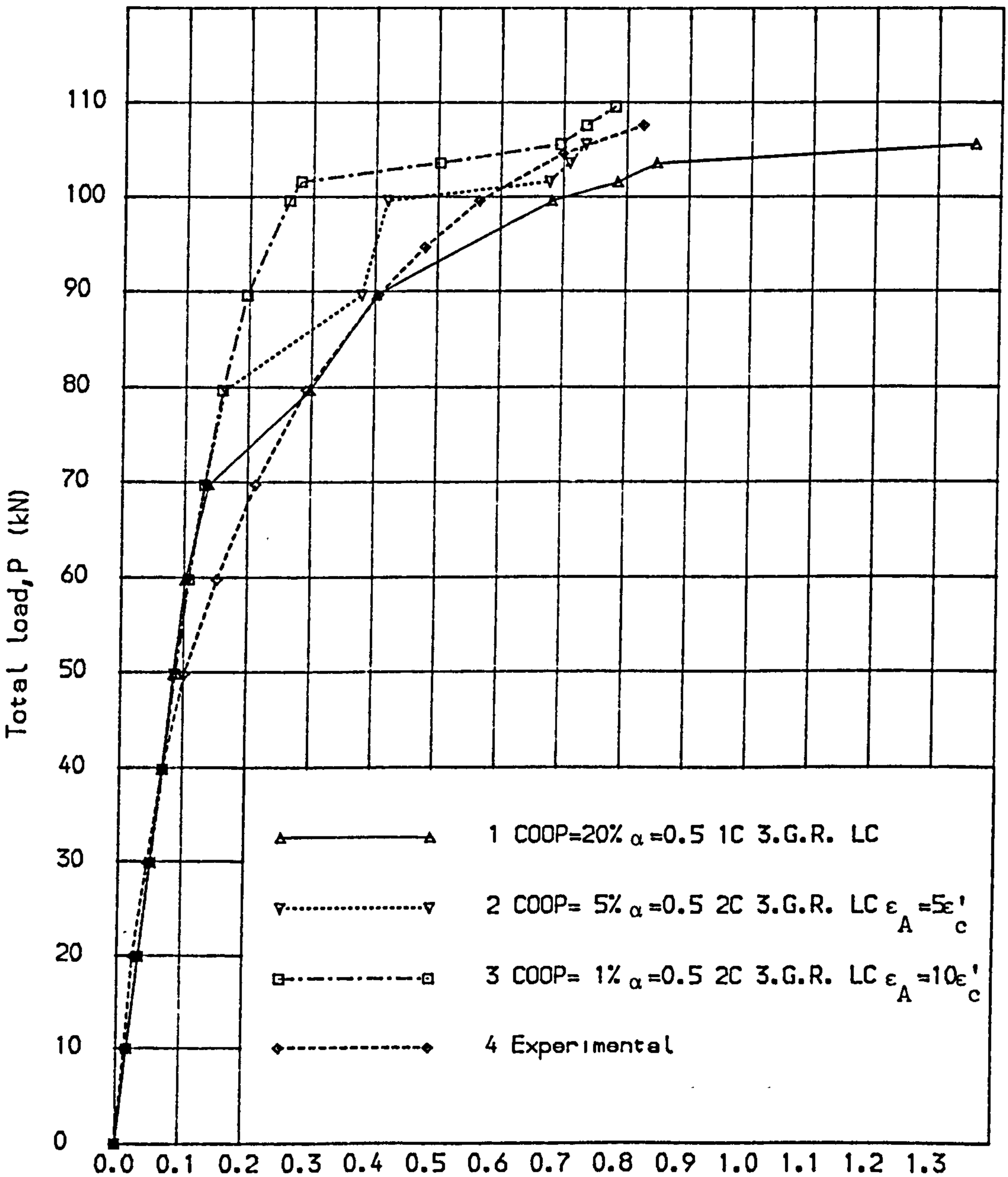

Fig. (6.47) Load deflection curves for deep beam, (V.S.M.1).

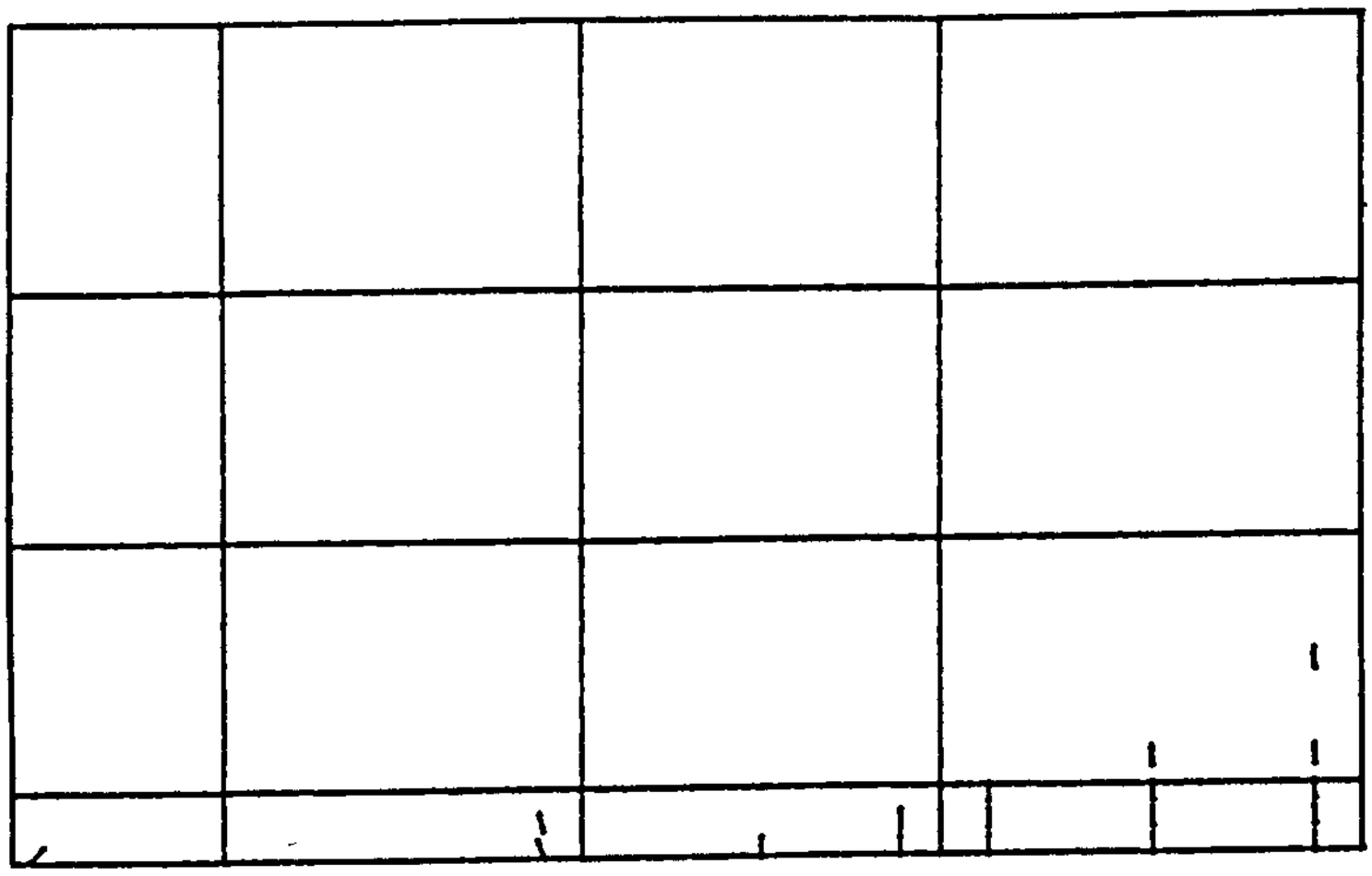

COOP = 20%, N.T.S.

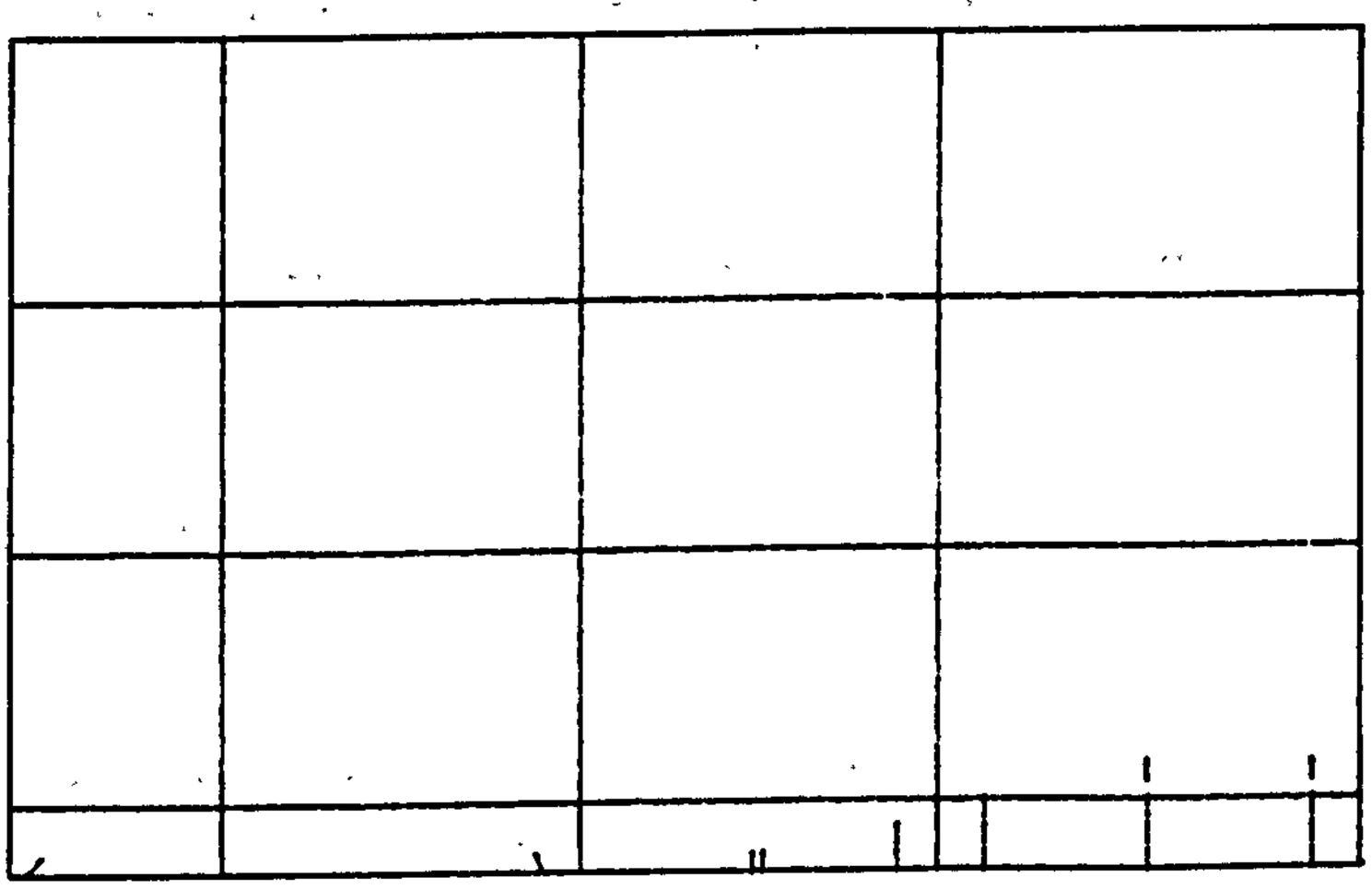

COOP = 5%, $\varepsilon_A = 5\ \varepsilon'_c$

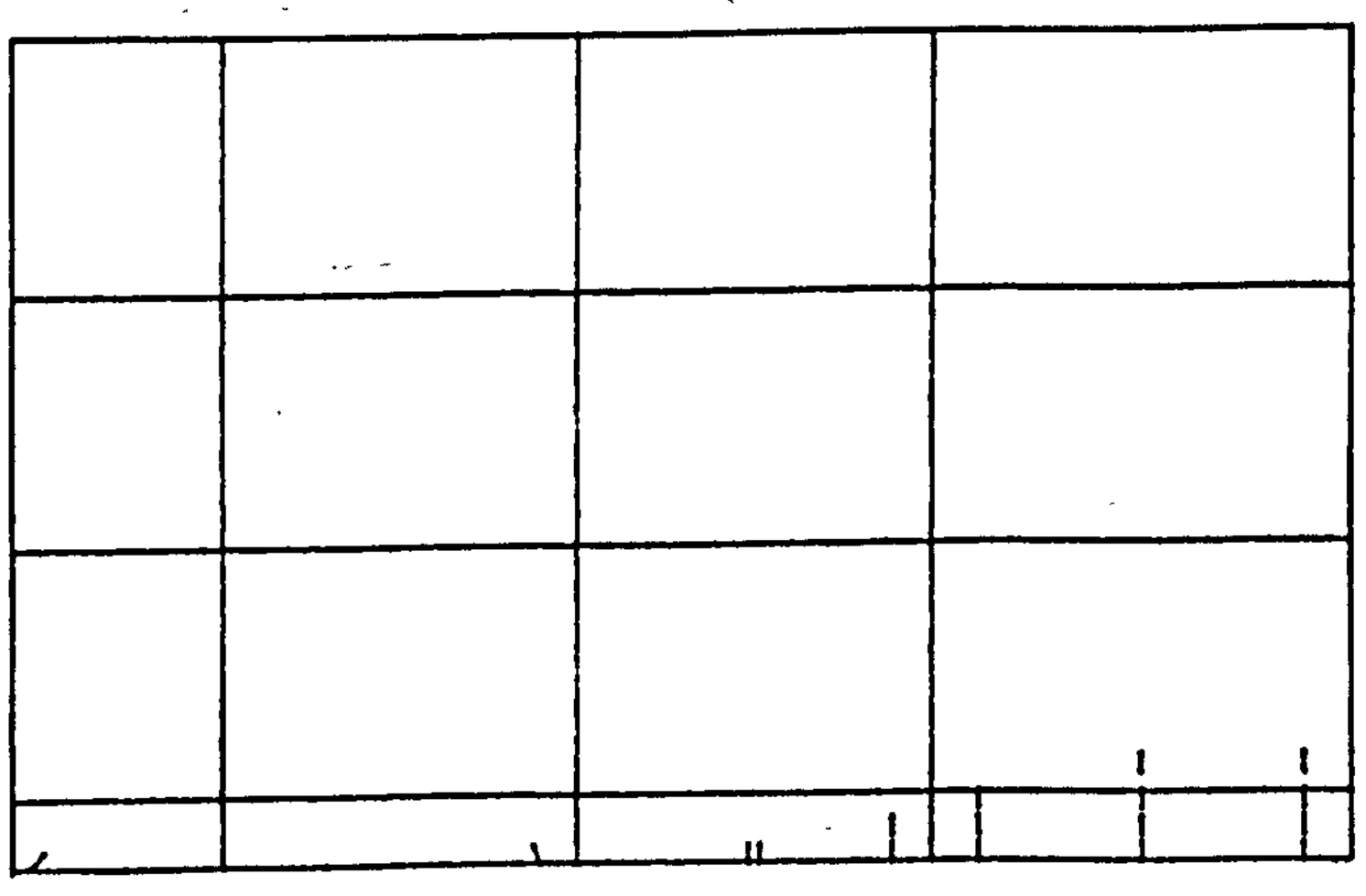

COOP = 1%, $\varepsilon_A = 10\ \varepsilon'_c$

Figure (6·48) Crack patterns at load = 69·7 kN.

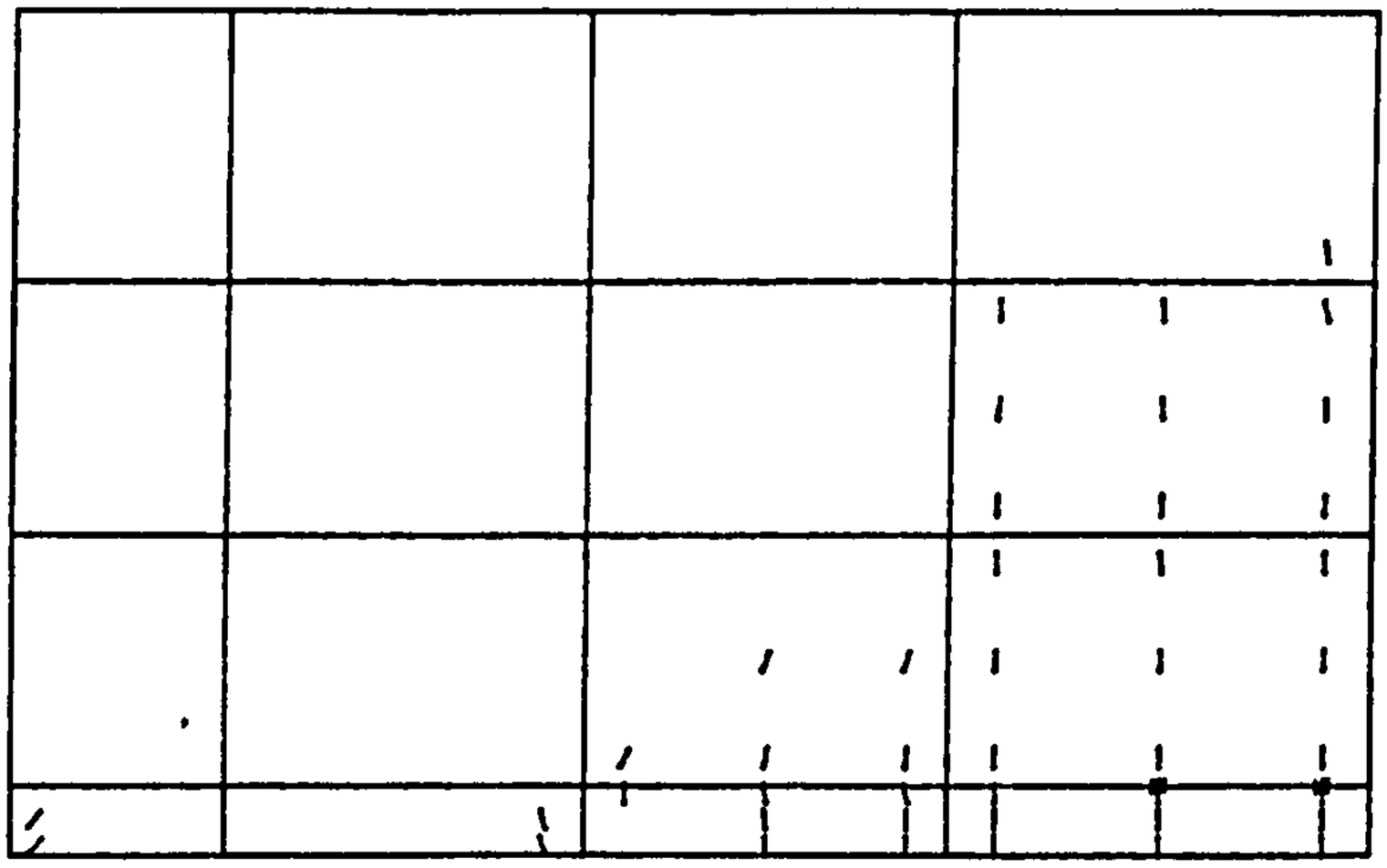

COOP = 20%, N.T.S.

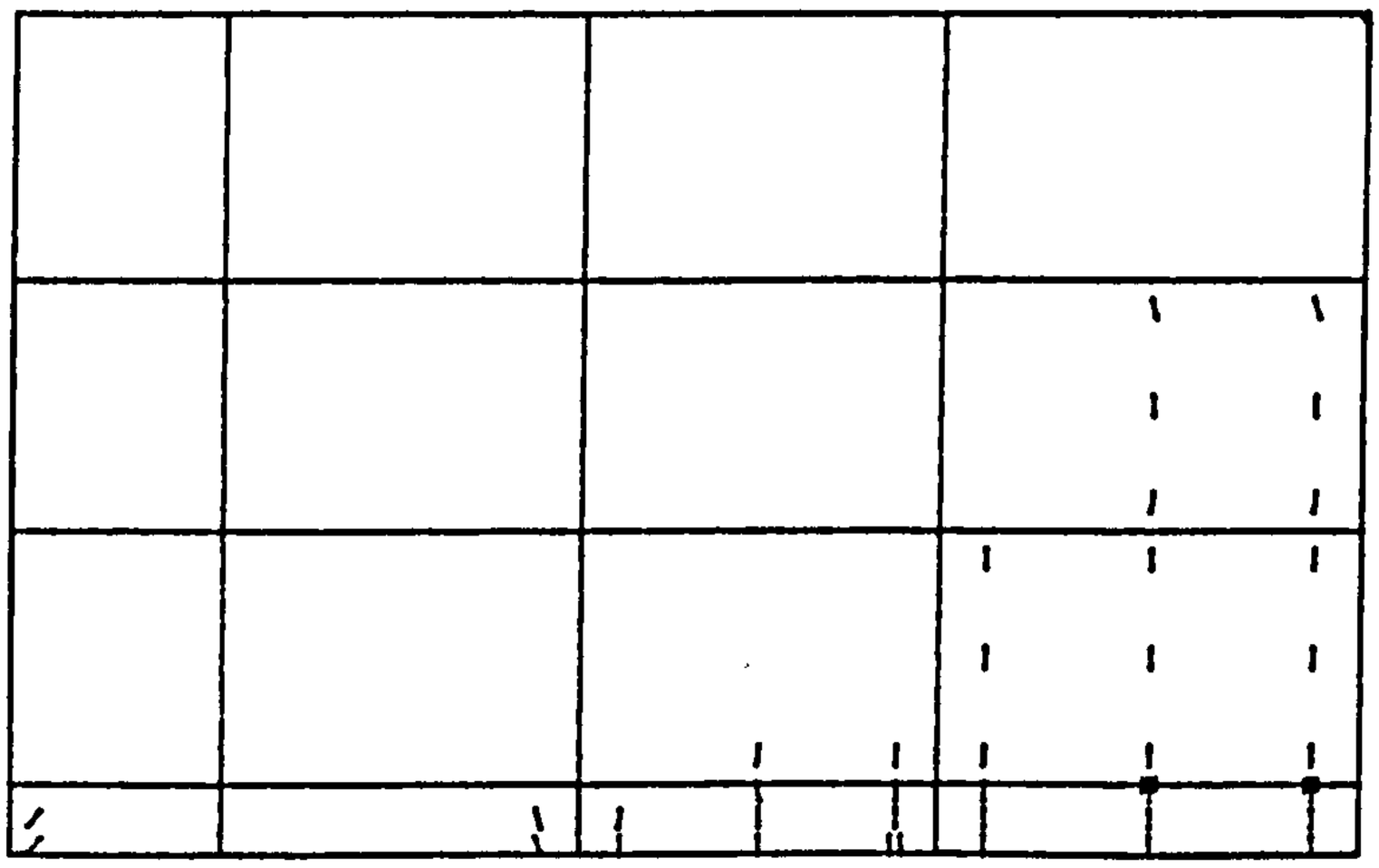

COOP = 5%, $\varepsilon_A = 5\,\varepsilon'_c$

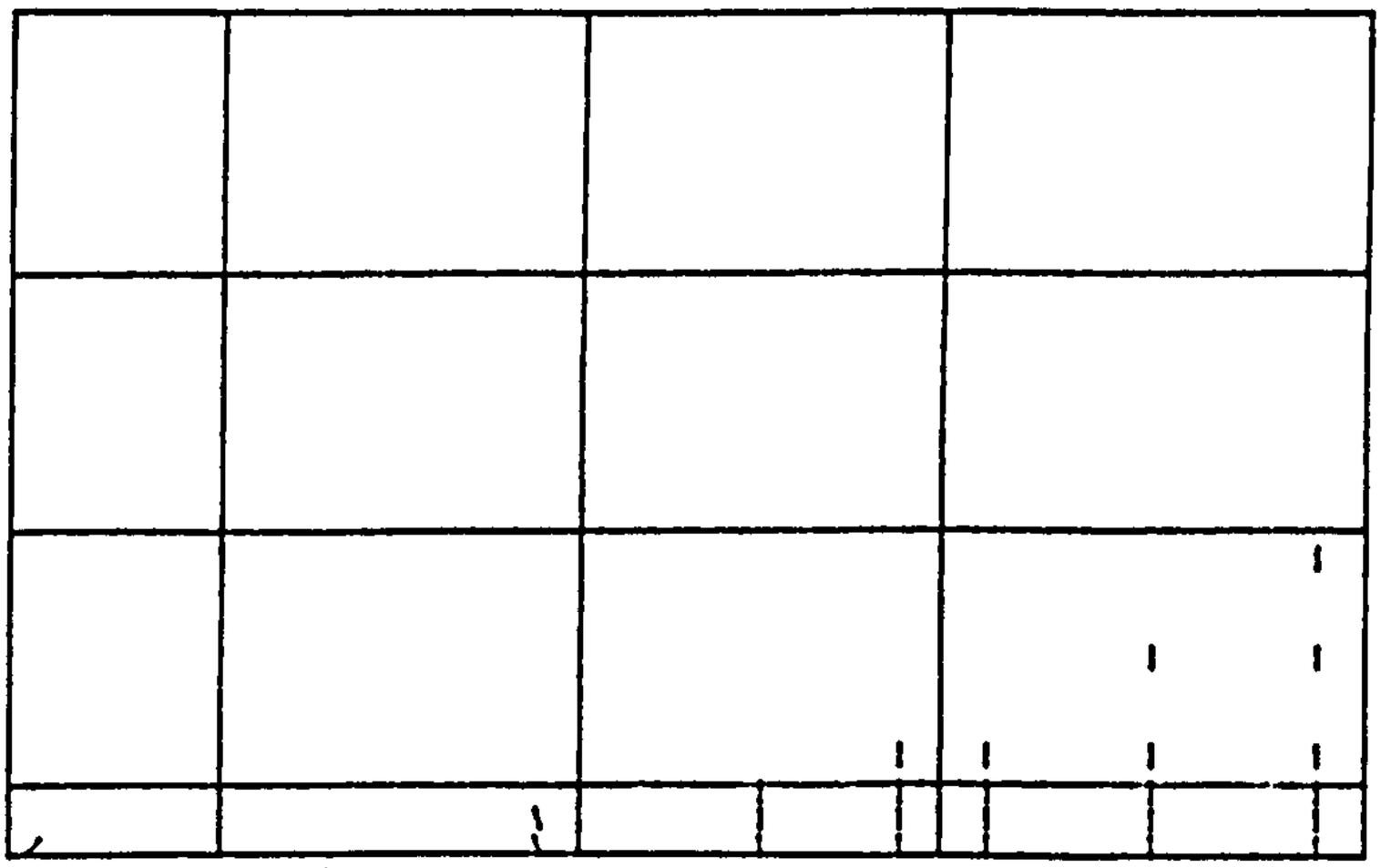

COOP = 1%, $\varepsilon_A = 10\,\varepsilon'_c$

Figure (6·49) Crack patterns at loads = 89·6 kN.

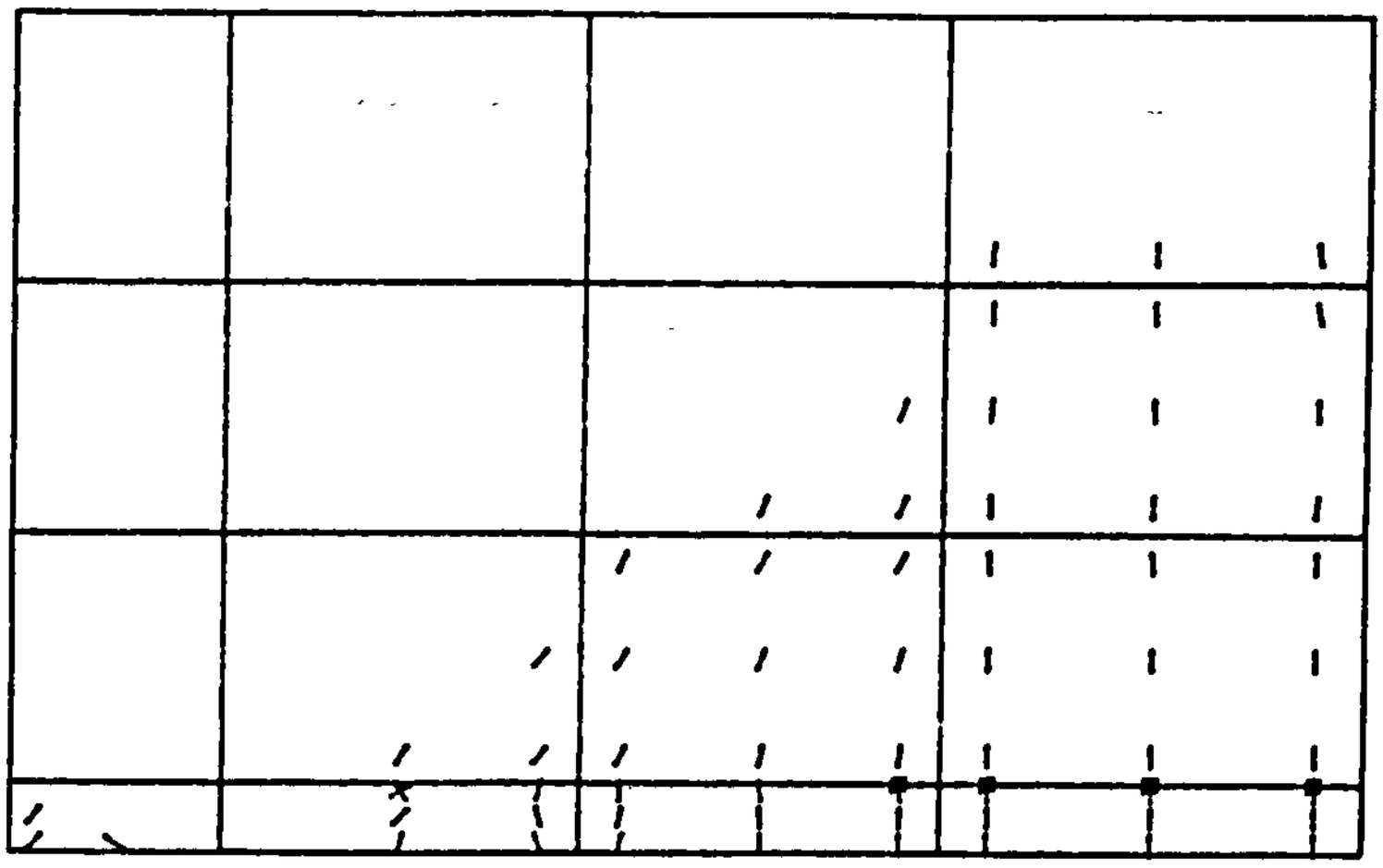

COOP = 20% , N.T.S.

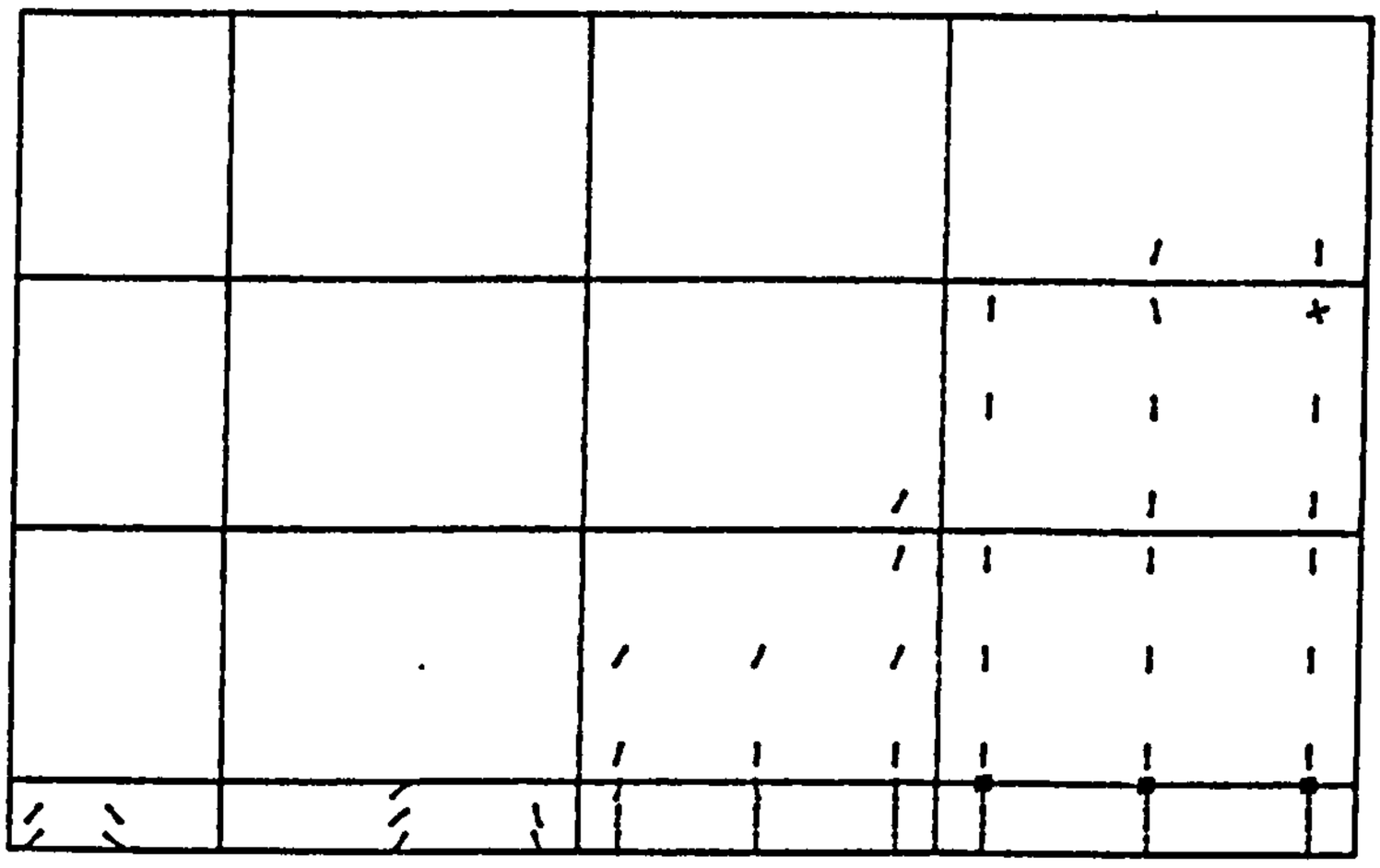

COOP = 5%, $\varepsilon_A = 5\ \varepsilon'_c$

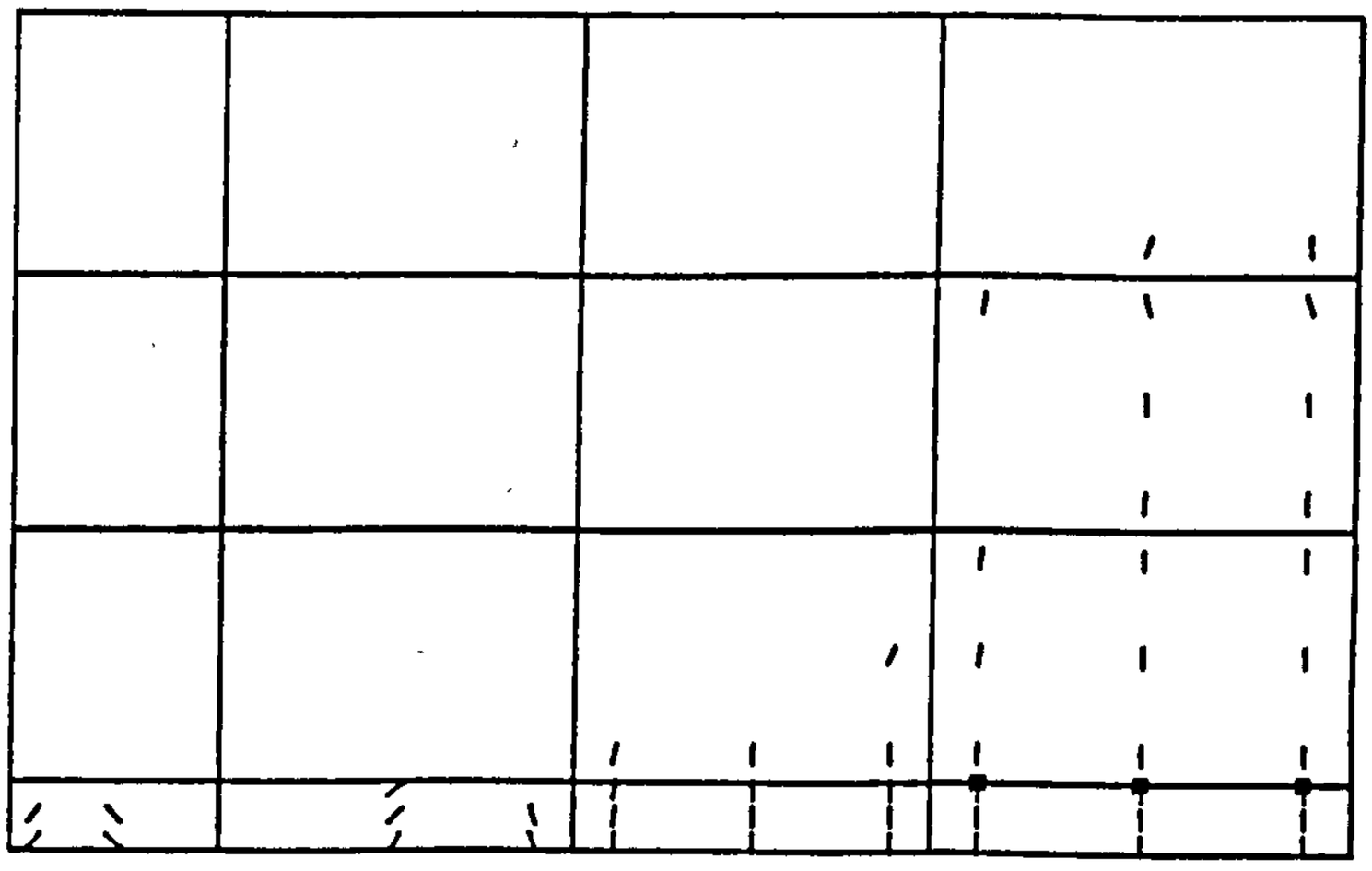

COOP = 1%, $\varepsilon_A = 10\ \varepsilon'_c$

Figure (6·50) Crack patterns at load = 103·6 kN.

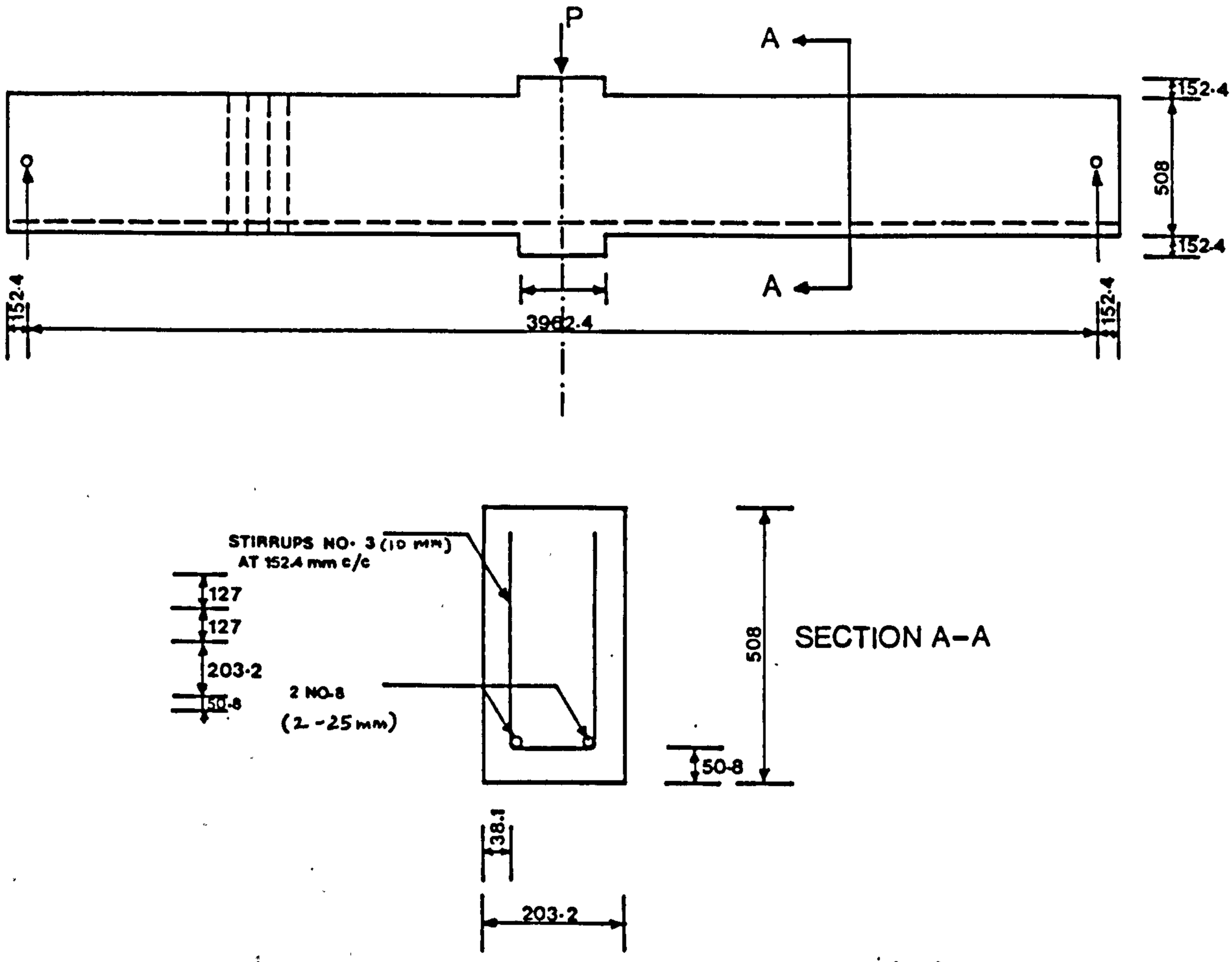

Figure (6·51) Simple beam J-4 tested by Burns & Siess.[12]

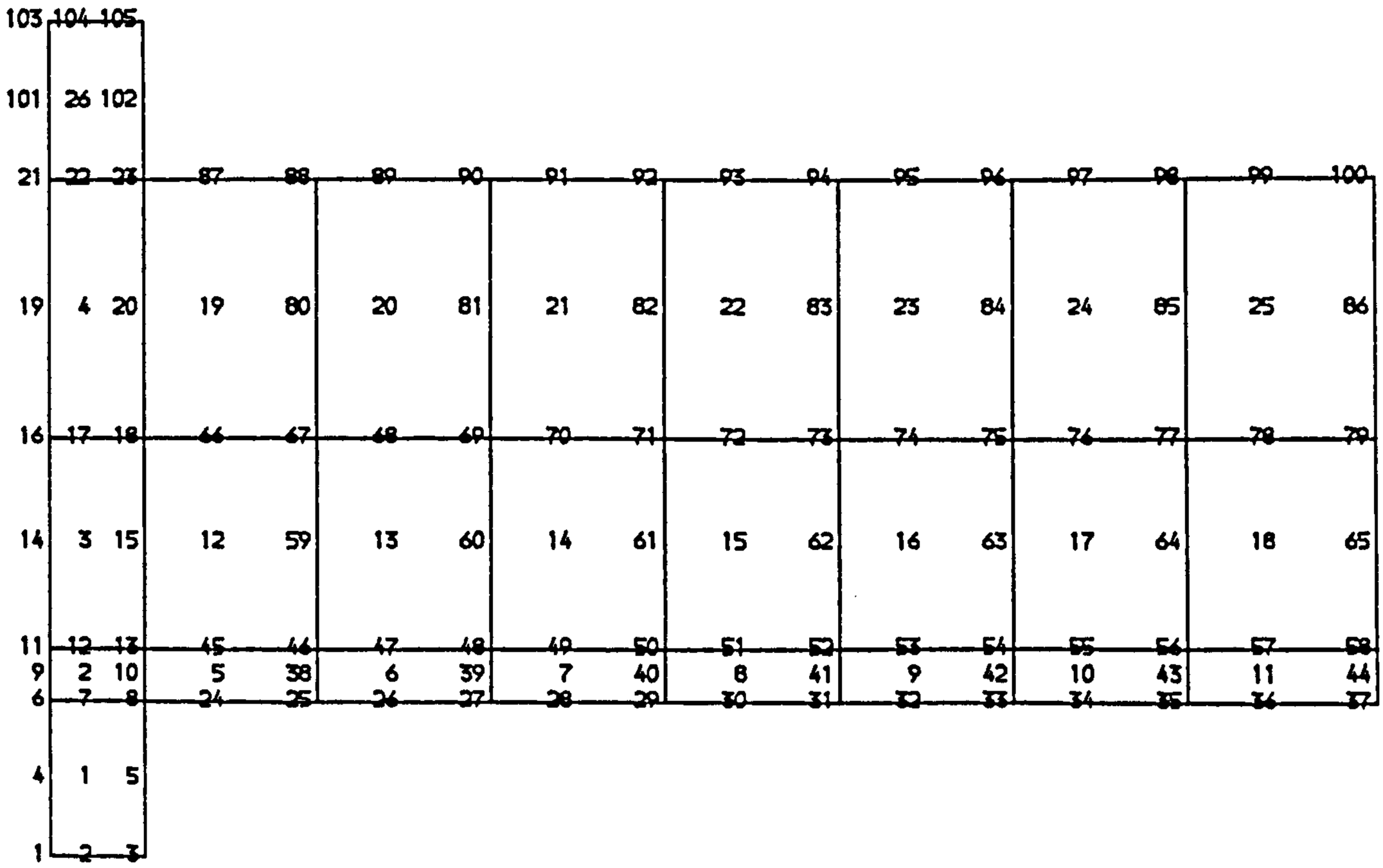

Figure (6·52) Mesh used for beam J-4.

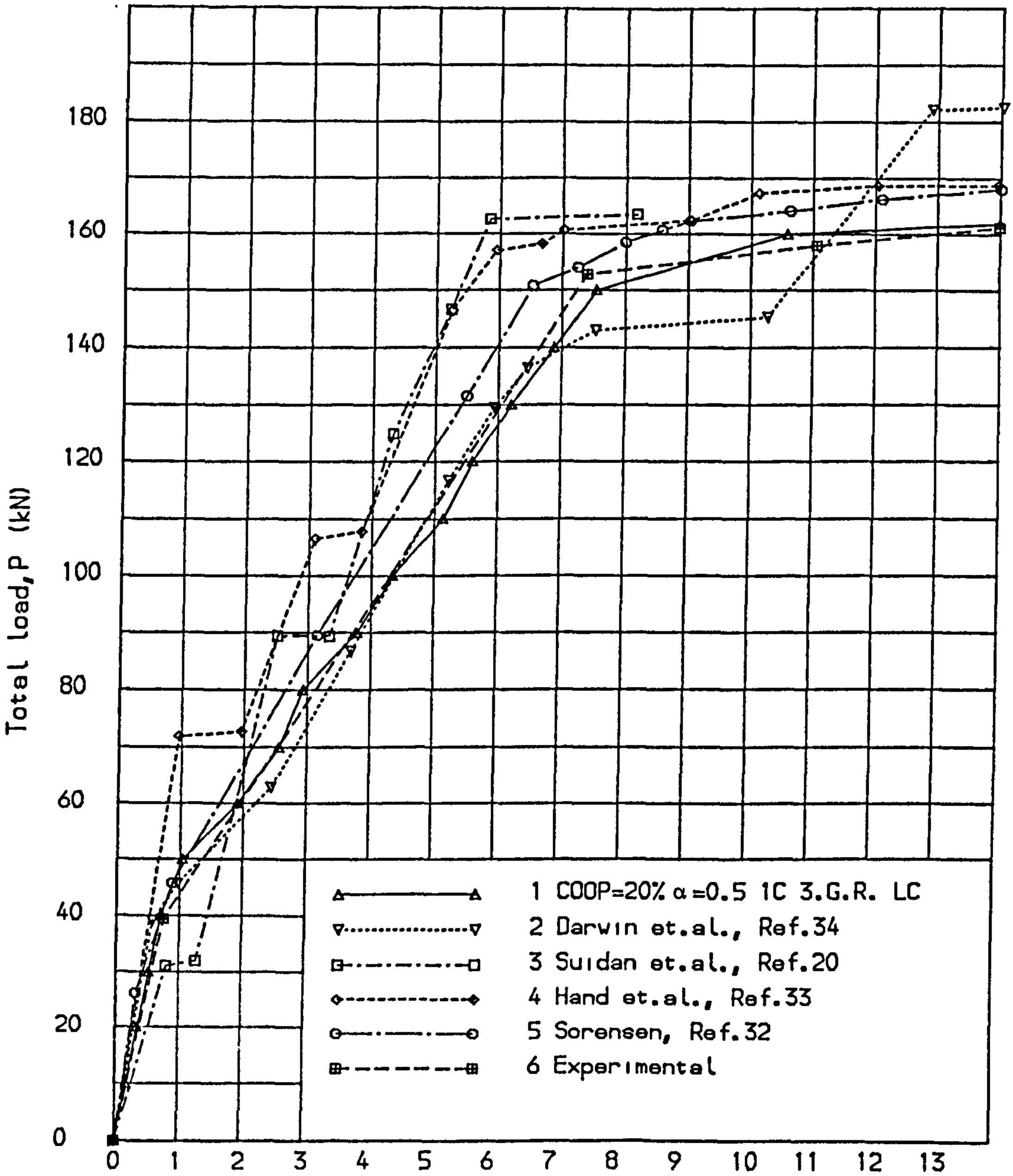

Fig. (6.53) Load deflection curves for simple beam.

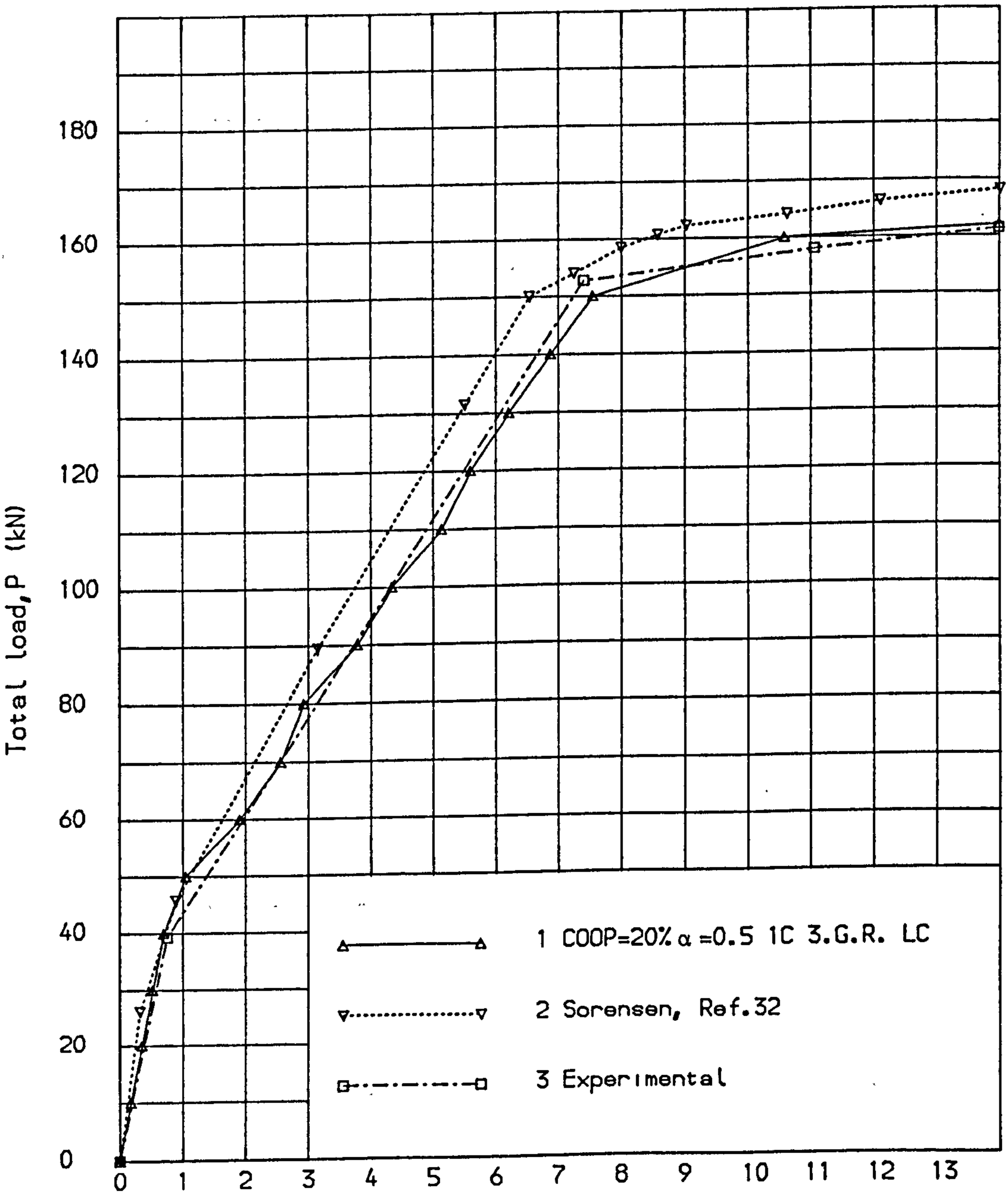

Fig. (6.54) Load deflection curves for simple beam.

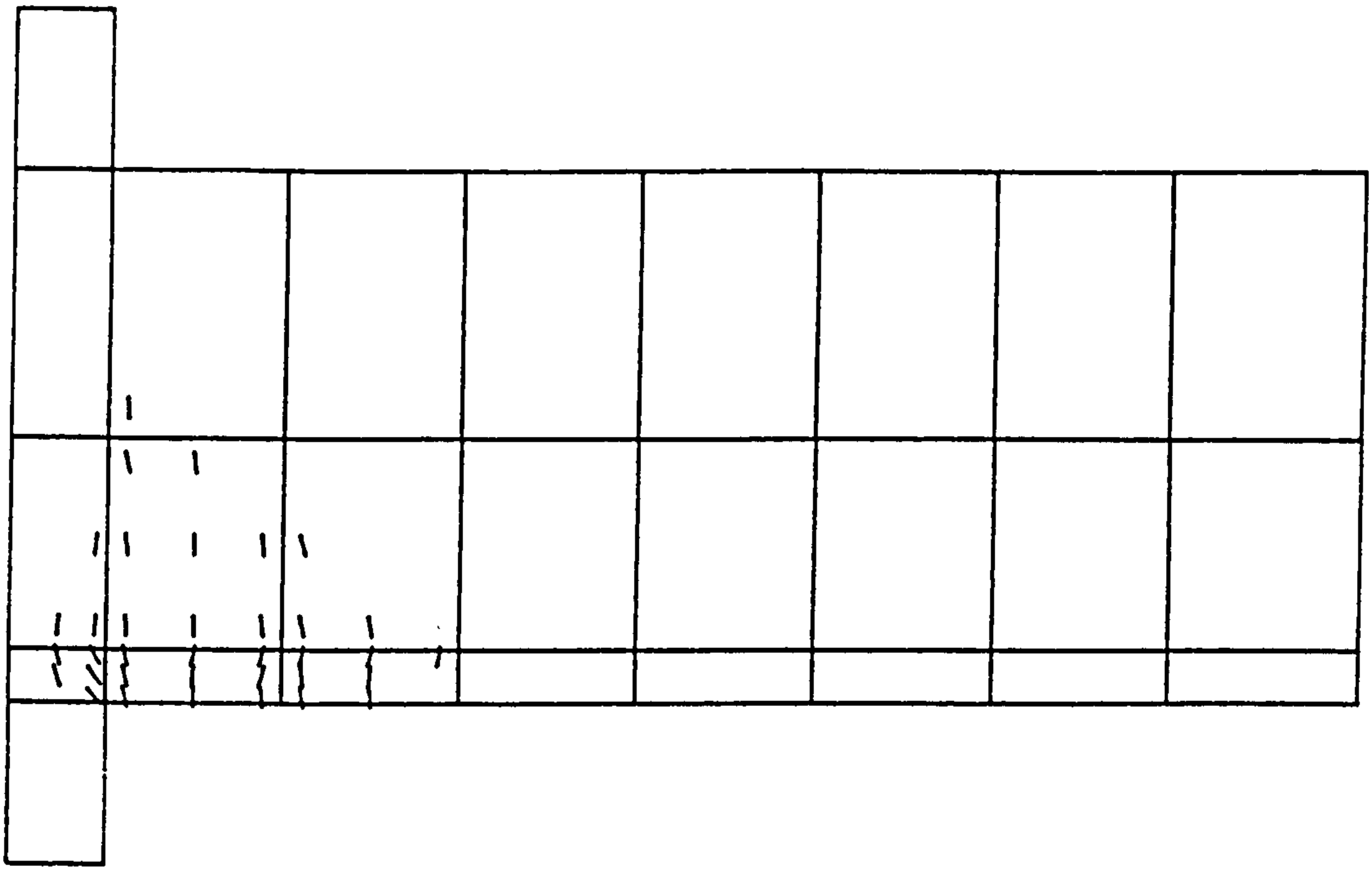

Figure (6.55) Crack patterns at load = 60·0 kN.

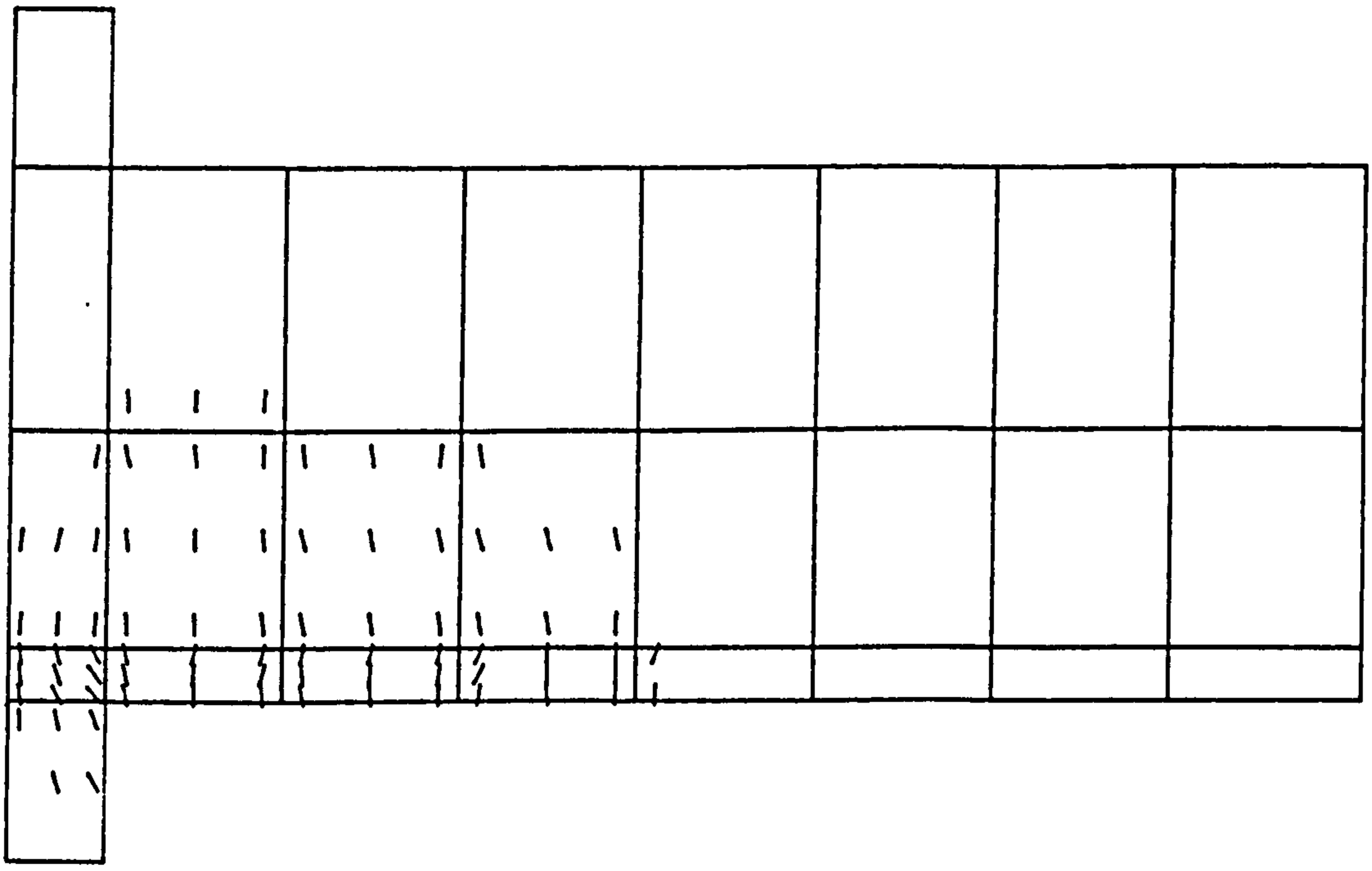

Figure (6.56) Crack patterns at load = 100·0 kN.

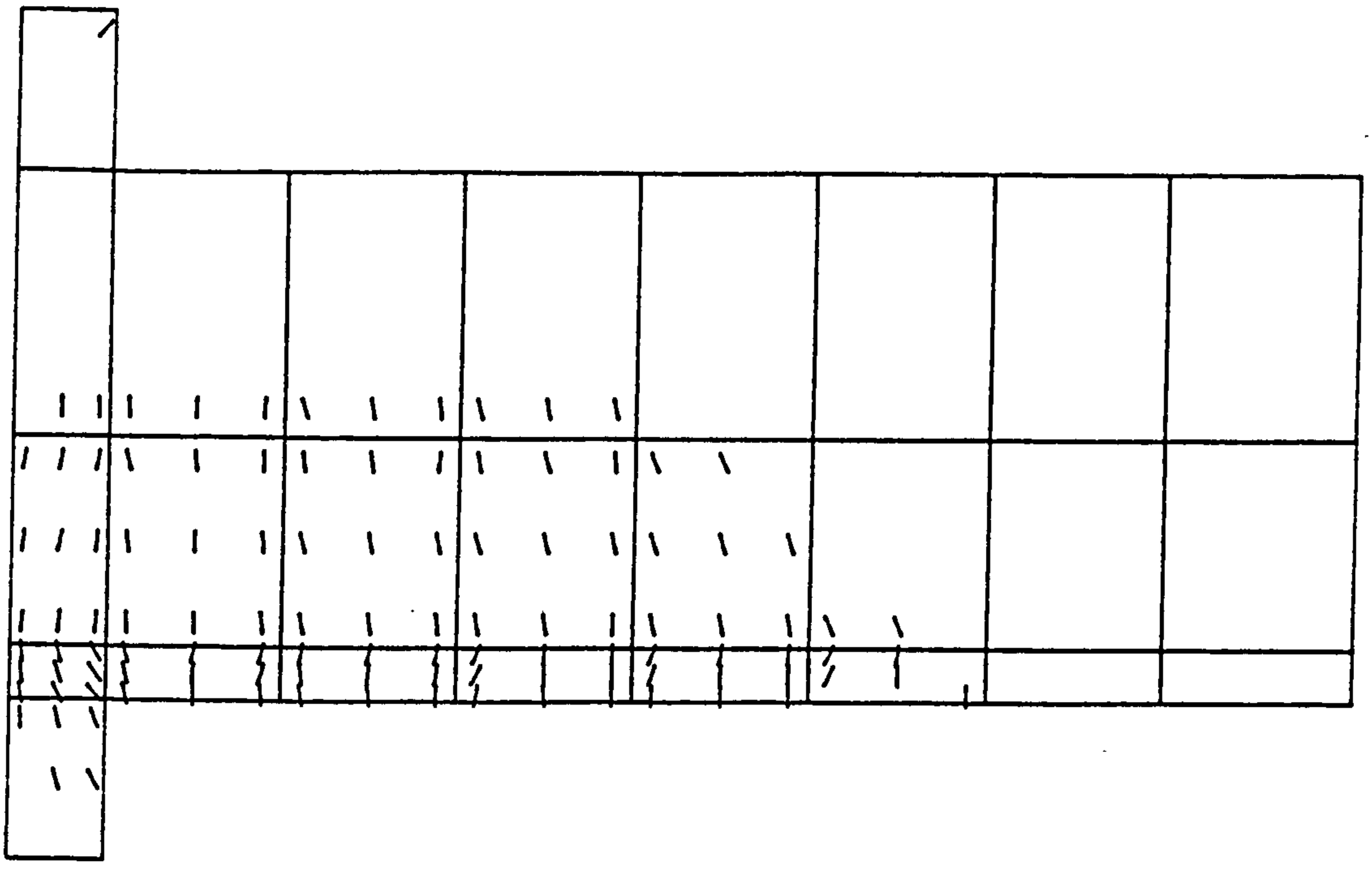

Figure (6.57) Crack patterns at load = 140·0 kN.

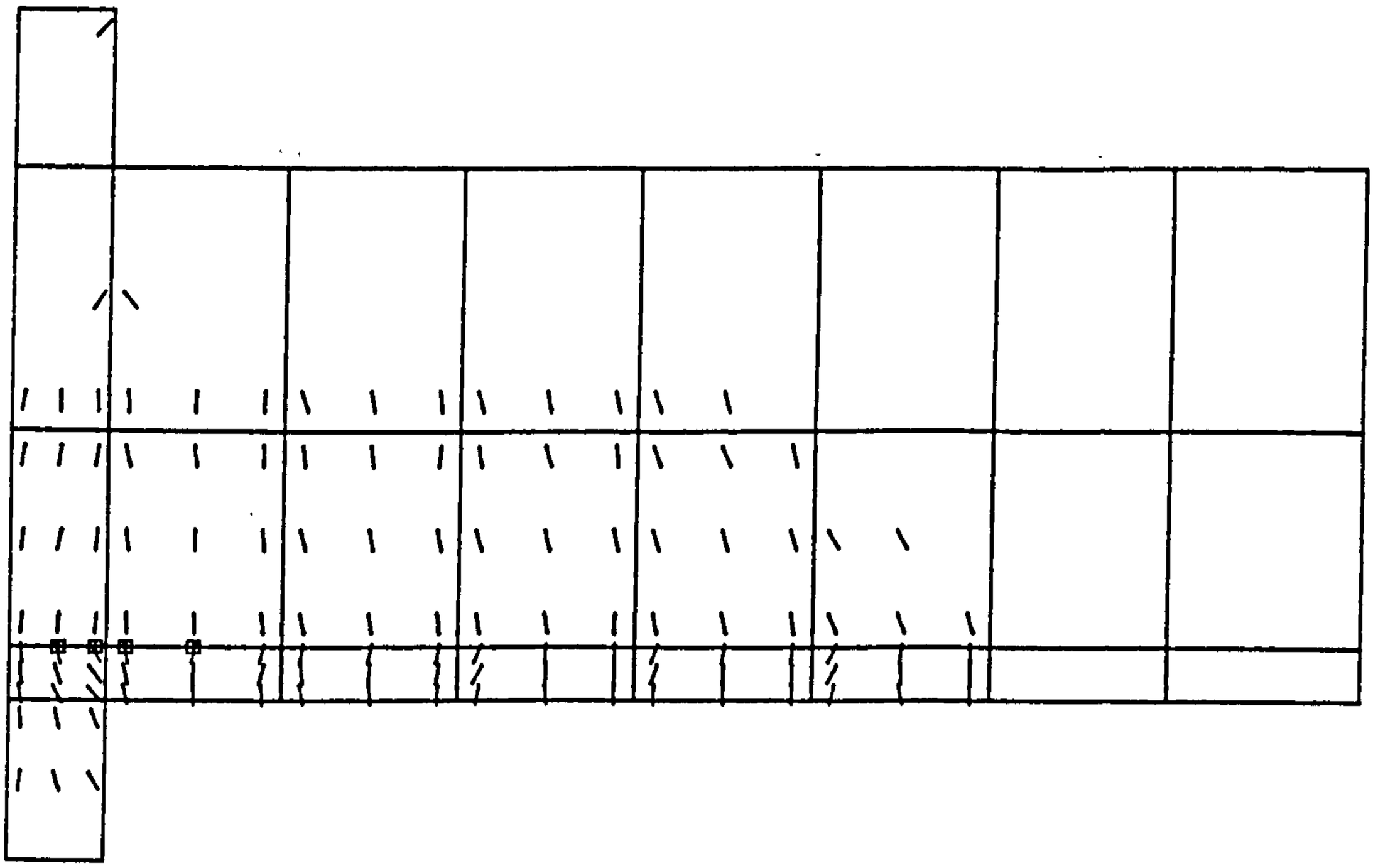

Figure (6.58) Crack patterns at load = 160·0 kN.

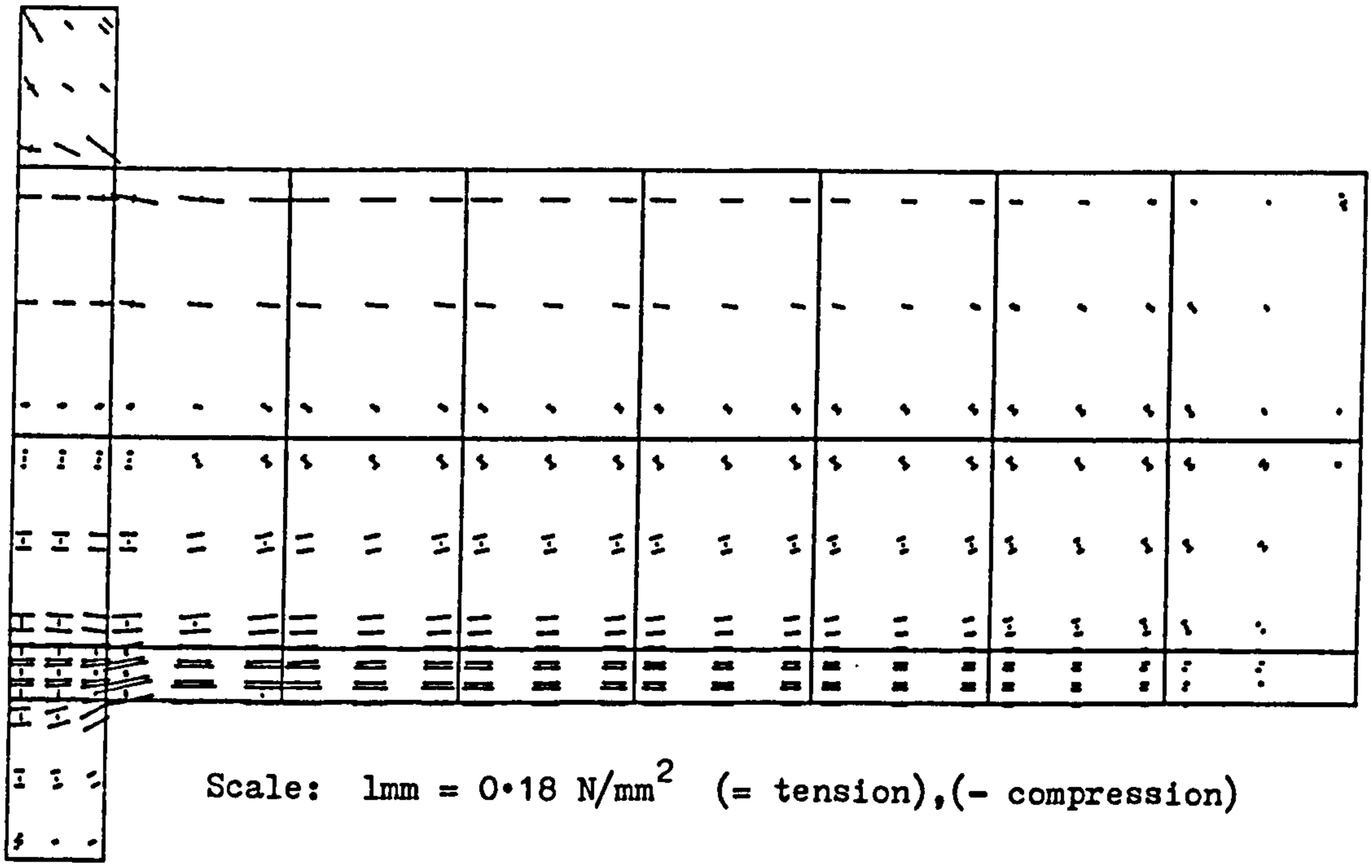

Scale: 1mm = 0·18 N/mm^2 (= tension),(- compression)

Figure (6.59) Principal stress directions at load = 10·0 kN.

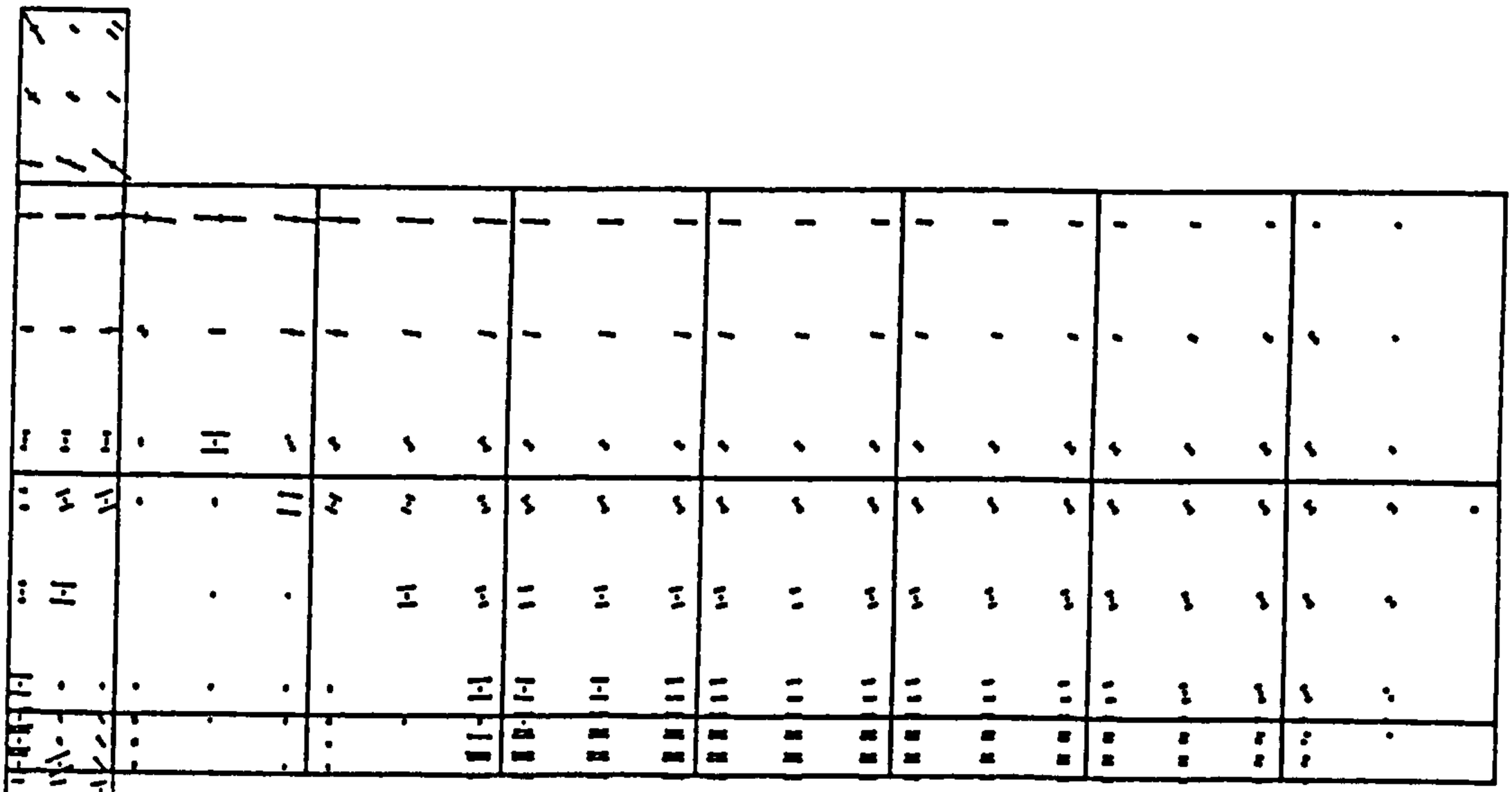

Scale: 1mm = 1·49 N/mm^2 (= tension),(- compression)

Figure (6·60) Principal stress directions at load = 60·0 kN.

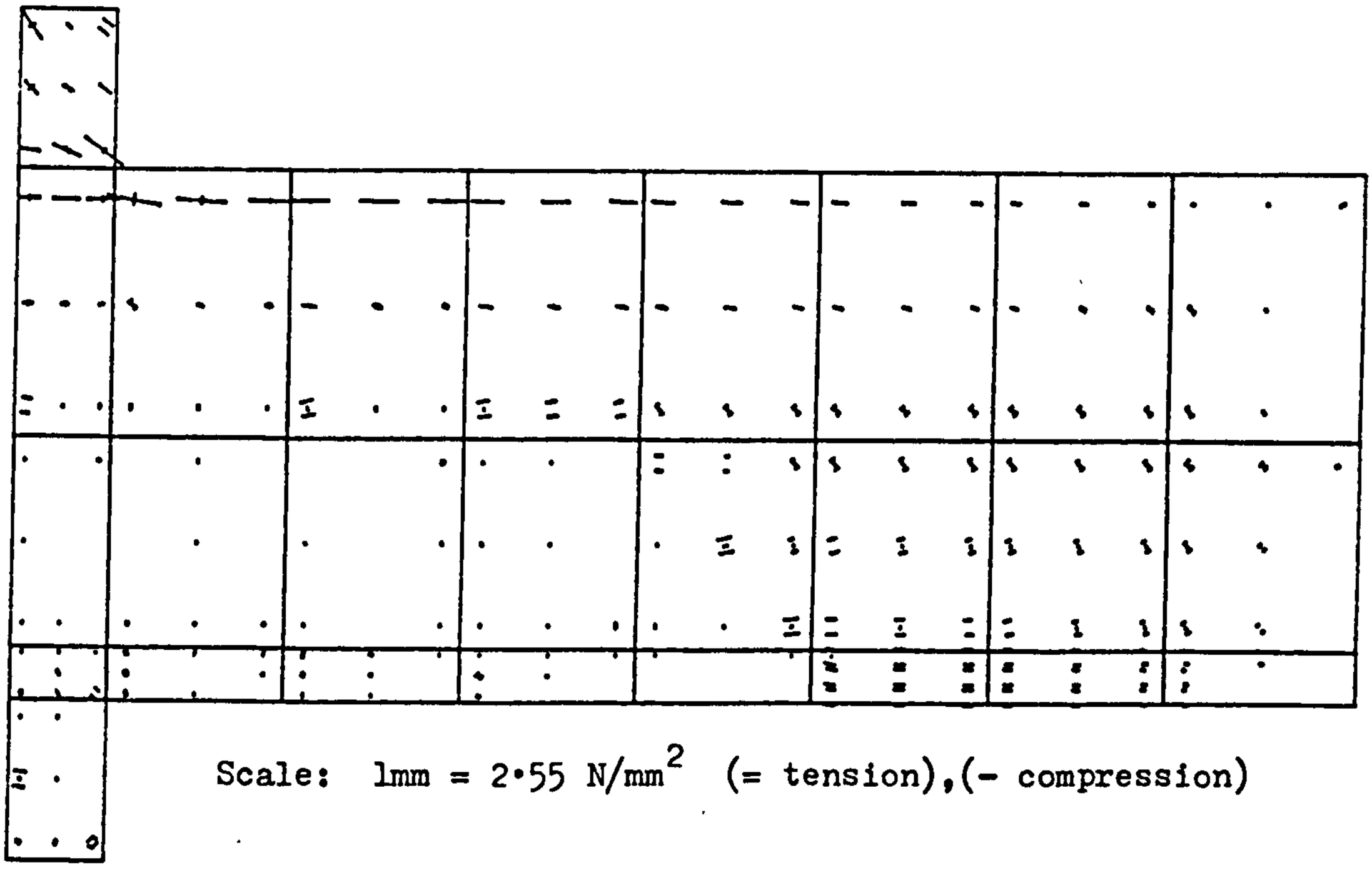

Scale: 1mm = 2·55 N/mm^2 (= tension),(- compression)

Figure (6·61) Principal stress direction at load = 110·0 kN.

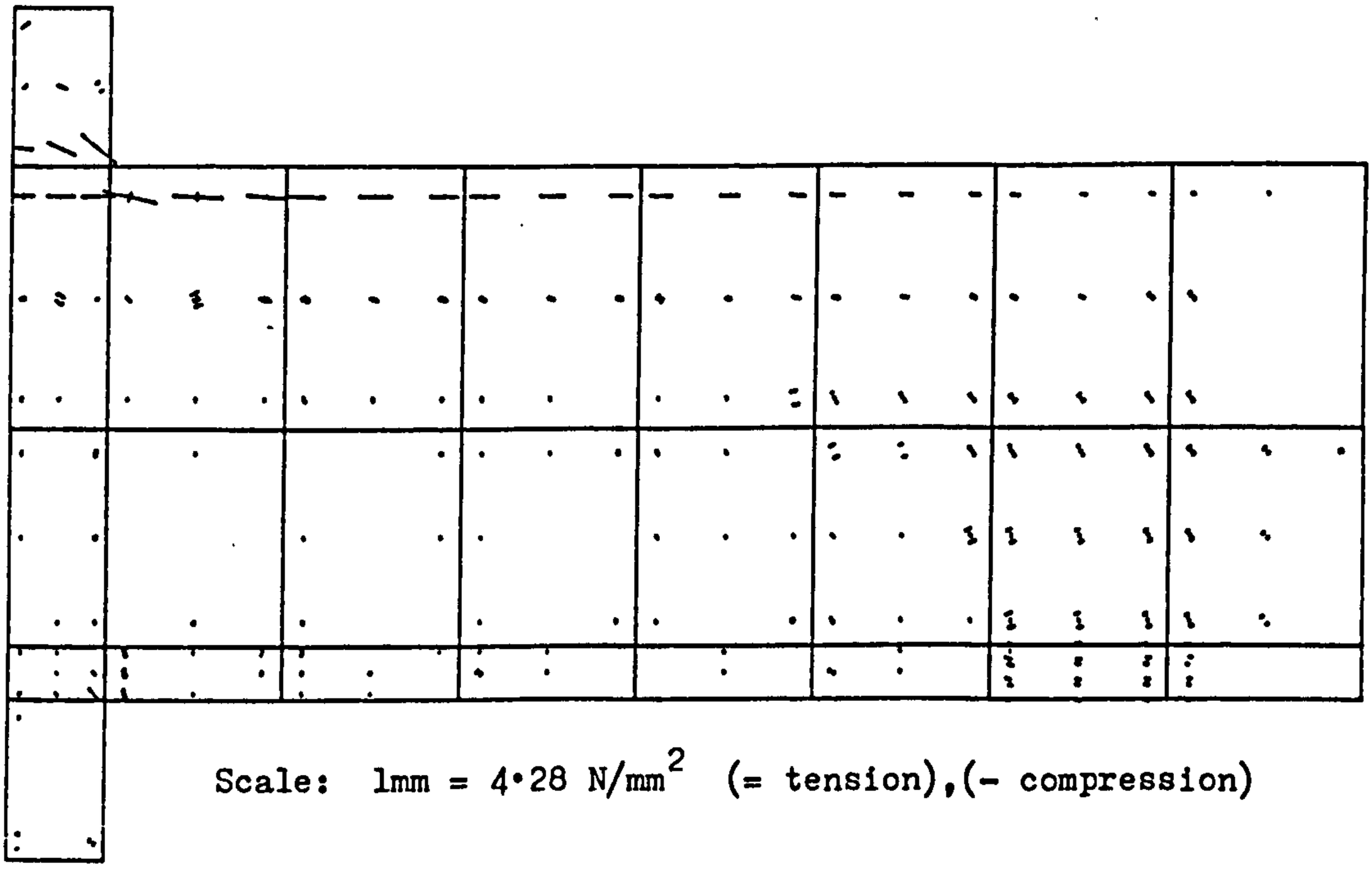

Scale: 1mm = 4·28 N/mm^2 (= tension),(- compression)

Figure (6·62) Principal stress directions at load = 160·0 kN.

REFERENCES

1. Scordelis, A.C., "General report - Basic Problem". IASS Symposium on the nonlinear behaviour of reinforced concrete spatial structures, Vol.3, 35-70, July, 1978.

2. Gerstle, K.H., "Material modelling of reinforced concrete". IABSE Colloquium on The Advanced Mechanics of Reinforced Concrete, Introductory Report, Delft, 41-61, 1981.

3. Phillips, D.V., "Nonlinear analysis of structural concrete by finite element method". Ph.D. Thesis, University of Wales, 1973.

4. Nilson, A.H; Cedolin, L., "A convergence study of iterative methods applied to finite element analysis of reinforced concrete". Int. J. Num. Meth. Eng., Vol.12, 437-451, 1978.

5. Duncan, W.; Johnarry, T., "Further studies on the constant stiffness method of nonlinear analysis of concrete structures". Proc. Inst. Civ. Eng., Part 2, 951-969, Dec., 1979.

6. Cope, R.J.; Rao, P.V.; Clark, L.A., "Nonlinear design of concrete bridge slabs using finite element procedures". Nonlinear Design of Concrete Structures, CSE-ASCE-ACI-CEB International Symposium, University of Waterloo, Ontario, Canada, 379-407, Aug., 1979.

7. Cope. R.J.; Rao, P.V.; Edwards, K.R., "Nonlinear finite element analysis techniques for slabs". Numerical methods for nonlinear problems, Proc. of the Int. Conf. held in University College, Swansea, 445-456, Sept. 1980.

8. Cope, R.J.; Rao, P.V.; Clark, L.A.; Norris, P.; "Modelling of reinforced concrete behaviour for finite element analysis of bridge slabs." Proc. of the Int. Conf. held in University College, Swansea, 457-470, Sept. 1980.

9. Cope, R.J.; Rao, P.V., "Nonlinear finite element strategies for Bridge slabs", IABSE Colloquium on The Advanced Mechanics of Reinforced Concrete, Final Report, Delft, 273-288, 1981.

10. Crisfield, M.A., "Local instabilities in the nonlinear analysis of reinforced concrete beams and slabs". Proc. Inst. Civ. Eng., Part 2, Vol.73, 135-145, 1982.

11. Ramakrishnan, V.; Ananthanarayana, Y., "Ultimate strength of deep beams in shear", J. ACI, Vol.55, 87-98, Feb., 1968.

12. Burns, N.H.; Siess, C.P., "Load deformation characteristics of beam-column connections in reinforced concrete". Report No.234, University of Illinois, Jan., 1962.

13. Cope, R.J.; Rao, P.V.; "Discussion on reference 5". Proc. Inst. Civ. Eng., Vol.69, Part 2, 873-874, Sept., 1980.

14. Cook, R.D., "Concepts and applications of finite element analysis". Wiley, 2nd ed., 1981.

15. Zienkiewicz, O.C., "The finite element method". McGraw-Hill, 3rd ed., 1977.

16. Bathe, K.J., "Finite element procedures in engineering analysis". Prentice-Hall, 1982.

17. Irons, B.; Ahmed, S. "Techniques of finite elements". Wiley, 1981.

18. Chen, E.Y.T.; Schnobrich, W.C., "Material modelling of plain concrete". IABSE Colloquium on The Advanced Mechanics of Reinforced Concrete, Final Report, Delft, 31-52, 1981.

19. Bathe, K.J.; Wilson, E.L., "Numerical methods in finite element analysis". Prentice-Hall, 1976.

20. Suidan, M.; Schnobrich, W.C.,"Finite element analysis of reinforced concrete". J. of Struct. Div., ASCE, Vol.99, 2109-2122, Oct.,1973.

21. Hand, F.R.; Pecknold, D.A.; Schnobrich, W.C., "Nonlinear layered analysis of RC plates and shells". J. of Struct. Div., ASCE, Vol.99, 1491-1505, July, 1973.

22. Cedolin, L.; Dei Poli, S., "Finite element studies of shear critical R/C beams". J. of Eng. Mech. Div., ASCE, Vol.103, 395-410, June, 1977.

23. Al-Mahaidi, R.S.H., "Nonlinear finite element analysis of reinforced concrete deep members". Report No.79-1, Cornell University, Jan., 1979.

24. Buyukozturk, O.; Connor, J.J.; Leombruni, P., "Research on modelling shear transfer in reinforced nuclear structures". Nucl. Eng. and Design, Vol.59, 67-84, 1979.

25. Scanlon, A.; Murray, D., "Time dependent reinforced concrete slab deflections". J. of Struct. Div., ASCE, Vol.100, 1911-1924, Sep. , 1974.

26. Gilbert, R.I.; Warner, R.F., "Nonlinear analysis of reinforced concrete slabs with tension stiffening". Report No. R-167, University of New South Wales, Australia, Jan., 1977.

27. Gilbert, R.I.; Warner, R.F., "Tension stiffening in reinforced concrete slabs". J. of Struct. Div., ASCE, Vol.104, 1885-1900, Dec., 1978.

28. Lin, C.S.; Scordelis, A.C., "Nonlinear analysis of RC shell of general form". J. of Struct. Div., ASCE, Vol.101, 523-538, March, 1975.

29. Mang, H.A.; Floegl,H., "Tension stiffening concept for reinforced concrete surface structures". IABSE Colloquium on The Advanced Mechanics of Reinforced Concrete, Final Report, Delft, 331-349,1981

30. Shirai, N.; Sato, T., "Inelastic analysis of reinforced concrete shear wall structures - Material modelling of reinforced concrete". IABSE Colloquium on The Advanced Mechanics of Reinforced Concrete, Final Report, Delft, 197-210, 1981.

31. Vecchio, F.; Collins, M.P., "Stress-strain characteristics of reinforced concrete in pure shear". IABSE Colloquium on The Advanced Mechanics of Reinforced Concrete, Final Report, Delft, 211-225, 1981.

32. Sorensen, S.I., "Endochronic theory in nonlinear finite element analysis of reinforced concrete." Report No.78-1, Trondheim University, March, 1978.

33. Hand, F.R.; Pecknold, D.A.; Schnobrich, W.C., "A layered finite element nonlinear analysis of reinforced concrete plates and shells". Technical Report UILU-ENG-72-2011, University of Illinois, Aug., 1972.

34. Darwin, D.; Pecknold, D.A., "Inelastic model for cyclic biaxial loading of reinforced concrete". Report No.409, University of Illinois, July, 1974.

CHAPTER 7

APPLICATION TO DEEP BEAMS

CHAPTER 7

APPLICATION TO DEEP BEAMS

7.1 Introduction:

Deep beams are found in various types of structure and have different useful applications. In modern construction, for example, departmental stores, hotels, municipal buildings and so on, it is often desirable to have the lower floor entirely free of columns. It may be simpler to utilise the external and partition walls as deep beams to span across the column free space and carry the whole building above them instead of using a heavy frame construction.

As there is a gradual transition from shallow beam behaviour to deep beam behaviour a distinct classification of deep beams is not strictly possible. Typically they are characterised by low span/depth ratios, L/D varying from less than 1 to about 5, and are usually relatively thin. Vertical normal stresses and shear stresses are more significant than flexural stresses, and strain distribution across a vertical section is not usually linear even under elastic conditions. The difficulties with these beams, especially ones having a span to depth ratio less than about 2, are that the simple theory of bending is not applicable in analysis, and that the stresses are highly effected by the application of the external loads and the location of the supports.

The behaviour of these beams depends on many factors such as, span/depth ratio, percentage of tension and compression reinforcements, amount and arrangement of web reinforcement, etc. These aspects are discussed in references 1-16, and are summarised in Section 7.2.1. One special type of deep beam is the web opening deep beam. It is only in the

last decade or so that any significant research has been carried out on a practical scale for these beams. This type of beam will be discussed in a later section of this chapter.

The purpose of this chapter is to examine the conclusions obtained from the previous chapter in the analysis of complex deep beams with and without openings failing in shear, and to study the effect of varying different numerical parameters on the nonlinear solution. The program will be used to predict different aspects of the behaviour of these beams. Stress distributions, crack patterns, and load deflection curves will be plotted and compared with available experimental results. This will then complete the appraisal of the proposed method of analysis on a comprehensive range of deep beam types and behaviour.

The following beams, tested experimentally by different authors, will be analysed.

(1) Cervenka[1] panel wall W-2 failing by flexural-shear.

This type of failure is characterised by a combination of diagonal cracks and flexural cracks as shown in Figure (7.1.a).

(2) Lin[2] deep beam 101 failing by diagonal-compression.

This type of failure starts with an inclined crack developing along the line joining the load and support points, after which parallel inclined cracks start to appear. The final failure occurs due to the destruction of the portion of concrete between these two cracks. This is shown in Figure (7.1.b).

(3) Lin[2] deep beam 102 failing by shear-compression.

This failure is due to the penetration of the inclined crack towards the compression zone at the top of the beam. The beam fails by crushing

above the upper end of the inclined crack. This is shown in Figure (7.1.c).

(4) Lin deep beam 204 failing by splitting-shear.

The failure is characterised by the growth of the inclined cracks which join the inside edge of the support point and outside edge of the loading point. The main cause of such failure was due to the high compression force in support region and the lack of confinement of concrete beyond the region where the reinforcement terminated under loading point. This is illustrated in Figure (7.1.d).

(5) Memon[3] deep beam B-5 with web opening failing by diagonal-compression

This type of beam fails as described in 2 and shown in Figure (7.1.e).

(6) Memon[3] deep beam B-7 with web opening failing by diagonal-compression

This beam fails in a similar manner to beam B-5.

7.2 Solid deep beams:

7.2.1 General review:

Complete recent reviews on solid deep beams have been reported in detail by Lin[2] and Memon[3]. The work on deep beams will be discussed in two categories; first the theoretical studies will be discussed and then the experimental work.

Early theoretical work on this topic examined the change in stress from engineer's theory of bending as span to depth ratio increased. Dischinger[4] in 1932 presented a Fourier series solution for beams of decreasing span to depth ratio resting on a series of supports as a continuous beam. In 1951 Chow et al.[5] produced a method of analysing

the stress distribution in deep beams of finite length by superimposing two stress functions, namely a Fourier series and the principal of least work. Other investigators, Ulham[6], Chow et al. have obtained solutions using the finite difference method to provide information on the stress distribution. Gyzman et al.[8], Archer et al.[9] used strain energy methods for determining stresses.

Most of these theoretical models have assumed that reinforced concrete is homogeneous and isotropic. In fact the stress-strain response of reinforced concrete in situations where cracking occurs is more complicated than these simple elastic homogeneous models predict. Some investigators, for example Chow et al.[6] and Ulhman[7], have based design recommendations on this simplified model. However cracking of the beam may lead to a redistribution of stresses which may invalidate the results of the elastic analysis upon which the design was based. The stress distribution is best determined by experimental tests, which can then be further examined by a finite element model to give complementary information.

Many investigators have studied the behaviour of solid beams experimentally. For example Leonhart et al.[10] summarized various research work on deep beams, and studied simply supported deep beams under different load conditions, and various arrangements of reinforcement. Concrete strains measured on the beam surface were converted to stresses, and found to give a good agreement with the theoretical elastic prediction at low load levels. Arching action was apparent from concrete and steel strain measured in all tests, and the crack widths were found to be noticeably reduced by distributing the main tension cord over the bottom part of the beam.

A formula which was dependent on the stress distribution in the concrete was proposed to calculate the main tension steel. De-Paiva et al.[11] studied simply supported deep beams with span/depth ratios varying from two to six. He found that the type and the amount of web reinforcement provided had no significant effect on the formation of the cracks or on the failure modes. However, the presence of such web reinforcement did significantly reduce the amount of visible damage to the beam. De-Paiva et al. also found that increasing the quantity of main reinforcement will change the failure mode, for instance changes from flexural to shear failure modes were reported. He also found that an increase in concrete strength increased the shear capacity but did not increase flexural capacity.

Ramakrishnan et al.[12] studied different single span deep beams. In his experiments he obtained shear failures which were actually diagonal tensile failures caused by splitting and there was little sign of any shear or sliding taking place during the process. He also proposed an equation to predict the value of ultimate shear for the case in which a beam fails in a diagonal tension mode.

Kong et al.[13,14] tested a very wide range of deep beams with different span/depth ratios ranging from 1 to 3 and clear shear span/depth ratios ranging from 0.23 to 0.7. From the results of these tests the authors showed that the percentage of web reinforcement had a great influence on the development of inclined cracks, contradicting De Paiva et al. results.

Manuel et al.[15] found that the ultimate strength appears to be significantly influenced by changing the span/depth ratio and clear shear span/depth ratio. He also found that the extent of arch action

for a beam of constant shear span at any load level is reduced as the length of the beam increases.

Lin[2] tested 11 simply supported normal weight concrete deep beams under central concentrated top loads. The beams were divided into two main groups, one group with span/depth ratio of 1.8 and one group with 0.9. The main objective of the test was to examine the effect of concrete strength and orientation of reinforcement directions. Concrete strength was found to be very important in these beams as an increase of its value produced an increase of the ultimate strength. An increase in the amount of reinforcement was found not to have an important influence on the load at which diagonal cracks appear, but has the advantage of restricting the crack width and thus increasing the ultimate load.

Smith et al.[16] tested 52 deep beams under two point loads in order to study the effect of vertical and horizontal web reinforcement, shear span/depth ratio on inclined cracks, ultimate shear strength etc. The results also indicated that web reinforcement produces no effect on the formation of inclined cracks and seems only to moderately affect the ultimate shear strength. Also they found that the addition of vertical web reinforcement improves the ultimate shear strength but the addition of horizontal web reinforcement had little or no influence.

In recent years there has been a growing interest in the analysis and design of deep beams, and many publications have appeared. However the behaviour is complex and still requires more investigation and confirmation because there are many variables which have not been well studied, including different distribution of loads and different angle of inclination for reinforcement. These should be identified and studied

by both experimental investigations and by the use of the finite element method.

The use of the finite element method on deep beams has been reported by some investigators, references 1, 17-21, 27. It has been found that the finite element method is a useful tool in studying deep beam behaviour, but its potential is still being developed (as in this work).

7.2.2 Cervenka panel wall W-2(1):

Cervenka carried out tests on different panel walls. In this section the panel W-2, shown in Figure (7.2), will be analysed. Because of symmetry only half of the beam will be considered. Details of the finite element mesh are shown in Figure (7.3). Material properties for concrete and steel are shown in Tables (7.1) and (7.2).

In the analysis the following assumptions were made:

(1) The first cracking model was used (i.e. no tension stiffening).

(2) The method V.S.M.1 was used.

(3) The three point Gauss rule was used.

(4) The shear retention factor was kept constant at 0.5.

(5) The load criterion was used to check convergence.

(6) The load was applied in equal increments of 5.0 kN until failure occurred.

Different load deflection curves are compared for convergence tolerances of 20% and 10% in Figure (7.4). Iterations were continued until convergence to the specified tolerance was obtained. It can be observed that COOP = 10% gave a better estimate than COOP = 20%, but in general a stiffer prediction was obtained for both when compared with the

experimental and theoretical work of Cervenka. The COOP of 10% was more expensive than that of 20% because many more iterations were required. However the differences in the load deflection curves were not great; COOP of 20% overestimated the ultimate load by 8% which is quite acceptable, as COOP equals 10% overestimated the ultimate load by 4%. The Cervenka load deflection curve under estimated the ultimate load by 4%, but it appears that he changed the positions of the applied load so that it was on the ends of the thick flange. This could give a slight difference in the lever arms which may have some effect on the structural behaviour and the stiffness of the load-deflection curve. Horizontal stress distributions at midspan are compared in Figure (7.5) for COOP = 20% and 10%. It can be observed that the variation of the stress distribution is significant at low load levels. However this distribution becomes more similar at higher load levels when most of the cracks have developed.

Crack patterns for COOP = 20% at load levels of 50.0 kN and 75.0 kN are shown in Figures (7.6) and (7.7), and comparisons with the experimental results at higher load levels are shown in Figures (7.8 - 7.11). Good agreement was obtained. Positions where steel yields and concrete crushes are also shown in the Figures.

The following points can be made:

(1) Using the parameters suggested in previous chapters for the numerical solution, fast convergence was obtained without any difficulties until the failure load was obtained. It appears that these parameters which were suggested from different failure modes, also produced a good prediction for the behaviour of this beam.

(2) When using COOP = 10%, a softer load deflection curve was obtained compared with COOP = 20%. This shows again the importance of this parameter on the prediction of the load deflection curve and ultimate load.

(3) There was no need for tension stiffening to obtain a good estimate of the load deflection curve and other aspects of behaviour.

7.2.3 Lin deep beams 101 and 102[2]:

Beams 101 and 102 have similar dimensions and are shown in Figures (7.12). The beams were simply supported on an effective span of 900.0 mm and were loaded at the centre. These beams were provided with the same amount of reinforcement, but different concrete mixes were used. All the beams were provided with bearing plates at the support and load points. Local cages were provided to increase the bearing capacity at the support and load point. Details of concrete and steel properties are shown in Tables (7.3) and (7.4).

Because of symmetry only half of the beams will be considered. The finite element mesh is shown in Figure (7.13).

The following assumptions were made in the analysis:

(1) The first cracking model was used (i.e. no tension stiffening).

(2) The method V.S.M.1 was used.

(3) The three point Gauss rule was used.

(4) The shear retention factor was set equal to 0.5.

(5) The load criterion was used to check convergence, and iterations were continued until the specified convergence tolerance was obtained.

(6) The load was applied in equal increments of 24.5 kN until failure occurred.

Two methods were proposed to account for the material representation in this analysis; 1 Mat. which assumes that all elements used in the analysis will have a similar property description for concrete; 2 Mat. which assumes that concrete has a different strength, which is to be higher than the proposed value in the region under the point of application of load where cages were provided. This is because concrete has a higher effective strength when confined by a cage under the load and this would prevent premature failure in that region.

Different load deflection curves for beam 101 are compared for COOP = 15% and 20%, (1 Mat.), in Figure (7.14). It can be observed that the predicted load deflection curve was stiffer in its response and failure was underestimated for both cases. The same beam was also analysed assuming, the effect of confinement is considered, i.e. 2 Mat., and a higher value of modulus of elasticity equal to 34.5 kN/mm^2 was used for element 25 in Figure (7.13). The predicted load deflection curve, i.e. Figure (7.14), 2 Mat., was also as stiff in its response as that predicted when using 1 Mat., but there was some improvement in the predicted ultimate load. However, the predicted ultimate load was still underestimated. It appears that the shapes of the load deflection curves have a dis similar description to that obtained experimentally. This variation could be obtained if values of concrete properties such as the modulus of elasticity, or compressive strength of concrete were not measured accurately, in the experimental work, and since no check can be made on these values, it is difficult to judge their accuracy. The other reason could be the approximation in the finite element method, for example the steel reinforcement in areas where cages were provided could have a different description from that in the

experiment, or the effect of the steel plates provided at the support and under the points of load.

Different load deflection curves are compared using 1 Mat. and 2 Mat., for beam 102 in Figure (7.15). This beam was tested experimentally using a lower concrete compressive strength than that for beam 101 as shown in Table (7.3). It can be seen that stiff load deflection curves were also obtained for both cases. The 2 Mat. mesh predicted a better estimate of ultimate load than the 1 Mat. This shows again that it can be important to account for the confining effect where cages are used.

Crack patterns for beam 101 (2 Mat.) with a value of COOP = 20% are shown in Figures (7.16 - 7.20) and the experimental failure crack pattern is shown in Figure (7.21). It can be observed that at low load levels vertical cracks appeared in the central half section and were located near the midspan. Also a few cracks appeared near the half clear shear span section. On further increase in load, the central vertical cracks extended vertically and the off-centre cracks inclined towards the centre line of the beam. These inclined cracks developed at further increase of load producing struts between the support points and the loading points. After this yielding occurred followed by crushing of the concrete along the strut during the final stages.

The predicted crack pattern was in good agreement with the experimental pattern at failure as shown in Figures (7.20) and (7.21). Stress distribution at the midspan section at different load levels is shown in Figure (7.22). It can be seen that at the elastic load level, there was some nonlinearity in the stresses at the top of the beam. However as cracks started to appear the stresses dropped to zero for the cracked region and compressive stresses increased in the top of the beam.

Horizontal, vertical and shear contour strains are shown for load levels of 171.5 kN and 392.0 kN in Figures (7.23 - 7.28). It can be seen that the zero contour horizontal strain shifts upward when the load is increased. This is accompanied by tensile strains developing in regions of the midspan section. For the vertical strain contours it appears that most of the areas have a compressive strain at the lower load level. This changes at the higher load level where tensile strains develop in the areas between the point of load and support In areas of the support a more complex distribution of strains was obtained. The shear strain contours show that their effect is not important in the midspan section and edges of the beam but that their effect is most significant on the line joining the point of load and support. These figures show how the strains can vary in these beams and will give a picture of the complexity of this type of structure. For the time being the finite element method is the only choice for describing these strains.

7.2.4 Lin deep beam 204(2):

This beam was simply supported on a span of 900.0 mm and has a depth of 1000.0 mm. Details of beam dimensions are shown in Figure (7.29). The loading as well as the bearing plate were the same as beams 101 and 102. Details of concrete and steel properties are shown in Tables (7.3) and (7.4). Because of symmetry only half of the beam was considered. The finite element mesh is shown in Figure (7.30). The following assumptions were made in the analysis:

(1) The method V.S.M.1 was used.

(2) The shear retention factor was set equal to 0.5.

(3) The load criterion was used to check convergence.

(4) The load was applied in equal increments of 49.1 kN until failure occurred.

Different load deflection curves for (1 Mat.) and (2 Mat.) are compared in Figure (7.31) for the 2 x 2, 3 x 3, and 4 x 4 Gauss rules. Iterations were continued until COOP reached a value of 20%. It can be observed for the cases when 1 Mat. was used, underestimation of the ultimate load was obtained. However as the order of Gauss rule was increased a stiffer prediction of the ultimate load was observed. When 2 Mat. was assumed (i.e. effect of confinement was considered by increasing the value of the modulus of elasticity of concrete to 34.5 kN/mm^2 in element 65, Figure (7.30)) in the analysis a better estimate of the ultimate load was observed in all cases. It can be seen that the 2 x 2 Gauss rules(2 Mat.) gave a similar load deflection curve to that obtained for the 4 x 4 Gauss rules (1 Mat.). The best load deflection and ultimate load was observed for the 3 x 3 Gauss rule, and a slight overestimation of the ultimate load was observed for the 4 x 4 Gauss rule.

Different load deflection curves are compared in Figure (7.32) using different values of COOP of 20%, 15%, 10% and 5%. Iterations were continued until convergence to the specified tolerance was obtained. It can be observed that COOP = 20% gave a fairly good fit to the experimental load deflection curve and also gave the closest ultimate load. However only a slight underestimation was produced for other values of COOP less than 20%.

The effect of tension stiffening is shown in Figure (7.33) where different load deflection curves are compared using 2 Mat. Two values of COOP of 20% and 5% were used, and ϵ_A was checked for $5\epsilon'_c$, $10\epsilon'_c$, and $100\epsilon'_c$. Underestimation of the ultimate load was obtained in all cases. It appears that increasing the value of ϵ_A produced a stiffer response as found in the previous chapter. Also for the same value of ϵ_A it was found that reducing the value of COOP produced a more flexible response. It appears that tension stiffening is not reliable in predicting the ultimate load, and very poor results were obtained for this heavily reinforced beam. This could be due to the effect of the tension stiffening causing the steel stresses to be underestimated, but the poor prediction of the load deflection curves is quite surprising. This point will require further study.

Different load deflection curves using both cracking models are compared in Figure (7.34) for different values of crushing strains. The effects of confinement were considered in some cases and the 3 x 3 Gauss rule was used for integration with COOP = 20%. It can be observed that the second cracking model produced a much stiffer load deflection curve compared with the first cracking model. It can also be seen that when the crushing strain of concrete is increased to 0.008, overestimation of the load deflection curve was produced. In all cases the use of 2 Mat. was much better in predicting the ultimate load.

Crack patterns for COOP = 20%, 1C, 3.G.R., ϵ_{cu} = 0.004, 2 Mat. are shown in Figures (7.35 - 7.37), and the experimental crack pattern at failure is shown in Figure (7.38). Fairly good agreement was obtained at failure. A similar description for crack development was obtained

as that for beam 101 except that a more well-defined crack was observed at the half clear shear span at failure. Crushing of concrete under the point of load application was the main cause of failure in this beam.

Horizontal stress distribution at the midspan section for different load levels is shown in Figure (7.39). It can be observed that a few tensile stresses have developed in the top half of the beams. These are caused mainly by the effect of shear cracks between the support and the point of application of load.

Experimental and theoretical horizontal strain distributions are plotted at midspan and half clear shear span for different load levels in Figures (7.40 - 7.43). It appears that fairly good agreement was obtained for the strains at the midspan section but there was some variation in the strain distributions at the half clear shear span especially at high load levels. However this variation could be due to other effects such as dowel or bond forces which become more significant at higher load levels or it could also be due to the slightly different positions at which the finite element and experimental strains were measured.

Experimental and theoretical strain distributions are plotted at midspan and half clear shear span for different load levels in Figures (7.44 - 7.47). Fairly good agreement was obtained at the midspan section, but there was some variation in the vertical strain distribution especially at high load levels. The reason for this variation could also be as explained in the previous paragraph.

Strain distributions along the bottom bar obtained experimentally and using the finite element method are shown in Figures (7.48) and (7.49).

Fairly good agreement was obtained at the different load levels.

Finally, horizontal, vertical and shear contour strain distributions at load levels of 196.1 kN and 883.0 kN are shown in Figures (7.50 - 7.55). It can be seen that the horizontal strains at the low load level do not vary significantly especially below the neutral axis. This becomes more complex at the higher load level especially in the half clear shear span. Vertical strains are almost all compressive at the low load level, but this changes at the high load level when tensile strains appear near the support and under the point of load application. The shear strain contours show that these are only important at the line joining the point of load and support. This is observed clearly at the higher load level; very high shear is also developed near the point of load application.

The following conclusions can be made from this study of Lin's beams.

(1) The conclusions obtained from the previous chapter were also applicable to the beams studied in this section. Stiff load deflection curves were obtained for beams 101 and 102 and a fairly good fit for 204.

A comparison of measured and computed ultimate loads predicted by this method and Lin's theoretical results is shown below:

Beam name	W_u Measured ultimate load (kN)	Q_s Computed ultimate load (kN)		Q_s/W_u	
		Lin	F.E.M.	Lin	F.E.M.
101	575.0	473.0	490.0	0.82	0.85
102	420.0	397.0	416.5	0.95	0.99
204	1431.0	1931.0	1422.6	1.35	0.99

Better predictions were obtained for the proposed model than those obtained by Lin's model. For beam 101, it seems that deformation occurred at a high load level which neither model could predict.

(2) The effect of approximating the confinement of concrete was important for these beams. This was not required for the Cervenka panel wall or for the deep beam tested in the previous chapter. It also produced a slightly stiffer load deflection curve but this was not very significant. It is not yet known when this confining effect is important and when it is not. However it appears that for the beam of L/D = 0.9, its effect has much more importance than when the L/D = 1.8.

(3) Tension stiffening was tested for beam 204, and gave a stiff load deflection curve and gross underestimation of the ultimate load. It appears that this method was not reliable for predicting the behaviour of this type of beam but this requires much more investigation, including a check on the strain and stresses in concrete and steel.

(4) Crack patterns for beams 101 and 204 were in good agreement with experimental results at failure loads. Strain distributions were tested for beam 204 and found to have a better agreement with the experimental results at the midspan section. Less agreement was obtained at the half clear shear span. Steel strain distribution in the bottom bar was fairly well predicted. However it seems that the results in general were well predicted with a minimum complexity in the models.

(5) The order of Gauss rule is an important parameter, and the 3 x 3 Gauss rule was found to give a quite reasonable description. This will also be suggested for the next beams to be described.

(6) Convergence tolerance is another important parameter, as was shown for beam 204. Its value can produce a significant effect on the predicted ultimate load. Using a high convergence gave a fast solution and reduced the prescribed convergence tolerance with the maximum number of iterations on any occasion.

(7) Changing the value of the crushing strain of concrete ε_{cu} has some effect on the predicted ultimate load. Again this illustrates the dependence of the solution on the material parameter. However the value of ε_{cu} is quite a variable experimental parameter and depends on various other factors such as the confinement of concrete.

7.3 Deep Beams with openings:

7.3.1 General review:

Openings in beams are generally provided for utility, ducts and pipes. These openings provide more economical structures if they are designed in a proper way, in order to carry external forces on solid beams

In fact the design of deep beams with openings is not yet widely covered by the major design codes of practice, for example the ACI (American Building Code), CEB-FIP (The European Recommendation), or the British Code (CP110). Recently the Construction Industry Research and Information Association (CIRIA) published a guide "The design of deep beams in reinforced concrete" which is the only design guide currently in use in the United Kingdon[22]. However the design problem

itself is not the concern of this work. The purpose of this investigation will be to examine some specific numerical parameters which are thought to affect the solution and hence the predicted behaviour. These parameters have already been examined for solid beams, but they will be examined again to confirm the previous findings on the present beams. However, deep beams with openings have not previously been tested numerically using the finite element method, and it will be interesting to see how they act when varying these numerical parameters.

The behaviour of deep beams with openings has been investigated by a few authors. Kong et al.[23] tested 72 beams made with normal weight and lightweight concrete. A wide range of opening sizes and locations were used with several arrangements of reinforcement.

The effect of the opening on beam behaviour was found to depend upon the extent to which the opening intersected at the "load path" which was considered to exist between the loading and supporting point. When the opening intersected at the above mentioned load path the strength of the beam was reduced, with the extent of the reduction depending upon the size and location of the opening. It was also found that the web reinforcement was highly effective in controlling crack width and therefore must protect both the diagonal regions above and below the opening. Inclined web reinforcement was found to be particularly effective for crack width control and for increasing the ultimate shear strength. The order of the formation of cracks was found to depend upon the size and the location of the opening, and crack widths were found to increase when the web opening intersected the load path.

Kong et al.[24,25] proposed an empirical formula to predict the

ultimate shear strength for these types of beams. Kubic[26] tested 26 light and normal weight concrete deep beams. He found that a deep beam with a web opening which interrupts the flow of stresses due to intersection of load path with the opening deformed mainly by the rotation of the three blocks of the beam; one above the opening, another below the opening and the third between the opening and the end of the beam. He confirmed the previous findings of Kong et al. that the location of the web opening can effect the crack propagation. He found that the inclined web reinforcement was more effective in controlling the maximum crack width than the orthogonal reinforcement of horizontal bars and vertical stirrups. A review of the available work on deep beams with openings was also reported in this study. A theoretical model was proposed to predict the ultimate flexural and shear strength of these beams, but the model was applicable only to the case when the opening intersects the line joining the load and support point.

Memon[3] carried out a wide survey on the existing literature of deep beams with openings and different theoretical methods of solution. He concluded that the elastic methods of analysis are not sufficient to provide useful information on the post cracking behaviour and the ultimate strength. He also noted that the present design rules for these types of beams are defined empirically because of their complexity. From the tests he carried out a formula for the prediction of ultimate strength was proposed, but he restricted this to the cases he tested and suggested that further tests should be carried out before the formula could have a general use.

The next section will discuss two of Memon's beams in more detail, in conjunction with the finite element analysis.

7.3.2 Memon deep beam B-5[3]:

Memon's deep beam with opening B-5, shown in Figure (7.56), will be analysed in this section. Because of symmetry only half of the beam will be tested. Details of the finite element mesh is shown in Figure (7.57). Material properties for concrete and steel are shown in Tables (7.5) and (7.6).

In the analysis the following assumptions were made:

(1) The first cracking model was used (i.e. no tension stiffening).

(2) The method V.S.M.1 was used.

(3) The load criterion was used to check convergence with a value of COOP = 20%. Iterations were continued until the specific tolerance was obtained.

(4) The load was applied in equal increments of 50.0 kN until failure occurred.

Different load deflection curves using a value of α equal to 0.5 are compared for different orders of Gauss rules of 2 x 2, 3 x 3, and 4 x 4 in Figure (7.58). It can be observed that the 2 x 2 Gauss rule underestimated the failure load, and the results were better for the 3 x 3 and 4 x 4 Gauss rules. However it can also be observed that the 2 x 2 Gauss rule predicted the load deflection curve satisfactorily up to about 85% of the experimental curve.

Different load deflection curves are compared using the 3 x 3 Gauss rule in Figure (7.59) for different values of α of 0.0, 0.5 and 1.0. It can be observed that changing the value of α from 0.5 to 1.0 did not affect the predicted load deflection curve and ultimate load. However underestimation of the failure load was observed for $\alpha = 0.0$ and this occurred approximately where the diagonal cracks started in the beam.

Different load deflection curves are compared using the 3 x 3 Gauss rule and α = 0.5 in Figure (7.60) for different values of crushing strains. It can be observed that changing the value of the crushing strain of concrete ε_{cu} has some effect on the final ultimate load. The best estimate was obtained for a value of ε_{cu} = 0.004, and it is suggested that a suitable adjustment to this value would give the exact ultimate load.

Crack patterns are plotted for COOP = 20%, 3.G.R., α = 0.5, ε_{cu} = 0.004 at different load levels in Figures (7.61 - 7.65). Experimental crack patterns are also shown in Figure (7.66). It can be observed that flexural cracks started in the initial stages in regions of maximum tensile strains above the opening. These propagated at higher load levels (see Figure (7.62)) and cracks started to appear in the bottom of the beam. At further increases of load the flexural cracks became deeper and diagonal cracks started to appear in the mid shear span section. At the final stages these propagated, and crushing appeared near the opening followed by the yielding of steel above the opening. Good agreement with the experimental results was obtained at failure load as shown in Figures (7.65) and (7.66).

Principal stress directions are plotted in Figures (7.67) and (7.68). It can be observed that at the high load level, a pure compressive region was developed between the point of load and the support acting as a column in the beam. Horizontal strains obtained in the midspan section for the experimental and finite element analysis are shown in Figures (7.69 - 7.74) at different load levels. It can be observed that fairly good agreement was obtained up to a load of 600.0 kN. Between 600.0 kN,

and 1000.0 kN a large variation was observed. This represents the stage at which the cracks are developing in the section below the opening, and shows that these cracks mostly occurred in the finite element method between a load of 900.0 kN and 1000.0 kN. After that load, and as the failure load was reached, agreement with the experimental result improved, and was within about 30% in the worst condition.

Vertical strains near the opening measured both experimentally and using the finite element method are shown in Figures (7.75 - 7.80) at different load levels. Fairly good agreement was obtained for these strains at all the load levels observed.

Steel load-strain curves for the top bar (i.e. above the opening) and for the bottom bar in the beam are shown in Figures (7.81) and (7.82). Good agreement was obtained for the top bar especially close to failure. For the bottom bar the agreement was less satisfactory, and the sudden change between loads of 900.0 kN and 1000.0 kN was associated with that change observed in Figure (7.72) in the horizontal strains which represent the stage when most cracks appeared in the beam, as shown in Figure (7.64).

7.3.3 Memon deep beams B-7[3]:

This beam has similar dimensions to beam B-5 except that the width of opening was reduced to 400.0 mm, (see Figure (7.57)for mesh used) and has a higher concrete strength. Details of concrete properties are shown in Table (7.5). The steel provided was the same as that for beam B-5. The same numerical assumptions made for beam B-5 were used in this analysis. The value of crushing strain was assumed to be equal to 0.004. Comparisons between the analytical and experimental load

deflection curves are shown in Figure (7.83). It can be seen that fairly good agreement was obtained in the predicted load deflection and ultimate load. The ultimate load was higher than that predicted in B-5, this is either due to the increase in the strength of the concrete, or due to the reduction in the opening size.

No description will be given for the crack and stress distributions, since the beam failed in a similar manner to that described for beam B-5.

The following points can be made about the study of deep beams with openings:

(1) Nonlinear analysis was carried out for the first time on these types of beams using the suggestions from the previous chapter. Good predictions of the load deflection curves and ultimate loads were obtained. A comparison of measured and computed ultimate loads predicted by this method and Memon's theoretical results are shown below:

Beam name	W_u Measured ultimate load (kN)	Q_s Computed ultimate load (kN)		Q_s/W_u	
		Memon	F.E.M.	Memon	F.E.M.
B-5	1600.0	1102.0	1550.0	0.68	0.97
B-7	1700.0	1314.0	1650.0	0.77	0.97

The finite element method gave better estimates for both beams. These predicted results will give guidelines for further investigations to study the same type of beams with different load conditions and openings, and also those with different material properties.

(2) Changing the order of integration rule had less significant effect

on the prediction of the load deflection curve and ultimate load, than the deep beam failing in flexure tested in the previous chapter. However the low integration Gauss rules did produce an underestimation of the ultimate load. The use of the 3 x 3 Gauss rule was also found to be best when analysing this type of beam.

(3) When the shear retention factor α was set equal to 0.5 or 1.0, the load deflection curves and the ultimate load were not affected. When α was set equal to zero the failure load was underestimated. This failure occurred suddenly after the development of the diagonal cracks observed at the half clear shear span. It appears that setting the value of $\alpha = 0.5$ was the best value for all beams, and that $\alpha = 0.0$ can cause some numerical difficulties.

(4) Increasing the crushing strain of concrete from 0.004 to 0.008 can produce a stiffer response and overestimate the ultimate load. This shows again the importance of material parameters on the predicted behaviour. Suggestions are made that the value of 0.004 is satisfactory for the tested beams.This is based on the grounds that confinement can produce a higher concrete strength and hence crushing will be delayed.

(6) No tension stiffening was required and convergence was satisfactorily obtained in both beams without any difficulties.

(7) The development of flexural cracks at the midspan section can greatly affect the predicted finite element horizontal strain distribution below the opening. However this cracking effect is found to be less significant on the predicted vertical strain distribution near the opening. Horizontal load strains for longitudinal steel below the opening was also affected by the development of flexural cracks at midspan section. A suggested

explanation for this is that if the applied load increments were less than 50.0 kN, it would allow a more gradual crack development and hence a more gradual change in strains. However this was not tested out. The value of f_t' can also have some effect on this but it was assumed to be the same as that measured experimentally.

7.4 Conclusions:

A numerical study was carried out on some of the parameters influencing the solution of different types of deep beams failing in shear. It was assumed that the method V.S.M.1 was the best method to use from the observations obtained from the previous chapter. Some of the parameters which were suggested in the previous chapter to give the best solutions on beams failing in flexure were again investigated on the ones failing in shear in this chapter. The following points were noted:

(1) The first cracking model was used on all tested beams and found to produce a fairly good estimate of the ultimate load in all cases. However the load deflection curve was sometimes overstiff. This could be due to the effect of material properties since a similar shape for the load deflection was obtained when compared with the experimental ones. Tension stiffening was tested for one beam of L/D = 0.9 which was heavily reinforced. The results showed a drastic underestimation of the ultimate load. It appears that tension stiffening was not capable of producing a good prediction for the experimental results in this beam. Further investigation to this matter may be required. However the no tension stiffening model produced good prediction as was found

in previous chapters, and it is suggested that this model is quite capable of preventing the complex aspect of the behaviour. Moreover it is far cheaper in computer running time.

(2) Using the shear retention factor α = 0.5 and 1.0 did not significantly change the shape of the load deflection curve. When this was set equal to zero failure was underestimated and occurred when the diagonal cracks started to appear. This parameter was only tested for the deep beam with opening B-5 and was assumed equal to 0.5 in all other beams. A value of α = 0.5 was able to satisfactorily predict the behaviour of these complex beams without great difficulty.

(3) The 3 x 3 Gauss rule was found to be the best in predicting the ultimate load, and a reasonable load deflection curve. The 2 x 2 Gauss rule must not be used, because it was found not to be adequate to describe the crack pattern and monitor the nonlinearized material properties with close precision.

(4) The load criterion was used with COOP = 20% in most cases. This value gave a fast convergence without any obvious difficulties. Lower values were investigated and were found to affect the predicted ultimate load to some extent. For beam 204 which failed in pure shear, the load deflection curve was not significantly affected at lower loads. However these lower values covered a value which affected the Cervenka panel load deflection curve, where the failure was due to a combination of flexure and shear cracks. It was found, for that beam, that a change of COOP from 10% to 20% only produced a change of 4-8% in the predicted ultimate load. COOP = 10% required a total number of 173 iterations whereas COOP = 20% required only 55.

(5) Changing the values of the crushing strain of concrete can effect the shape of the load deflection at high load levels before failure and can produce different ultimate loads. This shows the importance of material parameters on the solution and these must be considered carefully.

(6) The predicted ultimate load using the finite element model was found to be much better than that obtained using different formulae as proposed by the different investigators from their experimental tests. This method gives more generality, with a stronger mathematical basis. Moreover it can produce detailed information which seems to be of acceptable accuracy when compared with experimental tests.

(7) The effect of increasing the concrete strength in order to account for the effect of confinement under the loading point was important for all the Lin deep beams. This was not required for Memon deep beams with openings. This may be due to the different type of load applications since two point loads were applied for Memon beams, and only single loads were applied to the Lin beams. This matter may be difficult to judge in practical applications, but obviously needs to be borne in mind.

Beam name	L/D	Width (b) (mm)	Depth (D)(mm)	f_{cu} (N/mm^2)	f'_c (N/mm^2)	f'_t (N/mm^2)	E_c (kN/mm^2)	ν_c
W-2	1.13	76.5 (centre) 898.9 (edge)	762.0	34.30	26.75	3.65	20.0	0.18

Table(7.1) Properties of concrete for Cervenka panel wall.

Bar No.	E_s (kN/mm^2)	f_y (N/mm^2)	E_w (N/mm^2)
No.3 (in)	188.23	353.0	0.0

Table (7.2) Properties of steel for Cervenka panel wall.

Beam name	L/D	Width (b) (mm)	Depth (D)(mm)	f_{cu} (N/mm^2)	f'_c (N/mm^2)	f'_t (N/mm^2)	E_c (kN/mm^2)	ν_c
101	1.8	100.0	500.0	47.0	36.0	3.07	19.5	0.20
102	1.8	100.0	500.0	31.0	18.0	2.62	15.3	0.20
204	0.9	100.0	1000.0	49.0	32.3	2.94	20.7	0.20

Table (7.3) Properties of concrete for Lin deep beams.

Bar diameter (mm)	E_s (kN/mm^2)	f_y (N/mm^2)	E_w (N/mm^2)
6	217.3	245.8	0.0
8	188.7	225.9	0.0
10	293.6	229.7	0.0
12	263.5	323.0	0.0
16	276.7	322.5	0.0

Table (7.4) Properties of steel for Lin deep beams.

Beam Name	L/D	Width (b) (mm)	Depth (D) (mm)	f_{cu} (N/mm^2)	f'_c (N/mm^2)	f'_t (N/mm^2)	E_c (kN/mm^2)	ν_c
B-5	1.0	100.0	1000.0	54.1	42.2	4.16	25.97	0.20
B-7	1.0	100.0	100.0	58.0	45.2	4.93	26.70	0.20

Table (7.5) Properties of concrete for Memon deep beams.

Bar diameter (mm)	E_s (kN/mm^2)	f_y (N/mm^2)	E_w (N/mm^2)
6	251.5	503.0	0.0
8	252.0	531.0	0.0
10	252.0	504.0	0.0

Table (7.6) Properties of steel for Memon deep beams.

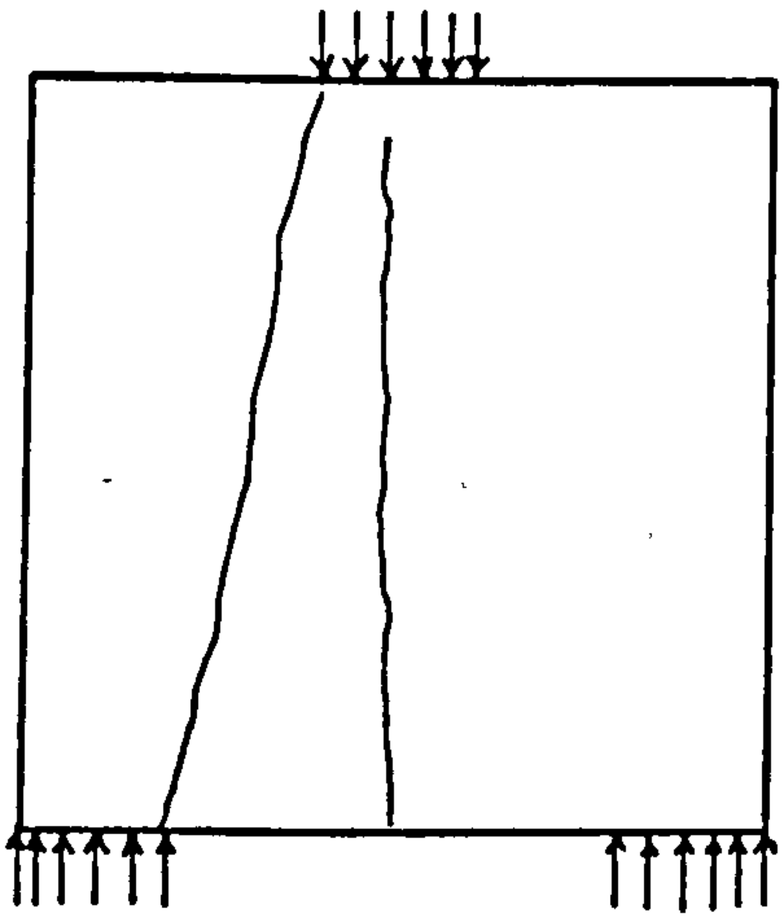

(a) Flexure - shear.

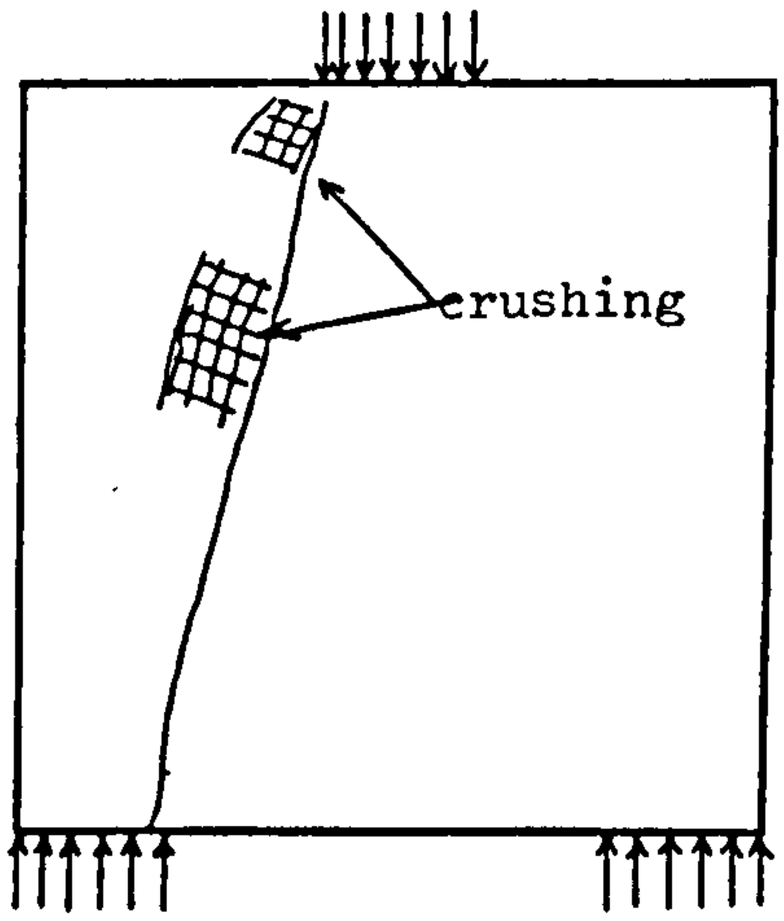

(b) Diagonal - compression.

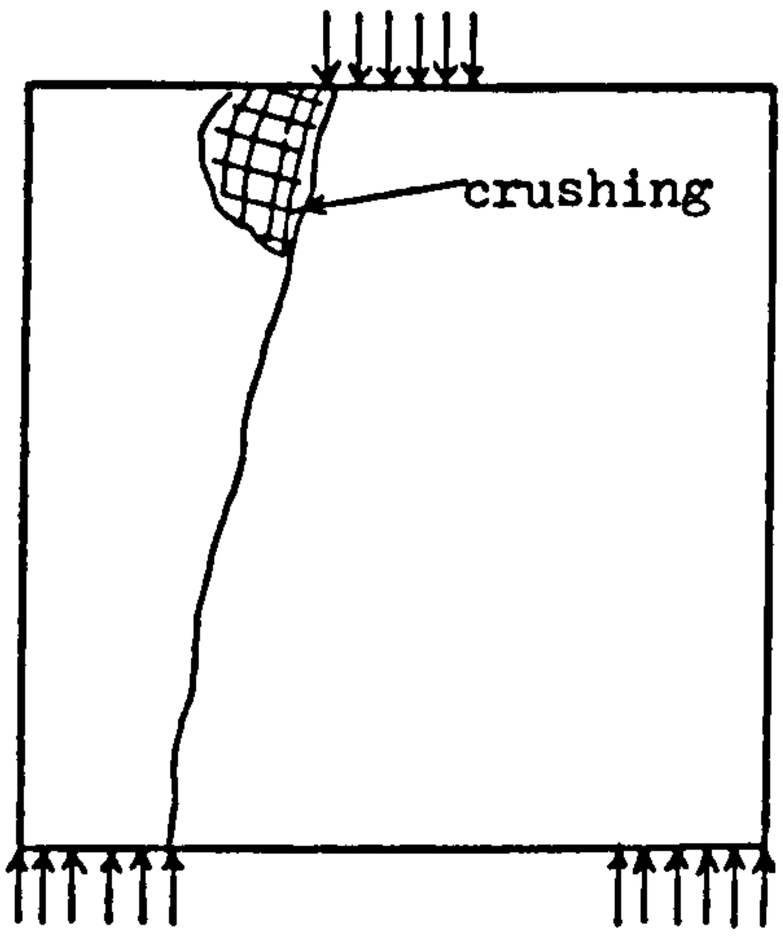

(c) Shear - compression.

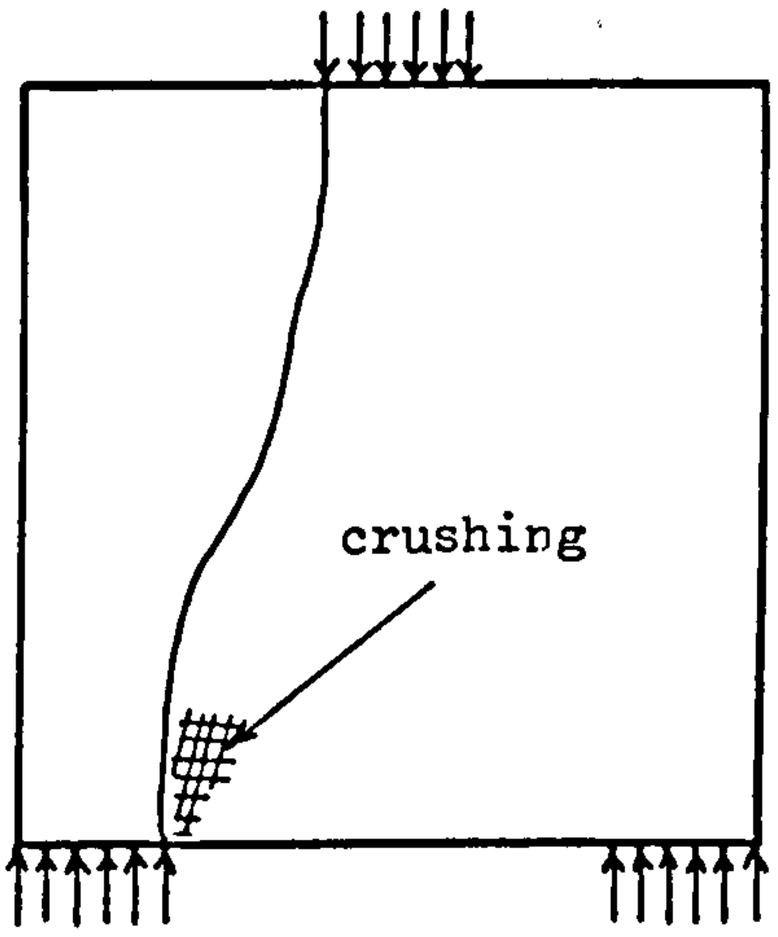

(d) Splitting-shear.

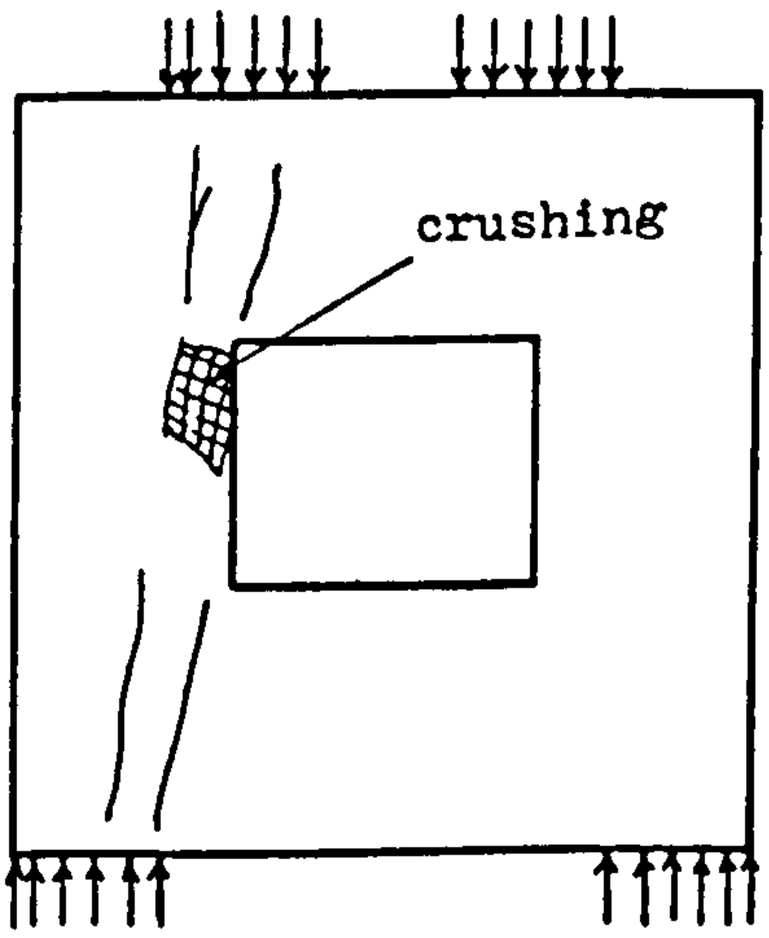

(e) Diagonal - compression.

Figure (7·1) Failure modes for tested beams.

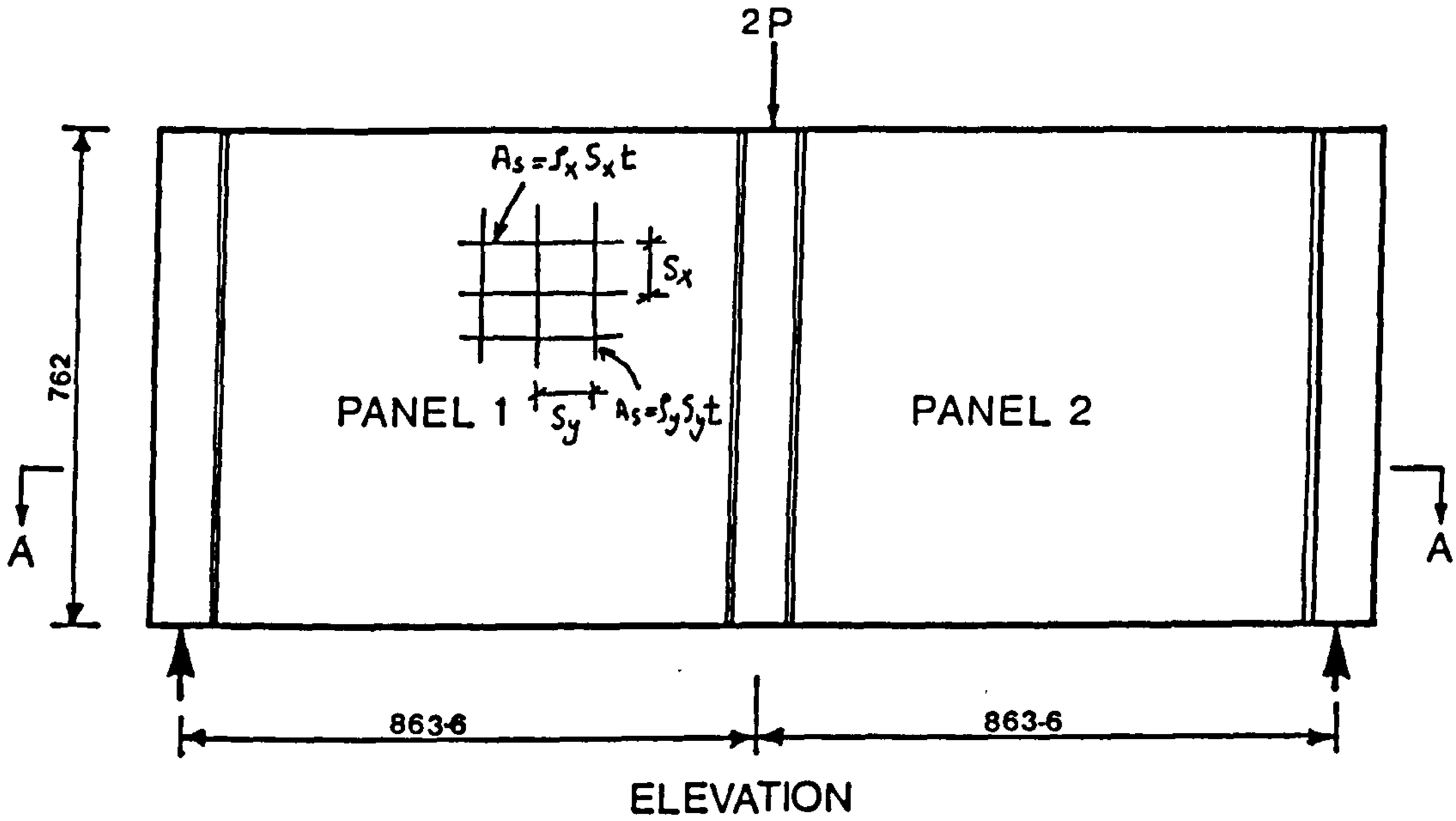

Type	S_x(mm)	ρ_x	S_y (mm)	ρ_y	
{3/8 in {10mm	101.66 50.66	0.00916 0.01832	101.6	0.00916	Top 610 mm Bot. 152 mm

Panel reinforcement

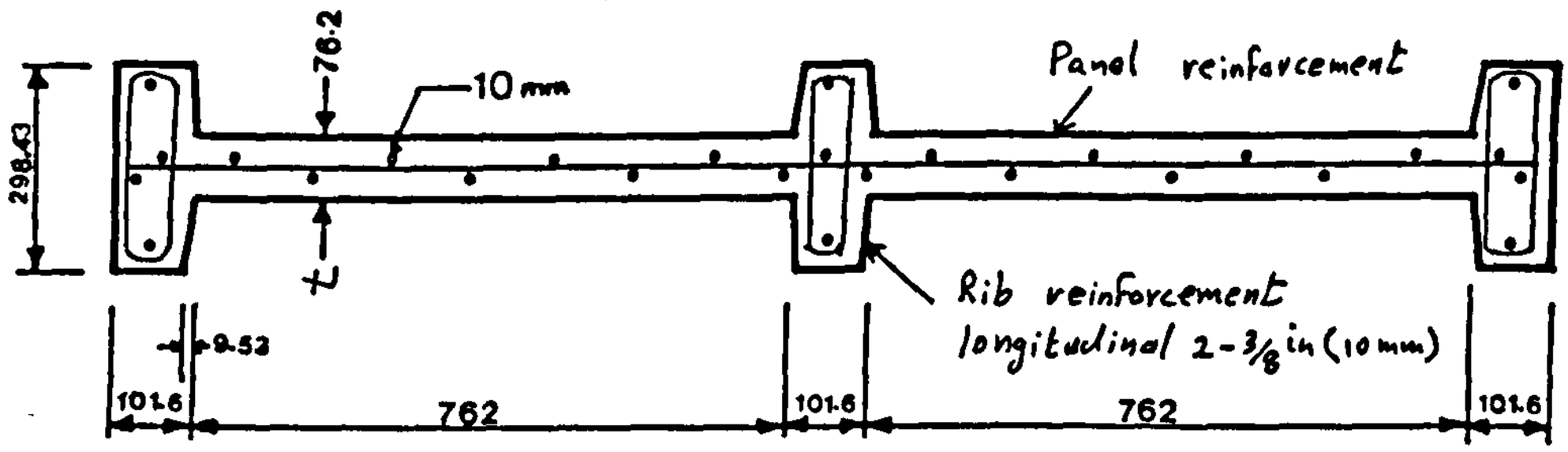

SECTION A–A

Figure (7·2) Details of Cervenka panel wall W-2.

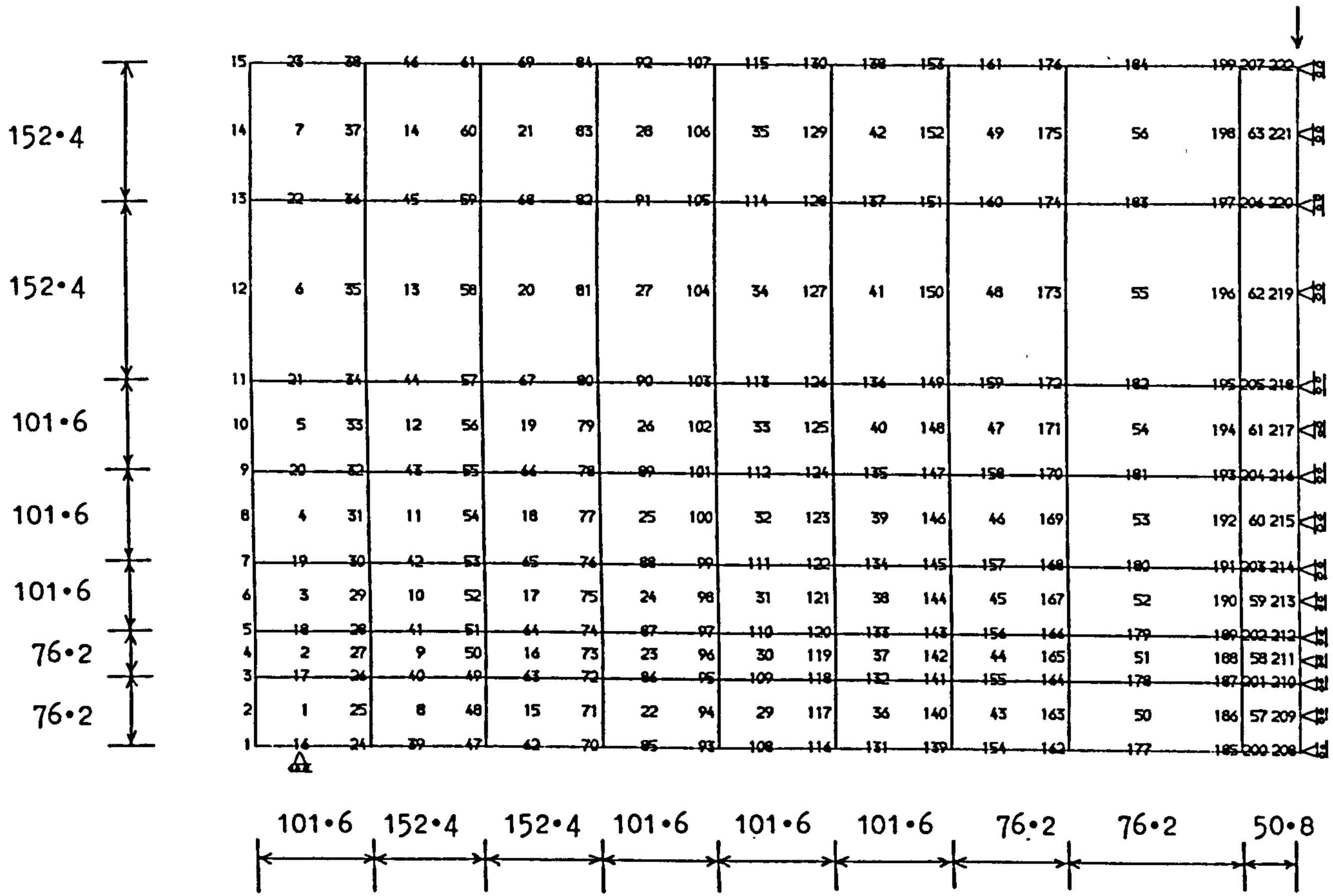

Figure (7•3) Mesh used for Cervenka panel wall W-2.

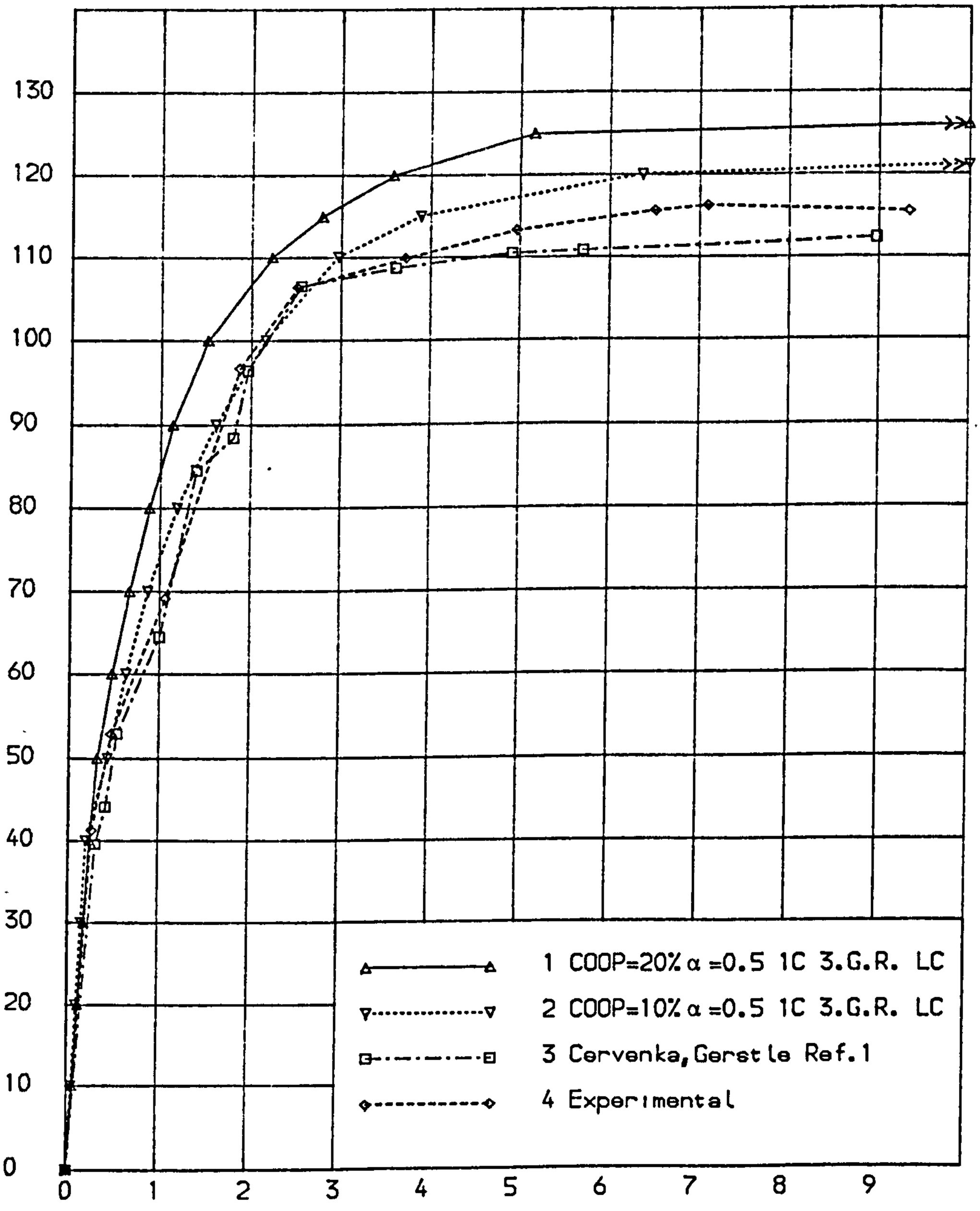

Fig. (7.4) Load deflection curve for Cervenka panel wall.

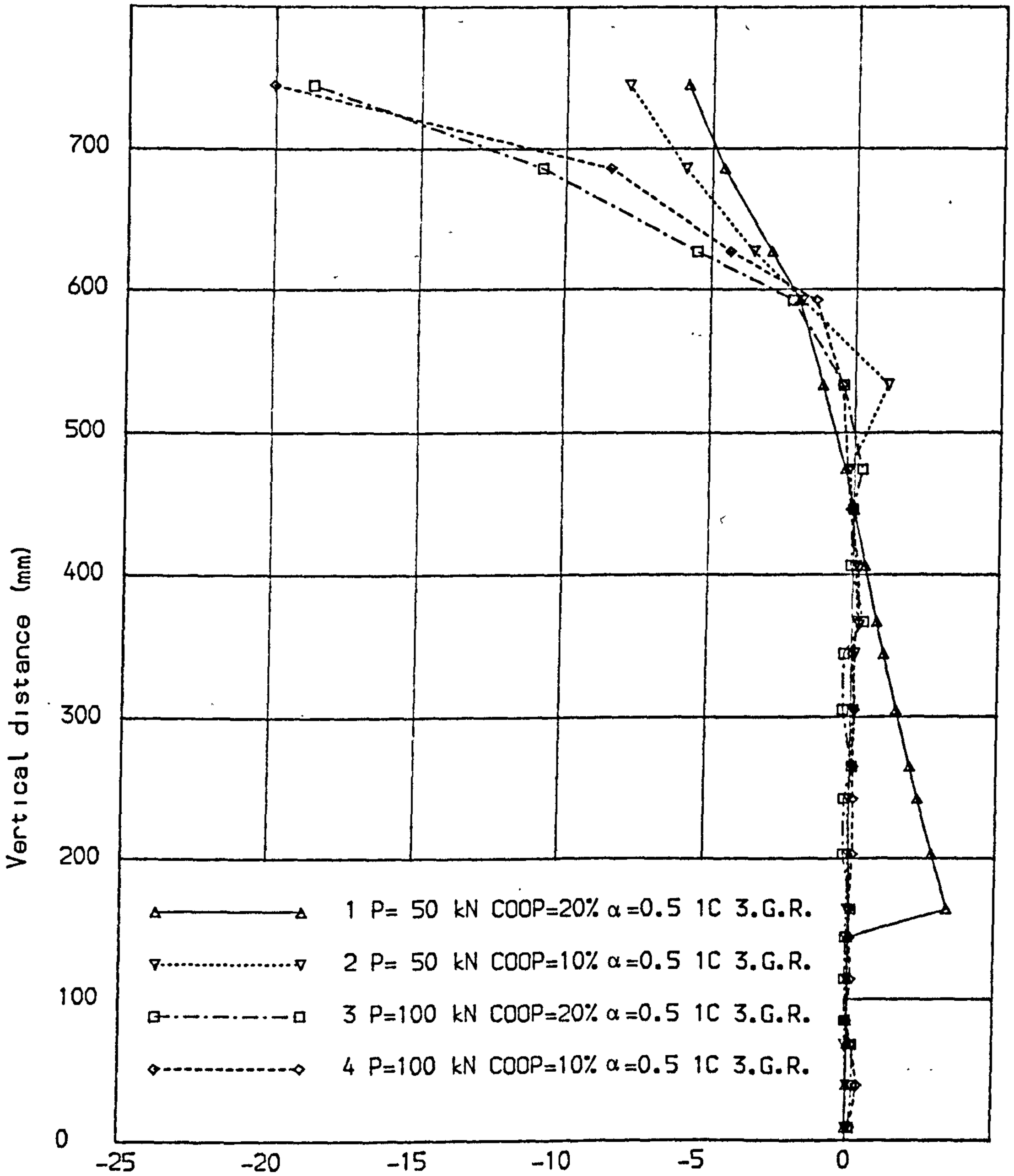

Fig. (7.5) Stress distribution at midspan section, (Cervenka).

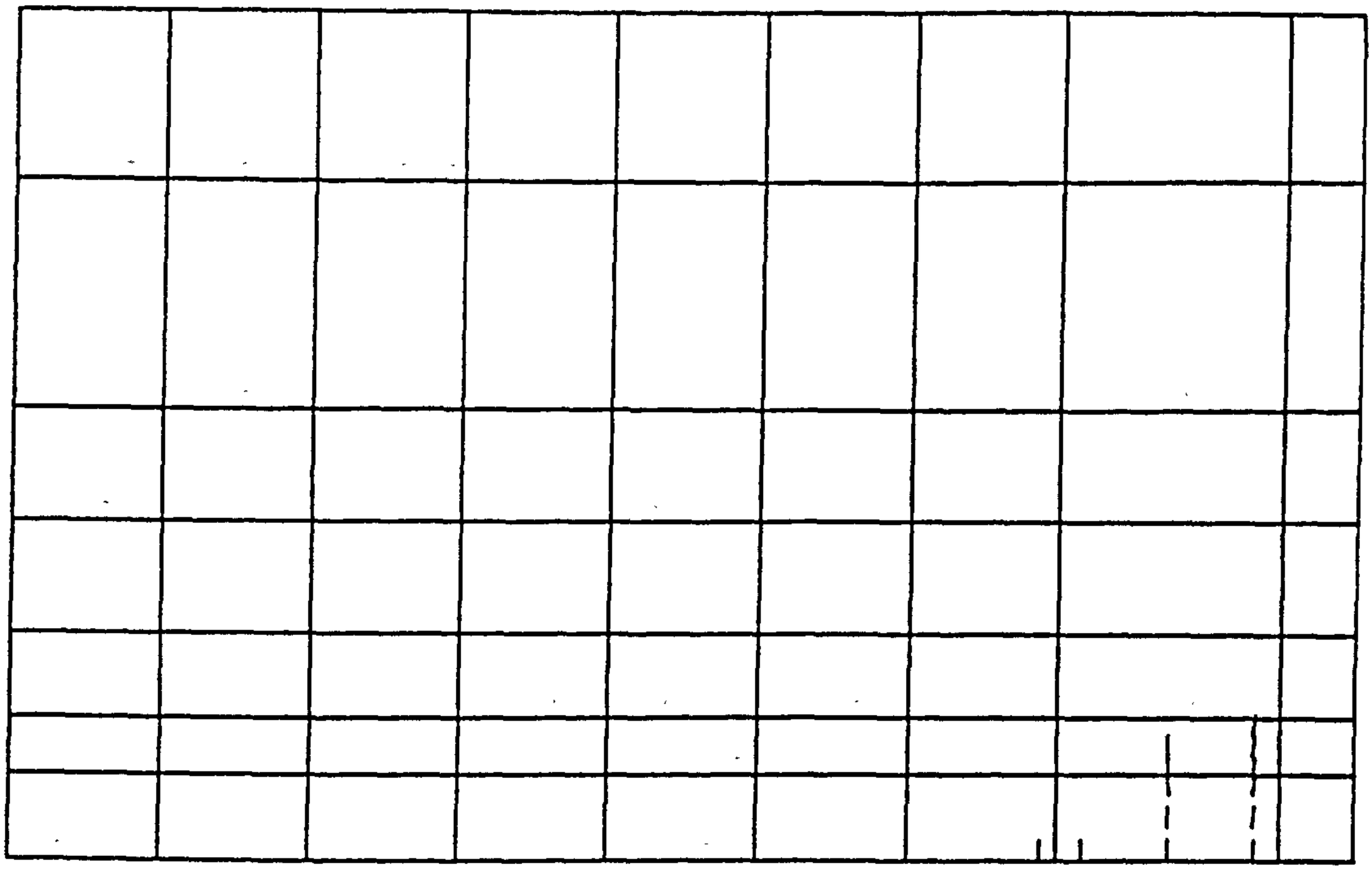

Figure (7·6) Crack pattern at load = 50·0 kN.

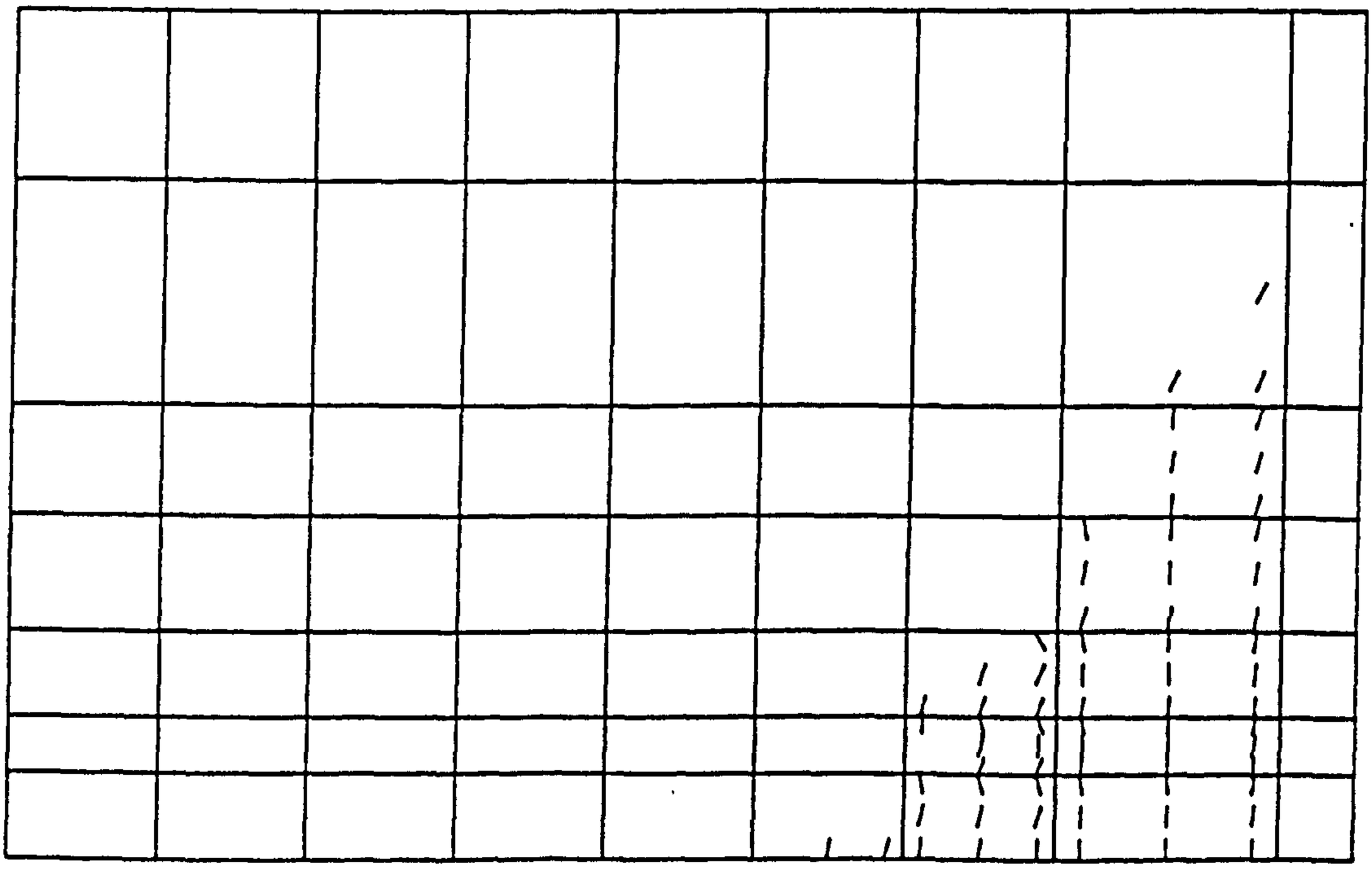

Figure (7·7) Crack pattern at load = 75·0 kN.

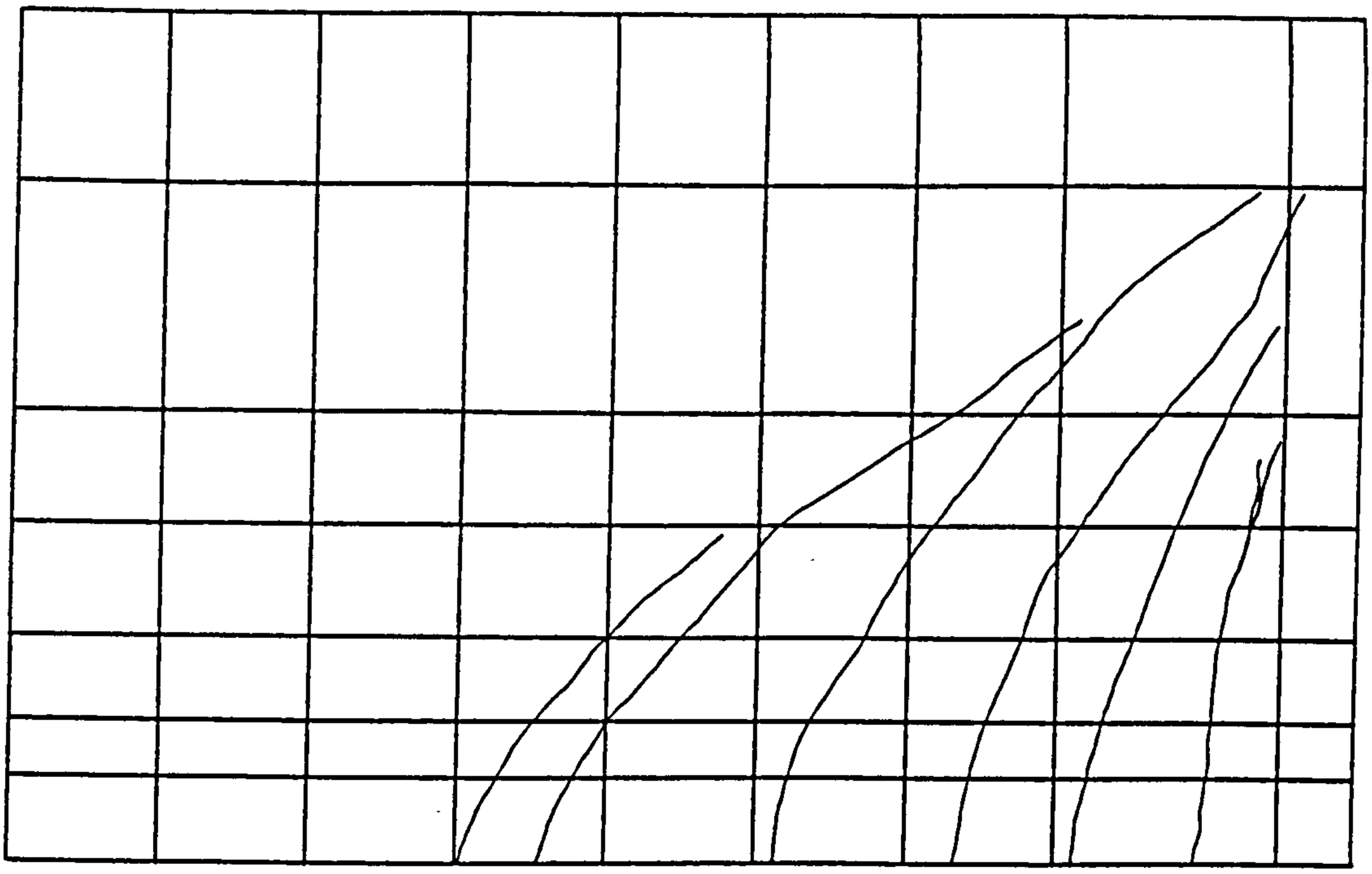

Figure (7·8) Experimental crack pattern at load = 106·8 kN.

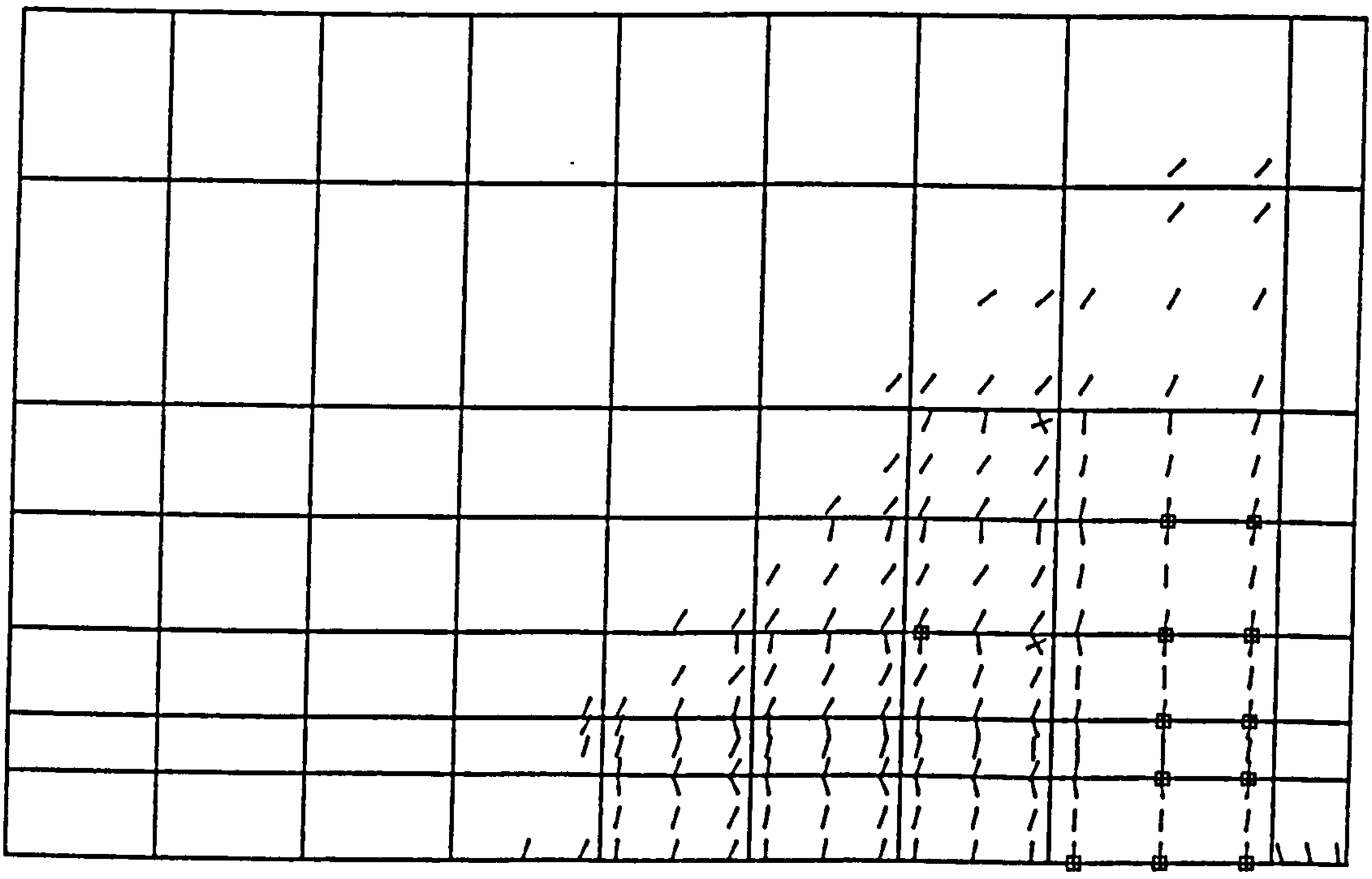

Figure (7·9) Crack pattern at load = 105·0 kN.

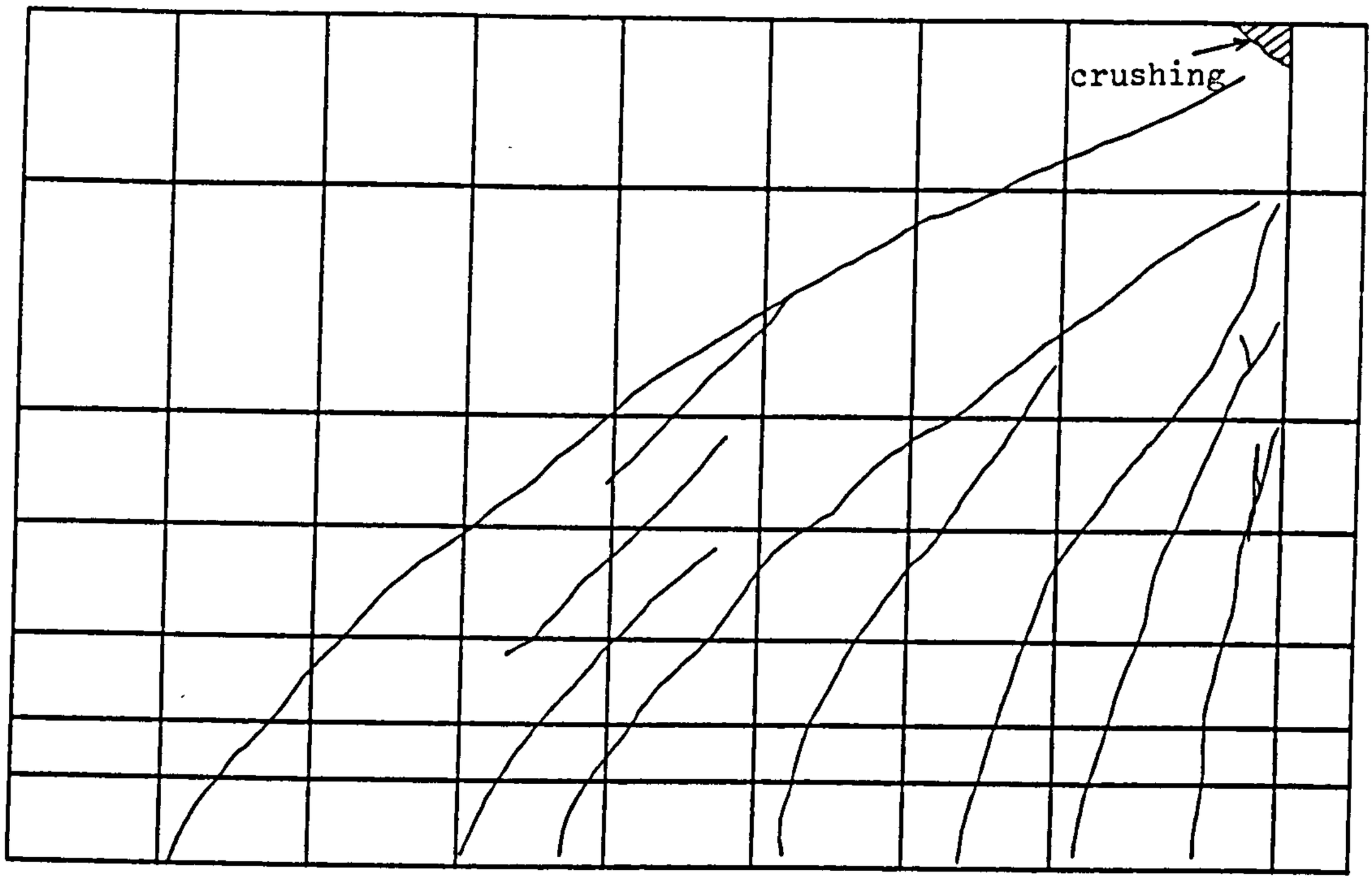

Figure (7·10) Experimental crack pattern at load = 113·4 kN.

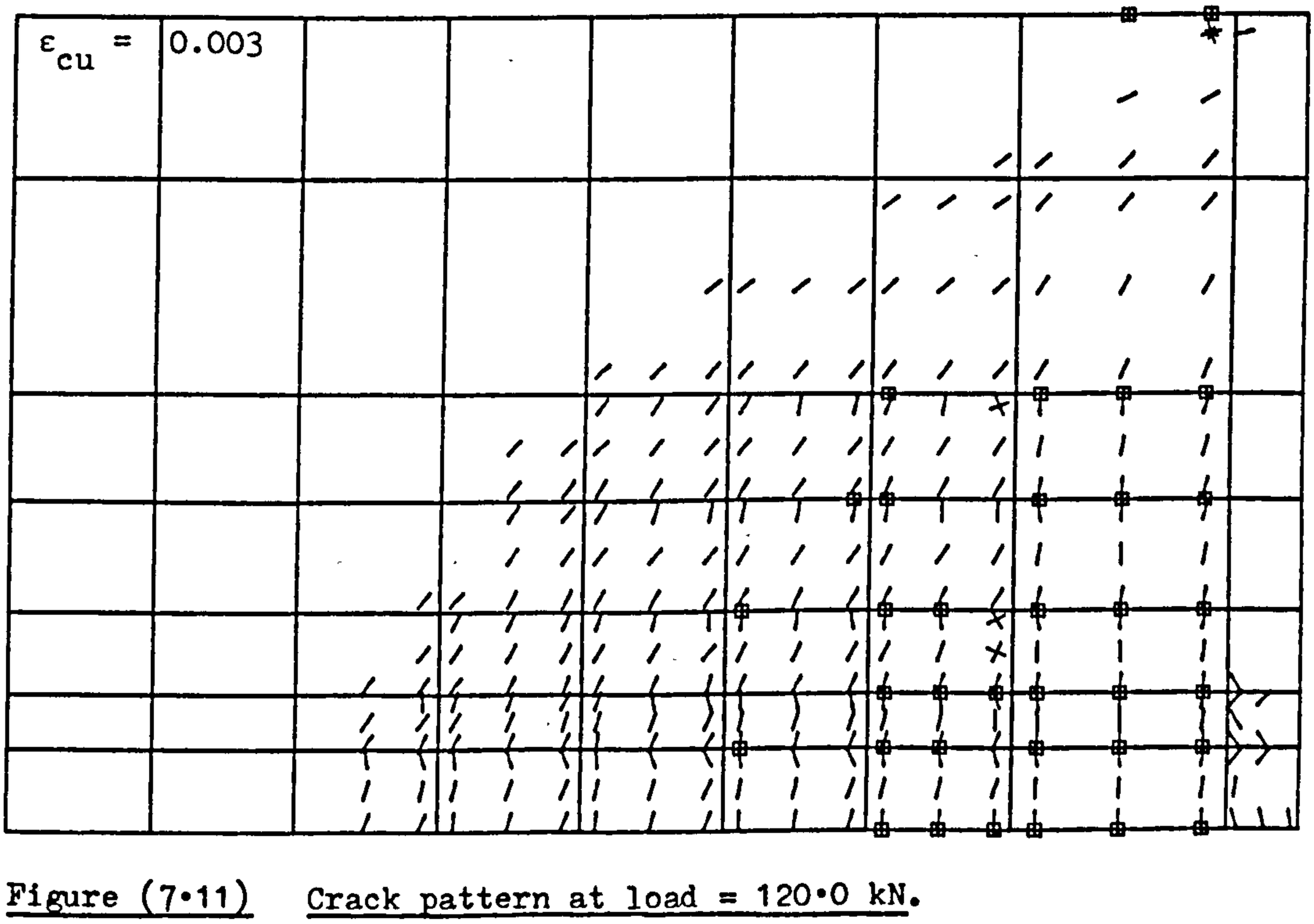

Figure (7·11) Crack pattern at load = 120·0 kN.

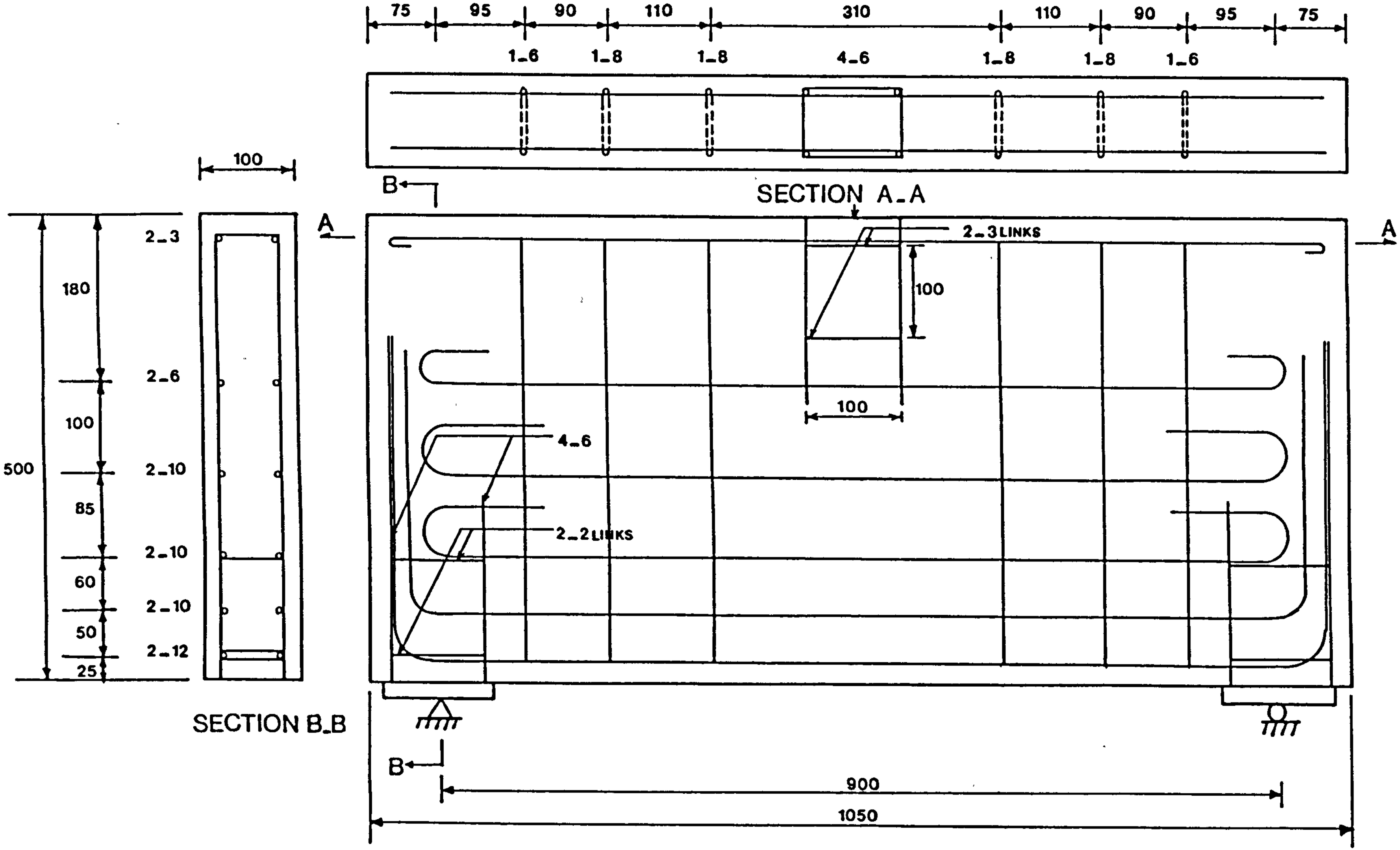

Figure (7·12) Details of Lin deep beams 101 and 102.

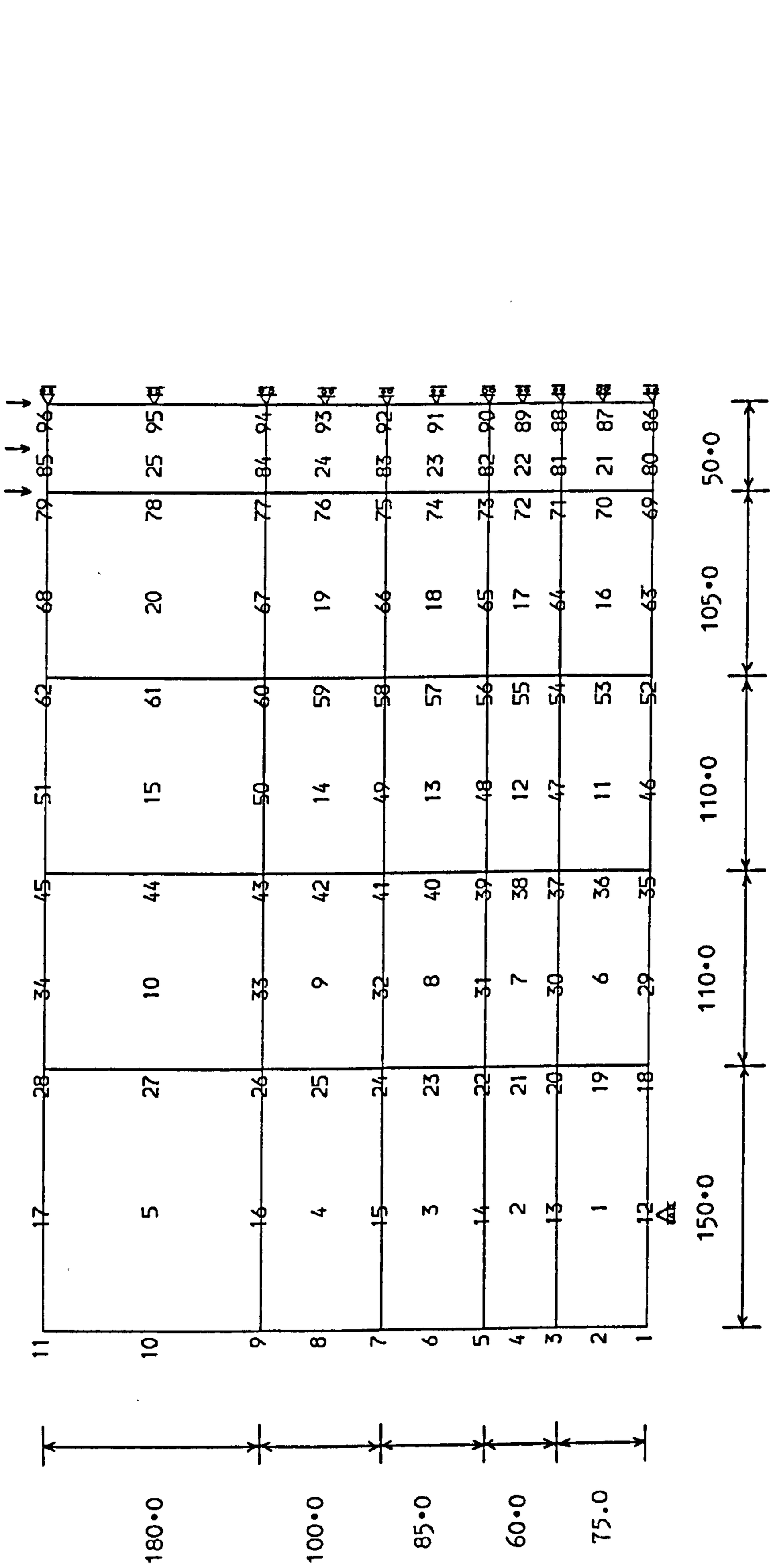

Figure (7·13) Mesh used for Lin beams 101 and 102.

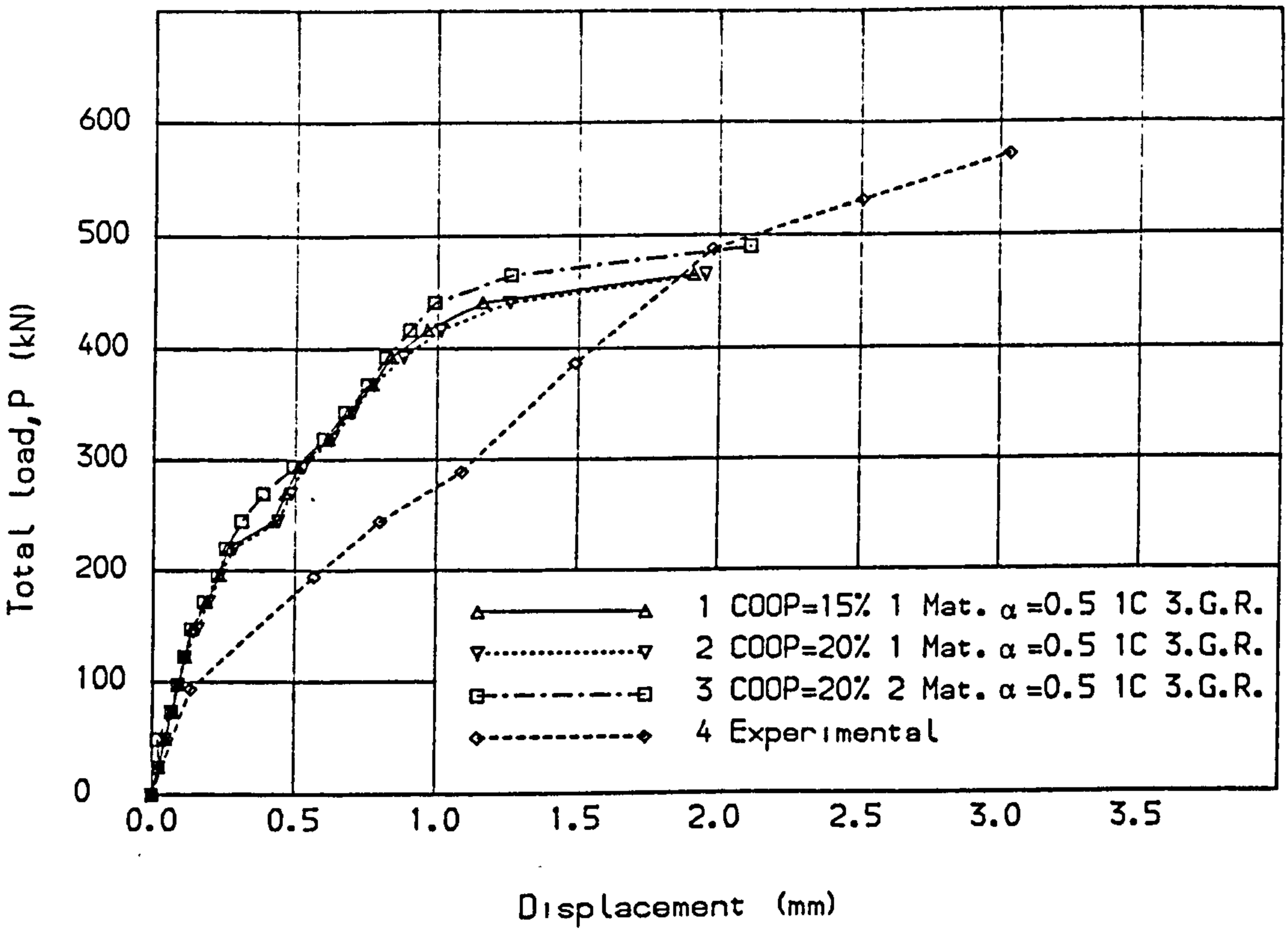

Fig. (7.14) Load deflection curve for Lin beam 101.

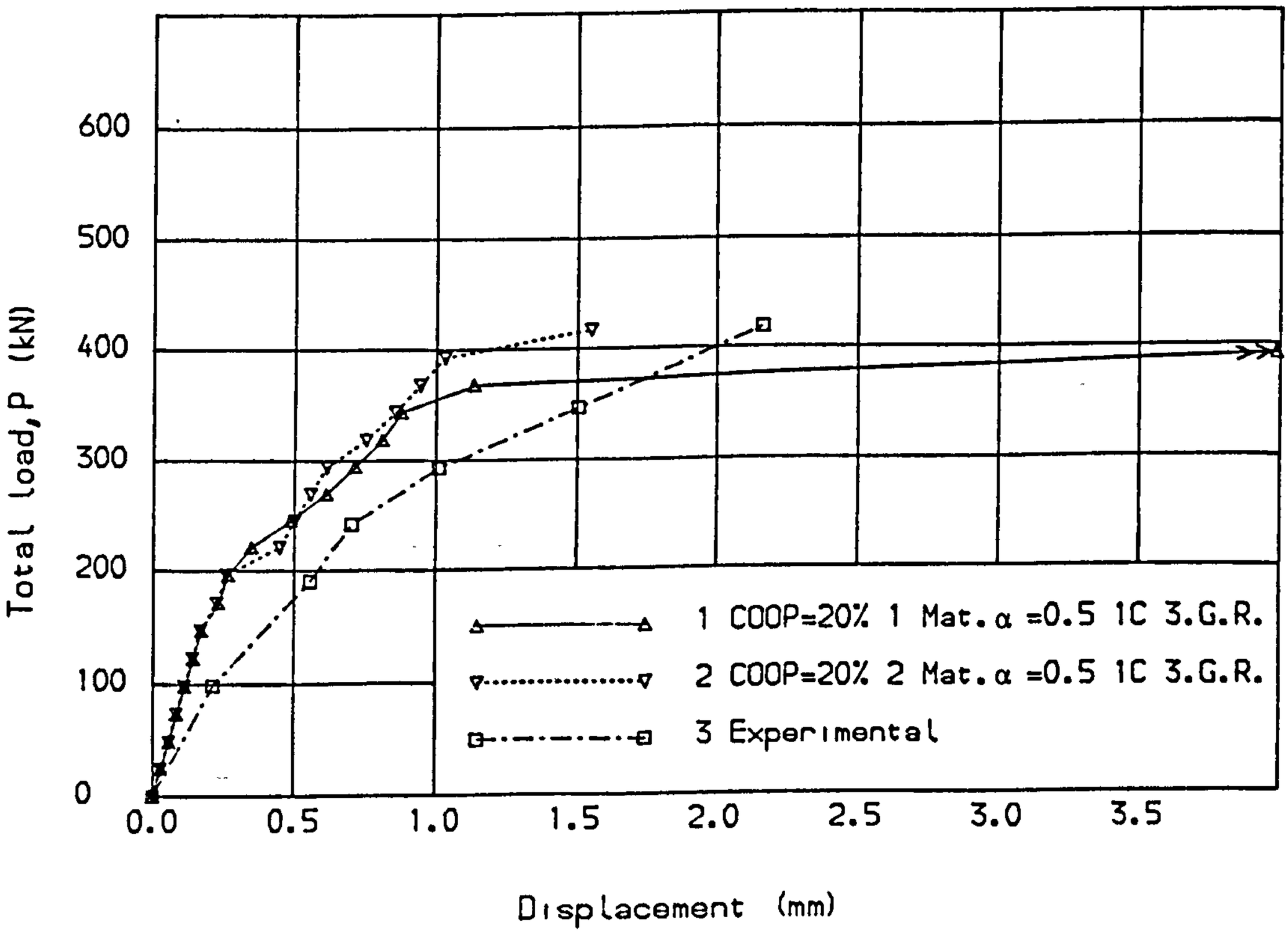

Fig. (7.15) Load deflection curve for Lin beam 102.

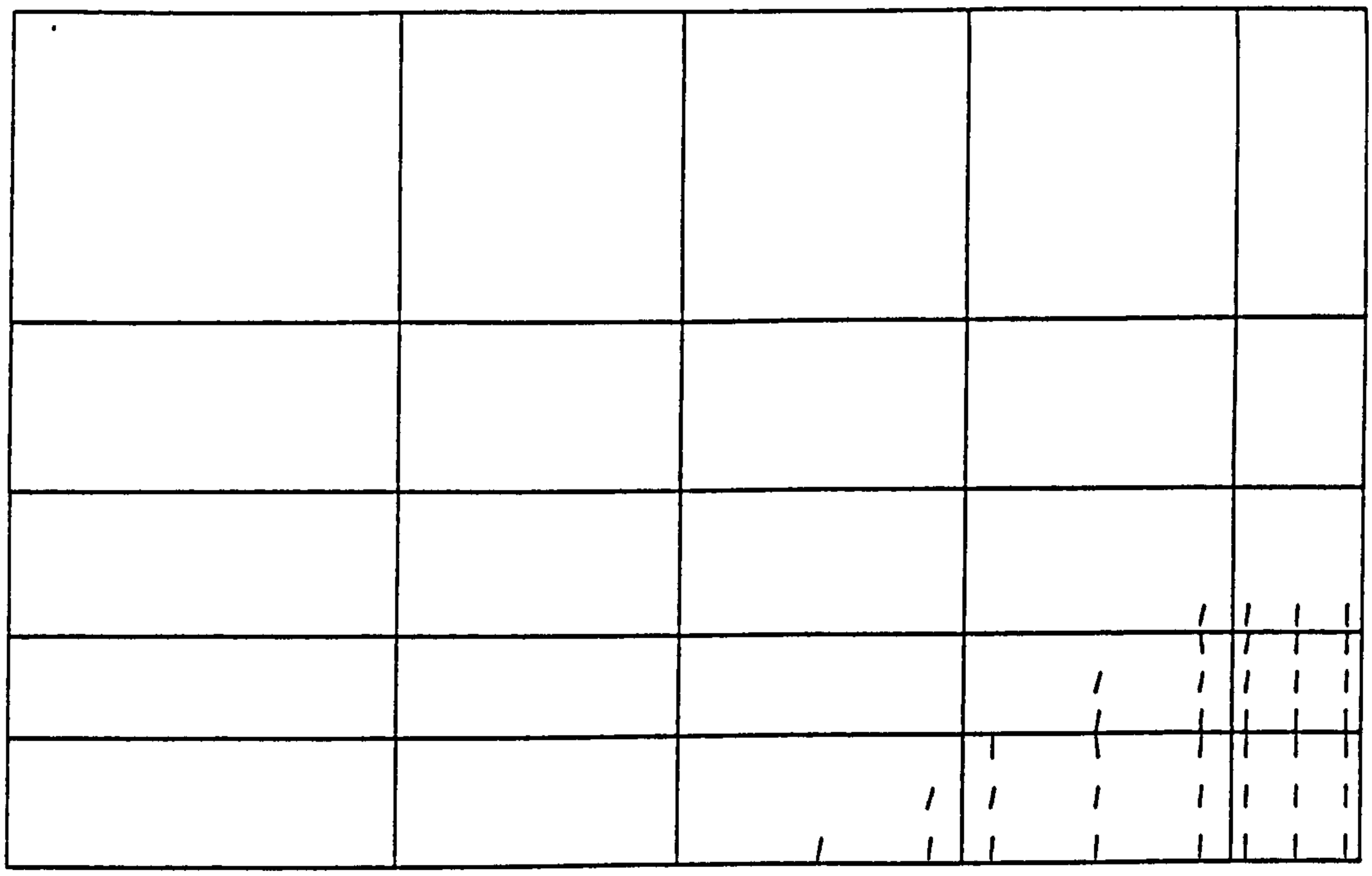

Figure (7•16) Crack pattern at load = 196•0 kN.

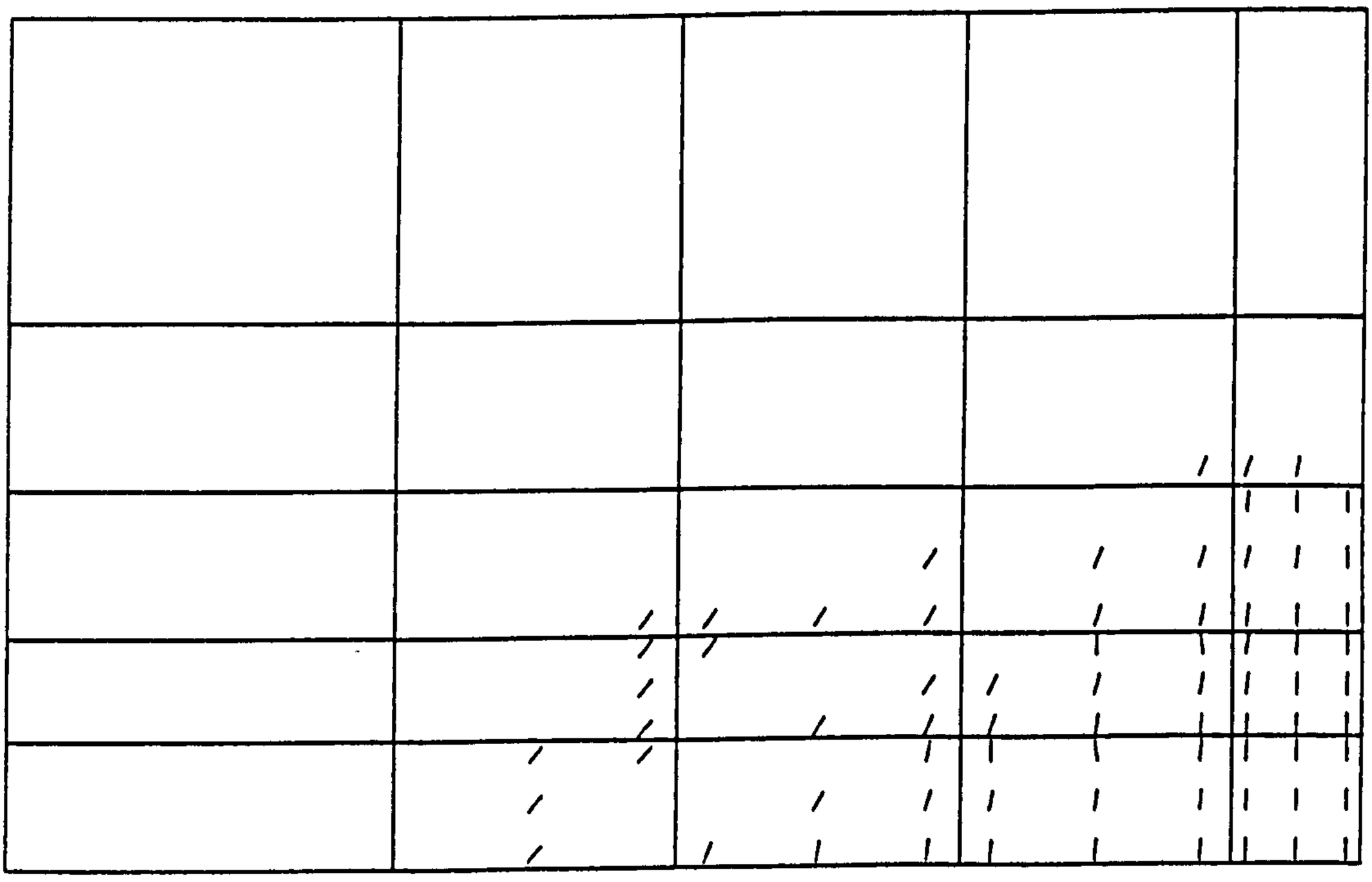

Figure (7•17) Crack pattern at load = 245•0 kN.

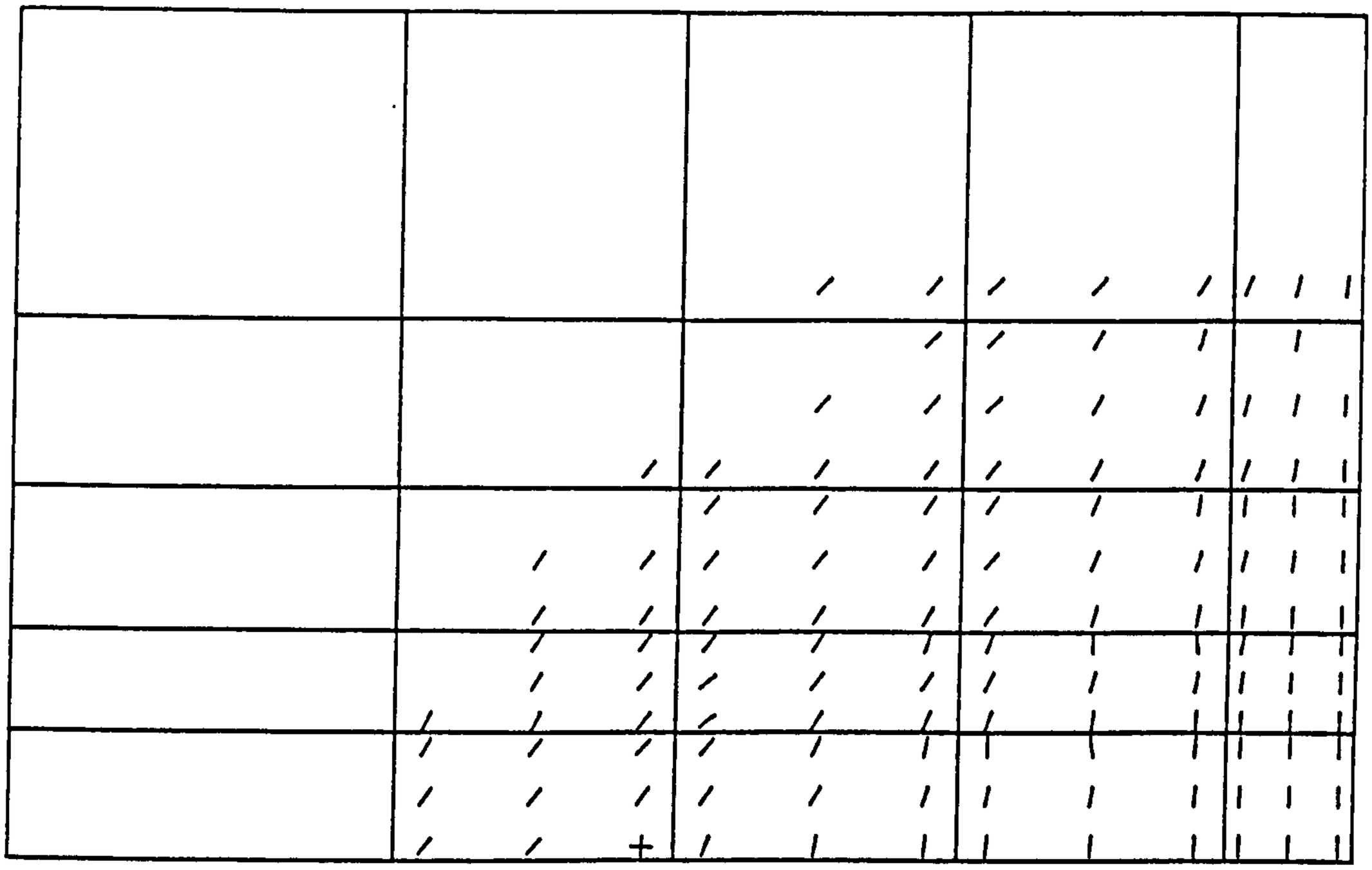

Figure (7·18) Crack pattern at load = 294·0 kN.

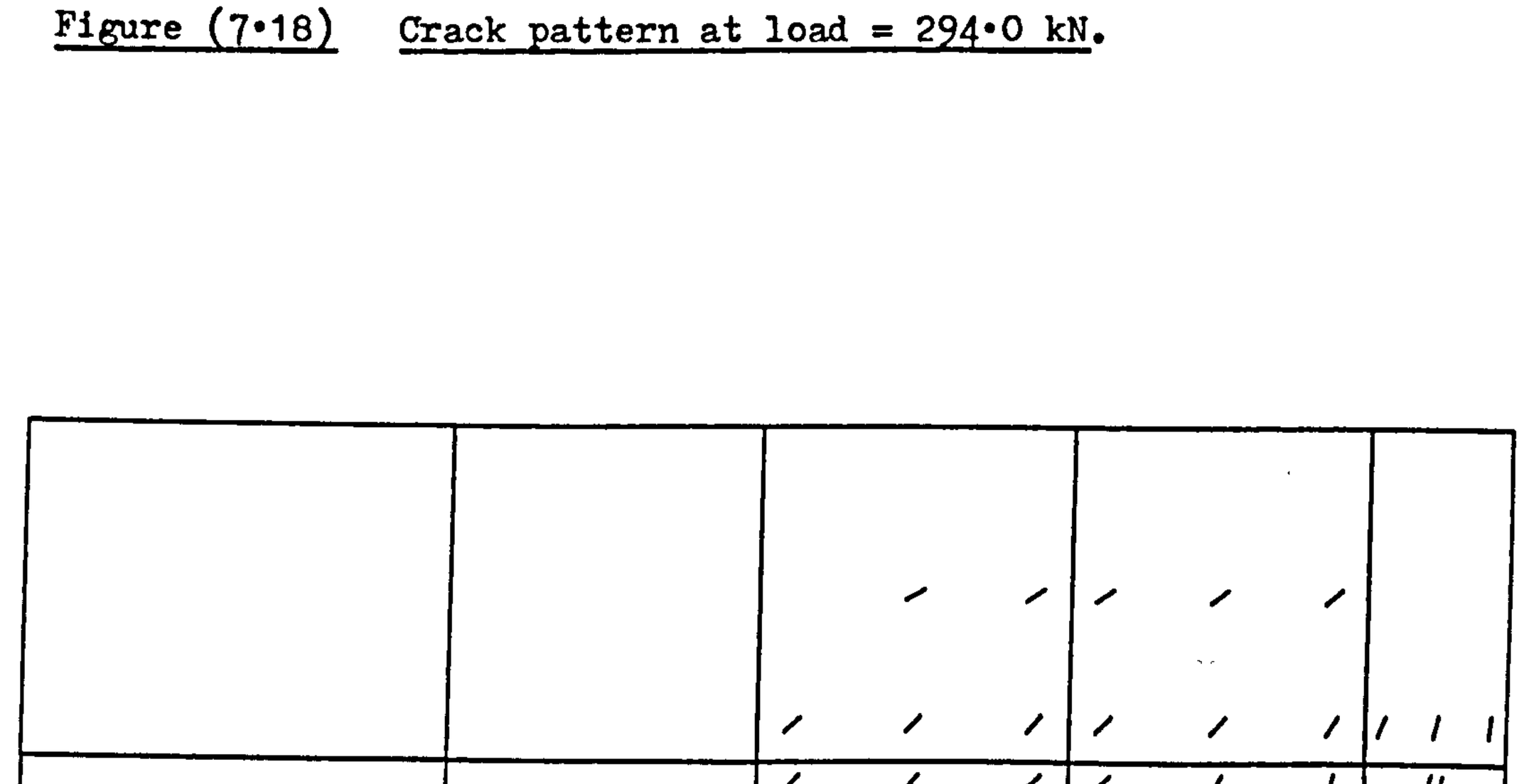

Figure (7·19) Crack pattern at load = 392·0 kN.

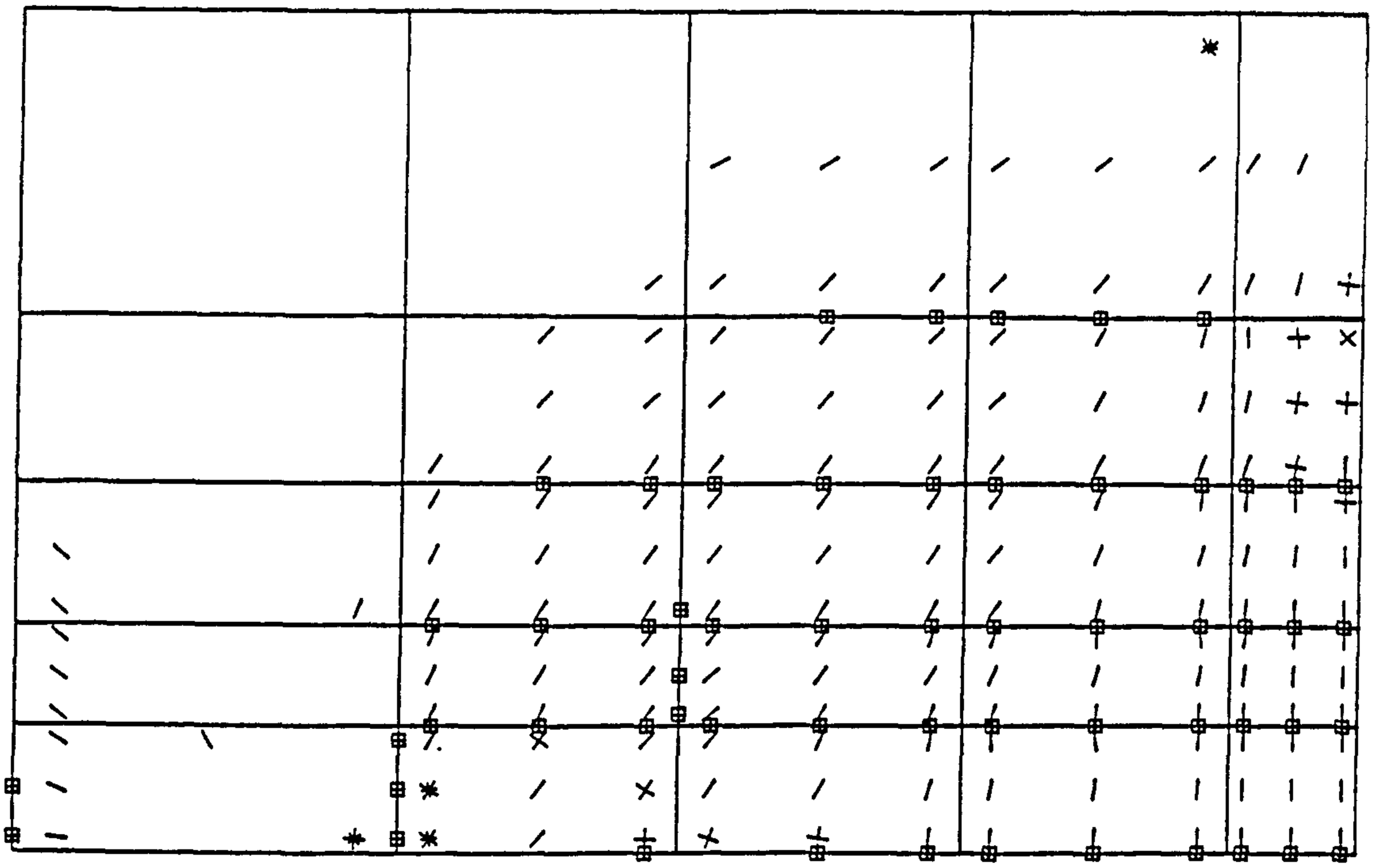

Figure (7·20) Crack pattern at failure load = 490·0 kN.

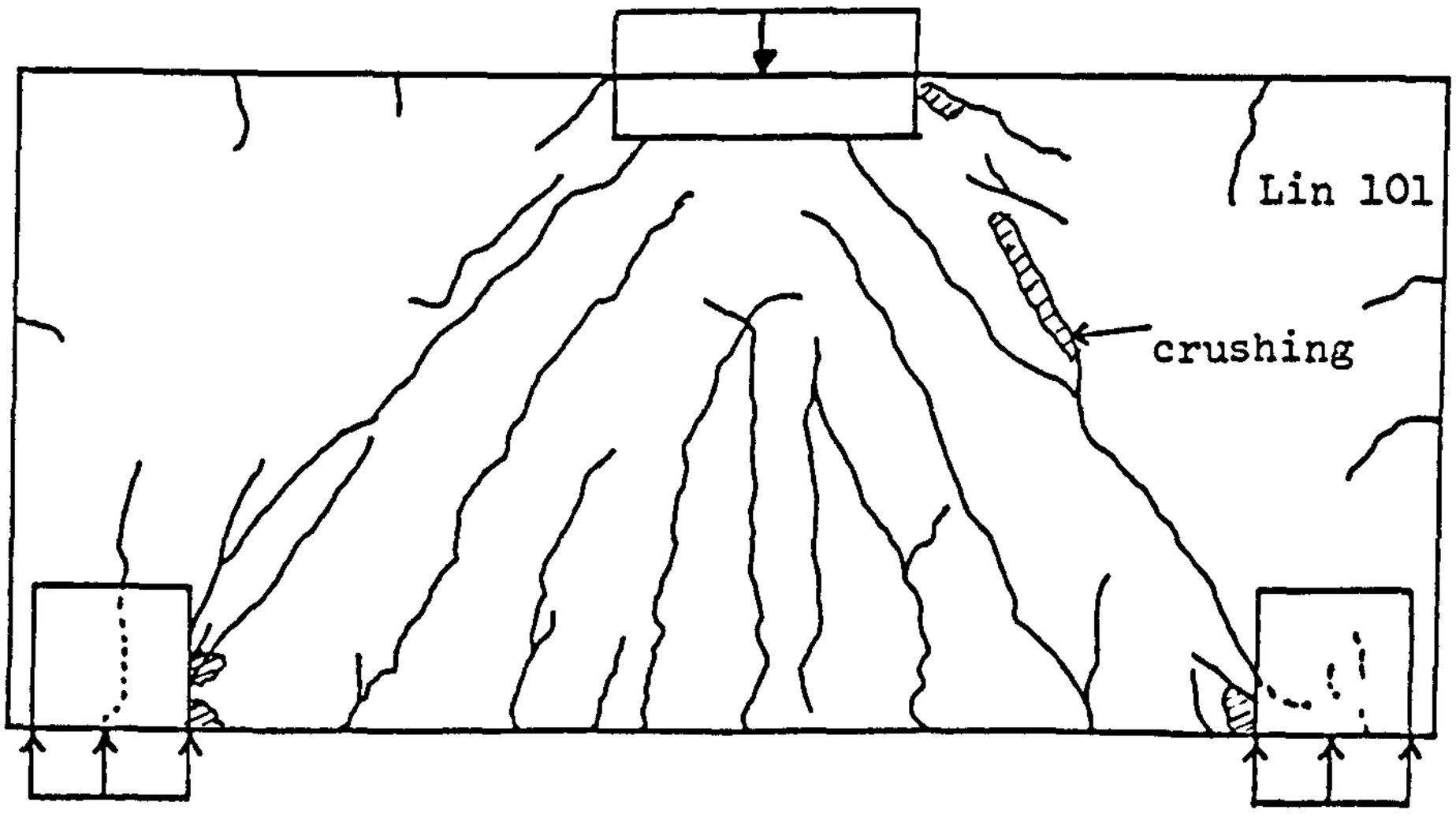

Figure (7·21) Experimental crack pattern at load = 575.0 kN.

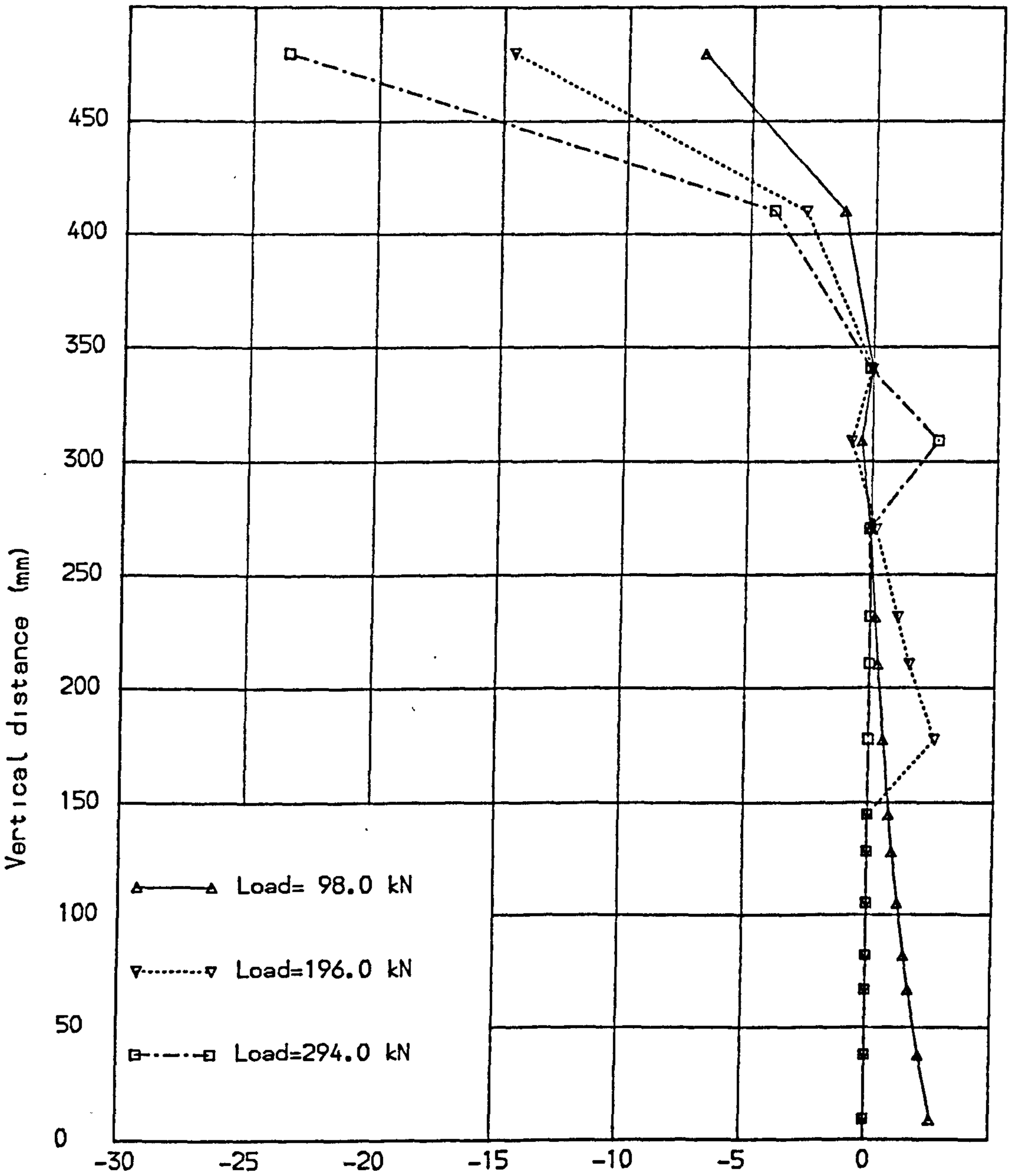

Fig. (7.22) Stress distribution at midspan section, (Lin 101).

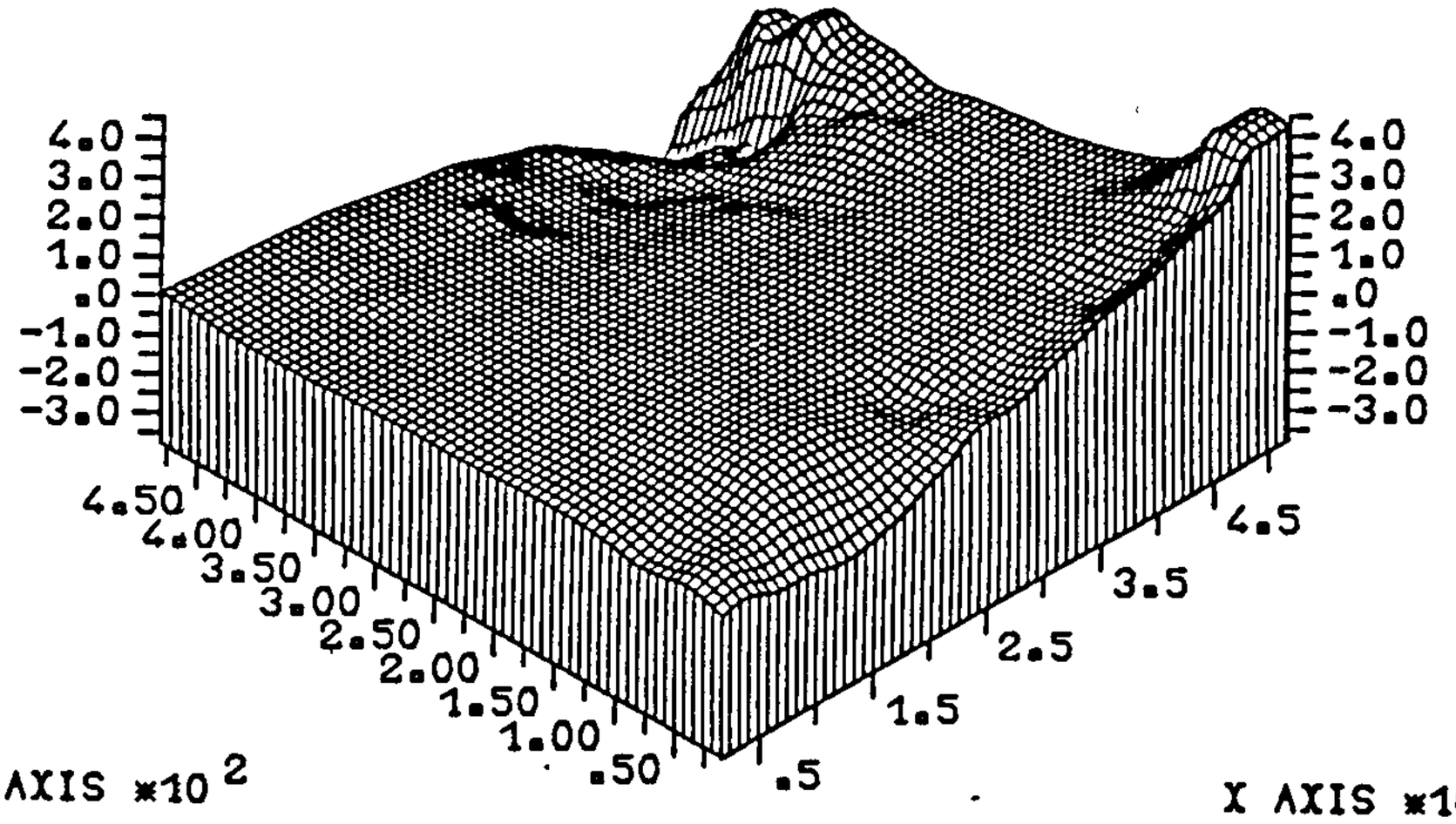

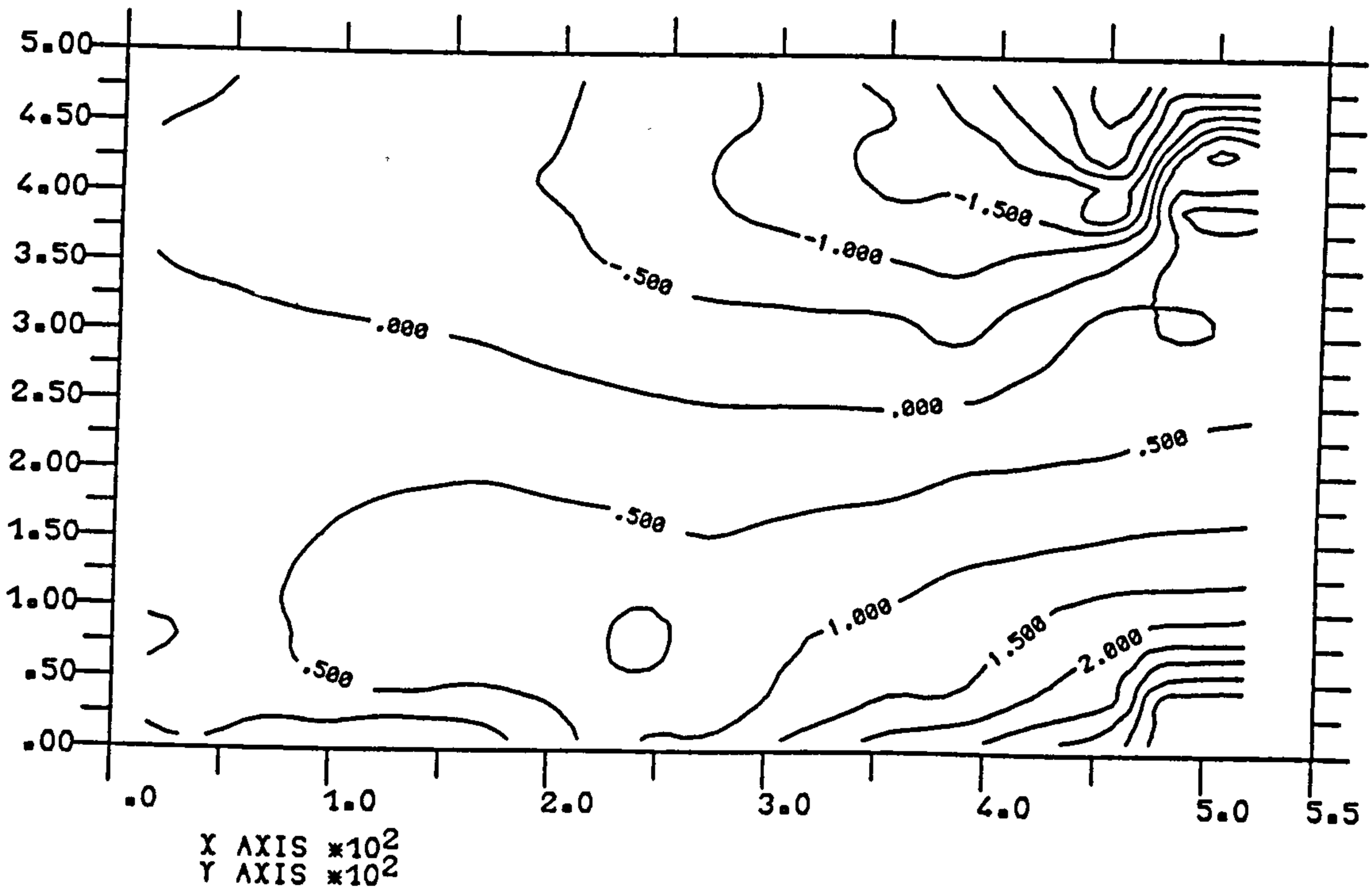

Figure (7·23) Horizontal strain x 10^{-4} at load=171·5 kN.

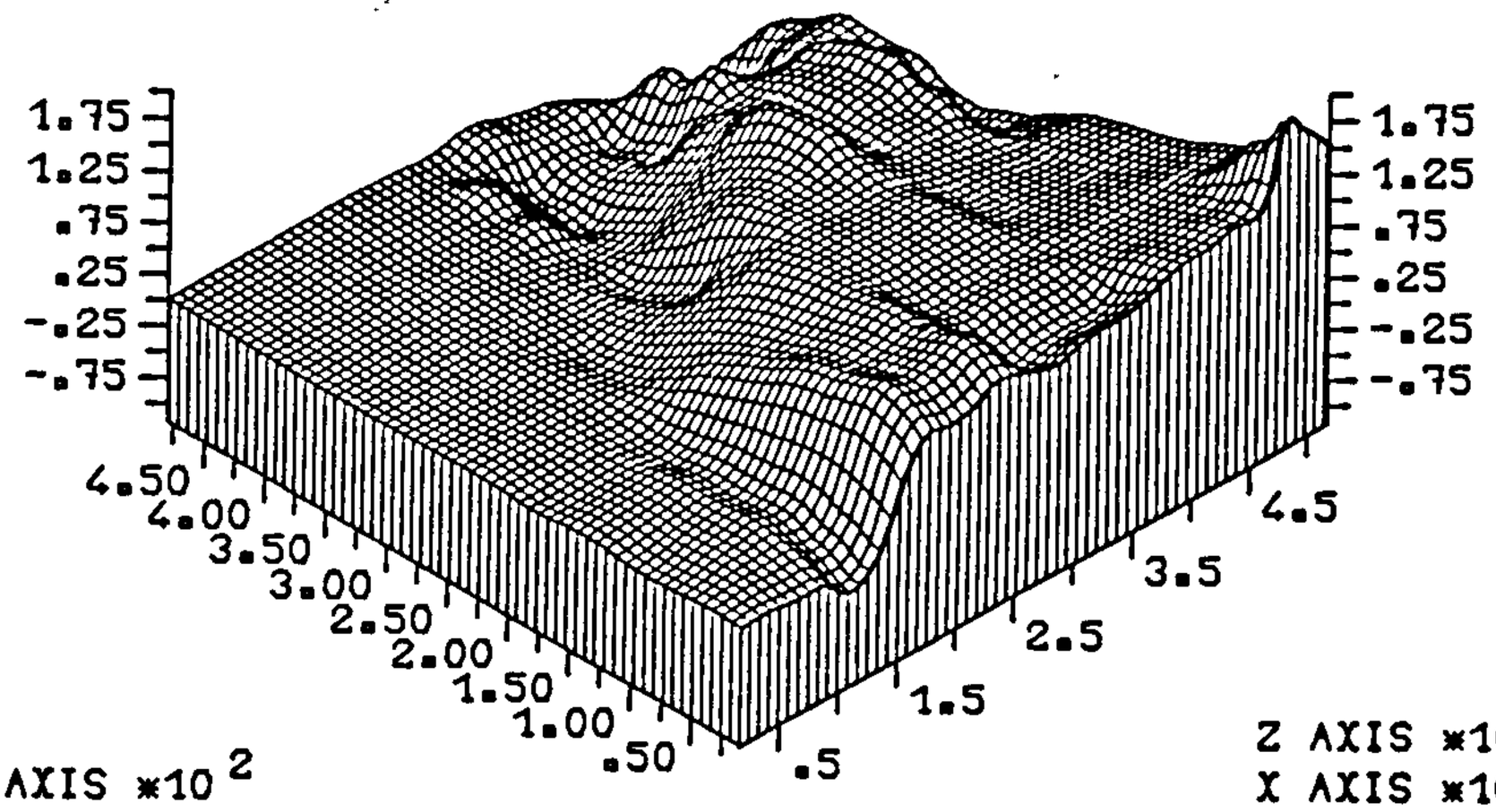

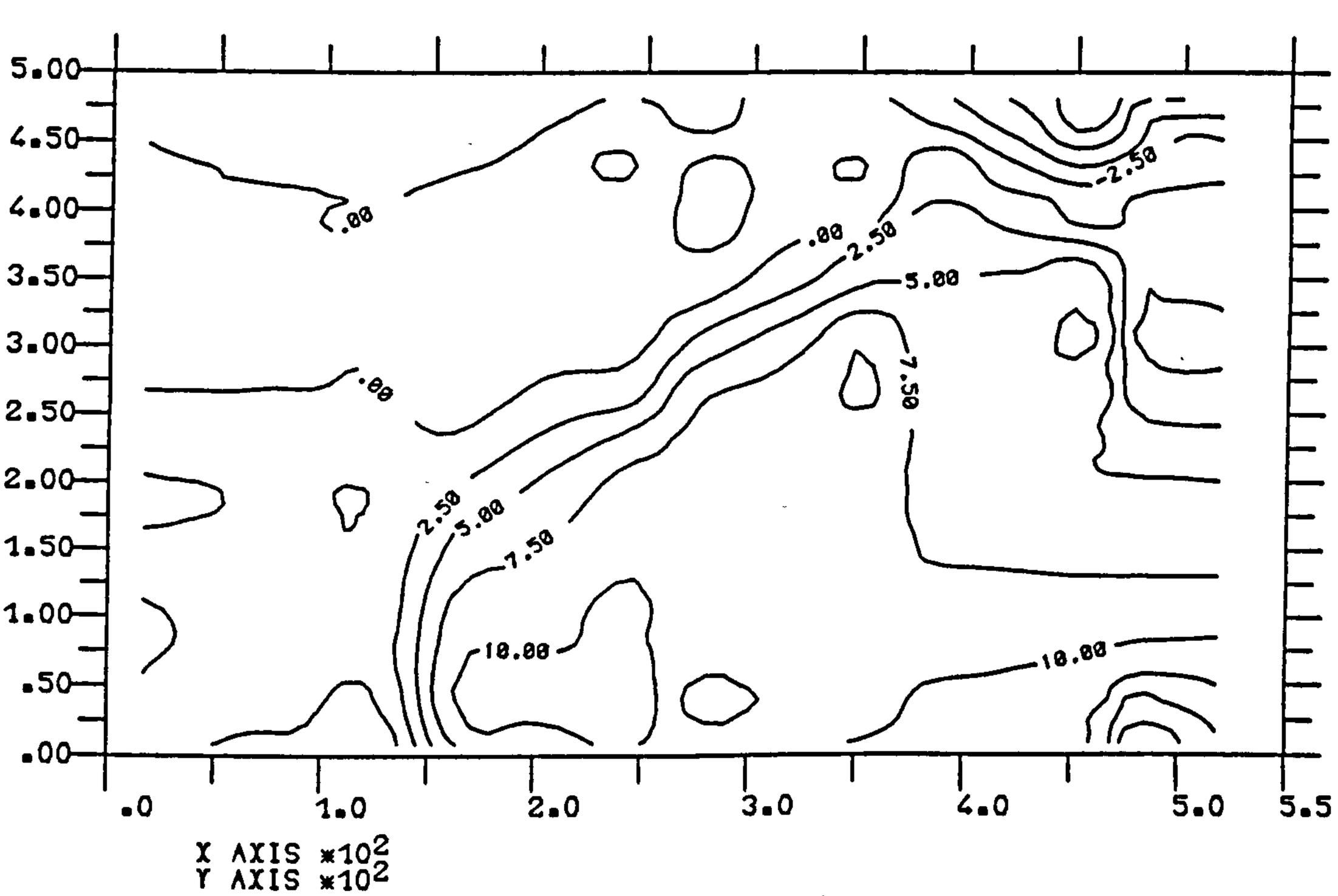

Figure (7·24) Horizontal strain x 10^{-4} at load = 392·0 kN.

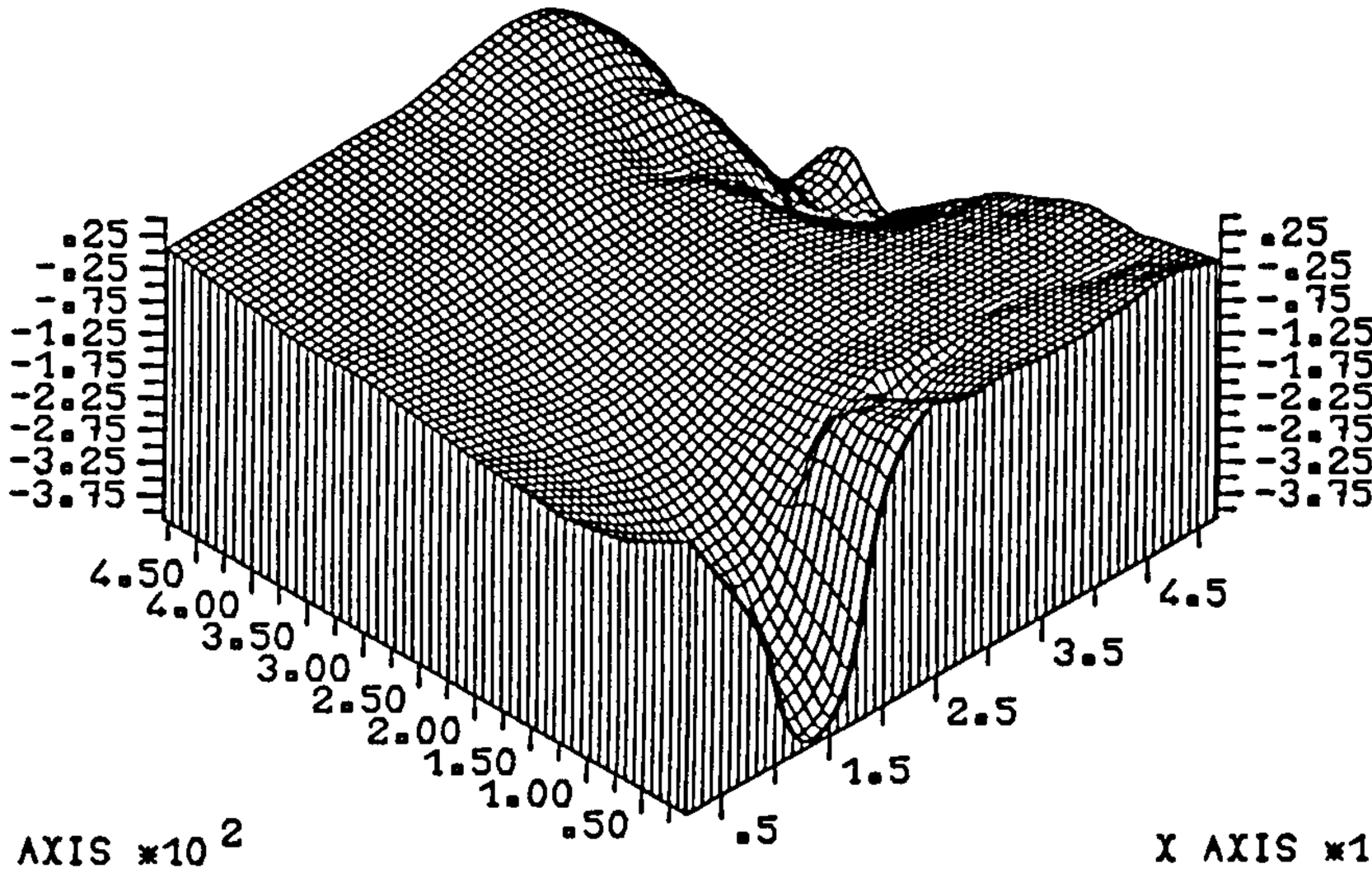

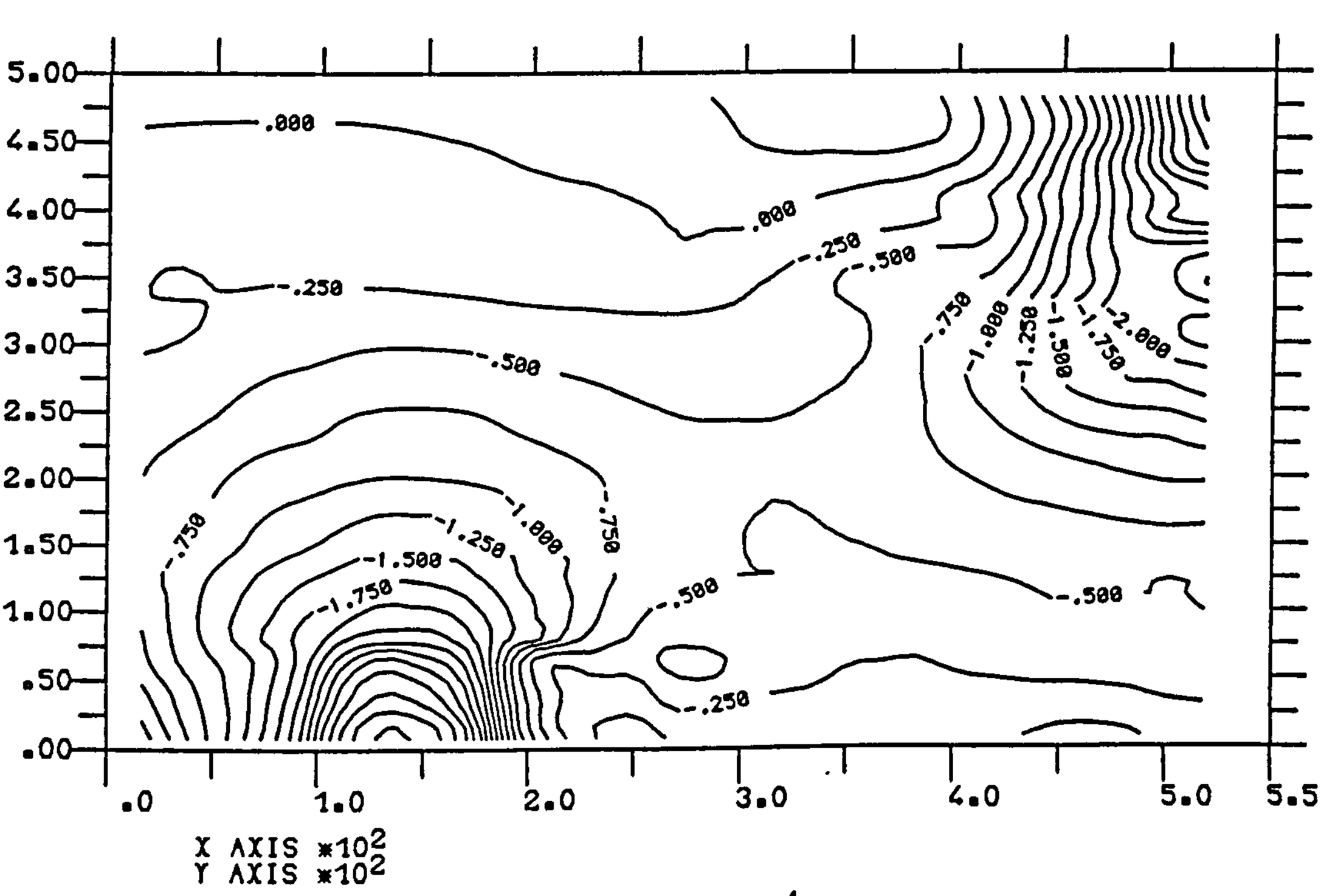

Figure (7·25) Vertical strain x 10^{-4} at load = 171·5 kN.

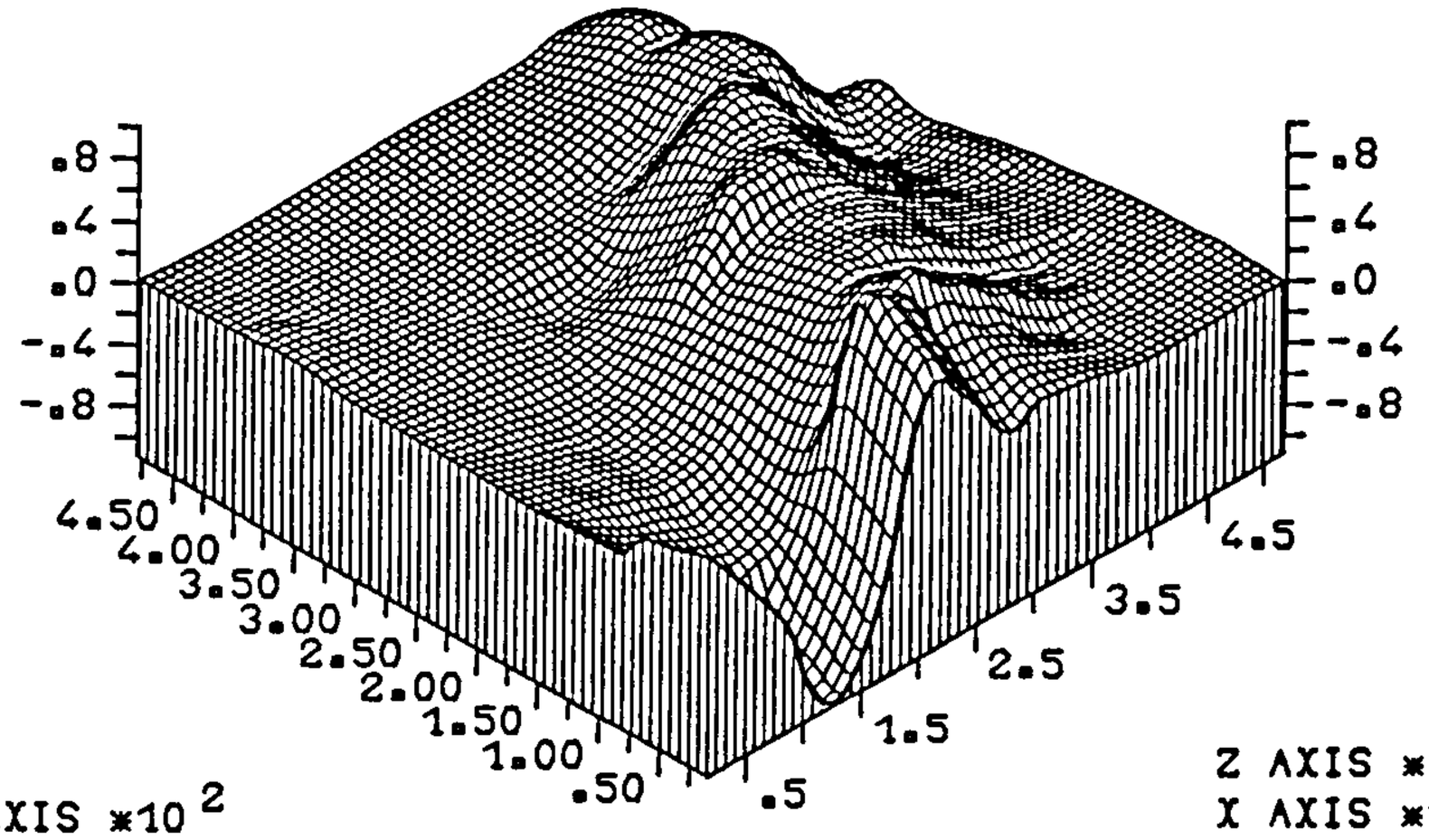

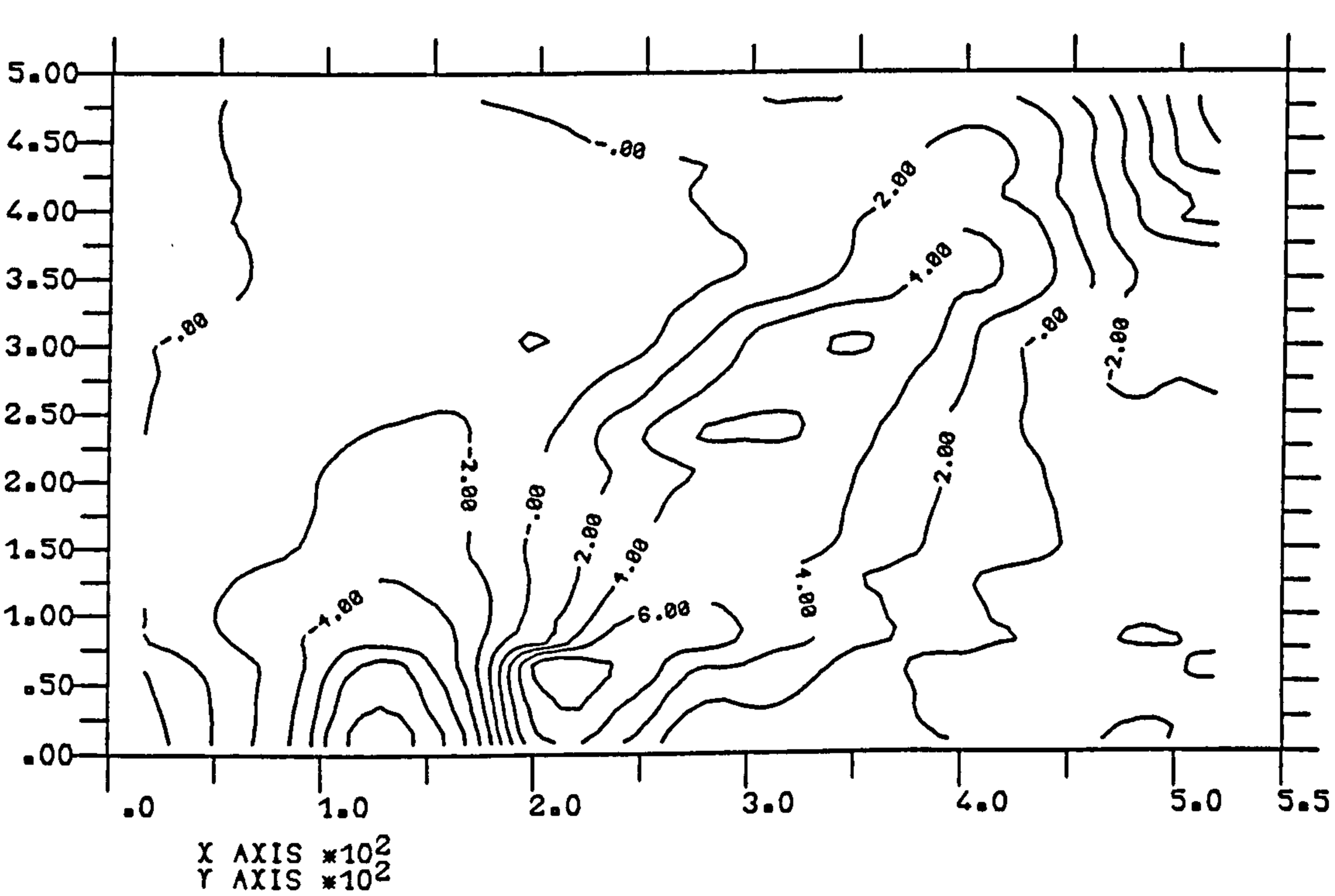

Figure (7·26) Vertical strain at load = 392·0 kN.

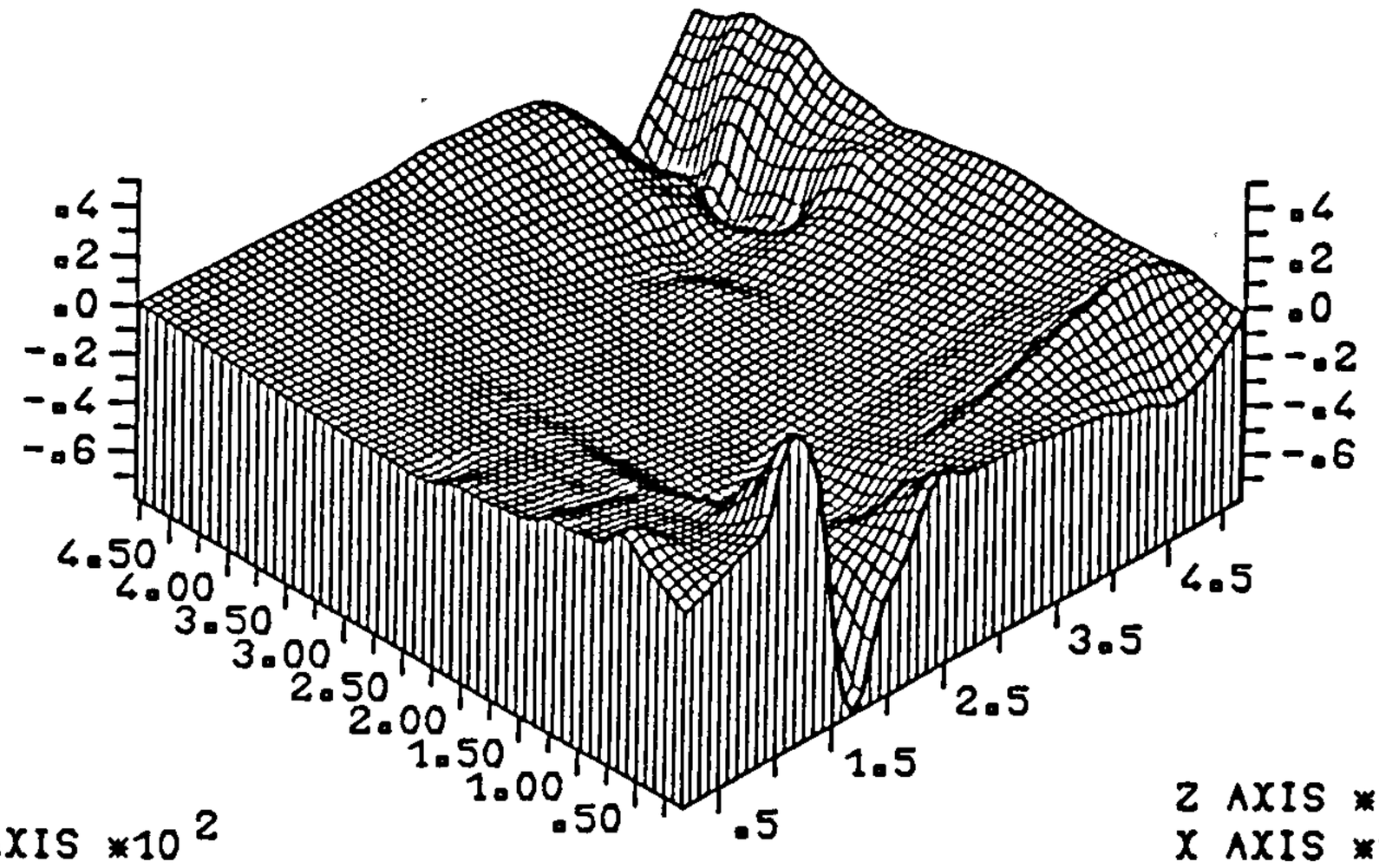

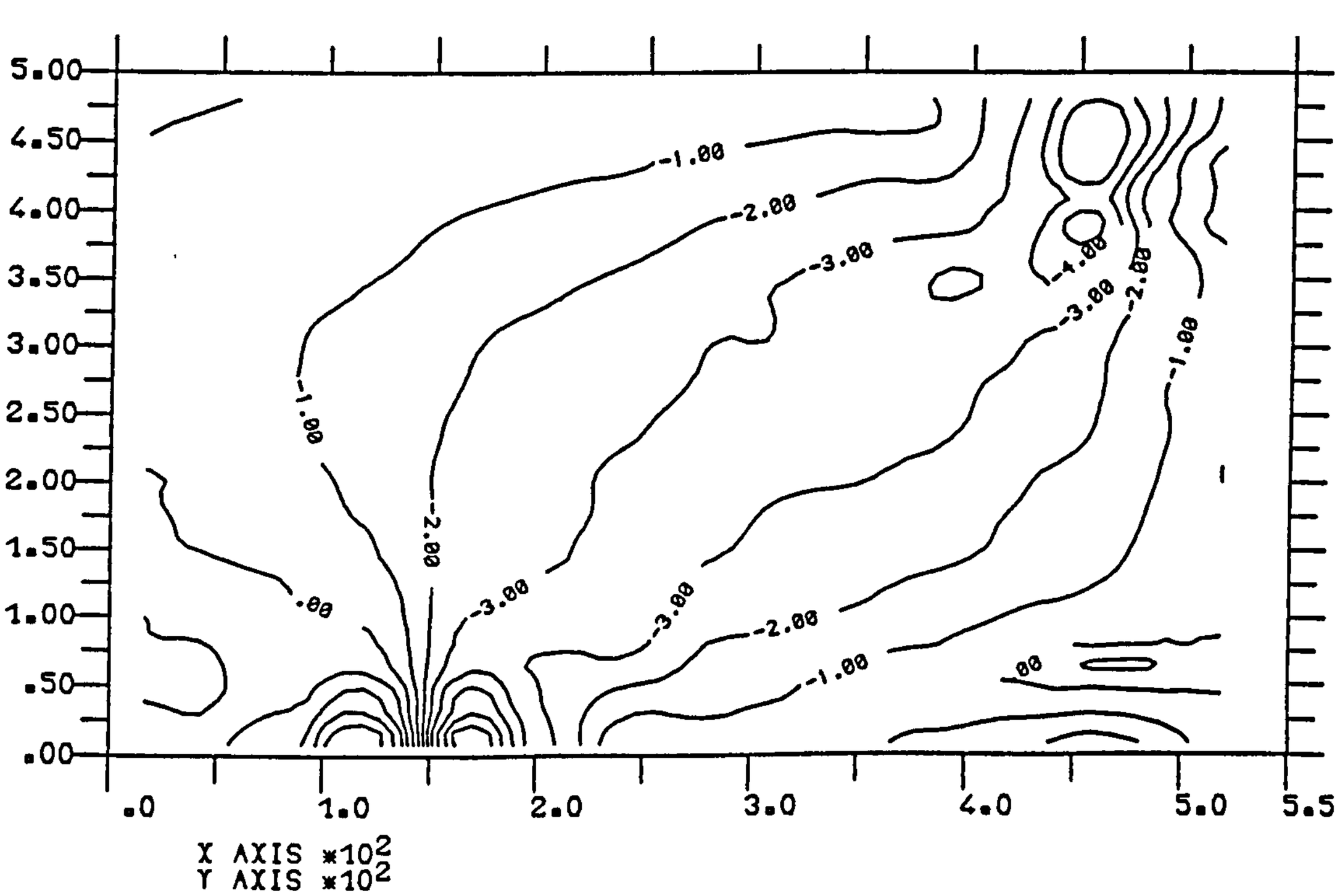

Figure (7·27) Shear strain x 10^{-4} at load = 171·5 kN.

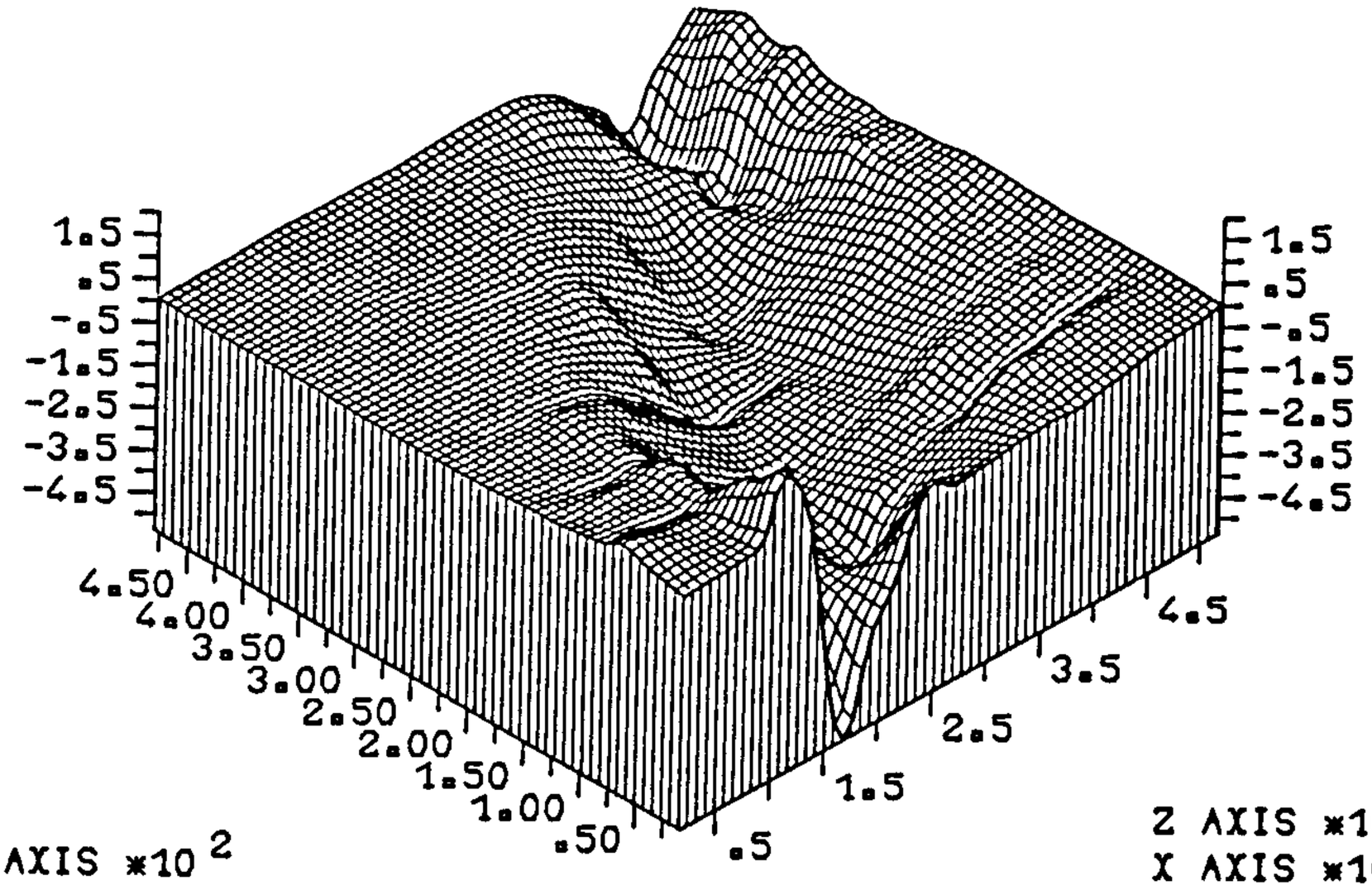

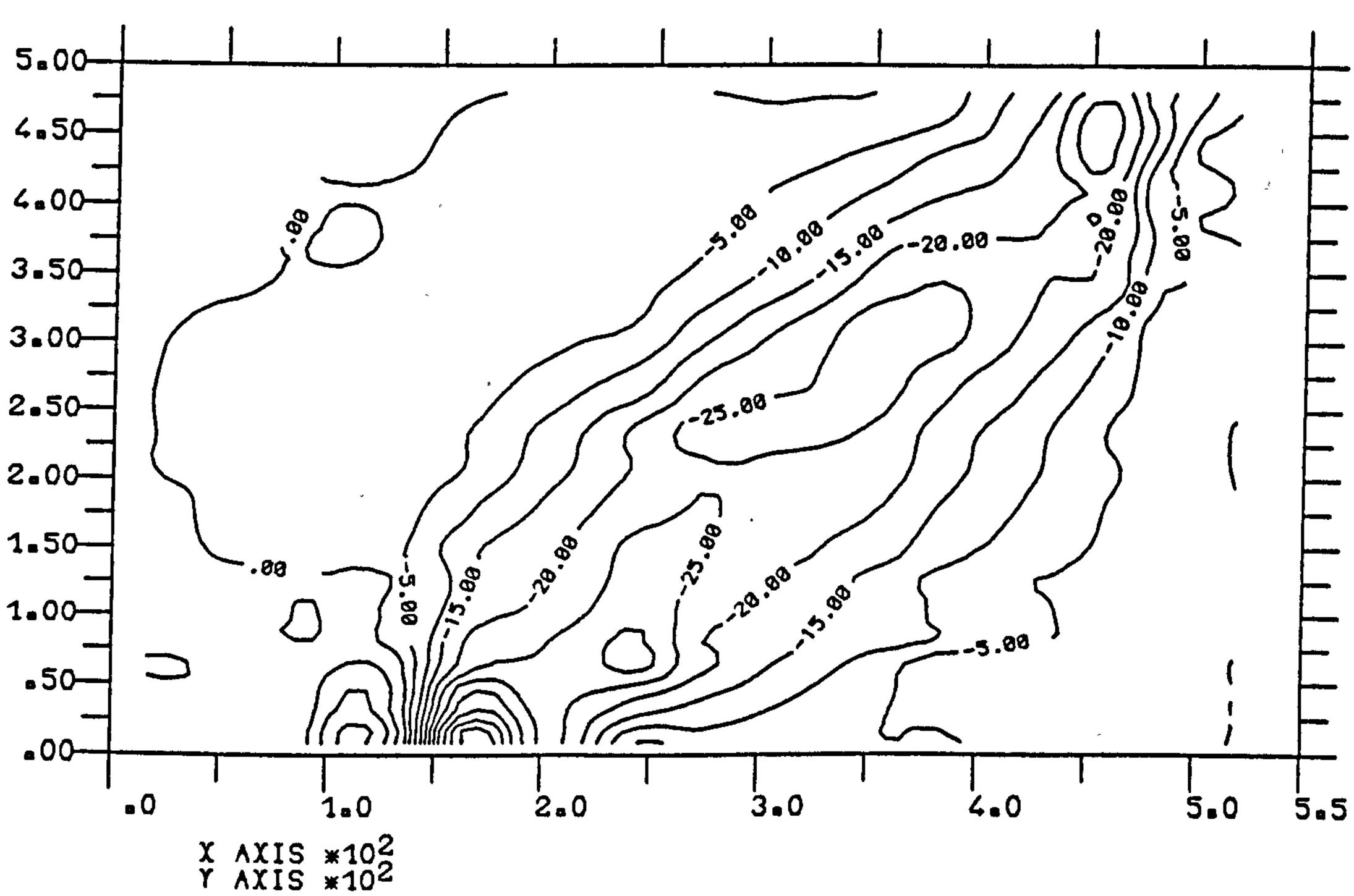

Figure (7·28) Shear strain x 10^{-4} at load = 392·0 kN.

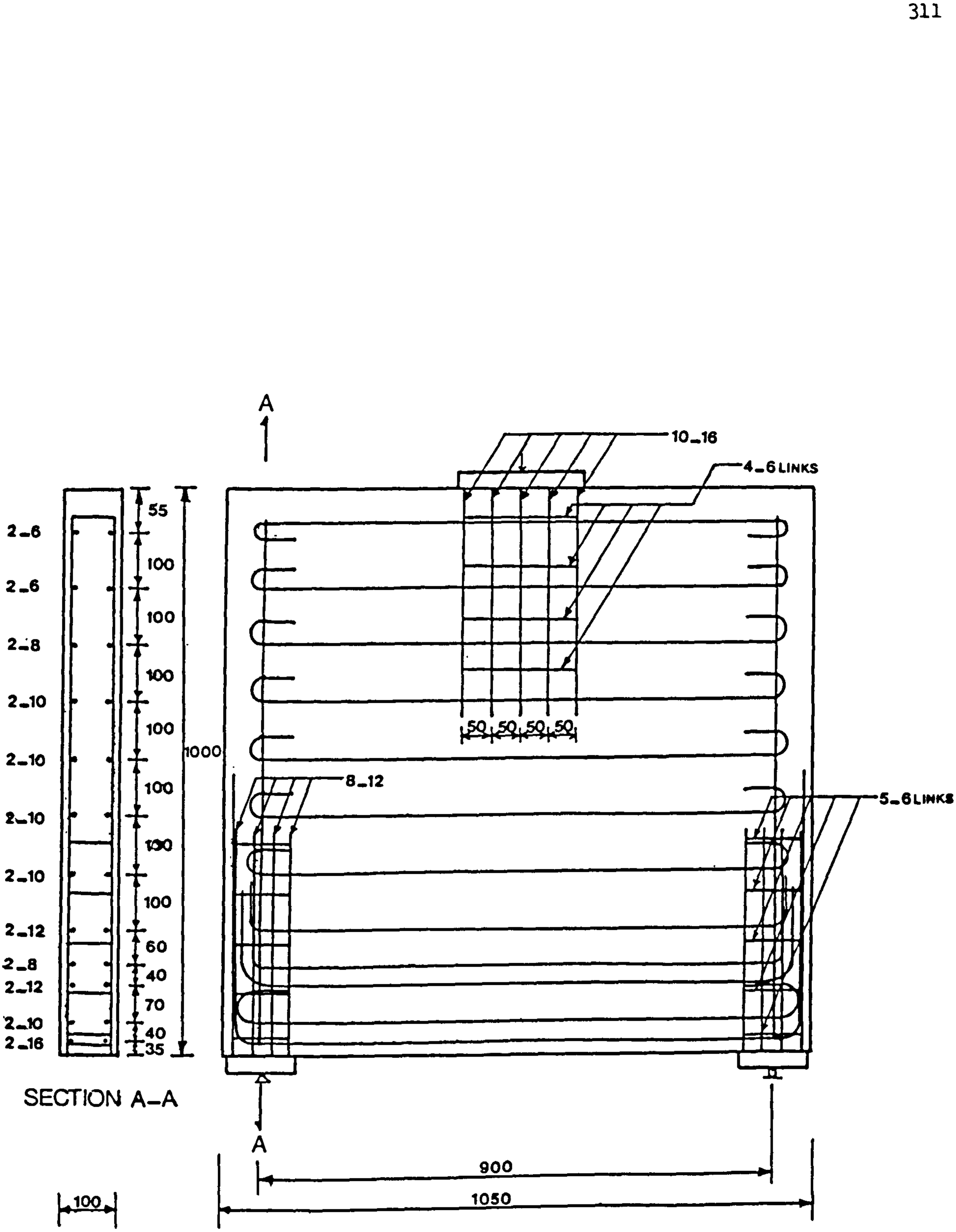

SECTION A–A

Figure (7·29) Details of Lin deep beam 204.

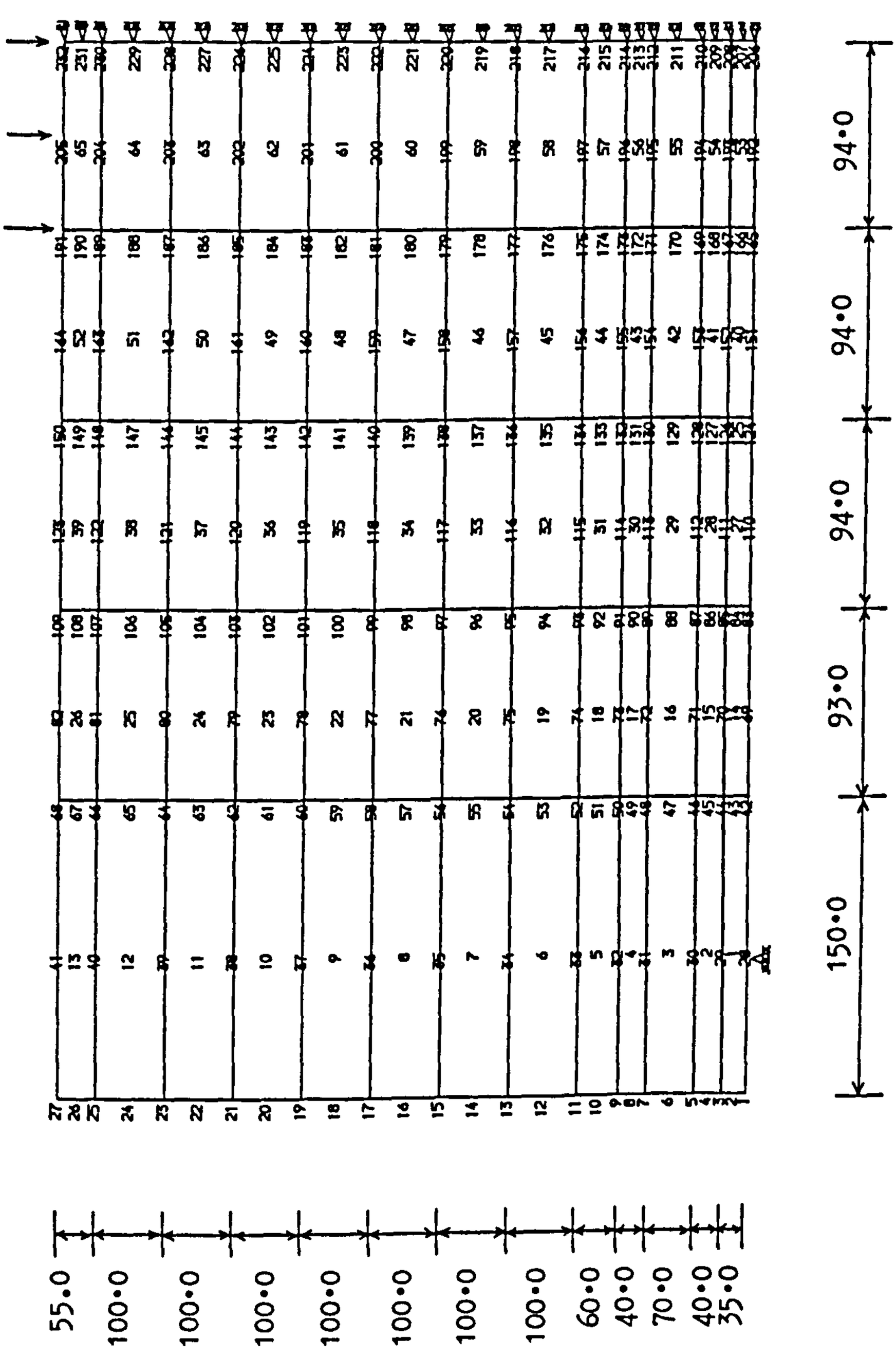

Figure (7·30) Mesh used for Lin beam 204.

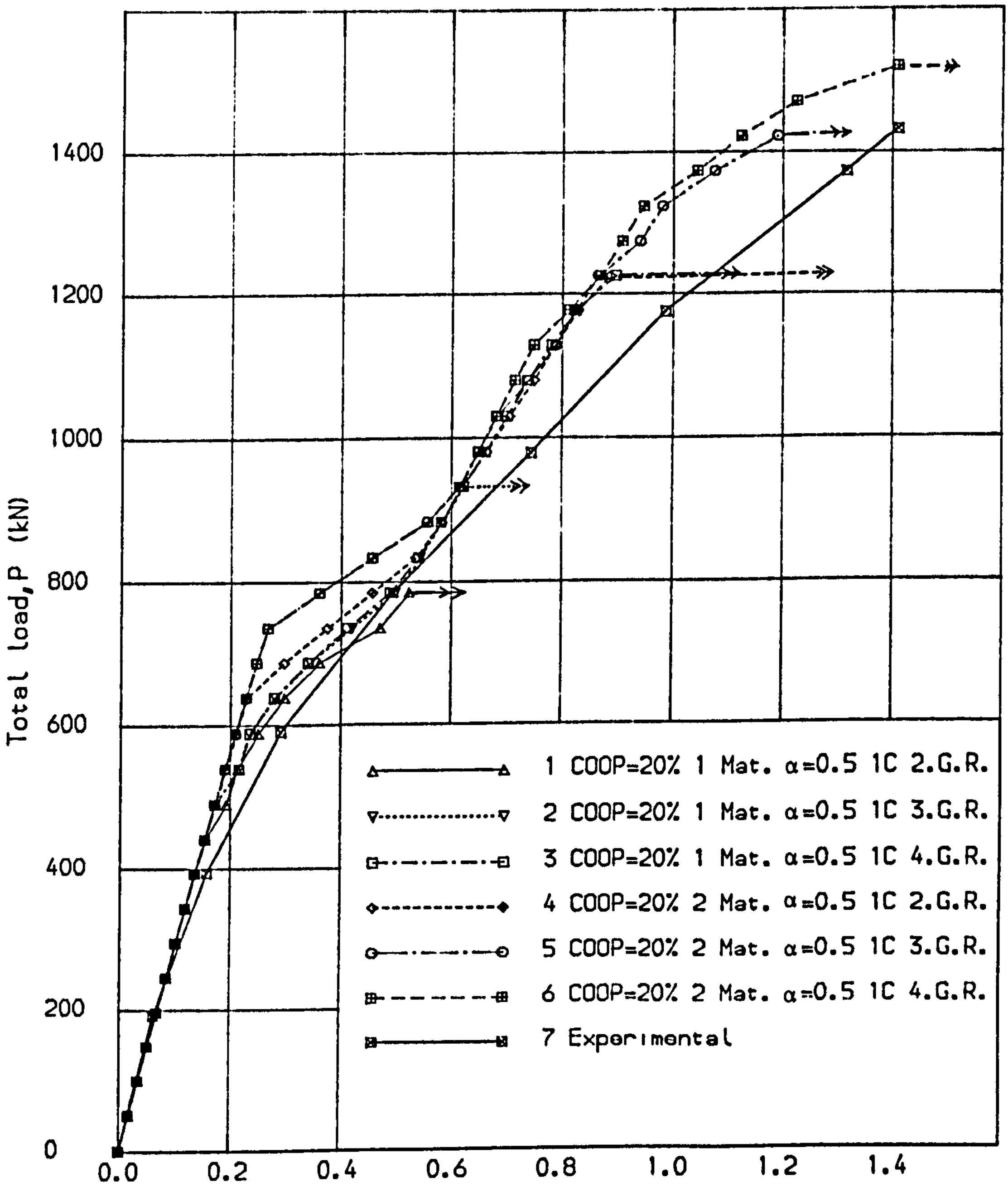

Fig. (7.31) Load deflection curves for Lin deep beam 204.

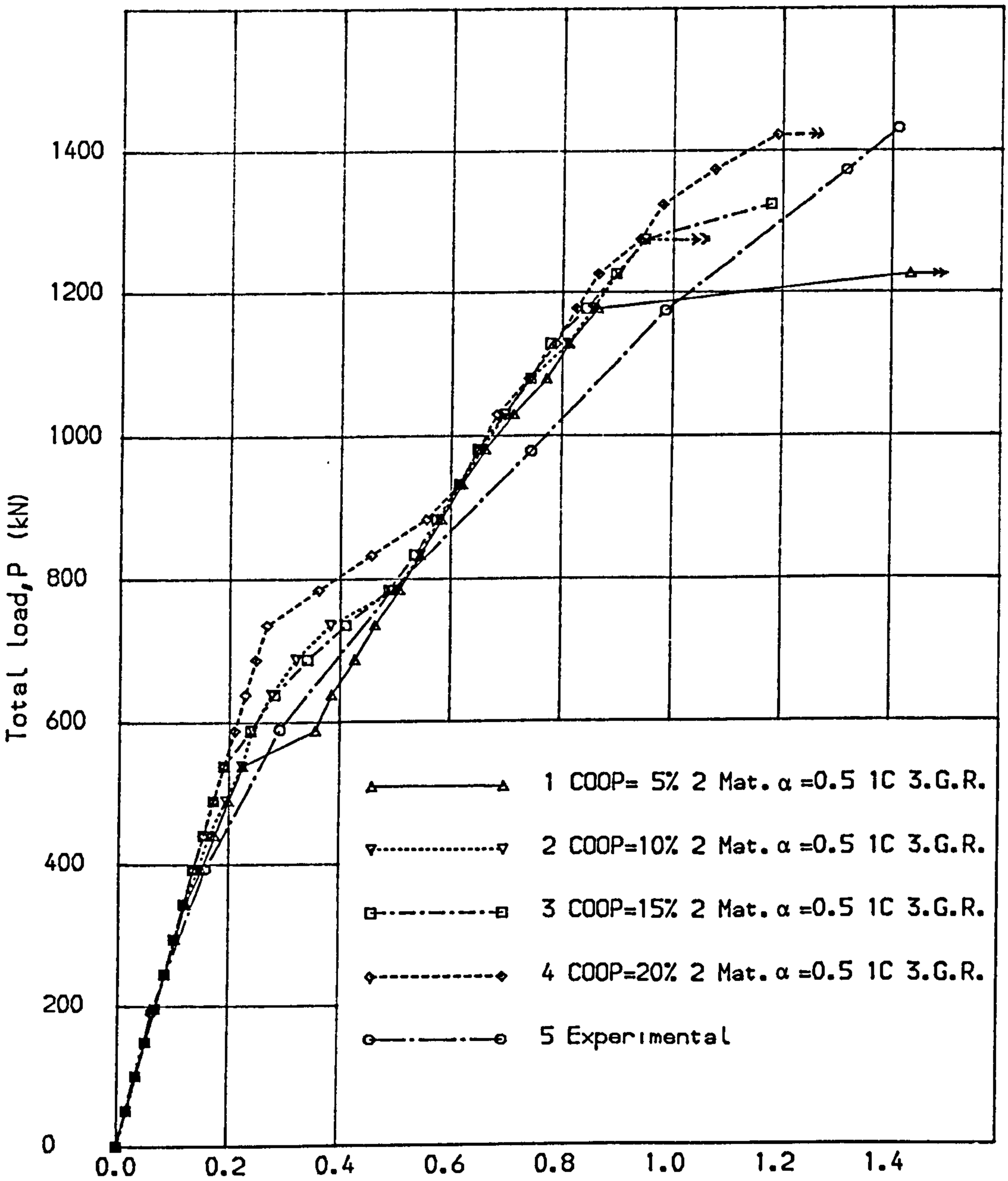

Fig. (7.32) Load deflection curves for L1n deep beam 204.

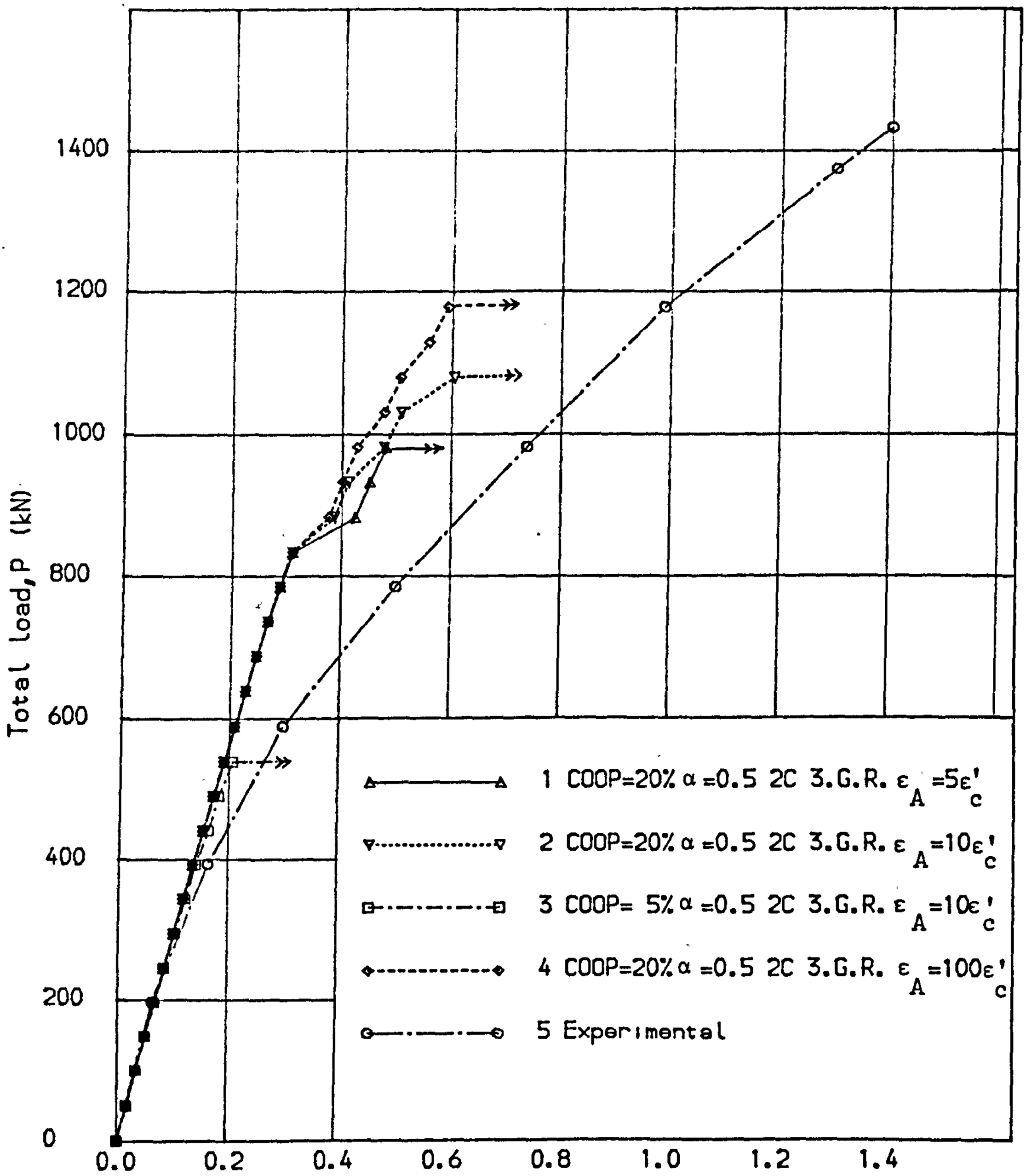

Fig. (7.33) Load deflection curves for Lin deep beam 204.

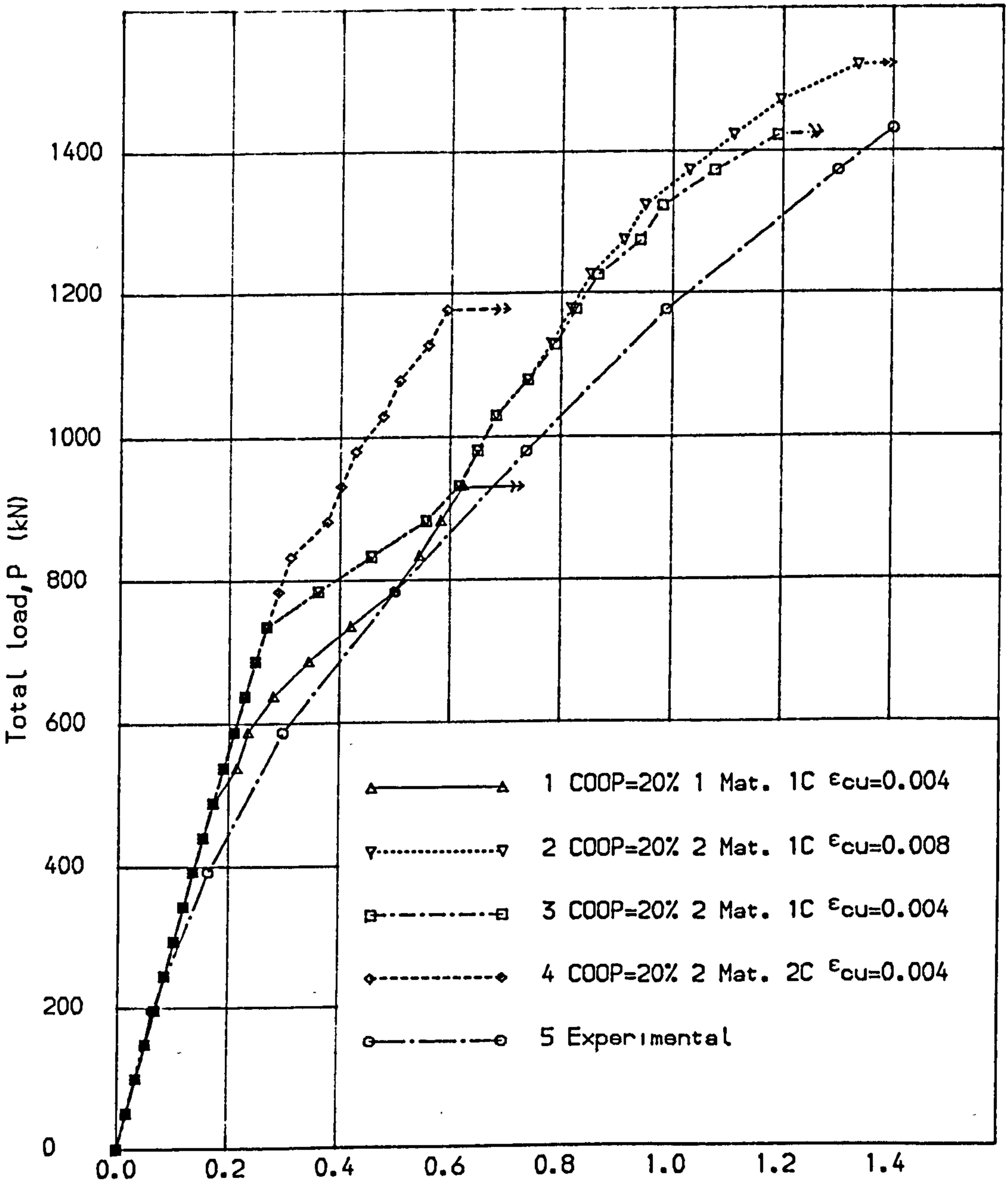

Fig. (7.34) Load deflection curves for Lin deep beam 204.

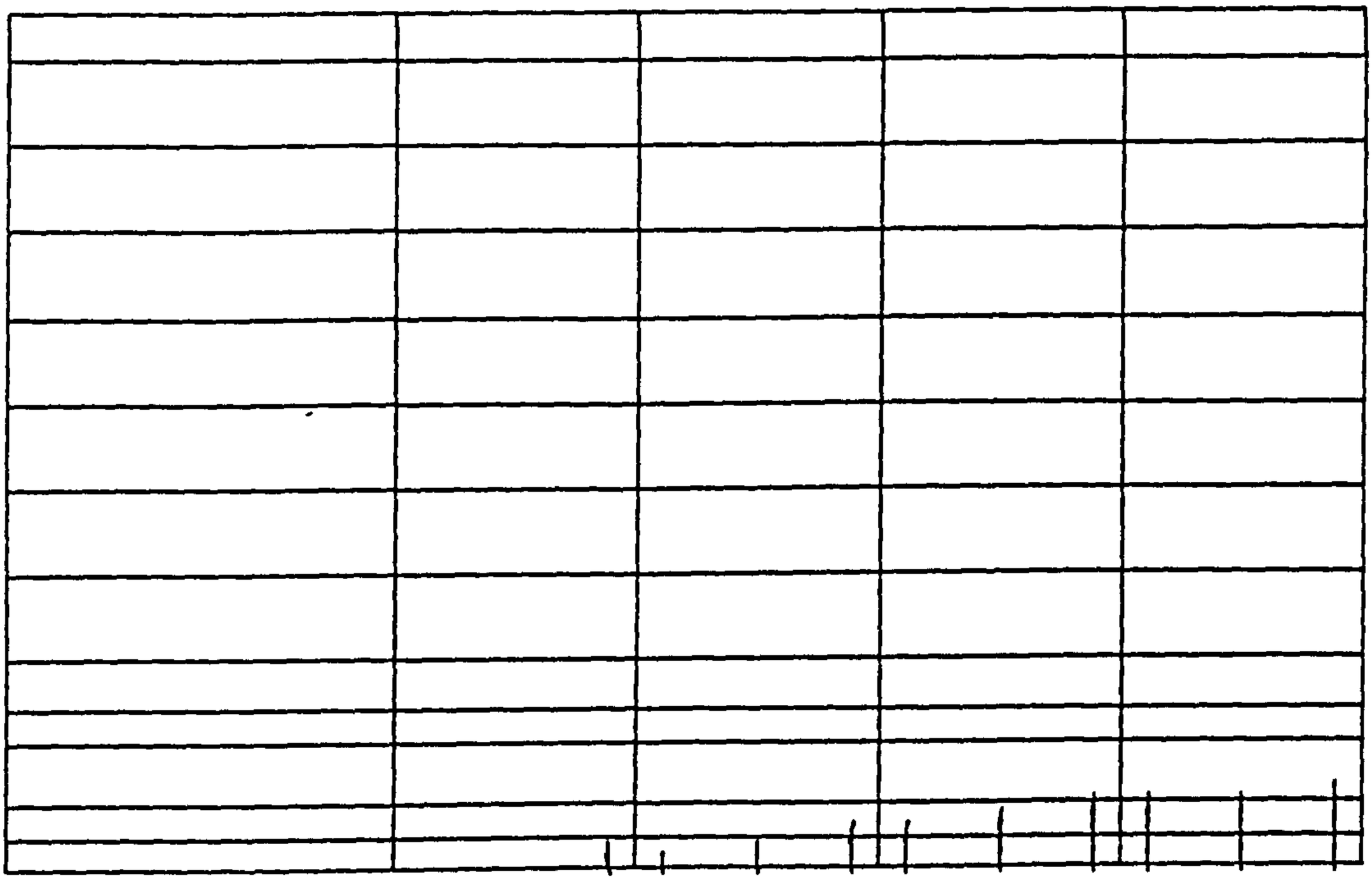

Figure (7·35) Crack pattern at load = 490·6 kN.

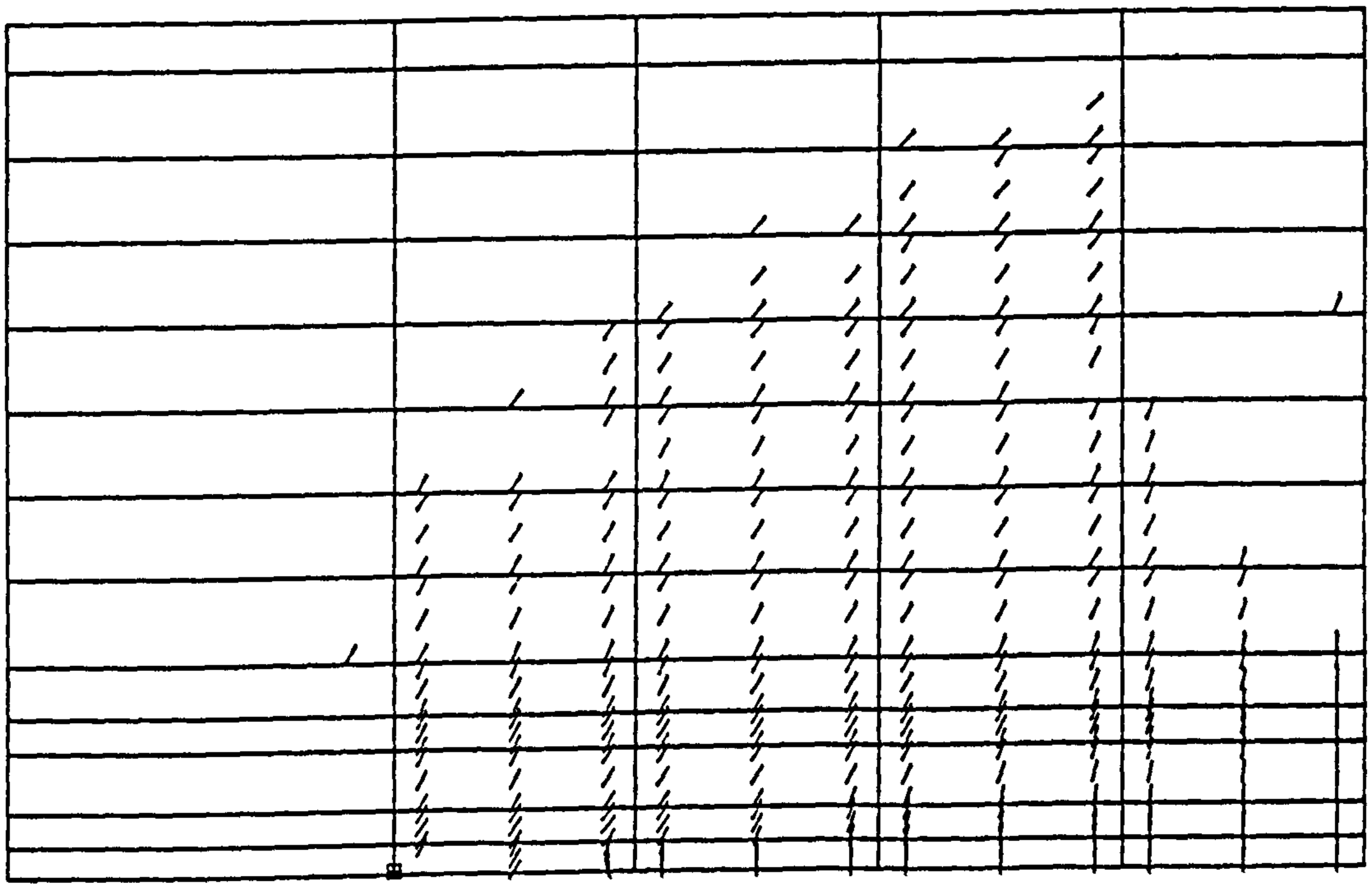

Figure (7·36) Crack pattern at load = 883·0 kN.

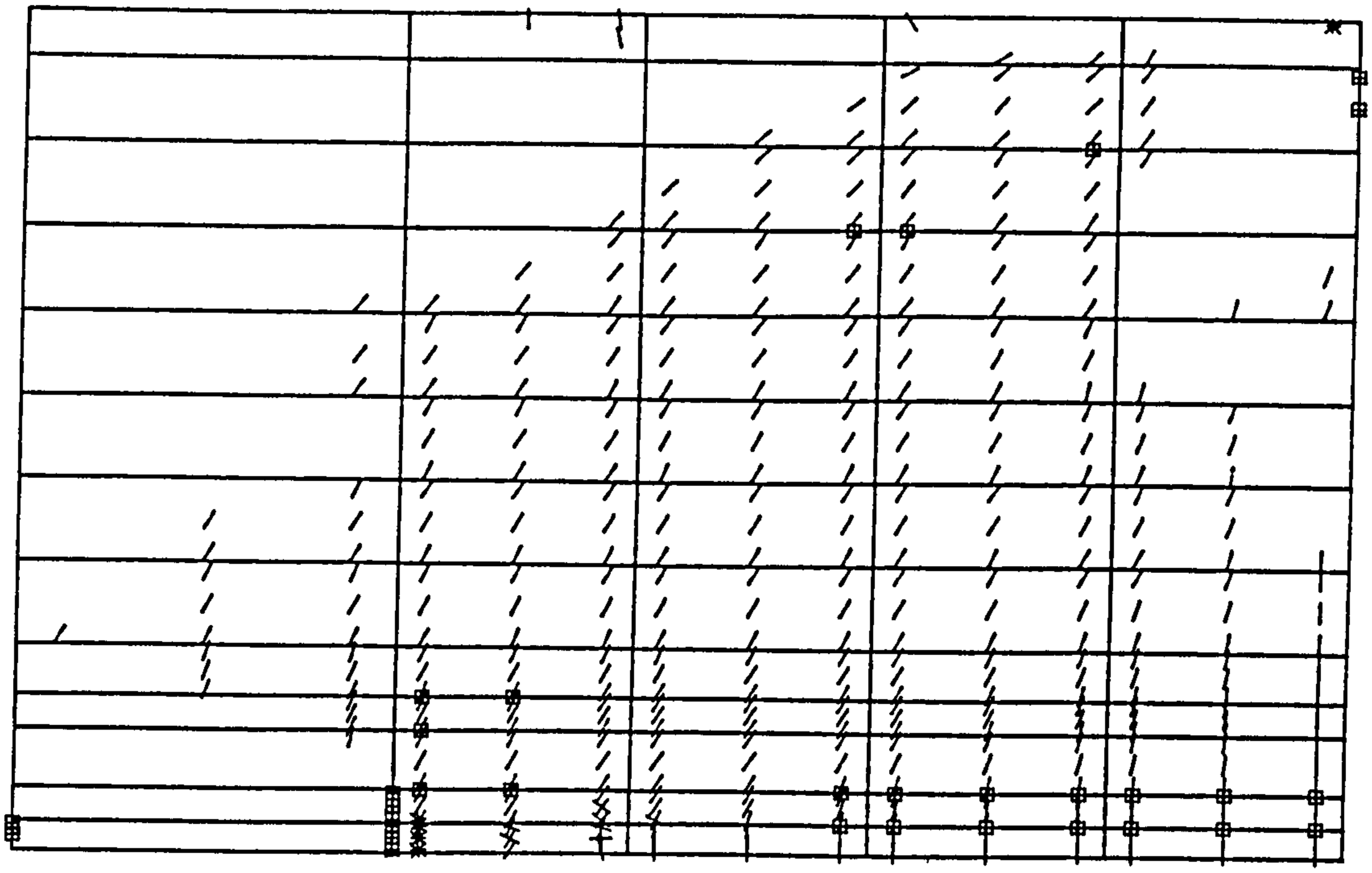

Figure (7·37) Crack pattern at load = 1422·6 kN.

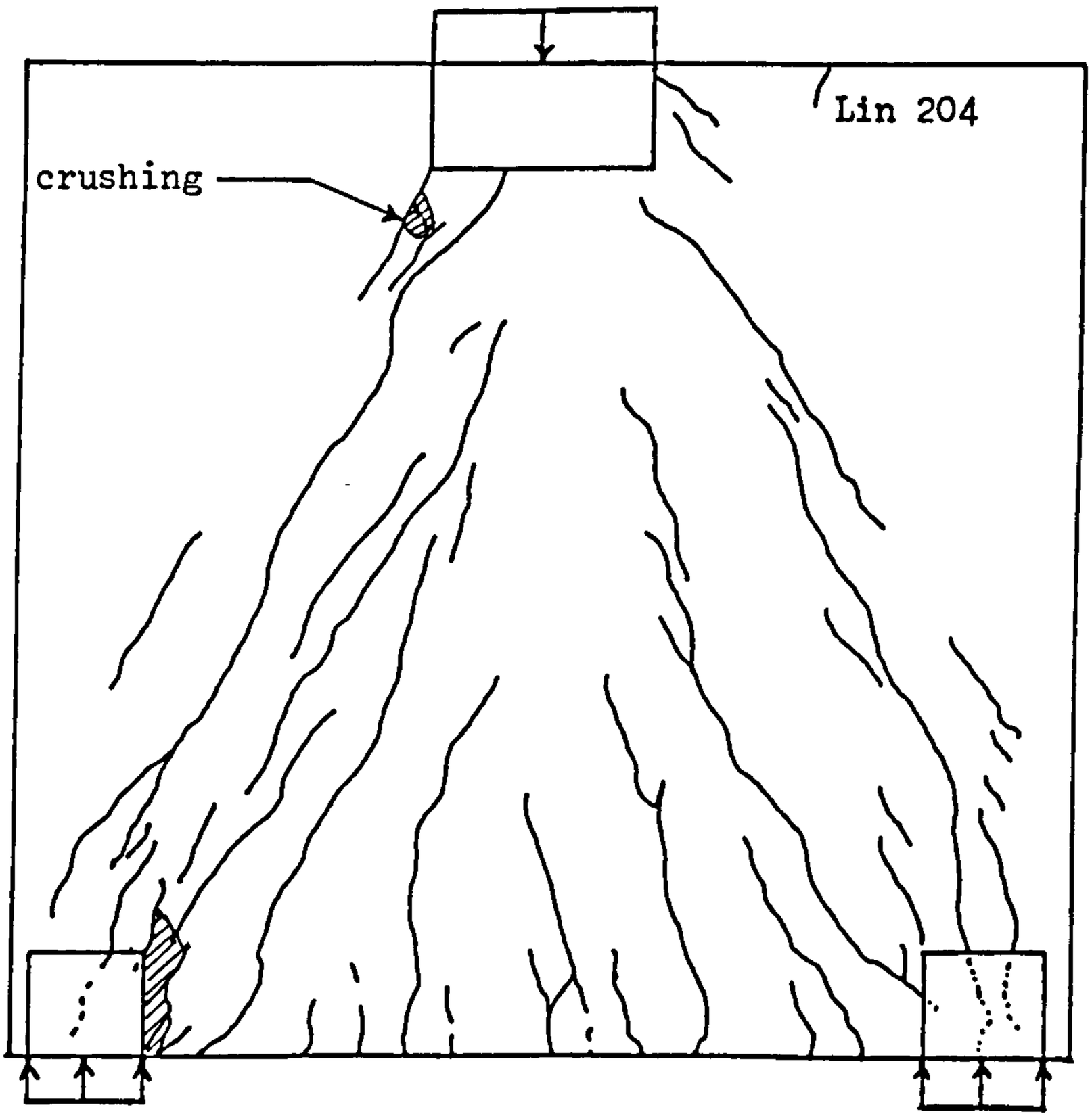

Figure (7·38) Experimental crack patterns at load = 1431.0 kN.

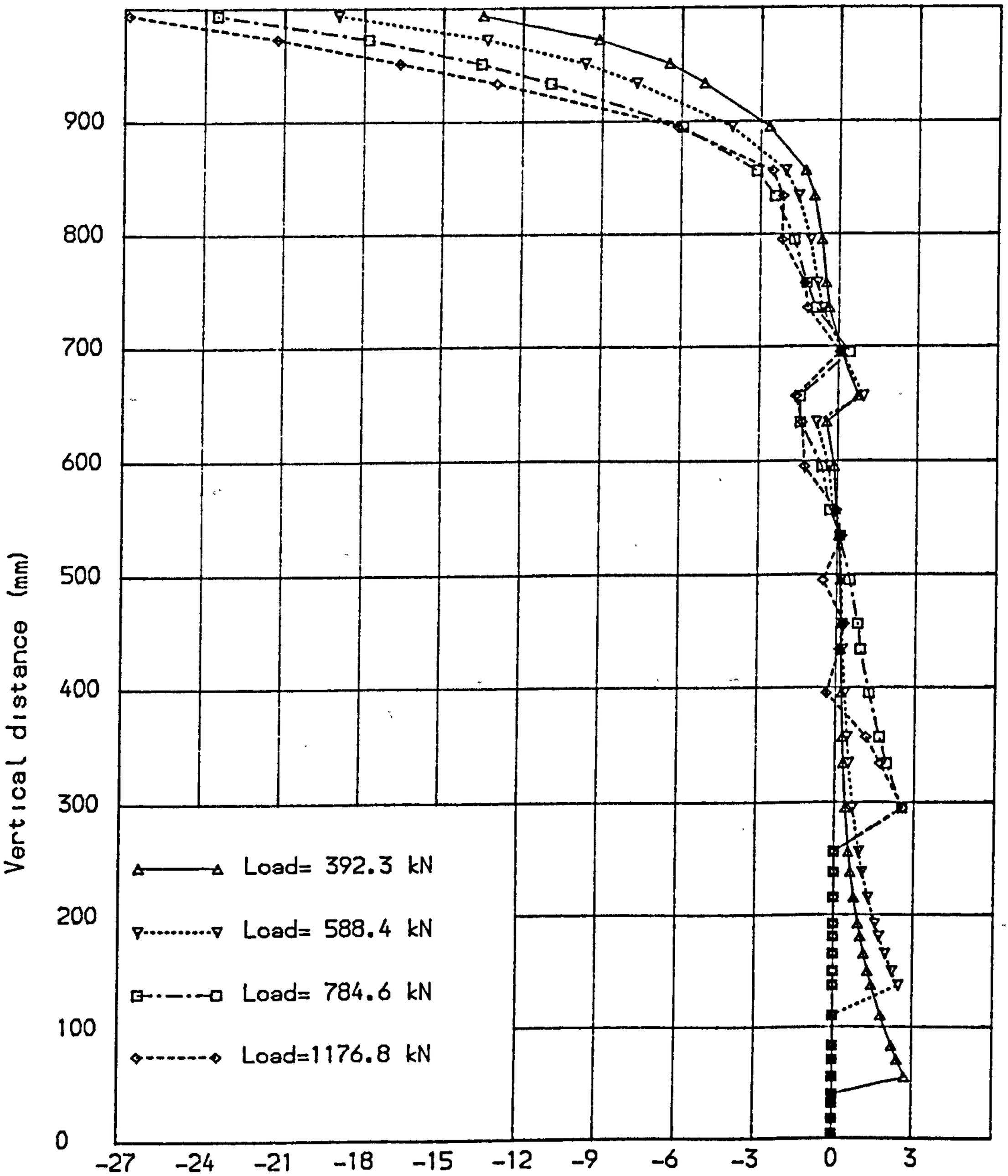

Fig. (7.39) Stress distribution at midspan section, (Lin 204).

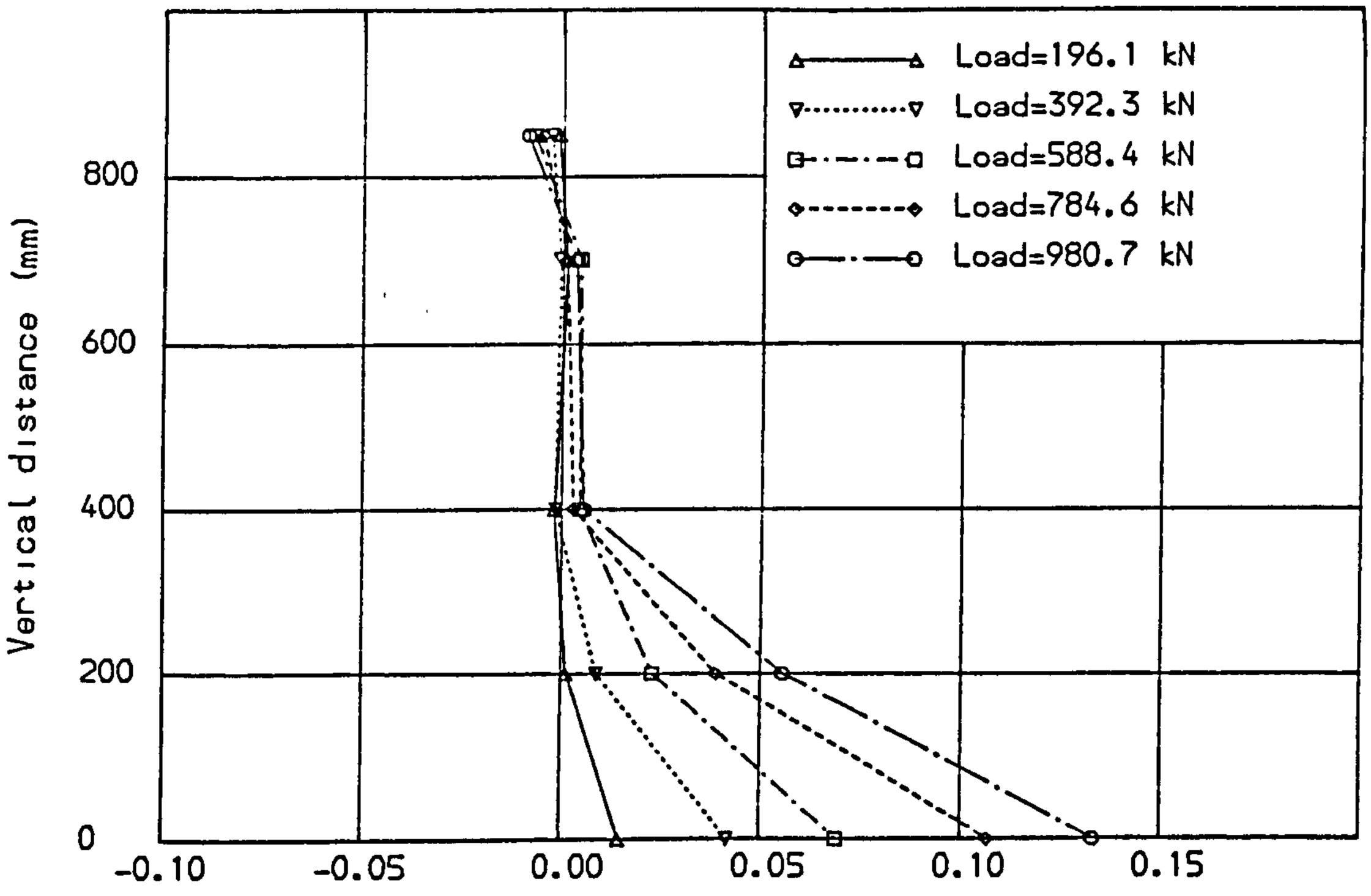

Fig. (7.40) Concrete surface strain for Lin deep beam 204.

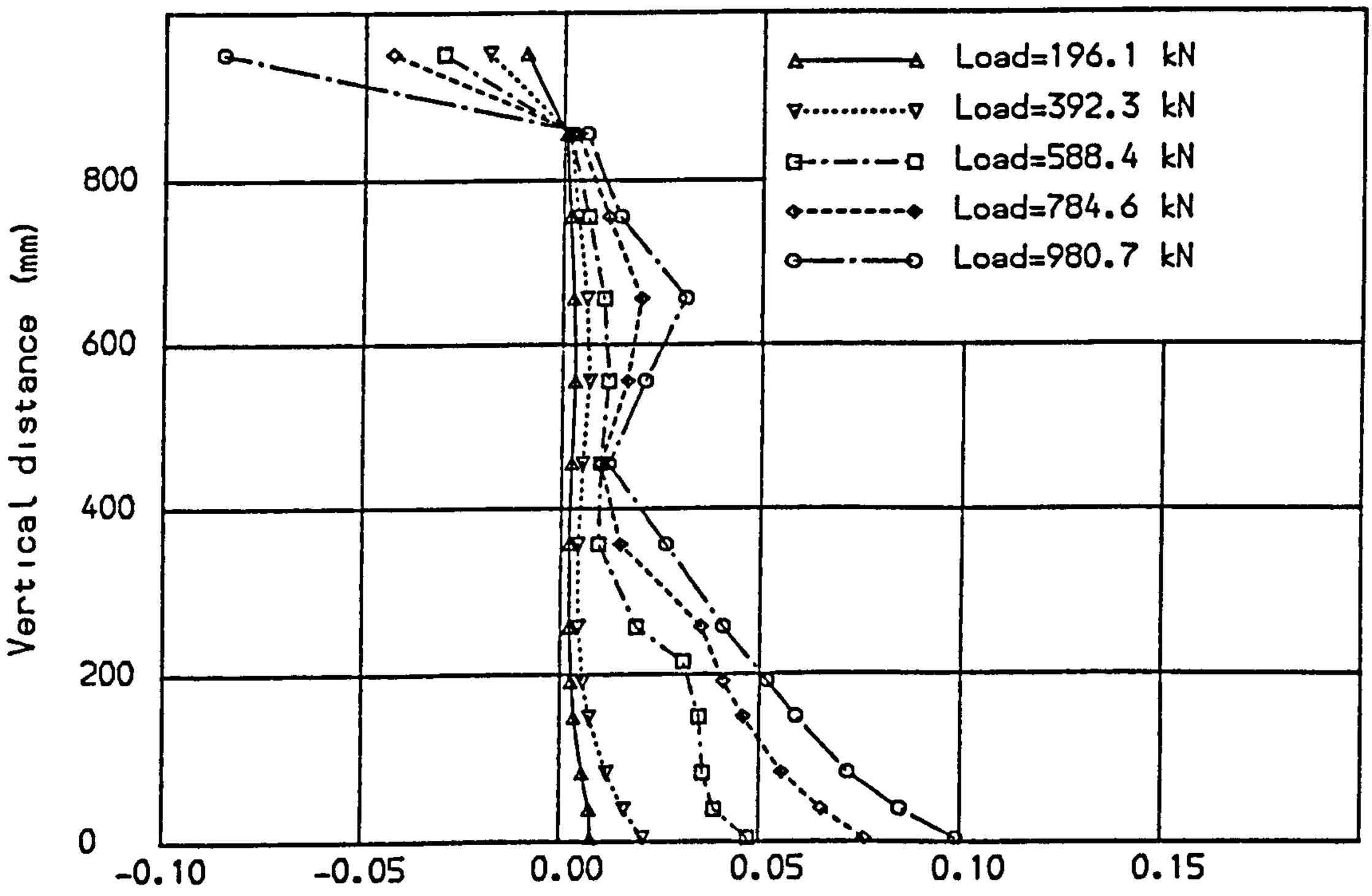

Fig. (7.41) Concrete surface strain for Lin deep beam 204.

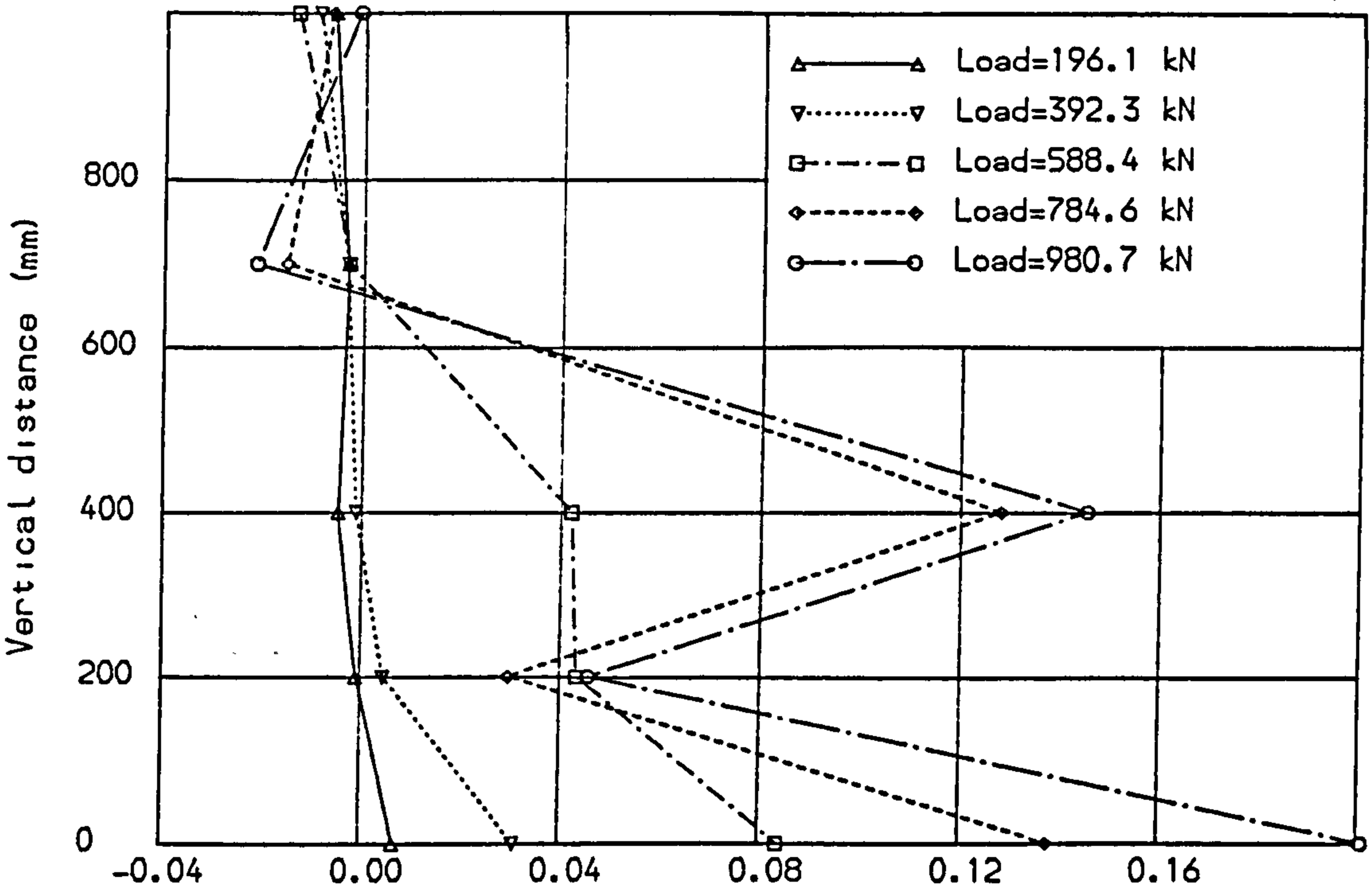

Fig. (7.42) Concrete surface strain for Lin deep beam 204.

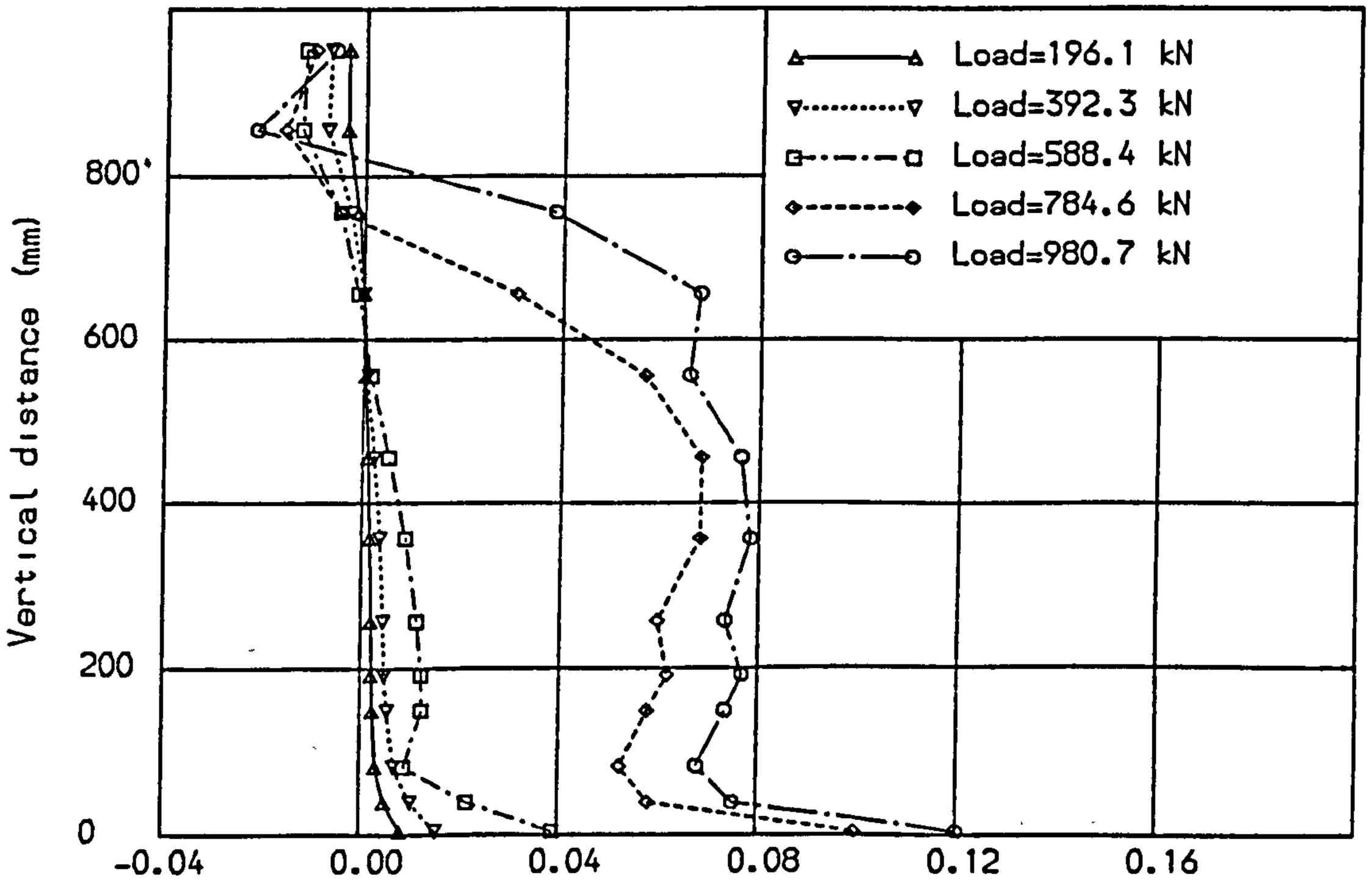

Fig. (7.43) Concrete surface strain for Lin deep beam 204.

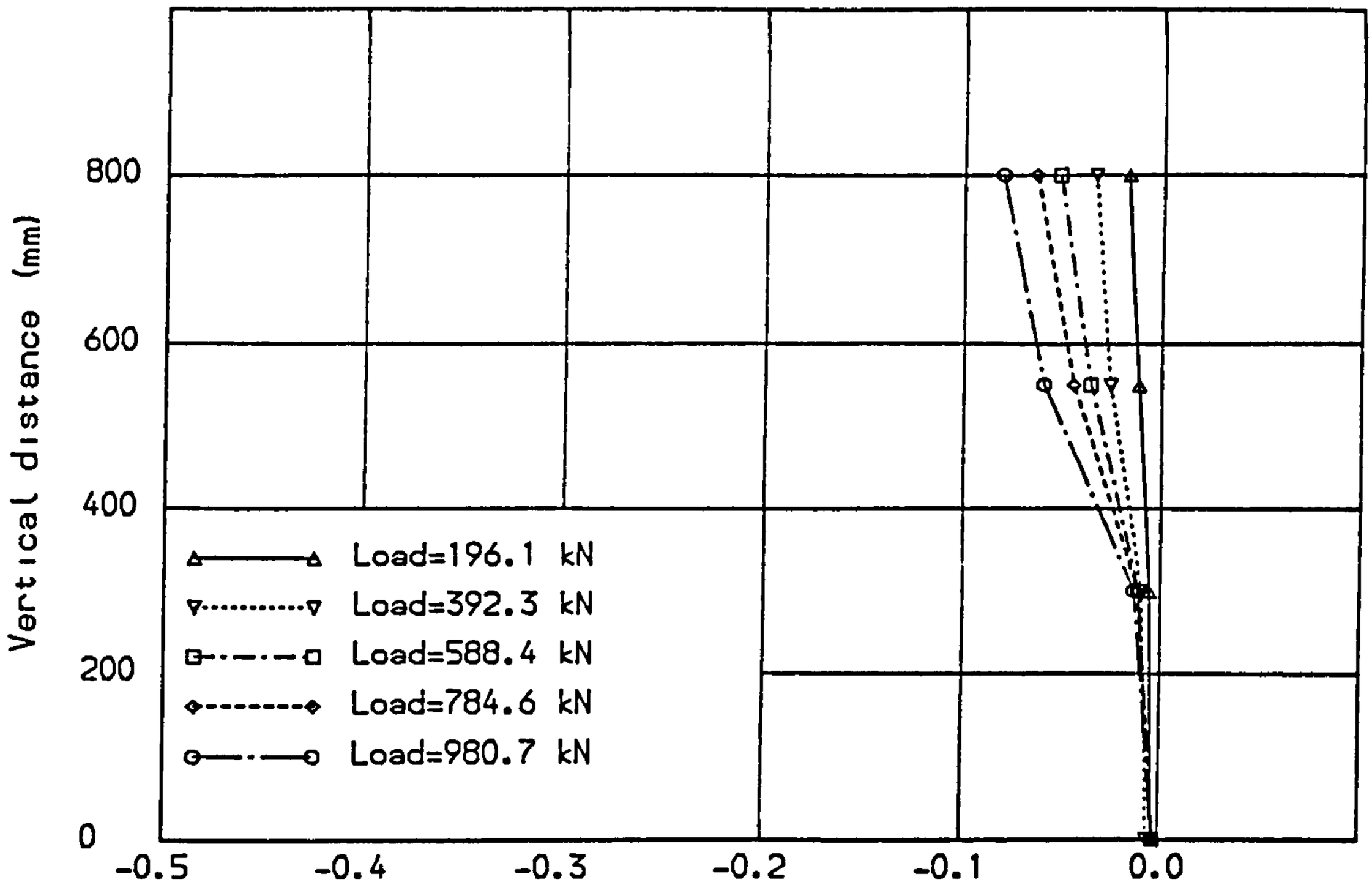

Fig. (7.44) Concrete surface strain for Lin deep beam 204.

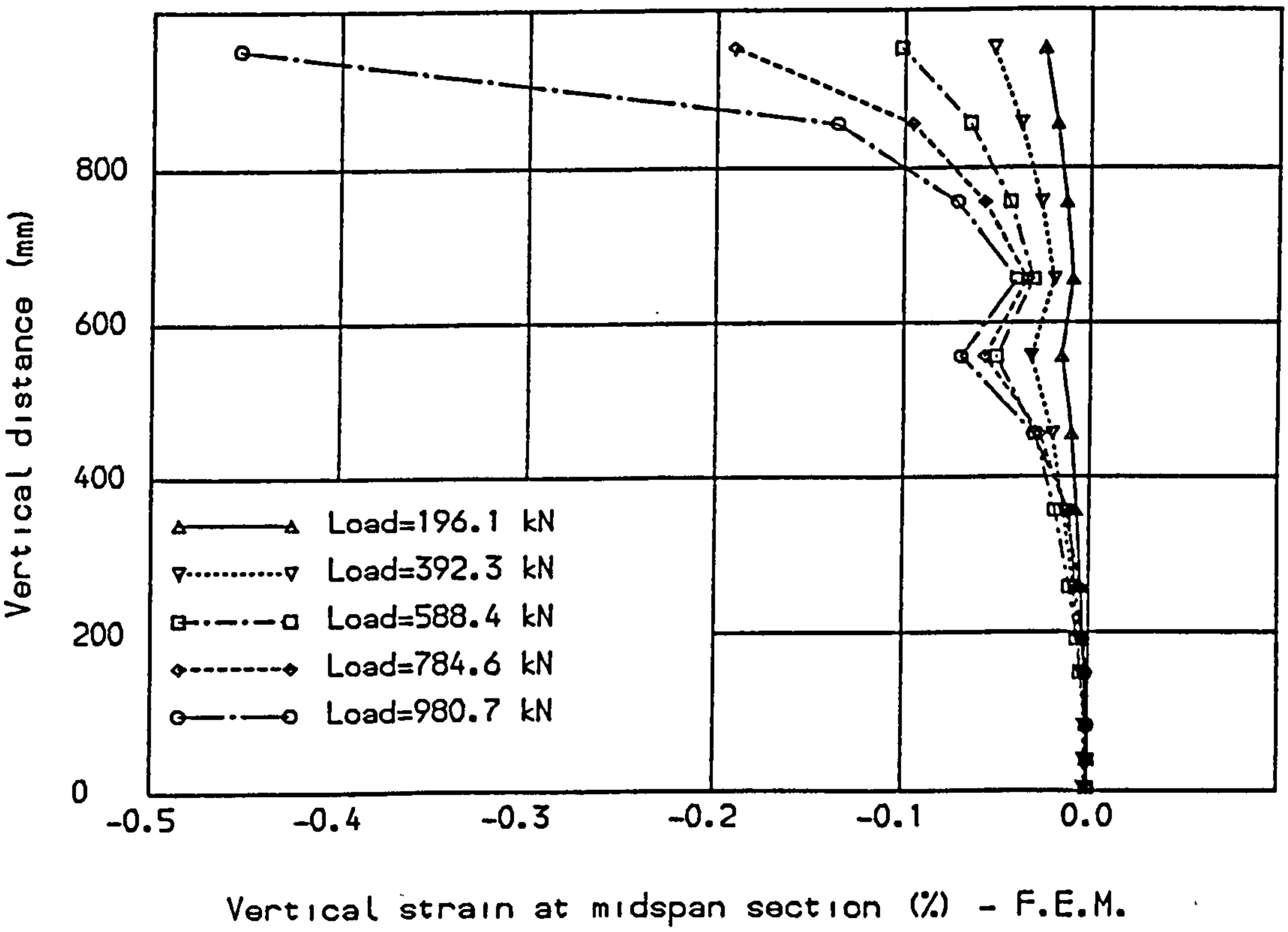

Fig. (7.45) Concrete surface strain for Lin deep beam 204.

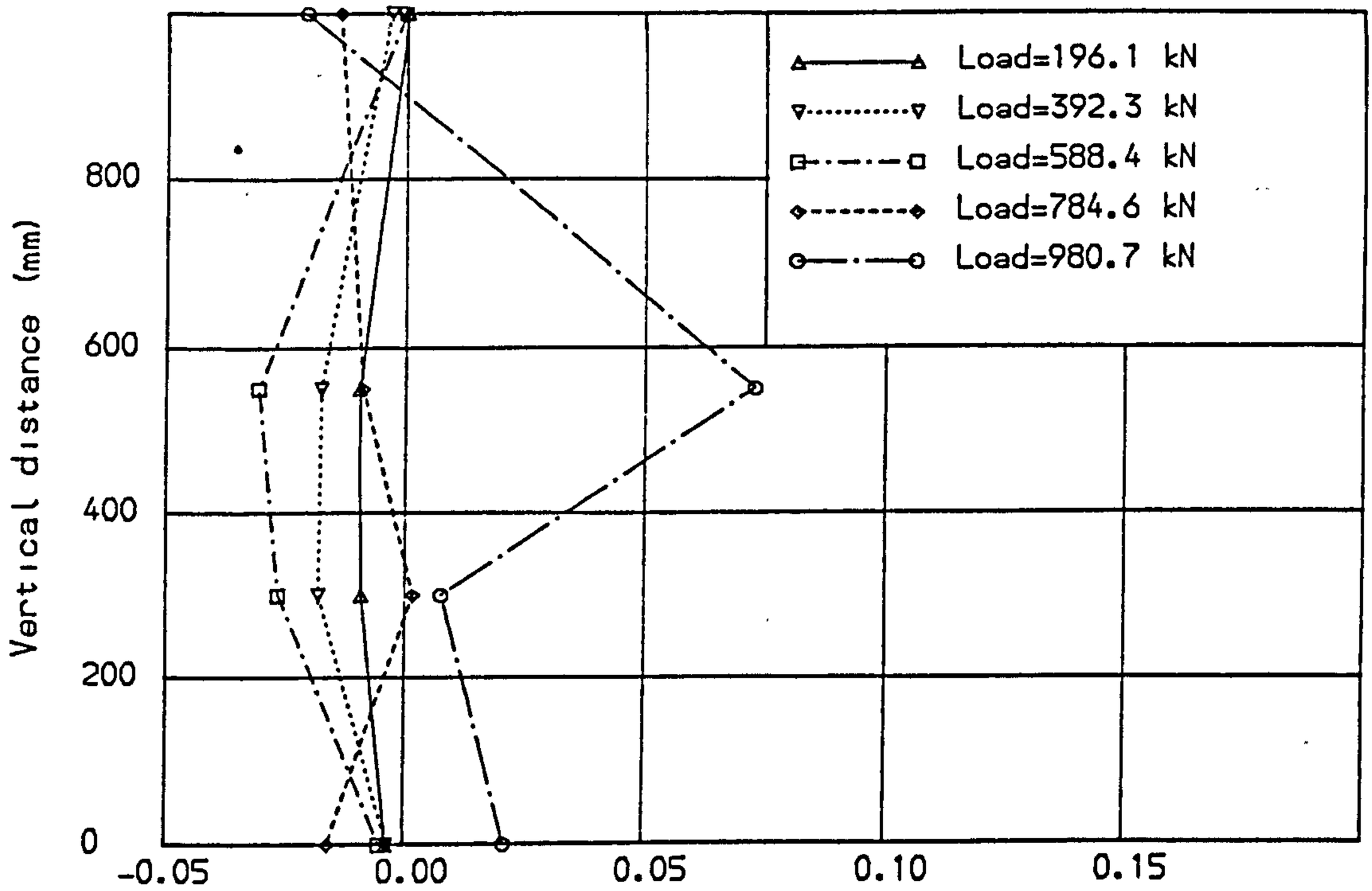

Fig. (7.46) Concrete surface strain for Lin deep beam 204.

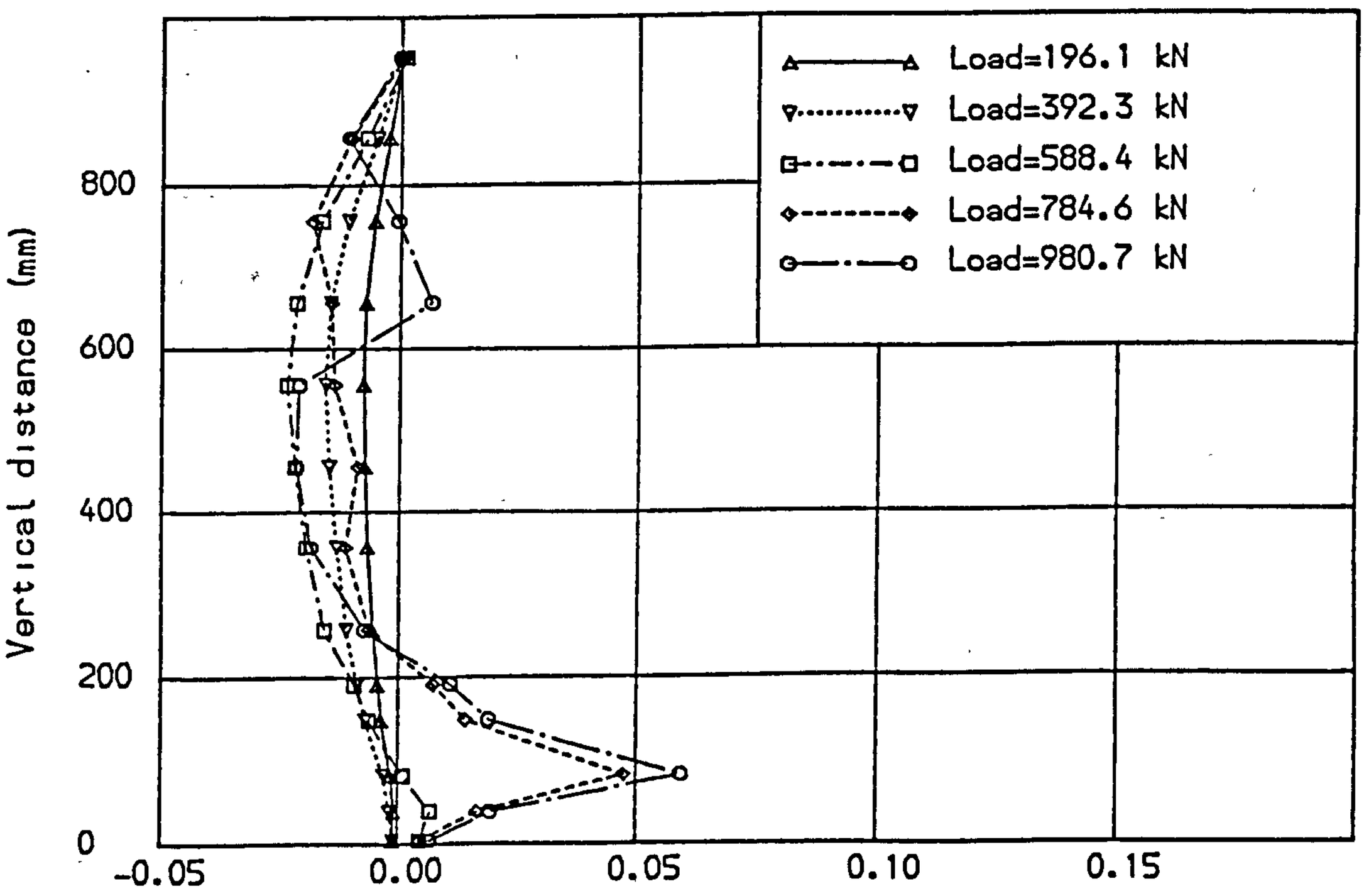

Fig. (7.47) Concrete surface strain for Lin deep beam 204.

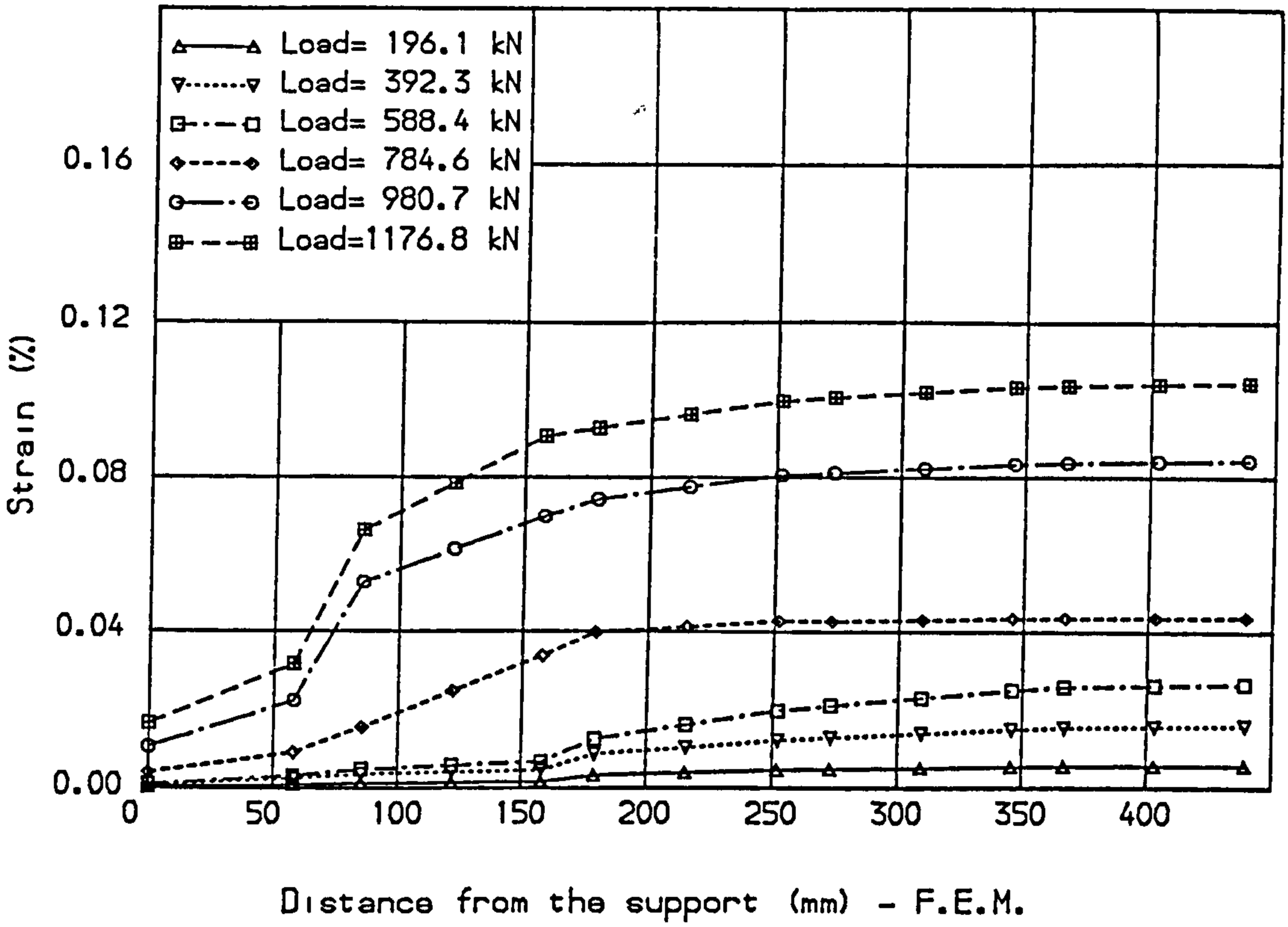

Fig. (7.48) Strain distribution along the bottom bar, (Lin 204).

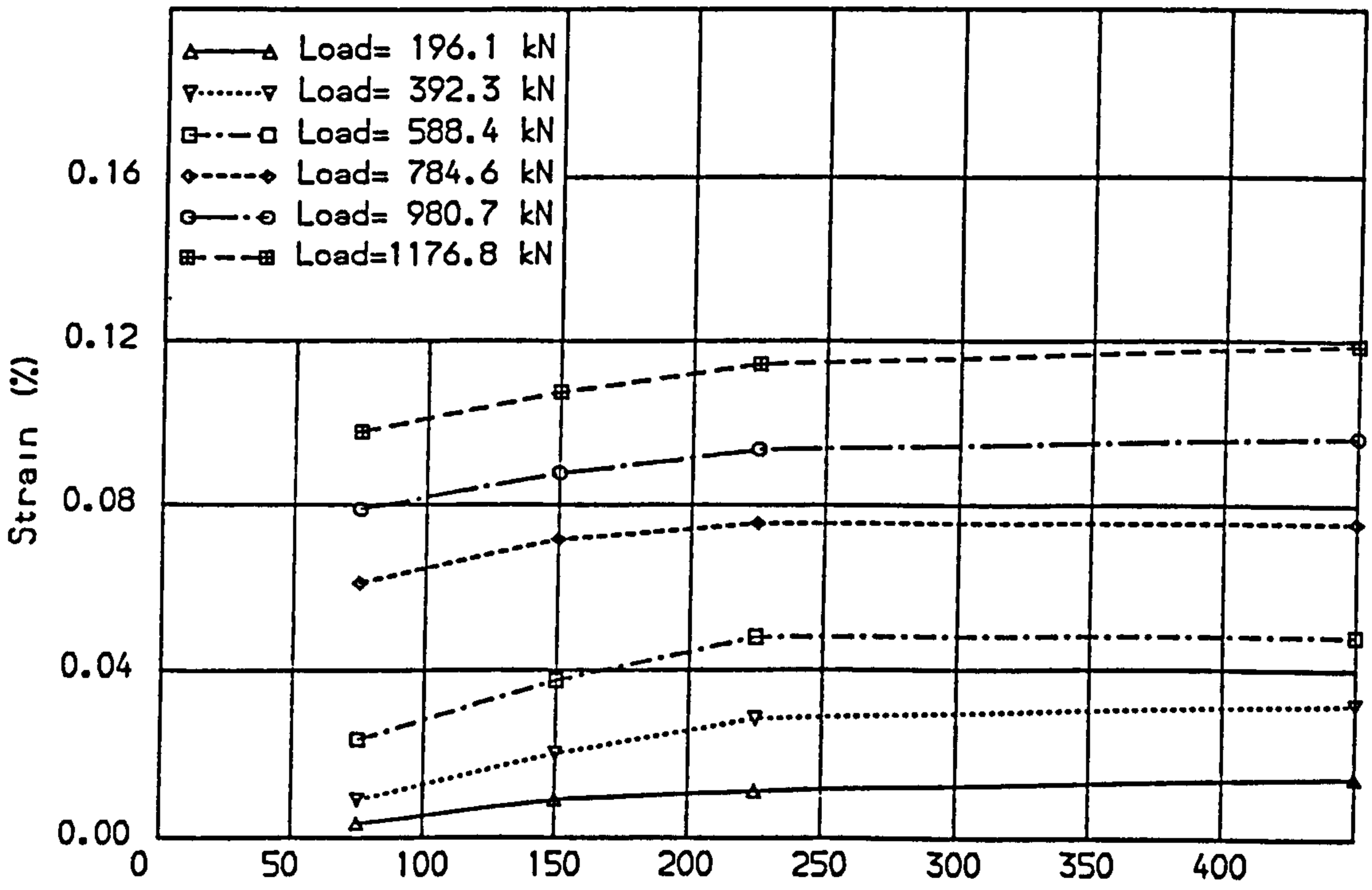

Fig. (7.49) Strain distribution along the bottom bar, (Lin 204).

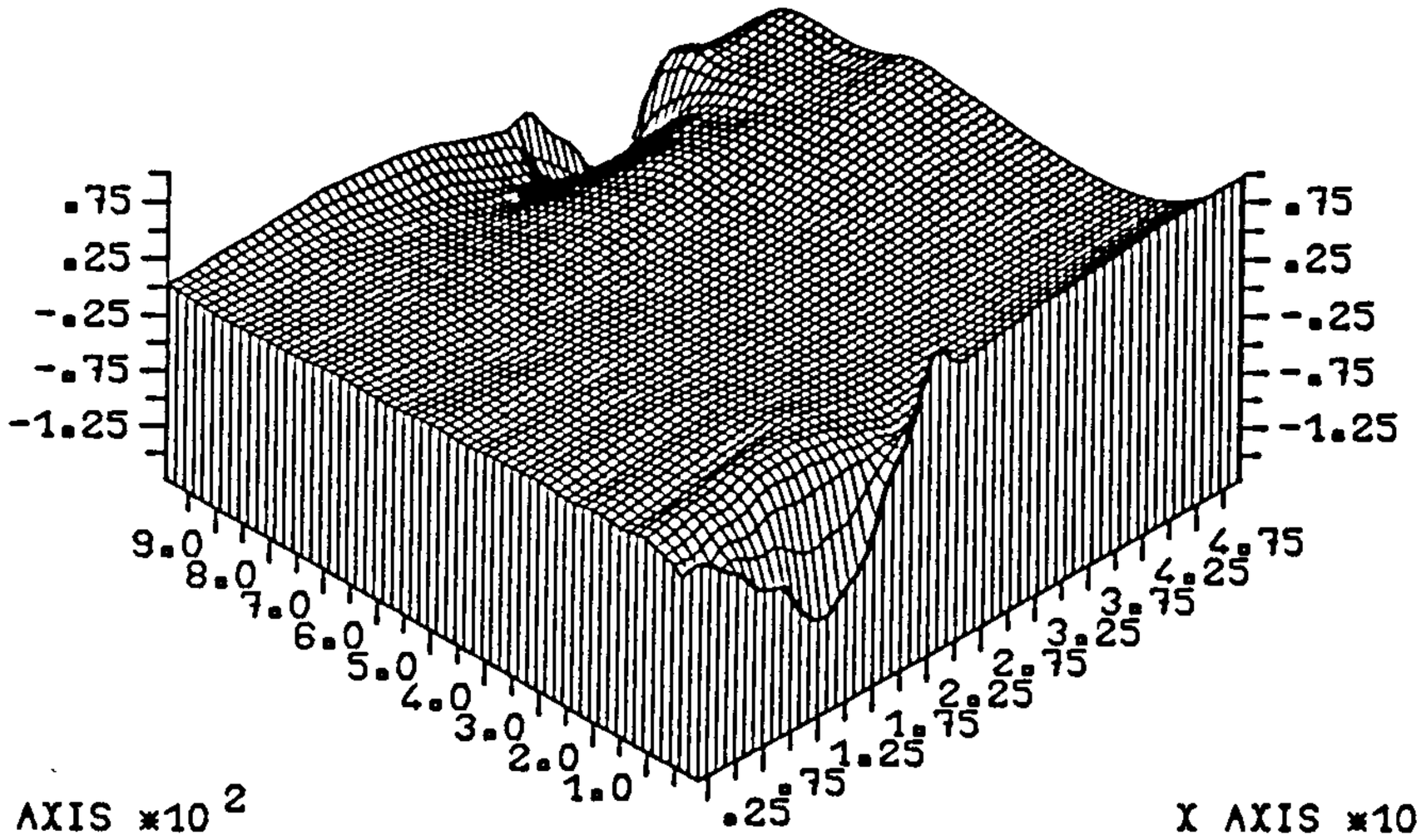

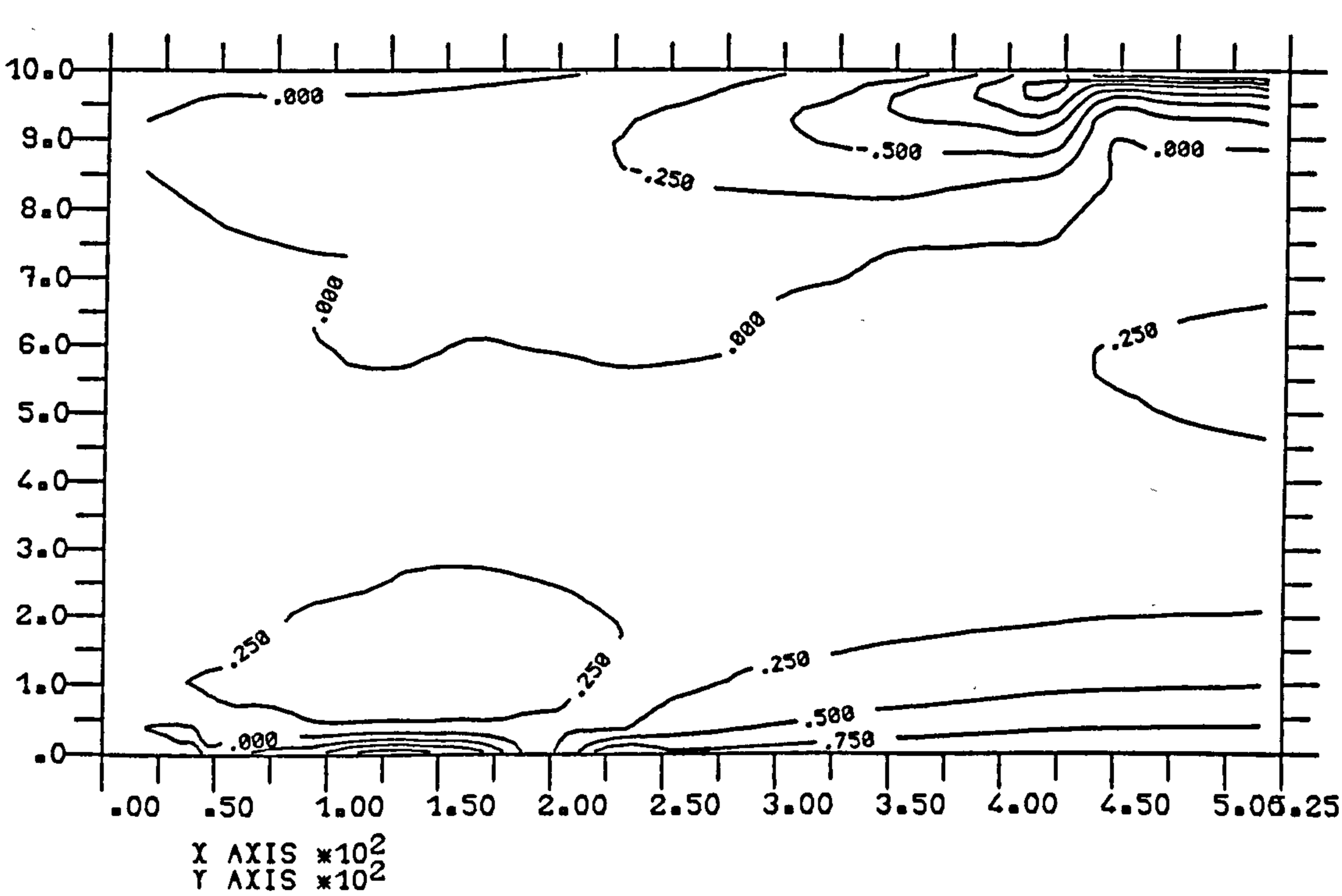

Figure (7·50) Horizontal strain x 10^{-4} at load = 196·1 kN.

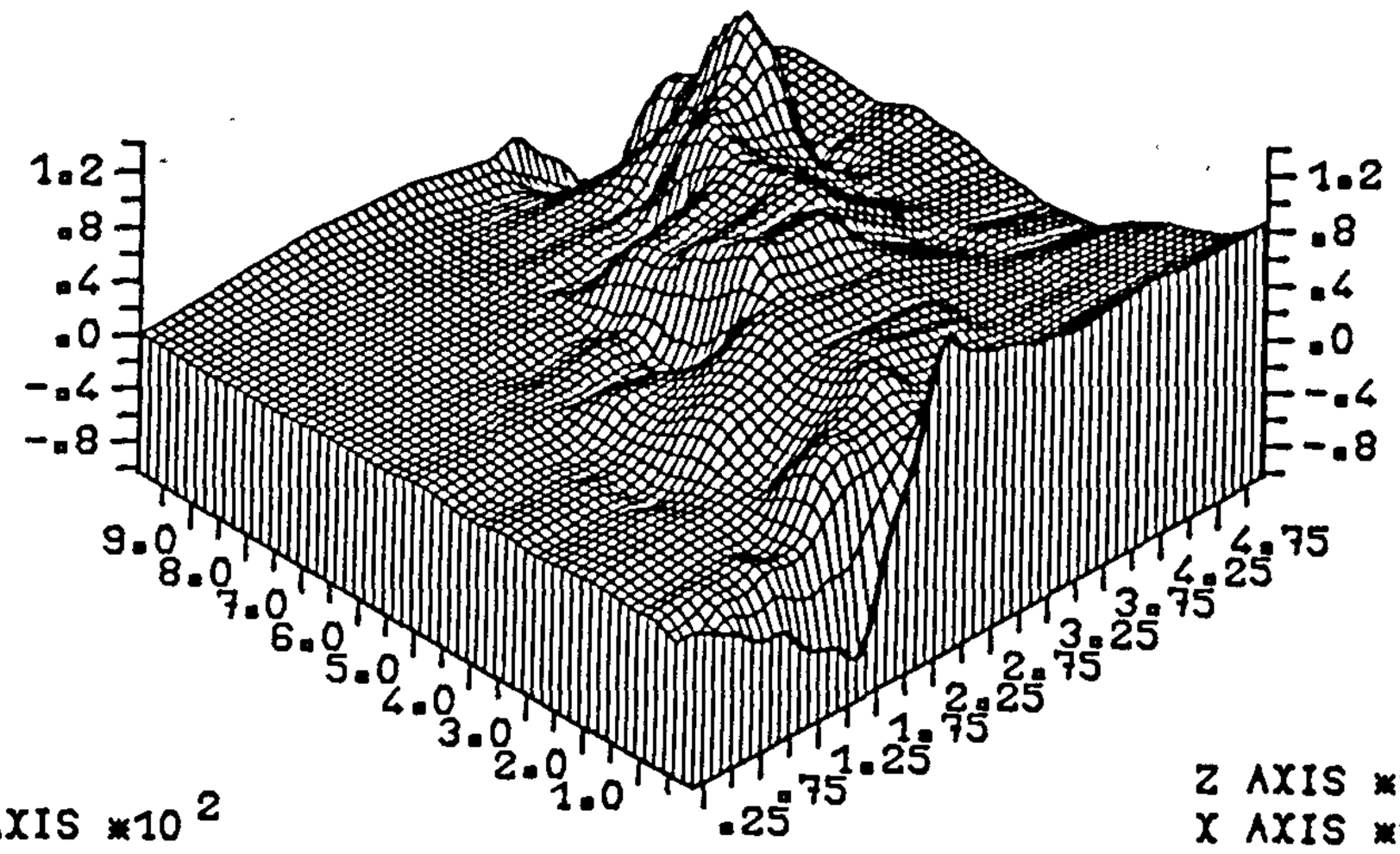

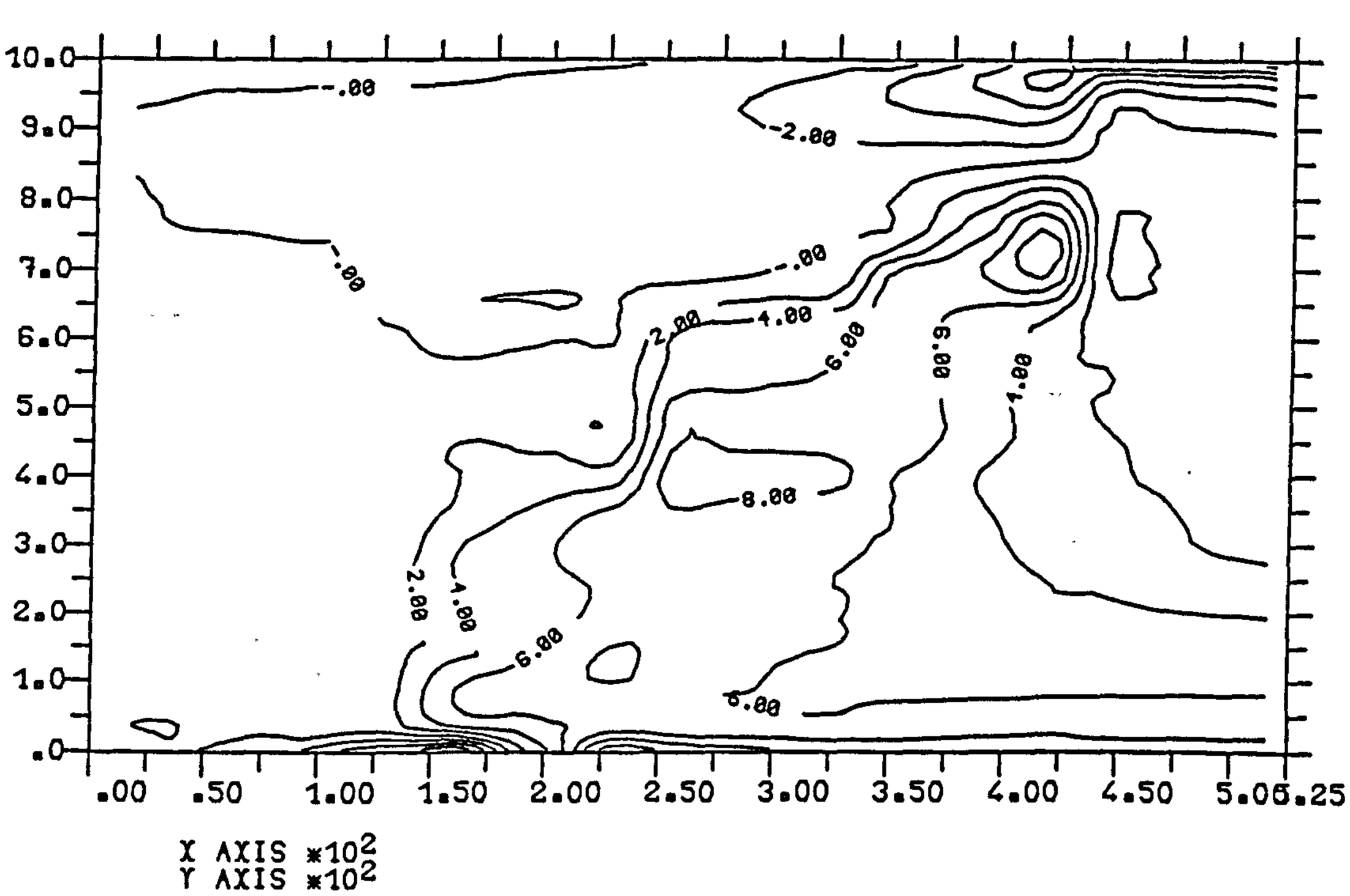

Figure (7·51) Horizontal strain x 10^{-4} at load = 883·0 kN.

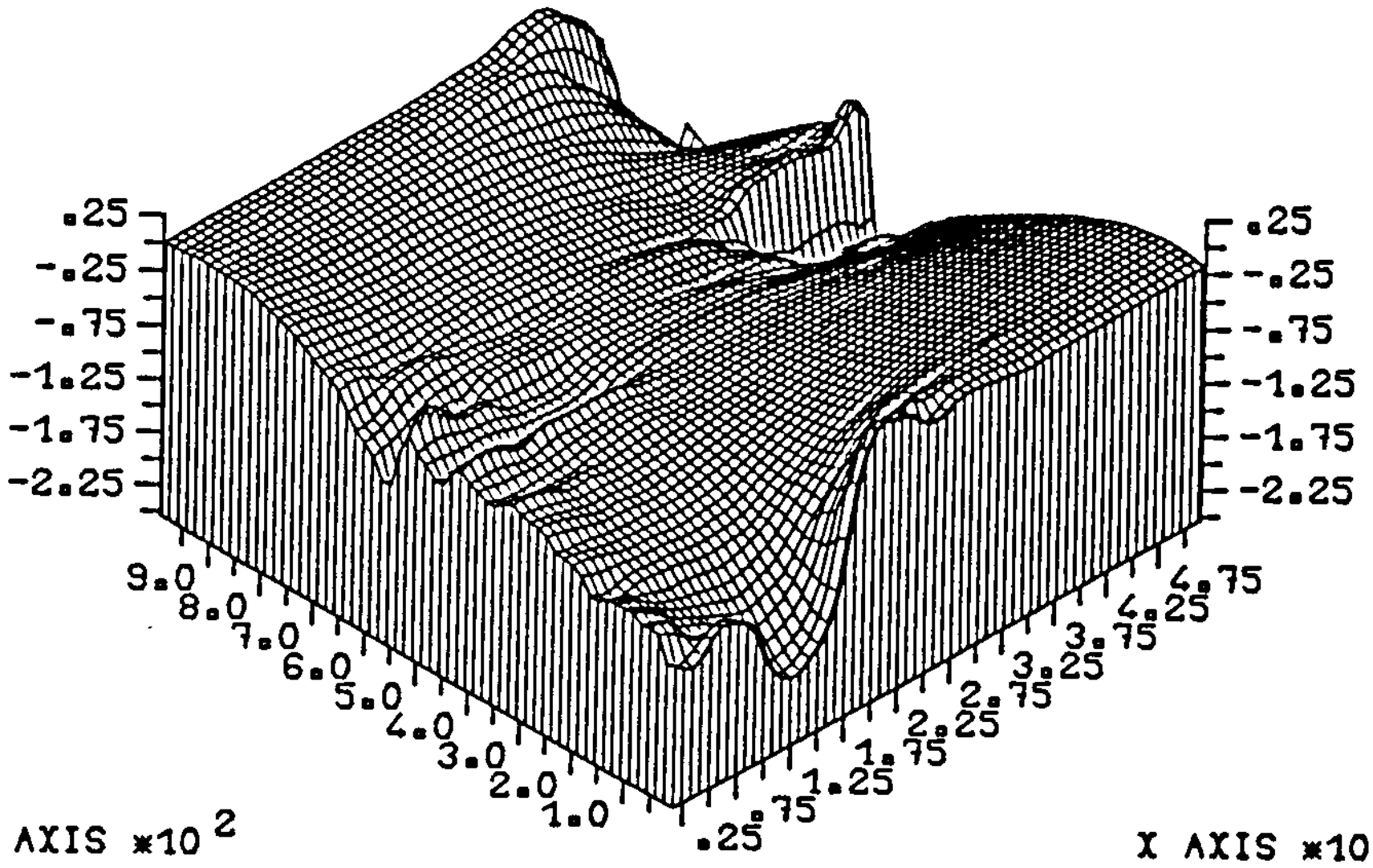

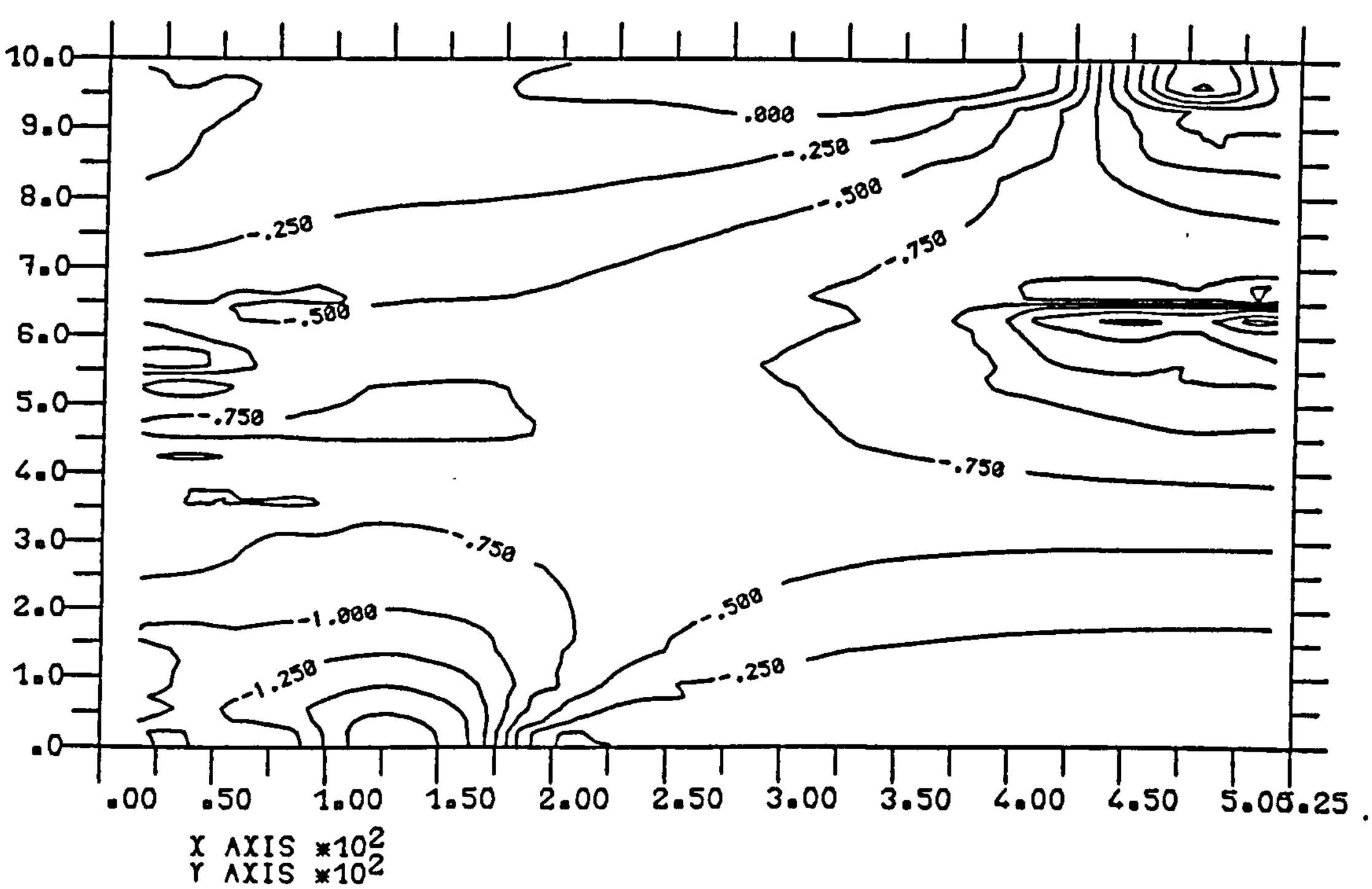

Figure (7·52) Vertical strain x 10^{-4} at load=196·1 kN.

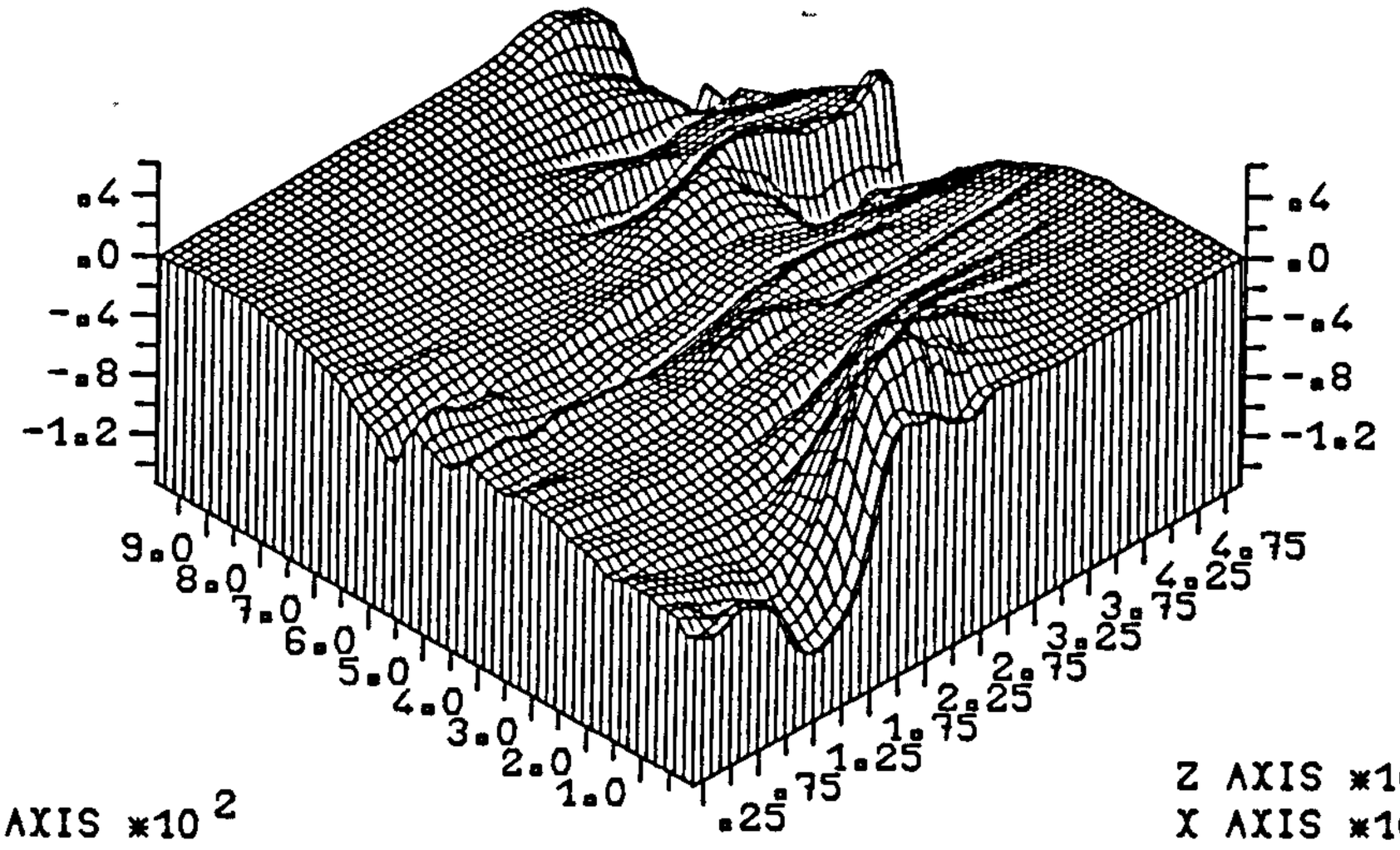

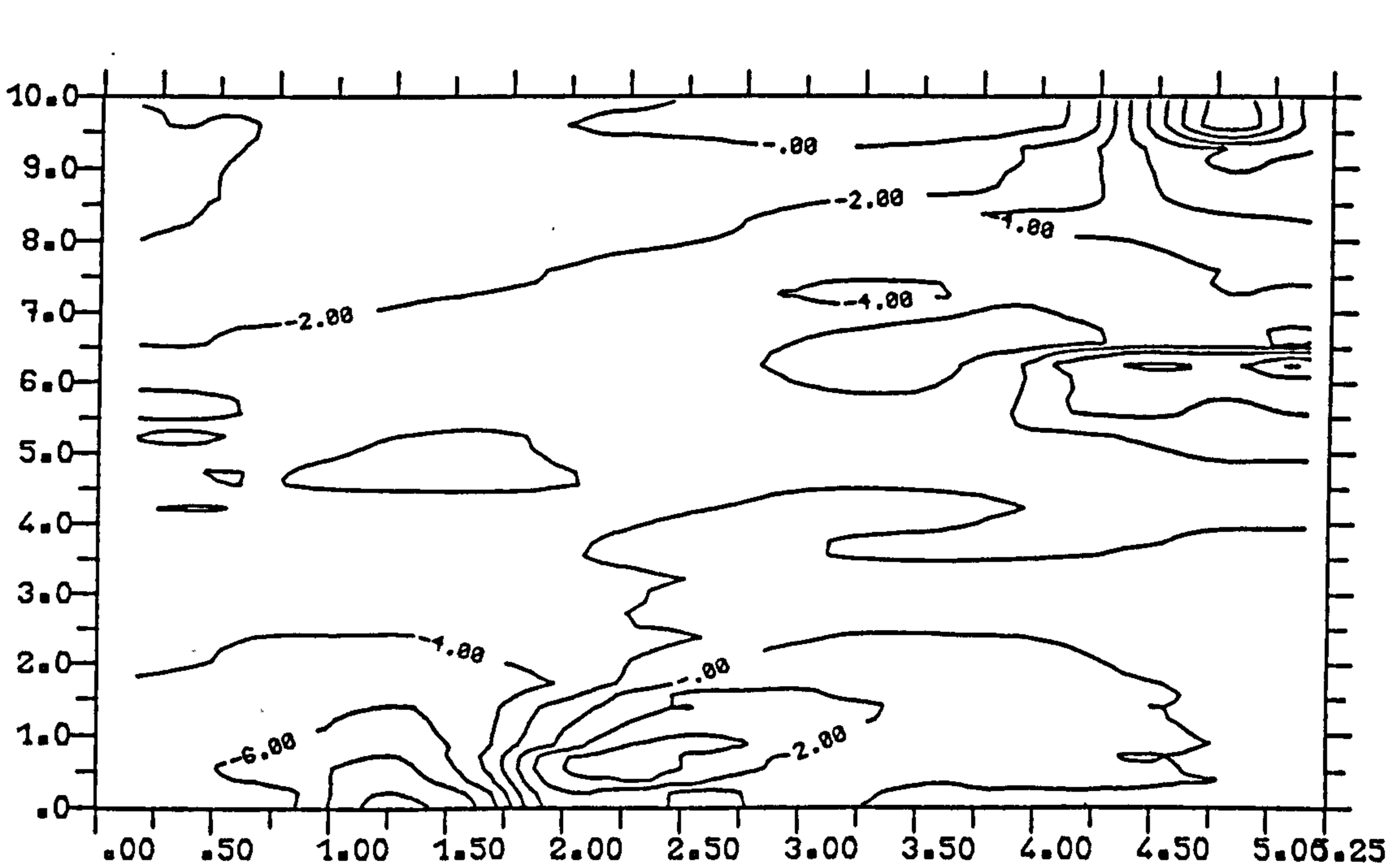

Figure (7·53) Vertical strain x 10^{-4} at load = 883·0 kN.

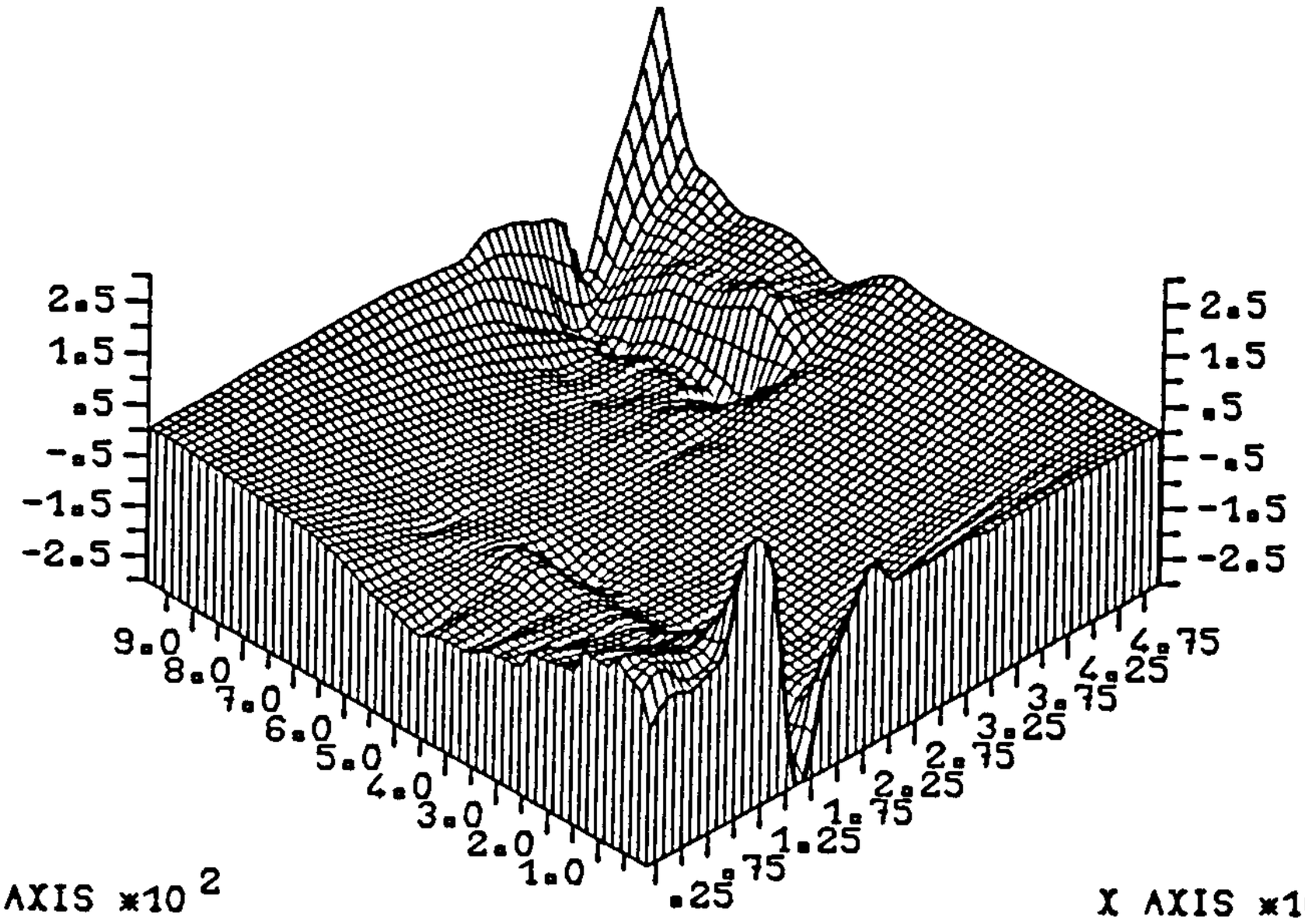

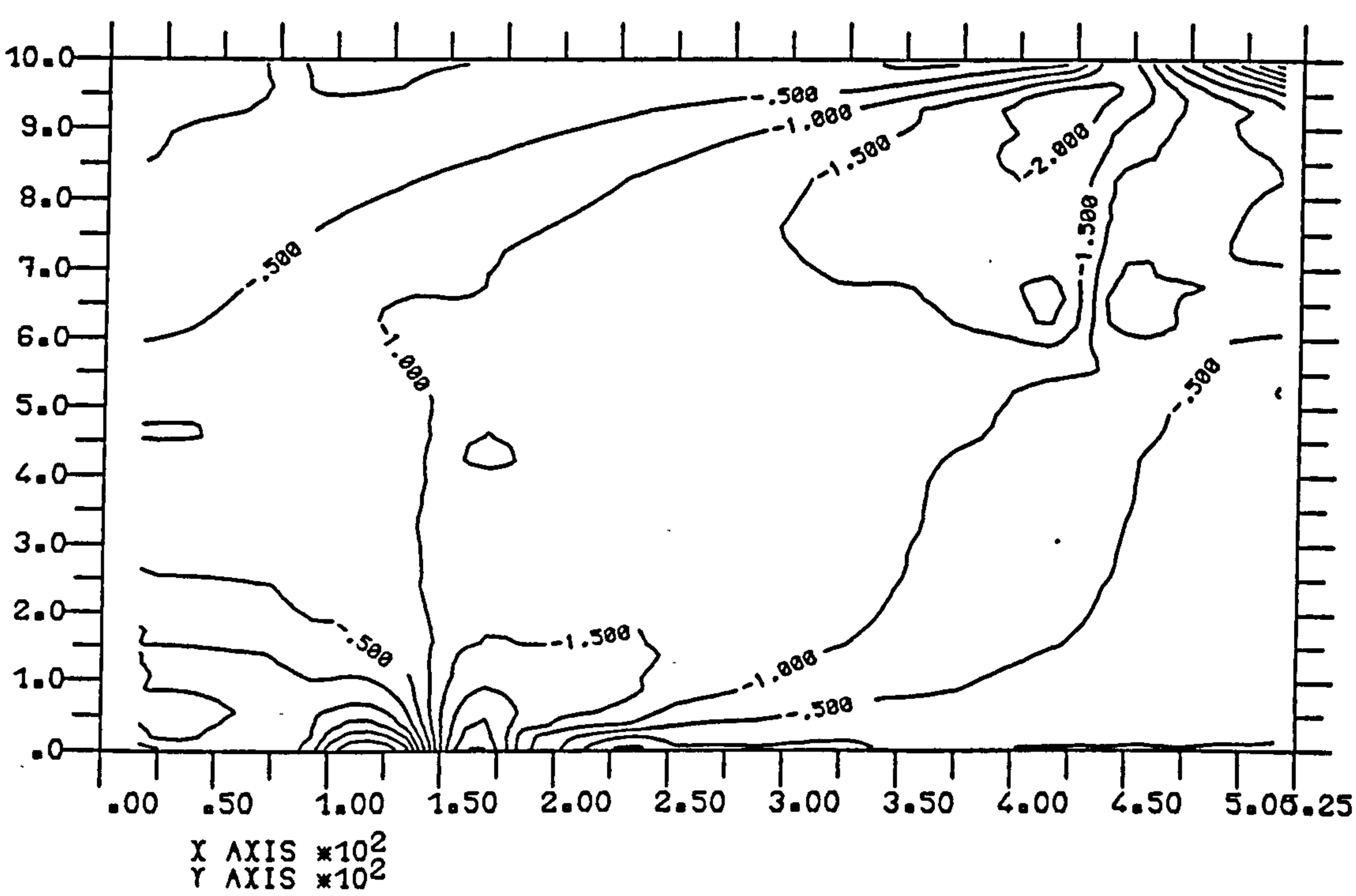

Figure (7·54) Shear strain x 10^{-4} at load = 196·1 kN.

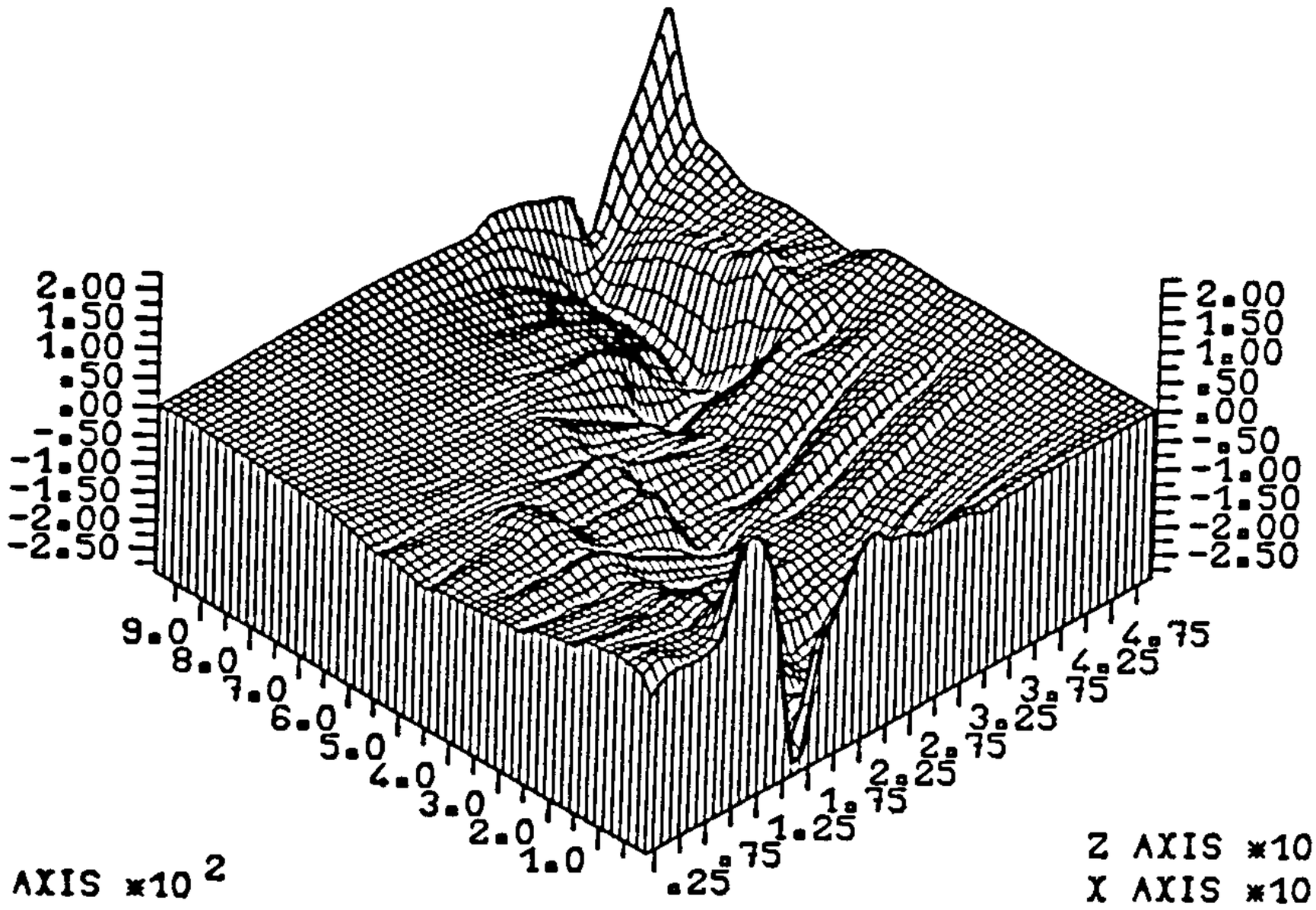

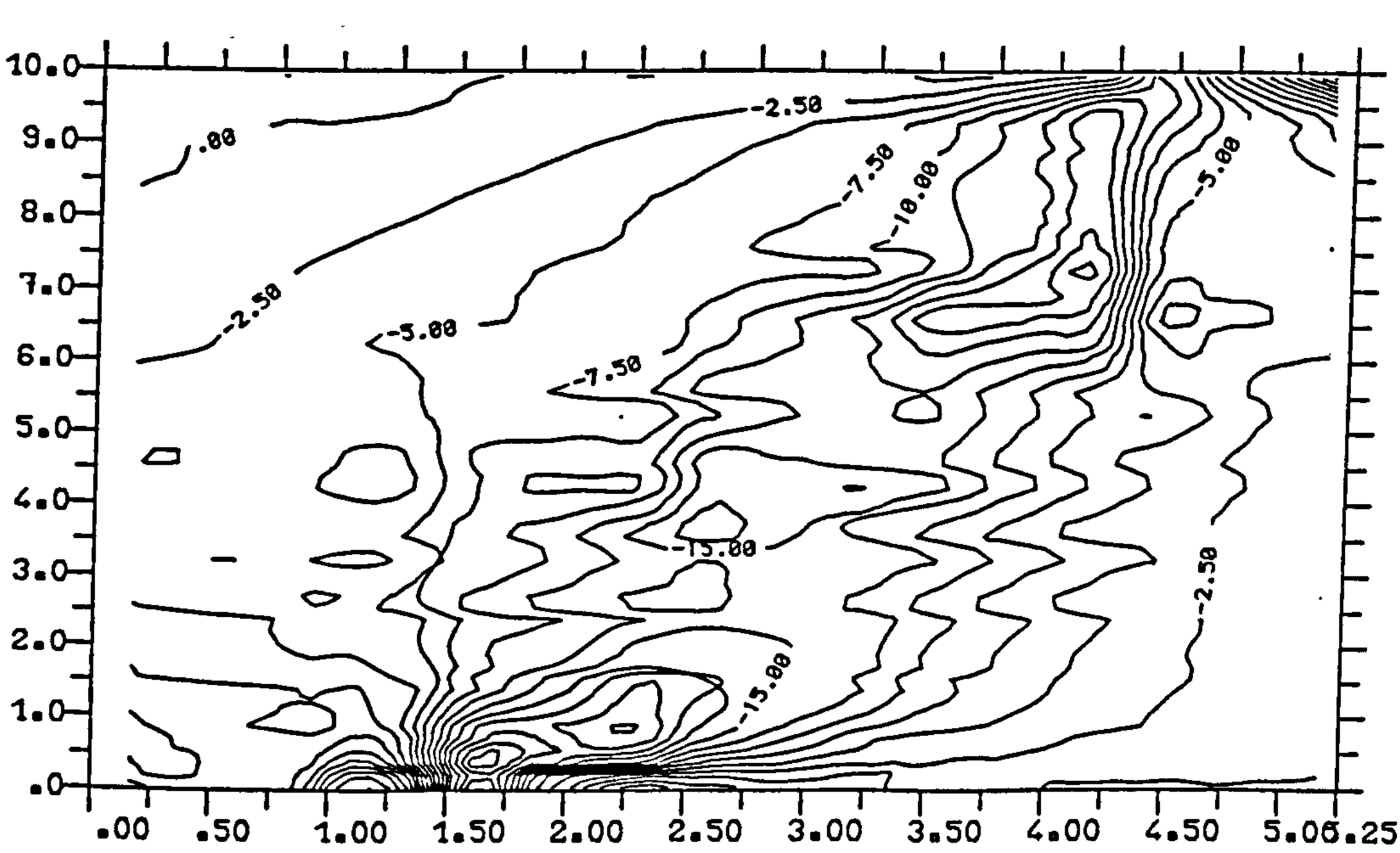

Figure (7·55) Shear strain x 10^{-4} at load = 883·0 kN.

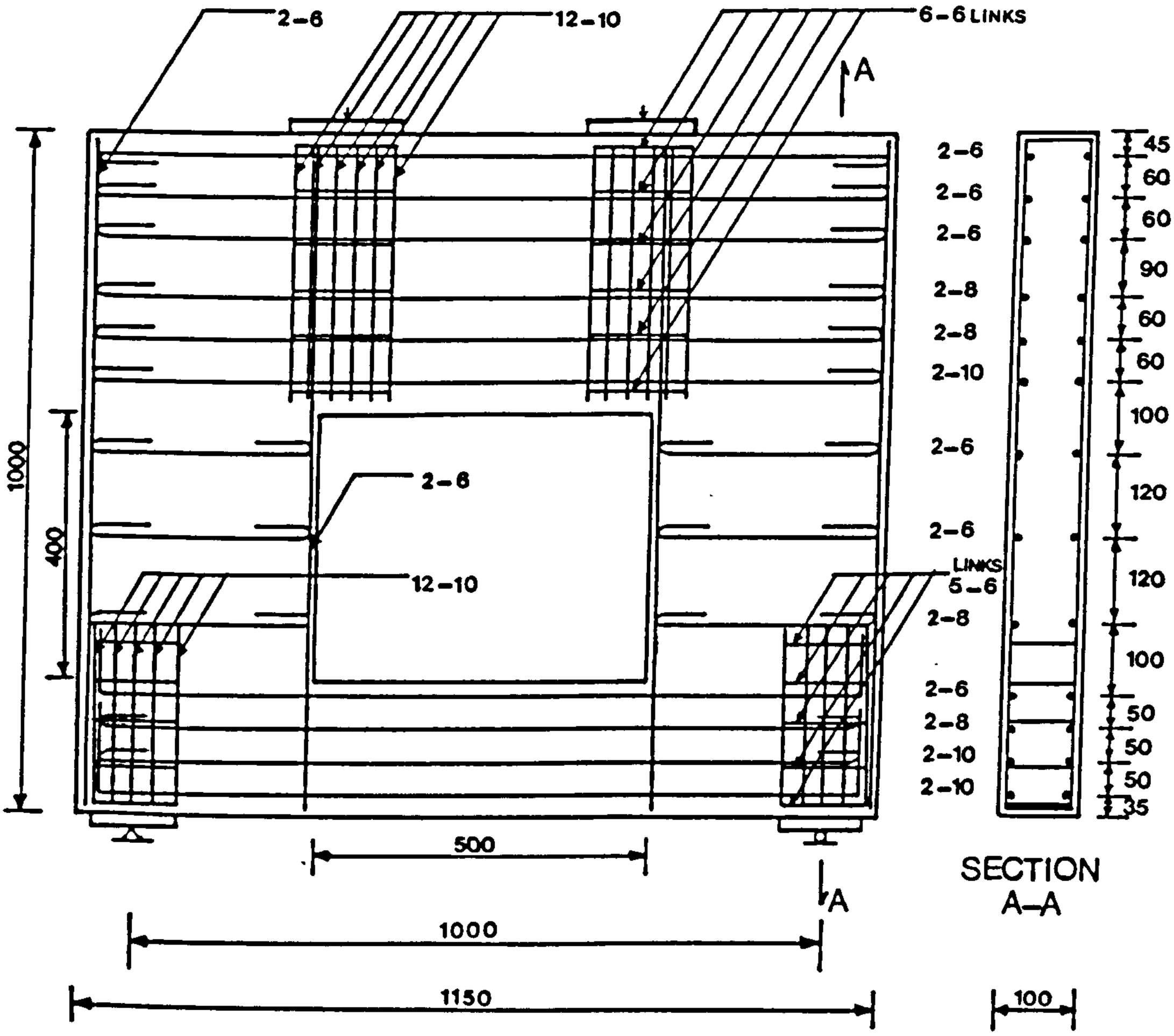

Figure (7·56) Details of Memon deep beam B-5.

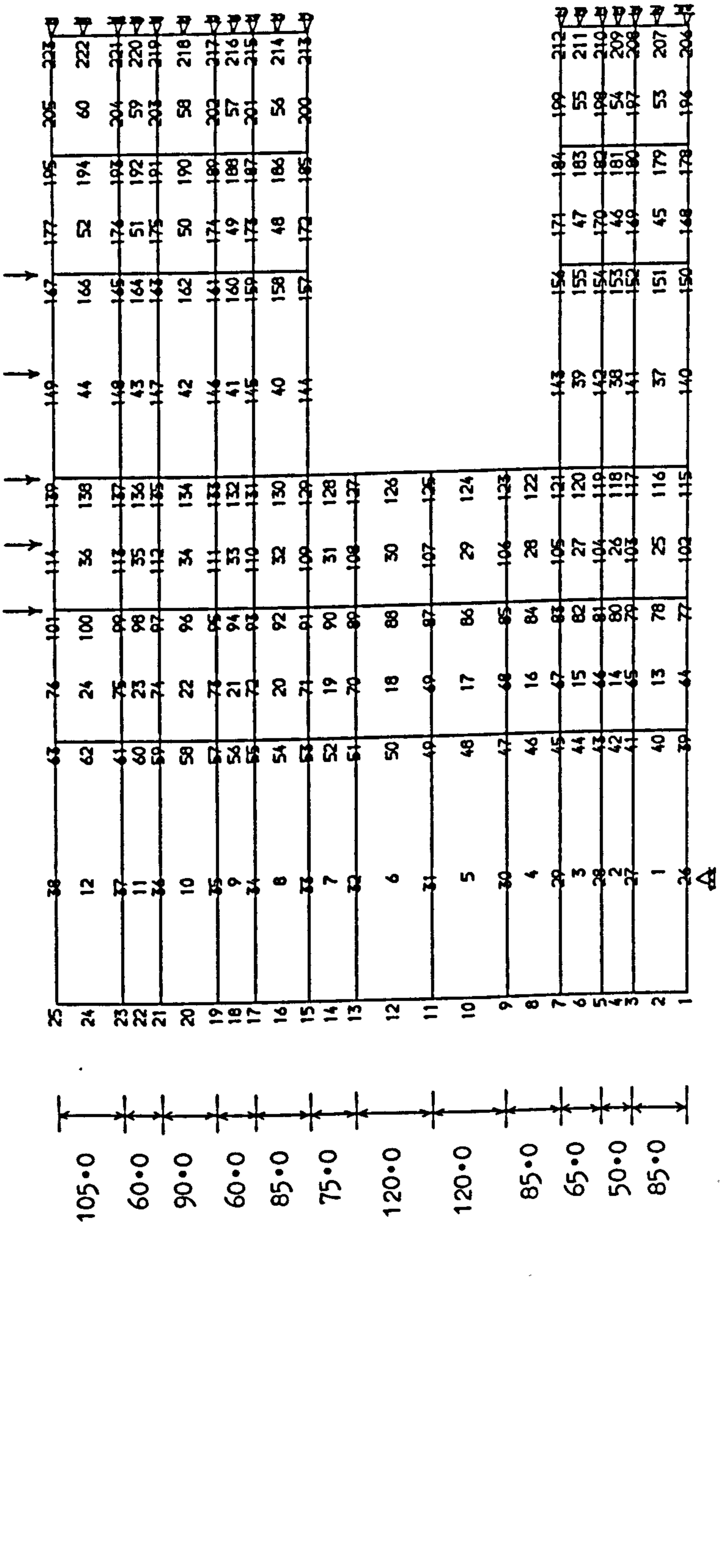

Figure (7•57) Mesh used for Memon beams B-5 and B-7.

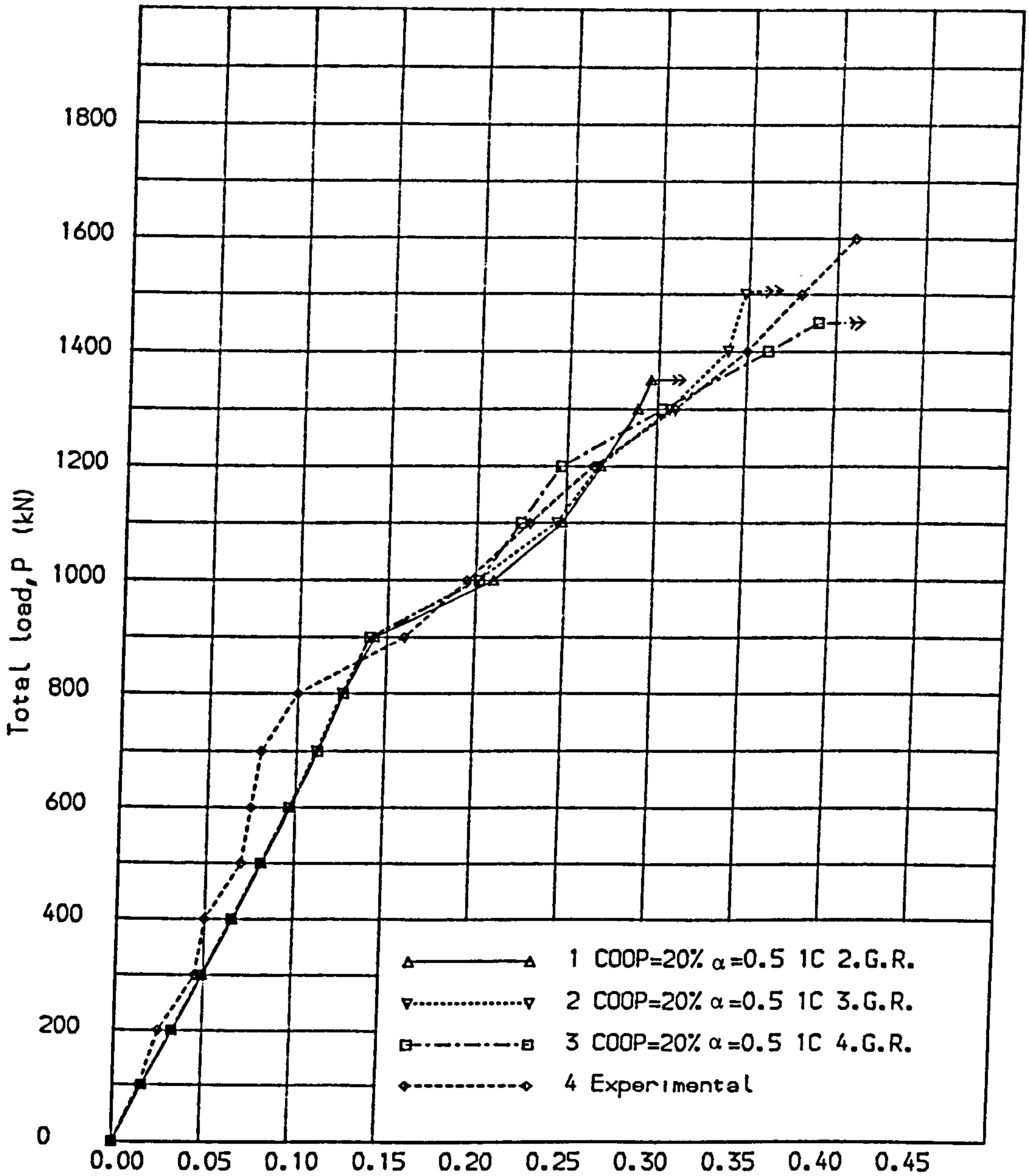

Fig. (7.58) Load deflection curves for Memon deep beam B-5.

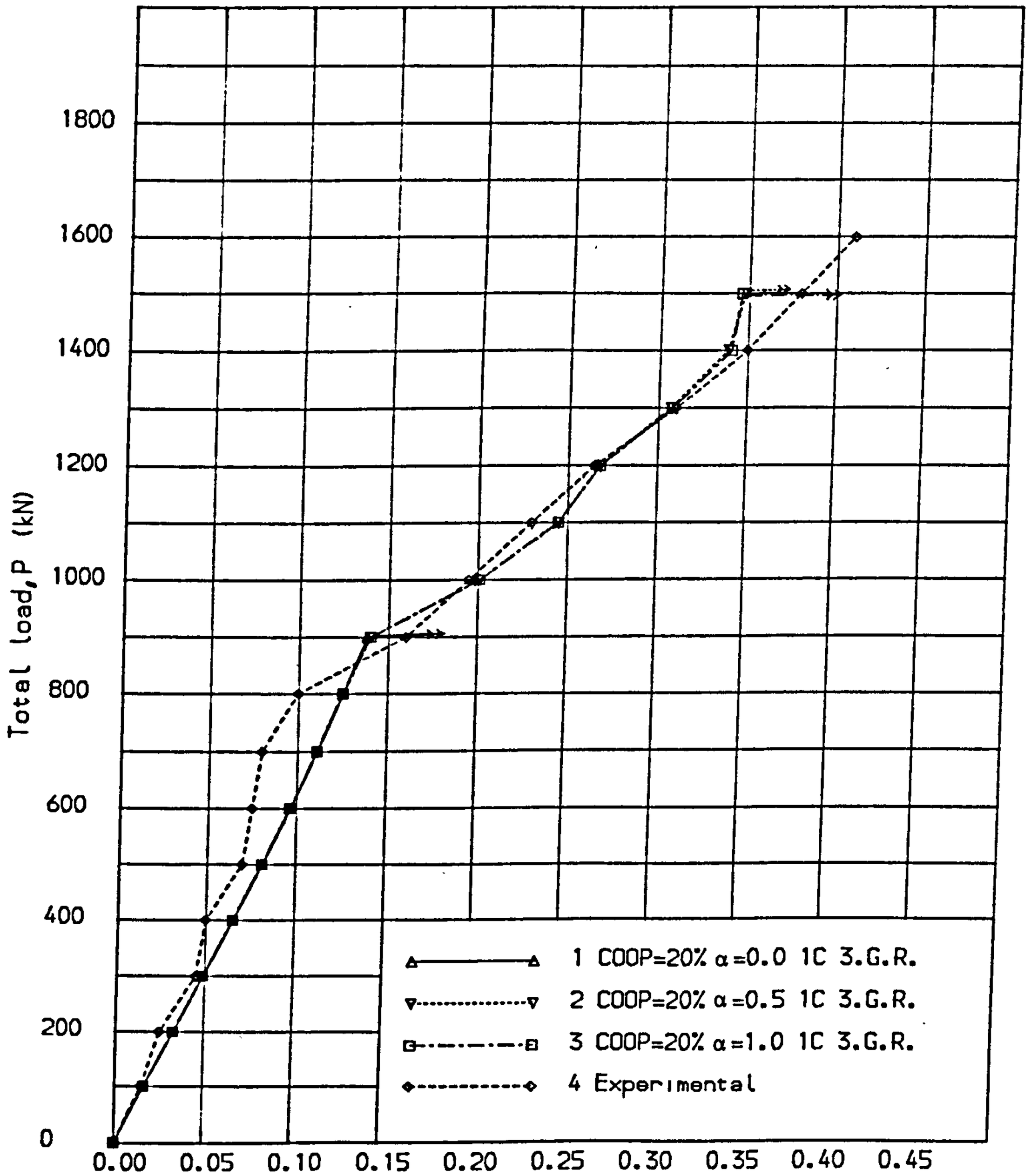

Fig. (7.59) Load deflection curves for Memon deep beam B-5.

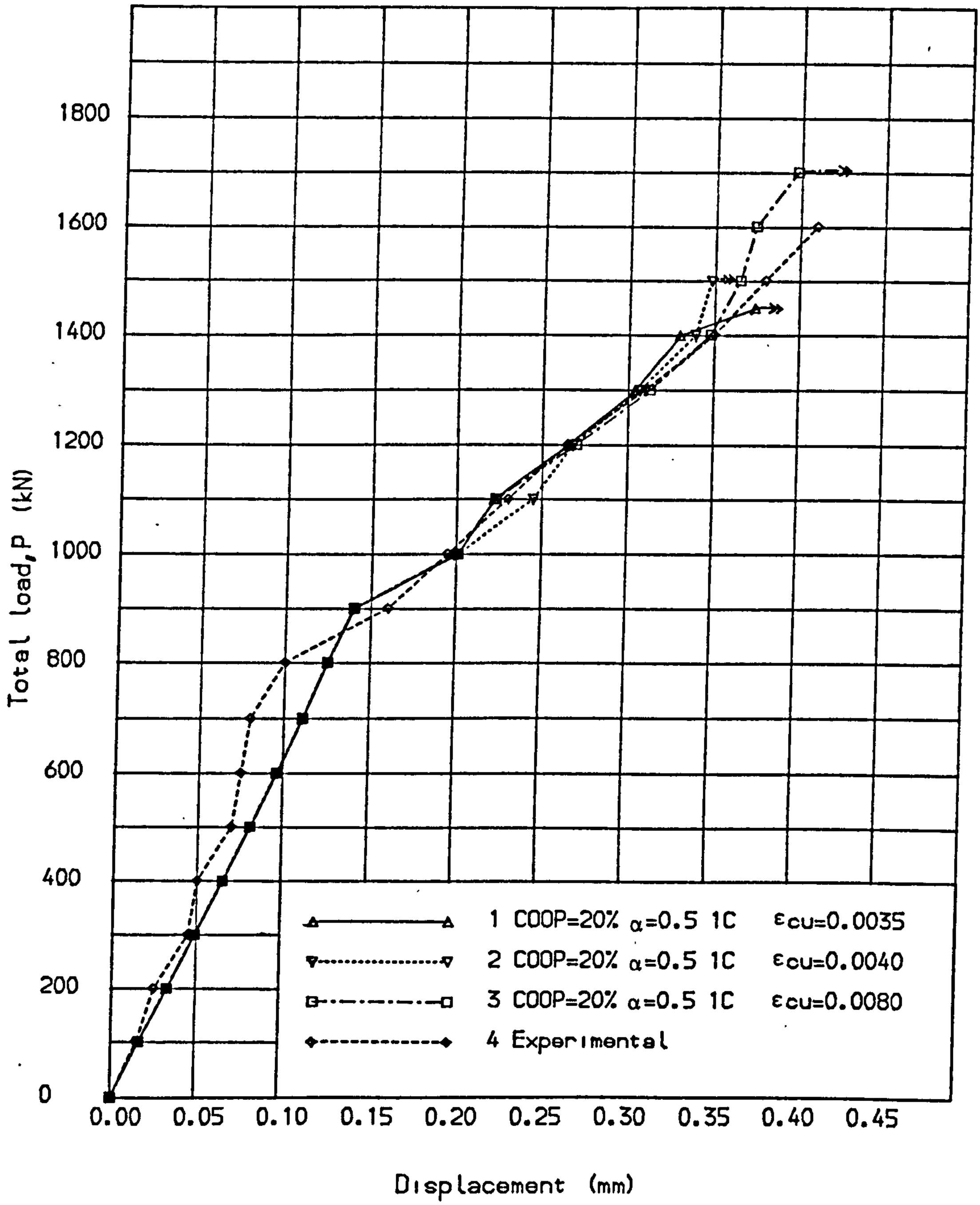

Fig. (7.60) Load deflection curves for Memon deep beam B-5.

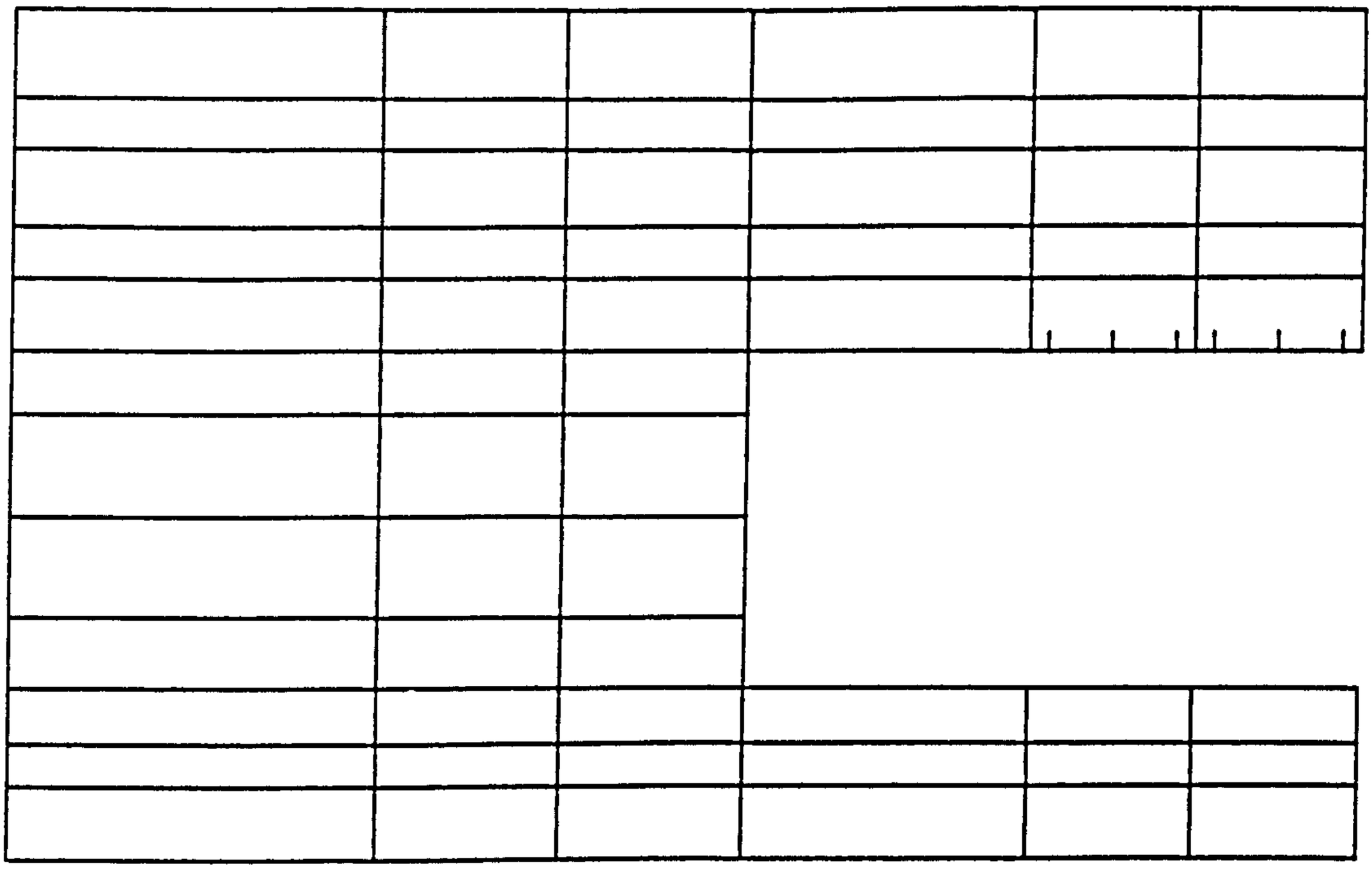

Figure (7·61) Crack pattern at load = 400·0 kN.

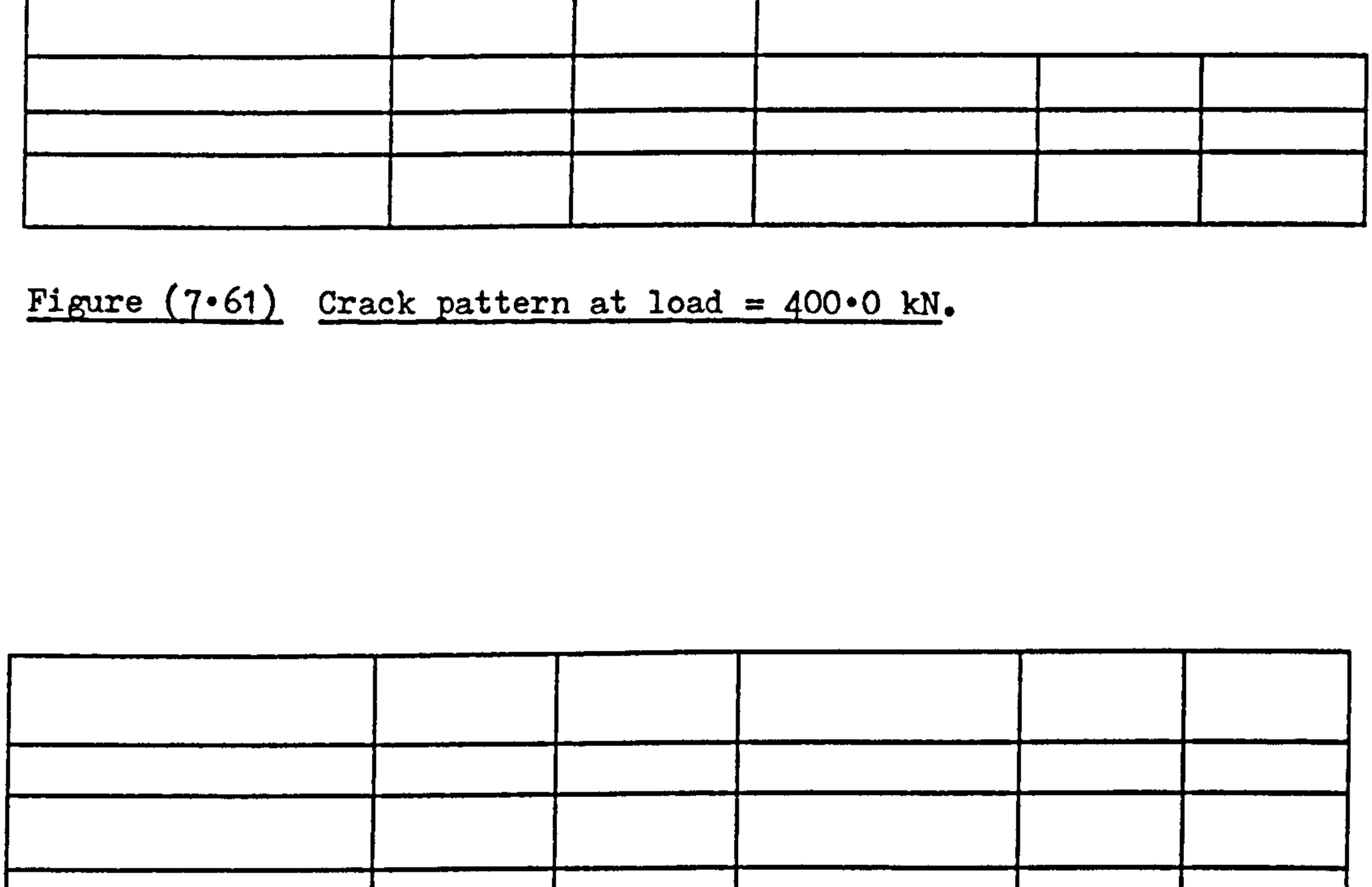

Figure (7·62) Crack pattern at load = 600·0 kN.

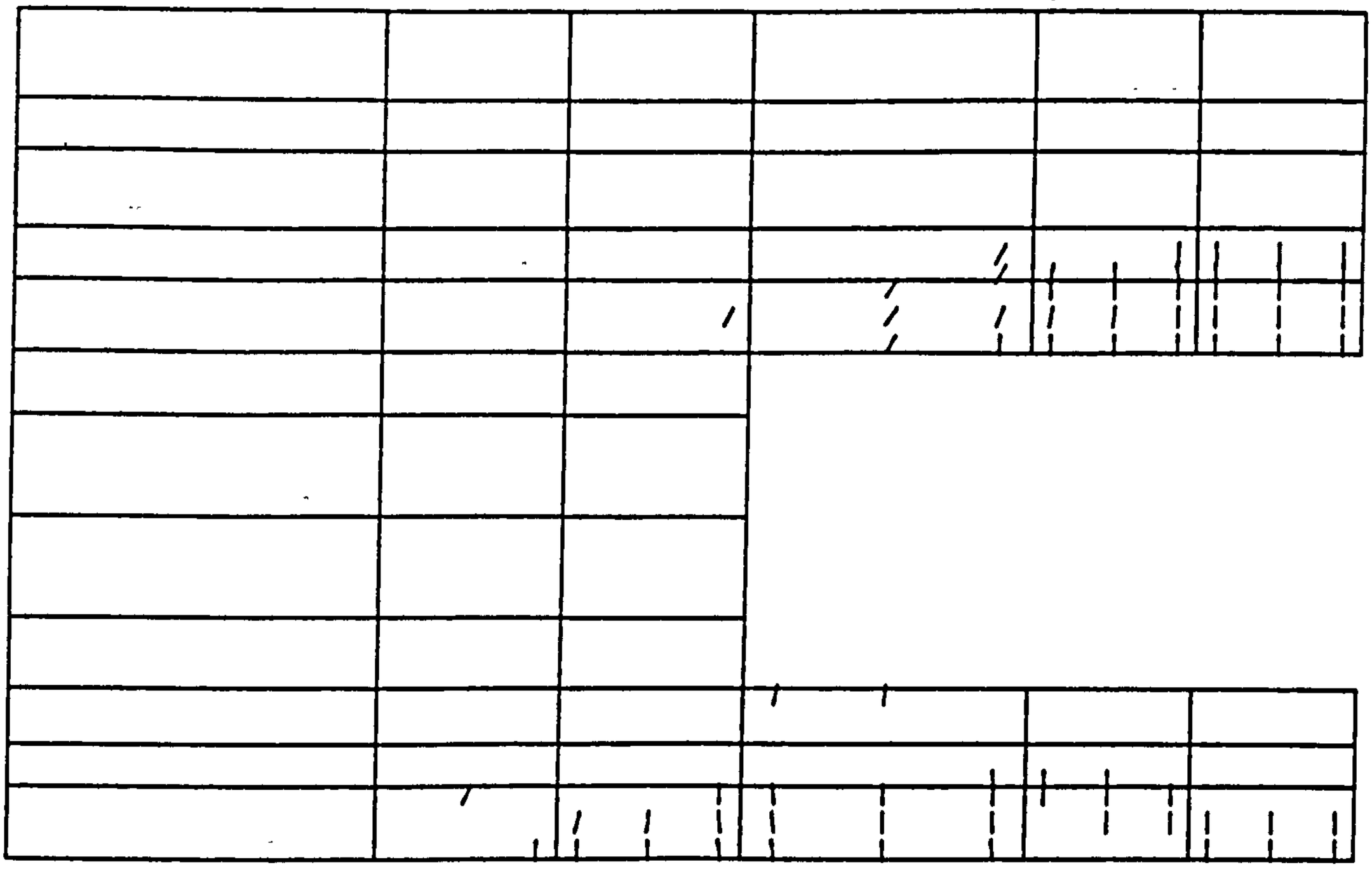

Figure (7·63) Crack pattern at load = 900·0 kN.

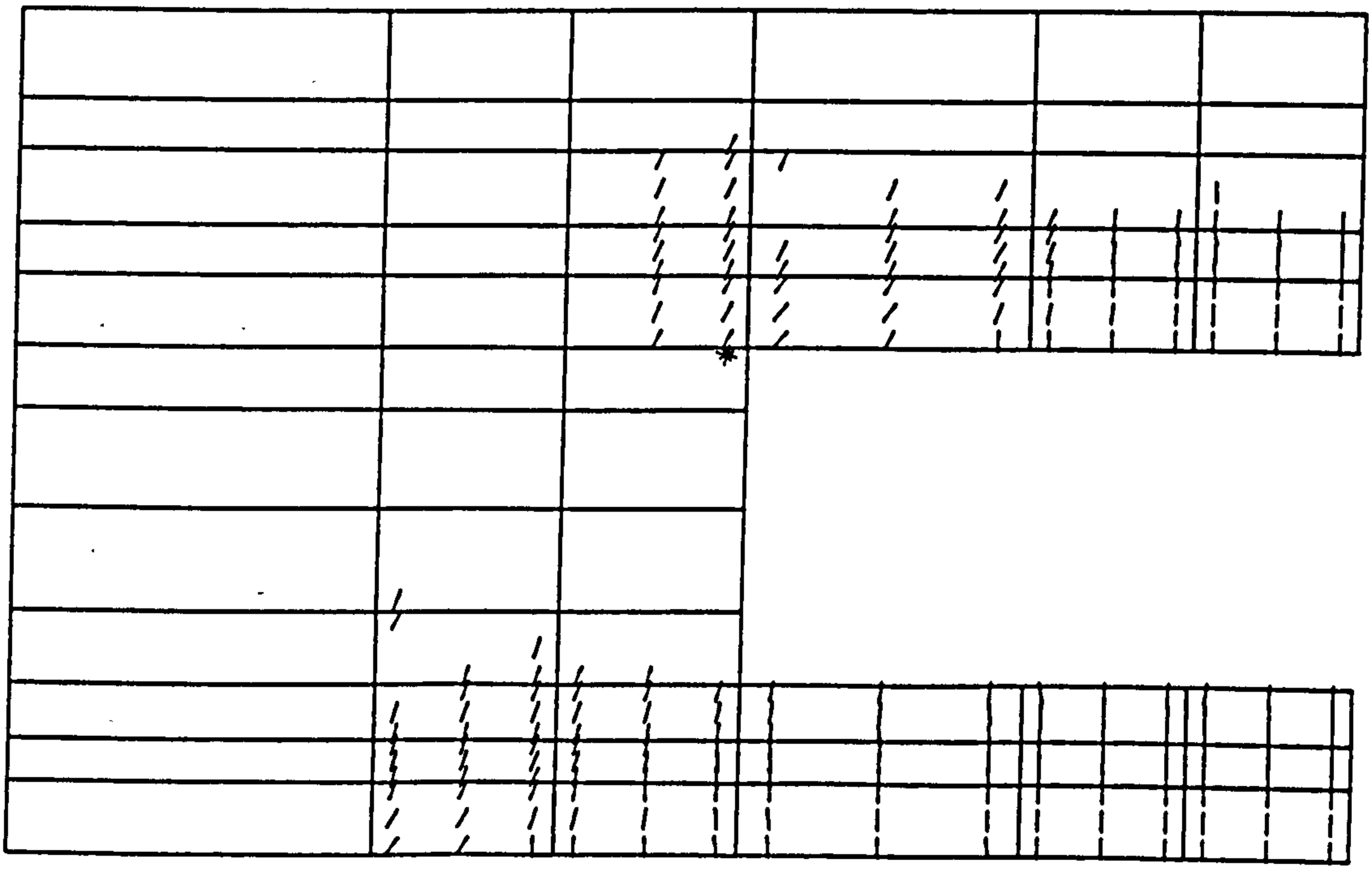

Figure (7·64) Crack pattern at load = 1000·0 kN.

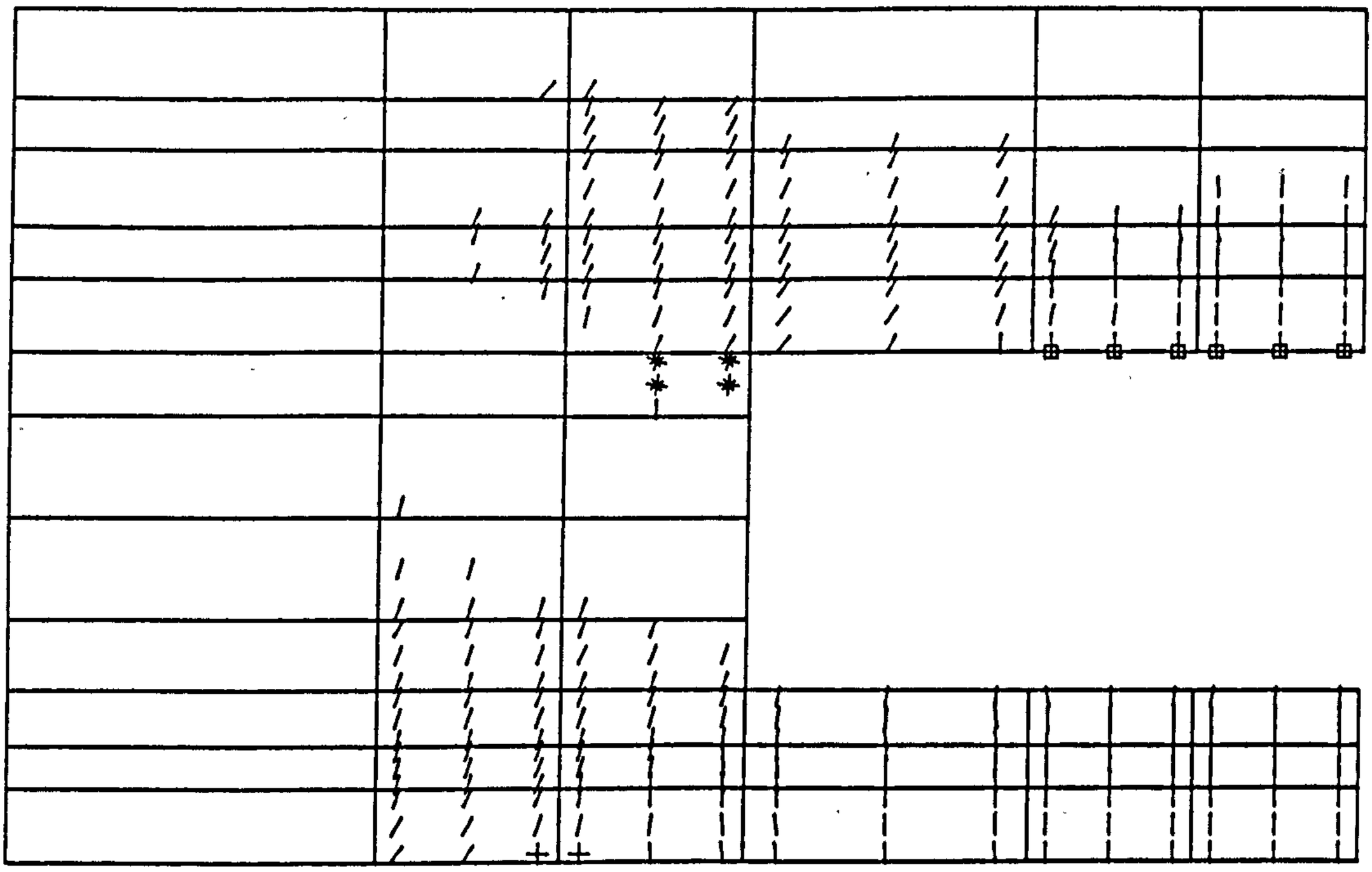

Figure (7·65) Crack pattern at load = 1350·0 kN.

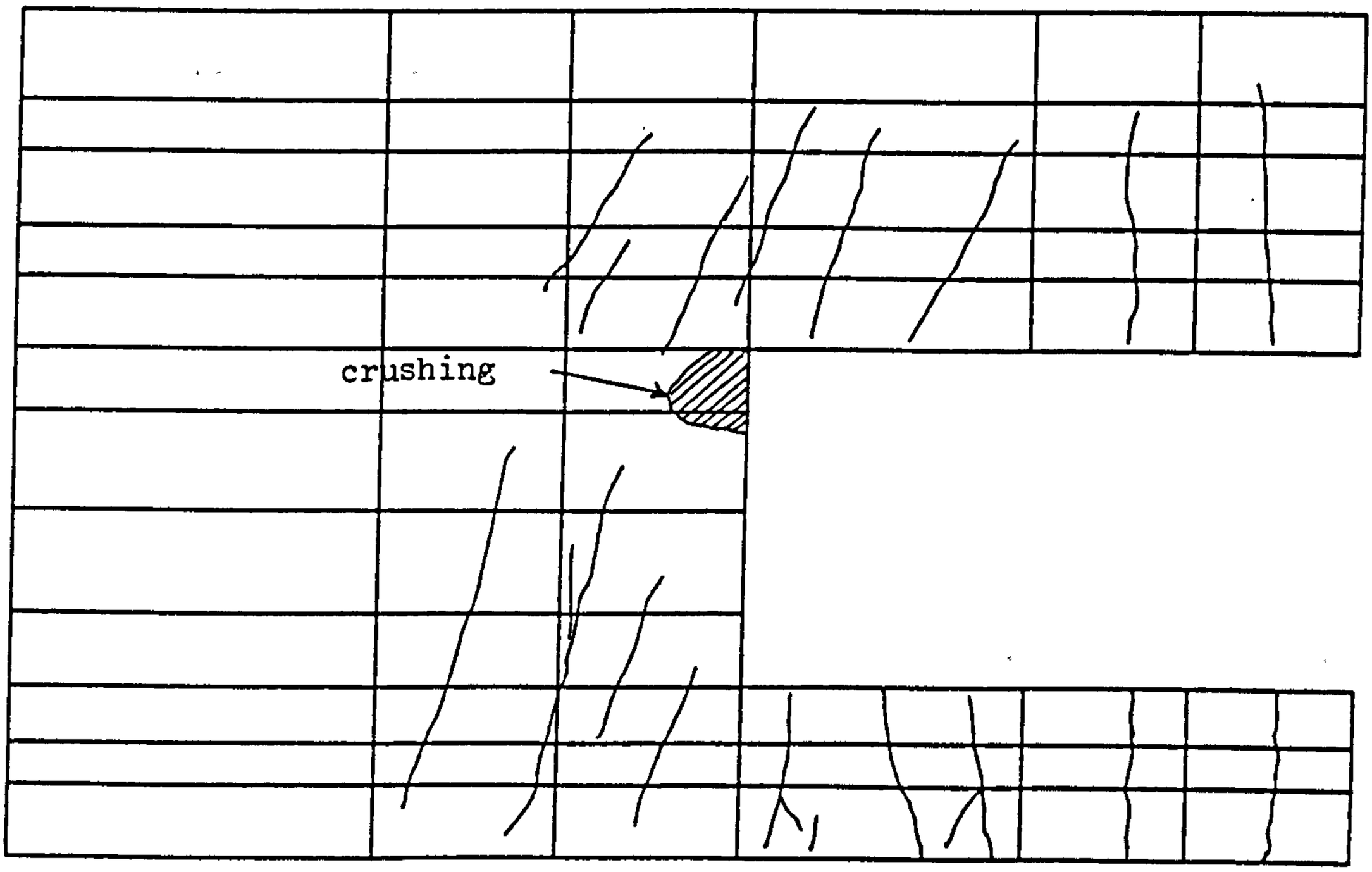

Figure (7·66) Experimental crack pattern at load = 1600·0 kN.

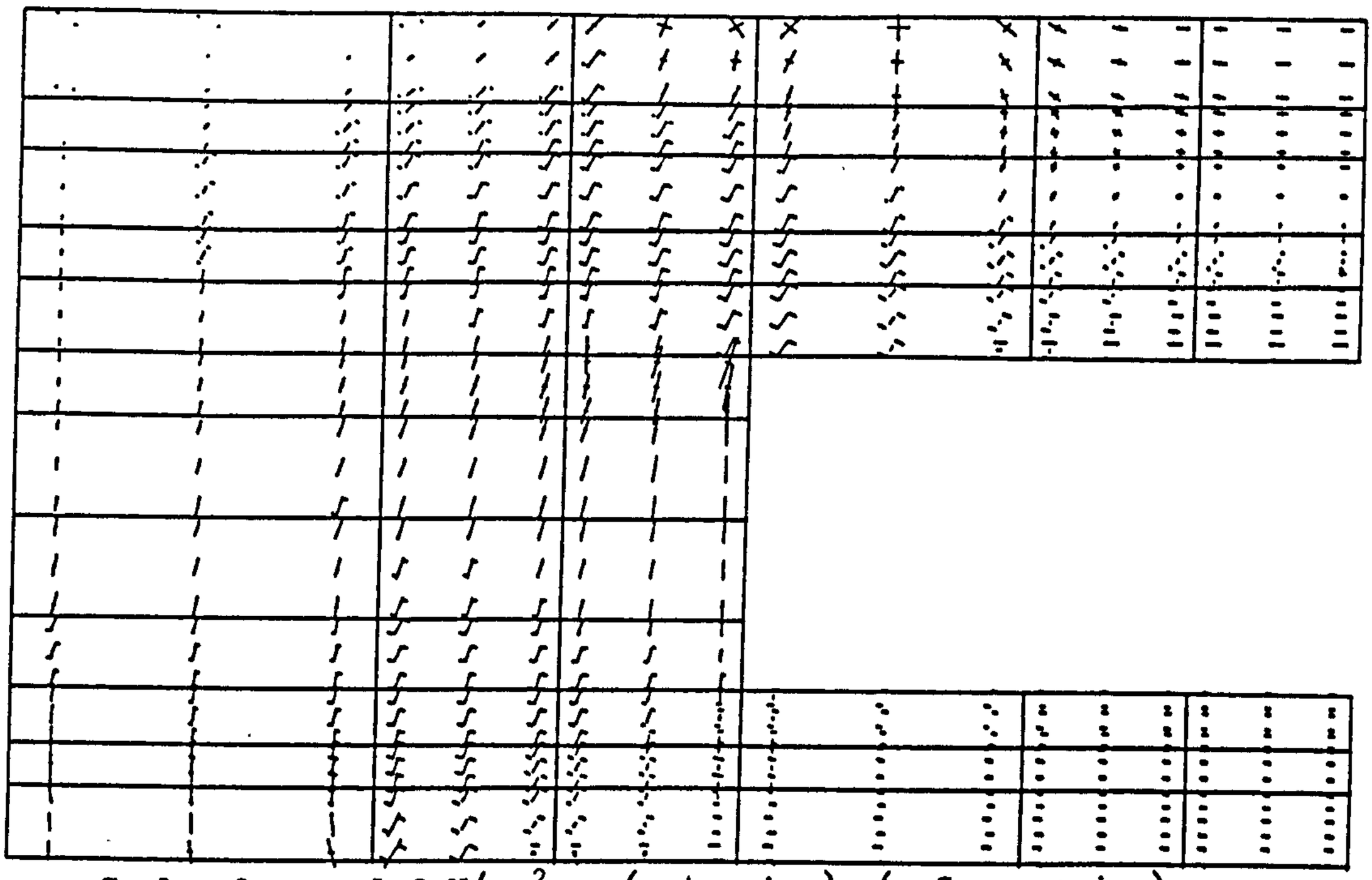

Scale: 1 mm = 1·2 N/mm^2 (= tension), (- Compression)

Figure (7·67) Principal stress direction at load = 150·0 kN.

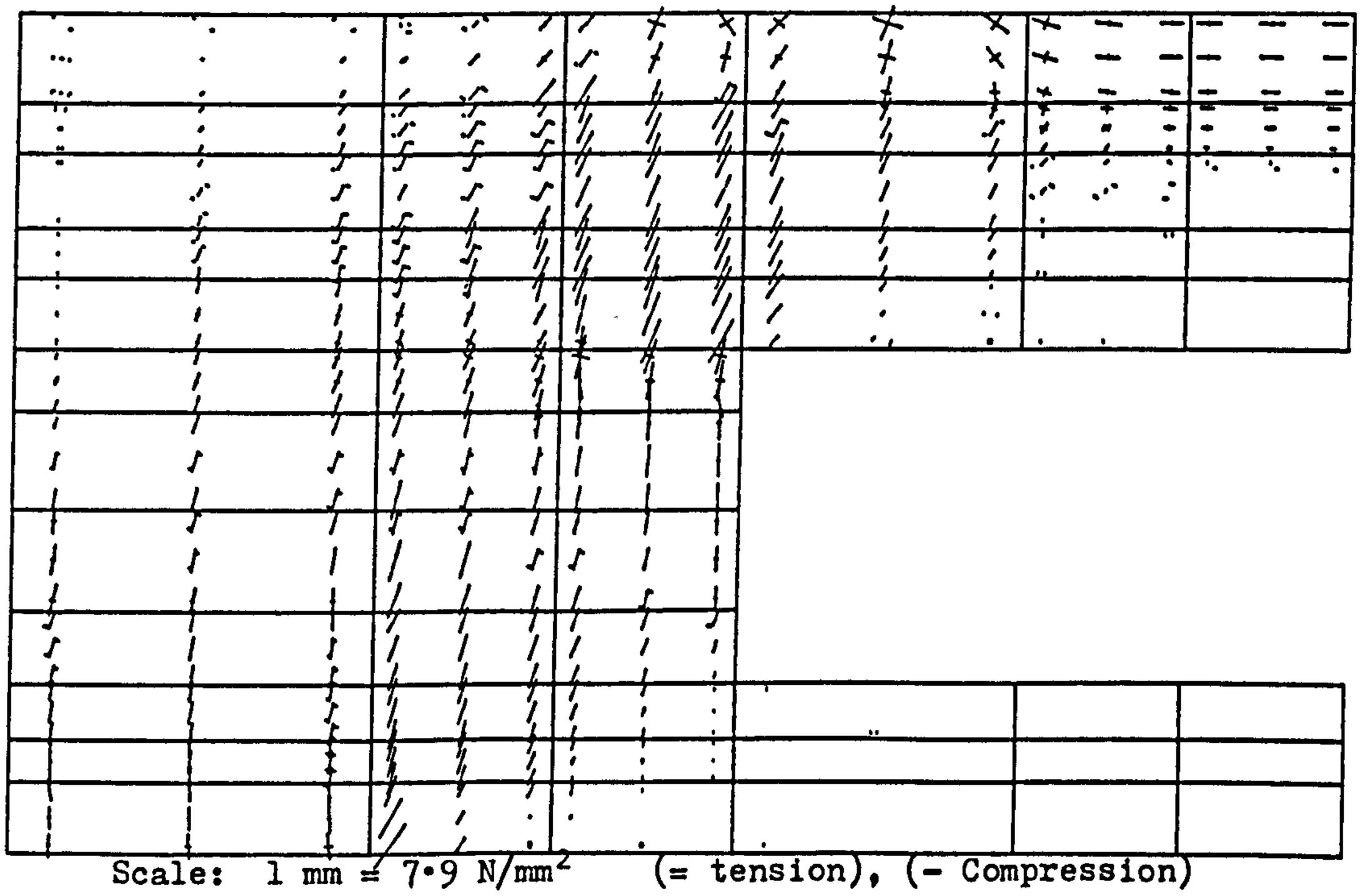

Scale: 1 mm = 7·9 N/mm^2 (= tension), (- Compression)

Figure (7·68) Principal stress direction at load = 1350·0 kN.

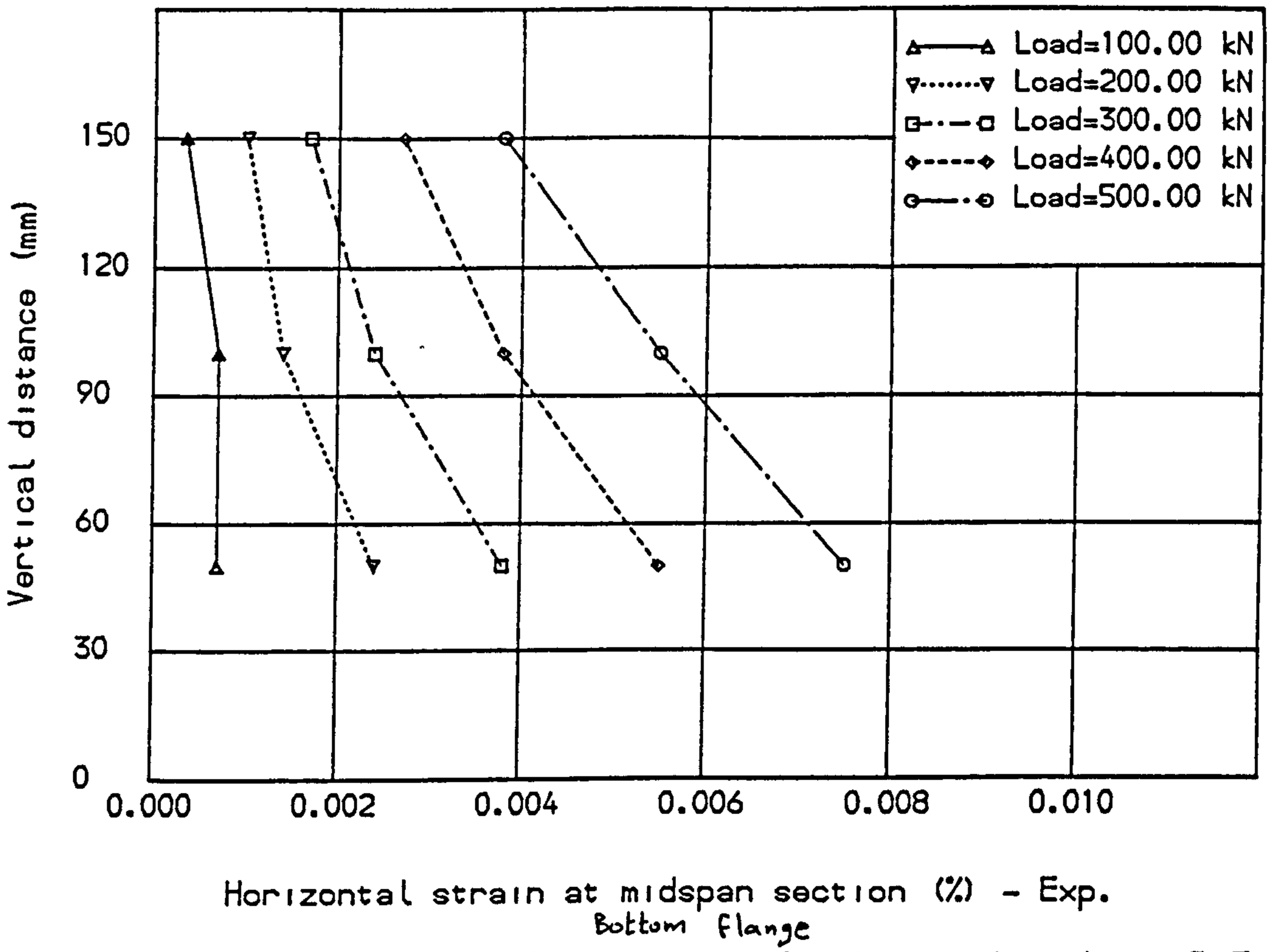

Fig. (7.69) Concrete surface strain for Memon deep beam B-5.

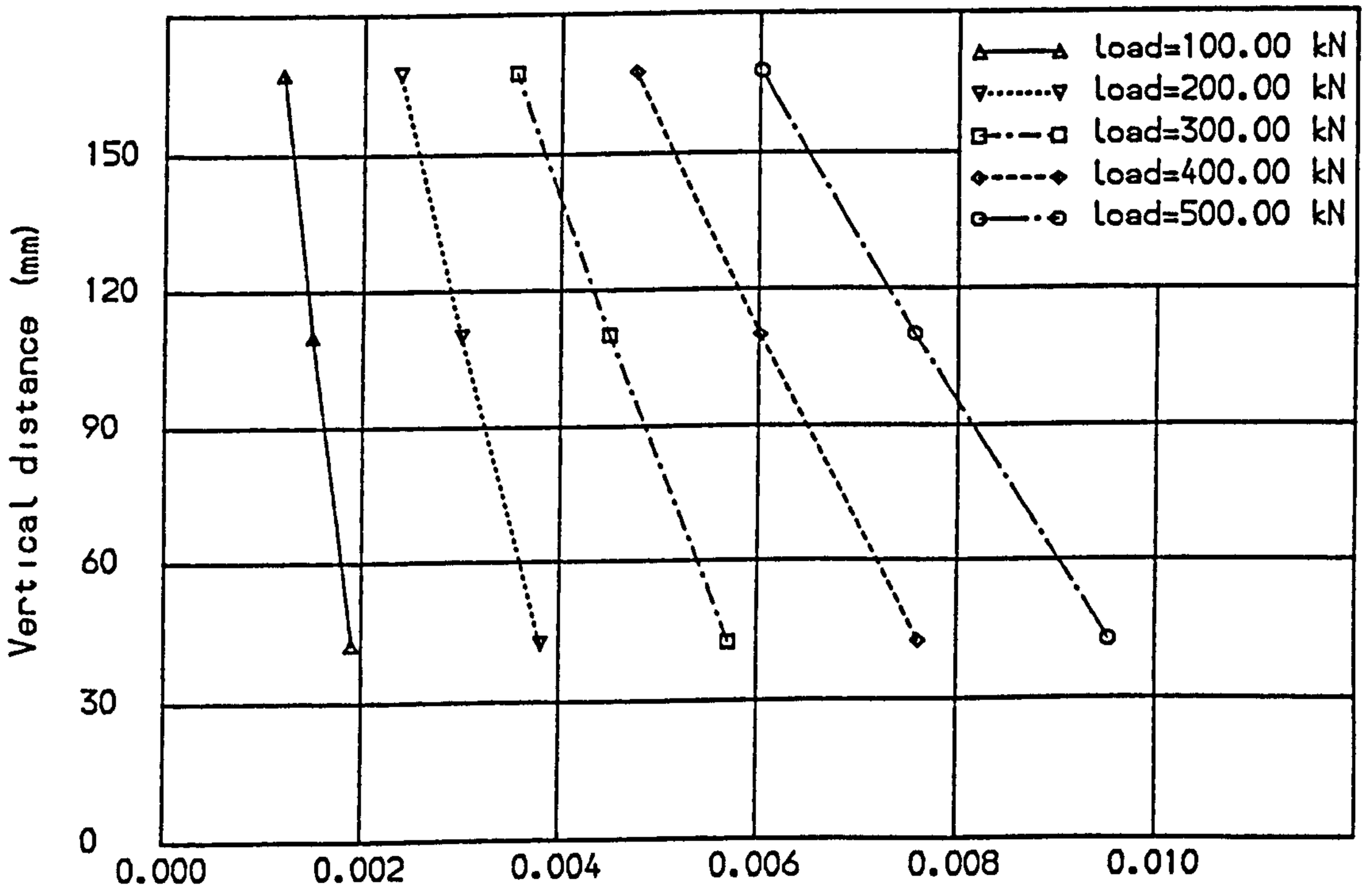

Fig. (7.70) Concrete surface strain for Memon deep beam B-5.

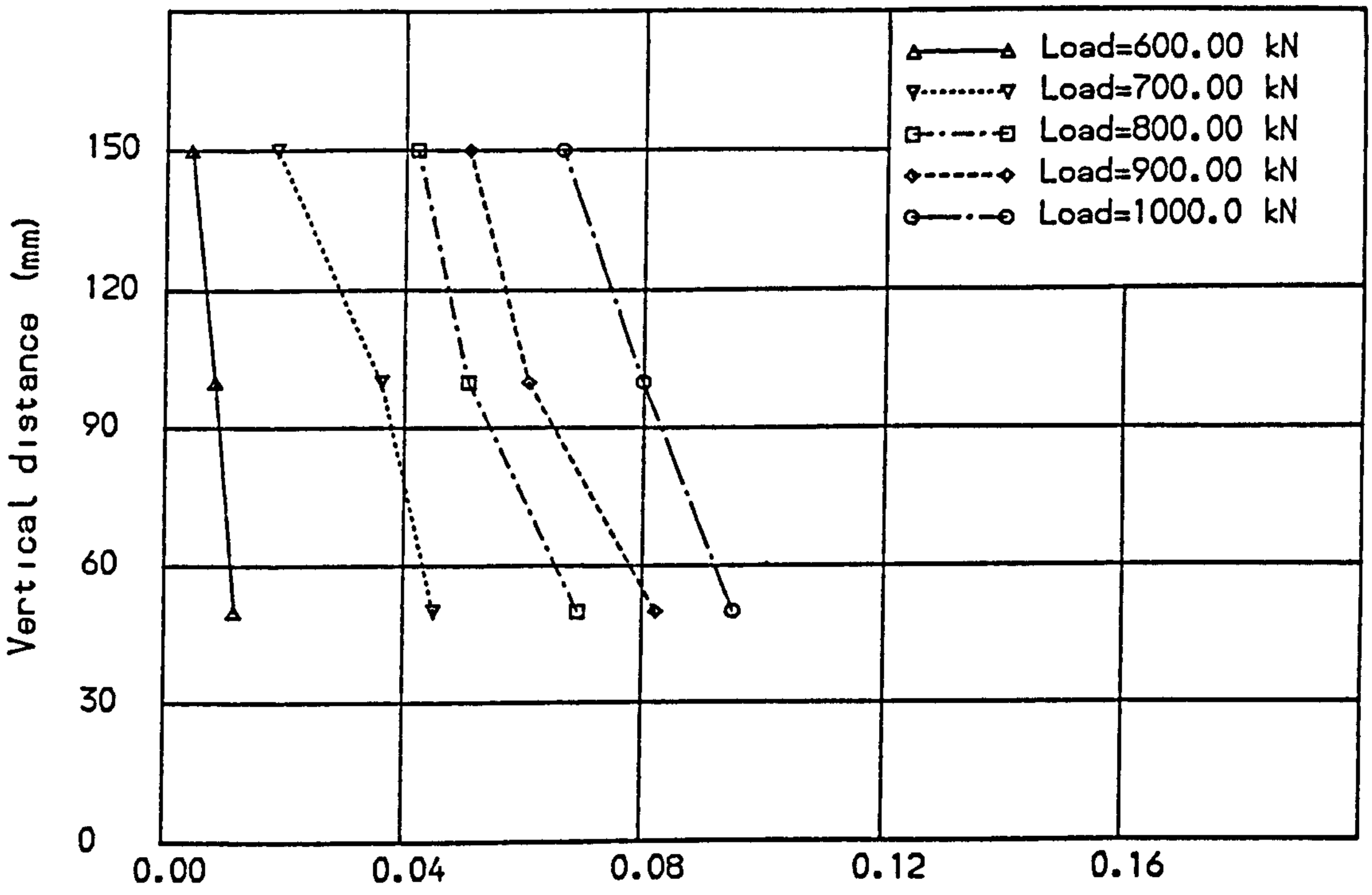

Fig. (7.71) Concrete surface strain for Memon deep beam B-5.

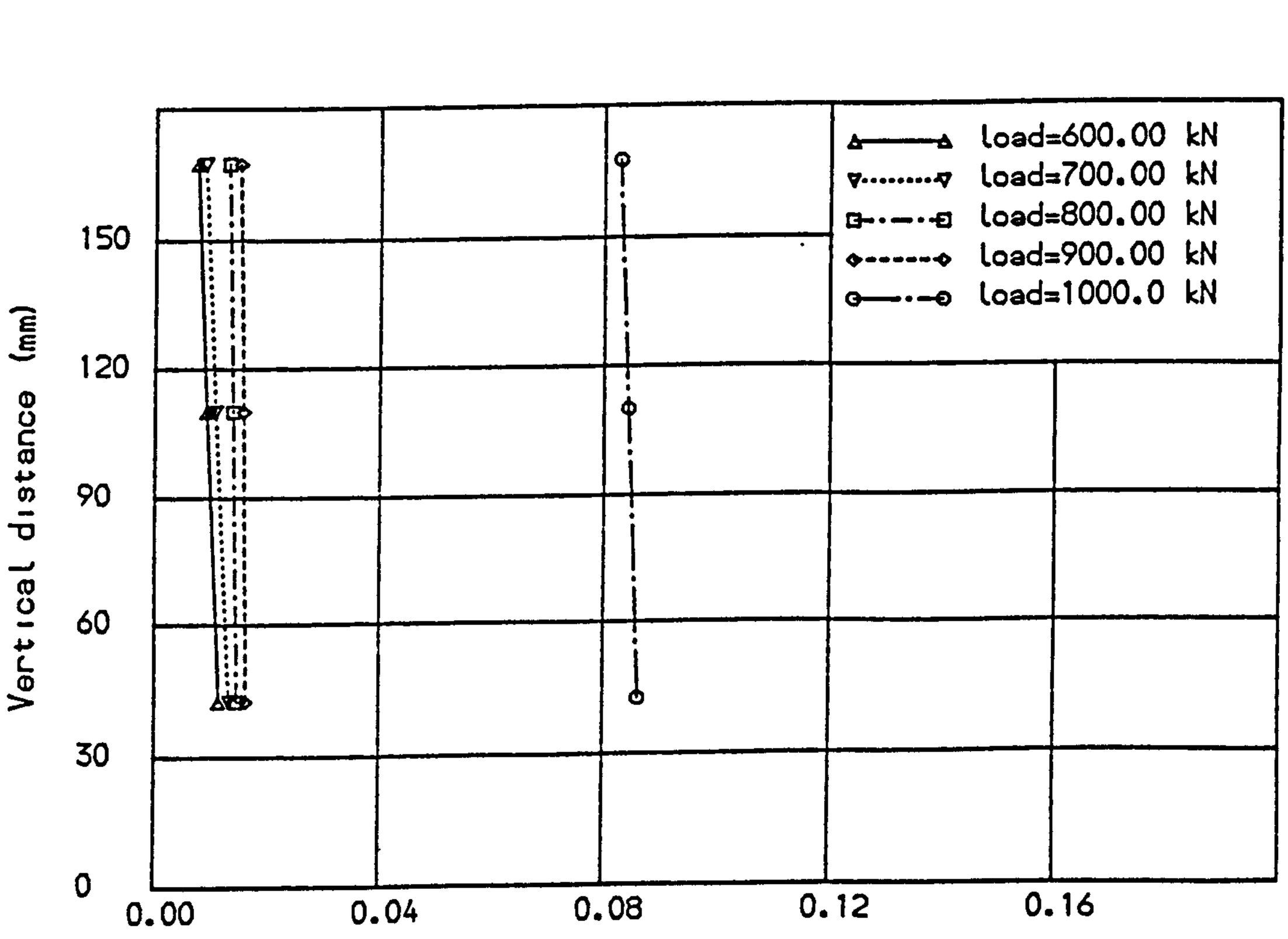

Fig. (7.72) Concrete surface strain for Memon deep beam B-5.

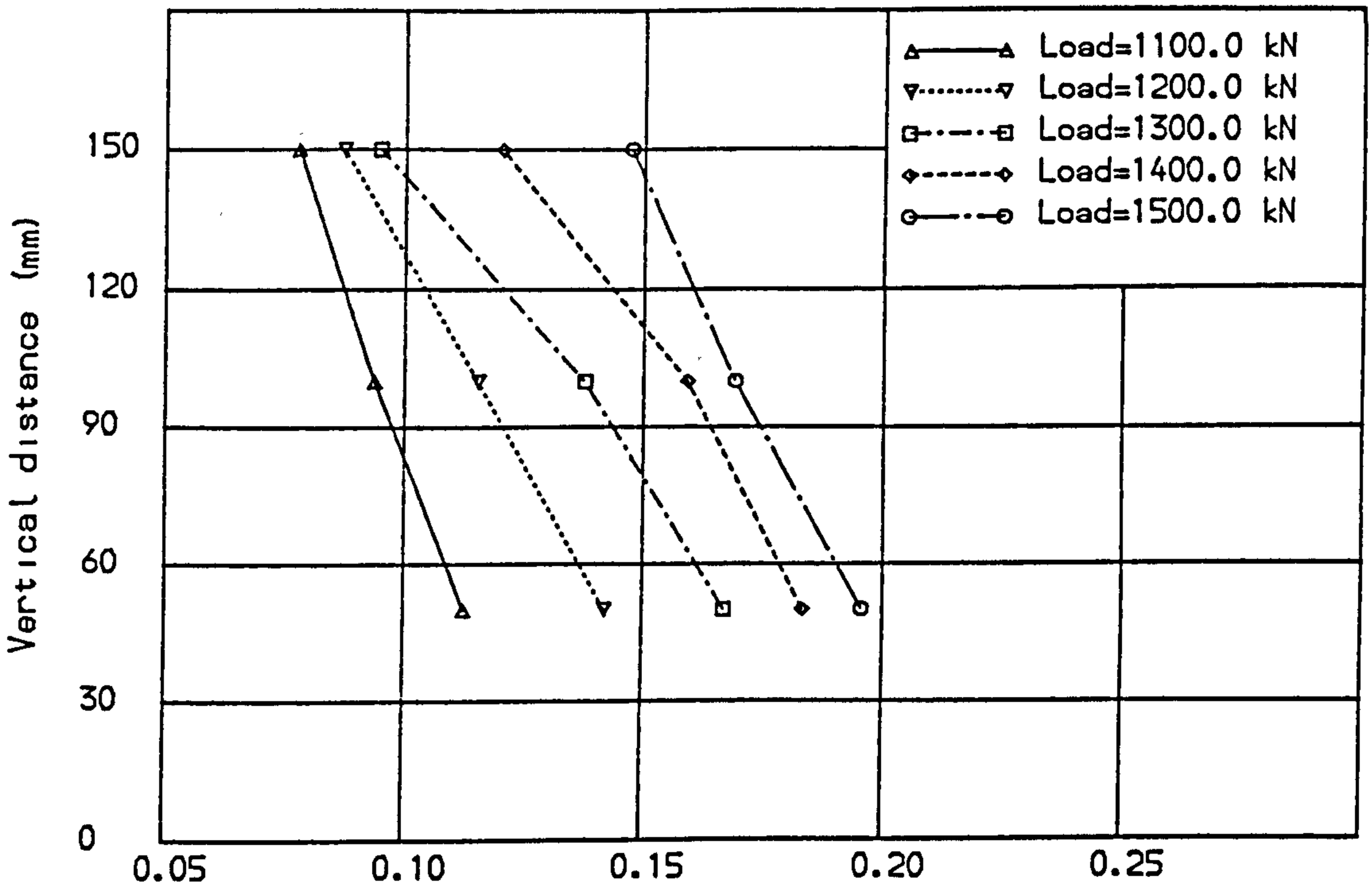

Fig. (7.73) Concrete surface strain for Memon deep beam B-5.

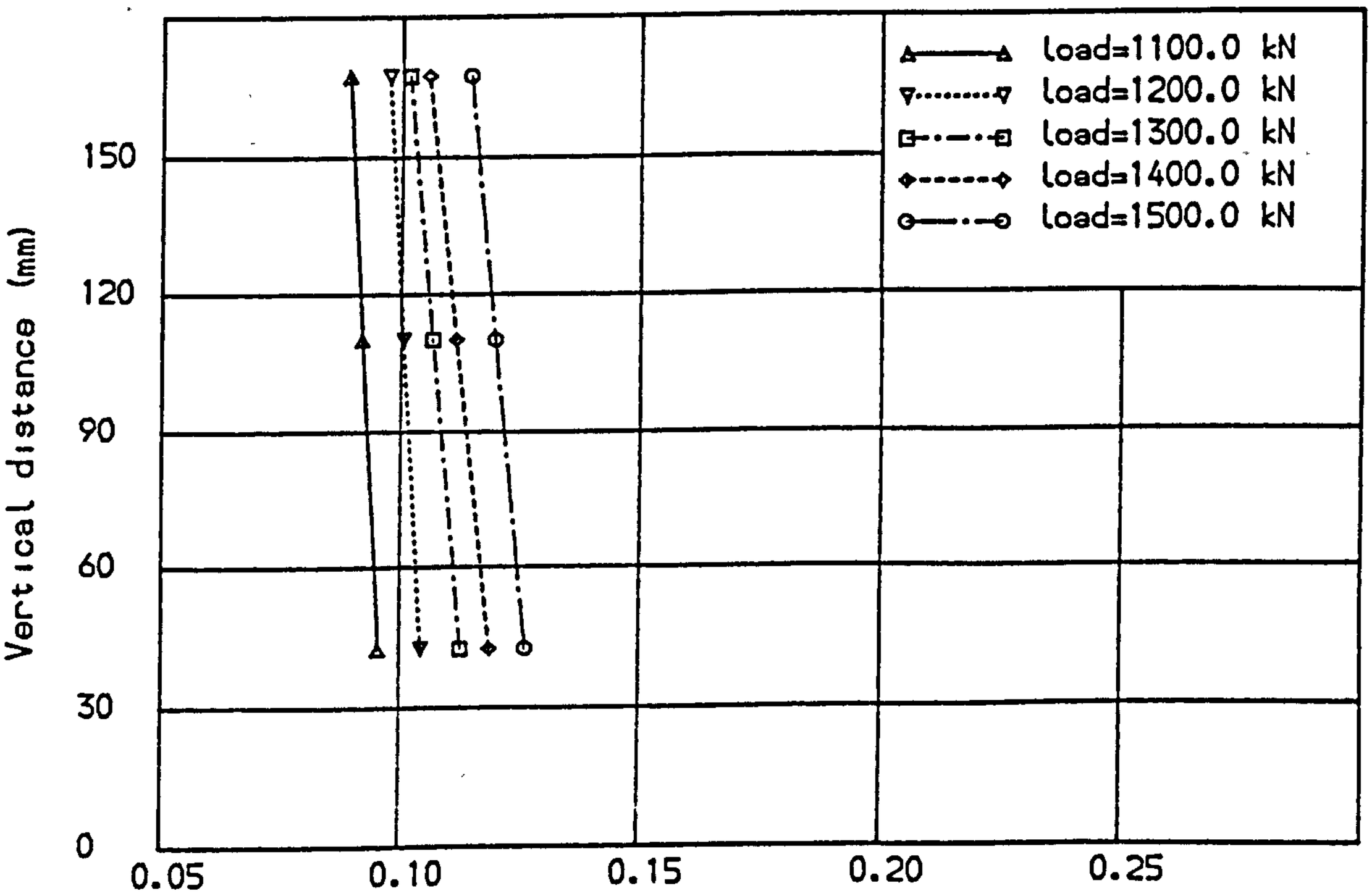

Fig. (7.74) Concrete surface strain for Memon deep beam B-5.

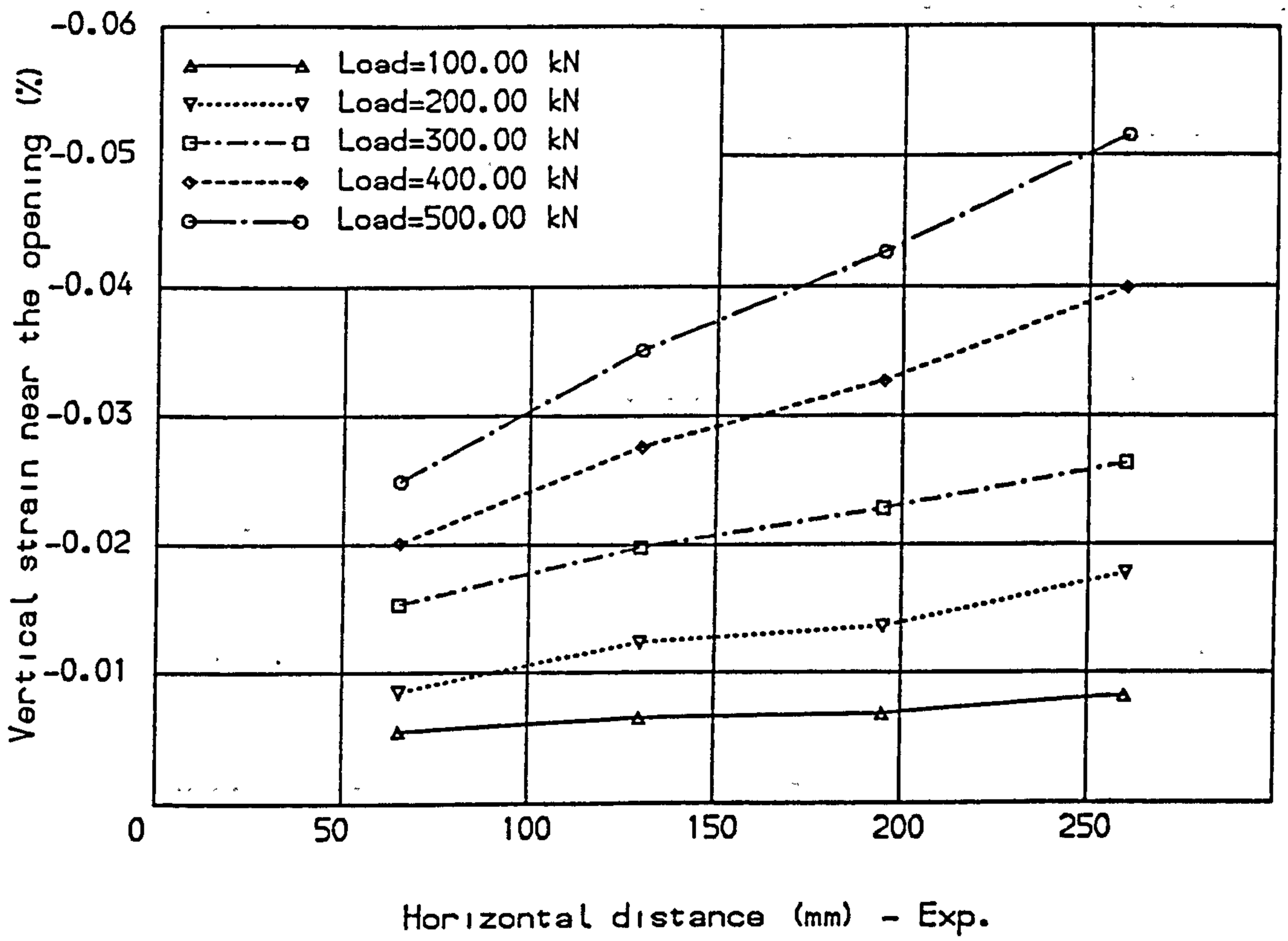

Fig. (7.75) Concrete surface strain for Memon deep beam B-5.

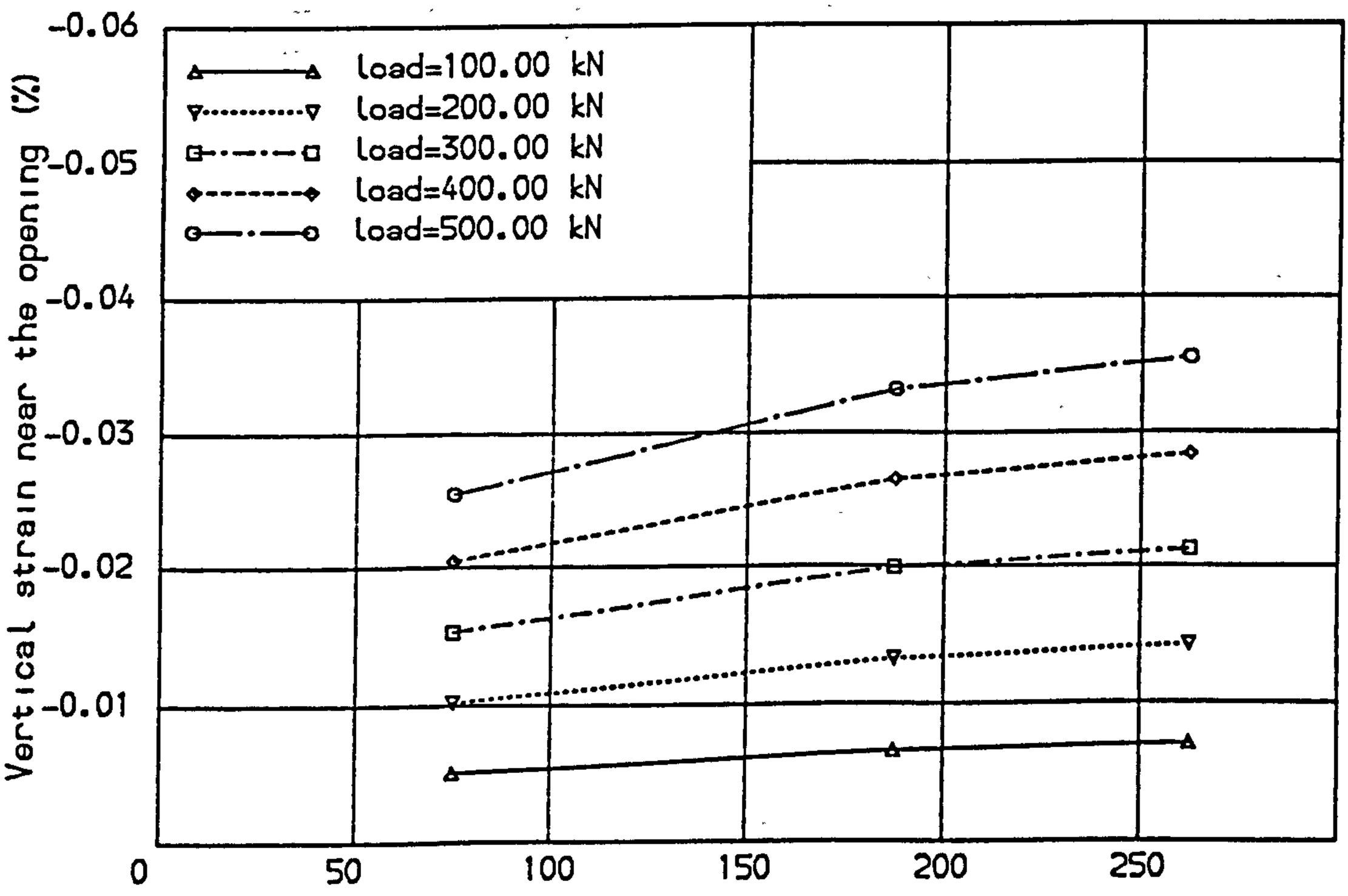

Fig. (7.76) Concrete surface strain for Memon deep beam B-5.

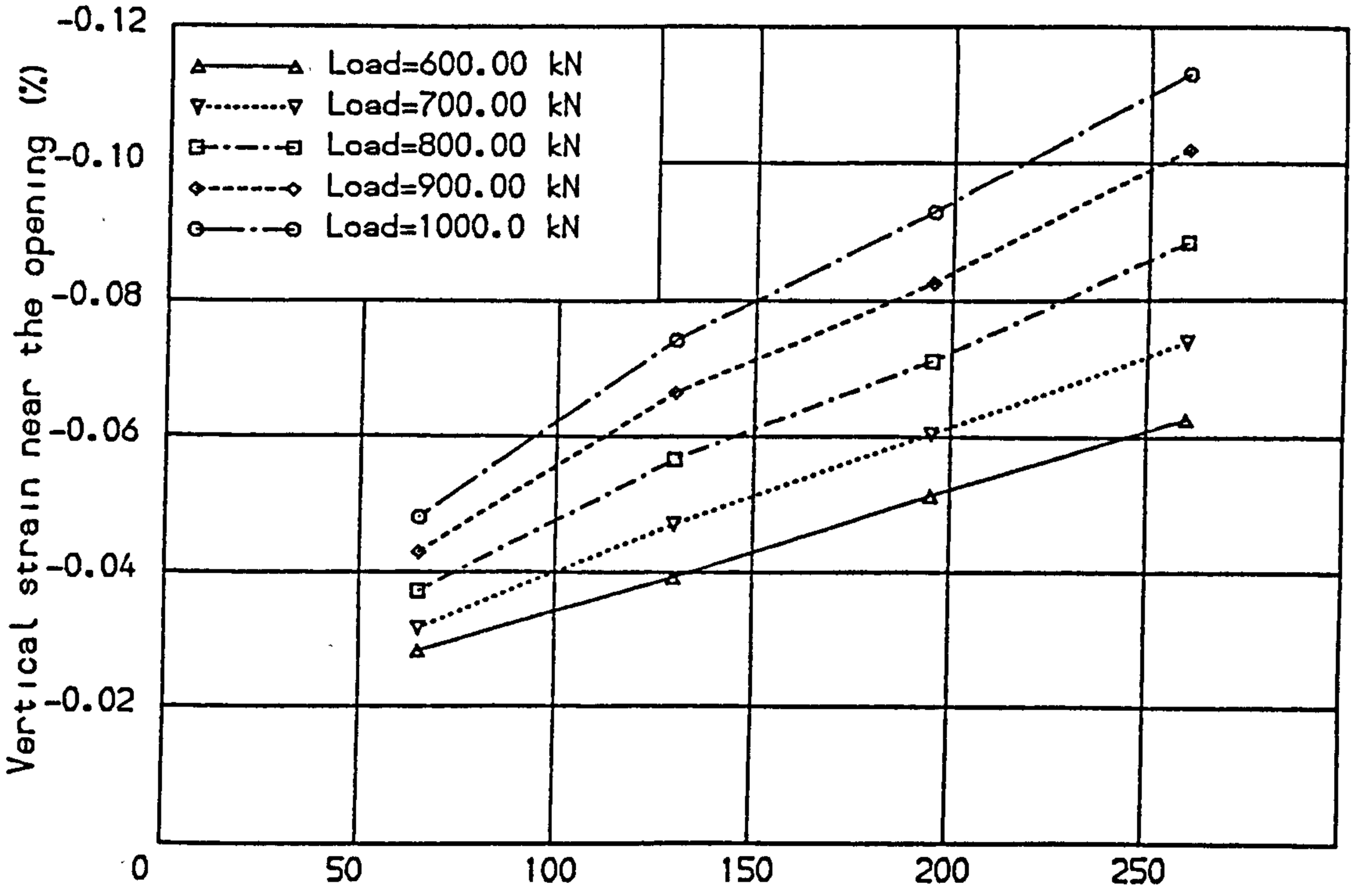

Fig. (7.77) Concrete surface strain for Memon deep beam B-5.

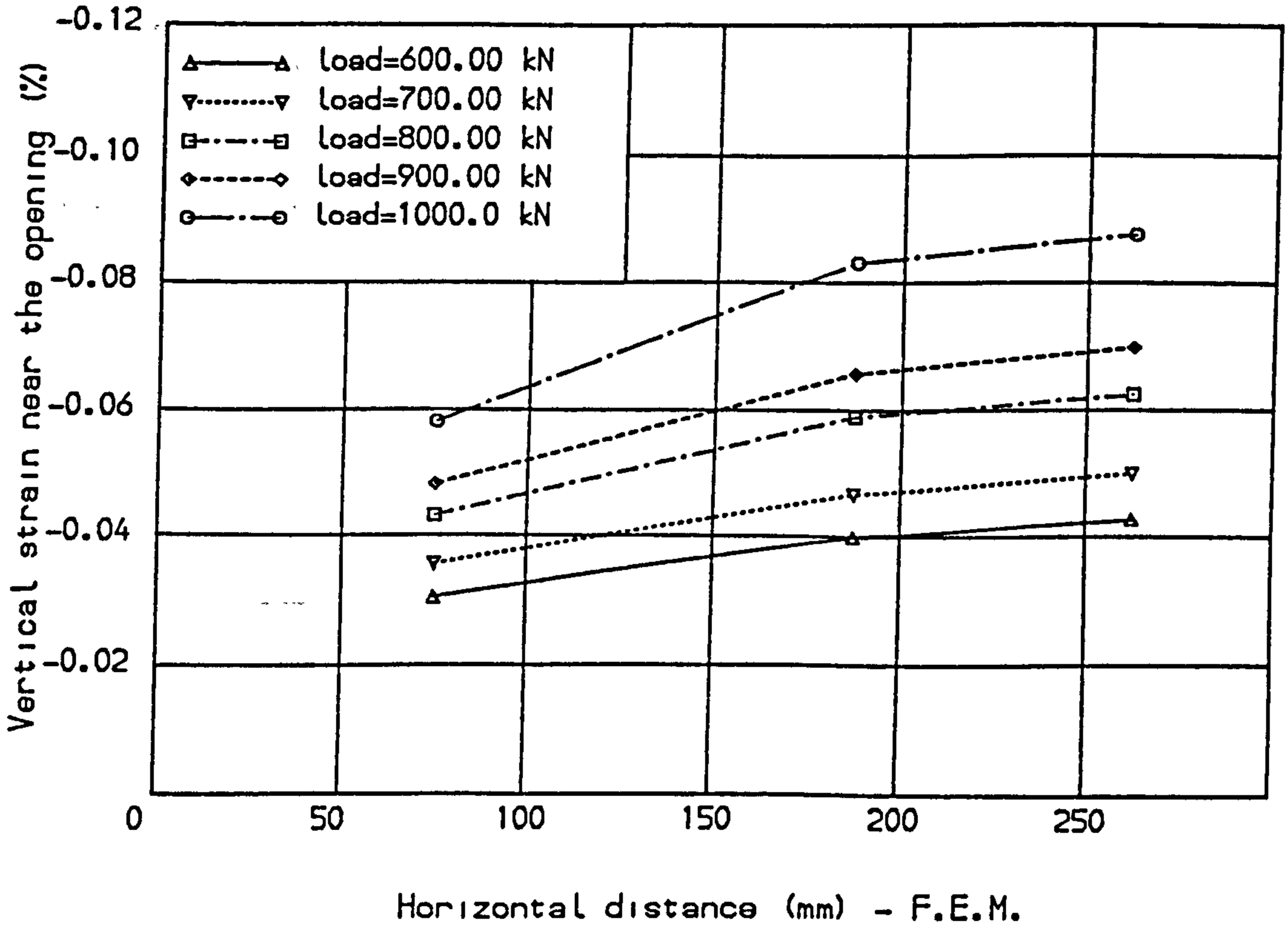

Fig. (7.78) Concrete surface strain for Memon deep beam B-5.

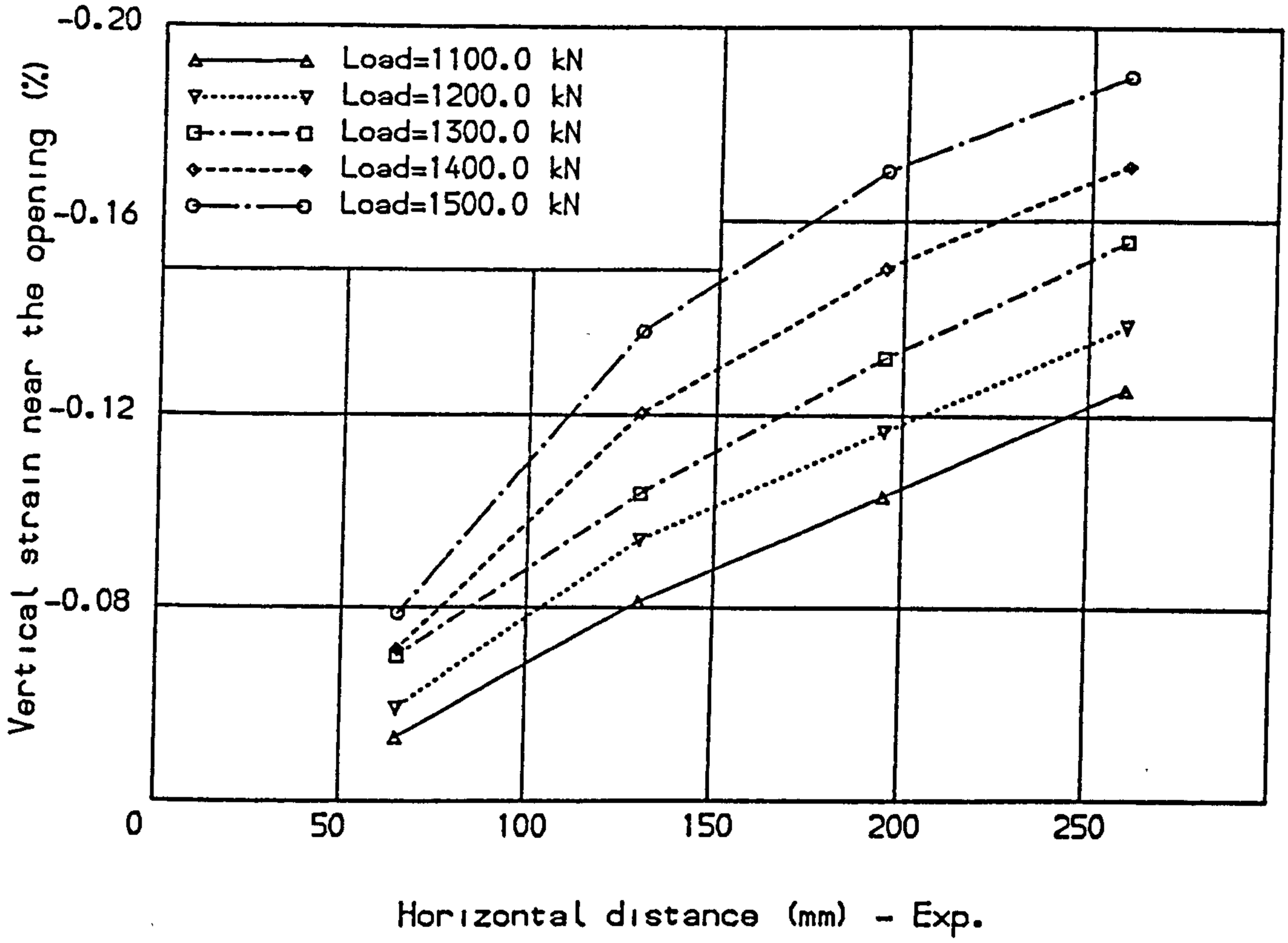

Fig. (7.79) Concrete surface strain for Memon deep beam B-5.

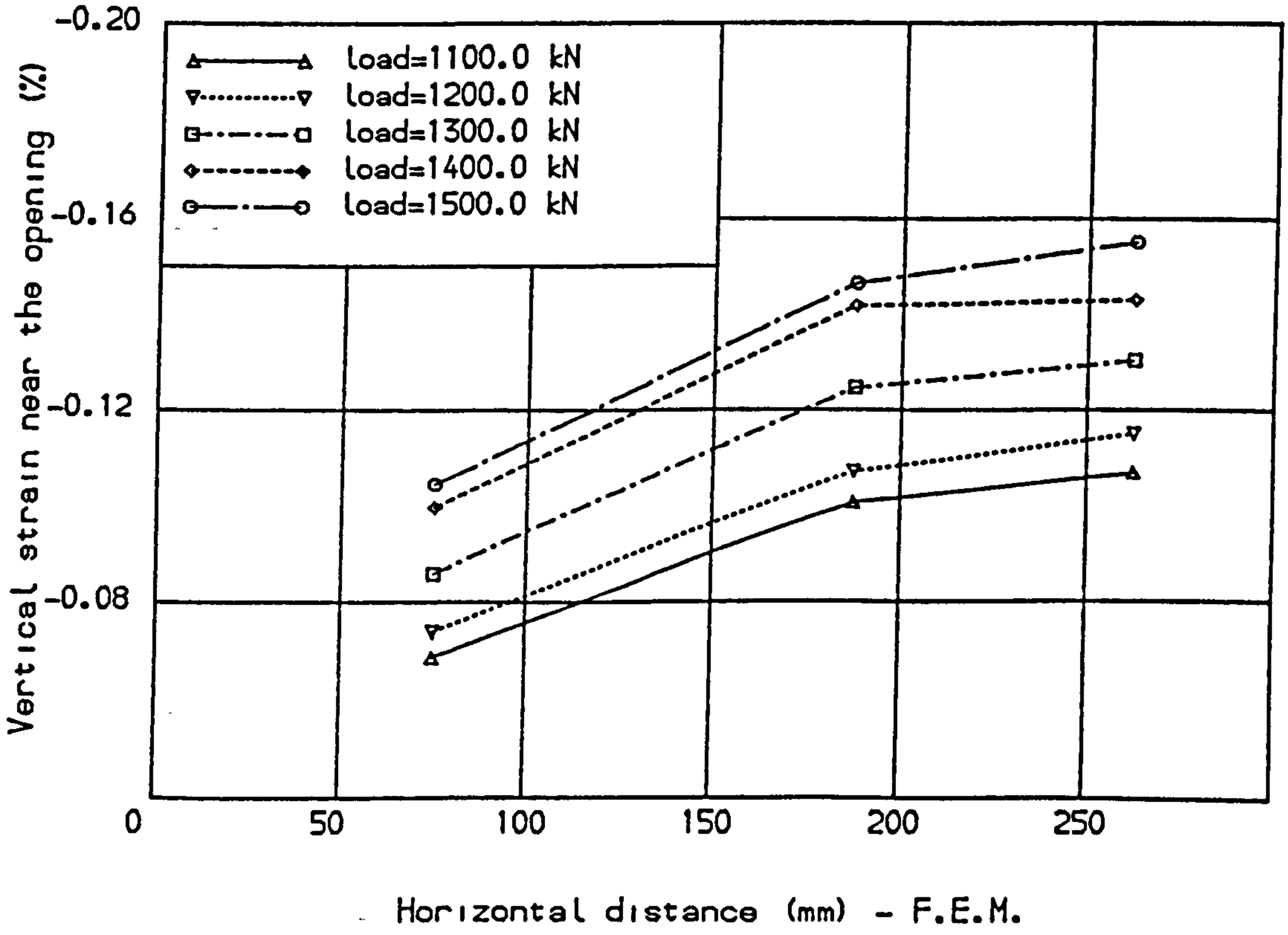

Fig. (7.80) Concrete surface strain for Memon deep beam B-5.

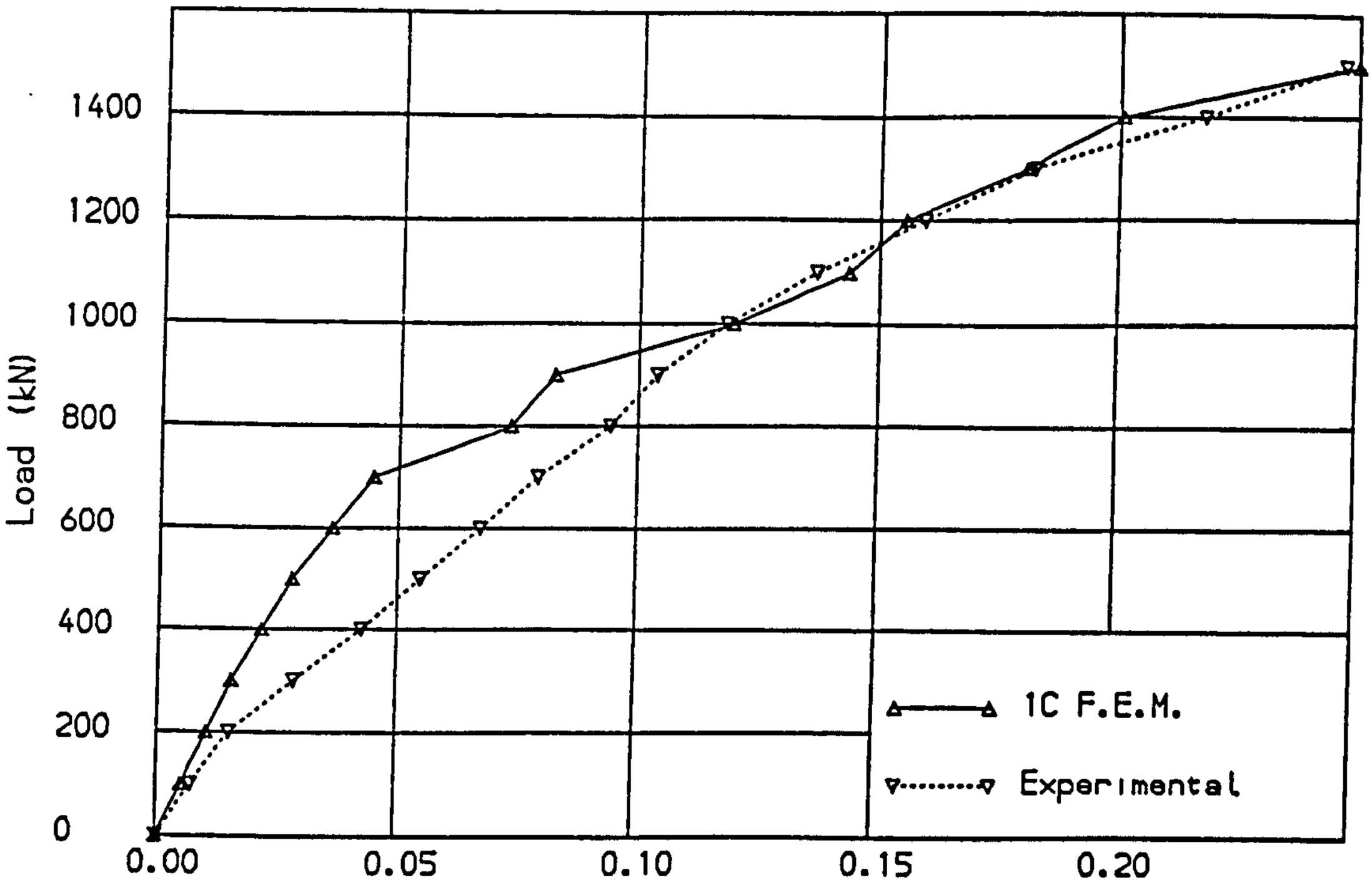

Fig. (7.81) Steel surface strain for Memon deep beam B-5.

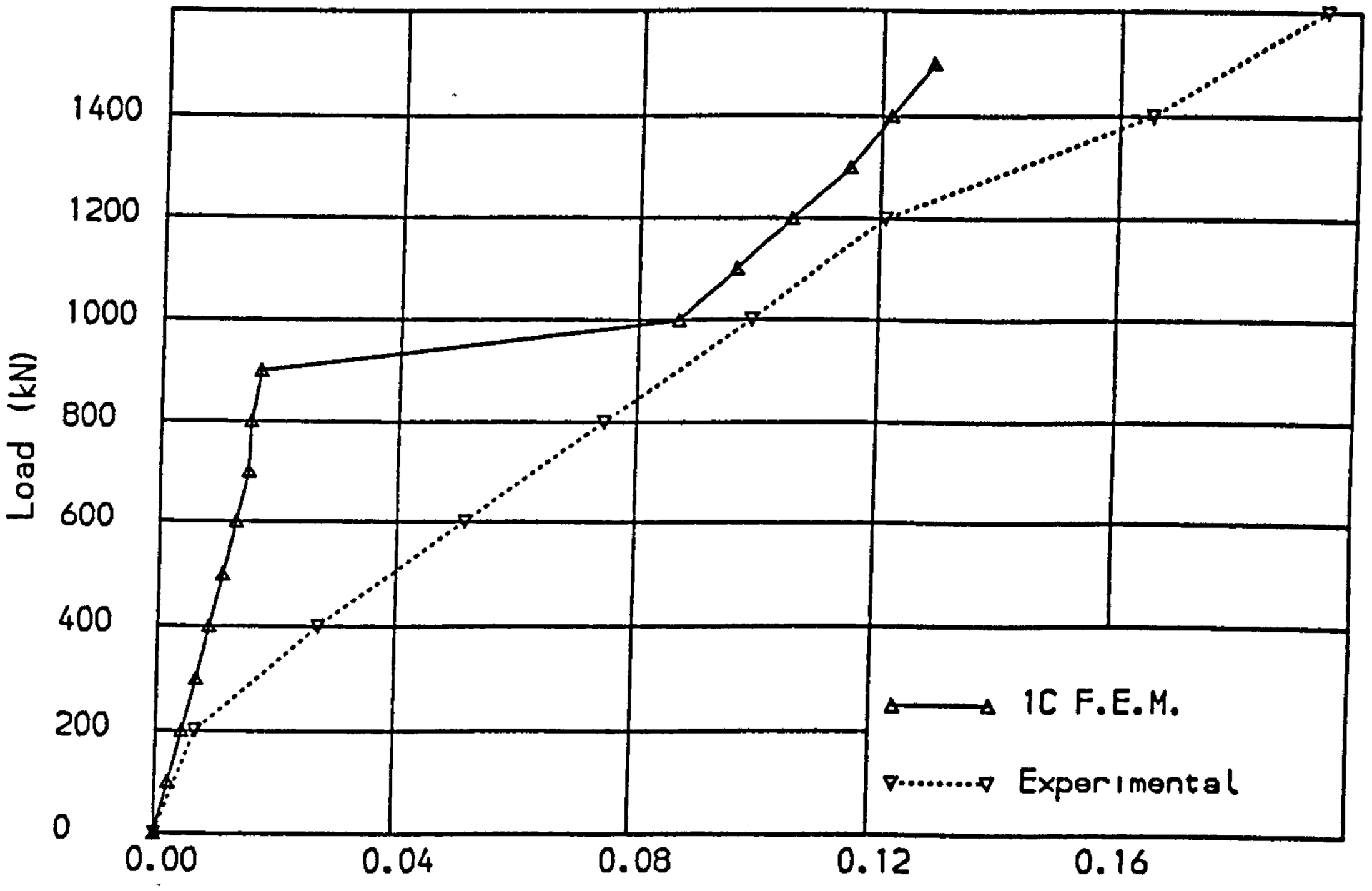

Fig. (7.82) Steel surface strain for Memon deep beam B-5.

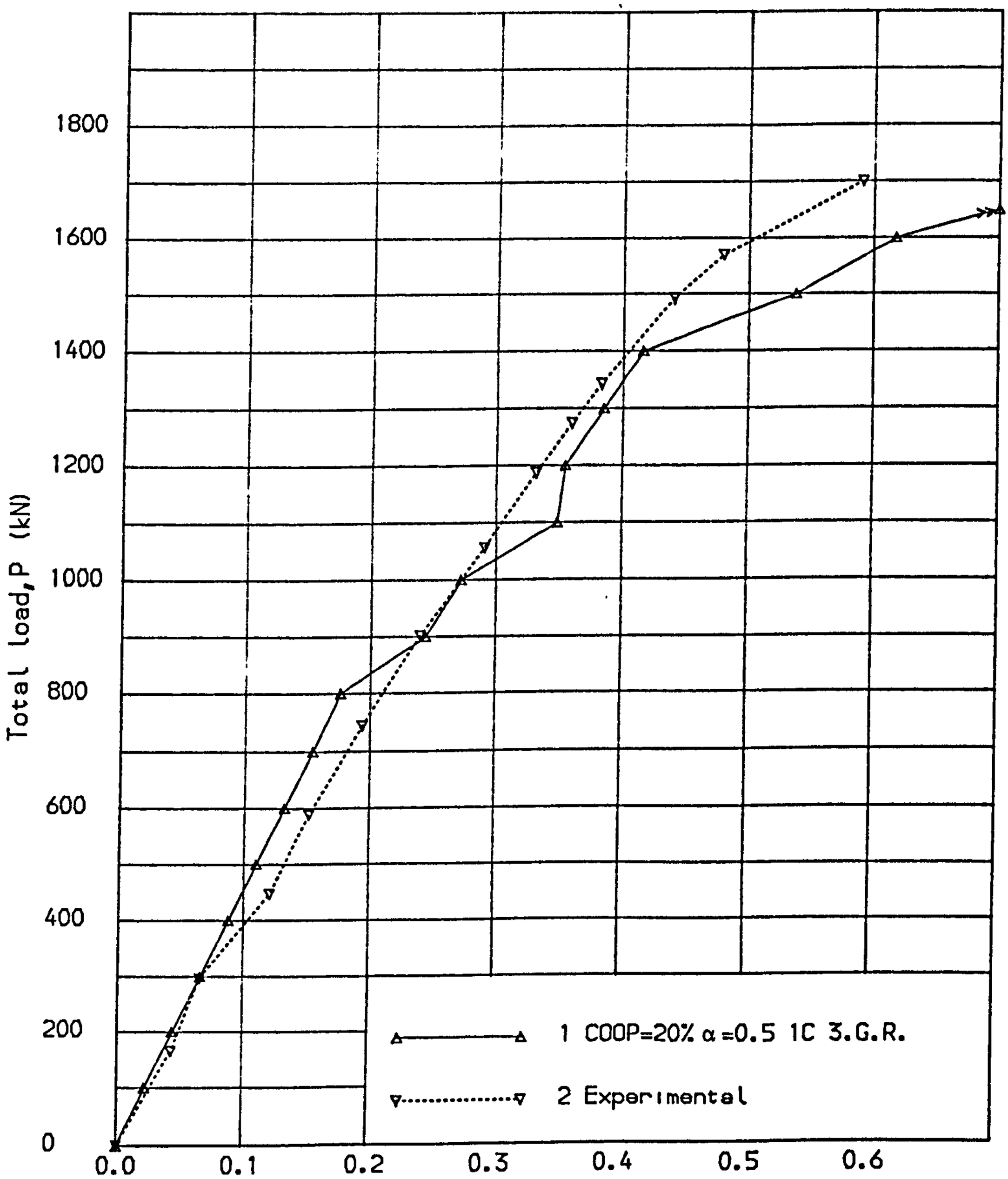

Fig. (7.83) Load deflection curves for Memon deep beam B-7.

REFERENCES

1. Cervenka, V., "Inelastic finite element analysis of reinforced concrete panels under inplane loads". Ph.D. Thesis, University of Colorado, 1970.
2. Lin, C. K., "Ultimate strength design of deep beams". M.Sc. Thesis, University of Glasgow, 1979.
3. Memon G. H., "Ultimate strength design of perforated deep beams". M.Sc. Thesis, University of Glasgow.
4. Dischinger, F., "Beitrag zur theorie der halbscheibe und des wandartigen balkens". Int. Association for Bridge and Structural Engineering, Zurich, Vol.1, 1932.
5. Chow, L.; Conway, H.D.; Morgan, G.W., "Analysis of deep beams". J. of Applied Mech., ASME, Vol.18, 163-172, June, 1951.
6. Uhlam, H. L. B., "The theory of girder walls with special reference to reinforced concrete design". The Struct. Eng., Vol.30, 172-181, Aug., 1952.
7. Chow, L.; Conway, H. D.; Winter, G., "Stresses in deep beams". J. of Struct. Div., ASCE, Vol.78, 17, May, 1952.
8. Guzman, A. M., Luisoni, C.J., "Solution variacional del problema de la viga rectangular simplements apoyada de gran altura". Cienciay Technica, Bueonos Aires 111, 1948.
9. Archer, F. E.; Kitchen, E.M., "Strain energy method for the solution of deep beams". Civil Eng. & Public Works review, Vol.52, 1375-1378, Dec. 1957.
10. Leonhardt, F.; Walther, R., "Deep beams". Wandartige Triger, Deutscher Ausschus Fur Stahlbeton, Bulletin 178, Berlin 1966, CIRIA Translation, Jan., 1970.

11. De-Paiva, H.A.R.; Siess, C.P., "Strength and behaviour of deep beams in shear". J. of Struct. Div., ASCE, Vol.91, 19-41, Oct., 1965.

12. Ramakrishnan, V.; Ananthanarayan, Y., "Ultimate strength of deep beams in shear". J. ACI, Vol. 65, 87-98, Feb., 1968.

13. Kong, F.K.; Robins, P.J.; Cole, D.F., "Web reinforcement effects on lightweight concrete deep beams". J. ACI, Vol.68, 514-520, July, 1971.

14. Kong, F.K.; Robins, P.J., "Shear strength of reinforced concrete deep beams". Concrete, Vol.6, 34-36, March, 1972.

15. Manuel, R.F.; Slight, B.W.; Suter, G.T., "Deep beam behaviour affected by length and shear span variations". J. ACI, Vol.68, 954-958, Dec., 1971.

16. Smith, K.N.; Vantsotis, "Shear strength of deep beams". J. ACI, Vol.79, 201-213, May-June, 1982.

17. Robins, P.H.; Kong, F.K., "Modified finite element method applied to RC deep beams". Civil Eng. & Public Work Review, Vol.68, 963-966, Nov., 1973.

18. Buyukozturk, O., "Nonlinear analysis of reinforced concrete structures". Comp. & Struct., Vol.7, 149-156, Feb., 1977.

19. Cedolin, L.; Dei Poli, S.; Kapru, S., "Finite element analysis of reinforced concrete deep beams", Costruzioni in Cemento Armato, Studie Rendiconti, Vol.14, Thechnical University of Milan, 1977.

20. Taner, N.; Fazio, P.P.; Zielinski, Z.A., "Strength and behaviour of beam-panels-tests and analysis". J. ACI, Vol.74, 511-520, Oct., 1977.

21. Niwi, J.; Maekawa, K.; Okamura, H., "Nonlinear finite element analysis of deep beams". IABSE Colloquium on The Advanced Mechanics of Reinforced Concrete, Final Report, Delft, 625-638.

22. Ove Arup & Partners, "The design of deep beams in reinforced concrete". Construction Industry Research and Information Association, CIRIA Guide 2, London, Jan., 1977.

23. Kong, F.K.; Sharp, G.R., "Shear strength of lightweight reinforced concrete deep beams with web openings". The Struct. Eng., Vol.51, 267-275, 1973.

24. Kong, F.K.; Sharp, G.R., "Structural idealization for deep beams with web openings". Mag. Conc. Res., Vol.29, 81-91, June, 1977.

25. Kong, F.K.; Sharp, G.R.; Appleton, S.C.; Beaumont, C.J.; Kubik, L.A., "Structural idealization for deep beams with web openings: further evidence". Mag. Conc. Res., Vol.30, 89-95, June, 1978.

26. Kubik, L.A., "Predicting the strength of reinforced concrete deep beams with web opening". Proc. Inst. Civ. Eng., Part 2, 939-958, Dec., 1980.

27. Phillips, D.V., "Nonlinear analysis of structural concrete by finite element method". Ph.D. Thesis, University of Wales, 1973.

CHAPTER 8

APPLICATION TO T-BEAMS

8.1 Introduction

8.2 General description of T-beams behaviour

8.3 Proposed theoretical model

8.4 Selection of axis of separation

8.5 Description of beams tested

8.6 Description of results

8.7 Conclusions

CHAPTER 8
APPLICATION TO T-BEAMS

8.1 Introduction:

The behaviour of T-beams is generally in the three dimensional category. This is because the flange exists in a plane perpendicular to the web. The objective of this chapter is to investigate whether the essential features of the behaviour of T-beams can be obtained by using a simple two dimensional plane stress approximation, which would be cheaper than using a three dimensional approach, or by using shell or plate approximations. This is especially attractive when it is considered that more expensive complex nonlinear approximations are not guaranteed to give satisfactory results anyway because of the influence of numerical parameters, material properties etc., as the previous chapters have shown.

Only a few investigators have reported the use of the finite element method to analyse T-beams. Cope et al.[1] used a composite shell element where compatibility of in-plane rotational displacement at common mesh lines of elements in different planes were ignored. The effect of changing the amount of reinforcement and the effect of web width on shear strength was studied. Deflections were underestimated in some beams at the beginning, but in general the predicted cracking patterns and failure loads agreed well with experimental results.

Razagpur et al.[2] studied the effect of shear transfer at the web-flange connection and the interaction of this shear with the transverse bending. The analysis was carried out using a combination of in-plane quadrilateral elements and quadrilateral plate bending elements. Satisfactory results were obtained in most situations except in the prediction of the stresses in the flange reinforcement, where

good results were reported only in some cases. This was thought to be due to the inadequate mathematical models where the effect of shear was dominant.

Much more experimental knowledge of T-beam behaviour exists. A wide survey on existing literature was reported by Fok[13] in 1972. Fok carried out an experimental study investigating the shear strength of simply supported T-beams under two point concentrated loads, and the effect of flange dimensions on the ultimate load. Recently Chong[4] in 1980 completed Fok's study by testing the same beams with uniformly distributed loads. Other investigators have studied different aspects, for example Swamy[5] studied the influence of flange width on shear behaviour, Taylor et al.[6] tested different T-beams with different types of reinforcement, Scribner et al.[7] studied cyclic behaviour using different types of stirrups, etc. These will not be discussed in this thesis and readers are referred to the appropriate references.

This chapter is concerned with presenting the proposed approximate method of T-beam analysis by comparing it with some beams presented in the literature; one beam was tested by Cope et al.[1] and failed in flexure, the other beams were tested by Chong[4] and failed in shear. Details of these are discussed in section 8.5.

8.2 General description of T-beams behaviour:

The variation of stresses for T-beams is more complex than that for ordinary beams because the flange has a dual function. It spans as a small cantilever, (or as a continuous slab) over the webs as support and it combines with the web to resist longitudinal bending. The direct stresses due to the flange acting as a cantilever are at

right angles to the stresses caused by longitudinal beam action, and there is little interaction between them. Typical variation in direct strain distribution under elastic conditions is illustrated in Figure (8.1), and compressive, shear and trajectory principal stress distributions are illustrated in Figures (8.2 - 8.4). The distribution of steel, cracking effects and the multiaxial compressive response of concrete are likely to affect these stresses and produce somewhat different behaviour. Some of these effects are not yet well understood and require further investigation.

The variation in flange compressive stress occurs because of shear deformations in the flange (shear lag), which reduces the longitudinal compressive strain with increasing distances from the web. The differences in longitudinal compressive stress resulting from different distributions of load, can be explained by referring to Figure (8.5). Under the action of a point load, Figure (8.5.a), the shear flow at the flange edge (i.e. connected to the web) is large right up to the point of the load, and the compression induced by shear flows near the midspan section cannot spread far across the flange. In contrast, the shear flows for the distributed load in Figure (8.5.b) are predominantly applied at the ends of the flange, and the compression they induce has most of the length of the flange to spread out. However, a rigorous analysis of the effect of load distribution and flange shape is extremely complex.

The distribution of longitudinal compressive stresses across the thickness of the flange become more uniform as the ultimate load is reached. This is because the concrete stress-strain curve shows a smaller variation of stress with strain at high stress levels.

As for transverse bending stresses, their effect is normally less significant than that of other stresses produced in narrow flanged T-beams as long as no loading is applied to the plane of the overhanging flanges. If this was the case, cracks could occur in the top of the flange over the web-flange junction, which would significantly affect behaviour.

In general, the stress distribution in T-beams depends on the relative dimension of the cross-section of the beam, the span, the arrangement of reinforcement, the type of material used and the type of loading.

8.3 Proposed theoretical model:

The model is based on a two dimensional plane stress approach and obviously introduces various techniques to achieve satisfactory results for what is essentially a three dimensional problem. The model is based on suggestions made by Iversen[8], and Macleod et al.[9] for linear-elastic behaviour. The method allows the shear stress developed in the web, due to the effect of bending in the longitudinal direction to be transferred to the flange. This will cause the stresses across the width of the flange to vary allowing longitudinal bending effects to be taken into account. This is illustrated in Figure (8.6).

The effect of bending in the direction perpendicular to the plane of the web and the flange is ignored. This is illustrated in Figure (8.7). This is not important in the web unless some torsional effects exist. For the flange this effect becomes more important for thicker or wider flanges, or when some forces are applied on the overhanging flanges. However once the assumption is made to ignore bending in the plane of the flange, the problem can be treated as a two dimensional plane stress problem.

The method assumes that the centre of gravity of the load is applied at the centre of the web-flange connection and behaviour will be essentially symmetric about the centre line of the beam. Also, because of symmetry, only one half of the T-beam needs to be analysed. In order to make the planes of the web and flange coincide, the flange is effectively rotated through 90^{o} as shown in Figure (8.8). The position of the axis of rotation is another assumption to be made in the analysis. These assumptions should adequately approximate the longitudinal and shear stress distributions in the flange and the web. The transverse stress in the flange will only be crudely approximated but its effect is assumed to be less significant, as previously explained.

A fictitious element composed of different linkage elements (i.e. similar to the element used by Ngo et al.[10]) having different stiffnesses in different directions, is used to connect the web to the flange. As shown in Figure (8.9) the element is assumed to be dimensionless and consists of eight nodal points connected by a series of springs which have high stiffnesses in the x-direction and small stiffnesses in the y-direction in the xy plane. The fictitious element is placed in the region between the web and the flange, and acts as a device to transfer forces for different degrees of freedom. A high stiffness of 0.1E + 10 is used for springs parallel to the web-flange in the x-direction (i.e. k_{3h}, k_{4h}, k_{7h}, k_{8h} in Figure (8.9)) to ensure compatibility. A small stiffness of 0.1E - 10 is used for springs in the y-direction of the plane (i.e. k_{3v}, k_{4v}, k_{7v}, k_{8v} in Figure (8.9)) to prevent any transfer of forces. Small values are given to avoid any numerical problems which may arise due to zero diagonals. The boundary conditions are assumed to be as shown in Figure (8.10). Rollers were provided in the flange

because symmetry requires that only half the flange need be analysed.

The main reasons for using the "8-noded" fictitious element rather than a simple "2-noded" spring element was to avoid difficulties in implementing it in the program. It meant that the mesh generator and frontal solution could be used without modification. It also has the possibility of being used for approximating bond-slip, aggregate interlocking, or other cracking aspects in much the same way as the Ngo et al.[10] linkage element, but the extra stiffnesses offer the prospect of a better approximation to actual behaviour. However this aspect was not developed in this work.

The procedure for the analysis can be summarized as follows:

(1) Assume the effect of bending is ignored in the z-direction for the web, and in the y-direction for the flange as shown in Figure (8.7).

(2) Rotate the flange thrcugh an angle of 90^{o} from the zy plane to the xy plane in order to keep the web and the flange in the same plane (see Figure (8.8)).

(3) Connect the web to the flange using the fictitious element shown in Figure (8.9), to allow transfer of forces from the web to the flange in the horizontal direction.

(4) Apply the load on the web and restrain the flange vertical movement in the xy plane as shown in Figure (8.10).

(5) In the calculation of residual nodal forces in the web-flange connection, check only for horizontal forces on the line parallel to the longitudinal direction. These forces should only be added in that direction. Other directions are ignored because they are out of plane.

The method is not capable of analysing loads acting on the flange outside the web-flange connection, and will assume that the strain and hence the stress distribution through the thickness of the flange is constant. This will effect the development of cracks in the flange in a nonlinear analysis as will be shown later. Also it would imply that the approximation would become less reliable for flanges of increased thickness.

8.4 Selection of axis of separation:

A problem in the idealization is to determine the best position at which the flange is separated from the web. This position will influence the results of an analysis by causing the effective second moment of area and other geometric properties, and hence the estimate of the ultimate load, to be under- or over-estimated.

Five different cases were investigated in which the centroidal axis and the second moment of area were calculated. These were studied to decide a web depth and a flange breadth which would give similar values to the correct ones for the actual T-beam. It is then assumed that this will give reasonable results in the finite element method. It was also assumed that the sections is solid concrete and steel were ignored. The different cases studied are shown in Figure (8.11) and these were tested for the beams shown in Figure (8.12), which represent the different dimensions for the beams investigated in this analysis.

Case 1 Figure (8.11.a):

Exact value.

Case 2 Figure (8.11.b):

This case assumes that the rotated flange gives a contribution to the second moment of area of $A_f(L_2 - \bar{y})^2$.

Case 3 Figure (8.11.a):

This case assumes that the rotated flange gives a contribution to the second moment of area of $A_f(L_1 - \bar{y})^2$.

Case 4 Figure (8.11.c):

This case assumes that the rotated flange gives a contribution to the second moment of area of $A_{f_1}(L_2 - \bar{y})^2 + A_{f_2}(L_3 - \bar{y})^2$.

Case 5 Figure (8.11.d):

This case assumes that the rotated flange gives a contribution to the second moment of area of $A_f(L_3 - \bar{y})^2$.

The different cases studied for the beams shown in Figure (8.12) are tabulated in Table (8.1). The best estimate, from Cases 2-5, which was nearest to the exact value was found to be case 5. This is fairly obvious in a sense, because it allows the constraint imposed by the flange to contribute to the overall stiffness which has been depleted by removing a part of the web at the top.

8.5 Description of beams tested:

In this study, one beam tested by Cope et al.[1], and another five beams tested experimentally by Chong[4], will be analysed. These will be studied in three groups; Cope et al. beam B-2 failing in flexure; Chong's beams B-10, E-10 and H-10 failing in shear; Chong's beams E-13 and G-14 which also failed in shear. The second group differ from the

third group in the way the stirrups were provided; the second group were provided with stirrups at the end and middle of the span to carry the main reinforcement, while the third group were provided with stirrups throughout the span to resist shear forces.

Details of beam B-2 and the mesh used are shown in Figure (8.13). Details and the mesh used for beams B-10, E-10, H-10, E-13, and G-14 are shown in Figures (8.14 - 8.16) and Tables (8.2) and (8.3). Details of material properties for concrete and steel are shown in Tables (8.4) and (8.5).

In these analyses the same assumptions as concluded from the previous chapters, were used as follows:

(1) The first cracking model was used (i.e. no tension stiffening).

(2) The method V.S.M.1 was used.

(3) The load criterion was used with COOP = 20%, and iterations were continued until this value was obtained.

(4) The aggregate interlocking factor α was kept constant at 0.5.

(5) The load was applied in increments of 5.0 kN for the first two groups, and in increments of 10.0 kN for the third group.

8.6 Description of results:

Group A:

Beam B-2 was tested by Cope et al.[1], under concentrated point load applied on the midspan of the beam. This beam failed in flexure at a load of 127.0 kN. The experimental load deflection curve as reported by the authors was discontinued at a lower load level, but the ultimate load was still recorded. It was found in the experimental work

that there was some evidence of local crushing of concrete in the top flange at failure.

As can be seen from Figure (8.13), 84 elements were used; 36 elements for the web; 36 elements for the flange and 12 elements as fictitious elements to connect the web to the flange.

Different load deflection curves are compared for values of f'_t ranging from 0.2 f'_t to its full value in Figure (8.17). The reason for studying this variation of f'_t is that microcracking which existed experimentally at the initial stages might have effected the value of f'_t and therefore the value assumed in the analysis might not give the exact prediction of the cracking behaviour.

It can be seen that a value of f'_t equal to 6% of f_{cu} gave the best possible prediction for the load deflection curve and ultimate load. In this case failure was obtained at a load of 125.0 kN, showing close agreement with the experimental value of 127.0 kN. Figure (8.17) also shows the finite element results obtained by Cope et al.[1] for a value of f'_t = 2% of f_{cu} using a different type of element. It appears that a stiff load deflection curve and a higher ultimate load is produced as the value of f'_t becomes smaller than that specified experimentally. Different crack patterns are plotted in Figures (8.18 - (8.21) for the case of f'_t = 6% of f_{cu}. The cracks initiated as flexure cracks and propagated with a small inclination towards the point of load application. A few cracks appeared later in the compression flange near the connected area. Yielding was observed at the high bending moment area which indicated failure. This caused divergence of the solution which stopped the analysis. Crushing occurred afterwards in the top flange, but this

is not reliable because it happened whilst the solution was diverging.

Longitudinal and shear stress distributions across the width of the flange were found to be similar in shape to those previously described, and they will not be plotted for this beam, but will be shown for a beam failing in shear in the next group.

Principal stress distributions are shown in Figures (8.22) and (8.23) for load levels of 20.0 kN and 110.0 kN respectively. The very small stresses in cracked regions and the high compressive stresses in the flange can be clearly seen.

Group B:

Beams B-10, E-10, and H-10 were tested experimentally by Chong[4], under uniform distributed load on the line above the flange junction. These beams failed in shear at load levels of 190.0 kN, 203.4 kN and 256.0 kN respectively. Three stirrups were provided at the end of each beam and one stirrup in the midspan section to hold the longitudinal reinforcement in place. The beams final failures were due to the cracking of concrete near the support, either in the regions just above the main tensile reinforcement, or in addition at the region immediately below the flange-web junction.

As can be seen from Figure (8.16), a total of 48 elements were required; 18 elements for the web, 24 elements for the flange, and 6 elements to connect the web to the flange. For simplicity the method described in this chapter will be termed the T.M.1 method. Another method will also be examined and compared with the T.M.1 method. This will be termed the T.M.2 method and it will use the straight forward plane

stress approximation with different thickness for the web and flange. This means that the stresses and displacements will be constant throughout the width of the flange. The T.M.1 method will be used for all beams in this group whilst the T.M.2 method will be used for beams B-10, and E-10 only.

Different load deflection curves are compared for beams B-10, E-10, and H-10 in Figures (8.24 - 8.26). It can be observed that using the experimental values of concrete properties produced a stiffer load deflection curve at the initial stages of loading. This was even more significant at the higher load levels especially before the failure stage. Also, it can be seen that the load deflection curves obtained by using the T.M.2 method for the beams B-10 and E-10 were similar to those obtained by using the T.M.1 method. The ultimate loads were overestimated for beams B-10 and E-10 when using the T.M.1 method. This was much more so for these beams when the T.M.2 method was used.

It appears that the stiff load deflection curve at the lower load levels using the T.M.1 method was not simply due to the approximations assumed in that method, because the T.M.2 method produced almost similar curves at those load levels. This stiff response could be due to other effects such as the inexact experimental value of Young's modulus which may produce this type of variation, or to other effects such as the existence of microcracking at the initial stages of loading which cannot be approximated early in the finite element model. This could be further confirmed if both methods show a similar crack pattern in the web in the initial stages. Since similar crack patterns were obtained experimentally in all these beams, only beam E-10 will be discussed. Different crack patterns are shown in Figures (8.27 - 8.30) using the T.M.1 method. It

can be observed that the beam developed flexural tension cracks at low load levels near the midspan section.

Further increase of load caused the appearance of diagonal cracks which were inclined at an angle of about 45^{o} to the beam axis. As this load is increased more cracks developed towards the compression zone accompanied by other cracks developing downward to the soffit or plunge. In the compression zone, after cracks had reached the underside of the flange, they started to propagate along the flange itself. The existence of these cracks led to a stage at which the beam was unable to sustain any increase in load. From Figure (8.30) it is clear that the failure is in shear and crushing appeared in the region immediately below the flange-web junction. This description of the crack propagation is very similar to the experimental descriptions except that there were some cracks reaching the outer side of the flange in the experimental results which this method could not produce. This could be another reason why a stiff load deflection curve was obtained compared with the experimental one.

Principal stress directions at two different load levels are shown in Figures (8.31) and (8.32). The existence of tension stresses in the web at the low load level can be seen. These stresses disappear at higher load levels when most of the cracks have appeared. Arching action is very clear in Figure (8.32).

Different crack patterns are plotted in Figures (8.33 - 8.36) with the T.M.2 method. It can be observed that the crack propagations in the flange at the low load levels are similar to that described by the T.M.1 method. However at higher load levels web shear cracks develop towards the flange but no cracks were predicted in the flange itself. After that,

the beam maintained its strength and eventually failed when the steel yielded in the maximum bending moment area in the midspan section of the web, and at the top of the flange. Crushing also occurs in the top of the flange at the midspan section. This type of failure was not exhibited experimentally. Principal stress directions using the T.M.2 method are plotted in Figures (8.37) and (8.38). These were not greatly different from the ones obtained using the T.M.1 method in the web, but they were different in the flange because of the stress variation throughout its thickness.

Horizontal stress distributions in the web at the midspan section for beams E-10 using the T.M.1 method are shown in Figure (8.39). Crack propagation occurred at early load levels, after which a situation was reached where the compressive stresses in the flange became dominant. This implies that the flange behaviour at higher load levels becomes more important and should be considered more carefully than the crude approximation made with the T.M.2 method where the steel in the transverse or even in the longitudinal direction cannot be represented in its actual position.

Horizontal stress distributions in the flange using the T.M.1 method under elastic conditions are shown in Figure (8.40). These were measured from the centre line of the web-flange connection to the outer edge of the flange. A nonlinear variation was obtained. This was not very significant, but it occurred mainly because of the effect of shear deformation in the flange. The horizontal stress distribution in the midspan section of the flange is also shown in Figure (8.41) for different load levels. It can be observed that with an increase of load, a more nonlinear distribution of the horizontal stresses is obtained especially

under the load itself. This is because the higher load levels produced higher strains in the midspan section than that obtained on the edges of the flanges, and since the stresses become more nonlinearly related to the strains at the high load levels, this type of distribution can be expected.

Shear stress distributions at different load levels in the midspan section of the flange are shown in Figure (8.42). These appear to have a maximum value at about one third of the width of the half flange and reduce linearly to the outside of the flange. The maximum value was obtained near the position of the compression reinforcement. This figure also shows how complex this variation actually is.

Group C:

Beams E-13 and G-14 were tested by Chong[4], under uniformly distributed load on the line above the flange junction. These beams failed in shear at load levels of 322.0 kN and 326.1 kN respectively. As shown in Figures (8.14.b) and (8.14.c), these beams differed from the beams in group B in that they were provided with web reinforcement in the form of vertical stirrups. Beam E-13 was provided with 4 mm stirrups and beam G-14 with 5 mm stirrups. Beam G-14 also has a wider flange of 500.0 mm than that of 300.0 mm described for the other beams.

Load deflection curves for both beams are compared in Figures (8.43) and (8.44) for the T.M.1 method. Although the load deflection curves were predicted fairly well, poor agreement was obtained for the ultimate load. Failure was due to the yielding of stirrups in the web at a distance of 800.0 mm from the midspan section. This failure is a valid characteristic of beams failing in shear with vertical stirrups, and occurs because

of the effect of shear cracks developing in the shear span section.

For beam G-14 different load deflection curves are also compared in Figure (8.44) using different values of f'_t. The change in this value did not produce any major effect on the load deflection curve and ultimate load. This was not the case for the beam which failed in flexure. It appears that the change in the predicted ultimate load in the beam failing in flexure was caused by the different loads at which the longitudinal reinforcement yielded at the midspan section. The steel stresses seem to be significantly affected at this position according to when the flexural cracks occurred which itself depends on the value of f'_t. However for the beam failing in shear, this was caused by the yield of vertical stirrups in the top of the web near the support. The stresses in these stirrups were not greatly affected by the initiation of the flexural cracks and the change of f'_t did not produce a major change in the stirrup stresses.

Crack patterns will be described for only one beam because a similar pattern was observed experimentally for both beams. These are shown for beam E-13 in Figures (8.45 - 8.48); flexural cracks appeared initially followed by diagonal cracks. The diagonal cracks appeared both as extensions of flexural cracks, and as isolated inclined web-shear cracks. The web shear cracks propagated towards the flange and the support regions, as the load increased. Failure occurred when stirrups yielded in the web and divergence of the solution occurred. The description is similar to that observed experimentally.

Principal stress directions are shown in Figures (8.49) and (8.50) for load levels of 50.0 kN and 250.0 kN. It can be seen that the tension stresses are very small in regions where cracks have developed. At high

loads compression stresses become more significant and arching action is very clear. Also, very high compressions were developed near the support which caused the vertical steel to yield and cause failure.

8.7 Conclusions:

(1) Using the plane stress approximation, a simple method was proposed to analyse different types of T-beams. The general trend in the shape of the load deflection curves was relatively acceptable but they did not always compare well with the experimental results. However the range of error in ultimate load was fairly reasonable. A comparison of measured and computed ultimate loads are shown below:

Beam name	W_u measured ultimate load (kN)	Q_s computed ultimate load (kN)	Q_s/W_u
B-2	127.0	125.0	0.98
B-10	190.0	215.0	1.13
E-10	203.4	225.0	1.11
H-10	256.2	250.0	0.98
E-13	322.0	280.0	0.87
G-14	326.0	270.0	0.83

The method requires more investigation regarding the improvement of the shape of the load deflection curve and in checking the validity of the stress distribution in the web and flange, compared with experimental results. Different values of Young's modulus should be examined, and the effect of using different values of the strain hardening part of the steel on the load deflection curve should be checked. The effect of flange behaviour also appears to be significant and should be examined

in greater detail. The effect of changing the axis of separation should also be studied in order to clarify the contribution of the rotated flange on the stiffness. However, the results for the longitudinal, and shear stresses in the flange, and the horizontal stresses at the midspan section of the web, gave a good indication of the distribution of these stresses.

In conclusion the method shows some potential in economically predicting various aspects of T-beam behaviour, but still requires further investigation and refinement to achieve more acceptable accuracy.

(2) The technique is not valid for describing the stress variation throughout the thickness of the flange. This may be important for thick flanges. It may be possible to improve this by using a layered element technique. However this will increase time and cost.

(3) In the nonlinear analysis, it appears that cracks never propagated beyond the point of compression reinforcement in the flange. This may not be true in practical situations, because cracks may propagate to the outer side of the flange at failure. This may be due either to the approximations which assume that stresses are constant through the thickness of the flange, or due to the effect of neglecting transverse stresses in the flange.

(4) The conclusions obtained in chapter 6 for the deep beam failing in flexure, and which were tested in chapter 7 for a deep beam failing in shear, also produced convergence throughout this study without much difficulty.

(5) The T.M.2 method agreed reasonably well with the proposed T.M.1

method for the stiffness of the load deflection curve. This implies that approximations in the T.M.1 method were not solely responsible for the shape of the load deflection curve compared with the experimental situation and the stiff response obtained in some curves could therefore be due to other factors.

(6) The T.M.1 method was better in predicting the ultimate load than the T.M.2 method. This suggests the importance of flange behaviour on a solution especially during the final load stages. This is because the T.M.1 method used a better approximation for the flange whereas the web simulation was similar in both methods. In particular the role of any crack development could be crucial. For the T.M.1 method this would be better simulated by using a layered element technique or by reducing the stiffness of the flange elements by some indirect means. This would require the identification of suitable parameters for determining cracks in the flange. Or, less importantly, the T.M.2 method could be improved by using more elements through the depth of the flange.

(7) It appears that the steel is a major factor governing failure in most of these beams. As steel started to yield (either in the stirrups or in the main tension reinforcement) failure occurred.

(8) The method developed in this chapter could also be used to analyse the nonlinear behaviour of L-beam and box girder structures with thin flanges. Certain changes in boundary conditions need to be considered, and further study would be required to work out the approximations.

Beam name	Centroidal axis/ Second moment of area	Case 1	Case 2	Case 3	Case 4	Case 5
Rao B-2	$\bar{y}$ mm I_{xx} mm^4	150.5 118.9E6	143.2 96.8E6	155.3 134.9E6	144.1 99.5E6	154.4 123.4E6
Chong B-10	$\bar{y}$ mm I_{xx} mm^4	145.0 88.1E6	137.5 70.8E6	150.0 100.8E6	138.4 72.9E6	140.8 91.3E6
Chong E-10 E-13	$\bar{y}$ mm I_{xx} mm^4	150.0 91.8E6	135.0 60.8E6	160.0 115.2E6	136.9 64.6E6	153.5 92.0E6
Chong H-10	$\bar{y}$ mm I_{xx} mm^4	152.0 92.6E6	128.0 47.8E6	168.0 126.7E6	131.0 53.6E6	154.5 87.9E6
Chong G-14	$\bar{y}$ mm I_{xx} mm^4	165.0 109.8E6	146.3 69.8E6	180.0 144.0E6	147.6 72.9E6	166.7 106.7E6

Table (8.1) Selection of axis of rotation.

Beam name	Total height (mm)	Web width (mm)	t_f Flange thickness (mm)	h_f Flange width (mm)
Rao B-2	250	120	40	360
Chong B-10	240	100	40	300
Chong E-10	240	100	60	300
Chong H-10	240	100	80	300
Chong E-13	240	100	60	300
Chong G-14	240	100	60	500

Table (8.2) Beam dimensions.

Beam name	x_1	x_2	x_3	x_4	x_5	x_6	x_7	x_8	x_9
B-10	40.0	90.0	90.0	0.0	40.0	36.7	36.7	36.6	370.0
E-10	40.0	85.0	85.0	0.0	40.0	36.7	36.7	36.6	360.0
H-10	40.0	80.0	80.0	0.0	40.0	36.7	36.7	36.6	350.0
E-13	40.0	85.0	85.0	0.0	40.0	36.7	36.7	36.6	360.0
G-14	40.0	85.0	85.0	0.0	40.0	70.0	70.0	70.0	460.0

Table (8.3) Details for mesh dimensions of Chong beams.

Beam name	f_{cu} (N/mm^2)	f'_c (N/mm^2)	f'_t (N/mm^2)	E_c(N/mm^2)	ν_c
Rao B-2	48.0	37.4	4.8	$.35 \times 10^5$	0.20
Chong B-10	37.2	29.0	4.2	$.25 \times 10^5$	0.18
Chong E-10	33.2	25.9	4.0	$.24 \times 10^5$	0.18
Chong H-10	35.0	27.3	4.1	$.25 \times 10^5$	0.18
Chong E-13	33.6	26.2	4.0	$.24 \times 10^5$	0.18
Chong G-14	38.5	30.0	4.3	$.26 \times 10^5$	0.18

Table (8.4) Concrete properties.

Beam name	Bar description	f_y (N/mm^2)	E_s(N/mm^2)	E_w(N/mm^2)
Rao beam	Longitudinal	340	$.20 \times 10^6$	0.0
	Stirrups	495	$.22 \times 10^6$	0.0
Chong beams	Longitudinal	479	$.19 \times 10^6$	57.23
	Stirrups	622	$.21 \times 10^6$	82.50
	Compression	399	$.20 \times 10^6$	0.0

Table (8.5) Steel properties.

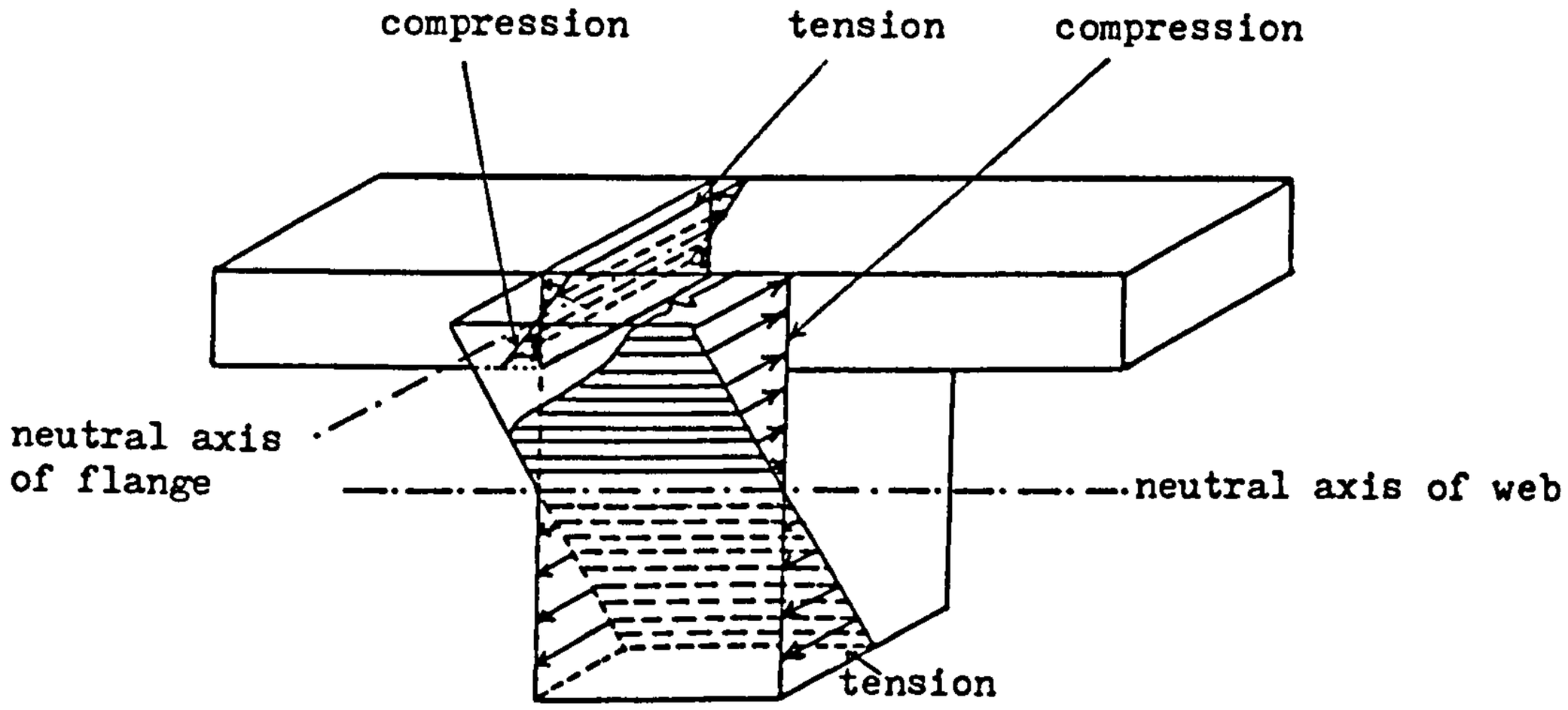

Figure (8•1) Direct strain distribution in a T-beam.

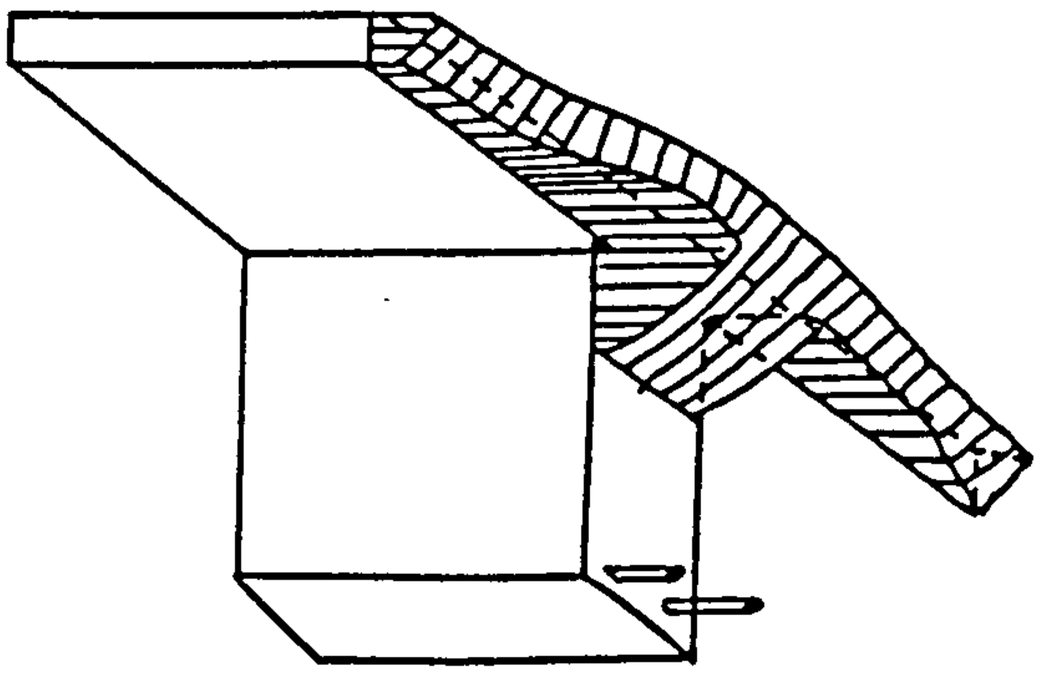

Figure (8•2) Variation of compression stresses above the neutral axis for a T-beam.

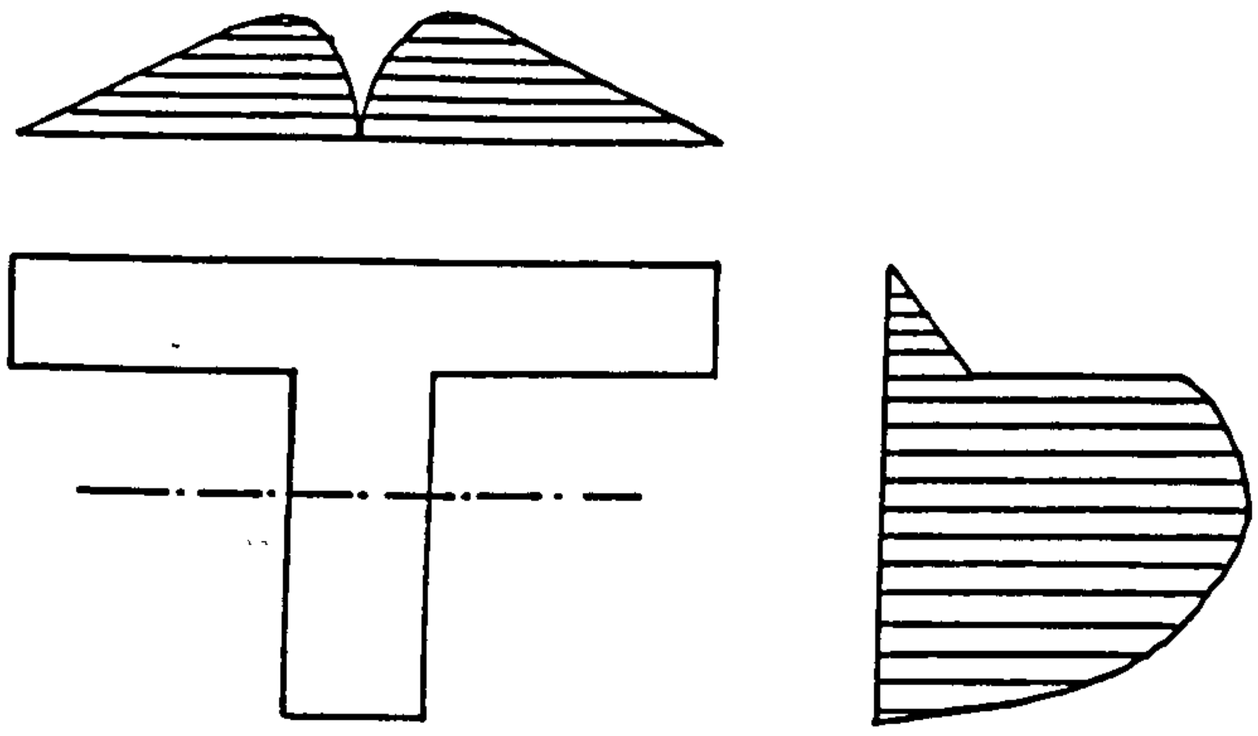

Figure (8•3) Shear stress distribution for a T-beam.

Figure (8•4) Principal stress trajectories.

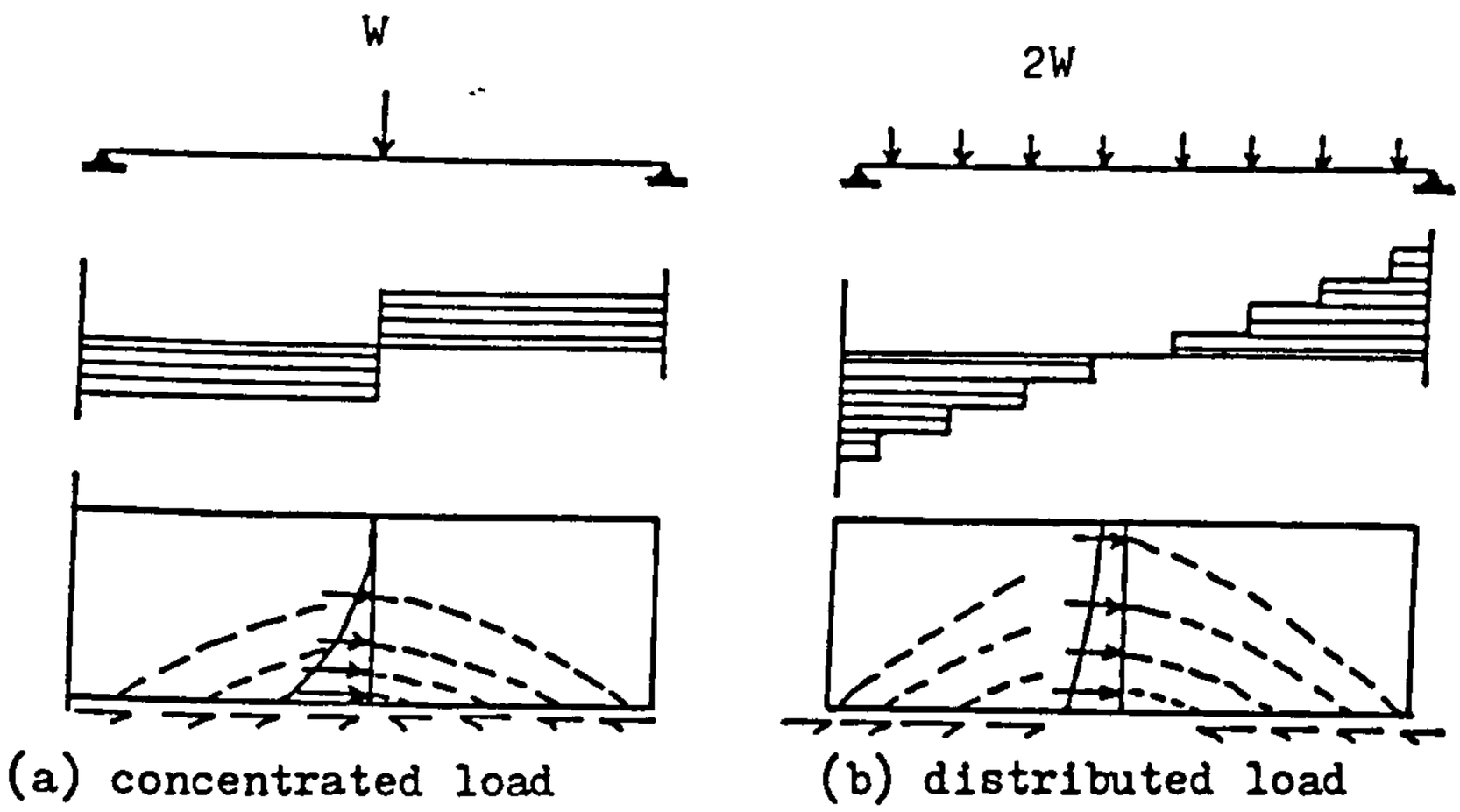

Figure (8•5) Different stress distribution in the flange.

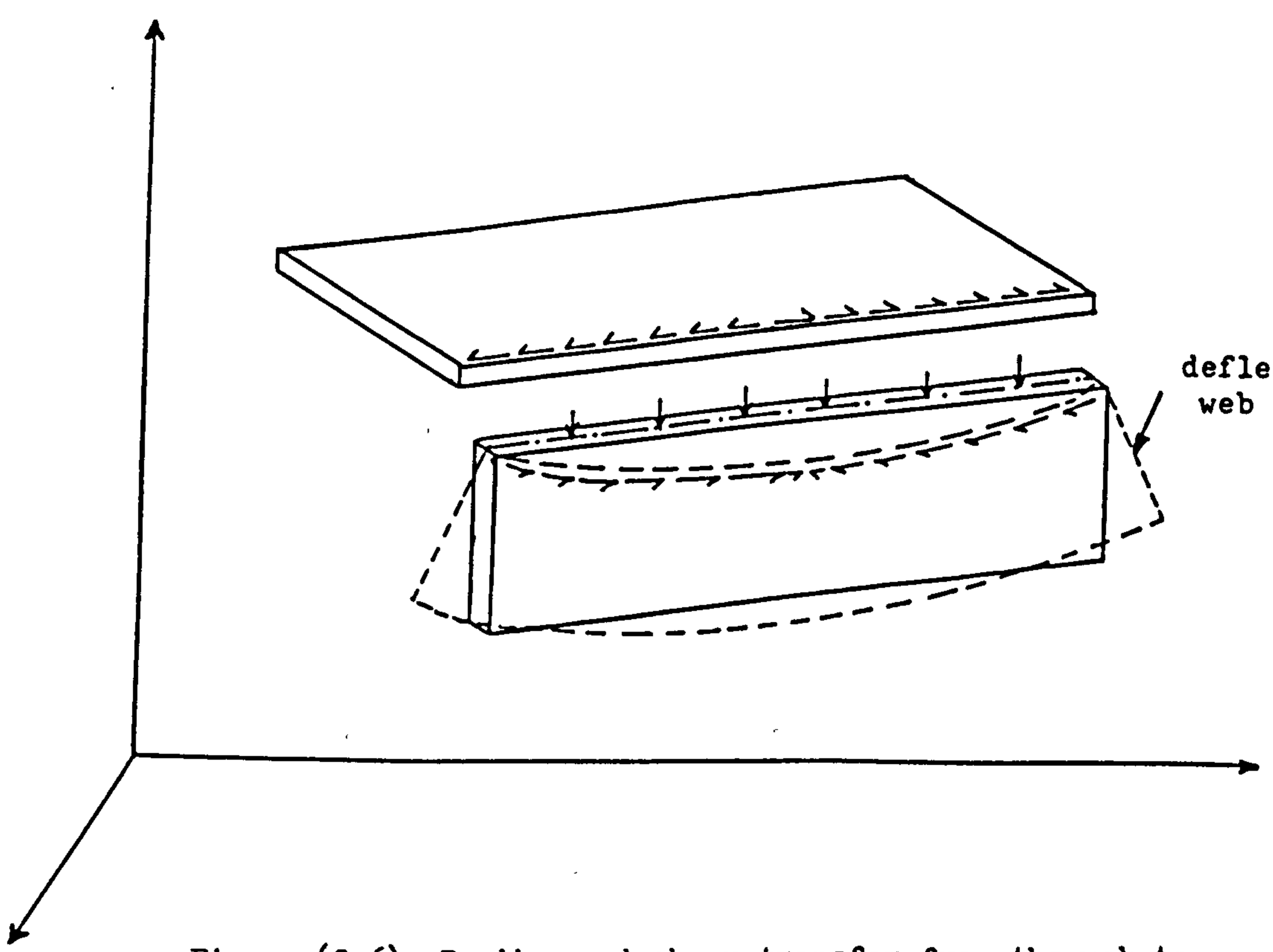

Figure (8•6) Bending and shear transfer from the web to the flange.

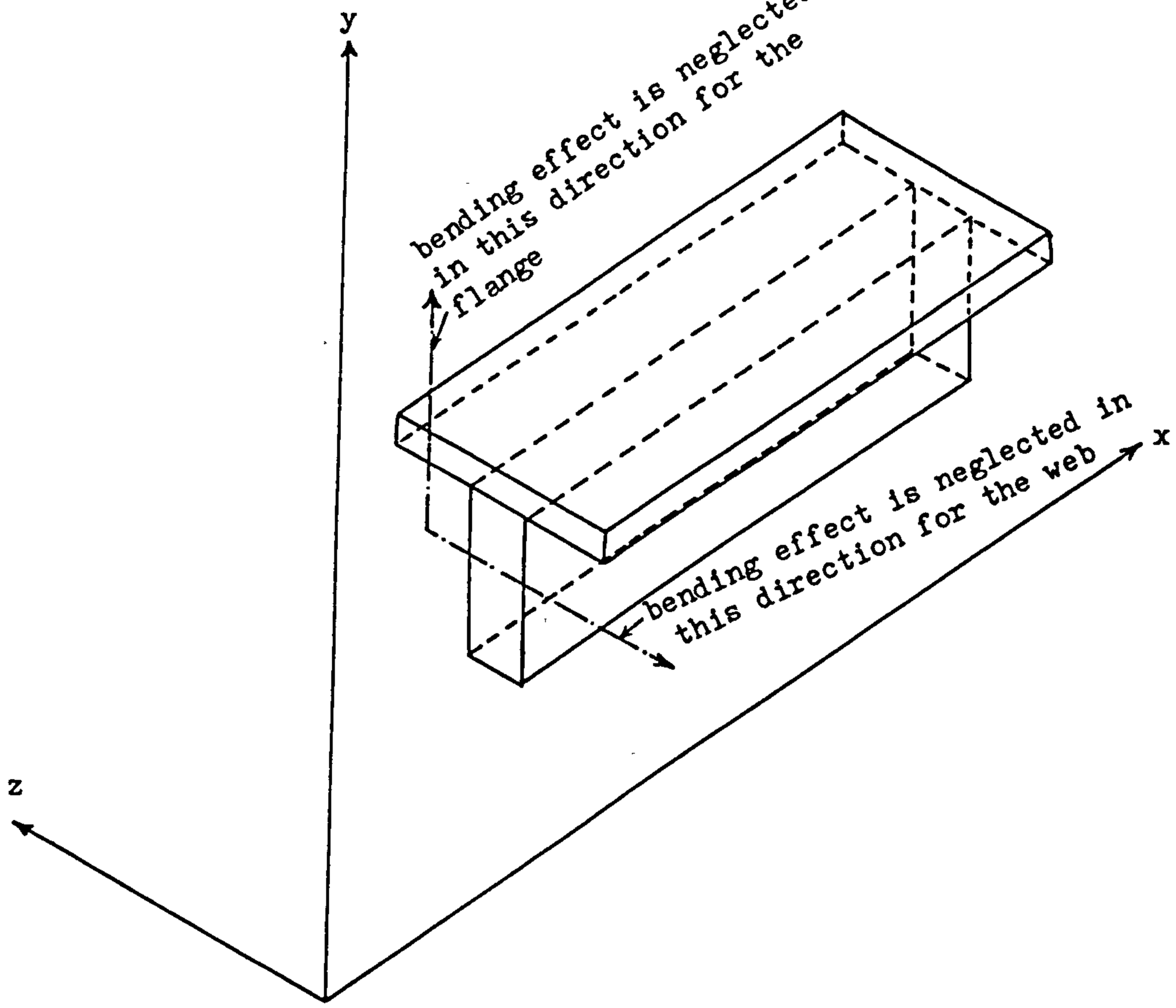

Figure (8•7) Diagram shows direction at which bending effect is neglected.

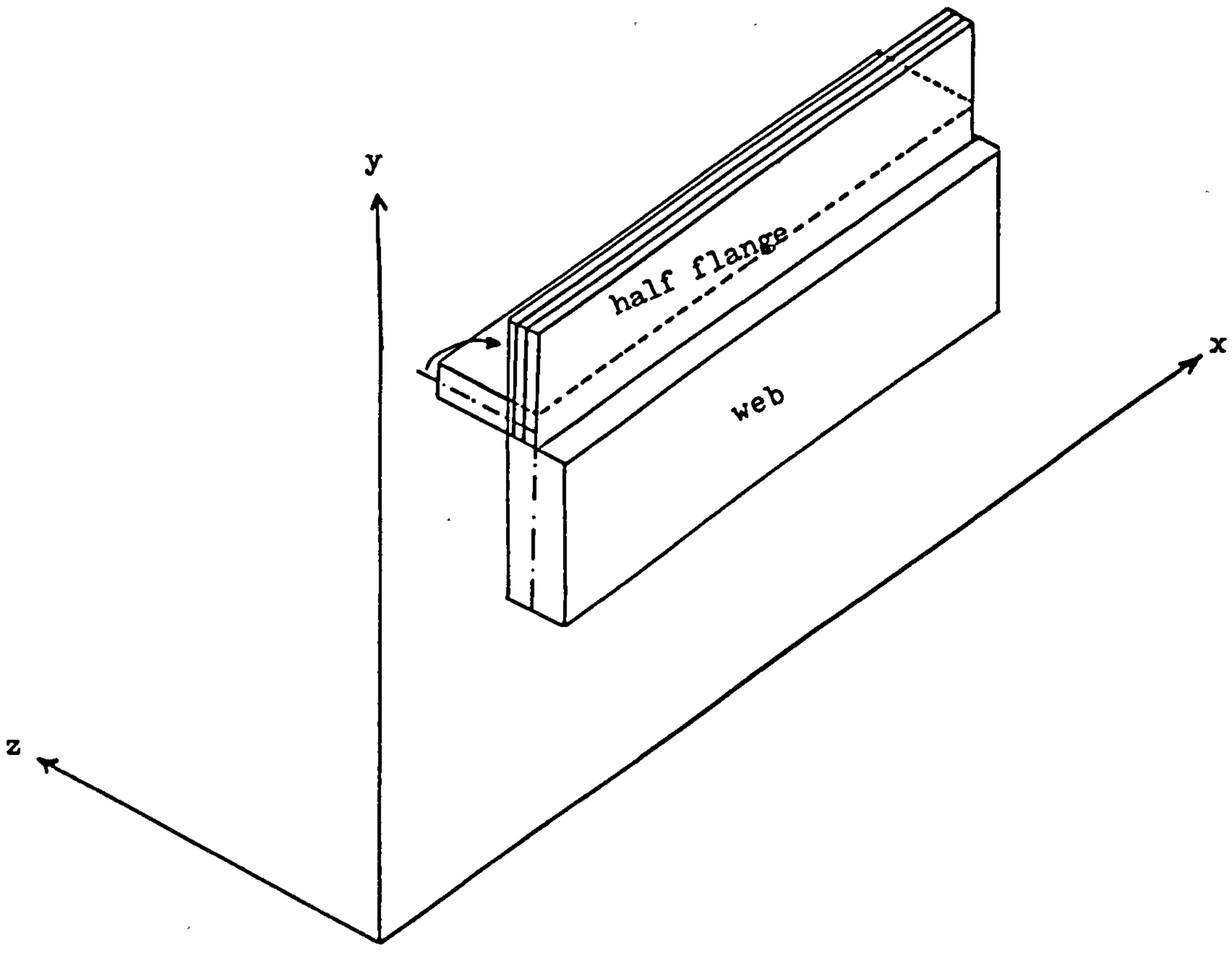

Figure (8•8) Rotation of flange to the plane of the web.

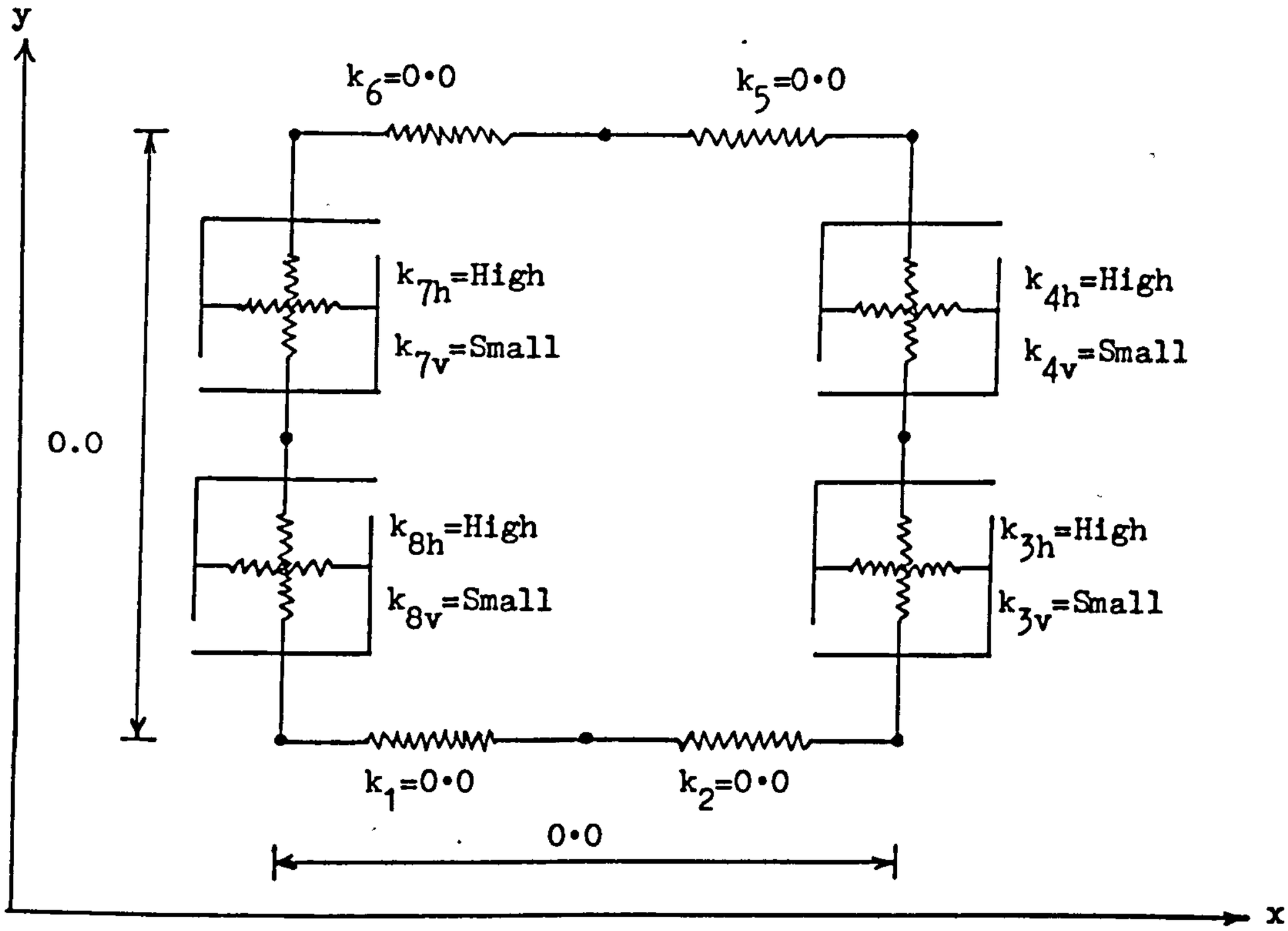

Figure (8·9) Fictitious element used to connect the web to the flange.

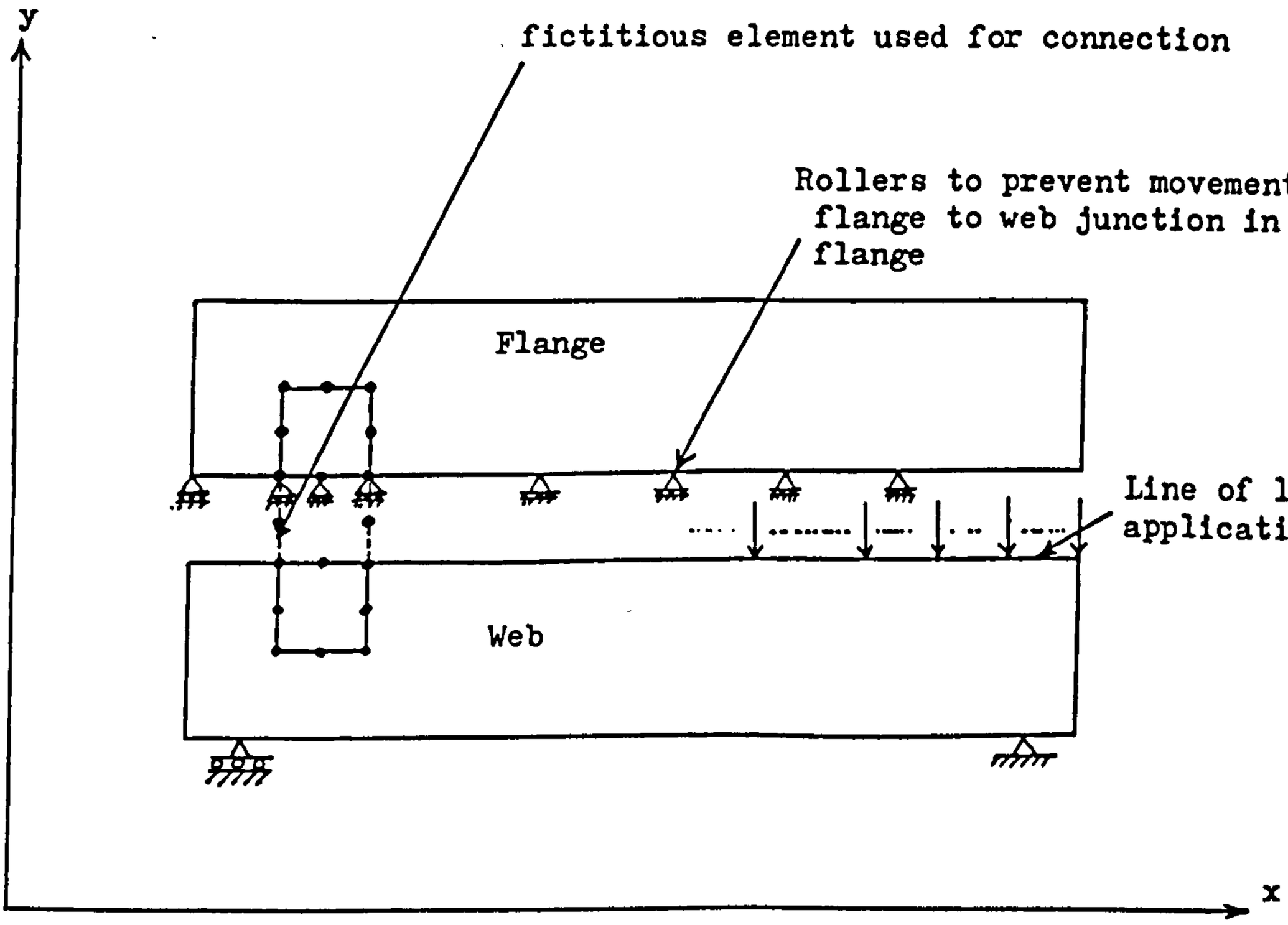

Figure (8·10) Finite element idealization for a T-beam.

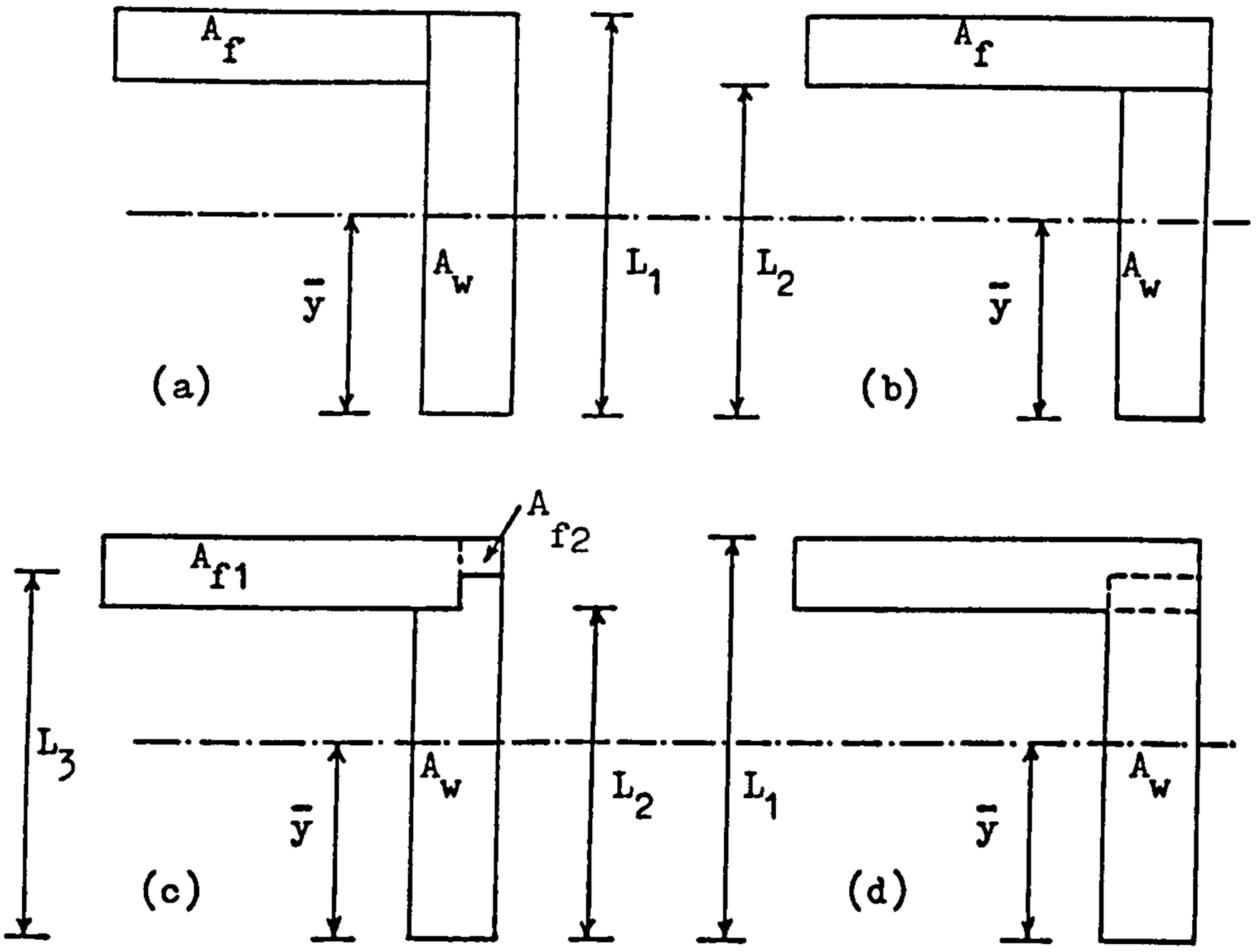

Figure (8·11) Different cases tested for the selection of axis of rotation.

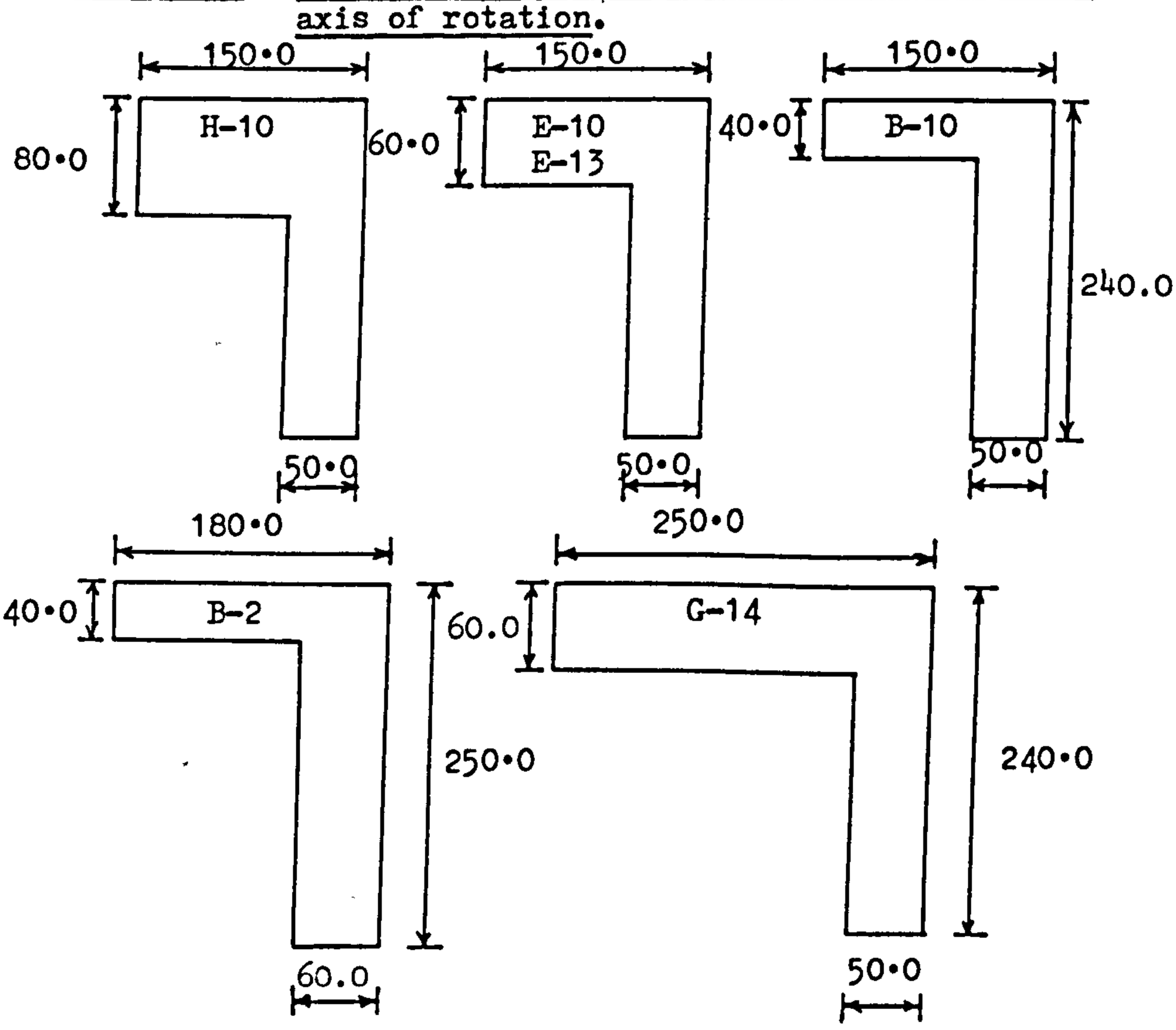

Figure (8·12) Different shapes used to test the selection of axis of rotation.

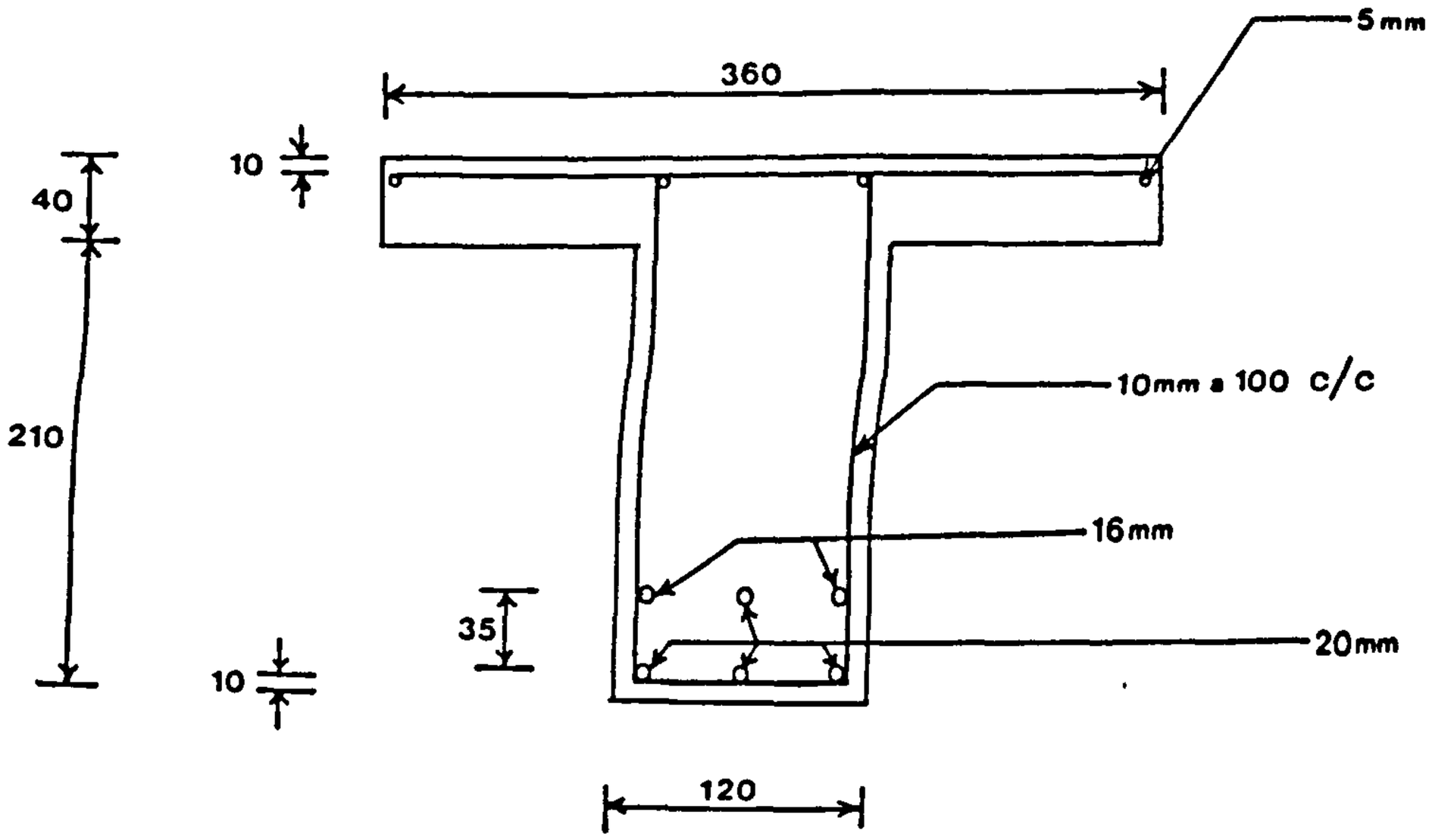

Section A-A

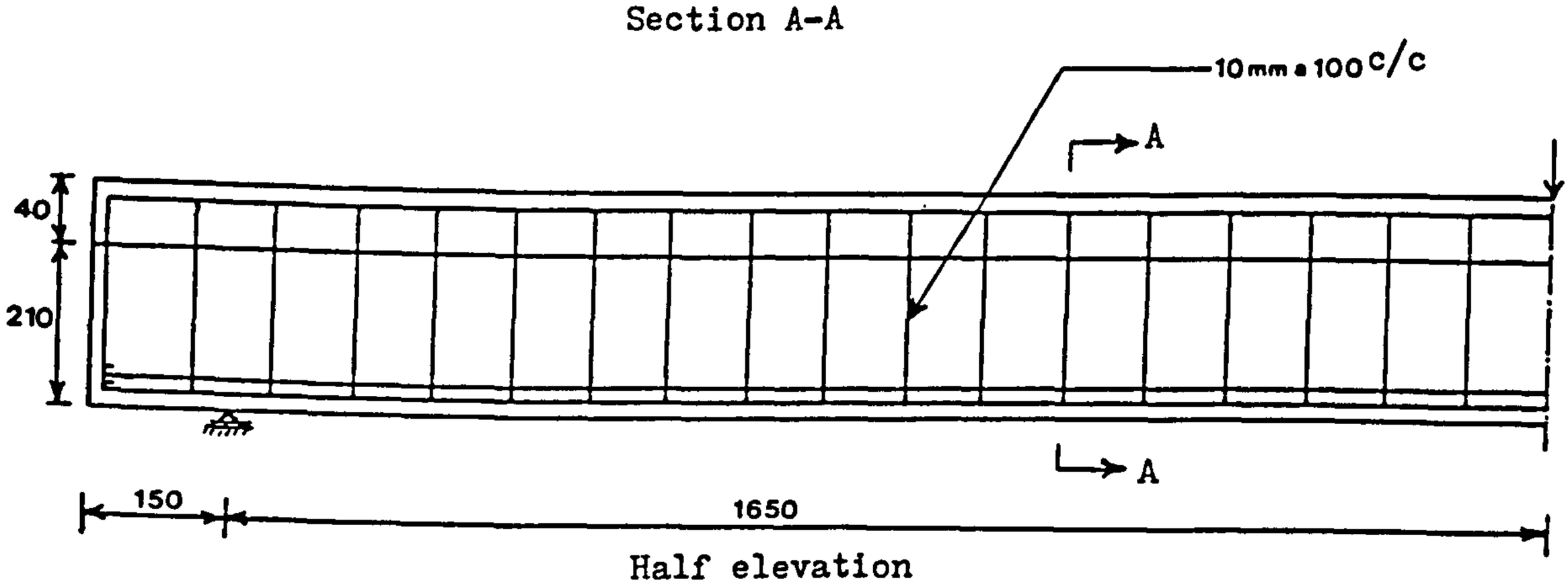

Half elevation

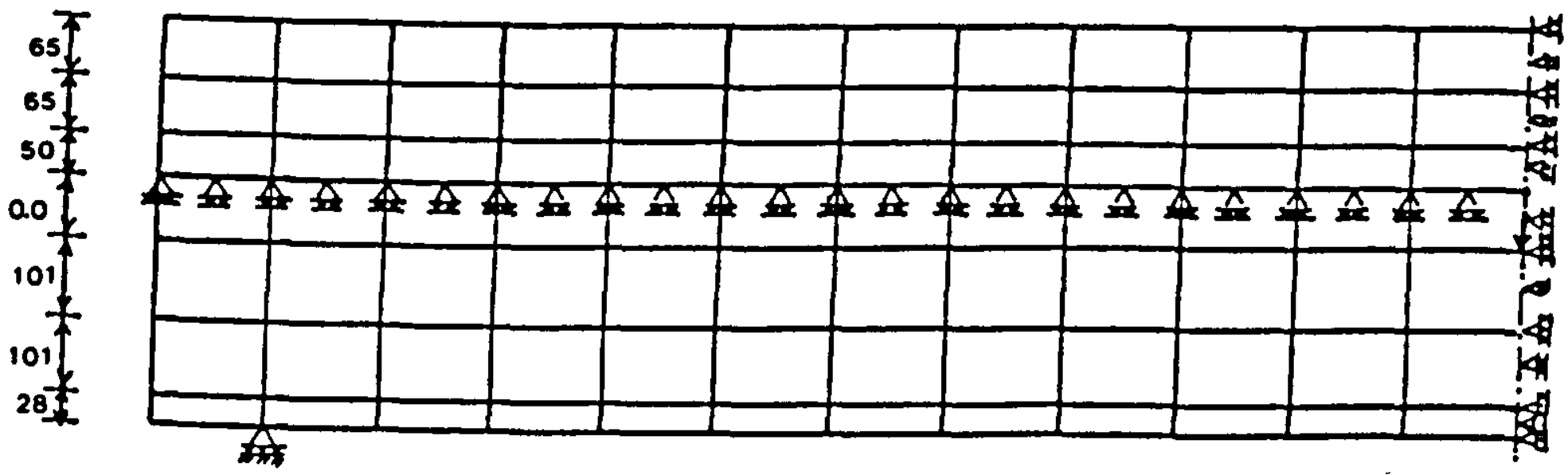

Mesh used

Figure (8•13) Details of Cope & Rao T-beam B-2.

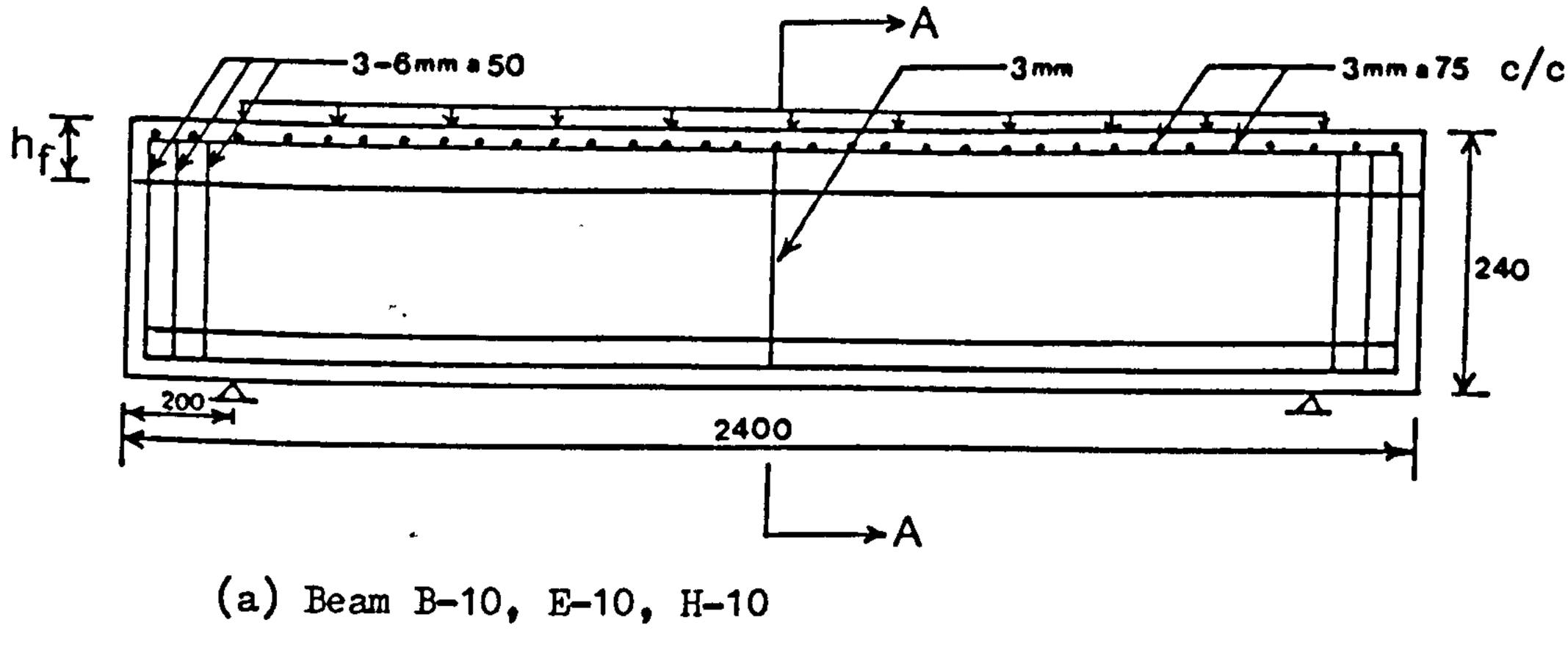

(a) Beam B-10, E-10, H-10

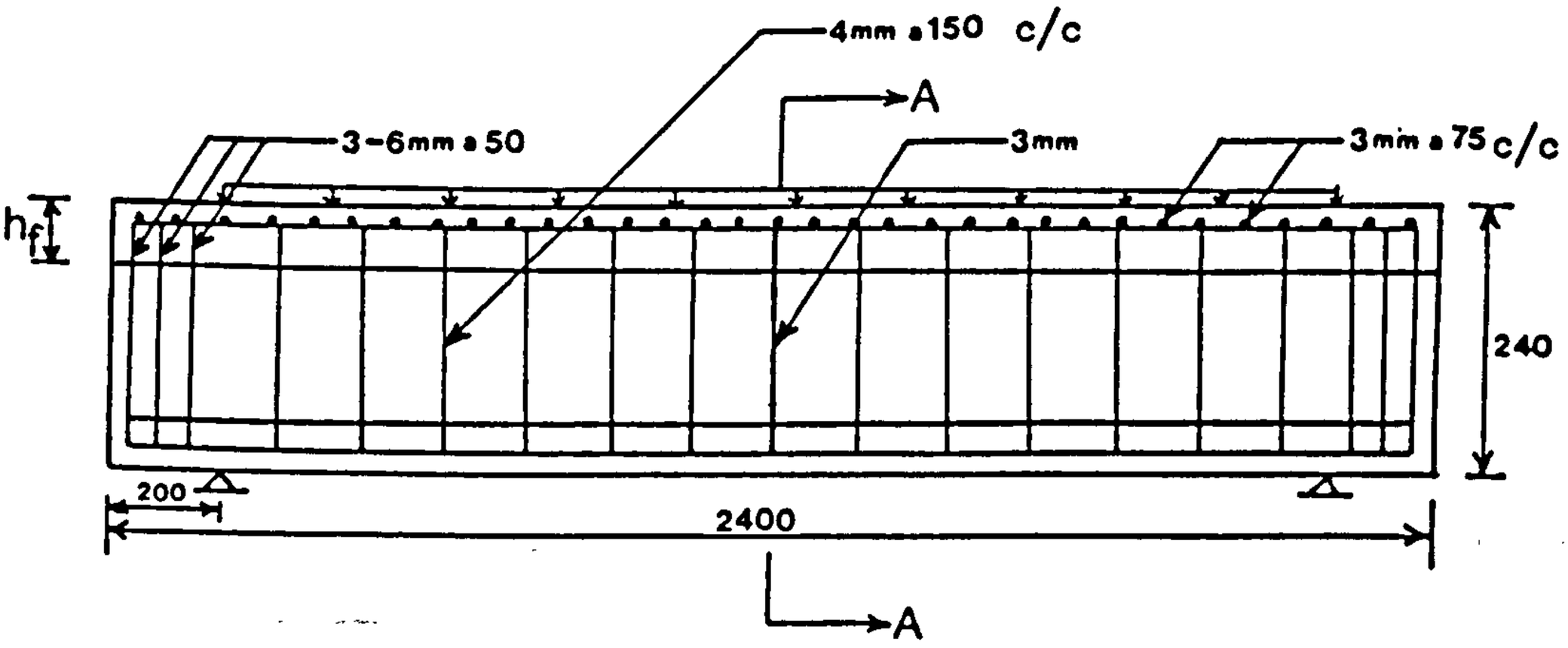

(b) Beam E-13

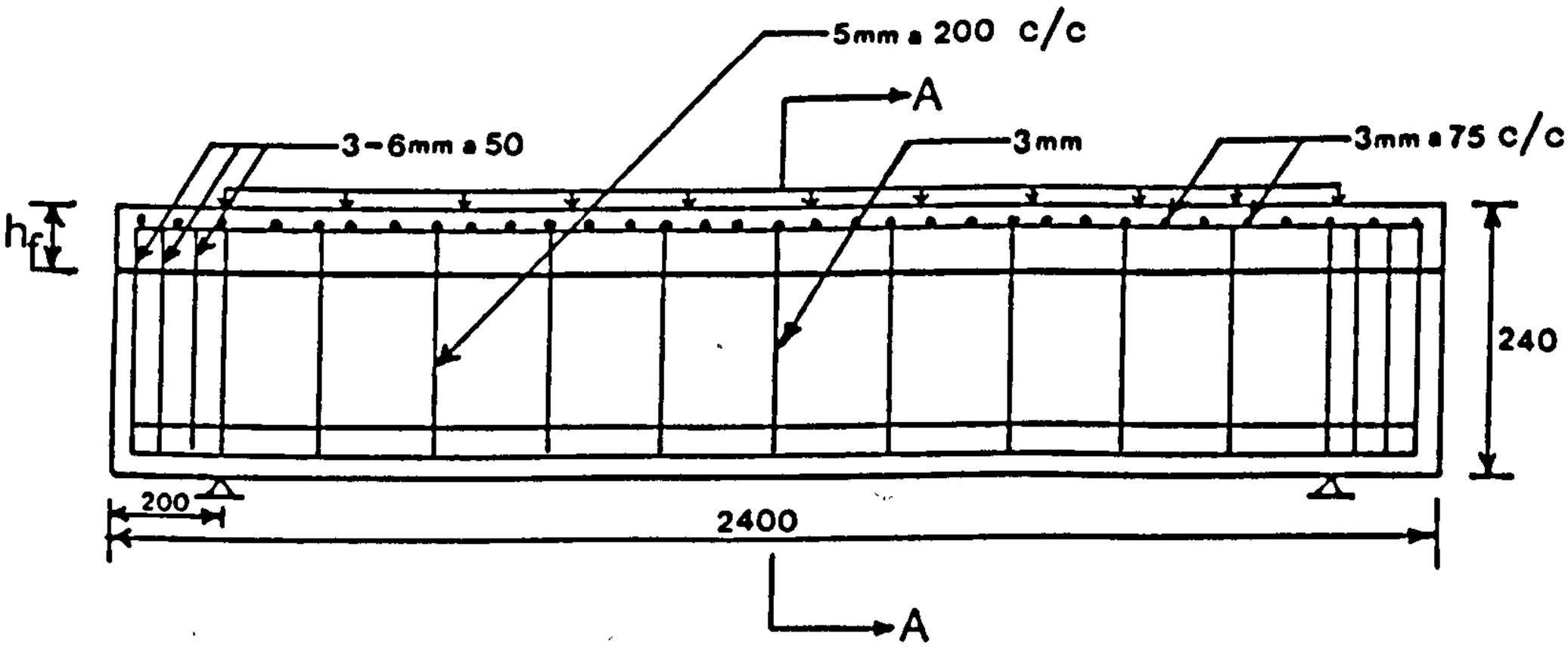

(c) Beam G-14

Figure (8·14) Details of Chong T-beams.

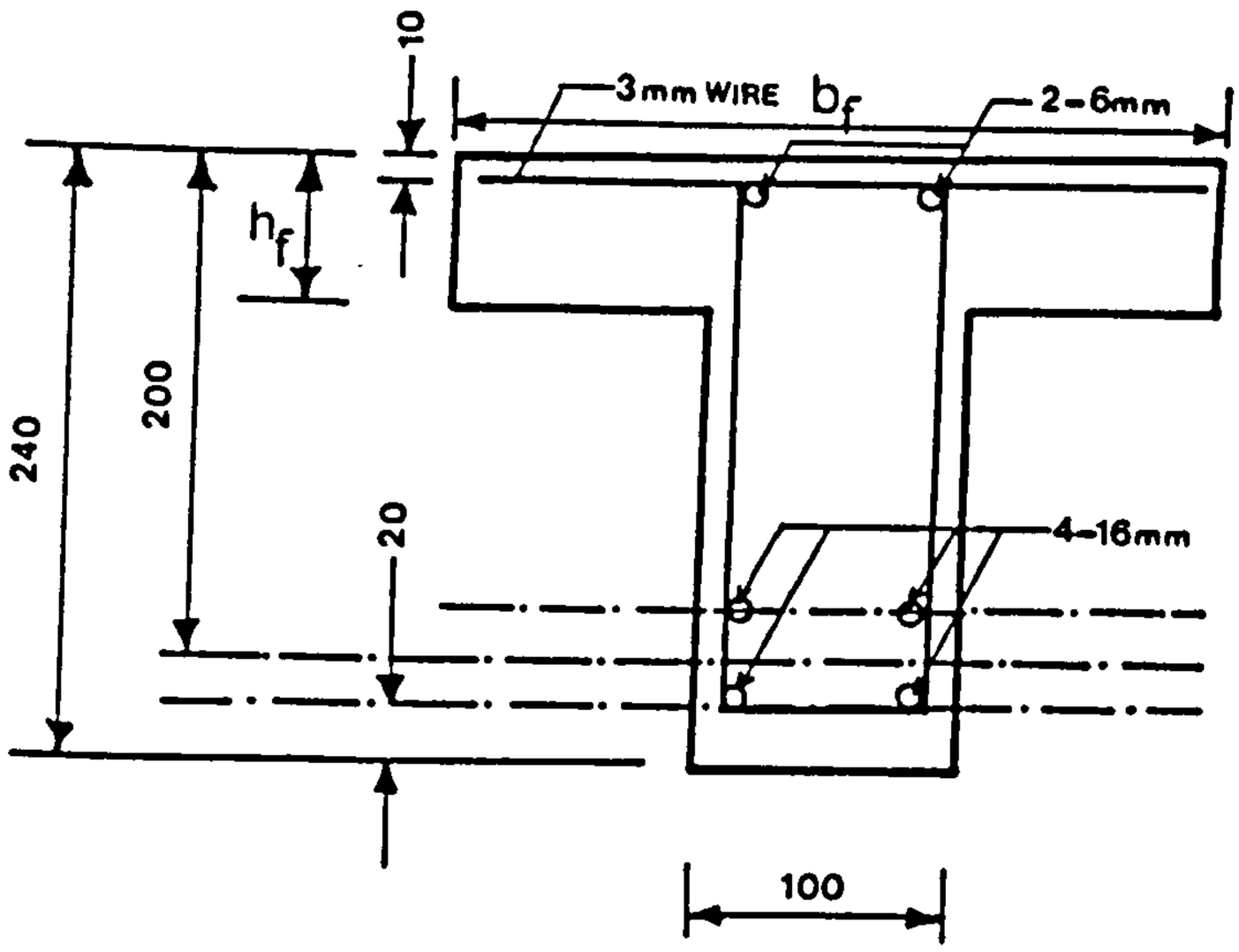

Figure (8•15) Section A-A from Figure (8•14).

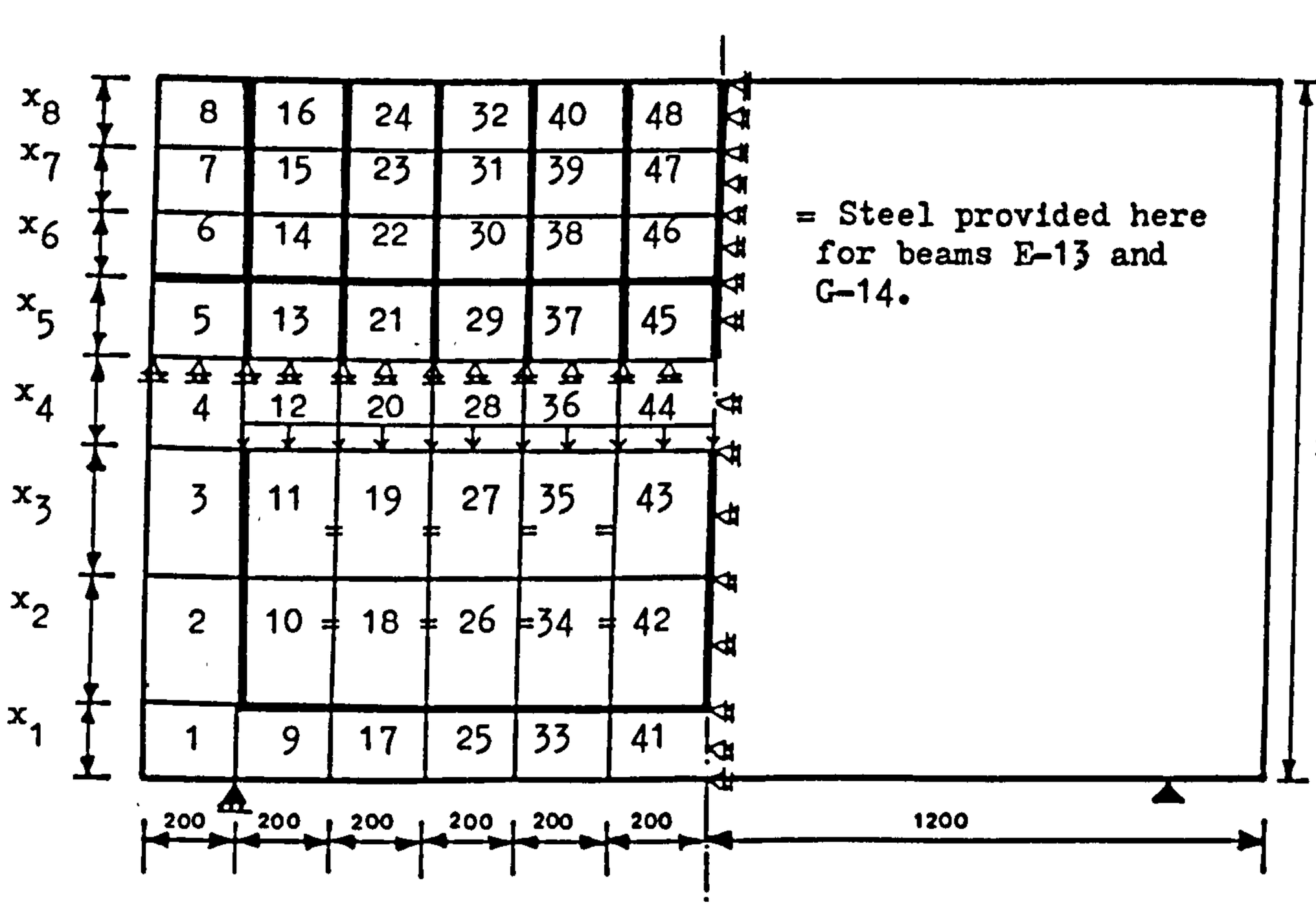

Figure (8•16) Mesh used for Chong T-beams.

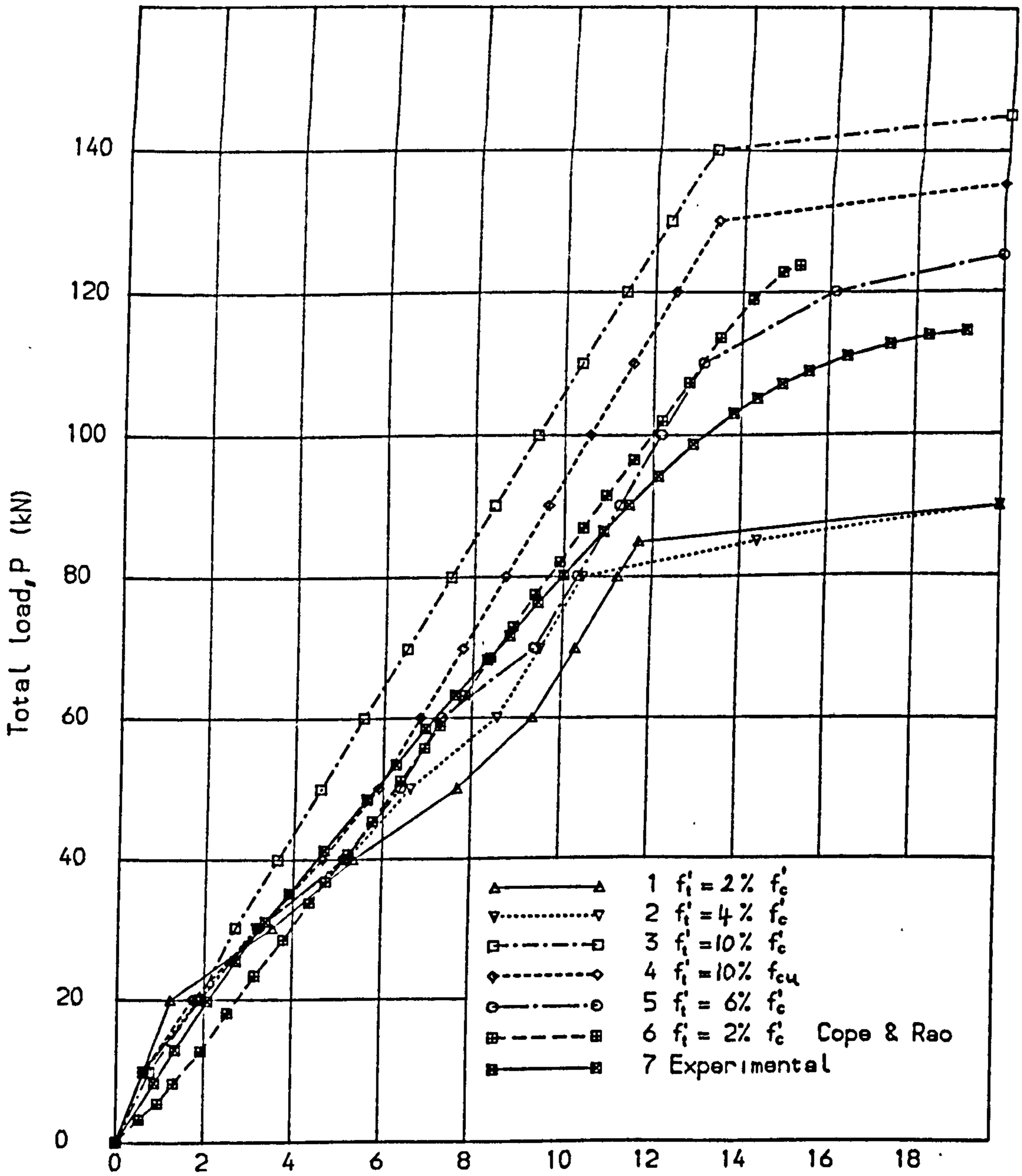

Fig. (8.17) Load deflection curves for Cope & Rao T beam B-2.

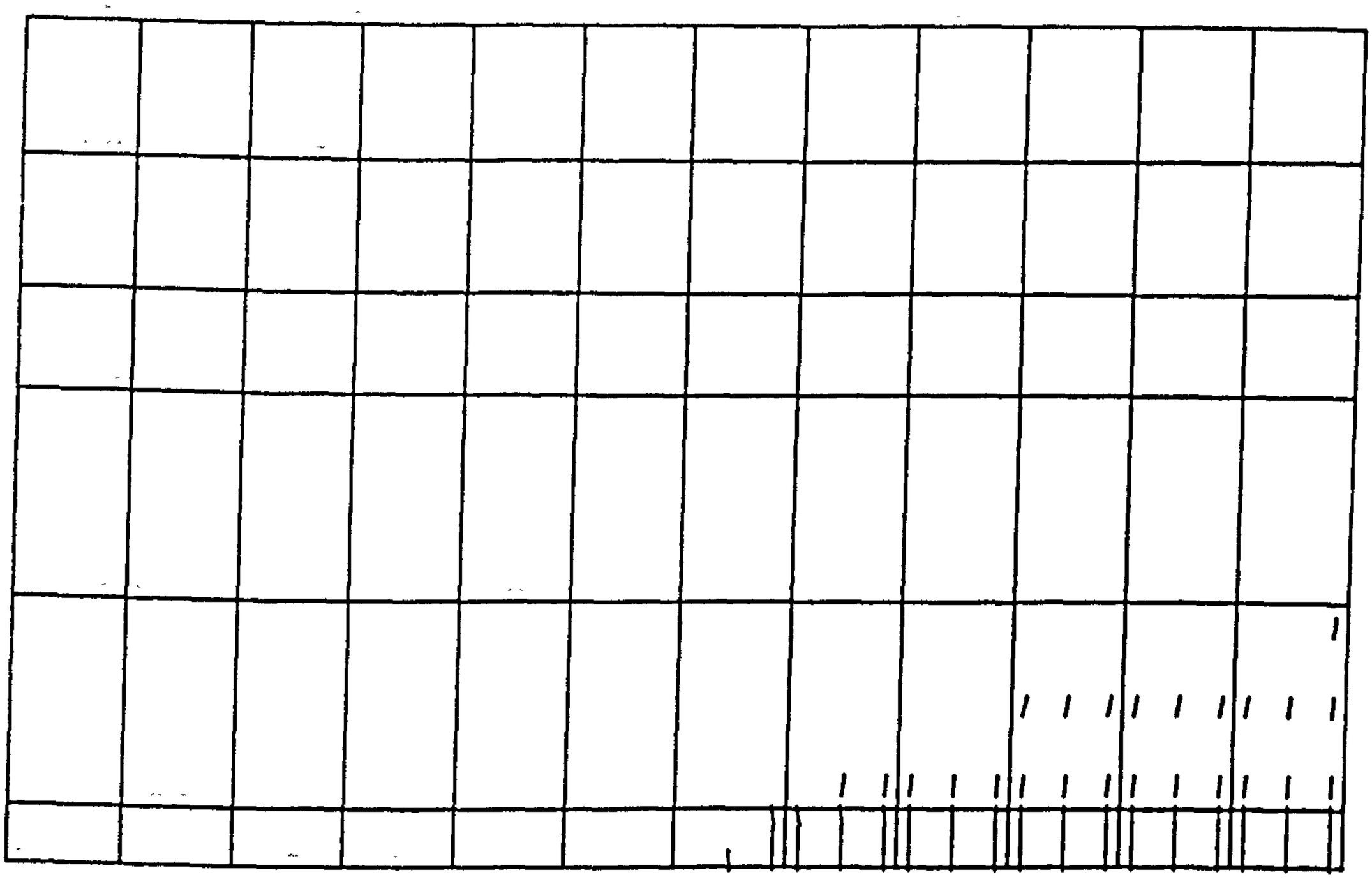

Figure (8•18) Crack pattern at load = 20•0 kN.

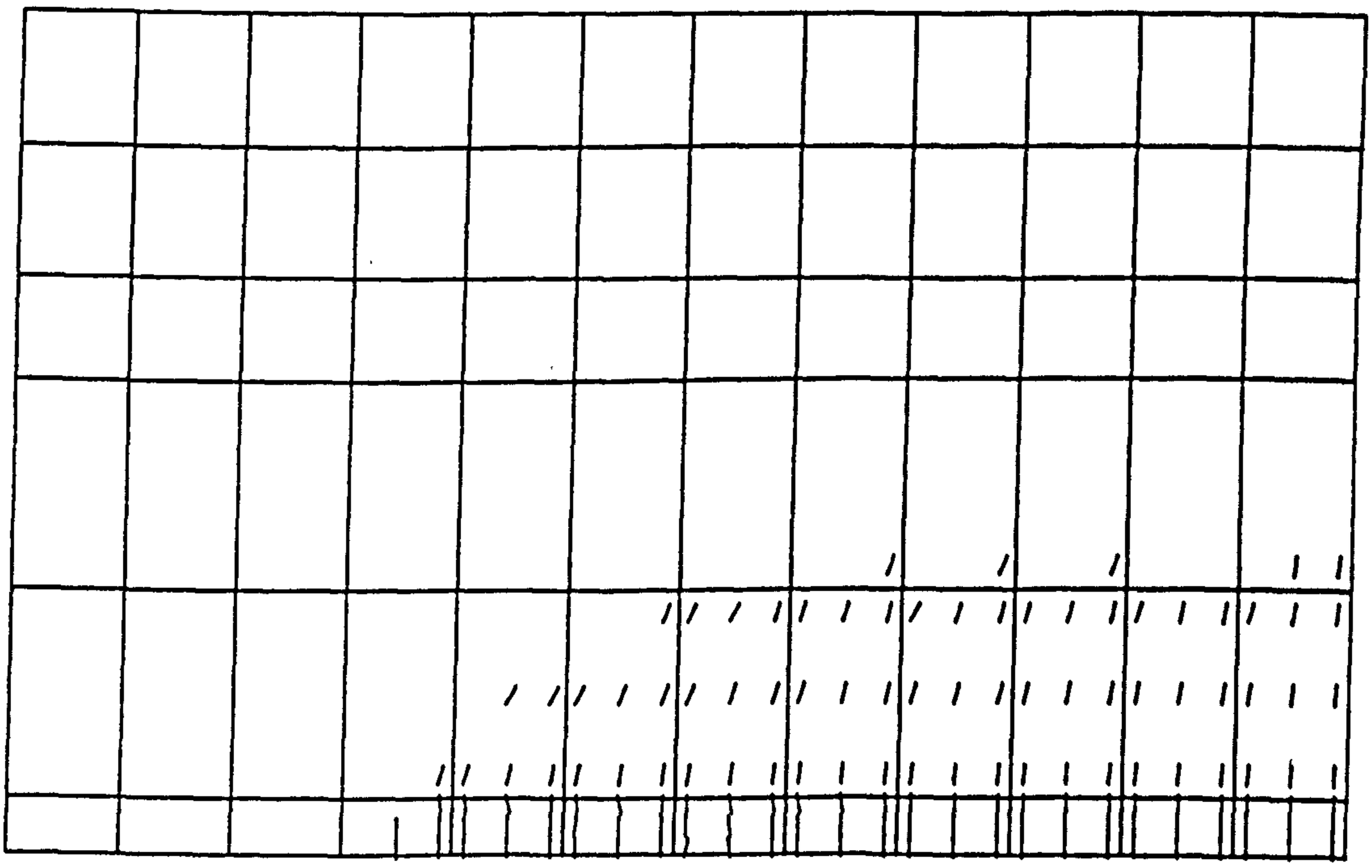

Figure (8•19) Crack pattern at load = 40•0 kN.

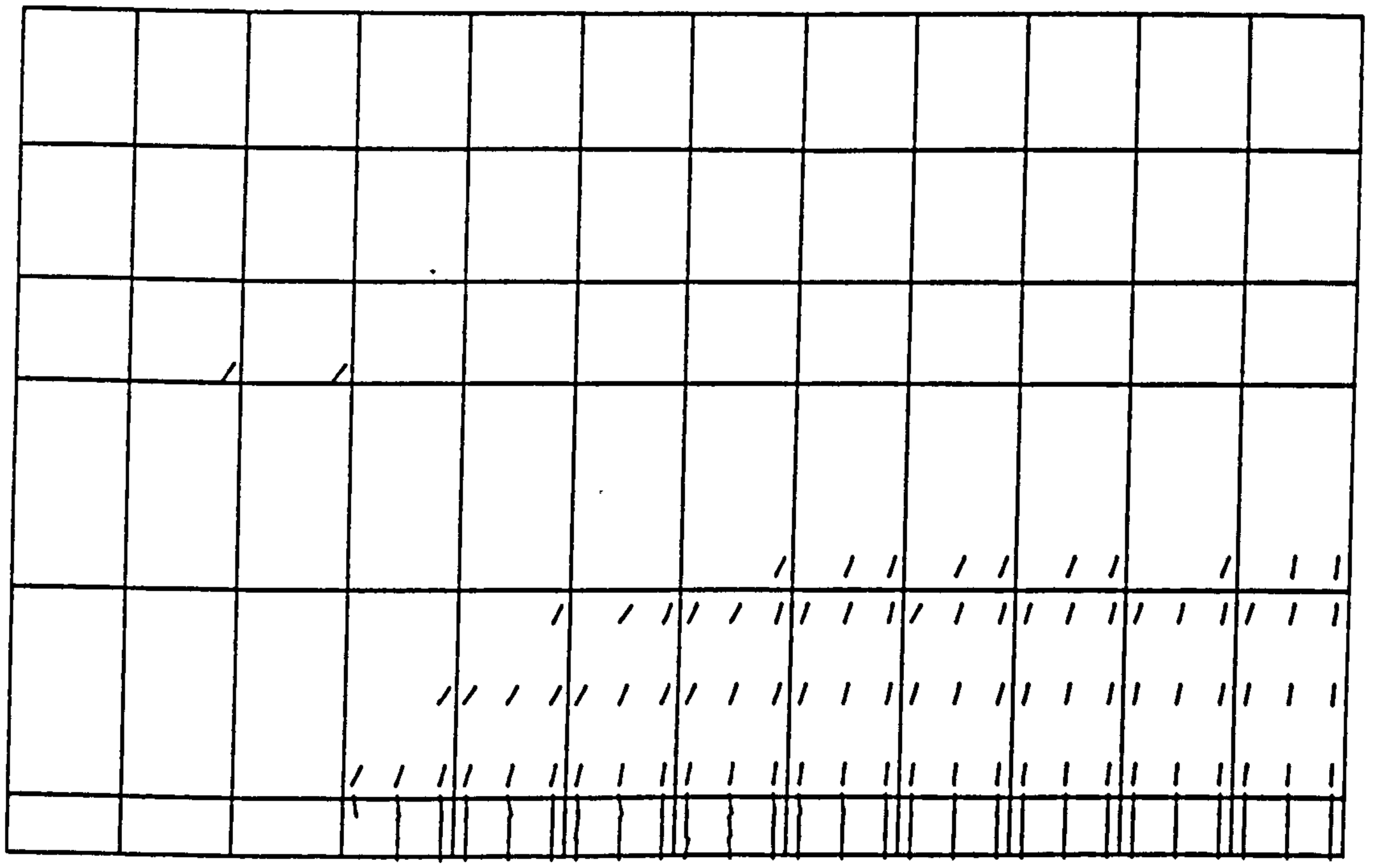

Figure (8•20) Crack pattern at load = 50•0 kN.

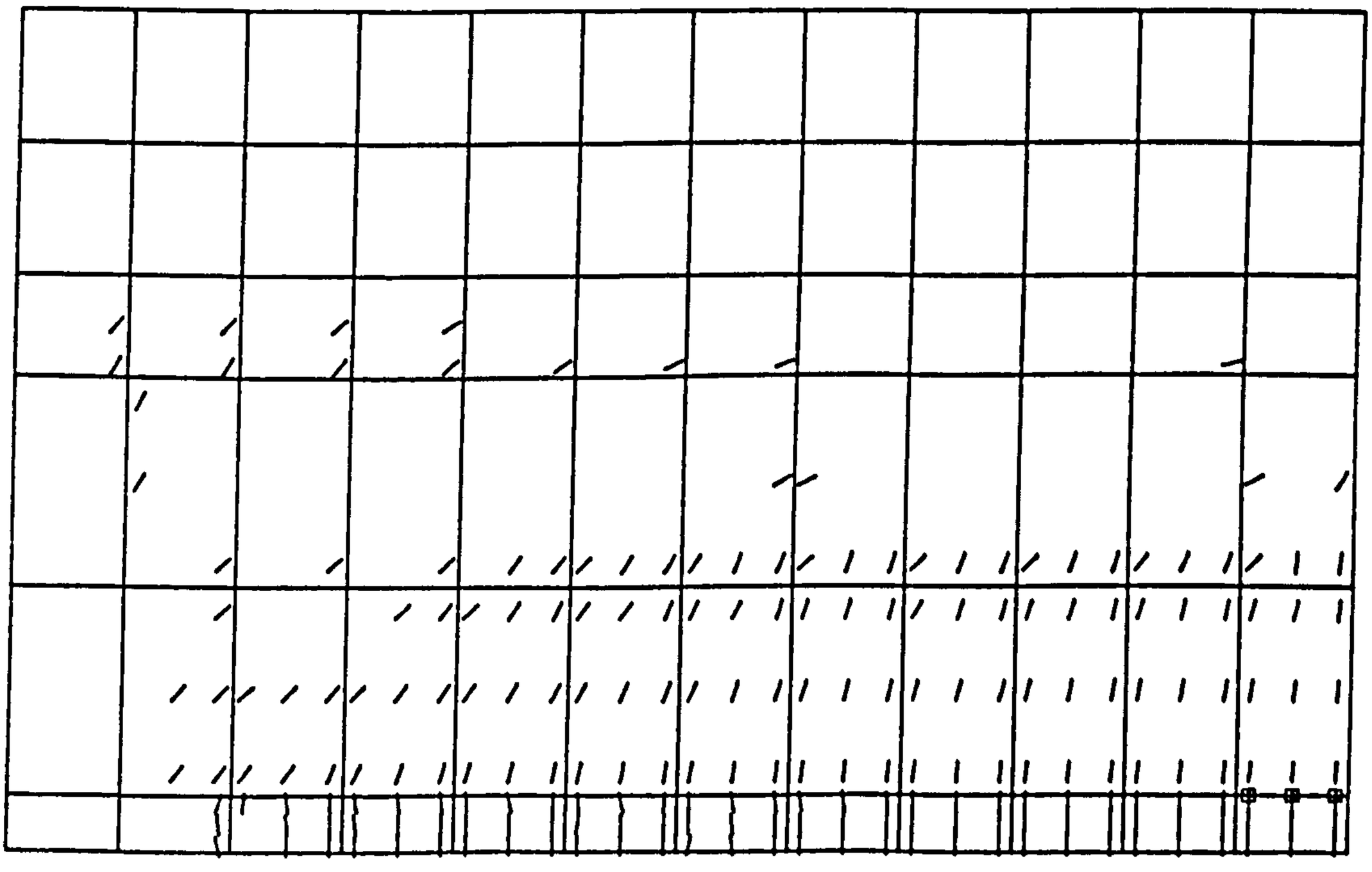

Figure (8•21) Crack pattern at load = 120•0 kN.

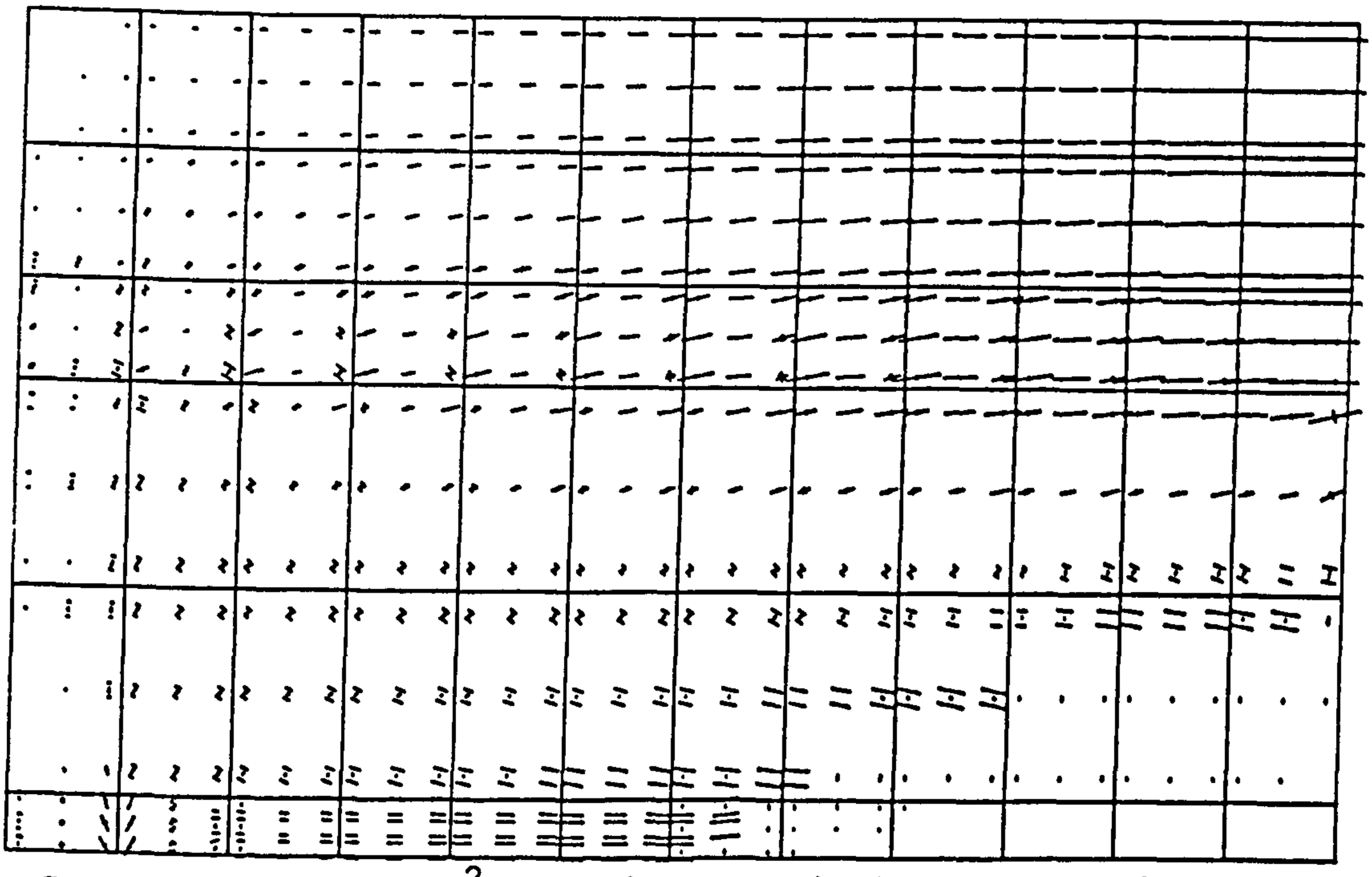

Scale:1 mm = 1·04 N/mm^2 (= tension), (- compression)

Figure (8·22) Principal stress direction at load = 20·0 kN.

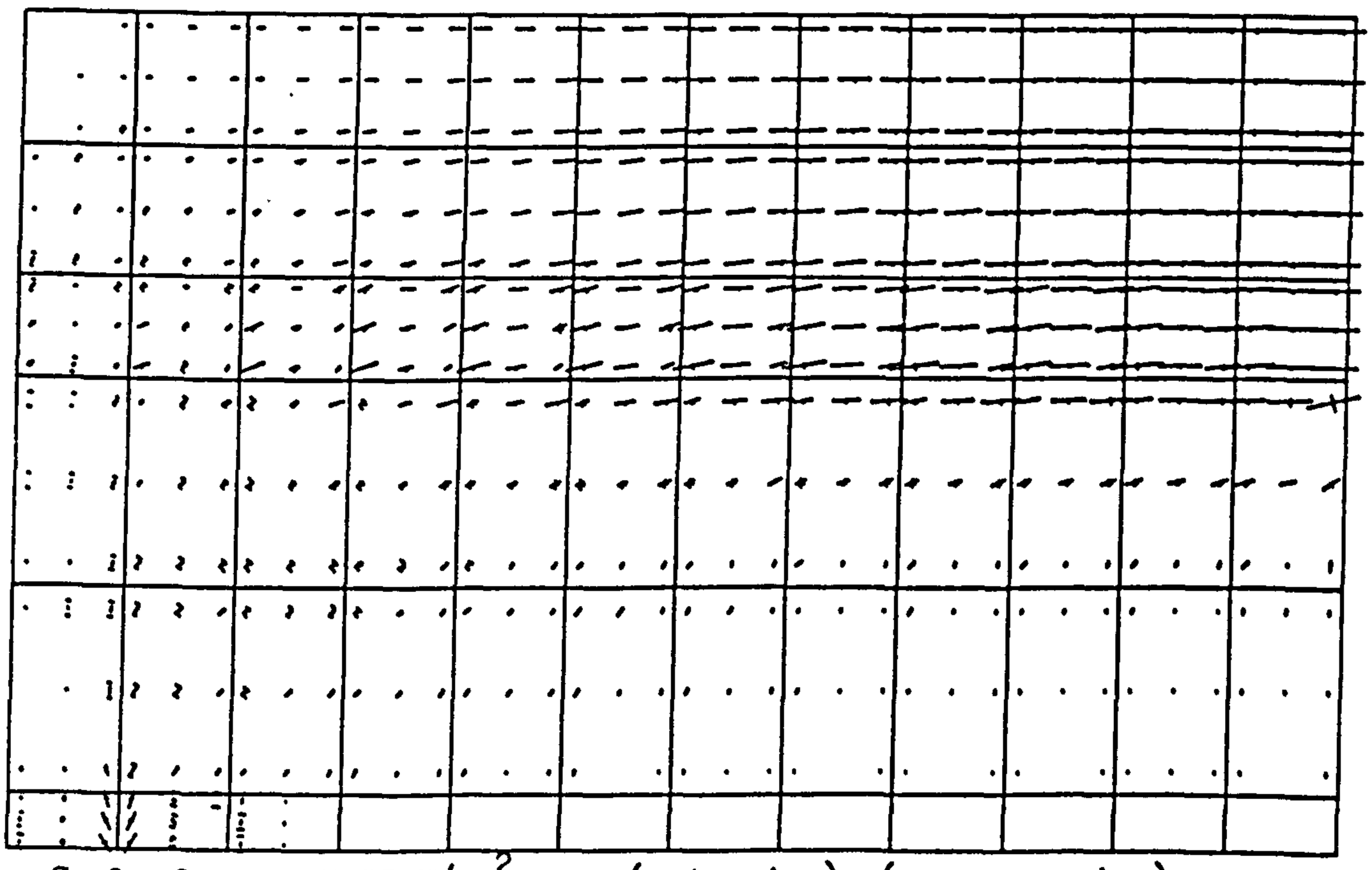

Scale: 1 mm = 5·03 N/mm^2 (= tension), (- compression)

Figure (8·23) Principal stress direction at load = 110·0 kN.

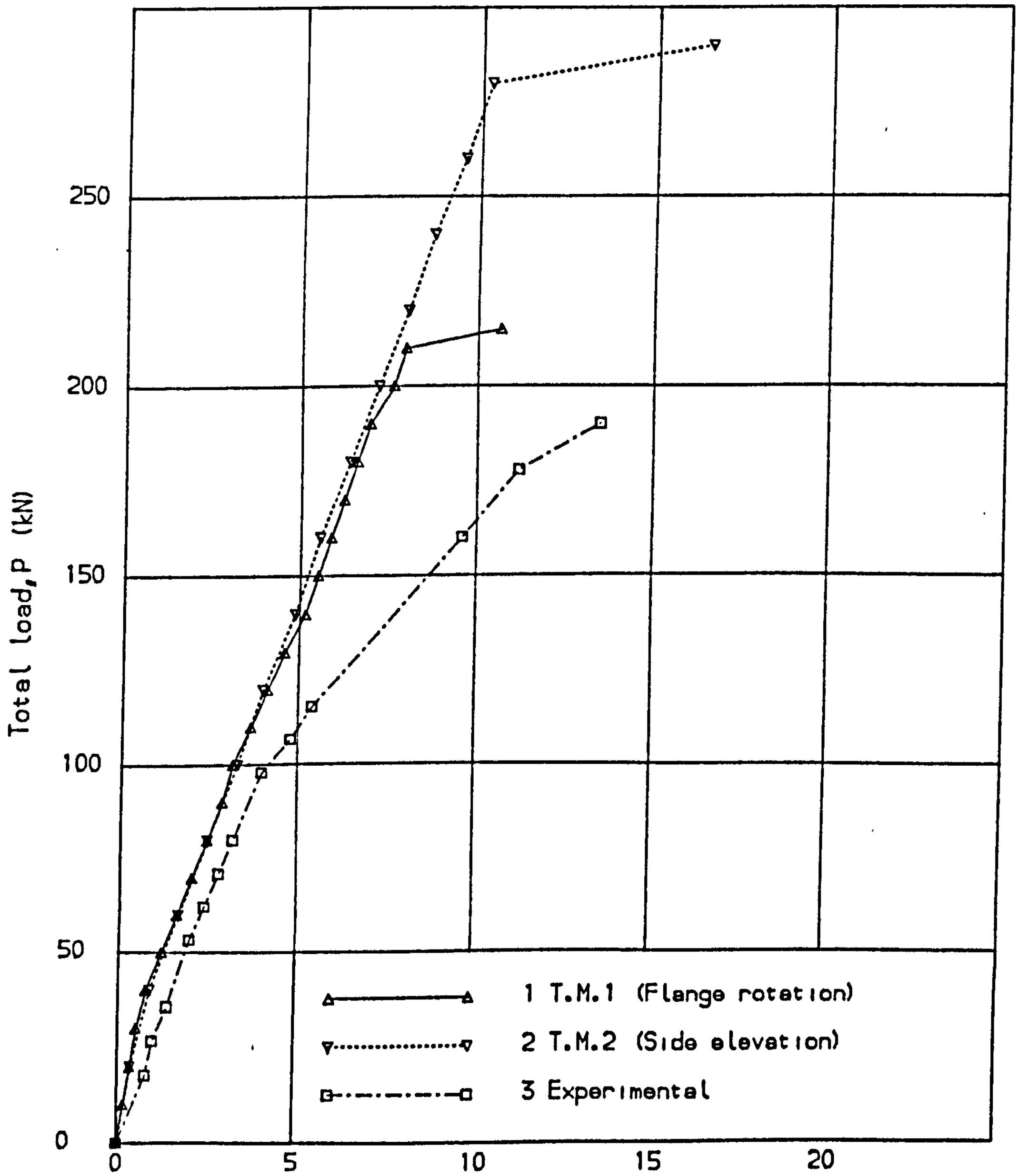

Fig. (8.24) Load deflection curves for Chong T beam B-10.

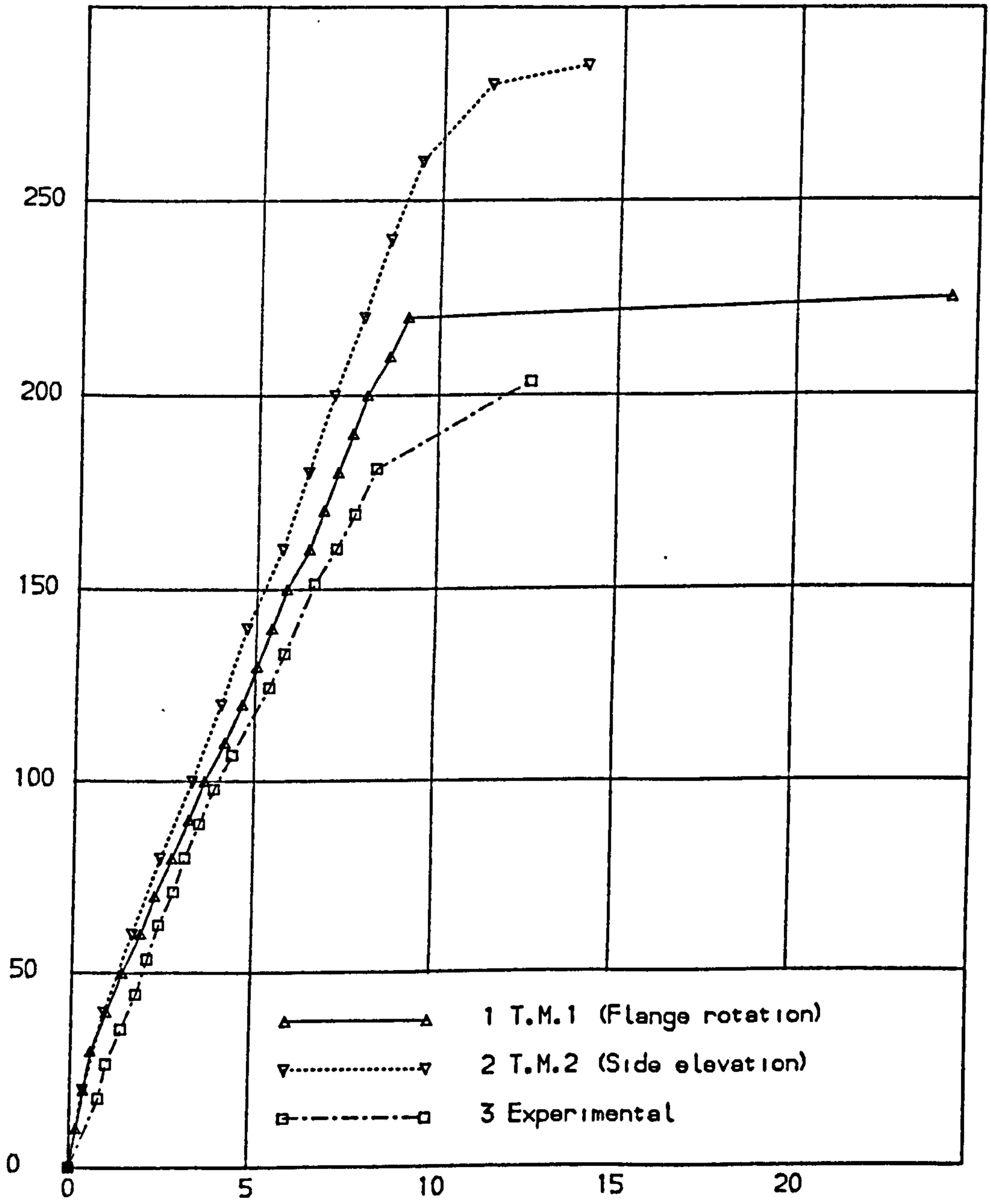

Fig. (8.25) Load deflection curves for Chong T beam E-10.

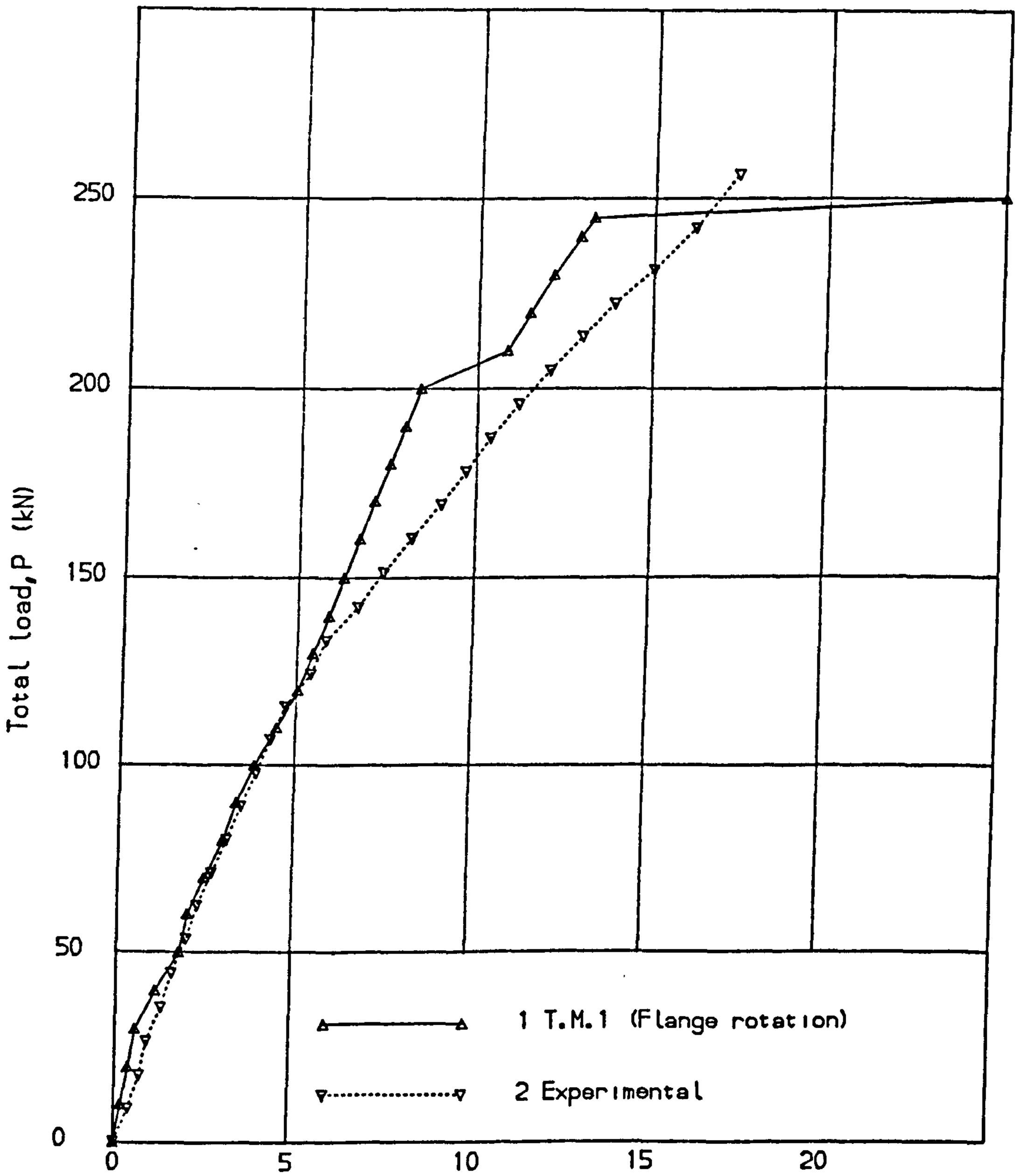

Fig. (8.26) Load deflection curves for Chong T beam H-10.

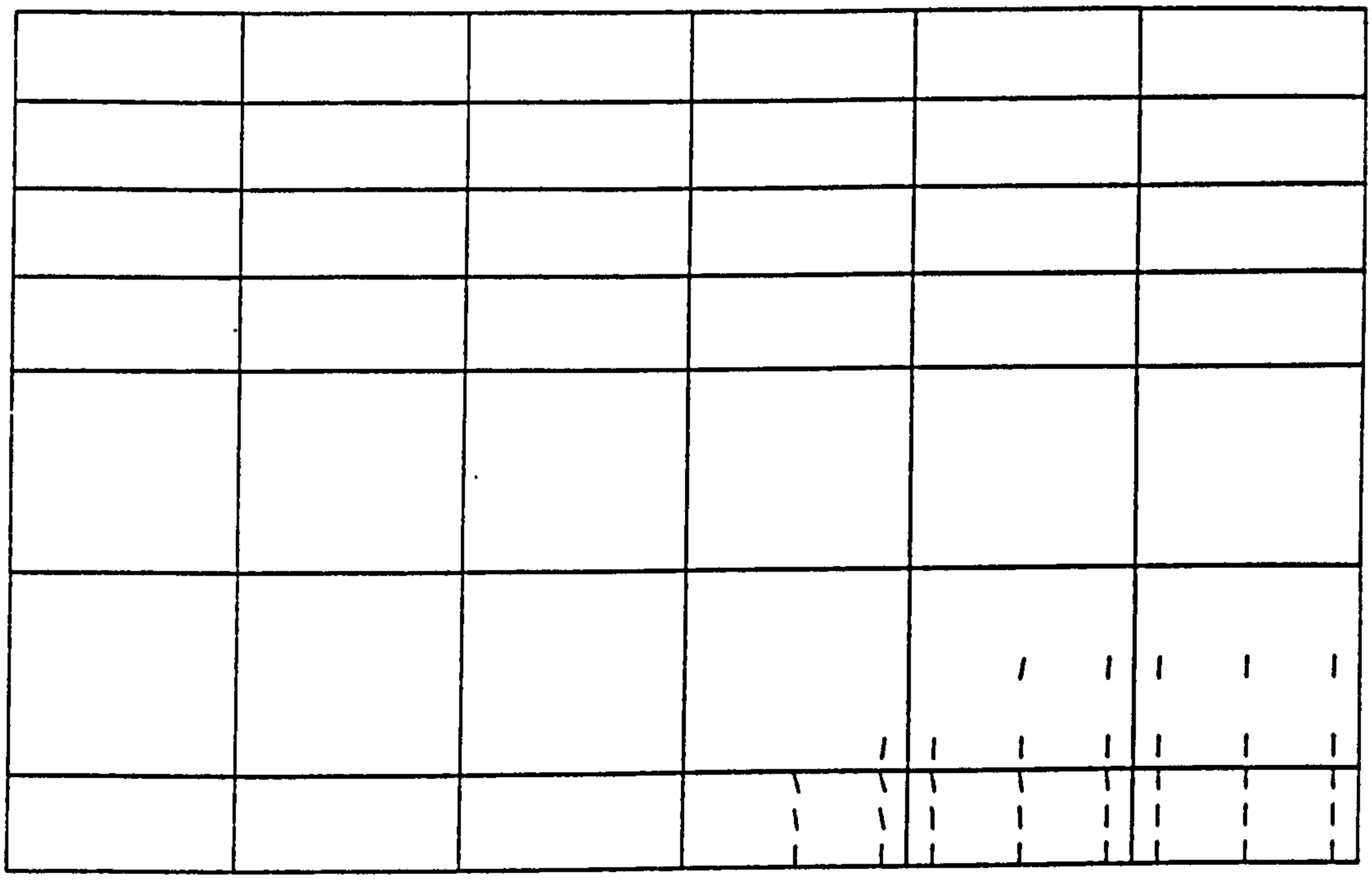

Figure (8•27) Crack pattern at load = 50•0 kN.

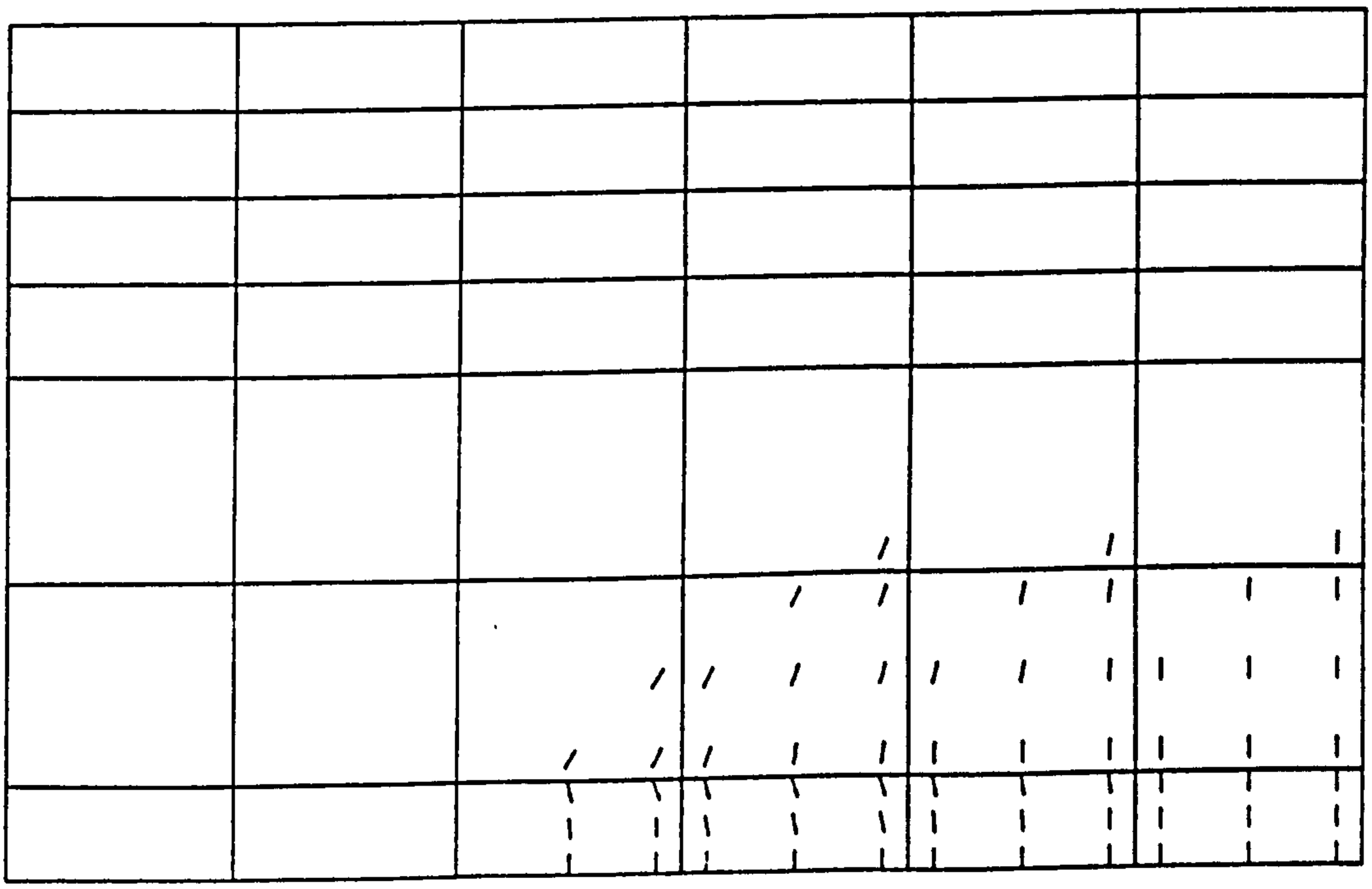

Figure (8•28) Crack pattern at load = 75•0 kN.

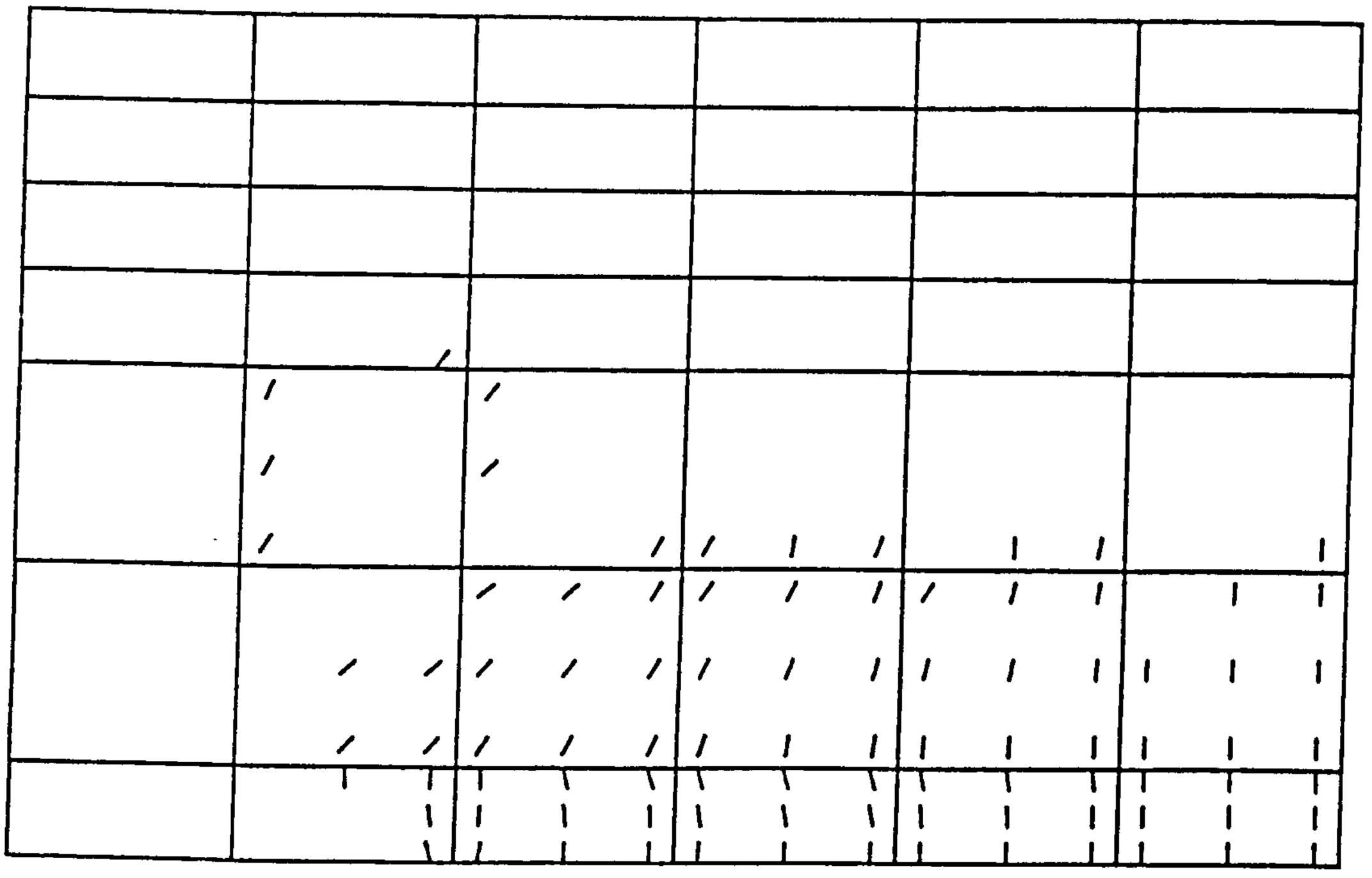

Figure (8·29) Crack pattern at load = 100·0 kN.

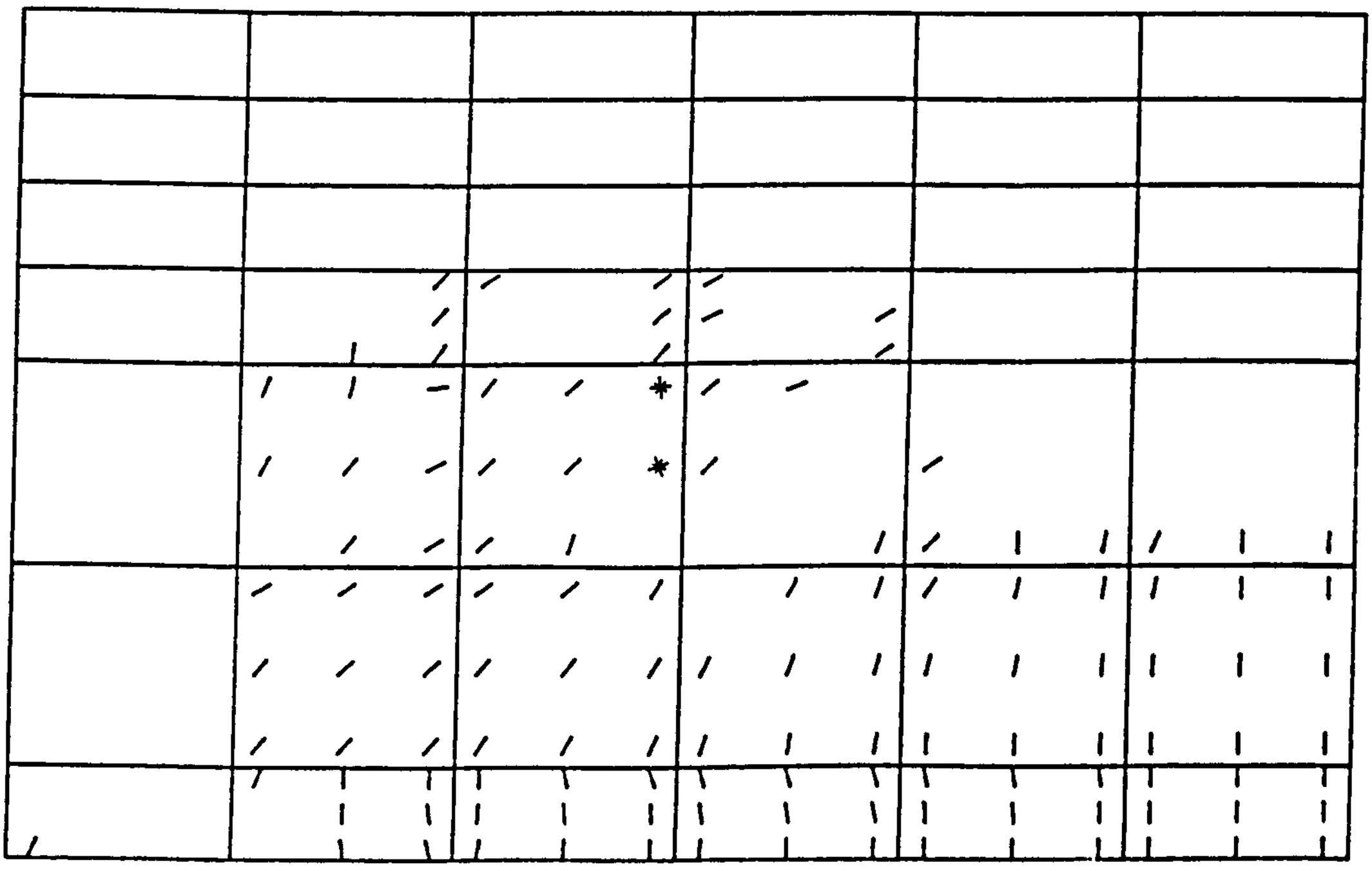

Figure (8·30) Crack pattern at load = 225.0 kN.

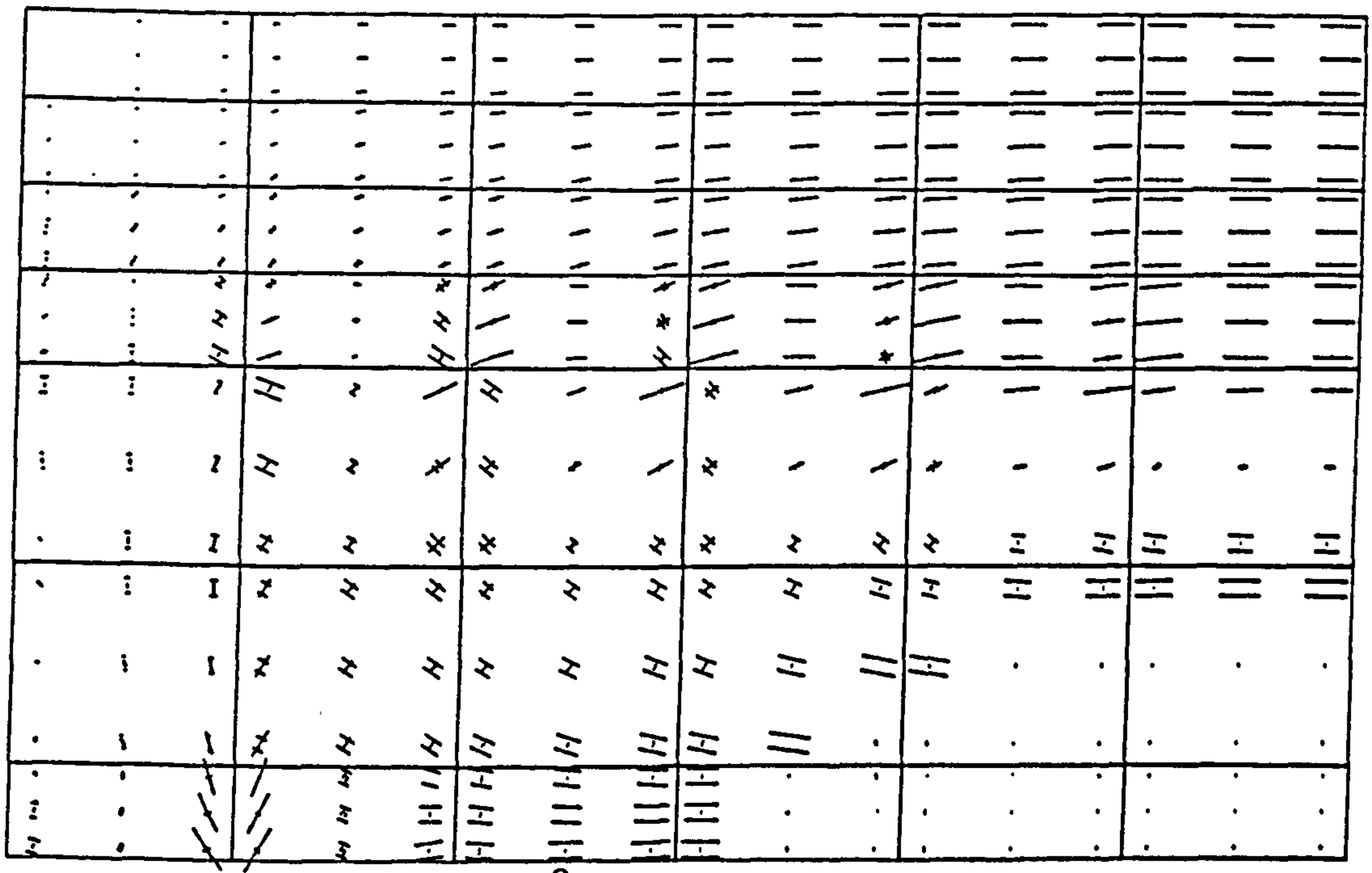

Scale: 1 mm = 0·82 N/mm^2 (= tension), (- compression)

Figure (8·31) Principal stress direction at load = 50·0 kN.

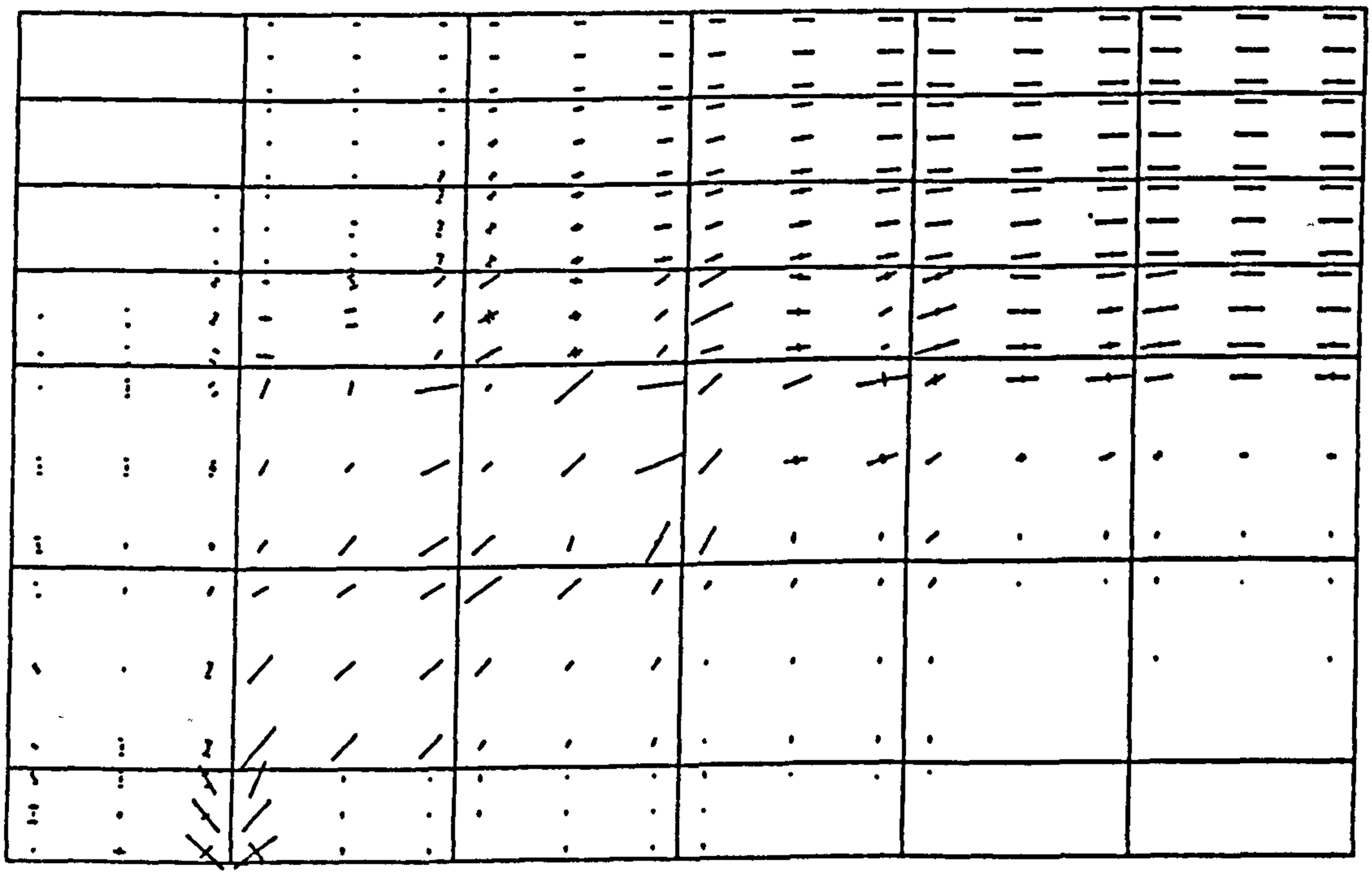

Scale: 1 mm = 3·76 N/mm^2 (= tension), (- compression)

Figure (8·32) Principal stress direction at load = 225.0 kN.

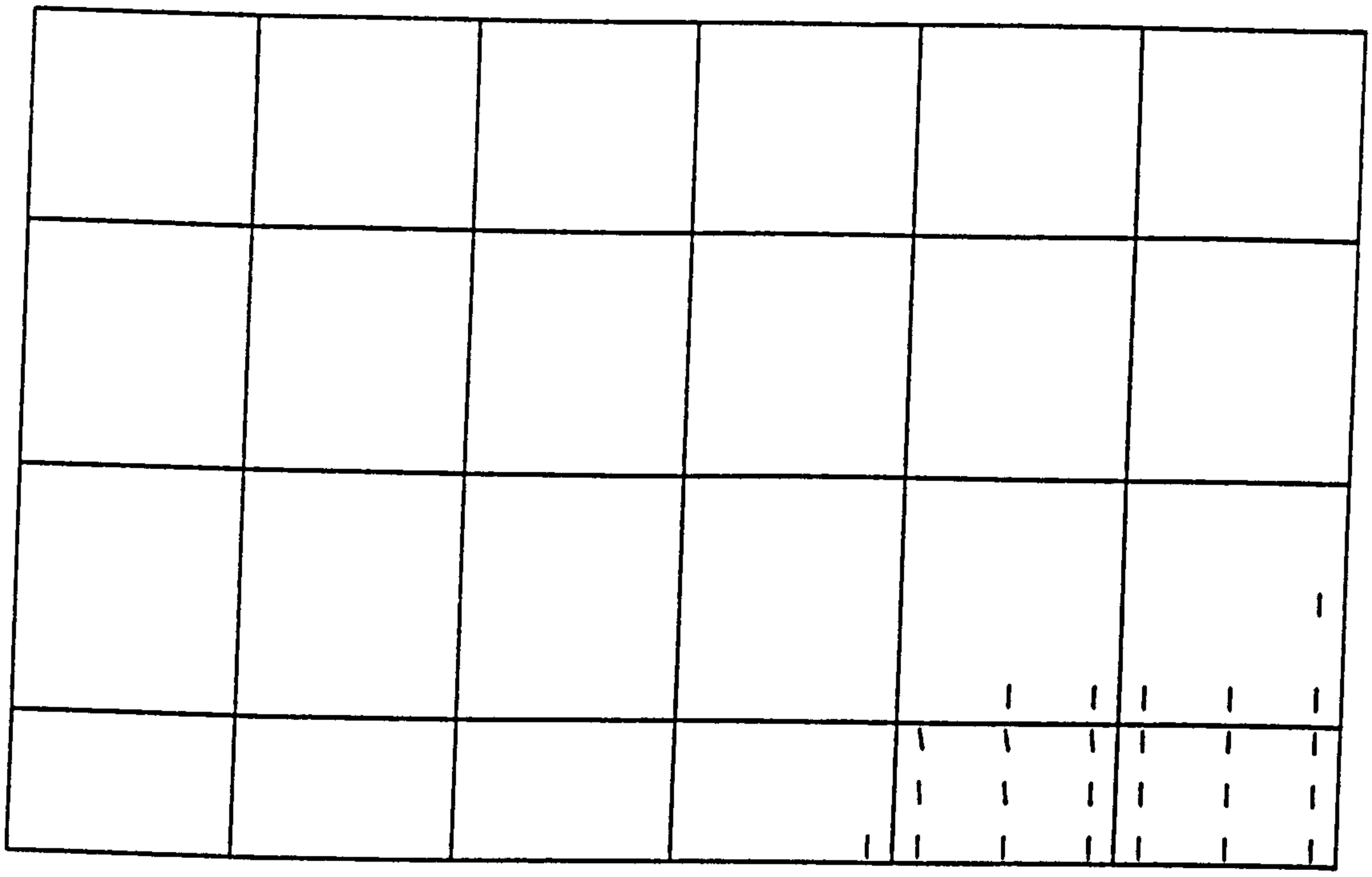

Figure (8•33) Crack pattern at load = 40•0 kN.

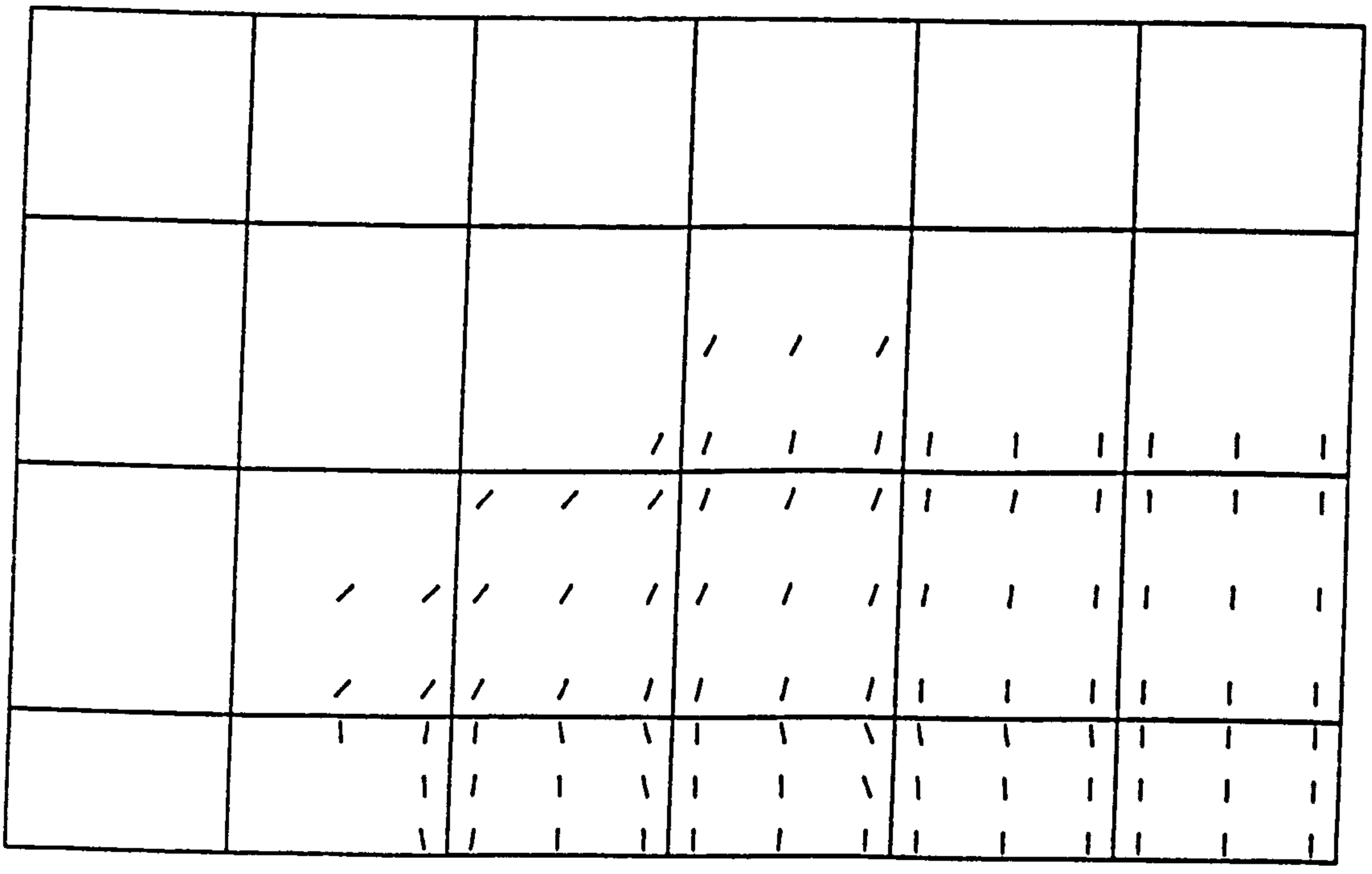

Figure (8•34) Crack pattern at load = 100•0 kN.

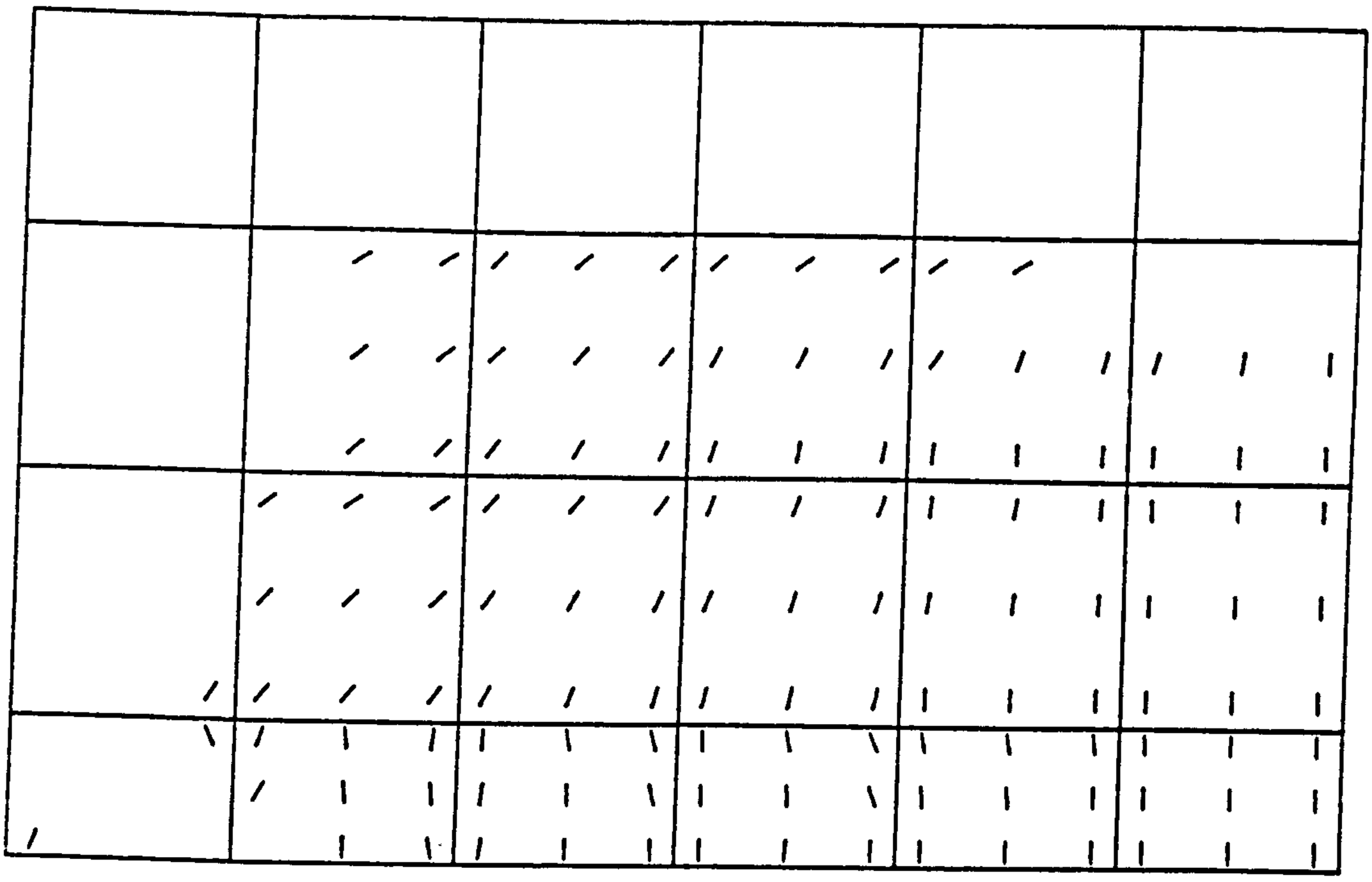

Figure (8•35) Crack pattern at load = 250•0 kN.

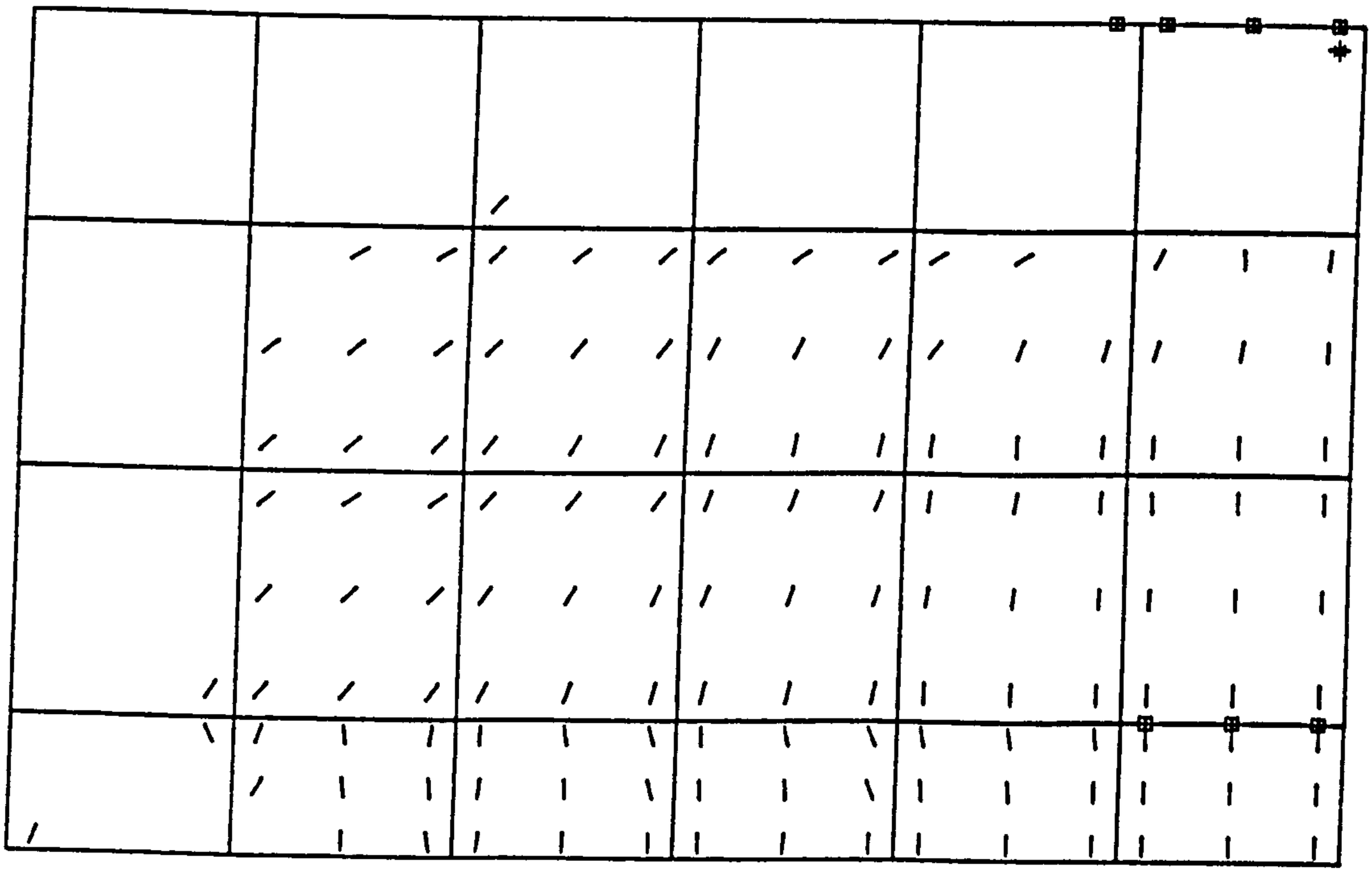

Figure (8•36) Crack pattern at load = 285.0 kN.

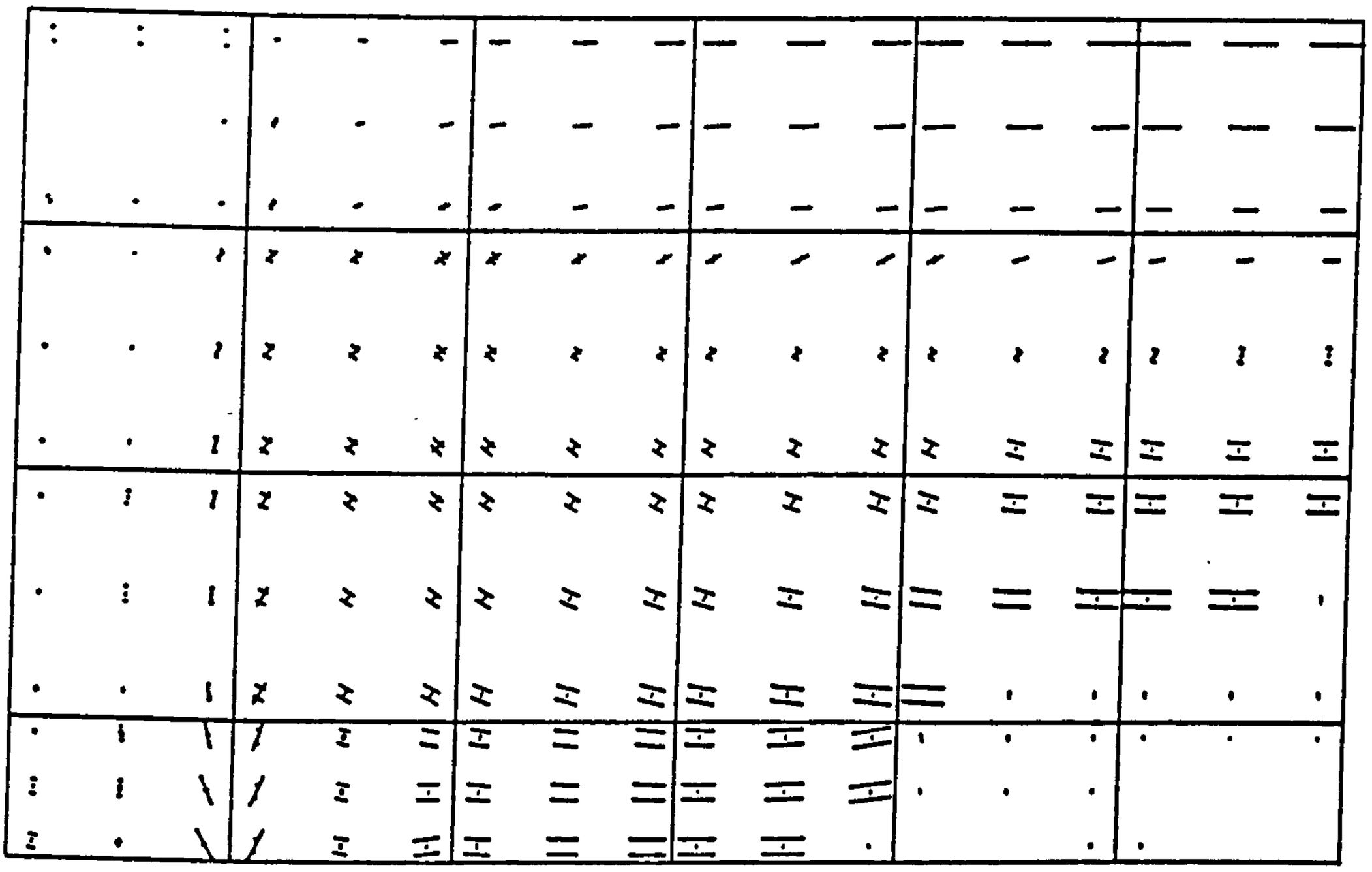

Scale: 1 mm = 0·76 N/mm^2 (= tension), (- compression)

Figure (8·37) Principal stress direction at load = 40·0 kN.

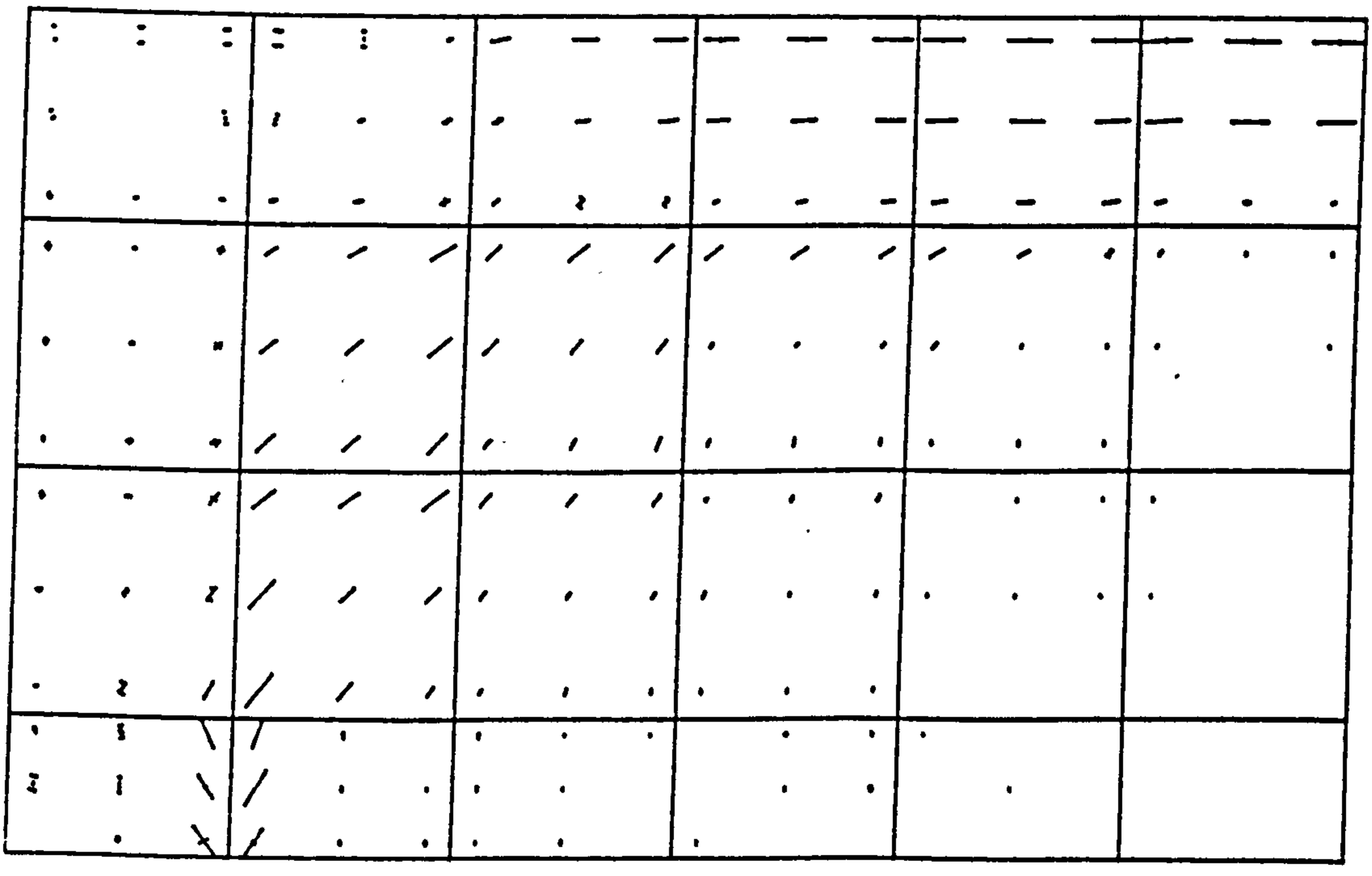

Scale: 1 mm = 5·35 N/mm^2 (= tension), (- compression)

Figure (8·38) Principal stress direction at load = 285·0 kN.

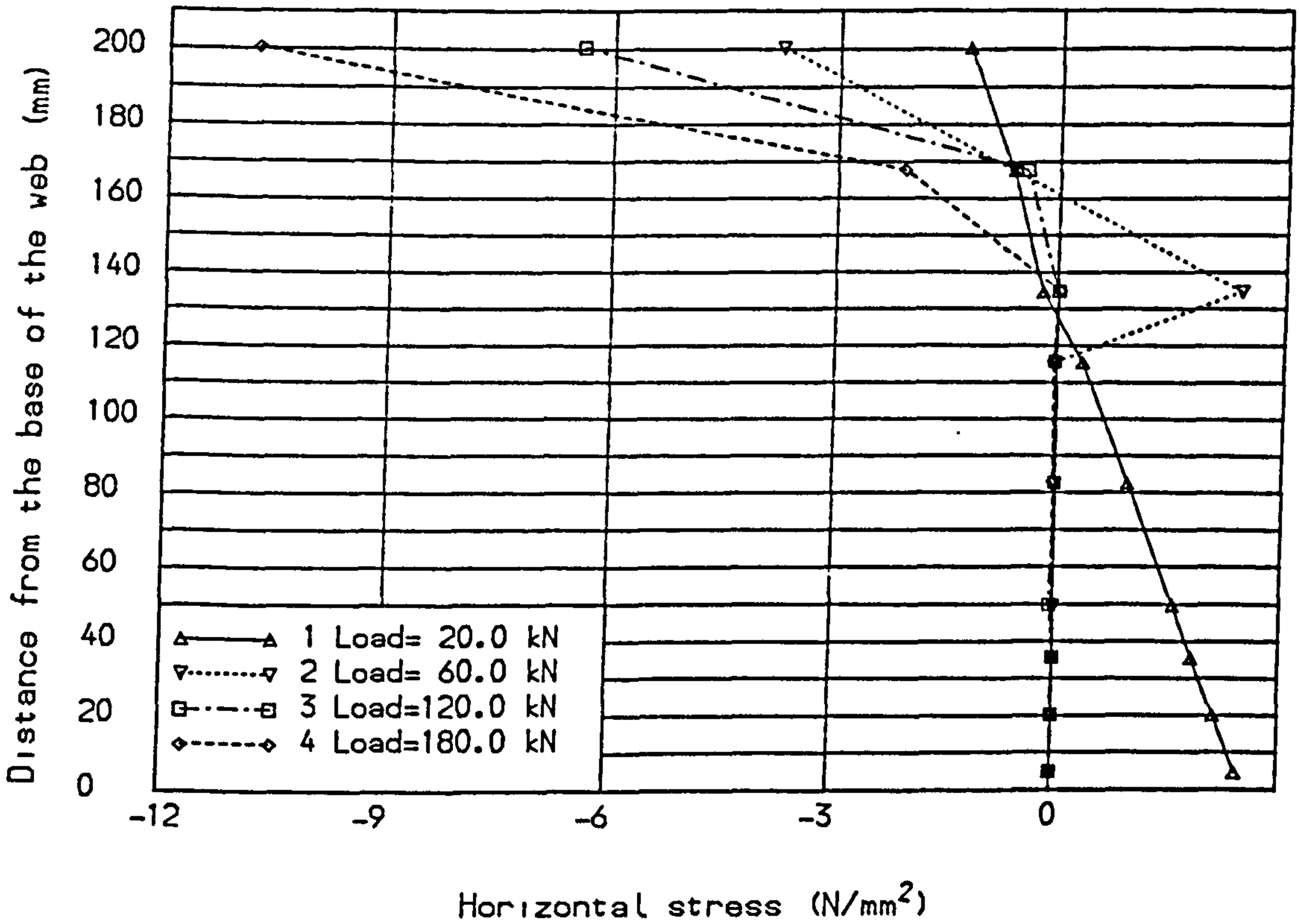

Fig. (8.39) Stress distribution at midspan section (Chong E-10).

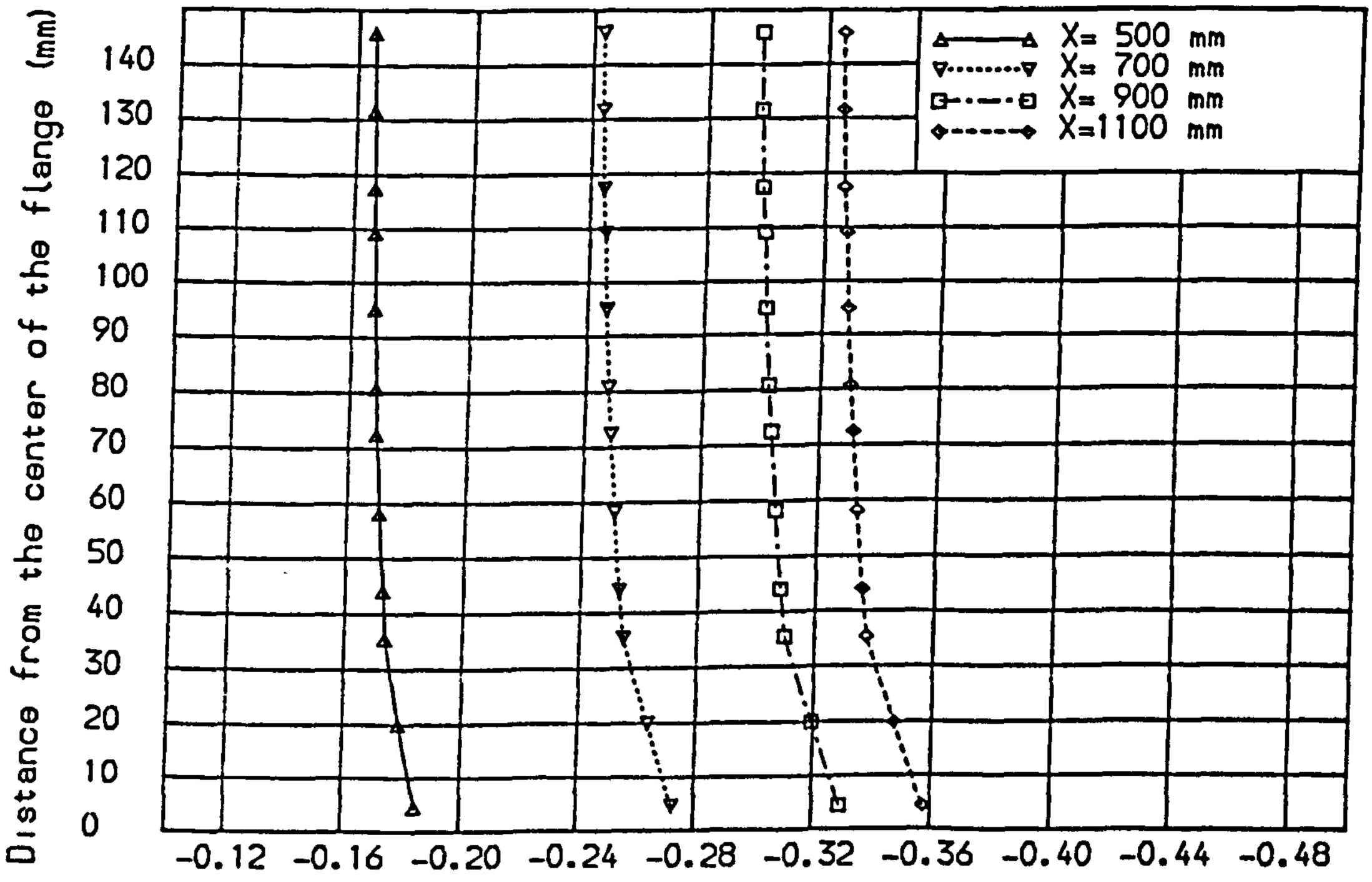

Fig. (8.40) Stress distribution for Chong T beam, (Load=5 kN).

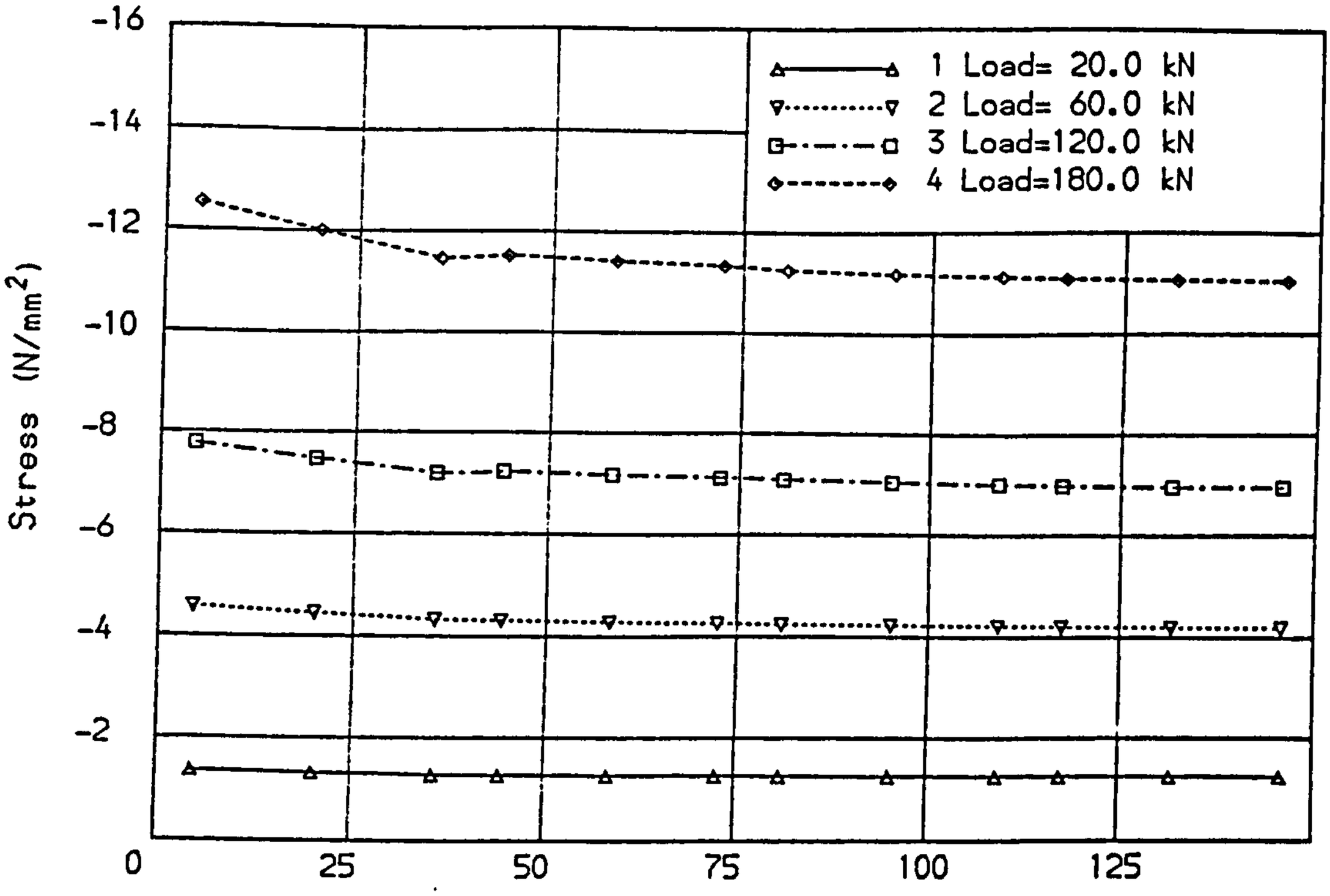

Fig. (8.41) Horizontal stress distribution for Chong T beam E-10.

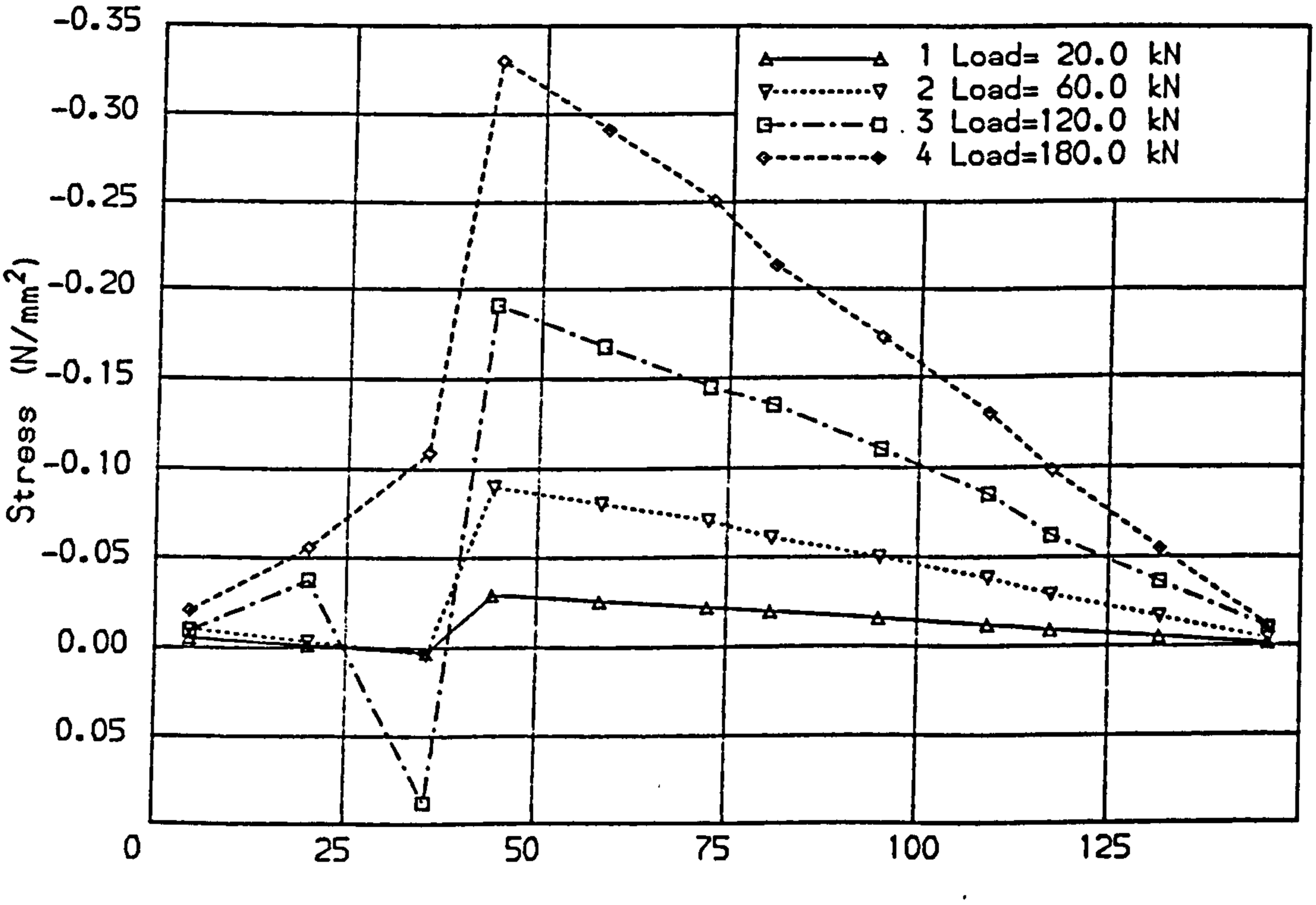

Fig. (8.42) Shear stress distribution for Chong T beam E-10.

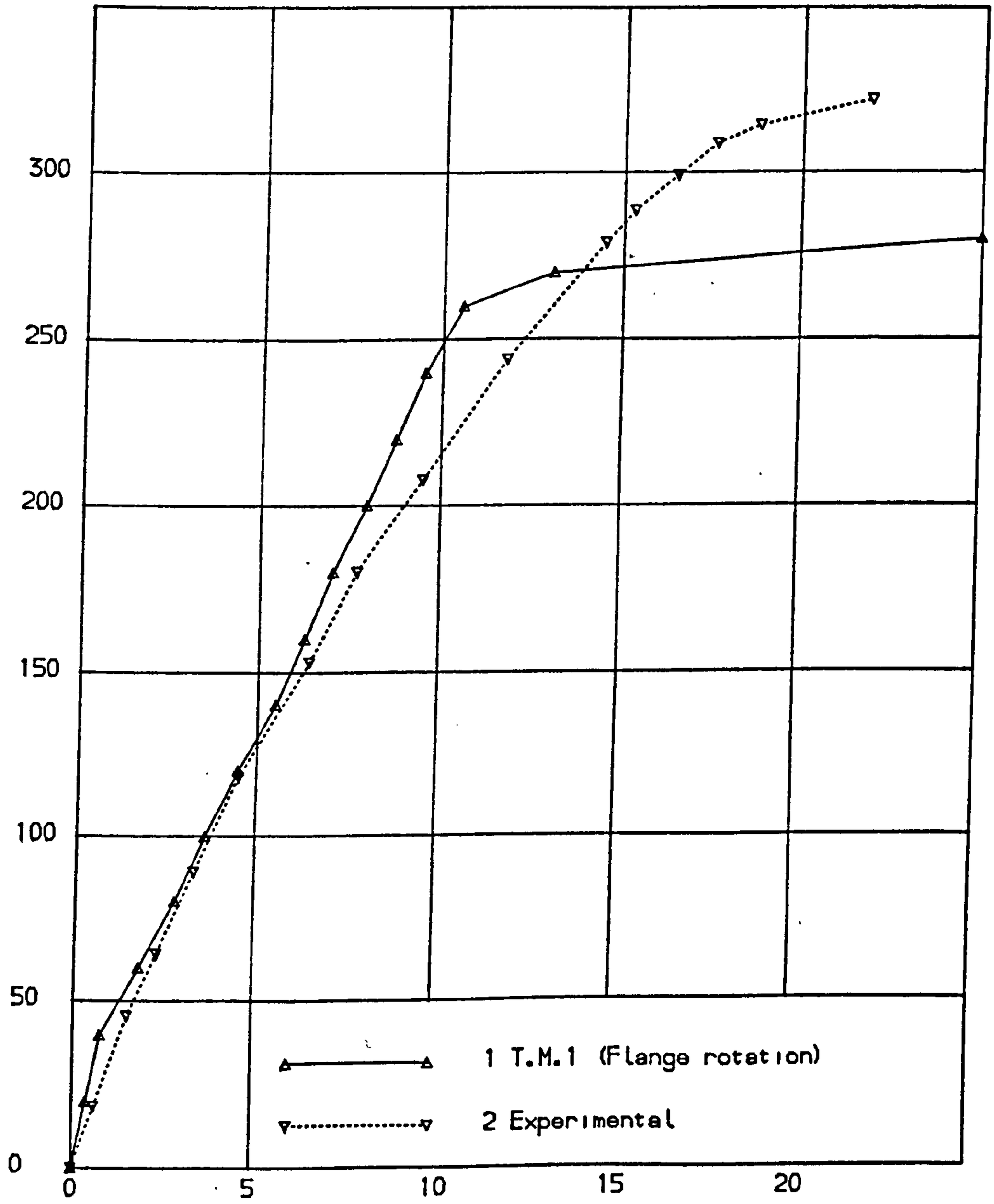

Fig. (8.43) Load deflection curves for Chong T beam E-13.

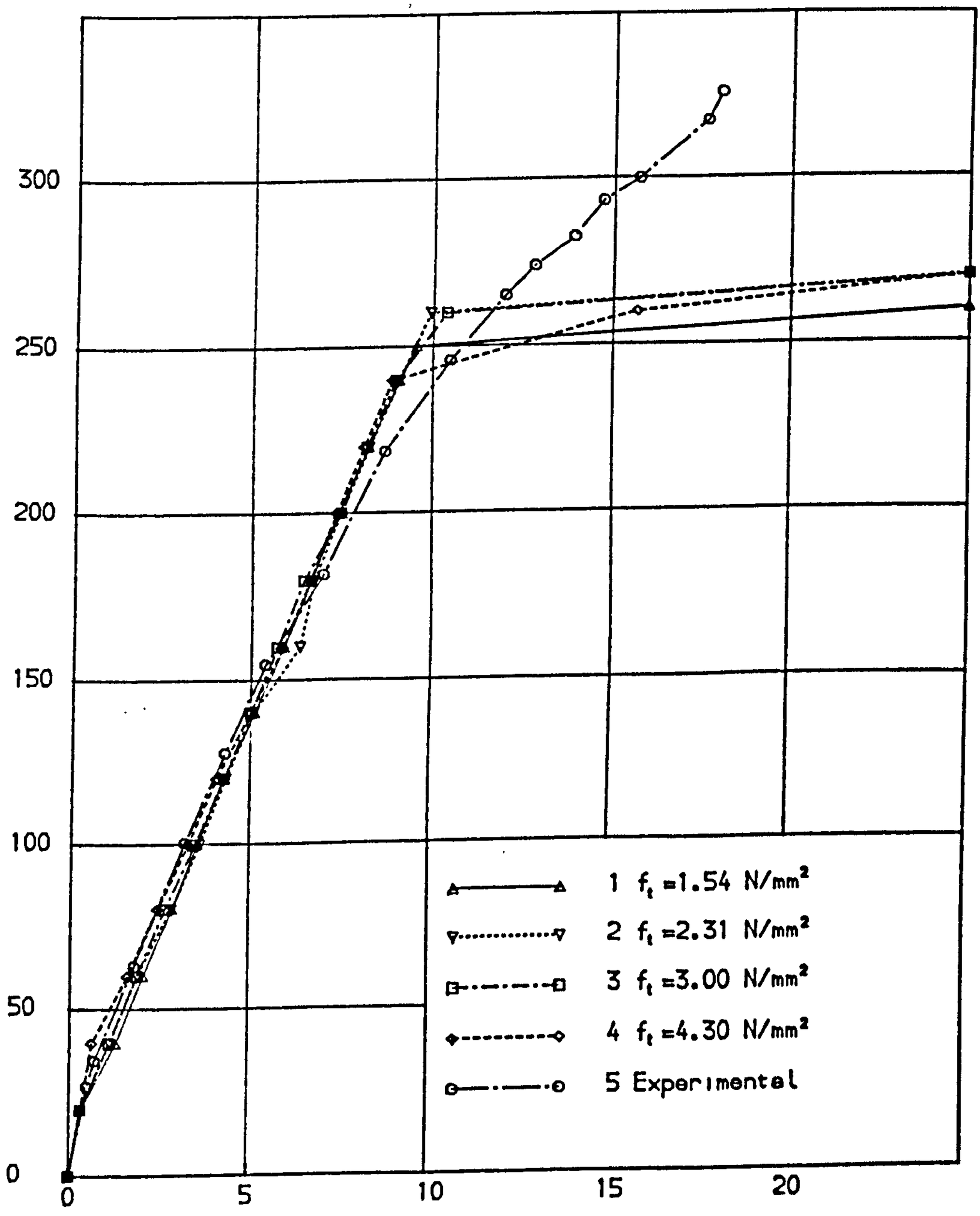

Fig. (8.44) Load deflection curves for Chong T beam G-14.

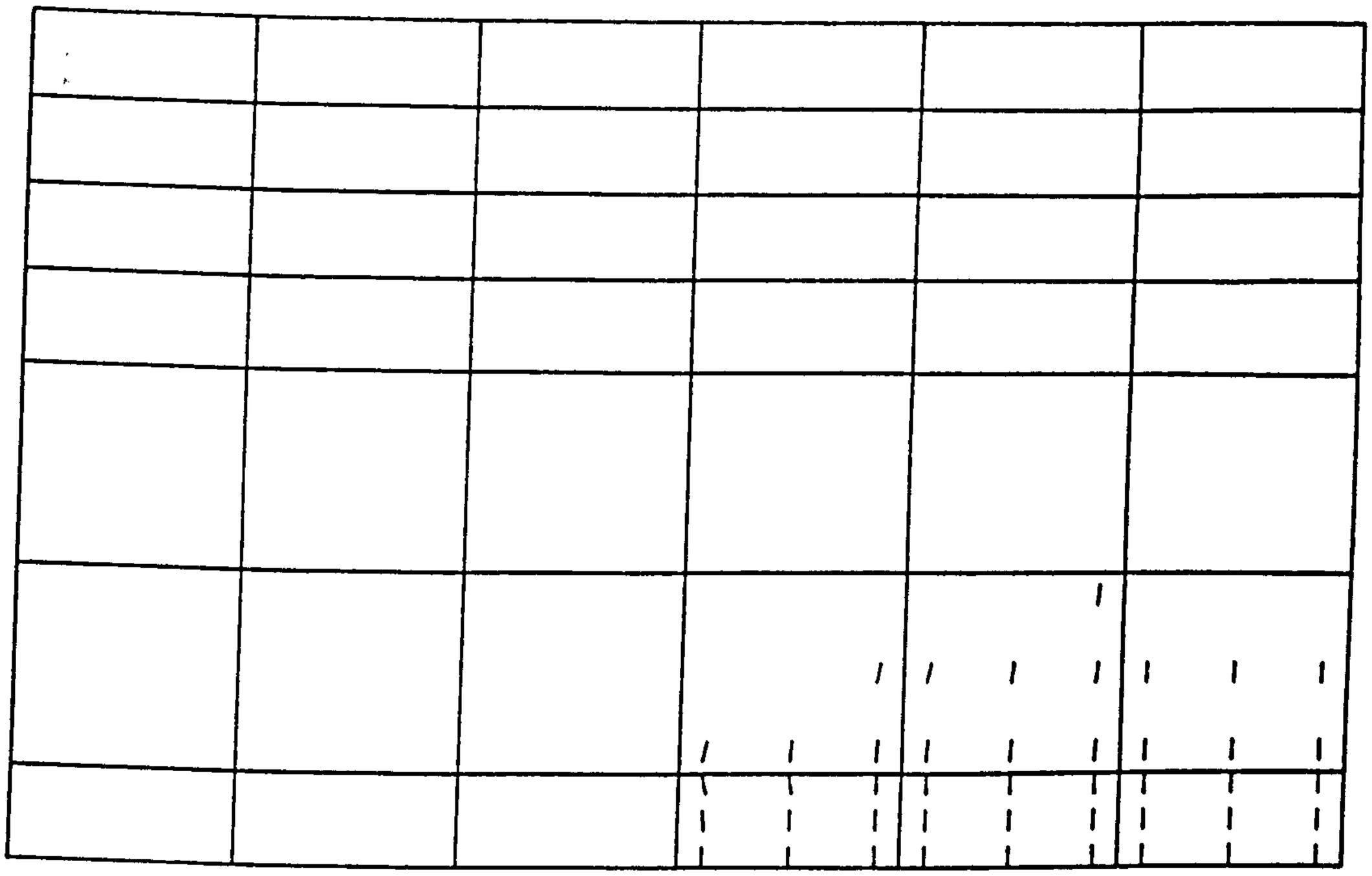

Figure (8·45) Crack pattern at load = 50·0 kN.

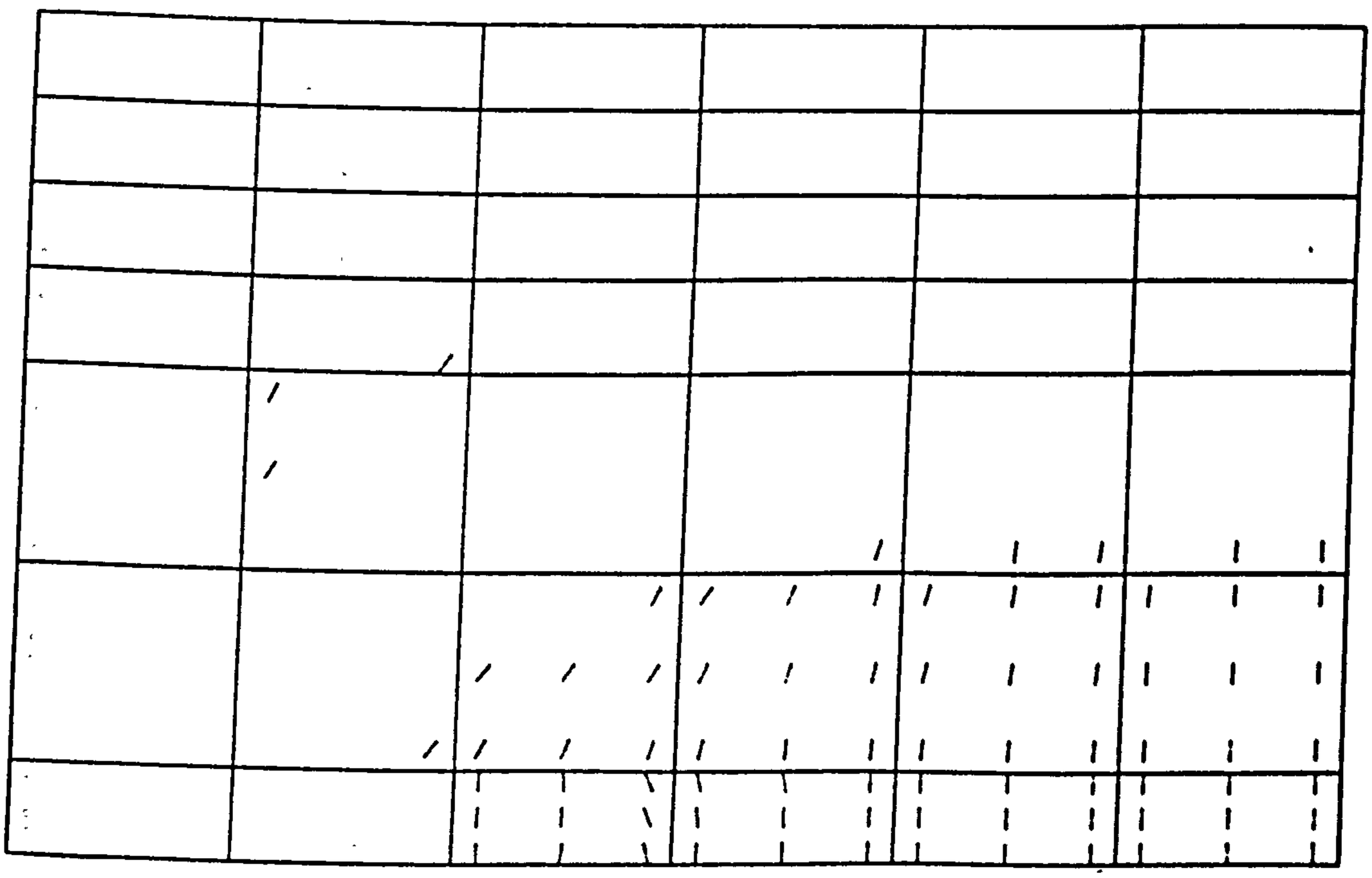

Figure (8·46) Crack pattern at load = 90·0 kN.

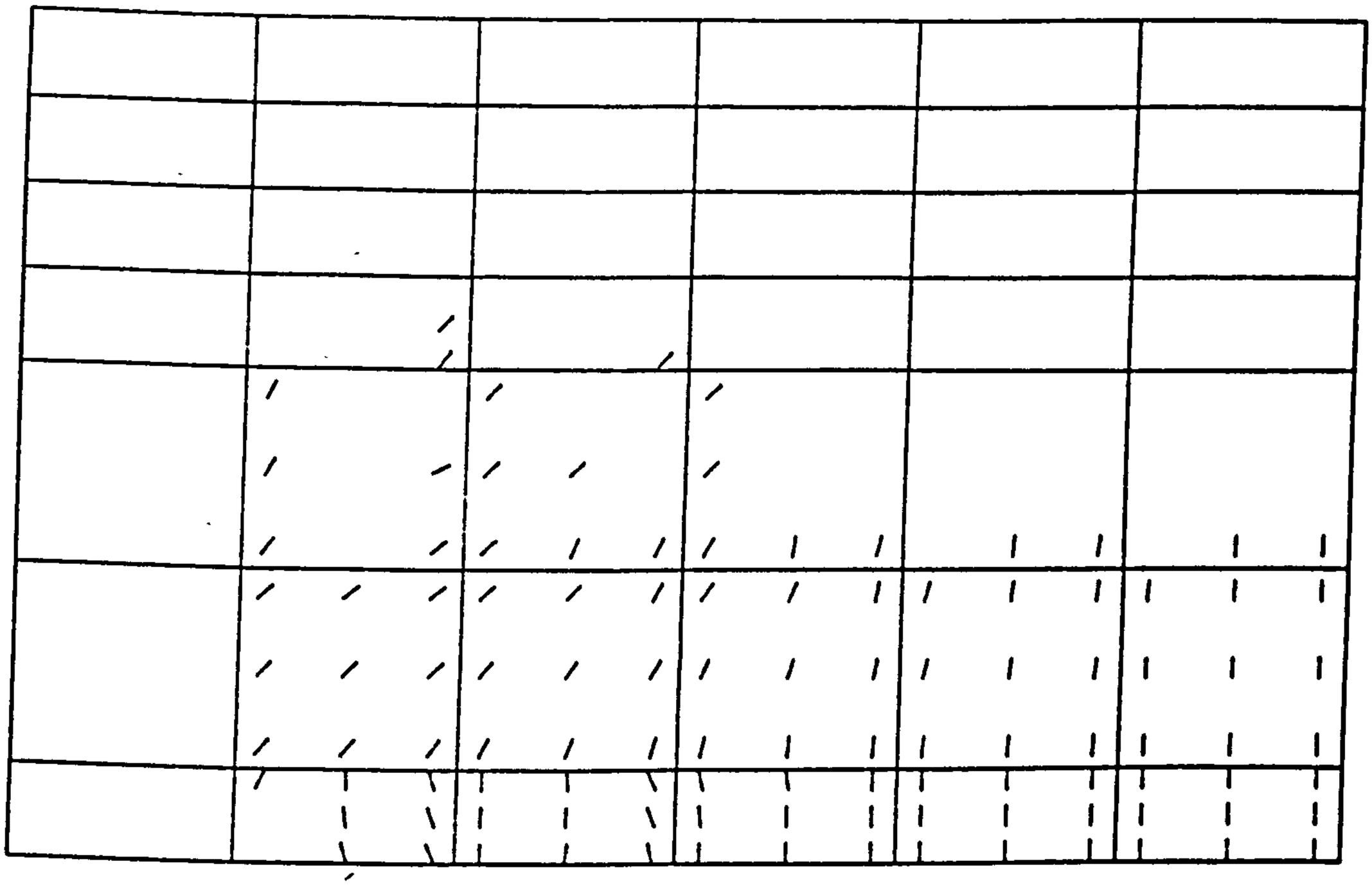

Figure (8·47) Crack pattern at load = 120·0 kN.

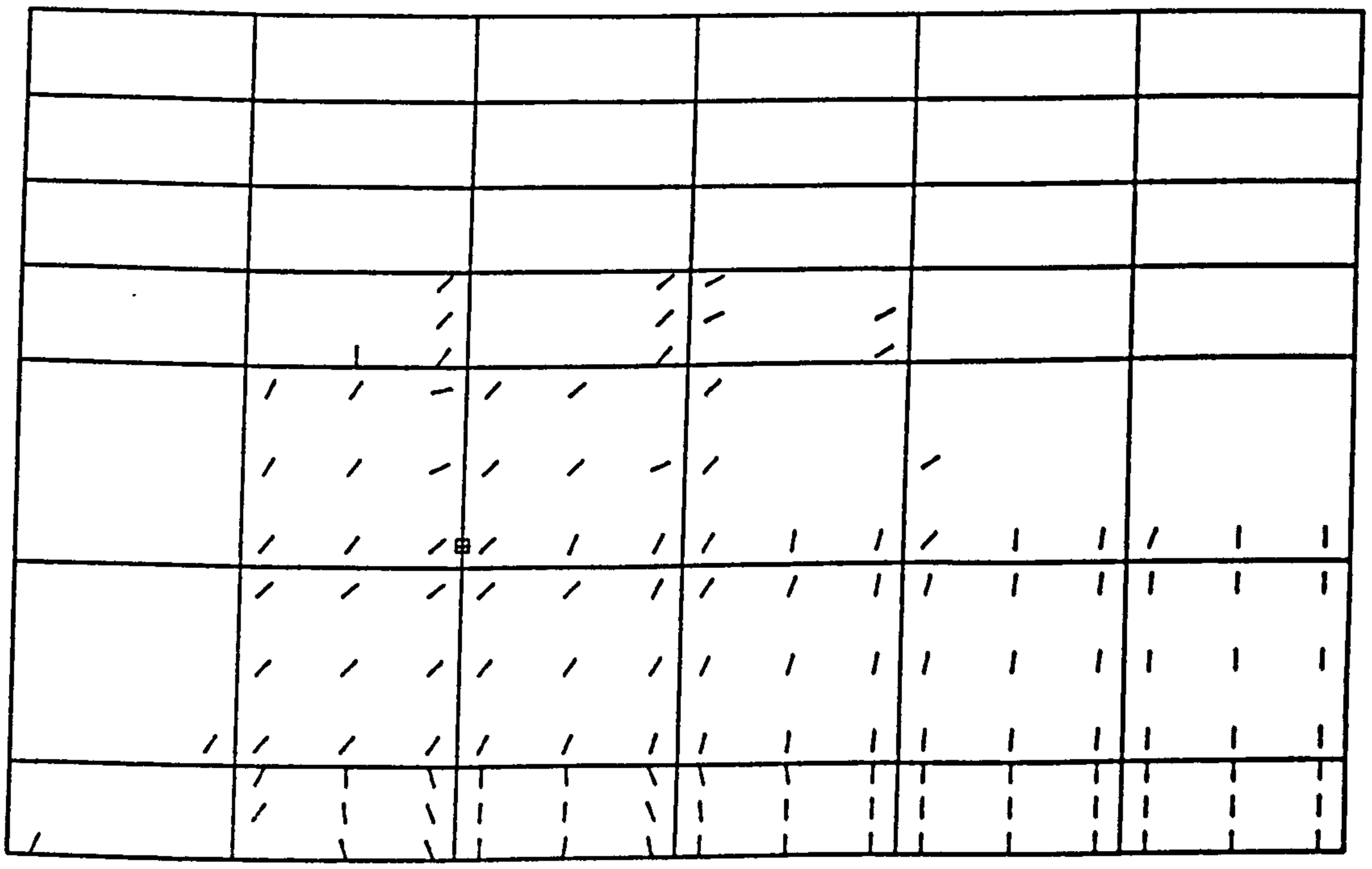

Figure (8·48) Crack pattern at load = 250·0 kN.

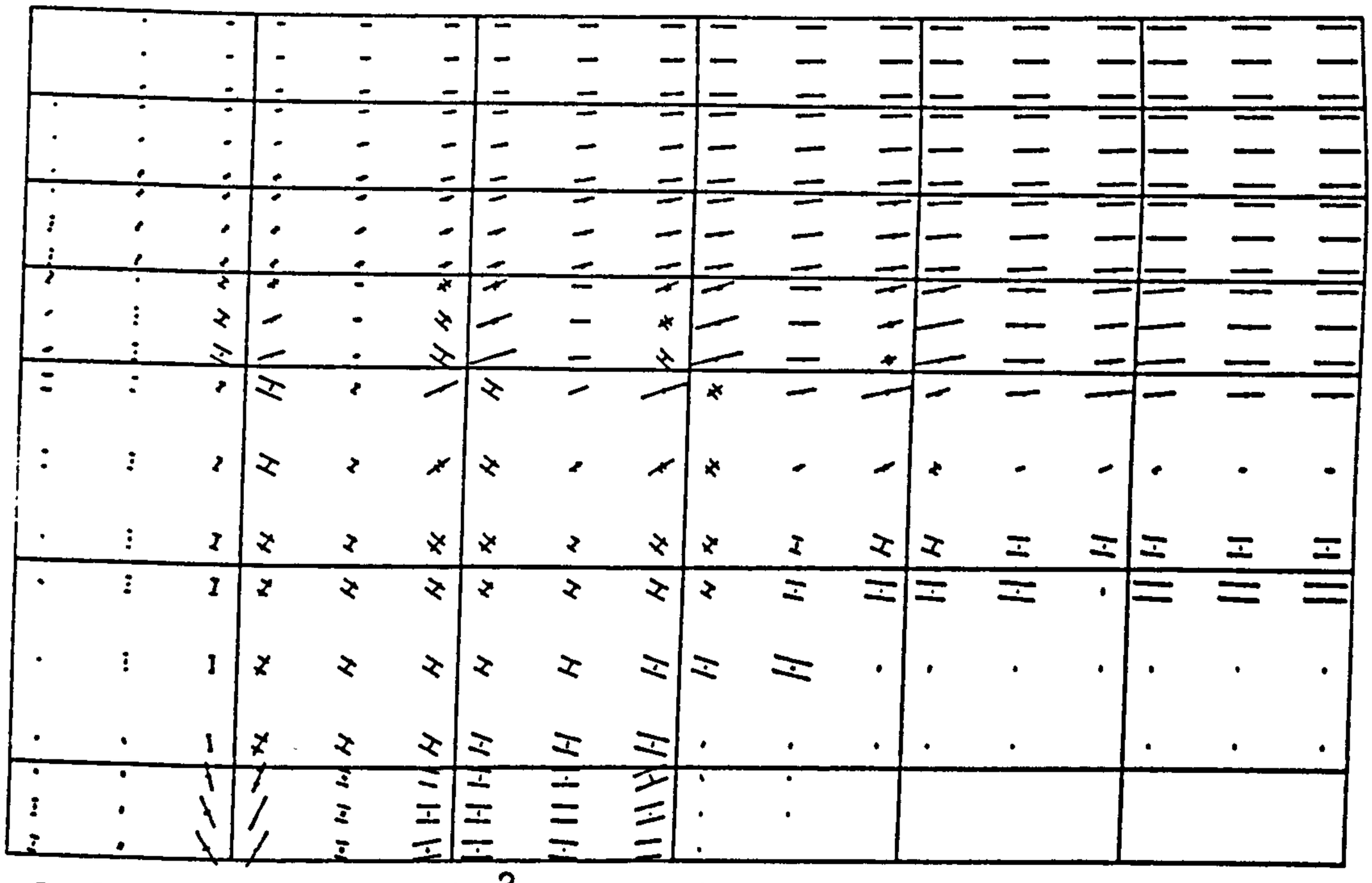

Scale: 1 mm = 0·86 N/mm^2 (= tension), (- compression)

Figure (8·49) Principal stress direction at load = 50·0 kN.

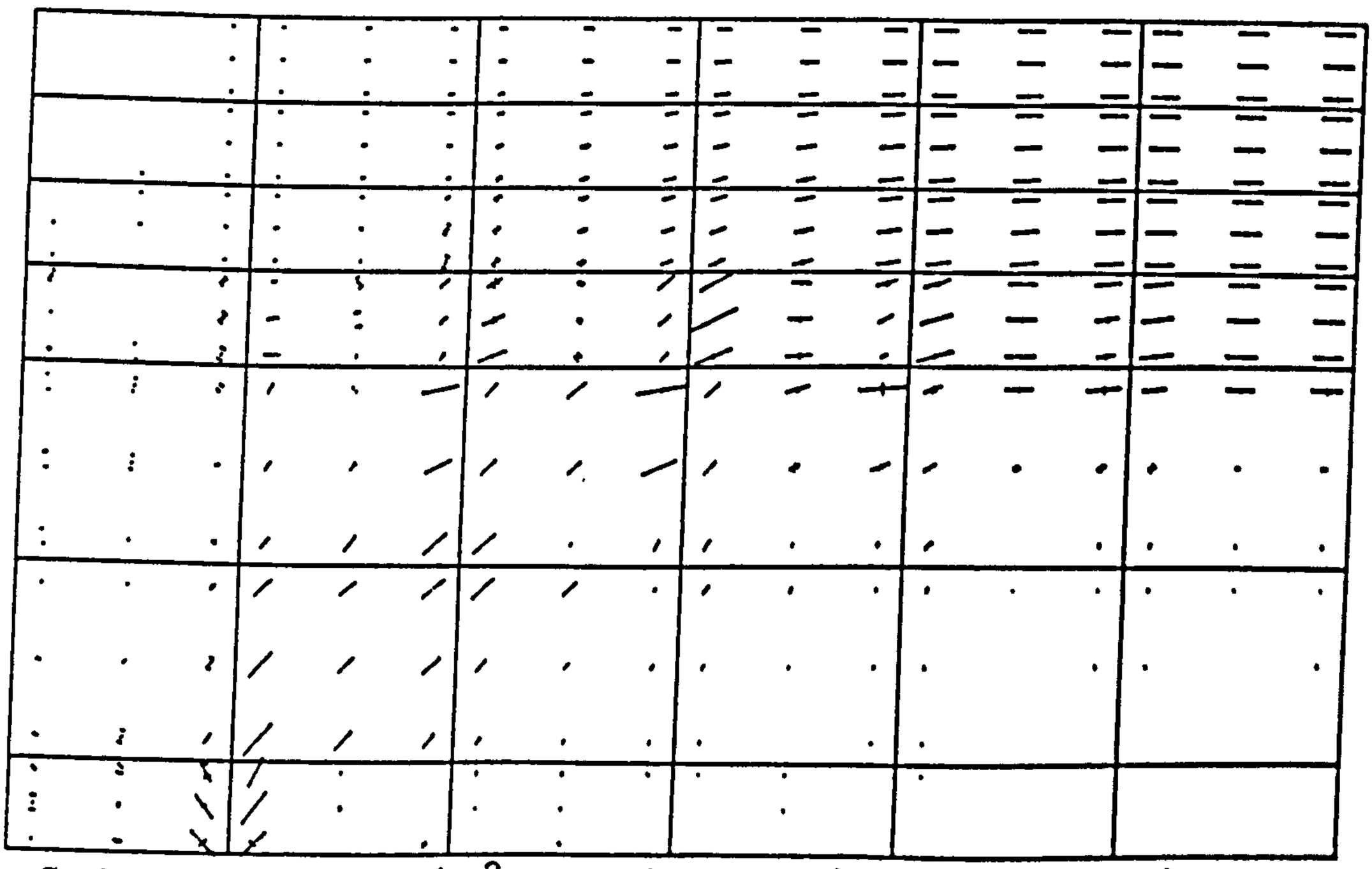

Scale: 1 mm = 5·22 N/mm^2 (= tension), (- compression)

Figure (8·50) Principal stress direction at load = 250·0 kN.

REFERENCES

1. Cope, R.J.; Rao, P.V., "Nonlinear finite element analysis of concrete slab structures". Proc. Inst. Civ. Eng., Part 2, Vol.63, 159-179, March 1977.

2. Razagpur, A.G.; Ghali, A. "Shear lag analysis in reinforced concrete". IABSE Colloquium on The Advanced Mechanics of Reinforced Concrete, Final Report, Delft, 671-686, 1981.

3. Fok, W.K., "The shear strength of reinforced concrete T Beams with unreinforced and reinforced web". Ph.D. Thesis, University of Glasgow, Sep., 1972.

4. Chong, O.W., "Ultimate shear strength of uniformly loaded reinforced concrete Tee beams". M.Sc. Thesis, University of Glasgow, Aug., 1980.

5. Swamy, R.N.; Bandopadhyay, A.K.; Erikitola, M.K., "Influence of flange width on the shear behaviour of reinforced concrete T Beams". Proc. Inst. Civ. Eng., Part 2, Vol.55, 167-190, March 1973.

6. Taylor, R.; Mills, P.E.; Rankin, R.I., "Test on concrete beams with mixed types of reinforcement". Mag. Conc. Res., Vol.30, No. 103, 73-88, June, 1978.

7. Scribner, C.F.; Wilhelm, D.R., "Behaviour of T-beam sections with varied shear reinforcement". J. ACI, Vol.79, 139-146, March-April, 1982.

8. Iverson, P.A., "Some aspects of the finite element method in two dimensional problems". Finite element method, Tapir, 110-111,1970.

9. Macleod, I.A.; Wilson, W.; Bhatt, P.; Green, D., "Two dimensional treatment of complex structures", Proc. Inst. Civ.Eng., Part 2, Vol. 53 , 589-597, Dec., 1972.

10. Ngo, D.; Scordelis, A.C., "Finite element analysis of reinforced concrete beams". J. ACI, Vol.64, 152-163, March, 1967.

CHAPTER 9

CONCLUSIONS AND RECOMMENDATIONS

9.1 General observations and conclusions

9.2 Recommendations for future work

CHAPTER 9
CONCLUSIONS AND RECOMMENDATIONS

9.1 General observations and conclusions:

The main observations and conclusions obtained from this thesis can be summarised as follows:

(1) The effect of numerical parameters in a nonlinear analysis are complex and significantly important in the prediction of the behaviour of reinforced concrete structures. These parameters must be defined clearly in any analysis so that a solution may be judged in relation to them, otherwise there might be an element of doubt in the adequacy of the results. Misuse of these parameters can lead to different solutions for load deflection curves, ultimate loads, cracking patterns and stress distributions. Variations can be obtained even if a single parameter is changed. In particular the following parameters were found to affect the results of an analysis:

(a) Solution parameters:- Convergence factor, convergence criteria number of iterations, nonlinear solution method, order of integration, aggregate interlocking, and tension stiffening;

(b) Quasi - material parameters:- aggregate interlocking and tension stiffening.

(2) Care must be taken when using low integration rules in a nonlinear analysis, because numerical problems may arise causing the solution to diverge. This was found for beams failing both in flexure and shear. It is well known that a 2 x 2 Gauss rule is the minimum required for a parabolic element, but this was found to be insufficient for a nonlinear analysis because it appears that higher orders are required to monitor the nonlinearized material

properties with closer precision. In this work a 3 x 3 Gauss rule was found to be quite adequate. However it appears that the order of Gauss rule is crucial rather than the total number of sampling points throughout the continuum.

(3) Shear retention factor α was examined for beams failing in both flexure and shear and it appears that using a value of 0.5 was satisfactory in both cases. This factor is quite adequate when used with the smeared crack approach and no further complications are required. The wide range of α between 0.01 and 1.0 did not significantly affect the predicted load deflection curves although as α increased towards 1.0 a slightly stiffer prediction was obtained. A value of $\alpha = 0.0$ produced very poor results. This would seem to suggest that α is a numerical device rather than an approximation to a physical phenomenon.

(4) No-tension stiffness cracking models produce large residual forces in comparison to the applied loads due to the discontinuity in the tension material law. Generally most cracks appear in the first two or three iterations of an increment. However, a crack could appear after a number of iterations have been applied, if the solution was close to convergence. This produces new residuals which are transferred to neighbouring nodal points even though a state of equilibrium has been almost reached at other points. This causes a completely new cycle of iterations to start because of the size of the new residuals. In general it is not significant whether these later cracks occur in the current or in the following increment. In such circumstances it is better to prevent the

occurrence of these cracks. This might be achieved if very small load increments were applied but on the other hand this tends to considerably increase the cost of the solution. However this point was not studied in detail in this work.

Alternatively iterations can be arbitrarily stopped after a given number of cycles but this is less satisfactory because the state of convergence is not known. Some authors have suggested the use of tension stiffening to counter this type of difficulty and satisfactory results have been reported. However this thesis suggests instead the use of a known but relatively high convergence tolerance with no-tension stiffening.

(5) Tension stiffening has been proposed by different authors and has been given various physical interpretations, ranging from a way of retaining stresses between discrete cracks to indirectly including bond-slip or aggregate interlocking effects. Moreover various models have been used for approximating this effect. It appears that the chosen shape of the stress-strain curve in the post cracking range is fairly arbitrary. This again suggests that it is a numerical device rather than a physical phenomenon.

(6) Tension stiffening can be replaced by a no-tension stiffening model with high convergence tolerance. This is because both approaches have the effect of retaining residual forces within the continuum, the former indirectly and the latter directly. However the no-tension stiffening model with high convergence has a considerable advantage in that it requires far less iterations and hence less computer time. Moreover, the results obtained using

tension stiffening methods are highly dependent on the combined effect of convergence tolerance and the value of strain at which the stress drops to zero, whereas the no-tension stiffening method depends only on the convergence tolerance which implies less complications.

A no-tension stiffening model using a 20% tolerance with the load criterion is suggested as the best combination.

(7) The V.S.M.1 method (where the stiffnesses are updated at the beginning of the first and second iteration of each increment) was found to be better than both the C.S.M. method and V.S.M.2 method in predicting the load deflection curve and ultimate load for a convergence tolerance of 20%. This conclusion must be slightly guarded because it has only been tested for a beam which failed in flexure.

(8) A general nonlinear solution procedure was established which gave satisfactory results although it may not necessarily be the best in a particular situation. This procedure uses the following:

(a) The variable stiffness method (V.S.M.1) where the stiffness are updated at the beginning of the first and second iterations.

(b) Between 20 to 30 load increments depending on the problem.

(c) The 3 x 3 Gauss rule.

(d) The no-tension stiffening cracking model.

(e) The constant shear retention factor with a value of $\alpha = 0.5$.

(f) The load criterion to check convergence to a tolerance of 20%.

(g) Iterations to continue until convergence is obtained; if convergence is not obtained by 30 iterations then failure is assumed to have occurred.

(9) The endochronic theory of concrete as presented by Bazant is difficult to modify because of the complexity of the form of equations and the difficulties of knowing just how the constants were determined. There appears to be much interdependence between the various parameters and the different effects they represent.

Simplifications need to be introduced so that the theory becomes more accessible, and can be more easily modified. However, despite these remarks the theory has proved both accurate and efficient in the prediction of concrete behaviour investigated in this work.

(10) Changing the values of the crushing strain of concrete affects the shape of the load deflection curve close to failure and can produce different ultimate loads. It is important to use a suitable value but this might be difficult to judge where confinement exists, particularly where reinforcement is closely spaced.

(11) The device of increasing the concrete strength in order to account for confinement caused by closely spaced reinforcement, such as under loading points, was found to be important in the analysis of some beams. Again this matter may be difficult to judge in practical applications, but obviously needs to be borne in mind.

(12) Despite the efficiency of the frontal solution, the peripheral operations of transfer to a backing disc file was found to be inefficient in a nonlinear analysis because disc transfers are very slow and costly. The introduction of the buffer area greatly improved this process and minimized the cost. However, the selection of buffer areas is highly dependent on the size of the main core

storage of the computer used and has to be carefully chosen.

(13) A simple method was proposed to analyse T-beam structures. Certain approximations were required in order to treat the structure as a two dimensional problem. The flange was treated separately from the web and was connected to the web through a fictitious element which transfers appropriate forces. Special boundary conditions and the selection of the point of separation of flange and web were important parameters. The method allows the prediction of the distribution of horizontal and shear stresses across the width of flange. The same numerical parameters proposed in the previous studies were used and full convergence was obtained for all solutions.

The results obtained for T-beams failing in flexure and shear showed different degrees of accuracy. The shape of the load deflection curves were relatively acceptable but they did not always compare well with the experimental results. The range of error in ultimate loads was fairly reasonable. Crack patterns in the webs were satisfactory, but they were not so in the flanges. Stress distributions in the flange were as expected. The approximation shows potential in predicting various aspects of the behaviour of T-beams, but requires further study and refinement.

9.2 Recommendations for future work:

This section recommends further work as follows:

(1) Reinforcing bar elements which can pass through the concrete element instead of the sides could be introduced. This will allow the use of less concrete elements and approximate the bar positions more

accurately. Hence cheaper solutions could be obtained, and more complex structures analysed. Also better aspect ratios could be selected which may give improved solutions.

(2) The effect of the different parameters used in the endochronic model should be studied in more detail to examine their relative significance in a finite element analysis. However, more important is that the endochronic theory is still under active development. Changes which appeared recently were found to be very efficient in handling more complex concrete behaviour such as cyclic loading and creep. Including new versions of this model would extent this program so that a much wider range of concrete behaviour could be studied.

(3) Further investigations are required to study the effect of varying the order of Gauss rule using different elements and mesh sizes under nonlinear conditions.

(4) Further studies on the calculation of residual forces at the nodes and checking their decay is required. It would be useful to confirm what influence cracks have on the decay of residuals using both methods of tension and no-tension stiffening, especially with different convergence tolerances and load increment sizes for a similar problem. This would provide more information and confirmation of the conclusion made in this work.

(5) The program in its present form is suitable for detailed numerical studies of different types of plane concrete structures. Numerical investigations could be carried out to study, for example, deep beams with openings of different geometry and loading conditions.

The use of the irregular mesh generator and plotting routines developed in this program will ease this process.

(6) The 8-noded element developed for the web-flange connection of the T-beams could be developed for other purposes such as introducing a bar between two concrete elements, similar to linkage elements. This would allow different nodes for the concrete and the steel which could then be connected by different stiffnesses which would account for such behaviour as bond-slip, dowel action etc.

(7) More detailed investigations are required to compare the experimental and theoretical stress distributions in the T-beams. For instance a layered element technique could be introduced for the flange in order to approximate the variation of stresses through the flange thickness. The method developed could also be extended for L-beams and box girder structures by introducing suitable modifications to the boundary conditions.

(8) The numerical procedure and models devised in this thesis could be tested for axisymmetric, and three-dimensional applications. In particular, the numerical parameters studies could be repeated for these cases.

APPENDIX

APPENDIX A

EQUATIONS OF ENDOCHRONIC THEORY FOR CONCRETE

For simplification the equations in the endochronic theory are divided into three parts:

1. Functions for intrinsic time parameters (z,z').
2. Functions for dilatation parameters (λ,λ').
3. Constants.

1. Functions for intrinsic time parameters:

$$F(\epsilon,\sigma) = F_1 + F_2$$

$$f(\eta,\epsilon,\sigma) = \left[1 + \frac{\beta_1\eta + \beta_2\eta^2}{1 + F_2/a_7} \right] F_3$$

$$H(\sigma) = b_1 \left[\frac{I_1(\sigma)}{b_2 - I_1(\sigma)} \right]^2$$

$$h(\eta') = 1 + \frac{\eta'}{\beta_3} + \left[\frac{\eta'}{\beta_4} \right]^2$$

in which

$$F_1 = \frac{a_o(1-\varepsilon_1)}{1-a_5(I_3(\sigma))^{1/3}(1+\varepsilon_2)}$$

$$F_2 = \frac{a_2\sqrt{J_2(\epsilon)}\ \ (1 + |a_6 I_2(\sigma)|^{1/4} + F_5)}{1-a_1 I_1(\sigma)+|a_8 I_2(\sigma)|^{1/2}F_4 - a_3 I_3(\sigma)\ [J_2(\epsilon)]^{1/8}(1+\varepsilon_2)}$$

$$F_3 = 1 + \frac{a_{10}}{J_2(\epsilon)\ (1+a_9/\eta^2)}$$

$$F_4 = \left[\frac{J_2(\epsilon)^{1/4}}{a_4 + J_2(\epsilon)^{1/2}} \right]^3$$

$$F_5 = a_{11}\,\sigma_{min}(1+a_{12}\sigma_{min}) \left[\frac{J_2(\epsilon)^{1/4}}{|a_{13}\sigma_{min}|^{1/4}+J_2(\epsilon)^{1/2}} \right]^3$$

$$g_1 = g_{11} \cdot g_{12}$$

$$g_2 = g_{21} \cdot g_{22} \cdot g_{23}$$

$$g_{11} = a_{14} J_2(\varepsilon)^{1/4} \left(\frac{\sigma_{med} - \sigma_{min}}{\sigma_{max} - a_{23}} \right) \left[a_{15} \left| \frac{\sigma_{med} - \sigma_{min}}{\sigma_{max} - a_{23}} \right|^{4/3} - a_{16} \right]$$

$$g_{12} = 1 - \frac{1}{1 + \left(\frac{\sigma_{min}}{a_{17}(\sigma_{max} - a_{23})} \right)^4}$$

$$g_{21} = \left[\frac{a_{18} \left(\frac{\sigma_{med} - \sigma_{min}}{\sigma_{med} - a_{23}} \right) - 1}{a_{19}\left(1 - a_{20} \left(\frac{|\sigma_{min}|}{\sigma_{max} - a_{23}} \right)(\sigma_{min} - a_{23})\right)} \right]^{5/4}$$

$$g_{22} = \frac{1}{1 + a_{21} \left(\frac{\sigma_{min}}{\sigma_{max} - a_{23}} \right)^4}$$

$$g_{23} = \left(\frac{J_2(\varepsilon)^{1/4}}{a_{22} + J_2(\varepsilon)^{1/2}} \right)^3$$

2. Functions for Dilatation Parameters:

$$\ell(\lambda) = 1 - \lambda/\lambda_o$$

$$L(\lambda) = \left(\frac{C_3}{1 - C_1 I_1(\sigma)} \right) \left[\left(\frac{\lambda}{\lambda_o} \right)^2 + \left(\frac{C_4 J_2(\varepsilon)}{C_2^2 + J_2(\varepsilon)} \right)^2 \right]$$

$$\ell'(\lambda') = C_6(1 - |\lambda'| / \lambda'_o)$$

$$L'(\lambda') = \frac{\sigma_{min}\, g_3^{1/3}}{1 + |g_3/C_8|^3}$$

in which

$$g_3 = |C_7 \sigma_{min}|^{0.93} - \sqrt{J_2(\varepsilon)}$$

In sections (1) and (2) $I_1(\sigma)$, $I_2(\sigma)$, $I_3(\sigma)$ and $J_2(\varepsilon)$ are defined by

$$I_1(\sigma) = \sigma_1 + \sigma_2 + \sigma_3$$

$$I_2(\sigma) = \sigma_1\sigma_2 + \sigma_2\sigma_3 + \sigma_3\sigma_1$$

$$I_3(\sigma) = \sigma_1\sigma_2\sigma_3$$

where σ_1, σ_2 and σ_3 are the principal stresses and

$$J_2(\varepsilon) = \frac{1}{2} e_{ij} e_{ij}$$

where e_{ij} is the deviatoric strain tensor.

Stresses σ_{min}, σ_{med} and σ_{max} are the principal stresses such that $\sigma_{max} < \sigma_{med} < \sigma_{min}$.

3. Constants:

The constants used in the previous equations were calculated by Bazant et al. using pound-inch units. These are summarized as follows:

$a_1 = 0.7$

$a_2 = 0.6/f_c'$

$a_3 = 1400 \left(\frac{f_c'}{4650\ psi}\right)^{1/2}$

$a_4 = \frac{90}{(f_c')^3}\left(\frac{3600\ psi}{f_c'}\right)$

$a_5 = 0.045$

$a_6 = \frac{0.6}{f_c'}\left(\frac{3600\ psi}{f_c'}\right)$

$a_7 = \frac{0.15}{f_c'^2}$

$a_8 = 0.05$

$a_9 = \frac{15}{f_c'^2}\left(\frac{f_c'}{3600psi}\right)^{1.5}$

$a_{10} = 0.000125$

$a_{11} = 0.2/f_c'$

$a_{12} = 0.8/f_c'$

$a_{13} = 2.2 \times 10^{-5}/f_c'$

$a_{14} = 25$

$a_{15} = 1.095$

$a_{16} = 1.216$

$a_{17} = 0.005$

$a_{18} = 0.94$

$a_{19} = \frac{1.0}{f_c'}\left(\frac{6300psi}{f_c'}\right)$

$a_{20} = 14$

$a_{21} = 1000$

$a_{22} = 0.04$

$a_{23} = 0.2\ f'_c$

$b_1 = 9.1\ \left(\frac{f'_c}{7020\text{psi}}\right)$

$b_2 = f'_c$

$C_1 = 2/f'_c$

$C_2 = 0.003$

$C_3 = 0.5$

$C_4 = 2$

$C_5 = 150$

$C_6 = 0.002/\text{psi}$

$C_7 = 1.05 \times 10^{-6}/\text{psi}$

$C_8 = 0.001$

$\beta_1 = 30$

$\beta_2 = 3500$

$\beta_3 = 0.08$

$\beta_4 = 0.23$

$z_1 = 0.0015$

$z_2 = 0.0125$

$\lambda_o = 0.003$

$\lambda'_o = 0.003$

These constants are applicable for normal weight concrete in the range of $3000 \leq f'_c \leq 7000$ psi (20 to 50 N/mm^2).

APPENDIX B

BRIEF DESCRIPTION OF THE PROGRAM

The program analyses nonlinear plane-stress problems using 8-noded isoparametric elements for concrete and 3-noded isoparametric elements for steel. The incremental iterative method is used to solve the nonlinear equations. The linear equations are solved by a Frontal technique, described by Hinton and Owen*. This was modified to include buffer storage areas in order to reduce the cost of analysis. The program also includes the endochronic theory, and different cracking, and crushing, models. Input and output were developed to be at a minimum and the selected output can be chosen as required.

Mesh generators are included for irregular and regular shapes of structure including the T-beam problems using fictious elements. Routines were built in for automatic plotting of meshes, crack patterns, principal stresses, contour stresses, and load deflection curves using the available GHOST and GINO plotting packages mounted on the ICL 2976 at Glasgow University.

A list of all subroutines is shown next followed by a brief description of their use. A chart which illustrates the relationship between each subroutine is provided at the end of this section.

* Hinton, E.; Owen, D.R.J., "Finite element programming". Academic,1977.

1. FES
2. INPUT
3. CONSTANT
4. GAUSSQ
5. LOADPS
6. FILL
7. FILL1
8. FILL2
9. NODEXY
10. RECTMG
11. GIN
12. INBLOC
13. GENER
14. GMESH
15. SFRQ
16. CHECK1
17. CHECK2
18. ECHO
19. INCREMENT
20. INPUT1
21. INPUT2
22. GOOUT2
23. GOOUT1
24. SFR2
25. JACOB2
26. BMATPS
27. MODPS
28. DMAT
29. DCRACK1
30. TMATRIX
31. BDB
32. DBE
33. STREPS
34. IFC
35. ENDOCA
36. ENDOC
37. CRUSH
38. POP
39. ELASTIC
40. PRINCIPAL
41. EMEM
42. SFRB
43. TEST
44. JACOB1
45. MODB
46. COUNT
47. STREB
48. DECIDES
49. IFCB
50. OUTPUTB
51. DECIDE
52. STIFPS
53. FRONT
54. GOOUT
55. PLMESH
56. SPACE
57. PLMESK
58. PLTXY
59. PLOTT

(1) Program FES:

This is the main controlling subroutine from which all other subroutines are called.

(2) Subroutine INPUT:

This reads the required information for geometry, boundary conditions, material properties for concrete and steel, and calls the required subroutines for data checking and mesh generation.

(3) Subroutine CONSTANT:

This sets up the initial values for all material property constants and stores them in the appropriate arrays by calling subroutine FILL.

(4) Subroutine GAUSSQ:

This sets up the sampling (Gauss) point positions and weighting factors for numerical integration. The order of Gauss rule is restricted to either 2 x 2, 3 x 3 or 4 x 4.

(5) Subroutine LOADPS:

This reads applied pressure and concentrated loads and distributes them onto specific nodes. It also handles gravity and temperature loads under elastic conditions.

(6) Subroutine FILL:

This stores the updated material parameters, in the proper positions. It also stores the angle of each crack and its identity (closed or open), and its type (single or double).

(7) Subroutine FILL1:

This subroutine stores the total stresses and strains.

(8) Subroutine FILL2:

This stores the endochronic variables to be used in other increments.

(9) Subroutine NODEXY:

The main purpose of this subroutine is to calculate the midside nodal coordinates for straight sided elements when no automatic mesh generator is used.

(10) Subroutine RECTMG:

This generates nodal coordinates and nodal connections for rectangular meshes only. Properties for different materials can be generated.

(11) Subroutine GIN:

This is the main subroutine calling the required routines for generating irregular (or regular) shaped meshes for the 8-noded element. It calls subroutines INBLOC, GENER, GMESH, SFRQ.

(12) Subroutine INBLOC:

This reads input data defining the main structure outline within which a mesh will be generated.

(13) Subroutine GENER:

This performs the mesh subdivision, for the given irregular (or regular) blocks, and eliminates repeated nodal points which occur during the mesh generating process.

(14) Subroutine GMESH:

This outputs the generated mesh and nodal connections calculated in the previous subroutine GENER.

(15) Subroutine SFRQ:

This sets up the required shape functions for mesh generating (which in general could be different from the shape functions defining the element properties).

(16) Subroutine CHECK1:

This checks the control parameters read in subroutine INPUT to ensure that they all have values ranging within the specified description in the manual. Any error detected is given an appropriate number which can be checked.

(17) Subroutine CHECK2:

This checks any identical information given with regard to coordinates and nodal connections. The most useful check in this subroutine is the one which ensures that the maximum frontwidth does not exceed the value specified in subroutine FRONT.

(18) Subroutine ECHO:

This is called if any error is detected in CHECK1 or CHECK2. The main purpose is to stop the program and to print out any remaining unread Input data.

(19) Subroutine INCREMENT:

This subroutine calls all the required routines for the nonlinear analysis, and for plotting the results. Also all stress, displacement and numerical control parameters are printed.

(20) Subroutine INPUT1:

This outputs the main control data of the finite element analysis.

(21) Subroutine INPUT2:

This subroutine outputs the documentary information which defines the printed output.

(22) Subroutine GOOUT2:

This subroutine outputs the nonlinear control numerical parameters.

(23) Subroutine GOOUT1:

This outputs the convergence information at each increment.

(24) Subroutine SFR2:

This calculates the shape functions and their derivatives for the 8-noded element.

(25) Subroutine JACOB2:

This calculates the coordinates of all gauss points, and the Jacobian matrix, its determinant and inverse for the 8-noded element.

(26) Subroutine BMATPS:

This subroutine calculates the strain matrix [B] for the 8-noded element.

(27) Subroutine MODPS:

This subroutine reads the material properties from subroutine FILL and sets up the elasticity matrix, for stiffness calculations.

(28) Subroutine DMAT:

This sets up the elasticity matrix for the calculation of stresses.

(29) Subroutine DCRACK1:

This sets up the required cracking matrix in the cracked directions for each gauss point.

(30) Subroutine TMATRIX:

This subroutine calculates the transformation matrix which is used to transform the stresses and strains to the required directions.

(31) Subroutine BDB:

This subroutine transforms the elasticity matrix to the cracked direction and back for the 8-noded element.

(32) Subroutine DBE:

This calculates the stress matrix [DB] for the 8-noded element.

(33) Subroutine STREPS:

This calculates the stresses at the Gauss points for the 8-noded element.

(34) Subroutine IFC:

This subroutine calculates the internal equivalent nodal forces for the 8-noded element.

(35) Subroutine ENDOCA:

This subroutine updates the stresses for all regions using the endochronic theory and checks the cracking and crushing of concrete.

(36) Subroutine ENDOC:

This sets up the endochronic equations to be used in subroutine ENDOCA.

(37) Subroutine CRUSH:

This subroutine checks for crushing of concrete using the required criteria.

(38) Subroutine POP:

This calculates the uniaxial stresses for a known value of strain using Popovics formula for concrete.

(39) Subroutine ELASTIC:

This subroutine calculates the stresses due to a defined $[D]$ and $\{\varepsilon\}$ matrix.

(40) Subroutine PRINCIPAL:

This calculates the principal stresses and strains and their directions.

(41) Subroutine EMEM:

This calculates and prints out the maximum and minimum major and minor principal strains and stresses for the 8-noded element throughout the whole mesh.

(42) Subroutine SFRB:

This subroutine calculates the shape functions and their derivatives for the 3-noded element.

(43) Subroutine TEST:

This subroutine selects the proper shape function for the four 3-noded elements which can be attached to the sides of the 8-noded element.

(44) Subroutine JACOB1:

This calculates the coordinates of all Gauss points for the 3-noded element and sets up the Jacobian matrix, its determinant and inverse.

(45) Subroutine MODB:

This calculates the stress matrix [DB] for the 3-noded element.

(46) Subroutine COUNT:

This sets up the 3-noded element stiffness in similar positions to an 8-noded element.

(47) Subroutine STREB:

This is used to calculate the stresses for the 3-noded element at the required Gauss points.

(48) Subroutine DECIDES:

This subroutine calculates the total stresses for the 3-noded steel element and checks for its yielding.

(49) Subroutine IFCB:

This calculates the internal equivalent nodal forces for the 3-noded element.

(50) Subroutine OUTPUTB:

This outputs the final stresses and strains for the 3-noded elements.

(51) Subroutine DECIDE:

This analyses the steel as a separate 8-noded two dimensional element with strain hardening included.

(52) Subroutine STIFPS:

This calls the required subroutines to calculate the stiffnesses for the 8-noded element and 3-noded element and adds them into the appropriate places in the stiffness matrix.

(53) Subroutine FRONT:

This solves the simultaneous equations by means of Gauss elimination and back substitution. The Front solution is used and a modified buffer storage facility is included.

(54) Subroutine GOOUT:

This outputs the required information for using the plotting routines. This includes a description of all parameters used to plot meshes, cracks and stresses.

(55) Subroutine PLMESH:

This subroutine plots the mesh, crack patterns and stress distributions in the two and three dimensional space, using the available GHOST routines (i.e. a general package for plotting).

(56) Subroutine SPACE:

This sets up the required plotting scales because the available GHOST package only plots on a specified distorted scale. (This would not usually be needed and is peculiar to the operating system on which this program was developed).

(57) Subroutine PLMESK:

This subroutine plots contour lines for horizontal, vertical and shear stresses for rectangular shapes using the GINO plotting package in the two and three dimensional space (The GINO package is also a general plotting routine, having better facilities for plotting contours than GHOST).

(58) Subroutine PLTXY:

This plots any two variables using the GHOST routines and is normally used to plot the load displacement curves.

(59) Subroutine PLOTT:

This subroutine plots stress-strain curves on the line printer.

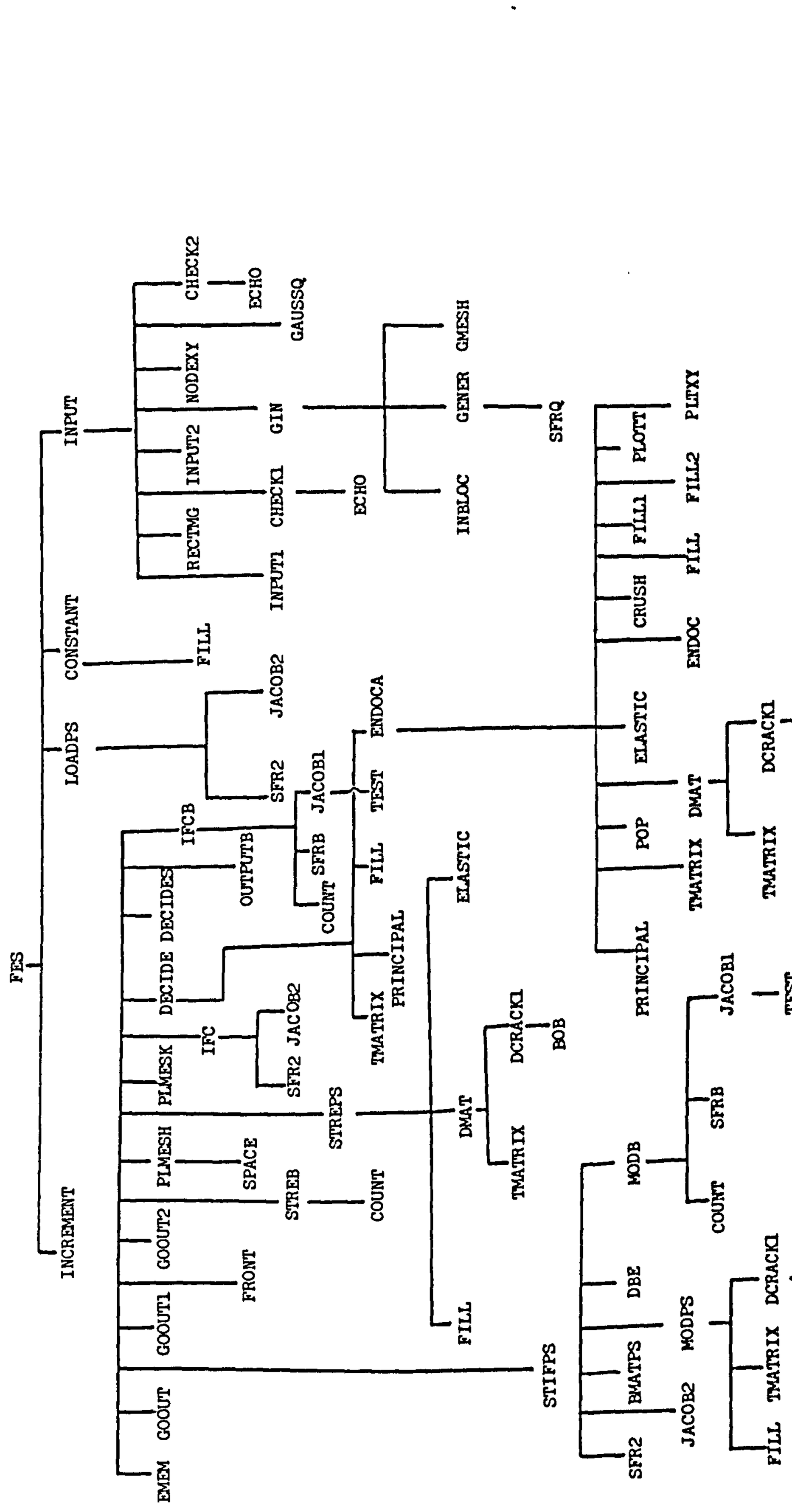

Chart showing the relationship between the subroutines used in this thesis.